THE SOLID STATE STRUCTURE AND PROPERTIES OF STIFF CHAIN ARAMIDS

by

GREGORY CHARLES RUTLEDGE

Bachelor of Science in Chemical Engineering
University of Virginia
(1983)

Submitted to the Department of Chemical Engineering
in Partial Fulfillment of the Requirements
for the Degree of

DOCTOR OF PHILOSOPHY

at the

MASSACHUSETTS INSTITUTE OF TECHNOLOGY
(January, 1990)

Signature of Author _____
Department of Chemical Engineering
January 18, 1990

Certified by _____
Professor Ulrich W. Suter
Thesis Supervisor

Accepted by _____
Professor William M. Dean
Departmental Committee on Graduate Students

'The time has come,' the Walrus said,
'To talk of many things:
Of shoes–and ships–and sealing wax–
Of cabbages–and kings–
And why the sea is boiling hot–
and whether pigs have wings.'

Lewis Carroll, *The Walrus and the Carpenter*

THE SOLID STATE STRUCTURE AND PROPERTIES OF STIFF CHAIN ARAMIDS

by

Gregory Charles Rutledge

Submitted to the Department of Chemical Engineering
on January 18, 1990 in partial fulfillment of the
requirements for the degree of Doctor of Philosophy

ABSTRACT

Stiff chain aramids are polymers composed of alternating aromatic ring and amide moieties which, due to the rigidity of the individual components and the parallel propagation of the chain contour, exhibit rodlike behavior in the individual macromolecule. This rodlike behavior leads to the formation of nematic liquid crystal mesophases above a critical concentration of polymer in solution and enables the realization of unusually high degrees of molecular orientation and crystallization in spun fibers. These aramids are characterized by high melting points and good thermal stability up to 550°C, and the practicality of high orientation of fully extended chains makes their fibers attractive as high strength, high modulus reinforcing materials. This work addresses the topic of the solid state structure and properties of such molecular architectures, with specific emphasis on poly(p-phenylene terephthalamide) (PPTA), at the scale of atomic level organization.

A static atomistic model was developed to simulate the geometry and potential energy characteristics in the ordered solid state of a crystal-forming polymer. This model represents the local atomic structure as an imperfect pseudocrystalline parallelepiped embedded within a larger crystalline matrix. It requires no adjustable parameters. Minimization of potential energy simultaneously with respect to both intramolecular and intermolecular degrees of freedom permits the prediction of detailed atomic structure and cohesive energy and estimation of the Hildebrand solubility parameter. Quantitative prediction and diagrammatic representation of the x-ray scattering pattern from these structures was made. Application of the simulation methods to PPTA yielded a plurality of viable polymorphs having cohesive energies on the order of 39 kcal/mole of repeat units; both energy and (in select cases) geometry predictions were in agreement with available literature information. Detailed analysis of interchain interactions was used to demonstrate the hierarchy of the primary behaviors leading to the formation of hydrogen-bonded sheets and three dimensional structure.

A series of simulated deformations of the minimum energy structures was used to predict the full twenty-one independent elements of the stiffness and compliance tensors. Thermodynamic and statistical mechanical analyses demonstrate that our values, calculated from considerations of potential energy only, overestimate the true elastic constants by 3% to 27%. Elastic properties of aramid fibers were estimated by symmetrizing the single crystal elastic tensors in the limits of uniform distribution of strain and stress to yield Voigt and Reuss bounds, respectively, for the elastic moduli. For one structure of PPTA the calculated extensional, transverse, and torsional moduli are in the ranges 215-325 GPa, 5.2-21.1 GPa, and 4.1-13.3 GPa, respectively, in good agreement with observed values.

Validation of the model was performed through an experimental program which included the design and construction of a dry-jet wet spinning apparatus suitable for the production of highly oriented crystalline monofilament of 20μm to 40μm dry fiber diameter from quantities of polymer less than one gram. Analysis by wide angle x-ray scattering of as-spun and annealed fibers confirmed the polymorphic behavior of PPTA and the accuracy of the structure predictions from the simulation.

The effects of atomic scale modification were addressed through the simulation of chlorinated PPTA's. Polymer chains having chlorines substituted in the 2 and 6 positions of the phenylene ring and their regular isomeric forms exhibiting entirely head-to-head, tail-to-tail or entirely head-to-tail linkages of asymmetric units were considered by simulation. Cohesive energies roughly 90% to 93% of that for

PPTA were found for these modified polymers. The primary cause for this reduction is the expansion of the atomic lattice. The hierarchy of structure-determining factors and the estimated fiber moduli are little changed from their PPTA counterparts.

Thesis Supervisor: Ulrich W. Suter

Title: Professor of Macromolecular Chemistry, Institut für Polymere, Eidgenössische Technische Hochschule, Zürich, and Visiting Senior Lecturer, Department of Chemical Engineering, Massachusetts Institute of Technology, Cambridge.

ACKNOWLEDGEMENTS

I would like to express my sincere thanks to many good friends and supporters who have assisted and sustained me through the realization of this work:

Ueli Suter, my thesis supervisor, provided philosophical inspiration, scientific freedom, and above all unwavering support, elements without which good research can not happen.

Professors Robert Cohen and Edward Merrill, my thesis committee, offered their guidance through advice and critique, and helped me to keep the computational development within perspective. Special thanks are due to Professor Cohen and to Dr. Gyula Vancso for providing access to state-of-the-art x-ray scattering equipment in Cambridge and in Zürich.

Dr. Frank Gentile, Dr. Werner Meyer, and Professor Costas Papaspyrides, my friends and fellow workers, through their efforts in and out of the lab, helped make this research possible.

Jeff Pribble, Friedrich Esch, and Urs Krebs have contributed indispensably to the development and realization of the experimental portion of this work.

Financial support was provided by the National Science Foundation Graduate Fellowship Program, the Amoco Oil Company, through the Amoco Graduate Fellowship in the Department of Chemical Engineering at MIT, and the Schweizerischer Nationalfonds zur Förderung der wissenschaftlichen Forschung.

Many friends, on this side of the Atlantic and that, have offered open companionship and provided welcome distraction from the pursuit of this research: Thankyou.

I wish to express special thanks to my family.

TABLE OF CONTENTS

LIST OF FIGURES

LIST OF TABLES

1. INTRODUCTION

1.1 Motivation

The rapidly expanding field of rigid rod polymers represents a commercially significant and scientifically fascinating class of new, high performance materials. Interest in this general class of polymers dates back to the work of Morgan and Kwolek in the sixties and seventies on wholly aromatic polyamides which resulted in patents [Kwolek, 1972; Morgan, 1975] to the Dupont Company and eventual commercialization of the trademark fibers Nomex® and Kevlar®. Today, this class has expanded to include, in addition to the original polyamides, a wide variety of new polyamides, polyesters, polyhydrazides, polyoxazoles and polythiazoles, to name a few. Commercially, these materials have attracted interest due to their unusual thermal stability and impressive mechanical properties, which hold promise for a new era of light weight, high strength composites and cords; an indication of the impressive strength-to-weight properties of these polymers, relative to conventional reinforcing materials, is illustrated in Figure 1.1 [Adams and Eby, 1987]. In the scientific arena, the rigid rod polymers have stimulated renewed interest in the theoretical and phenomenological ramifications of long range molecular rigidity to melt and solution behavior, processing, and solid state properties. The ease with which high degrees of molecular orientation may be realized and the impressive mechanical properties achievable with such stiff chains suggest the importance of atomic scale structural character to macroscopic structure and properties of the bulk polymer.

Efforts to develop improved high strength organic fibers have followed several paths. Some research has been directed towards modifications of aramids or development of entirely new chemistries to produce polymers which have a different combination of material properties or which may not be susceptible to some of the performance flaws characteristic of aramids, such as hydrolytic instability or poor compressive strength. Other efforts have sought to facilitate or improve processing methods to yield better performing fibers at reduced costs, either through chemical modification or process design. In our own laboratory research into the placement of substituents on the ring moiety of the diamide monomer and control of polymerization over the range of constitutional isomers which may result has led to the production of more soluble polymers which appear to retain the essential rigidity of the unsubstituted molecules. These new polymers are well-characterized in terms of the locus of substituents along the

Figure 1.1: Plot of specific strength versus specific modulus for a variety of fibers [Adams and Eby, 1987].

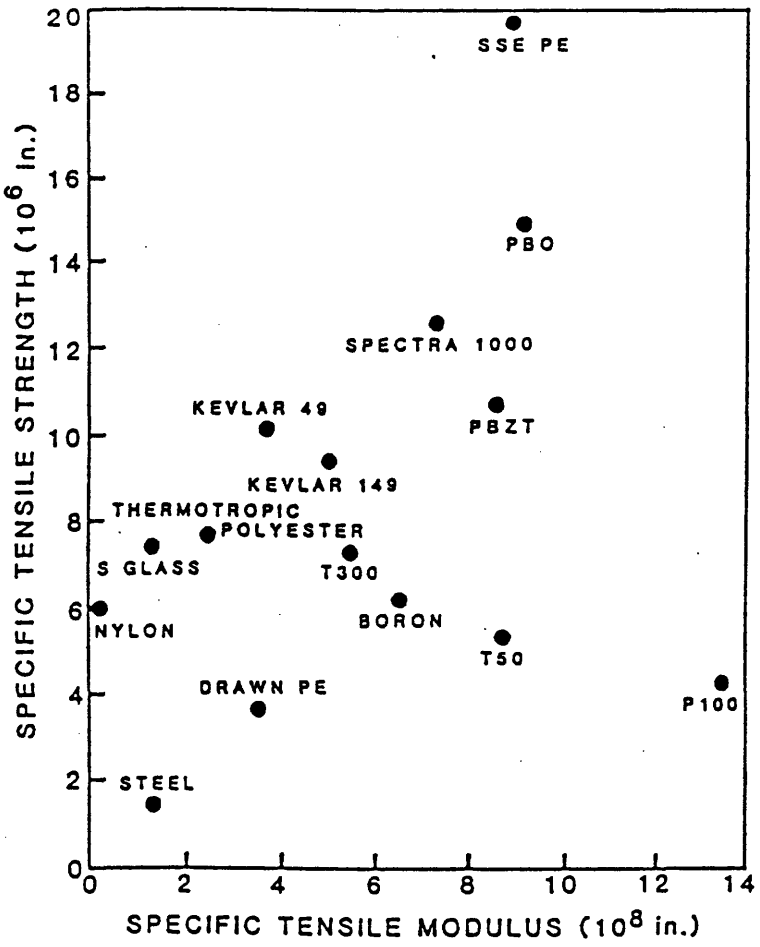

length of the chain; as such, they provide appropriate model polymers for exploring the effects of atomic level modifications on bulk properties.

Lacking to date is a complete description of the linkage between atomic scale detail and macroscopic material properties for these and other new, high performance polymers. Such understanding is required before one can proceed to the ideal of designed materials for engineered applications. The concept of perceptive design of new materials is a topic of great current interest. The goal is to understand the source of, and by so doing reliably predict, the properties of new materials in the bulk from knowledge of the constituent structure. In the past, such attempts have been largely empirical and phenomenological in nature, devised to mimic nature rather than provide an atomistic basis for understanding. With the ongoing explosion in computational resources, the application of more exacting and detailed approaches to property prediction than have heretofore been possible may now be attempted. Such methods as Molecular Mechanics (MM) and Molecular Dynamics (MD), and even the computationally demanding calculations of quantum mechanics, have been and are currently being developed for idealized conceptualization of increasingly complex systems, beginning with isolated molecules but including in a few instances polymeric liquids and solids of glassy and crystalline structure. However, no such attempt has previously been made to apply these techniques to the unique problems of conformationally constrained stiff chain macromolecules in their highly ordered solid state.

With the congruence of enhanced computational resources and the current emphasis on the design of new materials, the opportunity arises to further the development of novel computational techniques as well as establish a uniquely detailed basis for understanding the connection between structure and properties of a new class of materials. The insights gained should serve to expand our understanding of the fundamental relations between atomic structure and material behavior as well as augment the palette of computational software available for the development of such information. The results obtained should provide some direction for future synthetic efforts towards the next generation of high performance polymers.

1.2 Objectives

The goal of this work is to simulate the solid state structure of a commercially relevant aramid and its family of ring-substituted isomers and correlate calculated predictions with experimental results. For this purpose, we have selected the polymer poly(p-phenylene terephthalamide), referred to hereafter as PPTA, and its di-substituted isomers having chlorines on the aromatic ring of either the diamine or diacid monomer in the ortho positions. This broad scope entails the following specific objectives:

1) Development of a static atomistic model of a polymer chain in a highly ordered (i.e. pseudocrystalline, crystalline) solid state using available a priori geometric and energy information characteristic of the constituent subunits of the polymer, without the introduction of adjustable parameters. The model must be applicable to the specific features of extended chain conformation polymers and encompass all features relevant to the quantitative determination of geometry and potential energy.

2) Use of this model to derive predictions of structure, x-ray diffraction, selected thermodynamic properties, and detailed mechanical properties of the solid state of a model stiff chain polymer system and the atomic scale source of these properties.

3) Validation of the model by comparison with experimental data on structure and mechanical behavior. For this purpose, this work encompasses an experimental program to design and build an apparatus for spinning small quantities of fiber of sufficient crystalline perfection for comparison to simulation results. The validation procedure entails wide angle x-ray scattering (WAXS) analysis of such fibers produced under different processing conditions and direct comparison of simulation results with experimental data at both the atomic and the phenomenological levels.

4) Extension of the simulation process to the analysis of derivatives of the parent polymer for purposes of relating discrete atomic-scale variations to observable macroscopic properties. These derivatives may vary in the type of substitution (e.g. chlorine, methyl, nitro, or methoxy), the location of substitution (e.g. on the diacid phenylene ring or the diamine phenylene ring), and in the order of substitution along the polymer backbone (e.g. "head-to-head, tail-to-tail" polymerized comonomers or "head-to-tail" polymerized comonomers). For this purpose, 2,6-dichloro-substituted derivatives of poly(p-phenylene terephthalamide) are to be studied in detail.

The remainder of this document is organized to address these objectives in order. The state of the art leading up to this work is summarized in Chapter 2. Chapter 3 addresses the development of the computer model and discusses the special considerations required to simulate the oriented solid state. Chapter 4 details the application of the model to the parent polymer, PPTA. Chapter 5 then discusses the simulation procedure for the prediction of mechanical properties, again with application to the parent polymer. Chapter 6 deals with the experimental aspects of fiber spinning, x-ray analysis of fibers, and validation of the model. Finally, Chapter 7 deals with the extension of the method to the prediction of properties of the related polymers, with particular attention to the specific effects of atomic substitution and constitutional order.

2. STATE OF THE ART

2.1 Aramids

2.1.1 Early Development

Aromatic polyamides, or aramids, represent the first, chronologically, and to date commercially foremost of the high performance stiff chain polymers. By definition, aramids are synthetic long chain molecules containing amide moieties wherein at least 85% of the amide linkages are attached directly to two aromatic rings [Preston, 1987]. They are generally produced via step growth polymerization, or polycondensation, of (1) a monomer consisting of one or more aromatic moieties and having a primary amine at one end and a carboxylic acid or acid chloride at the other, or (2) comonomers comprised of an aromatic diamine on the one hand and an aromatic diacid (or diacid chloride) on the other. The introduction of aramids into the literature resulted from the work of Morgan, Kwolek, and co-workers at Dupont in the early seventies on the self-condensation of p-aminobenzoyl chloride to yield poly(p-benzamide) (PBA) and bipolymer condensation of m- or p-phenylene diamine with a phthaloyl dichloride to yield poly(m-phenylene isophthalamide) (MPIA) or poly(p-phenylene terephthalamide) (PPTA), commercialized under the trade names Nomex® and Kevlar® [Kwolek, 1972; Morgan, 1977; Kwolek et al., 1977; Bair et al., 1977; Schaefgen et al., 1979]; these polymers are shown in Figure 2.1. Of these, Kevlar® has attracted the greatest attention for its high temperature stability and good strength-to-weight properties; a list of its characteristics is given in Table 2.1. Since that time, numerous variations in the area of rigid and semirigid polymers that lead to high performance materials have been reported. These include molecular chains with modifications of the aromatic rings [Kwolek, 1972; Bair et al., 1977; Jadhav et al., 1988], terpolymers with flexible subunits [Lenk et al., 1977; Aoki et al., 1978], azomethines [Morgan et al., 1984], and poly(amide-hydrazides) [Morgan, 1978; Preston and Hofferbert, 1978], to name a few. As a result of their unusual properties, these aramids are finding application in such end uses as structural composites, ropes and cables, protective apparel, and abrasion-resistant moldings. The high performance tensile properties of these aramid fibers are commonly attributed to the unusually stiff extended conformational characteristics of the molecules and the relative ease with which these macromolecular chains may be aligned along the fiber axis during fiber formation. The resulting fibers and yarns are conjectured to bear tensile loads almost entirely along the molecular axis which,

Figure 2.1: Common aramid polymers.

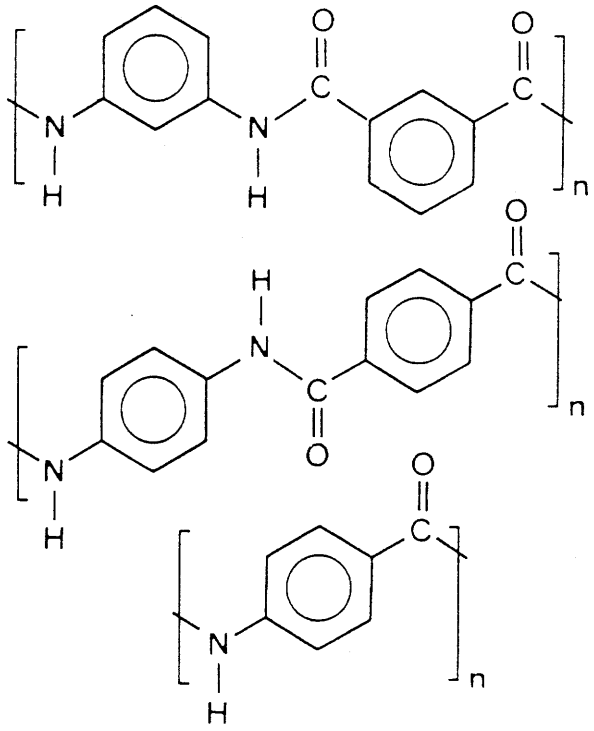

Table 2.1

Properties of Kevlar® aramid fiber[a,b]

High crystallinity (>95%)
High orientation
Extended chain structure
High melting point (ZST 640°C)
High glass transition temperature (375°C)
Low density (1.45 - 1.48 g/cm^3)
Low creep
High cut resistance
Good flex resistance and textile processability
Outstanding tensile properties (modulus: 180 GPa; strength: 3.5 GPa)
Low elongation at break (2 - 4%)
High damping vs. organic fibers
Nonconductive; good dielectric properties
Good abrasion resistance
Moderate compressive strength (500 MPa)

[a] from Schaefgen et al., (1979), as per Gentile [1988]
[b] Dupont Kevlar product literature

being extended, may not elongate significantly without bond scission. Tensile strengths approach the theoretical limits of chemical bond strengths.

2.1.2 Chain Rigidity and Solution Structure

π-bonding electron orbitals above and below the plane of the phenylene ring and the conjugated double bond character of the carbon-nitrogen and carbon-oxygen bonds in the amide link lend structural rigidity to the individual backbone moieties; thus molecular flexibility is possible only through rotation about bonds connecting successive moieties. The barrier to rotation and chain folding about the amide bond is on the order of 20 kcal/mol, with only a rare occurrence of cis conformations [Jorgensen and Swensen, 1985; Ramachandran and Mitra, 1976]. Rotation about the bonds connecting successive phenylene rings and amide groups is also restricted by the energetically advantageous tendency toward electron delocalization realized when these moieties are coplanar, on the one hand, and repulsive overlap of atomic spheres, on the other. Furthermore, such rotation produces little conformational change when the chain extending bonds on the ring are in the para positions. As such, these polymers resemble wormlike chains in solution, with typical persistence lengths on the order of 150 to 250 Å [Arpin and Strazielle, 1977; Zero and Aharoni, 1987; Millaud and Strazielle, 1978].

The lack of conformational flexibility and high degree of chain extension has two important ramifications. First, a relatively limited number of additional conformations are available to the polymer in solution or melt over that available in the solid state; for this reason, the entropies of solution and melting are expected to be unusually small. This contributes to the characteristically high melting points of aramids, on the order of 500+°C; these polymers typically undergo decomposition concurrent with or prior to melting. As such, they must be processed from lyotropic phases. However, since dissolution is little aided by entropic effects, the solubility of these aramids is largely determined by the enthalpies of dissolution. PPTA, for example, is only soluble in highly aggressive polar solvents, such as concentrated sulfuric acid, chloro or methyl sulfonic acids, or hydrogen fluoride, making processing difficult and expensive.

Second, above a critical concentration the polymer forms a stable anisotropic solution mesophase. In general, such anisotropic mesophases may arise upon cooling of the neat liquid (thermotropic liquid crystals) or upon increasing concentration in a solvent (lyotropic liquid crystals). This ordered phase formation in aramids has been anticipated through the use of lattice models predicting nematic liquid crystal phase formation for monodispserse and polydisperse rods [Flory, 1956; Flory and Ronca, 1979; Flory and Ronca, 1979; Flory, 1984]. In liquid crystals, the molecular chains are already ordered in local domains in the quiescent melt or solution. The nematic mesophase is characterized by coalignment of rods within each domain but with no preferred ordering perpendicular or translationally parallel to the

axis of local orientation; smectic and cholesteric mesophases, which will not be dealt with in detail here, exhibit additional translational ordering into molecular layers and rotational correlation between layers. The formation of the nematic phase results from directionally dependent interactions between molecular chains, which may be either hard (i.e. hard body steric exclusion) or soft (i.e. distance-dependent anisotropic intermolecular energetic interactions) in nature. The former case has been effectively described in terms of the aspect ratio x of the molecule, which may be calculated using the expressions:

$$x = (M_w/M_{ru})(l_{ru}/d_{ch}) \tag{2.1}$$

$$d_{ch} = (M_{ru}/\rho N_A l_{ru})^{1/2} \tag{2.2}$$

From this, the critical volume fraction at which a metastable ordered phase forms may be estimated by the equation:

$$V_p^* \approx (8/x)/(1 - 2/x) \; ; \quad x > 10 \tag{2.3}$$

While this equation was derived for *metastable* phase formation, its slight tendency towards overestimation has shown it to be a useful predictor for the onset of the *stable* nematic phase. The aspect ratio x must exceed $x_{crit} = 6.42$ for the formation of an ordered phase; as $x \rightarrow \infty$, the ratio of volume fractions in the two phases (ordered/disordered) at the transition approaches 1.465. The effects of polydispersity serve to widen the concentration range over which both isotropic and anisotropic phases are stable, and lead to fractionation of species such that higher aspect ratios are distributed preferentially into the anisotropic phase. During processing, imposition of an external field (e.g. flow or magnetic) induces common alignment of domains with minimal entanglement of molecules, which is important to achieving high orientation in conventional fiber-forming processes [Morgan, 1977].

Experimental studies on PBA, PPTA, and some of their chlorinated derivatives in dilute solution confirm the extended conformations of these chains (Table 2.2). Further studies [Papkov et al., 1974; Kwolek et al., 1977; Bair et al., 1977; Panar and Beste, 1977; Balbi et al., 1980; Gentile, 1988] of phase behavior for PBA and chloro-substituted PPTA in dimethyacetamide (DMAc) plus LiCl and PPTA in H_2SO_4 demonstrate (1) the tendency among these systems (including the chloro-substituted) to form nematic phases, (2) the reduction in critical polymer concentration for nematic phase formation at higher molecular weights (i.e. higher aspect ratio) in qualitative agreement with the lattice model (Figure 2.2), and (3) the critical point behavior associated with adding LiCl (i.e. increasing the interaction between

Figure 2.2: Critical volume concentration Vp* versus axial ratio and comparison between threory and experiments for PBA and PPTA [Flory, 1984].

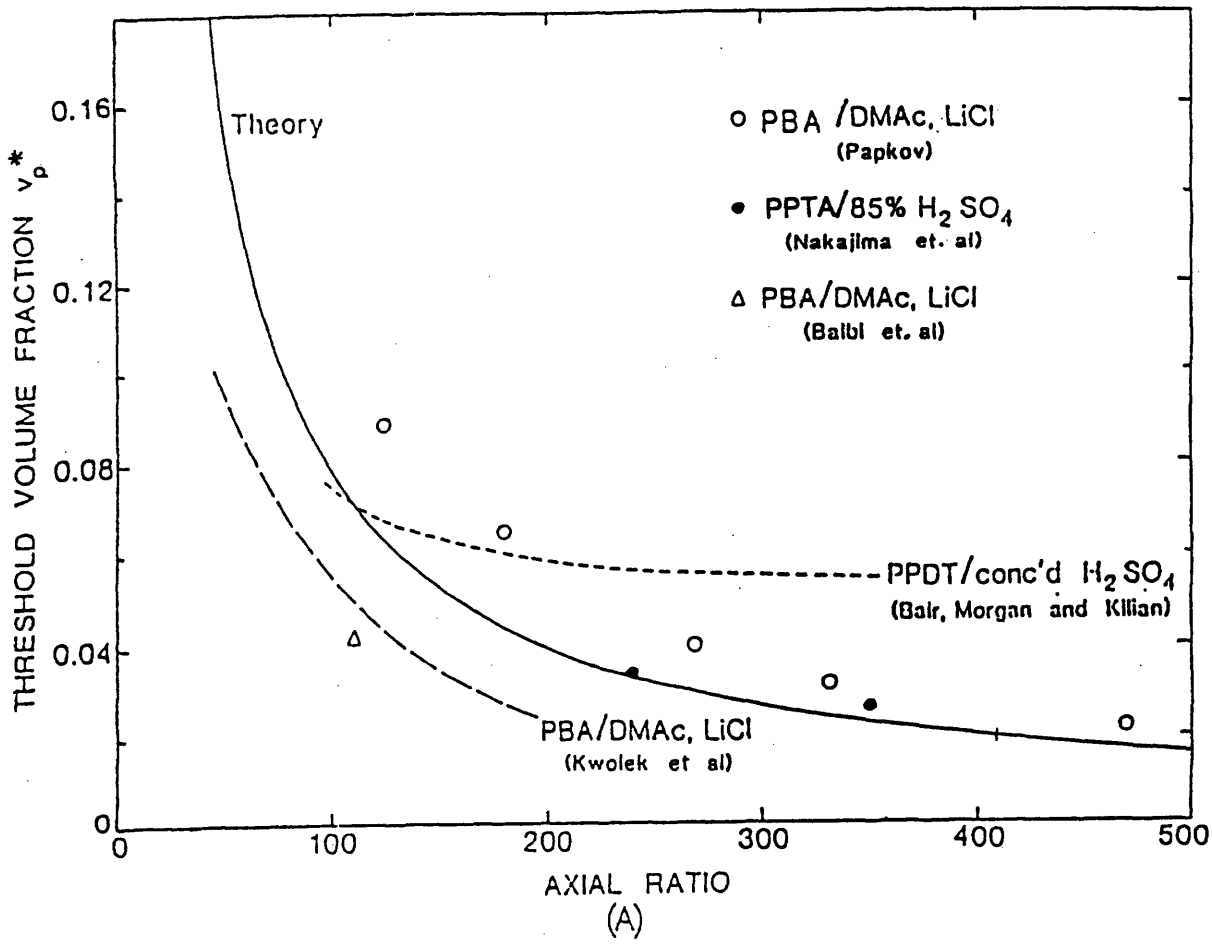

Table 2.2

Conformational behavior of some aramids

Polymer	Solvent	Persistence Length (Å)	Mark-Houwink Viscosity Dependence
PPTA[a,b]	96% H_2SO_4	150-200	1.09
PPTA[b]	HSO_3Cl	400-500	1.36
PBA[a,b]	96% H_2SO_4	400-600	1.5
Cl-PPTA[b]	96% H_2SO_4	150	-
Cl-PPTA[b]	HSO_3Cl	400	-
Cl-PPTA[c]	96% H_2SO_4	-	0.8
PPTA (calculated)[d]		420	-
PBA (calculated)[d]		410	-

[a] Arpin and Strazielle, 1977
[b] Millaud and Strazielle, 1978
[c] Aoki et al., 1978
[d] Erman et al., 1980

chains) to the solvent/polymer system. Deviations from theoretical behavior have been explained in terms of wormlike flexibility for PPTA at higher molecular weight (higher x in Figure 2.2) in concentrated sulfuric acid, resulting from protonation of the carbonyl oxygens and loss of double bond conjugation [Gardner et al., 1984].

2.1.3 Constitutional Isomerism

2.1.3.1 Definition

Recently, the possibility for control of constitutional isomerism in condensation polymers has been applied to the development of new and well-characterized substituted aramids from both theoretical and experimental perspectives [Murano, 1972; Korshak et al.,1975; Pino et al., 1978; Slonim et al., 1980; Steinman et al., 1981; Suter and Pino, 1984; Schmucki et al., 1985; Gentile, 1988]. Constitutional isomerism, as dealt with in this work, refers to polymers which have the same chemical composition and are produced from the same set of monomer reactants, but which differ in the nature or sequence of bonding, or atom connectivity. This is distinct from configurational isomerism and conformational isomerism, which refer to polymers of like constitution which differ either "permanently" in their sequence of sites of stereoisomerism or "nonpermanently" in the spatial arrangements of the constituent atoms such as might be induced by rotation about an internal bond. Such constitutional isomerism has long been recognized in vinyl polymers such as polystyrene, where the pendant phenyl rings may be on adjacent carbons (i.e. "head-to-head, tail-to-tail" isomer) or may be separated by an intervening carbon (i.e. "head-to-tail" isomer). Similar isomerism in condensation polymers is likewise possible in those cases where one or more of the monomers is nonsymmetric.

For the simplest case of bicomponent polycondensation, the nonsymmetric monomer may be denoted XabX and the symmetric monomer YccY, which may then be reacted to yield sequences of the type -acca-, -accb-, or -bccb-, with the elimination of XY. Polymerization may then result in a variation of molecular constitution between three possible extremes: 1) strictly alternating head-to-head, tail-to-tail sequences; 2) completely random distribution of head-to-head and head-to-tail sequences; 3) strictly head-to-tail sequences. The degree of order may be quantified using the parameter s, defined as [Suter and Pino, 1984]:

$$s = [accb]/([acca]+[accb]+[bccb]) \qquad (2.4)$$

where [ ] is the molar concentration of each sequence

By this convention, s = 0 describes the regular head-to-head, tail-to-tail isomer, s = 1 describes the regular head-to-tail isomer, and an equal distribution of head-to-head and head-to-tail junctions corresponds to s = ½. However, as noted by Gentile [1988], intermediate values of the order parameter provide no information about the *distribution*, or "blockiness", of the head-to-head and head-to-tail sequences; for this, one requires details of diad and triad statistics, which are currently unavailable.

Of particular interest to this work are the demonstrably large variations in physical properties with variations in structural regularity exhibited by constitutional isomers of polycondensates. Previous experimental work with polyesters, polyureas, and polyamides has demonstrated the anticipated variations in isomeric order and correlated this degree of regularity with changes in physical properties. Order parameters as low as s = 0.005 have been achieved with polyamide condensation and as high as s = 0.89 with polyurea condensation [Steinman, 1981]. Melting point decreases on the order of 30° to 40°C and solubility increases of an order of magnitude have been reported for several irregular isomers over their more regular head-to-head, tail-to-tail counterparts. The work of Gado [1985], and more recently Gentile [1988], have dealt directly with the considerations of atomic substitution on monomers composing the parent chain of PPTA. These works resulted in the realization of asymmetric constitutional units in the polymer chain and the controlled synthesis of polymers having different sequences of these asymmetric units (i.e. constitutional isomers).

2.1.3.2 Kinetic Model and Homogeneous Phase Amidation

The development of structural isomerism for homopolymer and bipolymer systems has been modeled under the assumptions of first order, single step, irreversible kinetics in a homogeneous reaction phase [Suter and Pino, 1984; Gentile, 1988]. By this model, structural order (s) at high conversion depends upon: (1) the degree of conversion X_n; (2) the relative reactivity (r) of the two functional groups of the asymmetric monomer XabX; (3) the reactivity induction parameters (g_a and g_b), indicative of a change in reactivity of the second -cY end of the symmetric monomer upon reaction of the first -cY end with either -aX or -bX, respectively; and (4) the rate and order of addition of each monomer to the reaction mixture; this refers to the possibility for immediate combination of both monomers, or the finite rate addition of one monomer to the other. Different combinations of these variables leads to several possible polymerization cases; these are summarized in Table 2.3, abstracted from Gentile [1988].

By means of controlled addition syntheses, wherein a novel homogeneous phase amidation system was required, ring-substituted derivatives of PPTA were successfully polymerized over a range of intermediate degrees of isomeric order. Ring substitutions were performed exclusively on the diamine monomer. Polymers included poly(2,6-dichloro-p-phenylene terephthalamide), poly(2-nitro-p-phenylene terephthalamide), poly(2-methoxy-p-phenylene terephthalamide), and poly(2,6-dimethoxy-p-phenylene terephthalamide). Of these, the first met with the greatest success, with inherent viscosities η_{inh} as high

Table 2.3

Polymer order versus kinetic parameters under different mixing mechanisms

Case A:	$r = 1$, $g_a = g_b = 1$		($s = ½$ under all mixing conditions)
Mixing mechanisms involving infinitely slow or fast addition of one monomer to the other:			
Case B:	$r \neq 1$, $g_a = g_b = 1$		$(0 \leq s \leq ½)$
	- YccY slowly added to XabX	$s = s(r)$	
	- XabX slowly added to YccY or infinitely fast mixing of XabX and YccY	$s = ½$	
Case C and Case D:	$r \neq 1$, $g_a = g_b \neq 1$ $r \neq 1$, $g_a \neq g_b \neq 1$		$(0 \leq s \leq 1)$
	- YccY slowly added to XabX (same as Case B)	$s = s(r)$	
	- XabX slowly added to YccY (same as Case B)	$s = ½$	
	- Infinitely fast mixing of XabX and YccY	$s = s(g_a, r)$ $g_a \rightarrow 0$, $s \rightarrow 1$ $g_a \rightarrow \infty$, $s \rightarrow 0$	
Mixing mechanisms involving finite rates of addition of one monomer to the other:			
Case B:	$r \neq 1$, $g_a = g_b = 1$		$(0 \leq s \leq ½)$
	- YccY added to XabX	$s = s(r,$ feed rate$)$	
	- XabX added to YccY	$s = ½$	
Case C: and Case D:	$r \neq 1$, $g_a = g_b \neq 1$ $r \neq 1$, $g_a \neq g_b \neq 1$		$(0 \leq s \leq 1)$
	- YccY added to XabX	$s = s(g_a,$ r, feed rate$)$	
	- XabX added to YccY	$s = s(g_a, g_b,$ r, feed rate$)$	
	- XabX and YccY added to each (slower controls as listed above)		

as 5.68 dl/g (for the s = ½ isomer) and order parameters ranging from 0.07 up to 0.60 (inherent viscosities around 0.5 dl/g were produced at the extremes of order). These dichloro-substituted polymers were further demonstrated to be soluble in N-methylpyrrolidone (NMP) up to 80 mg/ml (s = ½ isomer); maximum soluble concentrations decreased with increases in isomeric order in the polymer chain. It was further demonstrated that these substituted polymers exhibited nematic phase formation at concentrations comparable to those exhibited by the unsubstituted polymer; in the absence of changes in enthalpic interactions, such behavior confirms the retention of the essential rigidity of the chain in the modified polymers. Thus minute changes in atomic structure, and even more subtle variations in structural order, were shown to have measurable effects on polymer solubility without greatly altering chain flexibility. By process of elimination, one may conjecture that it is changes in enthalpic or energetic interactions between polymer chains and between polymer/solvent combinations that are responsible for the observed variation in macroscopic phase behavior, and that these changes arise due to subtle changes at the atomic level.

In light of these results, it seems clear that the ultimate cohesive behavior of the polymer is a function not only of composition, but of structural order as well. Qualitatively, one could argue simply that larger substituents and a higher degree of substitution serve to force main chain segments apart, disrupting specific interactions associated with the condensation linkages (e.g. hydrogen bonding of amide linkages), and that increasing disorder in the placement of substituents accentuates interferences. This work exploits our ability, by the methods described above, to preselect variations in (1) substituent composition and (2) isomeric order as part of the effort to clarify the relation between molecular level parameters and macroscopic material properties. These polymers have the advantages that they are well characterized and that they show changes in macroscopic behavior as a result of minute variations in atomic structure.

2.2 Solid State Structure and Properties

2.2.1 General

Because of the close proximity of atomic groups in the solid state, the specifics of molecular structure should play a large role in determining condensed phase behavior. Stereoregularity and tacticity in vinyl polymers are known to be important factors in determining whether these polymers can crystallize and in what form [Alexander, 1969]; regularity of structure is vital to the organization of crystalline order. In most cases, polymers which tend to crystallize do so only partially, resulting in a patchwork of crystallites embedded within an amorphous matrix, such as illustrated in Figure 2.3a, the degree of

Figure 2.3: Schematic representations of ordered phase formations in polymers: (a) semicrystalline matrix of unoriented crystallites embedded in an amorphous matrix; (b) quasinematic alignment of semicrystal domains; (c) microfibril paracrystal.

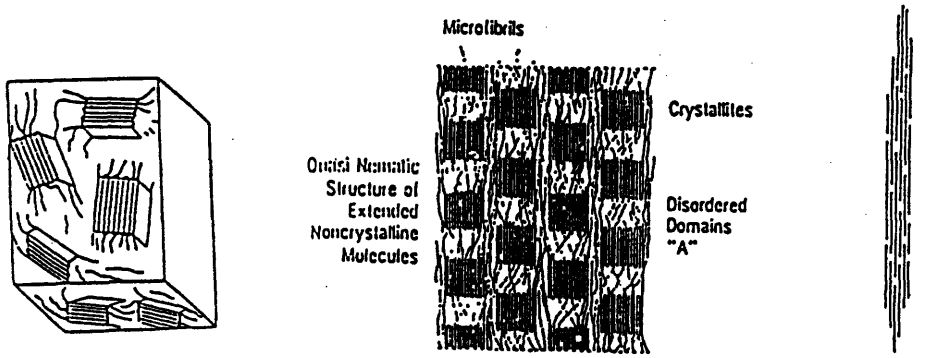

(a) (b) (c)

crystallinity and crystallite orientation being highly dependent upon processing history. In this morphology individual chains weave in and out of both phases. Flexible chain polymers may crystallize by chain folding, giving the common lamellar structures seen in polyethylene and the resulting spherulitic crystallites common in melt crystallization. In oriented (e.g. fiber) form, these flexible semicrystalline polymers may be represented by a two-phase composite model (Figure 2.3b) [Alexander, 1969; Prevorsek, 1982]. In this picture, crystal domains contain chains or chain folded lamellae aligned along the major orientation axis and are in turn separated from one another by discrete amorphous zones; this model is representative of aliphatic polyamides and polyesters, as well as polyethylene terephthalate. Depending upon the molecular rigidity, polymers which do not exhibit folding over long distances may be considered as a single phase "condensed nematic", wherein individual molecules are aligned along a common pseudocrystalline axis, and there is no distinct amorphous phase. This view is illustrated in Figure 2.3c. The solid state structure may also demonstrate translational registry between neighboring repeat units and dimensional order perpendicular to the fiber axis [Moncrieff, 1963; Norhtolt and Van Aartsen, 1977]. Ultimately, order in all three dimensions would denote a single crystal or polycrystal solid state.

In conventional crystallography of low molecular weight compounds, one identifies a unit cell, consisting of one or a few molecules, which when replicated periodically in three dimensions in space describes the long range ordered structure of the crystalline solid. By analogy, the common practice for crystal-forming polymers has been to define unit cells which consist of a finite and small number of constitutional repeat units of the polymer chain. However, in polymeric solids one encounters the additional constraints of intramolecular bonding between unit cells, which is not a priori compatible with the periodicity convention assumed by crystallography. In order to satisfy periodicity within a single macromolecule, the individual chain must assume a preferred helical (or degenerate helical, i.e. rodlike or zig-zag) conformation. These helices may then pack into one or more energetically favorable crystal lattice geometries, depending upon the helix itself and the possibility for interactions between helices. Translational periodicity along the unit cell dimension parallel to the chain axis implies commensuration of the helix over a finite section of the chain. The individual crystallites then exhibit dimensional periodicity, which may be classified using conventional crystallographic nomenclature. Multiple crystal forms may result where either two or more individual helix conformations or two or more packing geometries for the same helix are comparably stable.

Conventional crystal nomenclature begins to break down upon detailed consideration of real polymers, where the unit cells are composed of portions of molecular chains and must conform as well to intramolecular bond geometries. In this case one must consider the possibility of nonintegral, or incommensurate, helical structures, determined by preferred bond geometries, which preclude perfect translational periodicities over finite distances. Poly(oxymethylene) and poly(tetrafluoroethylene) are two polymers which have been proposed to have practically incommensurate helical structures in the solid [Carazzolo, 1963; Gramlich, 1976; Weeks et al., 1981]. Saruyama et al. [1985] have proposed periodic

defects (discommensurations) within a regular (commensurate) helix, as an alternative to the incommensurate helix description, in order to explain additional reflections in drawn poly(oxymethylene) and to suggest a means for interconversion between polymorphic forms.

A further categorization of crystalline structure relevant to these polymers has been described by Hosemann and Bagchi [1962] and is designated paracrystallinity. In this description of the atomic lattice, the true atomic positions are displaced from the regular lattice points according to some a priori distribution function. Hosemann postulates that real crystal structures are subject to two kind of distortions. *Distortions of the first kind* preserve the long range periodicity of the lattice; atomic positions are displaced about the points of the lattice described by the reference unit cell. Such distortions are indistinguishable from thermal vibration distortions. *Distortions of the second kind* involve fluctuations in the periodicity vectors in relation to the nearest-neighbor lattice points, rather than the ideal lattice points. Thus the absolute deviation of atomic positions from the ideal lattice points defined by the reference unit cell is cumulative and increases as the square of the distance from the reference cell.

2.2.2 Aramid Solid State

Previous investigators have reported on the considerable structural complexity of fibrous PPTA [Dobb et al., 1977; Dobb et al., 1977; Panar et al., 1983]. For length scales greater than tens of nanometers, one speaks of a supramolecular structure composed of superposed periodic defect layers (35nm period) and radially-oriented sheet structures with periodic pleats (500nm period), microfibrillar morphology (600nm diameter), and a skin-core differentiation in Kevlar® fibers; recently, Kelvar 149® has been reported to exhibit a higher degree of crystallinity and crystallite size and to be devoid of both pleat and microfibrillar macromorphologies as well as of skin-core differentiation [Kwolek et al., 1987]. On the molecular scale, chain ordering has been portrayed using crystalline and paracrystalline descriptions. Correlations of the breadths of meridional x-ray diffraction peaks with the square of reflection order, as predicted by a one-dimensional paracrystal model having distortions of the second kind, and with tensile modulus have been used to suggest a distorted lattice paracrystalline structure in PPTA [Northolt and Van Aartsen, 1977; Barton, 1985; Hindeleh et al., 1984]. In addition to unusual chain rigidity, the aramids experience strong intermolecular cohesive forces in the solid state due to interactions between the polar amide moieties on neighboring chains. This cohesive ability presumably improves the mechanical properties of the bulk polymer transverse to the axis of orientation, for resistance to shear and compressive failure, and leads to high thermal stability; however, this strong cohesion also causes the chains to associate and reduces the enthalpic driving force for mixing, thus contributing to the poor solubility of the polymer. The choice of balance in this trade-off has been previously considered only subjectively and the optimum condition has been unclear.

Other investigators have suggested that PPTA may coexist in several packing modes, or polymorphs [Northolt, 1974; Hancock et al., 1977; Haraguchi et al., 1979; Gardner et al., 1984]. To date, two different but related polymorphs for the pure polymer [Northolt, 1974; Haraguchi et al., 1979], as well as one crystal solvate structure, involving PPTA and sulfuric acid [Gardner et al., 1984], have been isolated and identified through the use of conventional x-ray analytical techniques. In the first, denoted Modification I, the derived unit cell is pseudo-orthorhombic with two chains per unit cell; this structure is shown in Figure 2.4a. The chain conformation is fully extended with ring rotation angles of -30° and +38°. The chains are rotated about their axes such that the amide planes lie 4° out of the bc crystallographic facet. The second polymorph, denoted Modification II and shown in Figure 2.4b, was derived as a variation of Modification I. Here, the same chain conformation is maintained, with location of the second chain shifted from [½,½] in the ab-facet to [½,0]; however, the resolution of the scattering data in this case was insufficient to determine a unique setting angle. The occurrence of the two polymorphs results from the different environments in which each is coagulated and the ability of the coagulant to interfere with interchain hydrogen bonding during solidification [Haraguchi et al., 1979]. Under certain conditions Modification II may transform to Modification I upon annealing. The unit cell descriptions for each of the pure polymer structures are listed in Table 2.4. The reported structure for the crystal solvate is essentially a swollen version of the pure polymer Modification I, wherein the sulfuric acid molecules coordinate primarily with the amide moieties of the polymer chains in a two-to-one ratio and incorporate into the hydrogen bonding sheets of the bc crystal facet, with the excess solvent nonstoichiometrically included between sheets.

2.2.3 Processing

Because of the multiple crystal forms often exhibited by polymers, processing history is a necessary consideration in solid state analysis. For aramids, the process of primary interest is fiber formation, which is best suited to achieving high uniaxial orientation for mechanical reinforcement applications. Fiber spinning operations usually fall into one of three categories:

(1) melt spinning; in this process, neat polymer is extruded as a melt, with solidification induced by cooling of the polymer filament below its melting temperature. Reported spin velocities may be quite high (e.g. 4000 m/min) [Montgomery, 1971] as solidification requires only thermal transfer and not diffusive transfer. Such processing is possible for aliphatic amides and even some stiff chain polyesters. However, as previously stated, the melt temperatures for aramids are typically comparable to the temperatures at which these materials decompose; thus this class of processes is precluded for aramid fiber spinning.

Figure 2.4: The two reported crystal structures for poly(p-phenylene terephthalamide): (a) Modification I [Northolt, 1974]; (b) Modification II [Haraguchi et al., 1979].

(a)

PPTA Modification 1

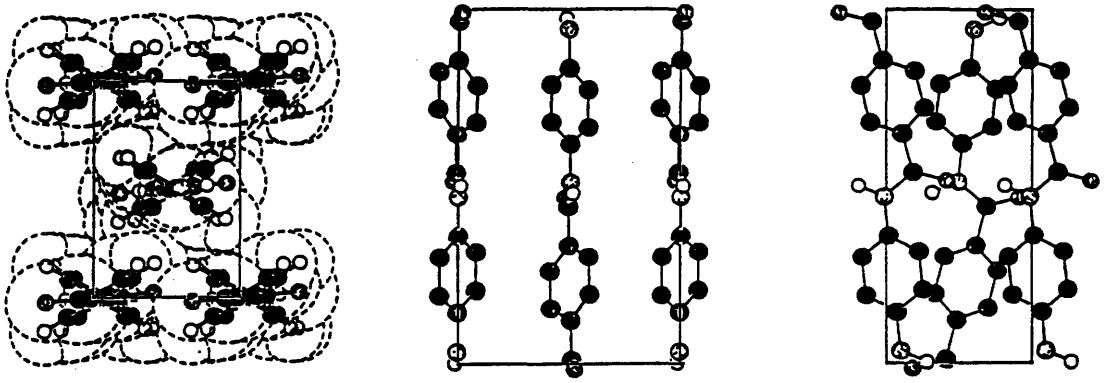

PPTA Modification 2

(b)

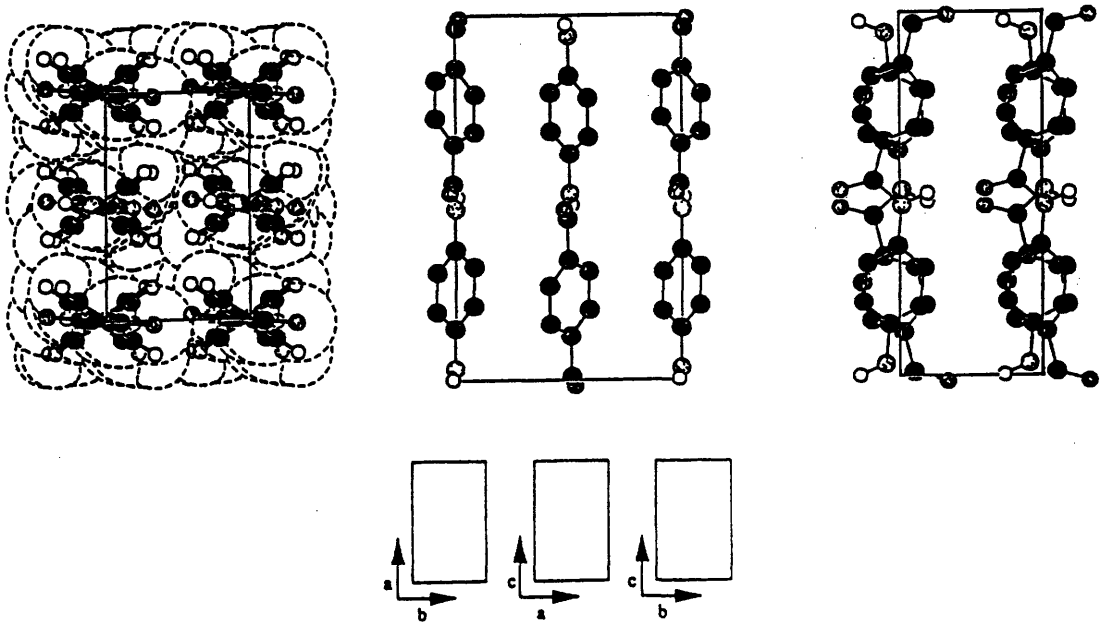

Table 2.4

Crystallographic parameters of previously reported modifications of PPTA

	Modification I[a,d]	Modification II[b,d]	Crystal Solvate[c,d]
a (Å)	7.87	8.0	16.35
b (Å)	5.18	5.1	9.59
c (Å)	12.9	12.9	12.9
γ (degrees)	90	90	90
chain locations	[0,0];[½,½]	[0,0];[½,0]	[0,0];[½,½]
# of H_2SO_4	-	-	ca. 9 per cell
Space Group	Pn or $P2_1n$	Pa or $P2_1a$	-
density (g/cm^3)	1.50	1.50	1.12

[a] Northolt, 1974.
[b] Haraguchi et al., 1979.
[c] Gardner et al., 1984.
[d] monoclinic cell type.

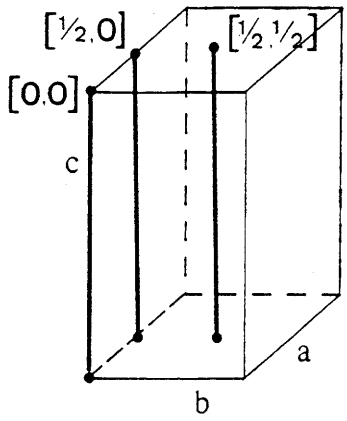

(2) dry spinning; in this process, polymer is extruded as a solution in a volatile solvent. Solidification of the extruded filament is induced by volatilization of the solvent species, which is then carried away by an inert gas. Because diffusion and volatilization of a light compound is required, process rates are generally slower (e.g. 1000 m/min) than those in melt spinning. Filament uniformity is affected by the relative rates of diffusion of solvent within the filament and evaporation of solvent at the filament surface. This in turn may be controlled by the temperature and flow rate of the carrier gas. Again, this process is precluded in aramid fiber manufacture due to the insolubility of these polymers in readily volatilized solvents.

(3) wet spinning; this process resembles dry spinning, except that solidification of the extruded filament is induced by diffusive exchange of solvent and nonsolvent species in a coagulating bath. This process typically requires the slowest spin rates (e.g. 100 m/min), depending upon the rates of diffusion of the solvent and nonsolvent species involved and the diameter of the filaments extruded. Best results are generally obtained when polymer concentrations are as high as possible, subject to the limits imposed by polymer solubility and solution viscosity [Knudsen, 1963 (from Montgomery, 1971)]. Coagulation should ideally occur as slowly as possible, to allow for uniform precipitation of the polymer filament and to avoid dissimilar morphologies within the cross section of the fiber. Coagulation rate may usually be reduced either by addition of solvent to the coagulant bath or by reduction of the coagulating temperature [Allcock and Lampe, 1981]. Because a ternary system is involved, filament solidification may actually entail separation into a biphasic system, from which the residual solvent/nonsolvent component must subsequently be removed.

(4) gel spinning; this process requires polymer of sufficient molecular weight to form a gel at polymer concentrations as low as 2% to 8% by weight. This gel phase is extruded as a filament which is precipitated in a coagulant bath such that up to 98% of the solvent/nonsolvent phase remains within the fiber. The primary difference lies in the character of the precipitated fiber, which consists of high molecular weight, unoriented, low entanglement density polymer chains. Hot drawing of this filament then results in primary extension and alignment of the unentangled chain segments between crossover points in the gel to yield well-oriented, high strength fibers upon removal of the solvent/nonsolvent phase. Elongation during the drawing process may range from 30 to 100 times the original length, but process rates are generally very slow compared even to wet spinning processes, on the order of cm/min [Jaffe, 1987]. Gel spinning essentially seeks to achieve, by means of dilution, the low entanglement densities in flexible polymers that are realized by stiff chain polymers upon microdomain formation in the quiescent liquid crystal phase. Low entanglement density is a prerequisite to achieving high alignment of polymer chains in the solid filament.

Aramids have been processed into both film and fiber form by means of solvent/nonsolvent exchange. For the formation of highly oriented, pseudocrystalline morphologies, the dry-jet wet spinning

process described by Blades [Blades, 1973; Blades, 1975], represents the best means currently available. By this process, the polymer in solution is extruded first through a "dry zone" prior to entry into the coagulation bath. While isotropic spin dopes may be used, the highest degrees of molecular orientation require the use of a liquid crystal solution dope. These domains may be conveniently oriented on a molecular scale prior to solidification [Hancock et al., 1977; White and Fellers, 1978; Valenti et al., 1981; Conio et al. 1987]. Without preorientation in solution, the long relaxation time for polymer motion prevents adequate molecular orientation within the time frame of the spinning process [Chung, 1986]. An extensional flow gradient, which is most pronounced in the dry zone, is realized by collecting the precipitated fiber at a greater linear velocity than that at which the solution exits the spinning die; increasing the extensional flow field improves the degree of orientation along the major axis of the fiber [Kwolek et al., 1977]. In the coagulation bath, a shear gradient is created due to the differential between filament and coagulant flow velocities, which may be reduced by providing for cocurrent coagulant flow in the vicinity of the fiber. Depending on the relative solvency strengths and diffusivities of the solvent and coagulant, a skin layer may form on the fiber, resulting in a differentiation between a fiber "skin", wherein solidification has occurred most rapidly, and a fiber core, where solidification and crystallization proceeds more slowly and to greater perfection. Thus the final product may be affected by changes in many processing factors, such as solution and coagulant temperatures, residence time and relaxation time of the solution/solid mixture in each zone, shear rates at the spin die and in the bath, the magnitude and distribution of extensional stresses along the fiber path, and the evolution of polymer/solvent/nonsolvent composition along the spin line. Such processing variables may enable the formation of kinetically-frozen structures, especially important in the morphology of the fiber skin, analogous to the concept of mechanically equilibrated structure in polymer glasses.

Postspin heat treatments near the melt temperature may provide the chains with sufficient mobility in the solid state to "melt out" kinetically frozen crystal forms in favor of the thermodynamically most favorable form. Table 2.5 demonstrates some reported variations in mechanical behavior for PBA and PPTA as functions of spin solution composition, draw ratio during spinning, and annealing. A significant jump in tensile modulus follows upon heat treatment and the average molecular weight increases due to end linking of chains [Kwolek et al., 1977]. The resulting increase in mechanical properties is illustrated for PBA in Figure 2.5. Tenacity and modulus both increase with decreases in orientation angle, a measure of crystallite alignment obtained through x-ray diffraction analysis. Orientation is improved by increased solution anisotropy in the quiescent state or by an increased extensional flow gradient during solidification.

Table 2.5

Some reported properties of aramid fibers as functions of process parameters

polymer	variable	η_{inh} (dl/g)	tensile strength (GPa)	tensile modulus (GPa)	orientation[c] (degrees)
[d]PBA	iso. soln.[a]	2.1	0.56	23.4	33
	low aniso.[a]	2.1	1.09	42.4	20
	high aniso.[a]	2.1	1.24	54.6	16
[d]PBA	free fall[b]	1.48	0.41	18.0	39
	1.90[b]	1.48	0.50	30.2	37
	2.56[b]	1.48	0.71	36.0	26
	3.83[b]	1.48	0.89	50.2	22
	5.11[b]	1.48	1.10	60.5	22
[e]PBA	-	-	2.11	72.1	-
[e]PPTA	-	-	2.53	53.6	-
[f]PBA	annealed	-	-	180.	-
[f]PPTA	annealed	-	-	139.	-

[a] solution morphology: isotropic or anisotropic fractions
[b] spin draw ratio: linear velocity of draw wheel over the linear velocity at the die exit
[c] orientation is expressed in degrees as the angle of orientation, which is calculated as the azimuthal peak width at which the intensity of x-ray scattering in a single reflection falls to half its peak intensity; the angle is a measure of deviation of the crystallites from perfect alignment, so that smaller angles correspond to more perfect crystallite alignment.
[d] Kwolek et al., 1977, p1390.
[e] Dobb et al., 1977, p237.
[f] Ii et al., 1986, p1809.

Figure 2.5: Effect of heat treatment of a few seconds duration on properties of poly(1,4-benzamide) fibers [Kwolek et al., 1977].

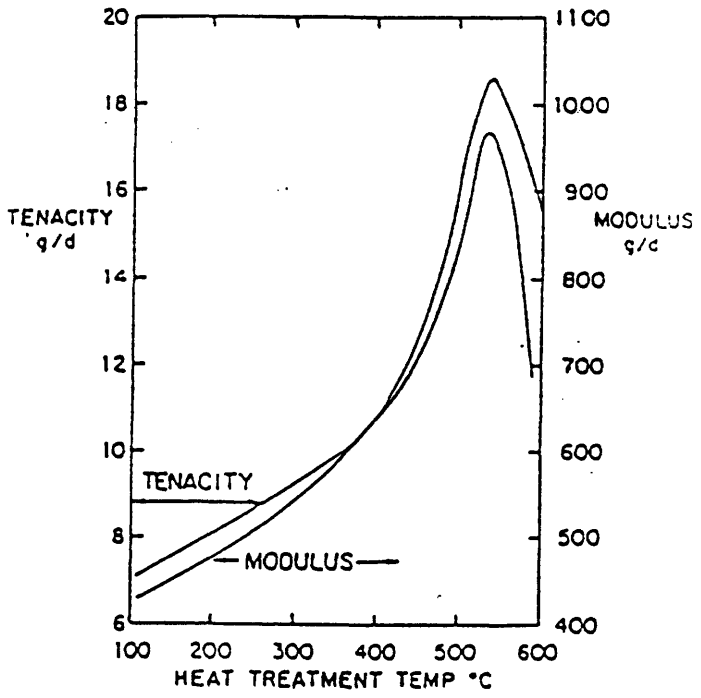

2.3 Atomistic Simulation of Dense Polymer Systems

2.3.1 General

The methods of Molecular Mechanics and Molecular Dynamics have proven considerably useful in the correlation of macroscopic behavior with atomic level structural detail. Usually, these methods are employed to obtain atomic potential energy functions in systems of experimentally known structure or, conversely, to elucidate the characteristics of a previously identified region of phase space. The methods prove especially useful in those instances where simplifying assumptions, such as independent behavior of single molecules, structural periodicity, or idealized stochastic disorder, are both realistic and quantifiable. Applications to isolated macromolecules are numerous [e.g. Brant and Flory, 1965; Suter, 1979; Brisson and Brisse, 1986; Allegra et al., 1970; Scott and Scheraga, 1966; Ooi et al., 1967; Tashiro et al., 1977]. However, the detailed treatment of atomic level interactions and chain packing of macromolecules at glass and crystal densities are considerably fewer.

2.3.2 Polymer Glasses

An extensive analysis of local structure in glasses originated in the work of Theodorou and Suter [1985, 1986]. This model entailed the simulation of a vinyl polymer glass, atactic polypropylene at -40°C, as a static structure in detailed mechanical equilibrium. A single chain of degree of polymerization (DP) 76 was generated in a cube having edge lengths of 18.15 Å by a Metropolis Monte Carlo procedure using the Rotational Isomeric State (RIS) scheme with fixed bond lengths and bond angles. The cube filling process employed periodic boundary conditions (i.e. a chain segment which extends through one face of the cube re-enters through the opposite face) and proceeded by means of an algorithm which took into consideration long range interactions in order to avoid large vacancies in the structure. The initial guess so generated was then relaxed to mechanical equilibrium by minimization of the potential energy of the system with respect to the torsional degrees of freedom of the chain. Here it is important to note that the final structure need not satisfy the criteria for thermodynamic equilibrium (i.e. minimum free energy) but instead satisfies the criteria for mechanical equilibrium (i.e. minimum potential energy in a static structure), consistent with the view of a polymer glass as a state of frozen liquid disorder. Nonbonded interatomic interactions were calculated explicitly up to a finite distance ($R = 2.3\sigma$, where σ refers to the minimum energy separation in the nonbonded interatomic potential function used, and is pairwise atom-dependent). The contribution to the system potential energy from long range interactions was then made by assuming a spatially uniform distribution of all species at large distances (i.e. no long range structural order) and integrating over all species pair interactions from 2.3σ to infinity. Macroscopic and microscopic properties of the glass were deduced from averages over fifteen such

minimized structures. Imposed deformations of the cube were then employed successfully to predict the elastic constants to within 15% of their experimental values.

This model was extended by Ludovice and Suter [1989] to include polar interactions and was applied to polyvinylchloride (PVC) of DP 76 (cube edge = 17.84 Å), and in a single instance to a chain of DP 200 (cube edge = 24.64 Å), at 25°C. Significant here was the introduction of charged atomic species, which was handled through the assignment of partial atomic charges to the individual atoms and the addition of a Coulombic interaction term. A distance-dependent dielectric constant was introduced to reflect the diminution effects due to induced polarization of the intervening medium on field strength experienced by charges separated by larger distances. This approach was shown to reproduce consistent dipole moments and reasonable cohesive energies in glassy PVC. This model of the glassy state has since been further employed to simulate constrained dynamics in PVC [Ludovice, 1989] and glassy polymer structure of atactic polypropylene confined between semi-infinite surfaces [Mansfield and Theodorou, 1989].

2.3.3 Polymer Crystals

Modelling efforts aimed at single crystals of flexible polymers tend to fall into two categories: (1) predictions of elastic properties of known crystal forms, or (2) derivation of structural and thermodynamic properties. For elastic constants, the investigator generally assumes that it is the response of potential energy to deformation that dominates elastic behavior in crystals. As early as 1967 Anand applied the concepts of atom-based force fields to predict the elastic constants for a known structure of orthorhombic polyethylene. McCullough and co-workers [1973, 1974] developed a matrix technique for representing crystalline assemblies of chains of fixed conformation, with consideration of certain chain defects (e.g. chain kinking or folding). Elastic constants in polyethylene were studied by considering potential energy interactions within a single chain and between selected nearest-neighbor chains in a given orthorhombic assembly. Crystal/crystal transformation pathways were proposed by mapping the potential energies of assemblies of chains as a function of selected packing parameters. However, minimization of the potential energies with respect to either intramolecular or intermolecular parameters was not attempted. Tashiro and co-workers also reported a method for the calculation of the three dimensional elastic moduli of assemblies of chains. This method relied largely upon a priori crystal symmetries to expedite calculations and was applied to polyethylene (PE), poly(vinyl alcohol), and Nylon 6 [Tashiro et al., 1978; Tashiro et al., 1978; Tashiro and Tadokoro, 1981].

Tripathy et al. [1981] dealt with the prediction of crystalline packing of chain molecules by minimizing the intermolecular interaction energies of assemblies of chains of fixed conformation using a row formalism for the single chain which enabled one to calculate interactions between infinitely long

chains. However, this formalism was not amenable to extension to three dimensions. From their study of PE, these authors concluded that, lateral to the chain axis, packing geometry was fixed primarily by interactions with the nearest-neighbor shell of chains, while for packing energy one required the additional inclusion of at least the next-nearest-neighbor shell. A limited investigation of poly(vinylidene fluoride) in a fixed geometry led these authors to conclude that a distance-dependent dielectric term such as that employed by Ludovice for glasses is most suitable for correct geometry predictions. These authors also recognized the problems associated with the identification of all local minima in such densely packed systems.

Recently, Sorensen et al. [1988] have incorporated the simultaneous minimization of packing energy with respect to both intramolecular conformation and intermolecular packing parameters, a feature important to the prediction of structure at solid state densities. These authors went on to deduce elastic constants, using the second derivative matrix of potential energy with respect to the independent variables at the minimum energy configuration, and vibrational dispersion curves, from which the thermodynamic quantities were calculated. Again, application to PE and poly(oxymethylene) showed remarkably good agreement between calculated and experimental values for packing geometry and lattice energy, and reasonable agreement for elastic constants and heat capacities between 50°C and 350°C. Lattice energy differences were proposed to explain the stability of the two polymorphs of poly(oxymethylene).

Despite this considerable attention to simulations of flexible chain aliphatic polymers, there have been no reports of application of these methods to the case of the rigid rod polymers. Flory and co-workers [Hummel and Flory, 1980; Erman et al., 1980] addressed the question of conformational energetics in p-phenylene polyamides and polyesters, with subsequent predictions of chain persistence lengths. Tashiro et al. [1977] also performed single chain calculations on the three relevant aramids, poly(p-benzamide), poly(m-phenylene isophthalamide), and poly(p-phenylene terephthalamide), in order to elucidate conformational energetics and tensile moduli, based on the assumption that intermolecular effects contribute negligibly to axial moduli, with reasonable success. Both groups produced parameterized force fields to describe the conformational behavior of the isolated chain and, in the latter case, its response to extensional deformation. However, in the solid state one encounters an environment that is both conformationally constrained and densely packed. Under such strong opposing forces, one cannot expect to decouple the problems associated with the possibly antagonistic criteria for optimization of chain conformation and long range crystalline regularity. It is especially important to recognize that intermolecular forces may be sufficient to induce changes in chain conformation and, by so doing, influence the intramolecular interactions. Conflicts between conformational intramolecular constraints and crystallographic intermolecular constraints are sufficient to induce the formation of nonrational helices or helix discommensurations such as those proposed by Saruyama et al. [1985]. One may further anticipate that intermolecular interactions between nonuniform helices or helices possessing some form of constitutional disorder would lead to anomalous packing behavior between neighboring chain segments.

It becomes apparent, then, that some attempts have been made to address the simulation of polymeric systems in the limit of isolated chain behavior and, in densely packed systems, at the extremes of crystalline order and liquidlike disorder. However, the emerging materials technologies include polymers which do not fit neatly into either extreme. For example, even in atactic PVC one observes local association of polymer segments and gelation. Ludovice and Suter [1987] have proposed subtle electrostatic interactions suggested by glass simulation results to account for this behavior. The presence of strong intermolecular as well as intramolecular forces and localized or anisotropic assemblages of chains or chain segments may be responsible for many of the desirable properties of the new polymeric materials, but pose particular problems of representation and numerical analysis to the materials investigator. The task remains to establish the quantitative connection between that which can be described and designed, and that which is actually observed in such cases.

3. ATOMISTIC SIMULATION OF ORDERED STRUCTURE

3.1 General Approach

The static atomistic modelling methodology assumes that the energy of the material in question may be calculated from a set of force interactions, corresponding to a total potential energy characteristic of the structure. It is composed of two fundamental parts: (1) a method for representation of the material as an ensemble of atoms, or atomic groups; (2) a realistic representation of the forces operating between individual members of the ensemble. In the ideal crystal representation, the first is defined completely throughout space by the local coordinates of the conformational repeat unit, in conjunction with transformations required to describe symmetry-related elements within the unit cell and the three periodicity vectors which define the replication of the unit cell in space. This periodicity may also be used to simplify the calculation of interatomic interactions, as will be described later. The approach which follows begins with the determination of the conformation behavior of the single chain, as prescribed by intramolecular interactions. From the single chain an explicit multichain structure is generated which reflects short-range intermolecular interactions in the nearest-neighbor and next-nearest-neighbor shells, and invokes periodicity simplifications only to estimate the appropriate long-range compaction forces. The calculations assume that the force interactions may be realistically represented by empirical bond length, bond angle, and bond torsion deformation functions, and additive two-body interactions in the case of nonbonded species or species whose interaction distance is conformationally dependent. Iterations along a decreasing potential energy trajectory are performed using a Quasi-Newton algorithm with simultaneous variation of all intramolecular and intermolecular degrees of freedom.

3.2 Structural Representation

3.2.1 Chain Generation and Helix Alignment

The generation of the representative chain involves the specification of the set of three dimensional coordinates locating the atoms or rigid moieties which comprise the chain and entails 3n-3 intramolecular

degrees of freedom, n being the number of atoms (or moieties) in the (finite) chain. This set may be specified directly in Cartesian space or generated as a function of internal parameters, such as bond lengths, bond angles, and dihedral angles, as is common in amorphous polymer glass simulations; the latter has been facilitated by the introduction of the generator matrix formalism of Flory [1969]. In the case of polymer glasses, successive atom placements are generated stochastically, so that one can not expect repetition in structure along the chain. One special feature of macromolecular crystals is the coupling between periodicity along the contour of the polymer chain and periodicity along the lattice dimension parallel to the chain propagation. In the case of ideal crystals the higher level order of the crystal implies translational periodicity along the chain and thus the formation of a rational helical conformation (one may consider rodlike and zig-zag conformations to be degeneracies of the general helix description); to ensure periodicity, one employs a feature of the multichain ensemble, a lattice dimension, in describing the structure of the helix and hence the chain conformation. Previous simulations of ideal crystals have taken advantage of the periodicity characteristic of perfect crystals to generate additional transformations whose elements involve intermolecular distances and orientations derived from the dimensions, angles, and symmetries of the crystal lattice [McCullough, 1974; Sorensen and Boyd, 1988]. The result is a perfectly periodic ensemble created by replication in three dimensions of the minimum basis set of coordinates belonging to a single repeat unit of the rational helix. If one assumes only the existence of a "conformational repeat unit" (referred to hereafter as CRU), a substructure which is internally indistinguishable from any other along the chain contour in terms of conformation, the chain generation method satisfies the more general condition of helical periodicity. The special case of translational periodicity, or rational helicity, may be superposed by substituting a helix axis translation parameter for one of the internal degrees of freedom. In these cases, the number of intramolecular positional degrees of freedom reduces to $3N_{CRU}$-3, where N_{CRU} is the number of atoms in the CRU. This repeat unit is typically taken to be one chemical repeat, but could just as well be an integer multiple thereof. This number of internal degrees of freedom may be further reduced through the introduction of virtual bonds or other conformational constraints.

In the procedure developed here, we treat the polymer chain as a finite segment of the general coiling backbone polymer. Following Flory [1969], the Cartesian coordinate vector **X** for all atoms i in a single chain in the frame of reference of the first atom is generated:

$$\mathbf{X}_i^1 = \mathbf{L}_1 + \mathbf{T}_1 \mathbf{L}_2 + \mathbf{T}_1 \mathbf{T}_2 \mathbf{L}_3 + \ldots + \mathbf{T}_1 \mathbf{T}_2 .. \mathbf{T}_{i-1} \mathbf{L}_i \tag{3.1}$$

$$\mathbf{L}_i = \begin{bmatrix} l_i & 0 & 0 \end{bmatrix} \tag{3.2}$$

$$\mathbf{T}_i = \begin{bmatrix} \cos(\vartheta_i) & \sin(\vartheta_i) & 0 \\ \sin(\vartheta_i)\cos(\phi_i) & -\cos(\vartheta_i)\cos(\phi_i) & \sin(\phi_i) \\ \sin(\vartheta_i)\sin(\phi_i) & -\cos(\vartheta_i)\sin(\phi_i) & -\cos(\phi_i) \end{bmatrix} \tag{3.3}$$

l_i, ϑ_i, and ϕ_i are the bond length, bond angle complement, and dihedral angle locating atom i in the frame of reference of atom i-1. In this convention, $\phi_i = 0$ corresponds to the trans dihedral conformation. This may be accomplished using the generator matrix **A**:

$$\mathbf{X}_i^1 = \mathbf{A}_{[1}\,\mathbf{A}_2\,\mathbf{A}_3\,\mathbf{A}_4 \ldots \mathbf{A}_{i-1}\mathbf{A}_{i]}, \quad i>1 \tag{3.4}$$

$$\mathbf{A}_j = \begin{bmatrix} \mathbf{T}_j & \mathbf{L}_j \\ \mathbf{0} & 1 \end{bmatrix} \quad 4 \times 4 \text{ matrix} \tag{3.5}$$

with $$\mathbf{A}_{[1} = \begin{bmatrix} \mathbf{T}_1 & \mathbf{L}_1 \end{bmatrix} \quad 3 \times 4 \text{ matrix} \tag{3.6}$$

and $$\mathbf{A}_{i]} = \begin{bmatrix} \mathbf{L}_i \\ 1 \end{bmatrix} \quad 4 \times 1 \text{ matrix} \tag{3.7}$$

In highly ordered polymer structures, it is appropriate to limit the set of unique conformational parameters to those of the CRU. The helical superstructure may be defined in terms of the translation along the helix axis (pitch, d_h), the directional rotation (twist, Θ_h) between identical points in successive structural units, and the radius (ρ_h), the distance from the axis to a reference point on the chain. The nonuniform helix is considered to be a perturbation of the uniform conformation. In order to capture local perturbations in helical structure, this model allows continuous variation of chain conformation during energy minimization through nonrational as well as rational helix conformations and includes the special cases of zig-zag and extended chain conformations. For the fully extended (i.e. zero helix twist) conformation it is necessary to introduce a switch from true helix representation and alignment to an approximation based on alignment of the major axis of the radius of gyration of the finite chain segment, in order to overcome the singularity in helix radius and consequent alignment problem which occurs in the helix treatment. These calculations are presented in greater detail in Appendix A. Imperfect helix alignment, rigorously interpreted, creates the possibility for steric interference between neighboring chains at points remote from the region explicitly described in the model. In allowing imperfect alignment of neighboring helices within the dominant explicit representation one must ensure that the deviation from alignment be quantifiably small over large distances; that is, either (a) minor, low energy torsional correc-

tions (e.g. discommensurations) spaced at large intervals along the chain are capable of "periodically realigning" the set of chain propagation vectors or (b) the correlation lengths of the "crystallites" are sufficiently small relative to the alignment deviation to preclude any significant remote steric interferences. The first condition may be allowed through minor torsions which produce changes in chain alignment but which are energetically insignificant (e.g. an amide torsion of only 1° out of plane requires less than 0.05 kcal/mol, but may alter the backbone contour vector by 2°, and can create a local helix twist displacement of approximately 10°); the second condition may be deduced from the minimum dimension at which energetically-significant steric overlap occurs.

3.2.2 Multichain Packing

The multichain structure is created through successive independent molecular coordinate generation accompanied by alignment of the primary chain axes. Again, the problem may be computationally simplified by assuming that individual chains are conformationally indistinguishable, analogous to the CRU assumption. In this case structure generation reduces to replication and reorientation of the parent chain conformation at points on a two-dimensional field. In a "disordered lattice", each neighboring chain may be located by a set of independent parameters describing orientation and translation of that chain from the "parent" position. In the paracrystalline structure, the vectors joining points in the "net" vary in magnitude and direction according to an a priori statistical probability. One may further limit the degrees of freedom by requiring correlation between the orientation of chains located at regular points in the net. In the perfect crystal, the net simplifies to a regular grid of translationally periodic points with only one or two characteristic orientations describing the setting of the chain at each of the grid points.

In these calculations, we employ the single conformation and periodic grid assumptions. The primitive cell parallelepiped has edge vectors **A**, **B**, and **C**, and angles $\angle\mathbf{AB}=\zeta$, $\angle\mathbf{AC}=\upsilon$, and $\angle\mathbf{BC}=\tau$. Figure 3.1 illustrates this description of the crystal. We define the translation lengths, A and B, and the angles, ζ, υ, and τ, that orient the point net with respect to the major chain propagation axis C, chosen to coincide with the z coordinate axis; the **A** vector is arbitrarily chosen to lie in the xz-plane of the parent frame of reference. Chains are located at $m\mathbf{A}+n\mathbf{B}$, m and n being positive or negative integers. Each of the N_c *independent* chains may be oriented about its center of mass through the use of appropriate Euler angles and N_c-1 chains may be translated (relative to the parent chain) along their axes. From this selection of A, B, τ, υ, and ζ, it follows that, in Cartesian coordinates:

$$\mathbf{A} = \begin{bmatrix} A\cos(90°-\upsilon) \\ 0 \\ A\sin(90°-\upsilon) \end{bmatrix} \qquad \mathbf{B} = \begin{bmatrix} B\cos(90°-\tau)\cos\zeta' \\ B\cos(90°-\tau)\sin\zeta' \\ B\sin(90°-\tau) \end{bmatrix} \tag{3.8}$$

Figure 3.1: Definition of chain packing parameters.

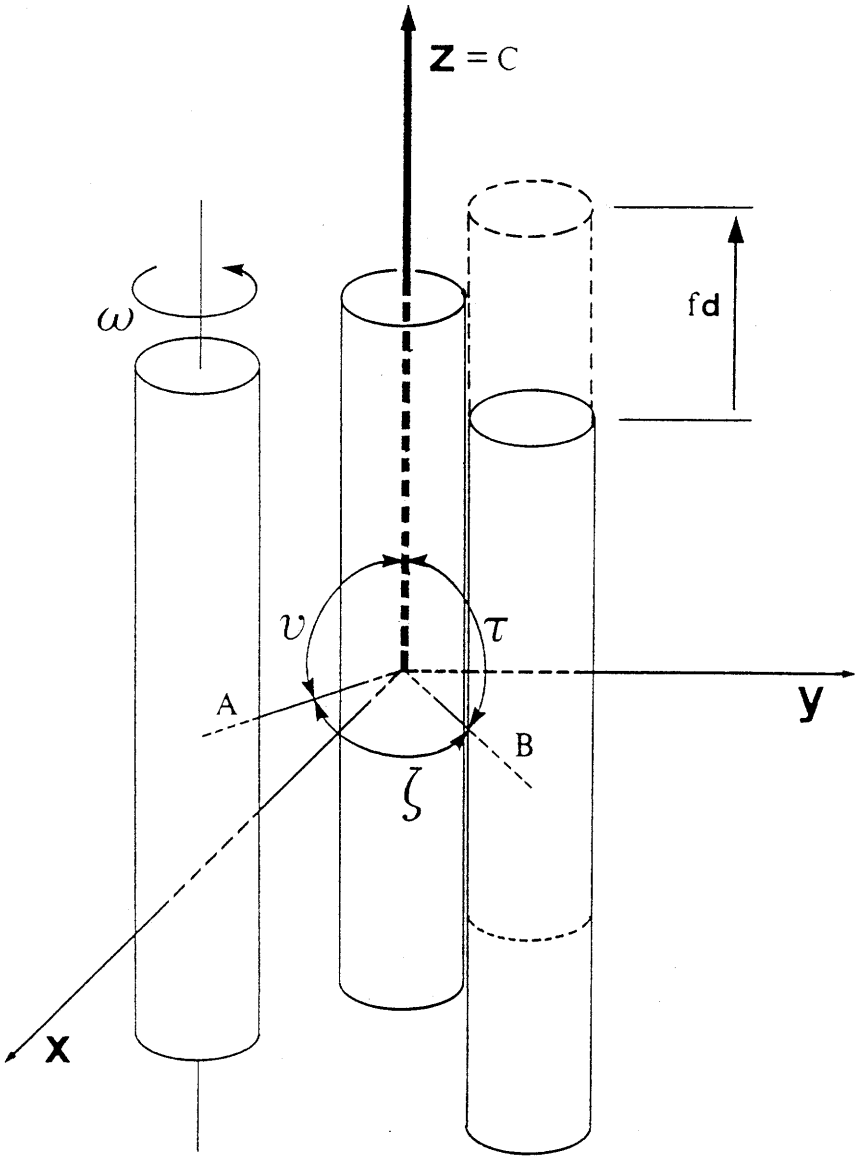

where $\cos\zeta' = (\cos\zeta - \cos\tau\cos\upsilon)/(\sin\tau\sin\upsilon)$

The calculation of individual atomic coordinates for each atom i in chain j (which is located at $\mathbf{R}_j=m_j\mathbf{A}+n_j\mathbf{B}$ in the frame of the "parent") is accomplished by:

$$\begin{bmatrix} \mathbf{X}_{i,j} \\ 1 \end{bmatrix} = \begin{bmatrix} \mathbf{W}_j & \mathbf{R}_j \\ \mathbf{0} & 1 \end{bmatrix} \begin{bmatrix} \mathbf{X}_{i,1} \\ 1 \end{bmatrix} + f_j d \begin{bmatrix} \mathbf{W}_j & \mathbf{0} \\ \mathbf{0} & 1 \end{bmatrix} \begin{bmatrix} 0 \\ 0 \\ 1 \\ 0 \end{bmatrix} \tag{3.9}$$

$$\mathbf{W}_j = \begin{bmatrix} \cos\chi_j\cos\psi_j\cos\omega_j - \sin\chi_j\sin\omega_j & -\cos\chi_j\cos\psi_j\sin\omega_j - \sin\chi_j\cos\omega_j & -\cos\chi_j\sin\psi_j \\ \sin\chi_j\cos\psi_j\cos\omega_j + \cos\chi_j\sin\omega_j & -\sin\chi_j\cos\psi_j\sin\omega_j + \cos\chi_j\cos\omega_j & -\sin\chi_j\sin\psi_j \\ \sin\psi_j\cos\omega_j & -\sin\psi_j\sin\omega_j & \cos\psi_j \end{bmatrix} \tag{3.10}$$

d is the helix translation per structural repeat length (pitch), f_j is the translation, expressed as a fraction of the pitch, of chain j along its axis, and χ_j, ψ_j, and ω_j are the Euler angles for placement of the jth chain (for details, refer to Appendix A: Figure A.2). For the crystalline case, A, B, τ, υ, and ζ are constant, while in the paracrystal these may vary. While the $\mathbf{W}_j$ matrix is formulated generally above, in long chain polymers ψ_j is limited to values near 0° and 180° due to constraints on helix alignment. Chains which are mirror images of the parent are handled through multiplication of $\mathbf{W}_j$ with an inversion matrix. Under these conditions, helix translation along its axis may be sufficiently considered by $-0.5 < f_j < +0.5$. With the introduction of the regular point net the number of intermolecular degrees of freedom becomes $4N_c+4$, while further simplification via $\chi_j=0$ and $\psi_j=0$ yields $2N_c+4$ degrees of freedom.

3.3 Energy Representation

3.3.1 Explicit Description

In order to calculate the potential energy for a representative crystal form, this method first assumes pairwise additivity of effective intermolecular interactions. The completely general description of the total potential energy for a construction consisting of L polymer chains may be represented as:

$$E^{expl} = \sum_{\substack{\text{all chains} \\ l}} E_l^{intra} + \tfrac{1}{2} \sum_{\substack{\text{all chains} \\ l}} \sum_{\substack{\text{all chains} \\ l' \neq l}} E_{l,l'}^{inter} \qquad (3.11)$$

l and l' refer to each of the L chains in the structure. Under the simplifying assumptions of structural repetition within and between chains, the average potential energy per structural repeat unit for a construction may be calculated explicitly as:

$$E^{unit} = E^{expl} / LN_r \qquad (3.12)$$

$$= (1/N_c N_r)\left[\sum_{m=1}^{Nc} E_m^{intra} + \tfrac{1}{2} \sum_{m=1}^{Nc} \sum_{\substack{l=1 \\ l \neq m}}^{L} E_{m,l}^{inter} \right] \qquad (3.13)$$

m refers to the each of the N_c chains in the structure which are not related by a symmetry operation. The first term represents the total of the intramolecular interactions. For a single chain of h helix units, each consisting of k interacting centers, the intramolecular energy may be calculated as:

$$E^{intra} = \sum_{i=1}^{k} \sum_{j=1}^{h \cdot k} E(i,j) \qquad (3.14)$$

where E(i,j) is the general form describing the interaction between two atoms i and j. The second term in Equation (3.13) represents the intermolecular potential energy. For two conformationally identical, parallel, interacting chains involving only distance-dependent interactions, one may take advantage of the nondirectional nature of spherically symmetric interactions to obtain the complete potential energy description from a reduced set of coordinates; this is employed only as an expedient to keep the memory requirements of the program to a minimum. For two interacting chains m and l, each of h helical repeat units consisting of k interacting centers per helical repeat, the interaction energy may be calculated as (where i_m refers to the ith atom of chain m):

in general:

$$E^{inter} = \sum_{i=h \cdot k/2}^{(h \cdot k/2)+k} \sum_{j=1}^{h \cdot k} E(j_l, i_m) \qquad (3.15a)$$

special case for parallel helices:

$$E^{inter}_{l,m} = \sum_{i=1}^{k} \sum_{j=1}^{h\cdot k} E(j_l,i_m) + \sum_{i=k+1}^{h\cdot k} \sum_{j=1}^{k} E(j_l,i_m) \qquad (3.15b)$$

3.3.2 Lattice Summation

While the above equations apply generally to multibodied systems, crystalline solids are most often idealized as perfectly periodic structures in three dimensions. This simplification precludes the representation of defects such as dislocations or discommensurations. However, it allows one to expedite the calculation of pairwise interactions through the use of lattice summations in three dimensions. A similar summation was employed by Anand [1967] in arriving at an analytical equation for the cohesive energy of the infinite crystal in the absence of electrostatic forces. The simplification is conceptually identical to a numerical approximation of the Madelung Constant for each new simulation. The translationally periodic infinite solid in three dimensions may be viewed as a construction consisting of unit cells displaced from a "parent" by an integer multiple of its edge vectors, where the only unique pairwise interactions that must be considered are those between the atoms making up one helical repeat unit of the parent chain and those of one helical repeat unit in each of the neighboring independent chains (i.e. those chains not displaced from the parent by a symmetry operation). The distance-dependent interaction may then be computed for an arbitrarily large construction through the use of a lattice summation:

$$E^{lattice} = (N_{CRU}/N_i) \sum_{n=1}^{Np} \sum_{i=1}^{Ni} \sum_{j=1}^{Ni} A_{ij,n} \; \Sigma_L \; V_n(d_{ij}) \qquad (3.16)$$

where i and j refer to the N_i interacting atoms that are crystallographically unique (i.e. belonging to the N_c independent chains). Thus if N_c=1, N_i is equal to k, the number of atoms comprising one period of the helix. In general, $N_i = kN_c$. The premultiplier ensures that E^{unit} and $E^{lattice}$ are calculated on the same basis. V_n is the distance-dependant potential function (e.g. d_{ij}^{-1}, d_{ij}^{-6} or d_{ij}^{-12}) having multiplier $A_{ij,n}$ for atoms i and j; $\Sigma A_{ij,n} V_n(d_{ij})$ is the potential energy of interaction between a pair of atoms i and j (summation over n implied). The summation over the distance-dependent function in Equation 3.16, $\Sigma_L \; V_n(d_{ij})$, is the lattice sum:

$$\Sigma_L \; V_n(d_{ij}) = \Sigma_{\lambda a} \Sigma_{\lambda b} \Sigma_{\lambda c} \; V_n(\; [\mathbf{d}^T_{ij,abc} \; \mathbf{d}_{ij,abc}]^{1/2} \;) \qquad (3.17)$$

$$\mathbf{d}_{ij,abc} = \mathbf{d}_j - \mathbf{d}_i + \lambda_a\mathbf{A} + \lambda_b\mathbf{B} + \lambda_c\mathbf{C} \quad (3.18)$$

$\mathbf{d}_i$ is the location vector of atom i. **A**, **B**, and **C** are, again, the parallelepiped edge vectors; the summation coefficients λ_a, λ_b, and λ_c are selected large enough to effectively capture all significant interactions. Values of λ_a, λ_b,and λ_c up to 20 (≈100Å for most organic crystals) have been explored in this work, but in general truncation of λ_a, λ_b, λ_c at values between 4 and 8 (depending upon geometry and potential energy description) was found to be adequate to approximate the energy of the infinite lattice to within 0.1 kcal/mole. This is in agreement with the findings of Tripathy et al. [1981], who concluded that the inclusion of a next-nearest-neighbor shell in the simulation of polyvinylidene fluoride was required to accurately estimate stabilization energy but that the inclusion of additional shells was unnecessary.

The above equations may be rewritten for helical periodicity as a summation over only the atoms of the helical subunits of each crystallographically unique chain. Then Equation (3.16) holds with N_i being the number of interacting centers in the helical subunit. The lattice sum becomes:

$$\Sigma_L\, V_n(d_{ij}) = \Sigma_a\, \Sigma_b\, \Sigma_s\, V_n(\, [\mathbf{d}^T_{ij,abs}\, \mathbf{d}_{ij,abs}]^{1/2}\,) \quad (3.19)$$

$$\mathbf{d}_{ij,abs} = \hat{\mathbf{W}}_s(\mathbf{d}_j - \mathbf{d}_{ij}^{\Delta}) + \mathbf{d}_{ij}^{\Delta} - \mathbf{d}_i + \lambda_a\mathbf{A} + \lambda_b\mathbf{B} + s\mathbf{F} \quad (3.20)$$

$$\mathbf{F} = \begin{bmatrix} 0 & 0 & d_h \end{bmatrix} \quad (3.21)$$

$$\hat{\mathbf{W}}_s = \begin{bmatrix} \cos(s\Theta_h) & -\sin(s\Theta_h) & 0 \\ \sin(s\Theta_h) & \cos(s\Theta_h) & 0 \\ 0 & 0 & 1 \end{bmatrix} \quad (3.22)$$

In this equation, $\mathbf{d}_{ij}^{\Delta}$ is the vector describing the displacement of a point on the axis of the helix containing atom j from that on the axis of the helix containing atom i. The latter representation, while more computationally demanding than the case of translational periodicity in three dimensions, has the advantage that it can simulate incommensurate helices throughout the lattice. However, time trials using code optimized for concurrency on an Alliant FX/80 superminicomputer resulted in roughly an eightfold increase in CPU time for the helical periodicity representation. Under the special condition of helix

commensuration (i.e. C=nd, s=nc, and $n\Theta_h$= m360°, m and n being integers) Equation 3.20 reduces to the form of Equation 3.18.

In our calculations we have retained the explicit potential energy calculation (Equation 3.13) within a central "core" region consisting of the reference chain segment and its nearest-neighbor shell (3 x 3 x DP6: an array of chain segments three chains on a side, each segment possessing six monomer units) or in some cases the next-nearest-neighbor shell (5 x 5 x DP10). This region contains the dominant energy contributions which define the geometry of the structure. The explicit calculation allows one to represent local inhomogeneities such as defects in chemical constitution or tacticity or helix discommensuration and accounts for over 90% of the total calculated energy (98% in the 5 x 5 x DP10 case). The lattice summation calculates the contribution to the system energy of interactions with the surroundings, which ensures an accurate estimate of densification and the total cohesive energy of the condensed phase structure. Thus the total energy to be minimized consists of both an explicit energy per unit contribution within a central parallelepiped and a lattice summation contribution for points outside of this parallelepiped:

$$E^{tot} = E^{unit}\,(\,K\times K \text{ array}, N_r \text{ repeat units}\,) + E^{lattice}\,(\,|\lambda_a|, |\lambda_b| > K/2,\ |\lambda_c| > N_r/2\,) \qquad (3.24)$$

The resulting picture, illustrated in Figure 3.2, may be viewed as a potentially defective pseudocrystalline parallelepiped embedded within a defect-free crystalline universe. In this manner the model attempts to capture both geometry and energy features of pseudocrystalline solid structures.

3.3.3 Force Field

The choice of a potential energy force field depends upon the molecular architecture. The potential energy summation must converge as its range is extended over successive interaction shells. Akin to earlier work described in the literature [McCullough, 1974; Tashiro et al., 1977; Pertsin and Kitaigorodsky, 1987], this model uses a modified Valence Force Field (VFF) description for bonded two- and three-atom deformations, and empirical torsional energy functions for bonded four-atom deformations. Nonbonded interactions are represented by a modified 12-6-1 Lennard-Jones/Coulomb energy function:

Figure 3.2: Representation of the packing structure as a local domain, described explicitly in terms of mutable atomic positions, embedded within an implicit perfect crystal.

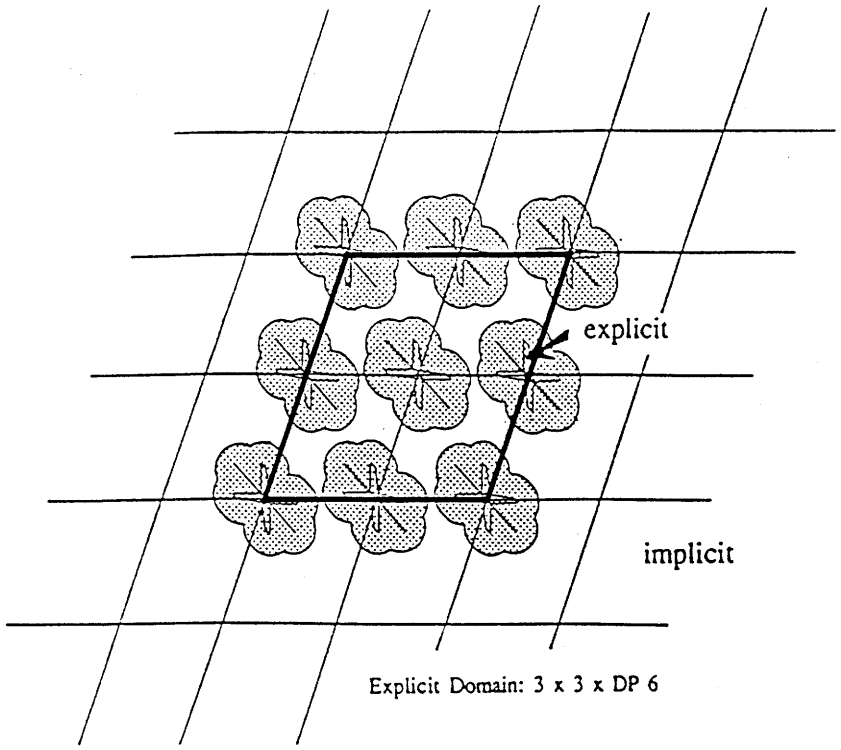

$$E_{ij} = A_{ij,12}/d_{ij}^{12} + A_{ij,6}/d_{ij}^{6} + A_{ij,1}/(Dd_{ij}) \quad (3.25)$$

where

$$A_{ij,12} = 0.5\ A_{ij,6}\ (r_i + r_j)^6 \quad (3.26)$$

$$A_{ij,6} = -(\varepsilon_i\varepsilon_j)^{1/2}\ (r_i + r_j)^6 \quad (3.27)$$

$$A_{ij,1} = q_iq_j\ /\ 4\pi\varepsilon_O \quad (3.28)$$

$$D(d_{ij}) = 1 \qquad ;\ d_{ij} < d^* \quad (3.29)$$

$$= D_B\ \exp(\ -\kappa/d_{ij}\ ) \qquad ;\ d_{ij} > d^*$$

$$\kappa = \ln(D_B)\ d^* \quad (3.30)$$

i and j refer to the atoms separated by the distance d_{ij}; ε and r are atom contributions to the van der Waals potential energy well depth and location, respectively, and the q are partial atomic charges, which may be derived from data on low molecular weight compounds or estimated using well-established quantum mechanical methods. ε_O refers to the vacuum permittivity. A distance-dependent dielectric constant has been employed, using the approximation of Block and Walker [1973] to reflect the different dielectric environments experienced by short and long range charge interactions. At short distances, the effective dielectric constant is unity; at larger distances, it asymptotically approaches its static bulk value, D_B. The constant κ is chosen to ensure convergence of the two portions of the dielectric function at the crossover distance d^*. A quintic spline in D between $1.0 < d_{ij}/d^* < 1.1$ is used to join the regions smoothly. A similar attenuation was employed with good results in the modeling of a polar polymer glass [Ludovice, 1989]. It is readily demonstrated that interactions of higher than third order in inverse distance (e.g. the sixth order and twelfth order induction/dispersion terms) are convergent as interaction distances become infinite (Appendix B); such is not necessarily the case of the first order electrostatic term. To ensure convergence of the summation over the electrostatic interactions one requires that the structure be electrically neutral; the electrostatic term then becomes equivalent to a summation of interactions only of dipoles and higher moments, which interact as functions of distance of third order or higher. Secondly, it is necessary in this method that the characteristic crossover distance d^* be constant for all atoms in the structure, in order to ensure that there is no net accumulation of residual electrostatic interaction as an artifact of the boundary between explicit energy calculation and lattice summation.

The representation of electrostatic interactions as partial atomic charges merits further discussion. An alternative to the use of a partial charge representation for polar species and subsequent use of a Coulombic potential would be to represent the polar character of each electrically neutral moiety by its dominant, or lowest nonzero, multipole and then to employ multipole interaction potentials. For all electrically neutral conformational subunits, the zeroth moment (total charge) is, by definition, zero. For

the amide moiety, the first nonzero moment is the dipole moment, and for the phenylene ring it is, by symmetry, the quadrupole moment. All higher nonzero moments depend on the choice of the frame of reference [Gray and Gubbins, 1984] and are of secondary importance. Thus one may employ an electrostatic interaction potential involving dipole-dipole, dipole-quadrupole, and quadrupole-quadrupole interactions, as shown in Equation 3.31.

$$
\begin{aligned}
E^{elec} = {} & [1/4\pi D(d_{ij})\varepsilon_O] \quad [\ (-\mu_i\mu_j'/d_{ij}^3)(2\cos\theta_1\cos\theta_2-\sin\theta_1\sin\theta_2\phi) \\
& + (3/2d_{ij}^4)(\mu_i\Theta_j\{\cos\theta_1(3\cos^2\theta_2-1)-2\sin\theta_1\sin\theta_2\cos\theta_2\cos\phi\} - \mu_j\Theta_i\{\cos\theta_2(3\cos^2\theta_1-1) \\
& -2\sin\theta_1\sin\theta_2\cos\theta_1\cos\phi\}) \\
& + (3\Theta_i\Theta_j/4d_{ij}^5)(1-5\cos^2\theta_1-5\cos^2\theta_2+17\cos^2\theta_1\cos^2\theta_2+2\sin^2\theta_1\sin^2\theta_2\cos^2\phi \\
& -16\sin\theta_1\sin\theta_2\cos\theta_1\cos\theta_2\cos\phi)\ ]
\end{aligned}
\tag{3.31}
$$

θ_1, θ_2, and ϕ are angles of orientation (see Appendix B: Figure B.1 for details). This representation requires the identification and assignment of higher order moments to subunits of the polymer chain. If we may assume that the distances over which interactions occur are large with respect to the separation of the poles of the relevant electrostatic moment, then the field may be approximated by a set of charges located at vectorial positions $\mathbf{r}_i$. One may then define a series of multipole moments [Maitland et al., 1981]:

zeroth moment: total charge	q	=	$\Sigma\ q_i$	(3.32)
first moment: dipole	μ	=	$\Sigma\ q_i\ \mathbf{r}_i$	(3.33)
second moment: quadrupole	Θ	=	$\Sigma\ q_i\ \mathbf{r}_i\ \mathbf{r}_i$	(3.34)
third moment: octopole	O	=	$\Sigma\ q_i\ \mathbf{r}_i\ \mathbf{r}_i\ \mathbf{r}_i$	(3.35)
etc.				

The use of partial atomic charges has the advantages that (1) the charge may be selected to reproduce any higher order moments for neutral moieties, (2) select atomic substitutions are readily handled through introduction of atomic potential parameters characteristic of the new atoms, and (3) the energy calculation is entirely a function of atomic separation distance, and not orientations of groups of atoms. This last feature facilitates calculation and reduces the simulation time requirements. This is especially crucial to

the implementation of the rapid lattice sum calculation, which assumes that interactions are only distance-dependent.

3.4 Prediction of X-ray Scattering

3.4.1 Structural Contributions to Intensity

Information about the microstructure of matter may be obtained experimentally only by indirect means. The most common approach to materials analysis proceeds by deduction of atomic structure from observations of scattered radiation; this is the method of conventional crystallography, whereby one proposes a unit cell *which is consistent with, but by no means unique to,* the observed scattering of x-rays at wide angles. Our detailed atomistic modelling approach instead predicts stable structures from a priori considerations of potential energy. This process of construction from atomic building blocks may be extended to the a priori prediction of the unique pattern of scattering of x-rays to be observed from such energetically stable structures. In this sense, our calculation of theoretical x-ray diffraction patterns is conceptually the reverse of the conventional crystallographic method and ensures the additional constraint of stability of structure with respect to potential energy.

The scattering of x-ray radiation at wide angles (i.e. at angles greater than 5° divergent from the incident beam) is the primary source of indirect information concerning atomic structure, where the scattering bodies are roughly 2 to 20 Å apart. Here, the incident radiation interacts with the electron cloud distribution centered around the atomic nuclei. Scattering, or secondary emission associated with the electrons, takes the form of *coherent* scattering, which is unmodified in wavelength and phase, and *incoherent* scattering, which is modified. The latter type, frequently termed Compton scattering, contributes to the diffuse background in x-ray diffraction and is not related to structural features, and for this reason is not considered further in the following discussion. The coherent scattering power f_j of an atom j at zero scattering angle 2θ, where all scattering is in phase, increases in proportion to the number of electrons around the atom and decreases with increasing scattering angle.

For two scattering bodies displaced from each other by the vector **r**, we define the scattering vector **S** as:

$$\mathbf{S} = (\mathbf{s} - \mathbf{s}_0)/\lambda \tag{3.36}$$

where s_o is the path of the incident radiation and s is the path of the diffracted radiation, forming an angle of 2θ with the incident beam path. λ is the wavelength of radiation. Thus the phase difference of the diffracted radiation is $2\pi\mathbf{S}\cdot\mathbf{r}$ and the magnitude of the scattering vector is given by Equation 3.37. We may express f_j, the atomic scattering factor alternatively as $f_j(S)$ or $f_j(2\theta)$.

$$S = |\mathbf{S}| = (2\sin\theta)/\lambda \tag{3.37}$$

For a system of N atoms, the intensity of the scattered radiation may be expressed in terms of the intensity I_e of x-rays scattered by an electron by defining the structure factor $F(\mathbf{S})$ and its complex conjugate $F^*(\mathbf{S})$ as follows:

$$I(\mathbf{S}) = I_e\, F(\mathbf{S})\, F^*(\mathbf{S}) \tag{3.38}$$

$$F(\mathbf{S}) = \sum_{1}^{N} f_j(S)\, \exp(2\pi i \mathbf{S}\cdot\mathbf{r}_i) \tag{3.39}$$

The nature of the problem then becomes to calculate the structure factor. In crystalline systems, where the entire structure is simply a composite of identical unit cells, one proceeds by describing all the atoms i=1 to N in terms of the unit cell k to which the atom belongs and the atom j within the unit cell which corresponds to i.

$$I_{cr}(\mathbf{S}) = I_e\, G(\mathbf{S})F_{cr}(\mathbf{S})\, G^*(\mathbf{S})F_{cr}^*(\mathbf{S}) \tag{3.40}$$

$$G(\mathbf{S})F_{cr}(\mathbf{S}) = \sum_{k} \exp(2\pi i \mathbf{S}\cdot\mathbf{R}_k) \sum_{j} f_j(S)\, \exp(2\pi i \mathbf{S}\cdot\mathbf{r}_j) \tag{3.41}$$

where now $\mathbf{R}_k$ is the placement vector which locates the kth unit cell and $\mathbf{r}_j$ is the local placement vector which locates the jth atom within the unit cell. By this decomposition of the spatial description, it is clear that:

$$\mathbf{r}_i = \mathbf{R}_k + \mathbf{r}_j \tag{3.42}$$

By invoking the familiar reciprocal lattice coordinate system, defined by

$$\mathbf{a}^* = (\mathbf{b}\times\mathbf{c})/V \qquad \mathbf{b}^* = (\mathbf{c}\times\mathbf{a})/V \qquad \mathbf{c}^* = (\mathbf{a}\times\mathbf{b})/V \tag{3.43}$$

$$V = \mathbf{a}\cdot(\mathbf{b}\times\mathbf{c}) = \mathbf{b}\cdot(\mathbf{c}\times\mathbf{a}) = \mathbf{c}\cdot(\mathbf{a}\times\mathbf{b}) \tag{3.44}$$

and expressing the scattering vector in reciprocal space and the coordinates of the jth atom in the unit cell in term of its fractional (real space) coordinates (x_j, y_j, and z_j), one can take advantage of the Laue functions for G(**S**) in the limit of a very large parallelepiped crystal having sidelengths **La**, **Mb**, and **Nc**, to obtain the following expression for the scattered intensity [Tadokoro, 1979]:

$$I_{cr}(hkl) = I_e\,(L^2M^2N^2)\,F_{cr}(hkl)F_{cr}^*(hkl) \tag{3.45}$$

where

$$\mathbf{S} = h\mathbf{a}^* + k\mathbf{b}^* + l\mathbf{c}^* \tag{3.46}$$

$$\mathbf{r}_j = x_j\mathbf{a} + y_j\mathbf{b} + z_j\mathbf{c} \tag{3.47}$$

$$F_{cr}(hkl) = \sum_{j=1}^{n} f_j(S)\,\exp[2\pi i(hx_j + ky_j + lz_j)] \tag{3.48}$$

$$= \sum_{j=1}^{n} f_j(S)\,[\cos 2\pi(hx_j + ky_j + lz_j) + i\sin 2\pi(hx_j + ky_j + lz_j)]$$

The summation in Equation 3.48 is taken over n, the number of atoms in the unit cell. h, k, and *l* are indices defined by

$$\mathbf{S}\cdot\mathbf{a} = h \qquad \mathbf{S}\cdot\mathbf{b} = k \qquad \mathbf{S}\cdot\mathbf{c} = l \tag{3.49}$$

Using the relation $F_{cr}(hkl)\, F_{cr}^{*}(hkl) = |\, F_{cr}(hkl)\,|^2$ we obtain finally

$$I_{cr}(hkl) = I_e\,(L^2M^2N^2) \sum_{j=1}^{n} f_j(S)\,[\cos^2 2\pi(hx_j + ky_j + lz_j) + \sin^2 2\pi(hx_j + ky_j + lz_j)] \qquad (3.50)$$

This is the structural contribution to diffraction intensity for a static periodic structure in the limit of large crystallite size. Since the atom positions are fixed on a three dimensional composite lattice, the diffraction pattern consists of a set of Dirac spikes of magnitude $I_{cr}(hkl)$ whose positions are described by the vectors S(hkl).

3.4.2 Modifications to the Structure Factor Intensity

Thermal Motion. In practice, several experimental factors contribute to modify the observed intensity. At finite temperatures the atoms vibrate about their lattice points. If we presume that these vibrations are isotropic for all atoms, then we may express the temperature factor correction to observed intensity in terms of the mean square displacement $\mu_{s,i}^2$ of each atom i. This effect is indistinguishable from that caused by isotropic displacements considered in the Hosemann theory of paracrystals of the first kind [Hosemann and Bagchi, 1962]. For simplicity, we may assume a single common μ_s^2 for all atoms and carry the temperature correction term out of the summation in Equation 3.50. The premultiplier becomes:

$$M_{iso} = \exp(-2\pi^2 S^2 \mu_s^2) \qquad (3.51)$$

$$= \exp[\, -8\pi^2 \mu_s^2 (\sin^2\theta/\lambda^2)\,]$$

In reality, due to atomic bonds and directionally-correlated interactions in the crystal, such motions are quite probably anisotropic. As a first approximation, one would expect the greatest anisotropy to occur between motions parallel to the chain axis and those lateral to it. To reflect this anisotropy, Equation 3.51 may be modified by recasting the dependence upon $(\sin\theta/\lambda)^2$ in terms of h^2, k^2, and l^2, the squared indices of the reflection, and introducing two mean square displacements $\mu_{\parallel}^2$ and $\mu_{\perp}^2$. The anisotropic thermal correction may then be expressed as:

$$M_{an} = \exp[\, -2\pi^2\{(h^2+k^2)\mu_{\perp}^2 + l^2\mu_{\parallel}^2\}\,] \qquad (3.52)$$

Absorption. The absorption factor A reflects the reduction in scattered intensity due to absorption of radiation as it travels through the specimen. This factor depends upon specimen size, shape and elemental composition, and the wavelength of x-rays used. The absorption correction is therefore addressed in the discussion of experimental x-ray measurement.

Multiplicity. The multiplicity factor J reflects the number of identical reflections which superimpose during the scattering experiment. This depends upon the crystal system and the distribution of crystallite orientations within a polycrystalline sample. For example, for the cubic crystal system and completely random orientation of crystallites, the vectors $\mathbf{a}^*$, $\mathbf{b}^*$, and $\mathbf{c}^*$ are of equal magnitude and equally distributed in all orientations; thus only the total magnitude of $|h|+|k|+|l|$ is significant. The multiplicity in this system of (h00) = (0h0) = (00h) is 6, while the multiplicity of (hhh) is 8 and that of (hh0)=(h0h)=(0hh) is 12. By including the entire set of hk*l* indices greater than, equal to, and less than zero in the calculation of the set of intensities I_{cr}(hk*l*) and summing redundant reflections, multiplicity due to crystal symmetry is implicitly considered. For the distribution of crystallite orientation in fiber samples, we assume cylindrical symmetry about the molecular chain axis, **c** in our convention, and uniform distribution of crystallite orientations lateral to this axis. In this case, those reflections which scatter in the equatorial or meridional planes contribute equally to two reflections, resulting in a halving of each reflection intensity prior to summing of redundant reflections, while those which scatter within a quadrant contribute equally to reflections in all four quadrants, resulting in a quartering of each reflection intensity.

Polarization and Lorentz Factors. The x-rays scattered by the electrons are plane polarized to a degree that is dependent upon the scattering angle. This correction may be expressed as:

$$P(hkl) = (1+\cos 2\theta)/2 \tag{3.53}$$

The Lorentz factor corrects for the relative fraction of time in which a given family of planes exists in a narrow angular range to reflect x-rays and is a function of the inclination of the planes to the axis of rotation of a crystal or the fiber axis in the case of cylindrical symmetry. Tadokoro [1979] suggests the use of the correction:

$$L(hkl) = \cos\theta/[\sin 2\theta(\cos^2\phi-\sin^2\theta)^{1/2}] \quad \text{for all reflecting planes} \tag{3.54}$$

Here, ϕ is the angle between the normal to the reflecting planes and the fiber axis. However, de Wolff [1962] suggests that in the case of fiber patterns, more satisfactory results may be obtained using:

$$L(hkl) = (\sin^2\theta \cos\theta \sin\phi)^{-1} \quad \text{for general reflections} \tag{3.55}$$

$$L(00l) = (t \sin^2\theta \cos\theta)^{-1} \quad \text{for meridional reflections} \tag{3.56}$$

t is given to a reasonable approximation in terms of the azimuthal angle $\beta_{1/2}$, in radians, at which the intensity of the reflection falls to one half of its peak value (at β=0°), by

$$t = 0.815\beta_{1/2} \tag{3.57}$$

The final observed intensity, then becomes:

$$I_{obs}(hkl) = A\ J\ M(hkl)\ P(hkl)\ L(hkl)\ I_{cr}(hkl) \tag{3.58}$$

In application, the structures generated by our model are highly ordered, pseudocrystalline geometries which deviate only locally from the ideal crystal description. Thus we consider it appropriate to apply the intensity analysis for periodic lattices to our structures; this is also consistent with the aforementioned view of our model as a local structure embedded within a perfect crystal matrix. The calculation first assumes a "pseudo unit cell", consisting of the domain of explicitly represented atoms or some sub-structure thereof. In this work, we have selected a substructure composed of one helix repeat unit or an approximation thereof from each chain type placed independently on the lattice. Then the Cartesian coordinates of all atoms comprising the cell are converted to fractional coordinates in a straightforward manner (see Appendix B). For all combinations of h, k, and l having $|h|$, $|k|$, or $|l|$ less than some preselected value (e.g. 6 to 9) we calculate the scattering vector, from which one obtains the scattering angle 2θ by Equations 3.46 and 3.37 and the azimuthal angle β by use of the relation

$$\cos\beta = (\mathbf{s}\cdot\mathbf{c} / |s|\,|c|) \tag{3.59}$$

which for a fiber sample oriented perpendicular to the incident beam, simplifies to

$$\cos\beta = (\mathbf{S}\cdot\mathbf{c} / |S||c|) \tag{3.60}$$

The structure factor square $F_{cr}^2(hkl)$ is obtained from a summation of Equation 3.50 over all atoms in the pseudo unit cell and the final intensity is corrected for thermal motion, polarization and Lorentz factors, Equation 3.58, and normalized by the most intense observed reflection; in this manner, all factors which moderate equally the intensities of all reflections are eliminated and we obtain a set of relative observable intensities which are directly comparable to experimental x-ray data. The following chapter details the specifics of application of these calculations to the case study of PPTA.

4. APPLICATION TO POLY(P-PHENYLENE TEREPHTHALAMIDE)

4.1 Introduction

This model was developed primarily with an interest in the particular features of highly extended, stiff chain polymers such as the wholly aromatic polyamides, polyesters, and other conformationally restricted long chain polymers. In the solid state, these materials are characterized by a high degree of molecular alignment. However, as a result of their relative inflexibility, they do not exhibit the conventional crystalline domain/amorphous domain segregation typical of more flexible polymers, as evidenced by the lack of an amorphous halo in x-ray diffraction measurement [Northolt and Van Aartsen, 1977]. Instead, the solid state structures tend to arrange into condensed phase nematic arrays. Aramid fibers specifically exhibit evidence of paracrystalline distortions of the second kind along the chain alignment axis. The modelling approach described above lends itself to the analysis of imperfection along the chain contour and the elucidation of the nature and molecular scale source of multiple orders (i.e. polymorphism).

For purposes of developing and testing the model we directed out attention to the in depth analysis of poly(p-phenylene terephthalamide). This structure possesses several features which recommend it for our purposes. First, PPTA has been discussed extensively in the literature and is the only such rigid rod polyamide for which there exists a sufficient set of experimental data, encompassing crystallographic and macromorphological descriptions, thermo-mechanical behavior, solution behavior, radiation absorption, and response to chemical exposure. Second, as was reviewed in the discussion of constitutional isomerism, a procedure exists to introduce controlled atomic substitutions on the parent chain and to vary the isomeric order of the PPTA derivatives; this is particularly useful in studying in a stepwise manner the sensitivity and range of applicability of the model. Third, PPTA is readily available, in the form of Dupont's Kevlar® fiber, for additional processing and testing against model predictions.

Even on a stand-alone basis, PPTA possesses several features of particular interest for molecular analysis. 1) This polymer consists entirely of alternating para-linked phenylene rings and amide linkages; each of these rigid moieties is a polyatomic group which acts in a concerted manner. The phenylene moiety may rotate without significant effect on the helical chain conformation, but with possibly major impact on chain packing. 2) The amide moiety is known to form intermolecular hydrogen bonds between

proximate hydrogens and oxygens. 3) There is the possibility for further energetically-favorable interactions due to π-bond overlap between adjacent phenylene and amide moieties within a chain or between proximate phenylene moieties between chains. These features create a vastly different environment from the neutral, flexible chain aliphatics addressed by other investigators. New problems of both intramolecular description and intermolecular behaviors must be addressed in order to produce a meaningful picture by atomistic modelling.

4.2 Chain Description

The polymer chain is described as an ensemble in Cartesian space of its constituent atoms, all of which are expressed explicitly. The repeat unit of the polymer chain is illustrated in Figure 4.1. All atoms in the chain are treated as point centers of force for calculation of interaction energies. We hold all bond lengths and bond angles constant, with the exception of the eight "backbone" angles (labelled ϑ_1 through ϑ_8 in Figure 4.1); during the course of this work, we discovered that the optimization trajectory was considerably improved when these crucial angles were allowed to change during ring rotation. The phenylene rings are represented as rigid, hexagonal constructions of the ten bonded constituent atoms. The bonding at the trivalent amide carbons and nitrogens in the amide group are fixed in the planar sp^2 hybridization configuration. In this way the number of internal degrees of freedom was reduced from eighty-four to fourteen: the eight bond angles and six torsion angles (ϕ_1 through ϕ_6 in Figure 4.1) of the structural unit.

4.3 Parameterization of the Force Field

Where possible, we have drawn upon proven force field parameterizations for use in this model. The reasons for this are twofold: first, the parameterizations taken from the literature have already been shown to reproduce structural features and thermodynamic quantities in related low molecular weight models and thus have some degree of credibility prior to their usage here; second, such a selection is philosophically compatible with the idea of the self-consistent force field and transferability of atomic parameters from one system to another, a concept central to the generalization of atomistic modelling methods.

A simple VFF description was employed for the eight bond angles, using values taken from Tashiro et al. [1977]. Table 4.1 gives the important parameters for the VFF description, along with all the bond lengths and bond angles required. Parameterization of the 12-6-1 nonbonded interatomic potential energy

Figure 4.1: A segment of poly(p-phenylene terephthalamide) (PPTA) with all torsion angles in their zero positions.

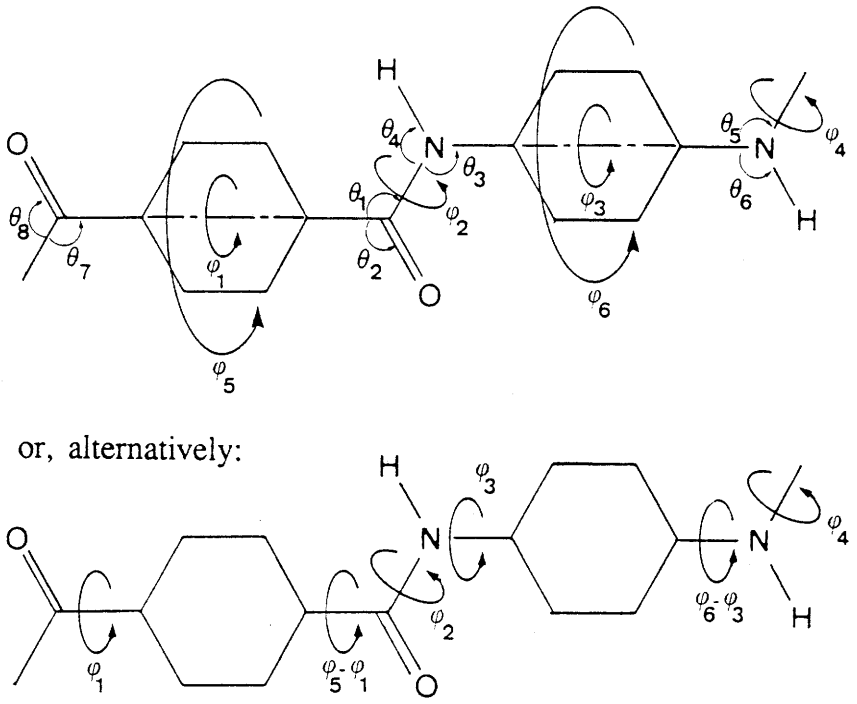

or, alternatively:

function for the amide moiety has been taken directly from the work of Lifson and co-workers on the development of a self-consistent force field encompassing low molecular weight alkane, alkene, amide, and carboxylic acid crystals [Lifson and Warshel, 1968; Warshel and Lifson, 1970; Hagler et al., 1974; Lifson et al., 1979]; this force field has been designed to reproduce hydrogen-bonding interactions implicitly. For the carbons and hydrogens of the aromatic rings, we initially attempted to use the values suggested by Lifson and co-workers for aliphatic carbons and hydrogens, as has been done previously by others [Bernstein and Hagler, 1978; Hummel and Flory, 1980]. The van der Waals radii for the aromatic carbons were eventually reduced by ten percent from the aliphatic carbon values suggested by these investigators, in order to improve the torsional energy approximation for ring rotation (see below). We deem this slight correction to be minor in light of the margin of error inherent in such estimates of van der Waals radii.

The partial atomic charges required for the atom-centered electrostatic interactions involving phenylene ring atoms, however, are not generally available. To estimate these, it was necessary to embark upon a series of calculations using various semiempirical quantum mechanics packages for a homologous series of low molecular weight aromatic amides. In each case, molecules in the series were completely optimized with respect to bond lengths, bond angles, and bond torsions, subject to the restriction of planar hexagonal phenylene rings, in accord with the model description. Results for the members of the series were compared for internal consistency of geometry and charge distribution. Where possible, individual members were checked for agreement with available experimental data for ring torsions and nonzero electrostatic moments. The procedures used and results obtained are detailed in Appendix C. The final atomic charges were chosen to reproduce dipole and quadrupole data through assignment of partial charges and to ensure local charge neutrality in the amide N-H, the amide C=O, and the phenylene ring. The calculated charges on the atoms of the amide group are comparable to those proposed independently by Hagler et al. [1974] and used in conjunction with their induction/dispersion parameters; the latter were retained in our work for purposes of consistency. Partial atomic charge and nonbonded potential energy parameters for all atoms are tabulated in Table 4.2.

For the C-N amide torsion, we have used the potential energy function of Jorgensen and Swensen [1985], derived from NMR data on N-methylacetamide. The interaction between the adjacent ring and amide moieties prefers coplanarity of the bond planes of these two groups in order to effect the delocalization of electrons in π-bond orbitals; however, this coplanarity is precluded by steric overlap between the hydrogens on the ring and the pendant atoms (O and H) on the amide group. Numerous (disparate) estimates for the phenylene-amide correlated torsion energy have been reported, indicating the general lack of consistent quantitative information on this type of distributed interaction. Estimates have originated from semiempirical quantum mechanics calculations [Lauprêtre and Monnerie, 1978], π-bond group additivity considerations [Tashiro et al., 1977, p413], and empirical fitting to experimental crystal data for low molecular weight analogues [Hummel and Flory, 1980]. We have further explored this

Table 4.1

Fixed bond lengths and Valence Force Field (VFF) constants for variable backbone angles

Angle[a,b]	k_i (kcal/deg^2)	Bond	l (Å)
CC_OO (ϑ_2)	0.088	C_{ar}-C_{ar}	1.40
CC_ON (ϑ_1,ϑ_7)	0.088	C_{ar}-H	1.10
C_ONH (ϑ_4)	0.050	C_{ar}-C_{am}	1.50
C_ONC (ϑ_3,ϑ_5)	0.088	C_{ar}-N	1.41
CNH (ϑ_6)	0.050	C_{am}=O	1.24
NC_OO (ϑ_8)	0.088	C_{am}-N	1.39
		N-H	1.00

[a] Angle bending energy = k_i (ϑ_i - ϑ_O) where ϑ_O = 120° in all cases.
[b] C_O is the sp^2-carbonyl carbon atom

Table 4.2

6-12 Nonbonded atomic potential parameters and elementary charges used in the electrostatic potential

Atom	ε (kcal/mole)	r (Å)	q[a] (elementary charge)
C (phenylene, 1 and 4)	0.039	1.96	-0.06
C (phenylene, 2 and 3)	0.039	1.96	-0.12
H (phenylene)	0.038	1.37	+0.14
C (amide)	0.147	2.03	+0.38
H (amide)	0.0	0.0	+0.28
N	0.169	1.96	-0.28
O	0.232	1.60	-0.38

[a] The value for the bulk dielectric constant D_B was 3.5, and the Block-Walker crossover distance d* was 3.3Å.

torsion using AM1 semiempirical quantum mechanics calculations, as described in Appendix C. Figure 4.2 shows several energy functions reported in the literature, along with AM1 results for the rotation of the phenylene ring connected to the amide nitrogen in benzanilide. Figure 4.3 shows similar predictions, including AM1 rotation results for the ring connected to the amide carbon in benzanilide. For parameterization purposes, we have employed two-parameter cycloidic torsion energy functions which, in combination with the nonbonded atomic interactions, are consistent with the available torsional energy estimates. These, along with the amide torsional energy function of Jorgensen and Swensen, are reproduced below, with parameters presented in Table 4.3. Because the nonbonded interactions are retained explicitly for interactions between atoms in the ring and the amide group, the torsional potentials describing ring rotation may be attributed to the phenomenon of electron distribution between the two moieties.

$$E^{tor,amide} = \tfrac{1}{2} V_{a,1} (1-\cos\phi_2) + \tfrac{1}{2} V_{a,2} (1-\cos 2\phi_2) \quad [\text{same for } \phi_4] \tag{4.1}$$

$$E^{del,phenylene\text{-}C=O} = \tfrac{1}{2} V_d (1 + \cos(y)) \tag{4.2}$$

$$\phi_5 = \tfrac{1}{2}(y - m_d \sin(y)) + \pi \quad [\text{same for } (\phi_5-\phi_1)]$$

$$E^{del,phenylene\text{-}N\text{-}H} = \tfrac{1}{2} V_d (1 - \cos(z)) \tag{4.3}$$

$$\phi_6 = \tfrac{1}{2}(z - m_d \sin(z)) \quad [\text{same for } (\phi_6-\phi_3)]$$

4.4 Simulation Procedure

The approach to structure optimization plays a major role in the validity of model predictions. Time and computational constraints limit the thoroughness of any such general investigation. Approaches to analysis by simulation may, however, be classified according to the goals they seek to achieve. Where one is interested primarily in elucidation of a known structure or defined region of parameter space, or in comparisons between such predefined domains, it is possible to take advantage of previous (e.g. experimental) information to limit the range of investigation, making it relatively straightforward to identify minima of immediate interest and to establish the nature of the local parameter space. This solution contains no assertions about the global nature of the minima thus identified and may depend strongly upon the choice of a starting point. Where one is concerned with a first principles approach to

Figure 4.2: Rotation energy functions suggested for the phenylene ring connected to the amide nitrogen in benzanilide: (a) π-bond additivity [Tashiro et al., 1977]; (b) empirical fit [Hummel and Flory, 1980]; (c) PCILO calculation [Lauprêtre and Monnerie, 1978]; (d) AM1 calculation (this work); (e) composite force field (this work).

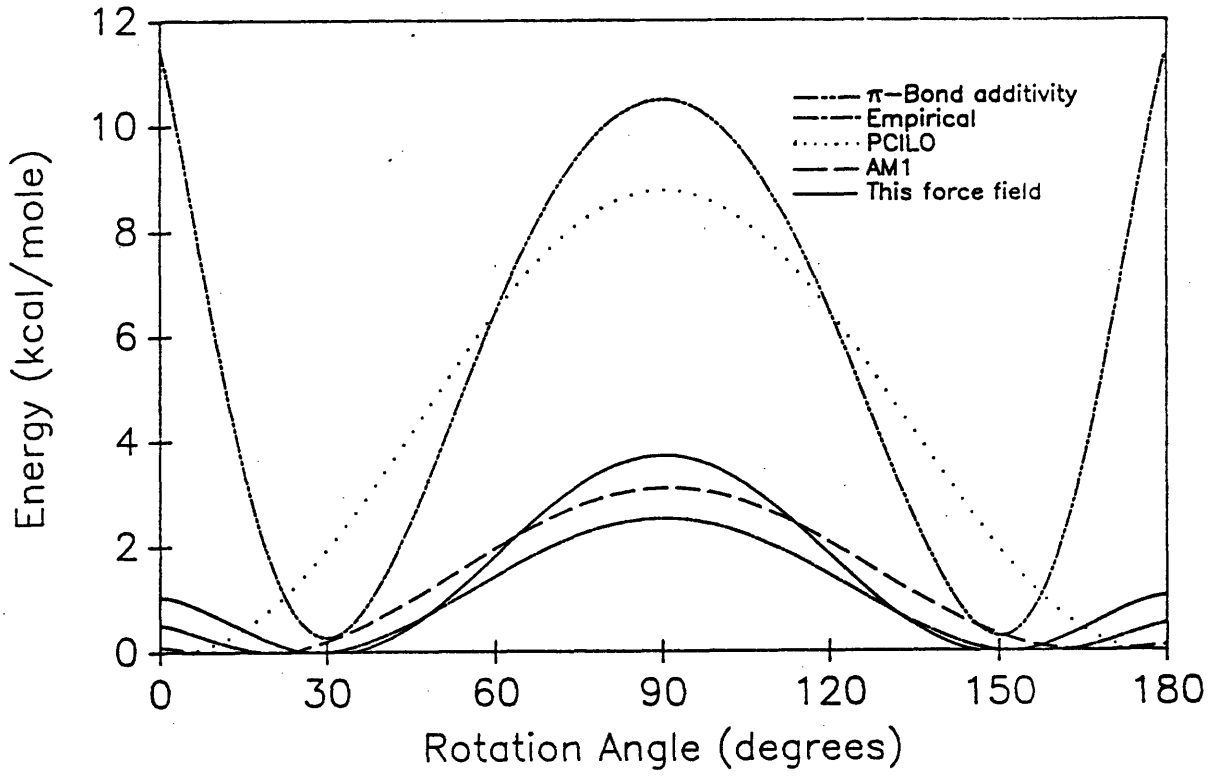

Figure 4.3: Rotation energy functions suggested for the phenylene ring connected to the amide carbon in benzanilide: (a) π-bond additivity [Tashiro et al., 1977]; (b) empirical fit [Hummel and Flory, 1980]; (c) PCILO calculation [Lauprêtre and Monnerie, 1978]; (d) AM1 calculation (this work); (e) composite force field (this work).

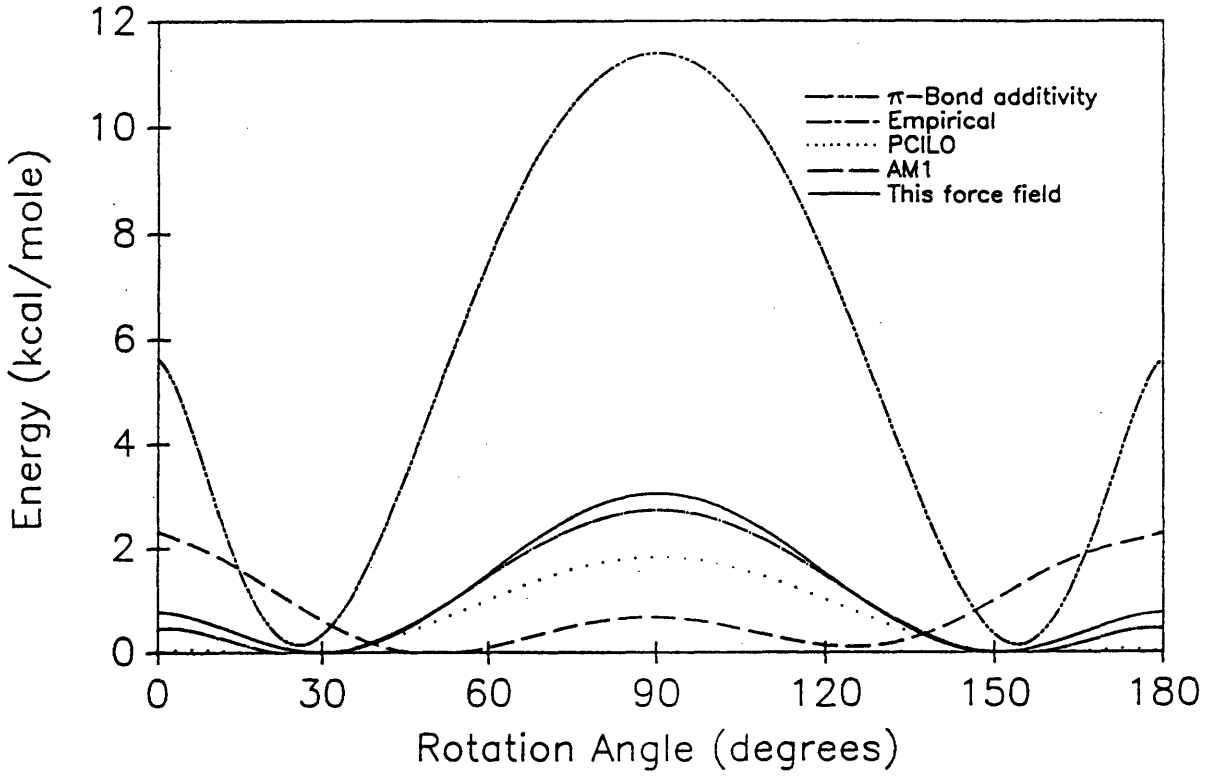

Table 4.3

Intrinsic torsional energy function parameters[a]

Torsion	$V_{a,1}$[b]	$V_{a,2}$[b]	V_d[b]	m_d
amide (ϕ_2,ϕ_4)	2.8	21.2	-	-
diacid ring (ϕ_5,ϕ_5-ϕ_1)	-	-	9.0	0.2
diamide ring (ϕ_6,ϕ_6-ϕ_3)	-	-	13.0	0.4

[a]see text for details, Equations 4.1 - 4.3
[b]all values in kcal/mol

materials investigation, it is necessary not only to locate minima, but to establish confidence in their global relation. Unfortunately, this may only be assured by investigating the whole of parameter space and identification of all minima therein, a time intensive process whose end cannot be a priori guaranteed. The latter problem necessitates an initial grid scan of parameter space, with a decision criterion established to identify relevant regions of the parameter field for further analysis. This approach, of course, suffers from grid density dependencies and response of the minimization algorithm to the convolution of the multivariate phase space.

Our analysis to identify likely structures for polymer packing proceeds according to the following strategy. As an initial approximation, we assume that chain conformation and chain packing considerations may be decoupled and considered independently. This is the most common approach taken in molecular mechanics and x-ray structure factor fitting procedures and, as was mentioned previously, is where most previous efforts have stopped. As a result of this approximation, we may first employ single chain simulations to identify those conformations which are of lowest energy and are most likely to meet packing density criteria. In addition, we are primarily interested in the highly oriented structures produced during fiber spinning. Such elongational processing steps are known to favor the formation of extended chain conformations prior to vitrification or crystallization and concurrent loss of conformational mobility. Based on this, we exclude conformations of low helical pitch from further consideration.

As a second step, we perform successive grid scans of the multivariate packing parameter space using fixed chain conformations at a predetermined packing density, initially without minimization of energy with respect to intermolecular packing parameters, starting with conformations of smallest helix diameter; we conclude the search with those conformations which are of sufficiently large helix diameter to preclude the realization of reasonable packing energies in the entire parameter space. In some cases, such scans are repeated with minimization of potential energy with respect to packing parameters. The grid density was chosen based on experience with the polymer in question and reflects a subjective trade-off between computation time and comprehensiveness. Table 4.4 lists the starting point mesh parameters, ranges, and mesh densities employed in PPTA.

In the third step, we drop the approximation of independent intramolecular and intermolecular behaviors and concentrate on those areas of conformation/chain packing space that signal the location of low energy local minima. The relevant domains thus identified are searched by means of nonlinear multivariate potential energy minimizations using an unconstrained Davidon-Fletcher-Powell Quasi-Newton algorithm with "approximate Hessian" estimation [Fletcher, 1972].

Table 4.4

Starting point mesh used in multichain search-minimization

Parameter	Range	Step Size
interchain distance (Å)	4.5 - 9.0	2.25
interaxial angle (degrees)	30 - 90	20
chain placement angle (degrees)	0- 360	20
chain translation[a]	-0.5 - +0.5	0.25

[a]chain translation is expressed as a fraction of the helix translation distance; values outside of this range are redundant with respect to rotation/translation

4.5 PPTA Simulation Results: Single Chain

In order to reduce the parameter space of relevance for chain packing calculations, we first looked for the preferred conformation behavior of the isolated chain. For this purpose, we consider the PPTA chain as a string of torsion angle triplets, composed of the phenylene-C-N, amide, and C-N-phenylene torsions (ϕ_3, ϕ_2 and ϕ_1, respectively, in Figure 4.4), each triplet being identical and alternating in order along the chain due to the symmetry of the monomer units. This simplification arises from the assumption that intramolecular interactions are essentially decoupled across the rigid phenylene moieties. Since the amide torsion exhibits a strong preference for the trans or cis conformation, it suffices to study the conformation energy as a function of ϕ_1 and ϕ_3, with ϕ_2 always assuming a position of minimum energy. Figure 4.4 shows such an energy contour map for benzanilide with the amide torsion optimized about its trans conformation; a similar map with minimization of the amide torsion about the cis conformation exhibits minima near [30°,150°] and [150°,30°], but these are energetically less favorable (by 4-5 kcal/mole of repeat units) compared to the trans amide conformation. Of the possible monomer conformations, only those of a highly extended character will pack to densities realized in the solid state for PPTA without unreasonable penalties in intermolecular energy. Based on this, we have concentrated on those conformations having rodlike or crankshaftlike conformations for chain packing studies. Of these, only the all-trans rodlike conformations appear in the final list of lowest energy packed structures, as will be seen in the next section. Table 4.5 lists the internal coordinates of the lowest energy rodlike conformations assumed by the PPTA chain in the current force field representation. This essential rigidity ensures that chain alignment plays a dominant role in packed structure formation.

4.6 PPTA Simulation Results: Multichain

4.6.1 Selection and Presentation of Results

A screening of the packing energy using the most probable conformations in a general grid assembly and minimizing simultaneously with respect to both intramolecular and intermolecular degrees of freedom indicates considerable correlation between chain orientations in the packed structures. This is demonstrated in Figure 4.5, where the concentration of packing minima along the diagonals of a plot of total potential energy versus chain setting angles ω (for a lattice composed of two independent chains initially in the all-trans conformation with successive phenylene rings oppositely rotated; ω is defined by the rotation of the first amide plane of the chain out of the AC-plane of the parallelepiped, Figure 3.1) is indicative of the predominant formation of sheetlike structures in PPTA; similar maps were found for packing of chains in other initial conformations.

Figure 4.4: Potential energy contour for benzanilide as a function of the ring torsions ϕ_1 and ϕ_3.

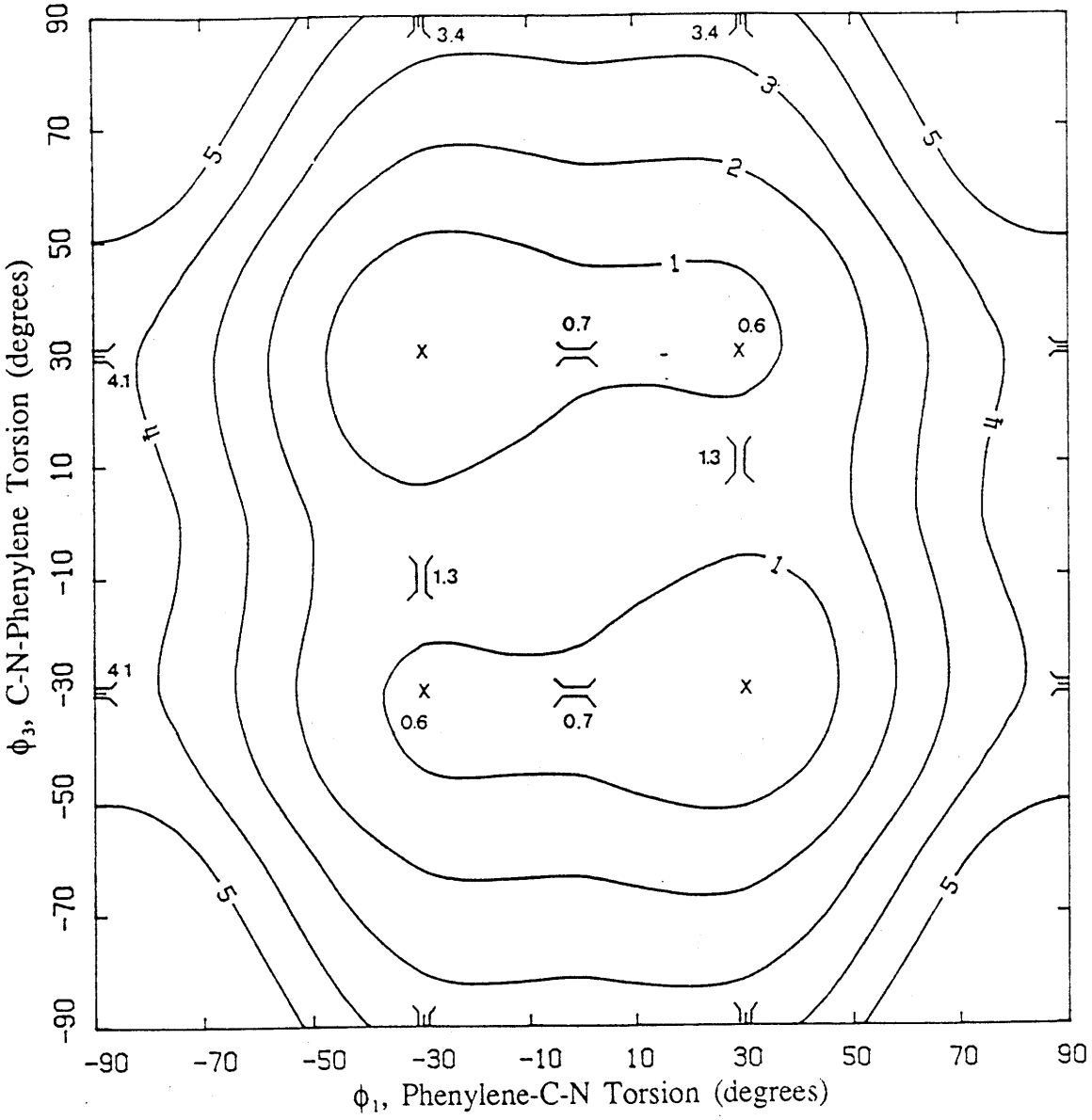

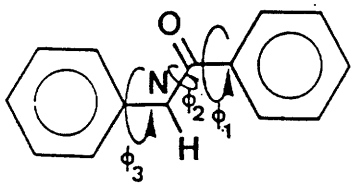

Table 4.5

Most favored isolated chain conformations

Structure →	1	2
Internal Coordinate ↓		
Bond Angles (degrees)		
C_{ar}-C_{am}-N	119.2	119.1
C_{ar}-C_{am}=O	120.6	120.5
C_{am}-N-H	117.4	117.2
C_{am}-N-C_{ar}	124.8	125.1
C_{ar}-N-H	117.7	117.6
C_{ar}-N-C_{am}	125.0	125.2
N-C_{am}=O	120.3	120.4
N-C_{am}-C_{ar}	120.5	120.5
Torsions (degrees)		
N-C_{am}-C_{am}-N	-0.4	55.0
C_{am}-C_{am}-N-N	8.5	8.9
C_{am}-N-N-C_{am}	1.1	62.6
N-N-C_{am}-C_{am}	-9.0	9.0
Out-of-Plane Ring Rotations (degrees)		
diacid phenylene	151	28
diamide phenylene	33	31
Helix Parameters		
Pitch (Å)	13.1	13.1
Twist (degrees)	0	128
Potential Energy (kcal/mol of repeat units)	0.0	0.469

Figure 4.5: Energy contours for packing of extended conformations of two independently orientable chains of like conformation of PPTA, as a function of the two setting angles ω_1 and ω_2.

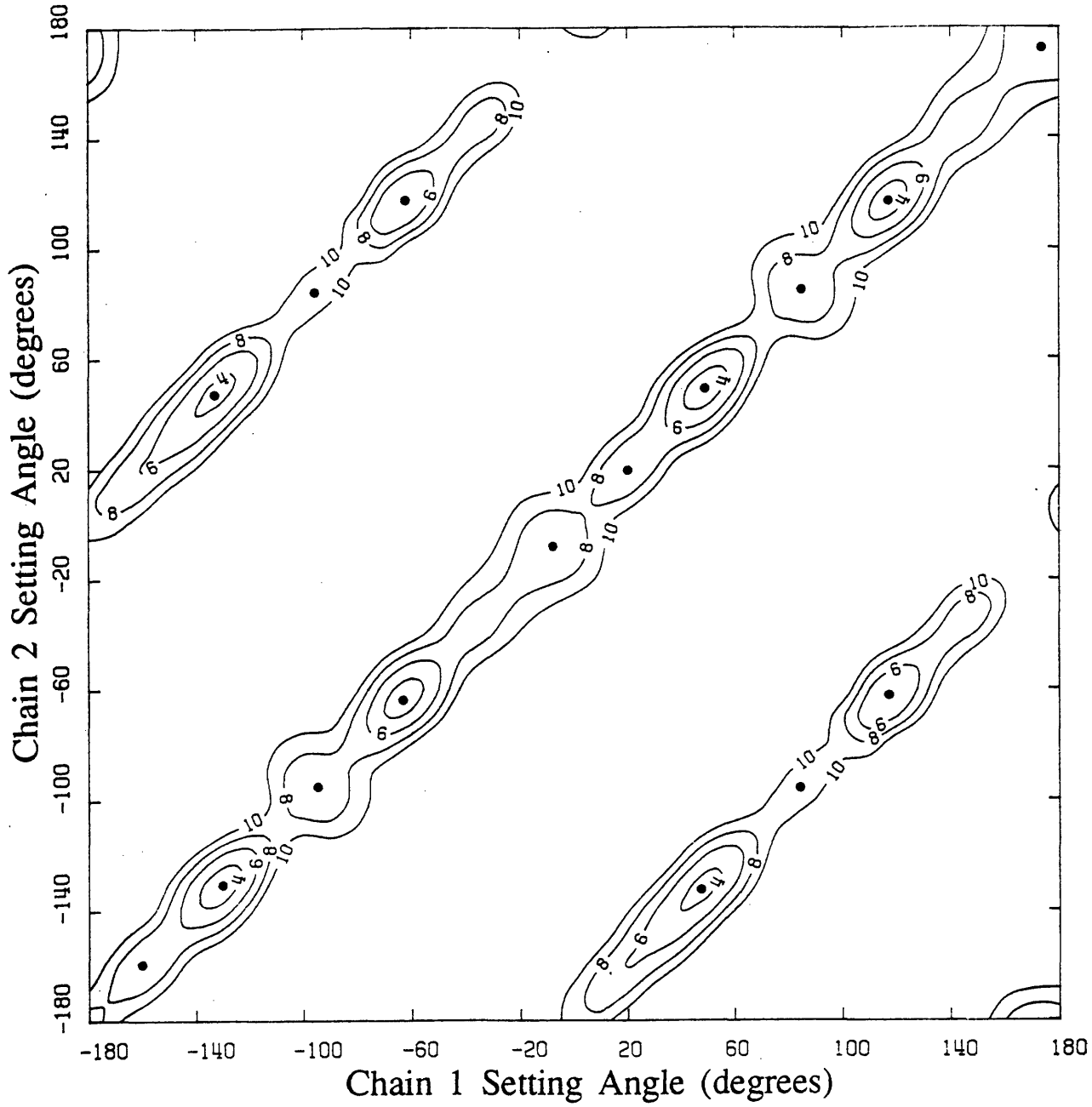

From such maps, those structures having the lowest total potential energy were identified as possible crystal structures. By means of the scan-and-search procedure, a listing of local minima is obtained; the length of this listing depends on the severity of the convolution of the potential energy hypersurface, the number of reasonably advantageous packing geometries available to the material in question, and the comprehensiveness of the scan-and-search employed. If we are only interested in the most probable polymorphs, we may discard as irrelevant those minima whose Boltzman-weighted probabilities fall below a designated significance level. That is, for some cut-off criterion $0 < f < 1$:

$$\Delta E_i = E_{\text{tot, allomorph i}} - E_{\text{tot, global minimum allomorph}} - 2\,\delta E \qquad (4.4)$$

where δE is the estimated accuracy of the energies calculated

$$\text{discard all allomorphs i such that:} \quad \exp(-\Delta E_i/RT) < f \qquad (4.5)$$

For a δE of roughly 1 kcal/mol and a cut-off criterion f of 0.2, or 20% probability of occurrence, at 298K, the cut-off in energy for a significant local minimum above that of the global minimum corresponds to 2.9 kcal/mol of repeat units (12 cal/g). On this basis, we discard those local minima whose energy exceeds this criterion to obtain a final basis set of significant energy-minimized structures.

The final analysis suggests up to eight distinct and viable crystalline polymorphs, all having cohesive energies within a variance of 6%, or a range of 2.4 kcal/mol (10 cal/g) between the highest and the lowest energies. These eight structures are demonstrated in the sets of orthographic projections presented in Figure 4.6(a)-(h). In these projections, the leftmost perspective looks down the chain axis, and van der Waals spheres (the dashed lines) have been included to illustrate the density of atomic packing in these structures. The middle perspective is perpendicular to the ac-facet of the structure, and the rightmost perspective is orthogonal to the previous two. In these perspectives, the carbons are black, the amide hydrogens white, the nitrogens lightly shaded, the oxygens more darkly shaded, and the ring hydrogens have been omitted from the second two perspectives for clarity. Quantitative description is given in Table 4.6. It may be noted that in the construction of this model we have intentionally favored a general parallelepiped description for chain packing, involving the vectors **A**, **B**, and **C**, over a presumed unit cell or superposition-of-unit cells description. There are also some minor quantitative differences between the parameters listed in Table 4.6 and those which may be deduced from Figure 4.5, due to refinements of the model and elimination of redundant structures prior to tabulation in Table 4.6. For ease of clarification, we have converted the structural parameters in Table 4.6 from the generalized parallelepiped description to a parameter set more amenable to crystallographic interpretation and have reported parameters in both conventions. The appropriate unit cell descriptions were selected from the infinite

Table 4.6

Multichain energy minimization results: structural parameters for eight most probable unit cells

Structure ID →	1	2	3	4	5	6	7	8
Structural Parameters ↓								
a (Å)	6.8	7.1	8.3	8.4	8.4	8.5	8.4	4.8
b (Å)	6.2	5.9	5.0	4.9	4.9	4.6	4.9	5.0
c (Å)	13.2	13.1	13.1	13.1	13.1	13.1	13.1	13.1
α (degrees)	90	93	90	86	80	79	85	55
β (degrees)	90	92	90	78	89	94	93	95
γ (degrees)	88	92	92	89	90	93	90	96
Chain Locations (ab projection)	[0,0] [½,½]	[0,0] [½,½]	[0,0] [½,½]	[0,0] [½,½]	[0,0] [½,0]	[0,0] [½,0]	[0,0] [½,0]	[0,0] -
Chain Setting Angles (degrees), relative to the bc-facet	6 -174	2 2	18 -161	12 13	-2 -1	-9 -9	2 1	2 -
Inter-sheet Translation (Å)	6.2	6.6	5.9	6.6	2.4	3.1	6.6	2.7
Helix Twist Θ_h (degrees)	0	0	4	6	3	0	1	4
Monomer Phenylene Ring Rotation (degrees)								
diacid ring ϕ_5:	-16	-30	-26	-35	-43	39	43	34
diamide ring ϕ_6:	15	21	43	36	40	38	33	29
Cohesive Energy (kcal/mole of repeat units)	40.5	38.5	38.3	38.2	38.1	39.3	39.7	39.6
Density (g/cm^3)	1.42	1.45	1.45	1.49	1.50	1.57	1.47	1.56
Parallelepiped Description:								
A (Å)	4.7	4.5	4.8	4.9	4.2	6.2	6.4	5.0
B (Å)	4.6	4.7	4.9	4.8	6.4	4.4	4.2	4.8
C (Å)	13.2	13.1	13.1	13.1	13.1	13.1	13.1	13.1
τ (degrees)	90	90	90	81	97	98	93	95
υ (degrees)	90	94	90	77	89	88	88	55
ζ (degrees)	85	81	62	61	50	48	50	96
ω_1 (degrees)	127	128	101	110	92	146	138	92
ω_2 (degrees)	-53	128	-79	110	92	146	138	92
f_2	0.47	0.50	0.45	0.50	0.18	-0.25	0.50	0.0

Figure 4.6: Orthographic perspectives of the eight primary structures for PPTA suggested by simulation. The sets (a) through (h) correspond to the structures labelled 1 through 8, in order, in Table 4.6. Left: z-axis perspective; Middle: perspective perpendicular to the ac-plane; Right: perspective perpendicular to the previous two perspectives.

(a)

PPTA Structure #1

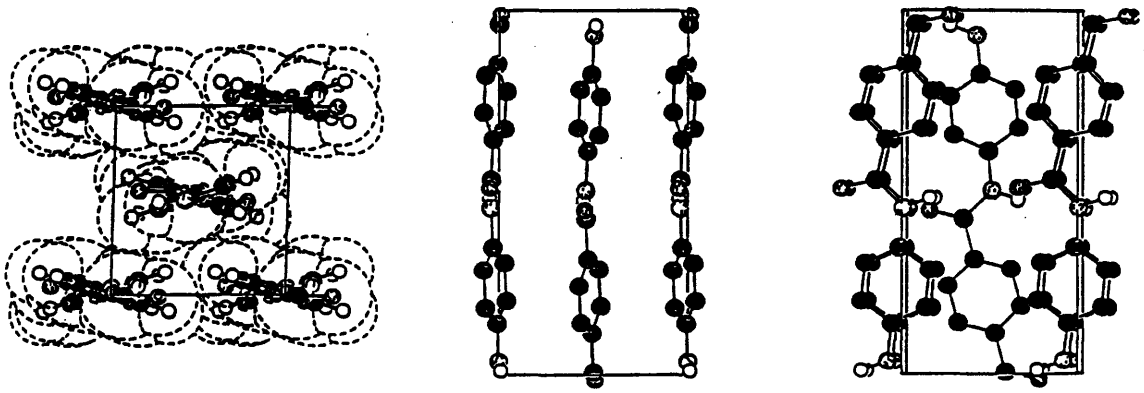

PPTA Structure #2

(b)

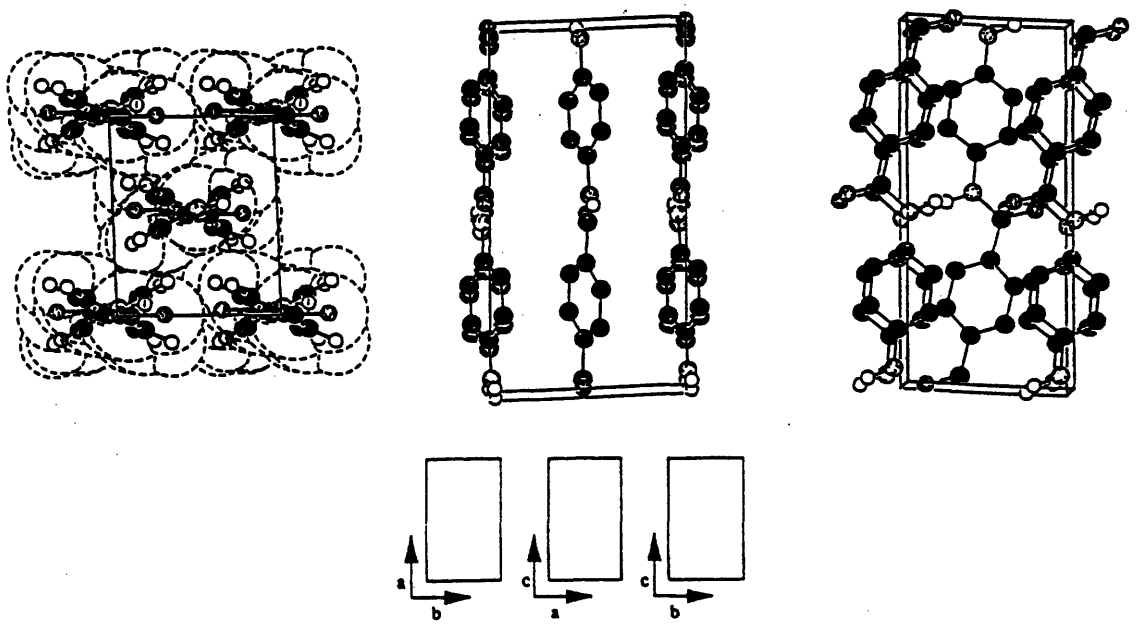

Figure 4.6: Orthographic perspectives of the eight primary structures for PPTA suggested by simulation (continued).

(c)

PPTA Structure #3

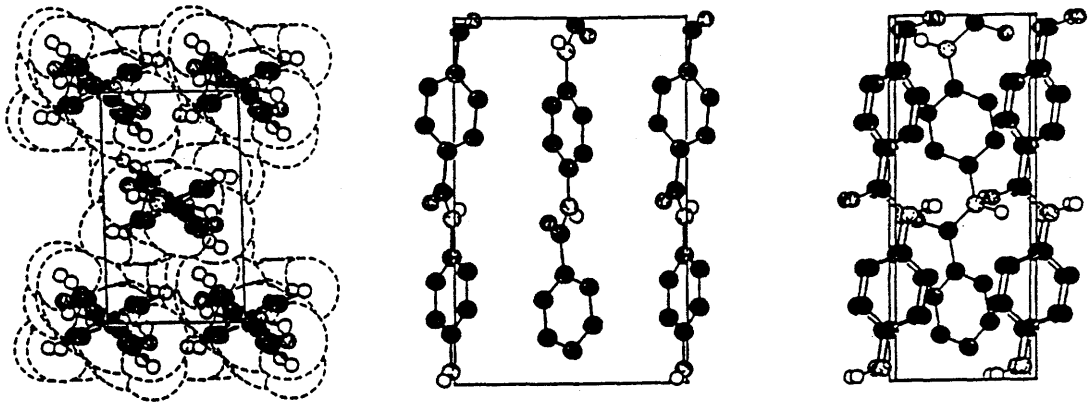

PPTA Structure #4

(d)

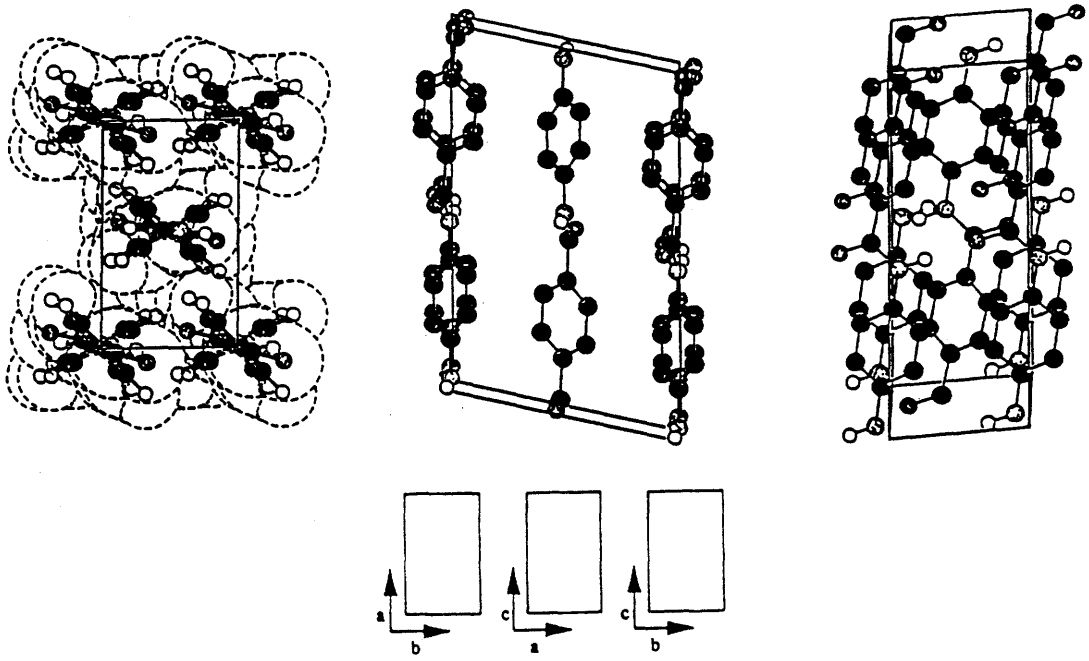

Figure 4.6: Orthographic perspectives of the eight primary structures for PPTA suggested by simulation (continued).

(e)

PPTA Structure #5

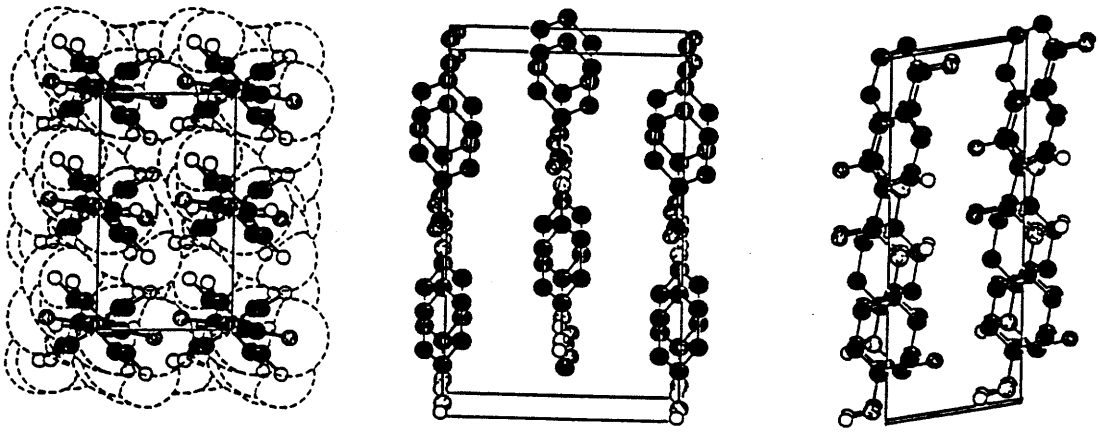

PPTA Structure #6

(f)

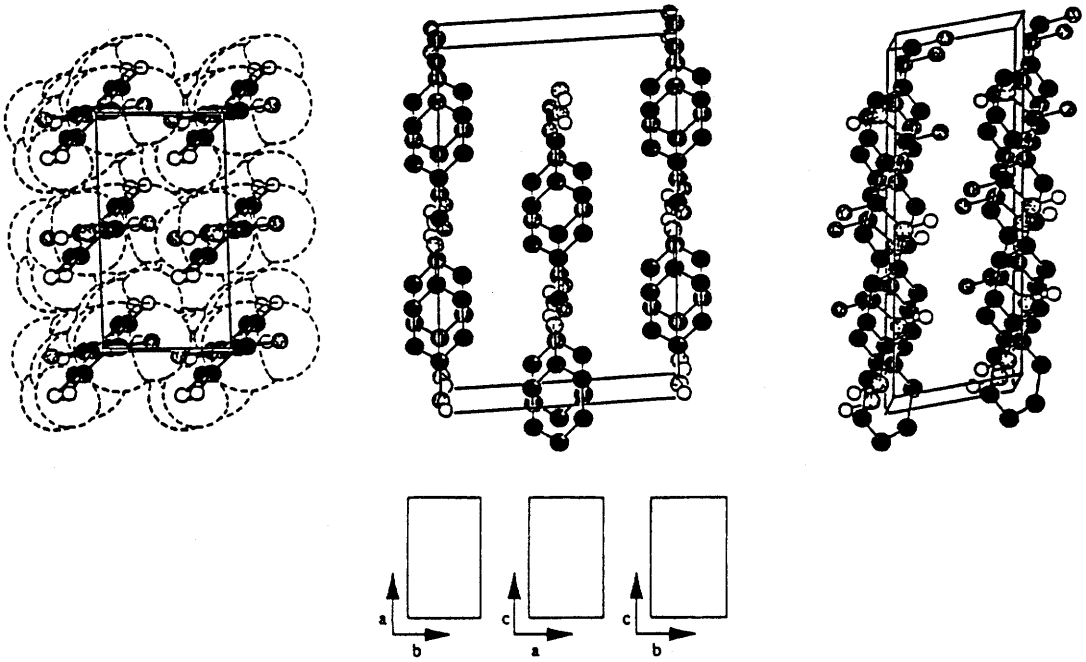

Figure 4.6: Orthographic perspectives of the eight primary structures for PPTA suggested by simulation (continued).

(g)

PPTA Structure #7

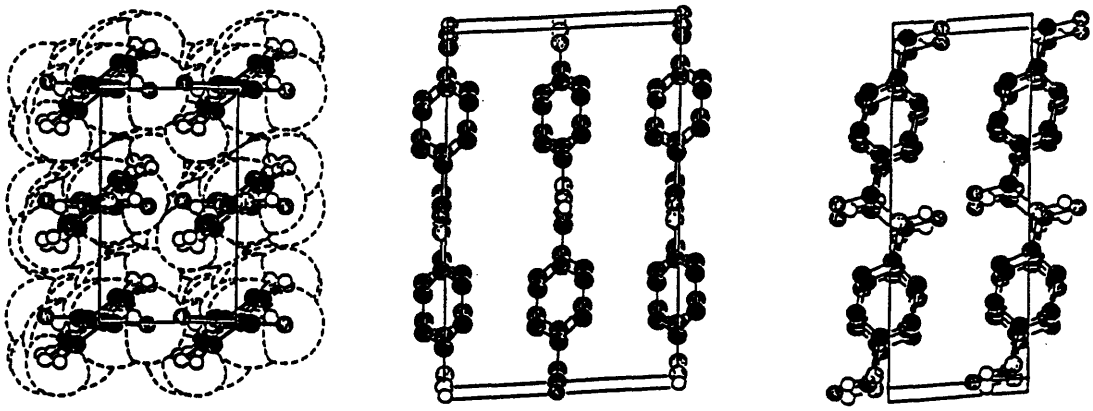

PPTA Structure #8

(h)

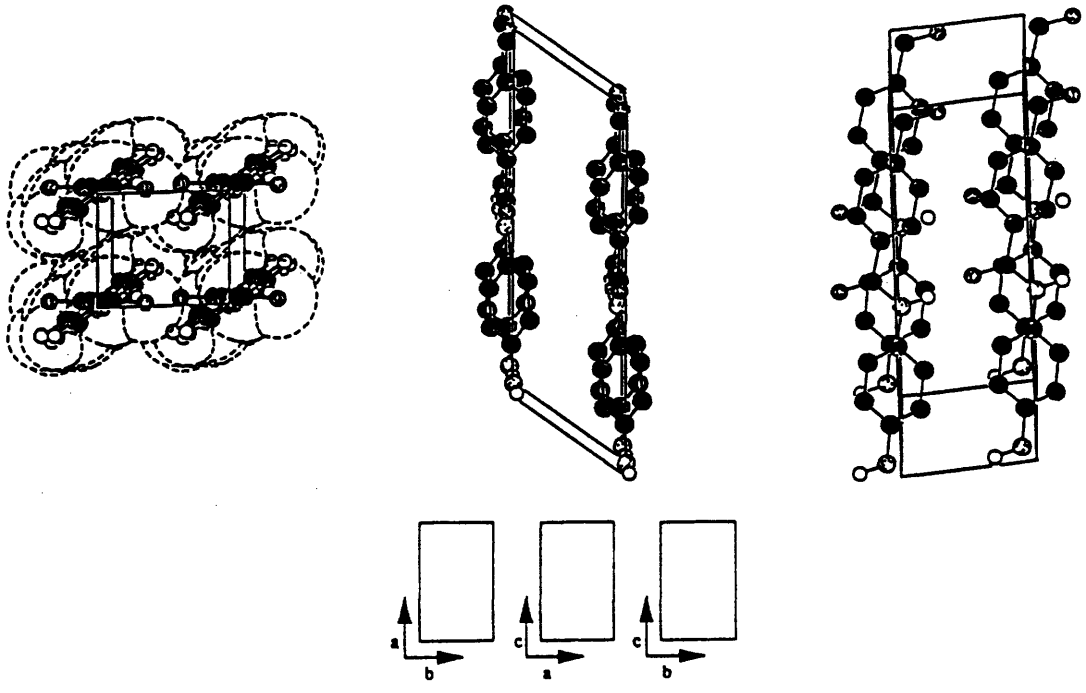

number of possible descriptions based on a preference for interaxial angles $\alpha=\angle\mathbf{bc}$, $\beta=\angle\mathbf{ac}$, and $\gamma=\angle\mathbf{ab}$ closest to 90°. It may readily be seen that the crystallographic cell, described by the vectors **a**, **b**, and **c**, obeys the relations: $\mathbf{c}\|\mathbf{C}$ and $\mathbf{a}\times\mathbf{b}\|\mathbf{A}\times\mathbf{B}$. Similarly, the chain setting angles are reported relative to the bc-facet (the **b**×**c** plane), as was done by Northolt for PPTA, rather than relative to the arbitrarily selected **A**×**C** plane of the parallelepiped.

4.6.2 Evaluation of Polymorphs

From this basis set of lowest energy packing minima, one may draw several conclusions concerning the preferred structure of PPTA:

1) The backbone features of individual chain conformations are in reasonable agreement with those employed by Northolt in his crystal structure analysis. Table 4.7 shows the final values of the important backbone angles and torsions of the chain conformation in the packed geometries. Angles of 10° ± 4° are formed between the phenylene rings and the chain propagation axis, and torsions about the amide bond vary from 2° to 7° and are generally balanced by alternate plus/minus torsions of equal magnitude in consecutive amide moieties. This conformation orients the amide dipoles in all cases in nearly antiparallel fashion as one travels along the chain axis. Phenylene ring positions about the C1-C4 axes relative to the plane of the adjacent amide bond show a preference for out-of-plane rotation (see Table 4.7), as expected from the isolated chain energetics reported in the previous section and from reports in the literature [Northolt, 1977; Tashiro et al., 1977 p413; Hummel and Flory, 1980]. Packing considerations do not appear to preclude either of the two possible directions of ring rotation. However, the chain packing does appear to have a considerable effect on the magnitude of out-of-plane rotation, with values ranging between roughly 15° and 43° for either ring.

2) While no hydrogen bonding potential energy function has been explicitly included, nevertheless the geometry and energy character of "hydrogen bonding" between amide groups in neighboring chains is reasonably reproduced. This is in good agreement with the findings of Hagler et al. [1974]. For the final eight structures, the average O···H "bond" distance is 2.3 Å, with a N-H···O angle of 160°. The interaction energy attributable to the hydrogen bond varies between 1.8 and 3.8 kcal/mole, and is largely due to the strong electrostatic attraction between the hydrogen-oxygen pair. Hagler et al. suggest that their force field for the amide moiety, employed unchanged in this work, yields an optimum hydrogen bonding distance of 2.1 Å and a "bond energy" of 2.4 kcal/mol; in their study of low molecular weight amide crystals, predicted hydrogen bond lengths were slightly lower, ranging from 1.9Å up to 2.1Å, with a N-H···O angle of 145° to 175°. Our calculated bond length of 2.3 Å lies intermediate between these values and the 2.9 Å proposed by Ladell and Post [1954] to be typical for amide crystals. The 160°

Table 4.7

Chain conformations realized in packed structures

Structure →	1	2	3	4	5	6	7	8
Internal Coordinate ↓								
Bond Angles (degrees)								
C_{ar}-C_{am}-N	118.6	118.9	118.9	119.3	118.3	118.6	118.7	119.0
C_{ar}-C_{am}=O	120.2	119.4	122.0	120.6	121.8	121.7	120.7	120.8
C_{am}-N-H	115.1	115.4	118.8	118.2	118.4	117.8	117.3	117.3
C_{am}-N-C_{ar}	129.3	128.3	123.1	124.1	123.1	124.2	124.8	126.0
C_{ar}-N-H	115.7	116.2	118.4	118.5	117.7	117.8	117.9	116.8
C_{ar}-N-C_{am}	129.1	128.4	122.7	123.9	125.0	124.5	124.8	125.9
N-C_{am}=O	121.3	121.7	119.2	120.4	120.7	119.6	120.6	120.4
N-C_{am}-C_{ar}	120.4	119.4	121.9	120.2	119.0	121.4	120.6	120.4
Torsions (degrees)								
N-C_{am}-C_{am}-N	0.3	0.5	-3.0	-3.3	-4.1	-0.4	-0.6	-5.7
C_{am}-C_{am}-N-N	7.3	7.3	5.6	3.8	4.4	3.1	4.1	7.8
C_{am}-N-N-C_{am}	-0.4	0.3	-0.8	-1.9	0.1	0.4	-0.1	-1.6
N-N-C_{am}-C_{am}	-7.1	-7.3	-6.6	-4.8	-3.5	-3.3	-4.4	-4.3
Out-of-Plane Ring Rotations (degrees)								
diacid phenylene	164	151	154	146	138	37	43	34
diamide phenylene	15	19	43	37	40	35	33	29
Helix Parameters								
Pitch (Å)	13.1	13.1	13.1	13.1	13.1	13.1	13.1	13.1
Twist (degrees)	0	1	4	6	3	0	1	4

angle is essentially identical to that assumed by Schroeder and Lippincott [1957] in their explicit potential function representation of the N-H···O hydrogen bond.

3) The nature of the chain-chain interactions are consistent across the set of eight structures, as suggested by the orientation correlation maps, and determine the extent of lateral order (perpendicular to the chain axis) seen in the polymorphs. The hydrogen bonding interactions for each chain lie roughly within a plane as a result of the chains' all-trans conformations; this leads to the association of chains by hydrogen bonding into sheets and allows one to distinguish between interchain energies within and between sheets. These energies may be broken down into their van der Waals and electrostatic components for each cell structure. Table 4.8 shows the sources of interactions within a sheet. In each case, the dominant contribution (66% to 90% of the total) is electrostatic. Furthermore, the electrostatic component may be decomposed into amide-amide interactions and phenylene-phenylene interactions as shown, with the remainder being a cross contribution from amide-phenylene interactions; clearly, the electrostatic interaction is predominantly between amide moieties and is quite specific in nature. Thus one finds an interaction of considerable magnitude and moiety-to-moiety specificity between chains within a hydrogen-bonded sheet, which ensures axial register and consistent interchain separation distances. This interaction takes priority in organizing the packing of chains lateral to the axis of chain alignment in the solid state. Table 4.9, on the other hand, illustrates the nonspecific nature of the interchain energetics between chains in neighboring sheets. Of particular interest is the magnitude of the total energy, which, contrary to previous conjecture, is comparable to that between chains within a sheet. However, the source of this interaction energy is evenly split between van der Waals and electrostatic contributions, and the latter in turn is relatively evenly split among the interactions between different moieties. From this one may conclude that while sheet-sheet separation is a high energy process, sheet-sheet slip remains a viable deformation mode, and the lack of preferred register between sheets is largely responsible for the multiplicity of crystal forms witnessed in the model analysis. This tendency towards slip is consistent with compressive failure observations reported in the literature [Knoff, 1987; Morgan et al., 1983].

4) The predicted densities lie between 1.42 and 1.57 g/cm^3; these values result largely from the choice of 12-6-1 potential energy parameters. While the model does not explicitly consider thermal effects, the force field parameters implemented were derived from experimental data on low molecular weight amide crystals at 25°C, and therefore incorporate thermal motion effects into the force field parameters themselves. The resulting densities are in good agreement with reported PPTA solid densities of 1.45 to 1.50 g/cm^3.

5) The cohesive energy is defined as the increase in internal energy per mole of a substance upon removal of all intermolecular forces [Van Krevelen, 1976]. This value is readily calculated as the difference between the energy of the packed structure and the energy of the most stable isolated chain

Table 4.8

Intermolecular bonding energy; component contributions to chain-chain interaction *within* a sheet (all values in kcal/mole of repeat units)

Cell ID	1	2	3	4	5	6	7	8
Total 12-6	2.1	2.6	2.8	2.2	2.6	1.4	2.5	0.9
Total electrostatic	5.8	5.1	5.4	6.9	7.1	8.1	7.5	8.3
Amide-amide electrostatic	3.8	3.3	3.5	5.7	5.9	7.4	5.7	6.8
Phenylene-phenylene electrostatic	0.7	1.1	1.9	1.7	1.5	1.9	2.1	2.1
Total	7.9	7.7	8.2	9.1	9.7	9.5	10.0	9.2

Table 4.9

Intermolecular bonding energy; component contributions to chain-chain interaction *between* sheets (all values in kcal/mole of repeat units)

Cell ID	1	2	3	4	5	6	7	8
Total 12-6	4.4	3.8	3.2	3.4	4.4	4.3	4.5	4.6
Total electrostatic	2.5	2.5	4.6	2.7	3.8	2.5	4.8	3.1
Amide-amide electrostatic	0.8	1.1	1.7	1.2	0.8	0.3	1.7	0.2
Phenylene-phenylene electrostatic	1.3	1.6	1.5	1.2	1.3	2.1	2.6	2.2
Total	6.9	6.3	7.8	6.1	8.2	6.8	9.3	7.7

conformation. The Hildebrandt solubility parameter may then be calculated as the square root of the cohesive energy density:

$$\delta = (E_{coh}/V)^{1/2} = (E_{coh}\rho/M_w) \qquad (4.6)$$

In this manner, for the cohesive energy and corresponding solubility parameter for PPTA based on the set of eight packing structures we obtain (per mole of repeat units):

$$E_{coh} = 39.0 \pm 1 \text{ kcal/mol}$$

$$15.3 \text{ [cal/cm}^3\text{]}^{1/2} < \delta < 16.1 \text{ [cal/cm}^3\text{]}^{1/2}$$

or $$31.2\times10^3 \text{ [J/m}^3\text{]}^{1/2} < \delta < 32.8\times10^3 \text{ [J/m}^3\text{]}^{1/2}$$

This range is quite reasonable in light of the relative insolubility and high temperature melting behavior of PPTA. While experimental values for solubility parameters of aromatic polyamides are not available, values for some related aliphatic polyamides are 12.7 and 13.6 $[cal/cm^3]^{1/2}$ (or 25.9×10^3 and 27.7×10^3 $[J/m^3]^{1/2}$) for poly(8-aminocaprylic acid) and poly(hexamethylene adipamide), respectively [Van Krevelen, 1972, p88]; we would expect the aromatic polyamide value to be somewhat higher, reflective of its reduced solubility in all but the most aggressive solvents.

Finally, significant differences between the eight final structures should be noted. All geometries except Structure #8 contain two chains per unit cell. The chains in Structures #1 through #4 all intersect the ab-plane at [0,0] and [½,½]. Of these, Structures #1 and #3 each contain conformations having oppositely rotated phenylene rings and sheet packing such that amide moieties in successive sheets are in register along the c dimension with alternating direction of the amide dipoles; Structures #2 and #4 are the analogues, respectively, of #1 and #3 with the distinction being the codirection of amide dipoles in successive sheets. The chains in Structures #5 through #7 intersect the ab-plane at [0,0] and [½,0]. Only Structure #5 has the adjacent rings rotated in the opposite sense as seen in the first four structures; Structures #6 and #7 have similarly rotated rings along the chain. The seventh structure is an analogue to the sixth, with the former having improved register between amide moieties in neighboring sheets. The eighth structure contains only one chain per unit cell but with an α angle of 55° that effectively creates the axial shift between hydrogen-bonded sheets seen in the other seven structures.

4.6.3 Calculation of X-ray Scattering

Applying the principles described in the previous chapter, we calculated the sets of x-ray diffractions anticipated from each of the eight possible structures for PPTA. Atomic scattering factors were calculated using exponential functions of $x = (\sin\theta/\lambda)$ in the range $0 \leq x \leq 1$, as described in Appendix D, using tabulated values of the atomic scattering factors readily available in the International Table for X-Ray Crystallography [1968]. By invoking fiber symmetry, the complete scattering pattern may be predicted from a plot of reflection intensity versus scattering angle 2θ and azimuthal angle β in a single quadrant (e.g. the $0 \leq 2\theta$, $0 \leq \beta \leq 90$ quadrant). The calculated intensities are normalized by the most intense reflection (generally the [200] reflection for PPTA) to yield values between 0 and 100%; these are tabulated for all reflections greater than 1% observable intensity in Appendix E, Table E.1. More illustrative, however, is the graphical recreation of the entire fiber diffractogram for immediate visual comparison to experimental films. We have presented patterns of intensity directly in polar form as functions of the scattering angle 2θ and the azimuthal angle β, which corresponds to projection of the scattering on a hemisphere with the sample positioned at its origin. For purposes of display, the calculated reflections were assumed to be distributed about their mean positions according to Gaussian probabilities in 2θ and β. The breadths of these distributions represent the expected peak broadening due to finite crystallite sizes, the crystal mosaic, and paracrystal displacements of the second kind, which are not available a priori from the model calculations. Additionally, we require an estimate for $\beta_{1/2}$ for the Lorentz correction of meridional reflection intensities. The peak broadening distributions were selected of the form:

$$y = A \exp[-\ln 2\ (2(x-x_O)^2/\omega_x^2)\ ] \tag{4.7}$$

A is the amplitude of the distribution at x_O and ω_x is the breadth of the distribution at y=A/2. Then the intensity at any point of the diagram may be calculated by summation of the contributions from all reflections at that point; the calculated intensity I_{obs} of each reflection i located at $(2\theta_i,\beta_i)$ equals the integrated volume of the distribution in 2θ and β:

$$I_{obs}(hkl) = A_{hkl}\omega_{2\theta}\omega_{\beta}\pi/4\ln 2 \tag{4.8}$$

$$I_{obs}(x_1,x_2) = \sum_{i=1}^{np} A_i\ (\exp\{\ -\ln 2[2(x_1-2\theta_i)/\omega_{2\theta}]^2\}) \times (\exp\{\ -\ln 2[2(x_2-\beta_i)/\omega_{\beta}]^2\}) \tag{4.9}$$

We require only three parameters not available through the model, the root mean square thermal displacement amplitude and estimates of $\omega_{2\theta}$ and ω_{β}, in order to recreate the entire fiber diffractogram. For our universal isotropic thermal displacement factor we employed the B value used successfully by Boon and Magré [1970] for poly(p-phenylene oxides) and by Northolt [1974] for the experimental analysis of scattering from PPTA:

$$B \equiv 8\pi^2\mu_s^2 = 5\times10^{-16}\ cm^2$$

corresponding to a root mean square displacement of 0.25 Å. For $\omega_{2\theta}$ and ω_{β} values of 1.5 degrees and 15 degrees, respectively, were found to be appropriate, corresponding to $\beta_{1/2}$ equal to 7.5 degrees. At this level of projection, it was not deemed justified to incorporate anisotropy of the thermal motion correction into the pattern simulations.

Due to the nature of the simulation, the calculated structures are inherently triclinic, so that observed reflections are actually groups of reflections of related diffraction planes; the slight displacement of these planes further contributes to the diffuseness of reflections expected in observable patterns and illustrates the potential complexity of reflections whose composite appears as a single "reflection" on film. The composites of reflections are illustrated in the recreated fiber diffractograms presented in Figures 4.7 (a) through (h), again corresponding to the eight PPTA structures described previously. These simulated fiber diffraction patterns were generated on an IRIS 4D series workstation with GT graphics and a 1280×1024 pixel display terminal. The grid density (2θ by β) was 500 points by 450 points per quadrant, or steps of 0.1 degrees in 2θ and 0.2 degrees in β. Visual resolution was enhanced using a nonproportional gray scale to achieve the greatest visual sensitivity at the lower intensities characteristic of the majority of reflections; a scale is provided in each diffractogram for clarification.

Diagrammatic representations of the calculated x-ray diffraction patterns provide a simple yet effective means for distinguishing between polymorphs at the phenomenological level, both for comparing and contrasting the various results of the model analyses, and for latter comparison to actual experimental data. For example, common to all the final polymorphs are the intense [002], [004], and [006] meridional reflections, characteristic of the extended chain conformations and the approximate 2_1 screw symmetry of chains; inclination of the normal to the ab-facet away from the chain axis results in these reflections appearing slightly off-meridian in a few cases. Only in the fifth, sixth, and eighth structures, where translation between neighboring sheets is 2.5 to 3.0 Å, are weak [001] and [005] meridional reflections observed. Most characteristic of the simulated PPTA patterns is the fingerprint of the equatorial and first layer lines of each structure. Here one can easily distinguish, by means of the

Figure 4.7: Simulated x-ray fiber diffraction patterns for the eight primary structures for PPTA. The sets (a) through (h) correspond to the structures labelled 1 through 8, in order, in Table 4.6.

(a)

(b)

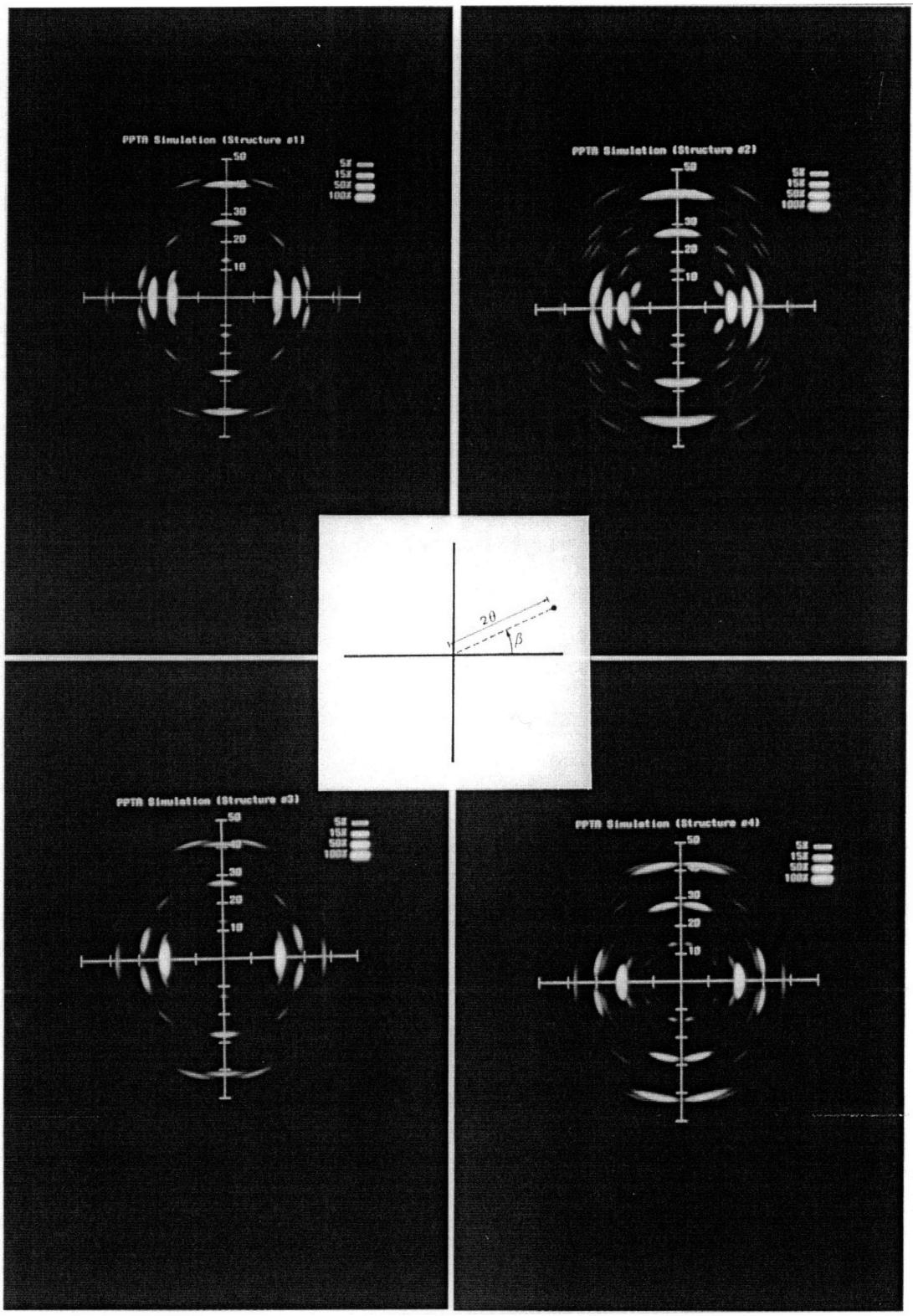

(c)

(d)

Figure 4.7: Simulated x-ray fiber diffraction patterns for the eight primary structures for PPTA (continued).

(e) (f)

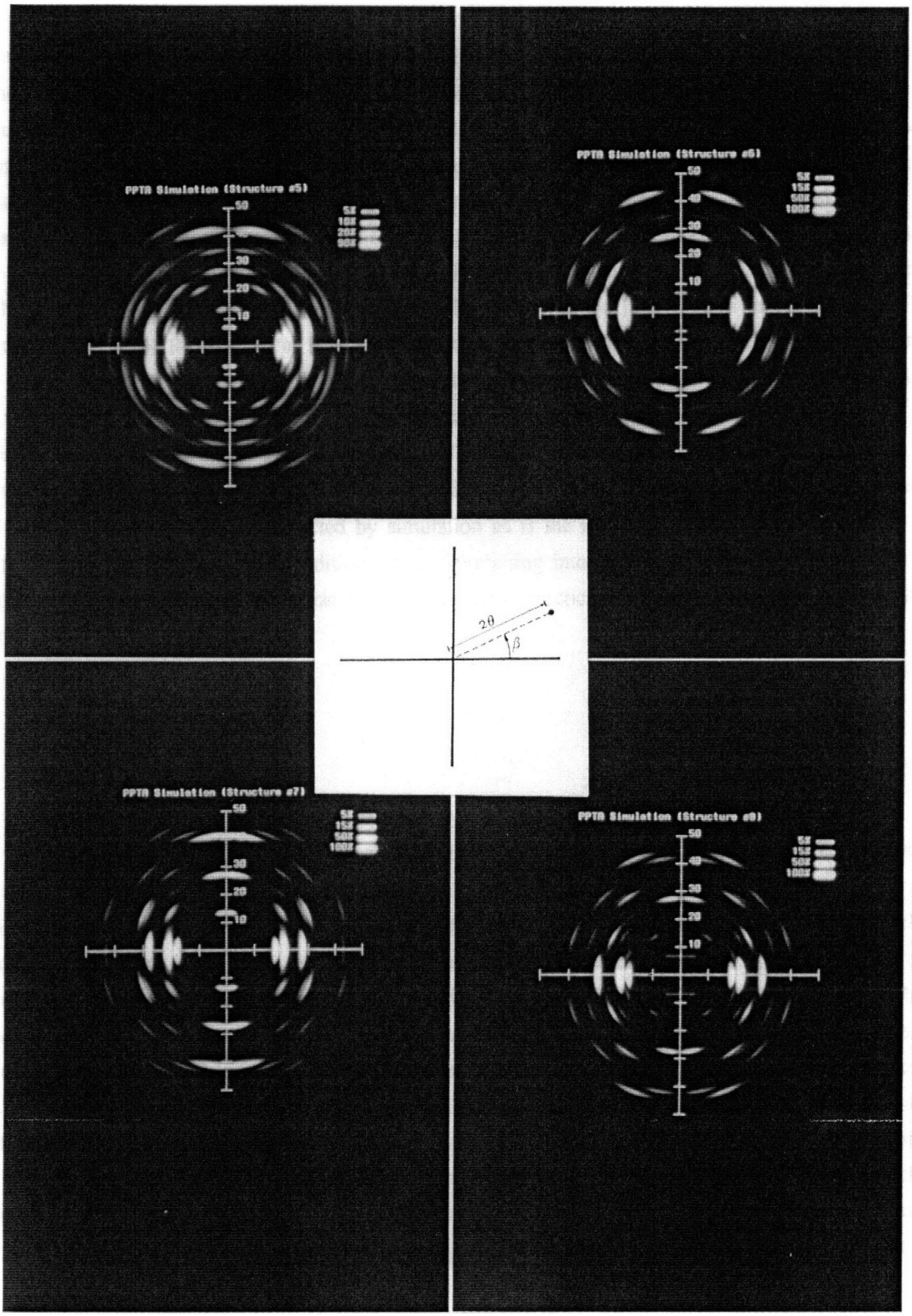

(g) (h)

presence or absence of [011] or [111] families of reflections (relative to the intense [110] reflection), between structures #1 and #3, having oppositely-directed amide dipoles in successive hydrogen-bonded sheets, and structures #2 and #4, having codirected dipoles in successive sheets. Structures #6 and #7, having face-centered unit cells and phenylene rings that are similarly rotated with respect to the amide bonding planes (and hence with respect to the hydrogen bonded sheets) have characteristically intense second layer reflections (i.e. [112] or [212] families of reflections). Structures #1 and #3 bear the hallmarks of the first modification of PPTA, reported by Northolt. As can be seen from a comparison of the unit cell parameters listed in Table 4.6 with those presented earlier in Chapter 2, Table 2.4, Structure #3 agrees most closely with the reported unit cell dimensions of Modification I. Only Structure #5 appears to exhibit any resemblance to Modification II reported by Haraguchi et al. (Table 2.4), most notably in the appearance of a [010] reflection and the combination of [210] and [211] sets of reflections, which reproduces the intensity attributed by Haraguchi entirely to the [211] planes in Modification II. However, in this case the agreement between simulation and experiment is not as satisfying in general. This is due in part to the considerable tilt (12°) of the normal to the ab-facet with respect to the chain axis in the simulated structure, resulting in the splitting of most reflections along the layer lines. However, it should also be noted that Modification II shows evidence of being a kinetically-frozen structure which can convert irreversibly to Modification I upon high temperature annealing. That this modification is not as faithfully predicted by simulation as is the first modification could be due in large part to the specific set of process conditions, namely spinning into an aqueous environment with no subsequent annealing, required to realize Modification II in practice, conditions which are in no way incorporated into the model.

4.7 Summary

The methodology presented in the preceding chapter serves to generate from a priori considerations predictions for the atomistic structural detail of highly ordered polymeric solids. In addition to its suitability in representing ideal periodic structures of packed helical molecules, such as have been almost exclusively dealt with in the past, this representation provides a method by which imperfections of either a periodic or local nature may be accurately incorporated into the analysis. This additional capability becomes especially important as interest increases in polymers of a paracrystalline or polycrystalline nature. Application of this procedure to the study of a representative stiff chain polymer, PPTA, reveals that, due to the convolution of the potential energy hypersurface, one may expect a multiplicity of viable candidates for stable geometries; the first point to address, then, becomes the selection of what information one chooses to derive from such an analysis and reduction of the output data to a minimum relevant basis set. Second, in the presence of strong intermolecular packing forces, one encounters competing trends of similar magnitude, one driven by bonded interactions within a chain and the other by non-

bonded interactions of the type commonly attributed to hydrogen bonds between chains. One may prioritize the development of structure according to the magnitude and specificity of interaction energies; for PPTA, the key traits are the chain stiffness arising from the rigidity of the moieties, the coplanar hydrogen bonding between chains arising from the rodlike conformation of each chain and the consequent persistent formation of sheet structures, and the relative variety of packing of sheets which leads to the occurance of distinguishable polymorphs having comparable stability and capable of coexistence at the microscopic level. Lastly, where several polymorphs are equally stable, each may be distinguished and identified by its characteristic x-ray diffraction pattern. This enables one to address the comparison between different simulated structures and between simulation and experimental data at the level of the identifying phenomenon (i.e. scattering) itself. Such analysis allows one to group the polymorphs according to intensity and location of reflections and to identify those which most closely agree with experimental observations.

5. MECHANICAL PROPERTIES BY SIMULATION

5.1 Thermodynamic Analysis

5.1.1 Classical Thermodynamics of Deformation

Thermodynamic stability of structure is defined by minimization of the free energy with respect to the degrees of freedom describing the structure; as such, it is composed of both an internal energy contribution (potential and kinetic) and an entropic contribution, as described by Equation 5.1. It is worth emphasizing at this point that so far we have spoken entirely of the relative stability of geometries based on a criterion of minimum potential energy, as is common practice in molecular mechanics methods. The justification for this simplification is several fold. First, we speak only of static structures in which atoms are assumed to behave as stationary centers of force; kinetic energy effects enter only through the selection of the force field parameters themselves, such as the effective van der Waals radii, which are derived from crystal data at finite temperatures. Thus for determination of relative stability of structure, kinetic energy factors are lumped into the potential energy implicitly. Second, we relax our criterion of *thermodynamic equilibrium* in favor of one of *mechanical equilibrium*, a condition more suitable to the visualization of dense polymer systems, which is by definition the minimum internal energy with respect to the degrees of freedom describing the structure. It may be mentioned that to the extent that we are simulating crystalline or pseudocrystalline solids at room temperature or lower, we would not anticipate large entropic contributions to stabilization energy. For example, Tadokoro [1979] calculates a total contribution of roughly 1 kcal per mole of CH_2 units in crystalline polyethylene between 0 K and 300 K. This translates into 17 kcal/mole in the PPTA case, on an equivalent per gram basis, or less than 50% of the stabilization potential energy. This estimate should be even smaller for stiff chain polymers such as PPTA. Even so, it is not the absolute magnitude of the entropic contribution, but its difference from structure to structure, that affects the relative stability; this is certain to be smaller yet.

The calculation of elastic compliances and elastic stiffnesses, however, is another matter. Here, we require the second derivatives of the Helmholtz free energy A with respect to deformation stress or strain:

$$A = U - TS \tag{5.1}$$

$$dA = dU - TdS - SdT \tag{5.2}$$

$$= dU - TdS \qquad \text{for isothermal deformations} \tag{5.3}$$

The elements of the fourth order elastic stiffness tensor are defined as:

$$(\partial^2 A/\partial\varepsilon_{LM}\partial\varepsilon_{NK})\big|_O = V_O C_{LMNK} \tag{5.4}$$

where the elements of the Lagrangian (material) strain tensor ε_{LM} are defined using:

$$2\varepsilon_{LM} = \partial u_L/\partial x_M + \partial u_M/\partial x_L + \sum_{I=1}^{3} \partial u_I/\partial x_L \, \partial u_I/\partial x_M \tag{5.5}$$

u is the displacement vector describing deformation. The subscript LM refers to deformation of the L surface acting in the M direction. For small deformations, we may neglect the terms of second order in displacement.

Consider first an arbitrary elastic solid subjected to an arbitrary isothermal small deformation; the internal energy U may be expressed as a Taylor series expansion about the undeformed state. Neglecting terms higher than second order, one writes for the difference in internal energy between the deformed state and the ground state:

$$dU = U_{def} - U_O$$

$$= \Sigma_{LM} (\partial U/\partial\varepsilon_{LM})\big|_O \varepsilon_{LM} + \tfrac{1}{2} \Sigma_{LM} \Sigma_{NK} (\partial^2 U/\partial\varepsilon_{LM}\partial\varepsilon_{NK})\big|_O \varepsilon_{LN} \varepsilon_{NK} \tag{5.6}$$

From Weiner [1983], we have the following relations:

$$(\partial U/\partial\varepsilon_{LM})\big|_O = (\partial A/\partial\varepsilon_{LM})\big|_O - T(\partial S/\partial\varepsilon_{LM})\big|_O \quad \text{(isothermal)} \tag{5.7a}$$

$$(\partial A/\partial\varepsilon_{LM})\big|_O = V_O\sigma_{LM} \tag{5.7b}$$

$$(\partial S/\partial \varepsilon_{LM})\big|_O = \gamma_{LM} C_\varepsilon \tag{5.7c}$$

$$(\partial^2 U/\partial \varepsilon_{LM}\partial \varepsilon_{NK})\big|_O = (\partial^2 A/\partial \varepsilon_{LM}\partial \varepsilon_{NK})\big|_O - T(\partial^2 S/\partial \varepsilon_{LM}\partial \varepsilon_{NK})\big|_O \tag{5.7d}$$

$$(\partial^2 S/\partial \varepsilon_{LM}\partial \varepsilon_{NK})\big|_O = -V_O(\partial \sigma_{LM}/\partial T \partial \varepsilon_{NK}) = -V_O(\partial C_{LMNK}/\partial T) \tag{5.7e}$$

which in conjunction with Equation 5.4 may be used to rewrite Equation 5.6 as follows [Theodorou and Suter, 1986]:

$$dU = \Sigma_{LM}\, V_O[\sigma_{LM} + \rho_O C_\varepsilon T \gamma_{LM}]\, \varepsilon_{LM} + \tfrac{1}{2} \Sigma_{LM} \Sigma_{NK}\, V_O[C_{LMNK} - T(\partial C_{LMNK}/\partial T)]\, \varepsilon_{LN}\, \varepsilon_{NK} \tag{5.8}$$

For direct application to the model description presented in Chapter 3, we convert this equation to an expression for the change in internal energy on the basis of a mole of polymeric repeat units:

$$dU = \Sigma_{LM}\, M_{ru}[\sigma_{LM}/\rho_O + C_\varepsilon T \gamma_{LM}]\, \varepsilon_{LM} + \tfrac{1}{2} \Sigma_{LM} \Sigma_{NK}\, (M_{ru}/\rho_O)[C_{LMNK} - T(\partial C_{LMNK}/\partial T)]\, \varepsilon_{LN}\, \varepsilon_{NK} \tag{5.9}$$

The first term in Equation 5.9 is the internal residual stress, which by formulation is zero in our simulations where we have allowed for variation of density during minimization. The second term reflects the connection between the elastic stiffnesses and the second derivatives of internal energy with respect to strain. To assess the relative importance of the contributions of internal energy and entropy to the elastic constants, we may proceed to evaluate the second derivative of Helmholtz energy with respect to strain:

$$V_O C_{LMNK} = (\partial^2 A/\partial \varepsilon_{LM}\partial \varepsilon_{NK})\big|_O = (\partial^2 U/\partial \varepsilon_{LM}\partial \varepsilon_{NK})\big|_O - T(\partial^2 S/\partial \varepsilon_{LM}\partial \varepsilon_{NK})\big|_O \tag{5.10}$$

Entropic effects are relatively unimportant if:

$$\left| T(\partial^2 S/\partial \varepsilon_{LM}\partial \varepsilon_{NK})\big|_O / (\partial^2 A/\partial \varepsilon_{LM}\partial \varepsilon_{NK})\big|_O \right| << 1 \tag{5.11a}$$

or

$$\left| T(\partial C_{LMNK}/\partial T)/C_{LMNK} \right|_O = \left| \partial \ln C_{LMNK}/\partial \ln T \right|_O << 1 \tag{5.11b}$$

The subscript O indicates the minimum internal energy (i.e. reference) structure. Evaluation of this inequality requires data for the elastic stiffnesses as functions of temperature at constant strain levels. Because such constant strain data is generally difficult to obtain, this criterion has been re-expressed in terms of constant stress derivatives [Theodorou and Suter, 1986]:

$$\left| (T/C_{LMNK}) \left[(\partial C_{LMNK}/\partial T)\big|_{\sigma} - \Sigma_{LM} \Sigma_{NK} C_{LMNK} \alpha_{NK} (\partial C_{LMNK}/\partial \sigma_{LM})\big|_{T,\sigma(LM)} \right] \right| << 1 \qquad (5.12)$$

For an *isotropic* solid characterized in the reference (undeformed) state by an isotropic stress distribution, the above criterion simplifies to:

$$\left| (1/C_{LMNK}) \left[T(\partial C_{LMNK}/\partial T)\big|_{P} + (\alpha_P T/\kappa_T)(\partial C_{LMNK}/\partial P)\big|_{T} \right] \right| << 1 \qquad (5.13)$$

However, such is not the case for the crystal lattice, where elastic response to imposed stress is generally anisotropic; instead, one requires the complete thermal expansion tensor α, expressed alternatively by the Grüneisen tensor components γ_{LM}:

$$\alpha_{PQ} = (C_e/V_O) S_{PQLM} \gamma_{LM} \qquad (5.14)$$

Unfortunately, the complete thermal expansion tensor or the Grüneisen tensor are rarely available for the *anisotropic* solid. One must usually settle for a few select elements, typically the diagonal elements, of either tensor. This issue will be readdressed in Section 5.1.3.

5.1.2 Statistical Mechanics of Deformation

Alternatively, in order to understand the contributions to the macroscopic thermodynamic properties of changes in structural description at the atomic scale, we may recast these state variables in terms of the canonical (ensemble) partition function for an N body system:

$$Q(N,V,T) = \sum_j \exp(-\beta E_j(N,V)) \tag{5.15}$$

where $\beta = 1/kT$ and the E_j are the total (free) energies of the states j available to the system. The thermodynamic state variables then become:

$$A = -kT \ln Q \tag{5.16}$$

$$U = kT^2 (\partial \ln Q/\partial T)_{N,V} \tag{5.17}$$

$$S = kT (\partial \ln Q/\partial T)_{N,V} + k \ln Q \tag{5.18}$$

For a system of distinguishable particles, such as the lattice points in a crystal, the canonical partition function may be decomposed into parts for additional treatment by either classical or quantum mechanical methods:

$$Q(N,V,T) = q_{trans} q_{rot} q_{vib} = Q_{class} Q_{quant} \tag{5.19}$$

Now, we choose to treat the crystal lattice in the vicinity of its minimum internal energy configuration as a regular structure of discrete lattice points at which are located the N bodies (or atoms) of the system; each body vibrates about its local lattice point. The total internal energy may then be expressed as a function of an arbitrary set of structure-defining variables s as a Taylor series expansion about the minimum energy configuration $s=s_O$:

$$U(s) = U(s=s_O) + \sum_{i=1}^{N} (\partial U/\partial(\Delta s_i))|_0 \Delta s_i + \tfrac{1}{2} \sum_{i=1}^{N} \sum_{j=1}^{N} (\partial^2 U/\partial(\Delta s_i)\partial(\Delta s_j))|_0 \Delta s_i \Delta s_j \tag{5.20}$$

where the first term, the potential energy at the minimum, is a function only of the soft variables and will be referred to hereafter as U^{pot}_{min}, and the second term, the kinetic term, is a function of vibratory displacements about this static minimum, due either to oscillations in such hard variables as bond lengths and bond angles or small oscillations in soft variables such as bond torsion or interchain distance, which are further assumed to be independent of s_O.

The positions described by the vector of change $\Delta s = 0$ correspond to the minimum energy configuration, where by the definition of mechanical equilibrium $(\partial U/\partial(\Delta s_i))\big|_0 = 0$. The quadratic term represents a set of coupled harmonic oscillators. By next assuming that the crystal behaves as a large polyatomic molecule whose atoms occupy lattice points connected by "springs", and introducing normal coordinate analysis, one may decompose the system into a set of independent oscillators, with a *maximum* of 3N-6 ≈ 3N (for N on the order of 10^{20} atoms) normal mode vibration frequencies ν_j, each contributing its own component $q_{vib,j}$ to the quantized portion of the partition function. Equating U(s) with the set of energies E_j available to the system in the vicinity of the lattice minimum and substituting the independent partition functions $q_{vib,j}$ for the component oscillators in the quadratic term, one obtains:

$$Q(N,V,T) = \exp(-\beta U^{pot}_{min}) \prod_{j=1}^{3N} q_{vib,j} \tag{5.21}$$

where $$q_{vib,j} = \exp(-\beta h\nu_j/2)/(1 - \exp(-\beta h\nu_j)) \tag{5.22}$$

For the Helmholz energy and its second derivatives, this yields:

$$A = U^{pot}_{min} + kT \sum_{j=1}^{3N} \ln(q_{vib,j}) \tag{5.23}$$

$$(\partial^2 A/\partial\varepsilon_{LM}\partial\varepsilon_{NK}) = (\partial^2 U^{pot}_{min}/\partial\varepsilon_{LM}\partial\varepsilon_{NK}) + kT \sum_{j=1}^{3N} (\partial^2 \ln(q_{vib,j})/\partial\varepsilon_{LM}\partial\varepsilon_{NK}) \tag{5.24}$$

For the calculation of elastic stiffnesses, our interest lies in the term $(\partial^2 A/\partial\varepsilon_{LM}\partial\varepsilon_{NK}) = VC_{LMNK}$. Clearly, if the normal mode frequencies are independent of deformation in the small deformation regime, then the second term on the right hand side drops out and $(\partial^2 A/\partial\varepsilon_{LM}\partial\varepsilon_{NK})$ may be replaced by $(\partial^2 U^{pot}_{min}/\partial\varepsilon_{LM}\partial\varepsilon_{NK})$, suggesting that oscillatory freedom makes at most a minor contribution to elastic response; this is the strict Harmonic Approximation. Thus for evaluation of the significance of entropic contributions to elastic stiffnesses, one requires either normal mode vibrational frequencies for deformed structures as well as undeformed structures, or experimental data for elastic constants versus temperature. Applying the same criterion for significance of entropic contributions as given in Equation 5.11a, one obtains:

$$kT \sum_{j=1}^{3N} (\partial^2 \ln(q_{vib,j})/\partial\varepsilon_{LM}\partial\varepsilon_{NK}) \,/\, VC_{LMNK} << 1 \tag{5.25}$$

Both the numerator and the denominator of this equation are size dependent, the numerator on the number of oscillators in the system and the denominator on the volume of the system. Taking advantage of the equality $(N/V)_{system} = (N/V)_{unit\ cell} = N_O/V_O$ and differentiating Equation 5.22 with respect to the components of strain, one may write:

$$N_O kT \sum_{j=1}^{3N} (\partial^2 \ln(q_{vib,j})/\partial\varepsilon_{LM}\partial\varepsilon_{NK}) \,/\, NV_O C_{LMNK} \ll 1 \tag{5.26}$$

or

$$(N_O/\beta NV_O C_{LMNK}) \sum_{j=1}^{3N} h\beta(\tfrac{1}{2} + \Lambda)(\partial^2\nu_j/\partial\varepsilon_{LM}\partial\varepsilon_{NK}) - (h\beta)^2(\Lambda+\Lambda^2)(\partial\nu_j/\partial\varepsilon_{LM})(\partial\nu_j/\partial\varepsilon_{NK}) \ll 1$$

$$\Lambda = 1/(\exp(h\beta\nu_j) - 1) \tag{5.27}$$

As will be suggested by the data presented in the next section, if we assume that:

(1) $\partial\nu_j / \partial\varepsilon_{LM} = K_\nu$, a constant for all j, LM

and (2) $\partial^2\nu_j / \partial\varepsilon_{LM}\partial\varepsilon_{NK} = 0$ for all j, LM, NK

then for a new criterion we obtain:

$$-(N_O/\beta NV_O C_{LMNK})\ (h\beta K_\nu)^2 \sum_{j=1}^{3N} (\Lambda+\Lambda^2) \ll 1 \tag{5.28}$$

For large N, we may approximate the summation by introducing a distribution function g(ν) for the normal mode frequencies and integrate over all frequencies:

$$-(N_O/\beta NV_O C_{LMNK}) \quad (h\beta K_\nu)^2 \int_0^\infty \exp(h\beta\nu)g(\nu)/(\exp(h\beta\nu)-1)^2\, d\nu \ll 1$$

$$\int_0^\infty g(\nu)\, d\nu = 3N \tag{5.29}$$

It only remains to determine the distribution function g(ν), which should be easier than the complete set of individual frequencies. According to McQuarrie [1976], the normal frequencies of a crystal vary from essentially zero to some value of the order of 10^{13} cycles per second. Normal frequencies are not due to the vibrations of single atoms, but are concerted harmonic motions of all the atoms; such concerted motion is called a normal mode. Unfortunately, complete distributions are not generally available. Nevertheless, we may proceed by introducing the same approximations for the normal mode vibrations of a crystal as have been employed so successfully in the prediction of low temperature heat capacities, namely the Einstein and Debye approximations:

Einstein Approximation: Here it is assumed that each normal mode has the same frequency ν_E, i.e. each member of the lattice sees the same environment and acts as an independent oscillator:

$$g_E(\nu) = 3N\,\delta(\nu-\nu_E) \tag{5.30}$$

which, when substituted into Equation 5.29, yields:

$$-(3N_O/\beta V_O C_{LMNK})\,(h\beta K_\nu)^2\,[\,\exp(h\beta\nu_E)/(\exp(h\beta\nu_E)-1)\,] \ll 1 \tag{5.31}$$

Debye Approximation: Here it is reasoned that only low frequencies, up to a characteristic frequency ν_D, are important; these long wavelength oscillations are insensitive to the detailed atomic character of the solid and may be calculated by assuming that the crystal is a continuous elastic body. This leads to:

$$\begin{aligned} g_D(\nu) &= 9N\nu^2/\nu_D^3 \qquad 0 \le \nu \le \nu_D \\ &= 0 \qquad\qquad\quad \nu > \nu_D \end{aligned} \tag{5.32}$$

which, when substituted into Equation 5.29 and making the substitution $x=h\beta\nu$, leads to:

$$-(3N_O kT/V_O C_{LMNK})K_\nu^2/(h\beta\nu_D^3)\int_0^{h\beta\nu_D} x^2\exp(x)/(\exp(x)-1)\,dx \ll 1 \tag{5.33}$$

which may be integrated numerically for a given ν_D. These criteria for the significance of the entropic contributions to the elastic moduli, expressed in equations 5.12, 5.31, and 5.33, are addressed in the next section with respect to the particular case of the stiff chain polymer.

5.1.3 Estimation of Entropic Contributions

Ii et al. [1986, 1986, 1987] in a series of papers reported lattice thermal expansion data and some thermomechanical properties for PPTA and PBA aramid fibers obtained by means of x-ray analysis of the crystal lattice spacings under given axial (c-axis) loadings. Relevant properties which may be deduced from this work are reproduced in Table 5.1. Based on these values, we may calculate the stiffness criterion for $\partial^2 A/\partial\varepsilon_{33}^2$, assuming that only the axial stiffness constant C_{3333} is significantly affected by the introduction of an axial stress σ_{33}. In the second term of Equation 5.12, one would expect that for such oriented chains $\partial C_{3333}/\partial\sigma_{33}$ should far exceed all other $\partial C_{LMNK}/\partial\sigma_{LM}$ due to the deformation of internal bond lengths, angles, and torsions required by an imposed stress in this direction, rather than the deformation of weaker intermolecular interactions allowed under stress in the other directions; the possible exception in the aramid case is the $\partial C_{1111}/\partial\sigma_{11}$, which involves deformation of the hydrogen bonds. However, the fact that C_{3333} should also be much greater than the other moduli, and that α_{11} and α_{22} are greater than zero and thus would offset somewhat the negative α_{33} contribution, should ensure that the estimate calculated below is a worst case scenario:

$$\left| (T/C_{3333})[\, \partial C_{3333}/\partial T|_{\sigma} - C_{3333}\alpha_{33}\partial C_{3333}/\partial\sigma_{33}|_{T} \,\right| = 0.27 \text{ (PPTA)}$$

$$= 0.32 \text{ (PBA)}$$

These numbers imply that the true modulus of PPTA is at least 79% of the value calculated solely from internal energy contributions.

For our consideration of the analysis based on statistical mechanics, we refer to the work of Galiotis et al. [1985], who have investigated the strain dependence of the Raman frequencies of Kelvar 49® fiber, in the range 1100 to 1700 cm^{-1}, between 0% and 2% axial strain (ε_{33}). The frequencies and peak shifts of six vibrational modes are reproduced in Table 5.2. From their data, the gradients in frequency appear to be roughly independent of both frequency and strain. Hence we make the simplifications suggested in the previous section, i.e. that the second derivatives of frequency with respect to strain are essentially

Table 5.1

Thermomechanical properties of PPTA and PBA[a]

	PPTA	PBA
α_{11}	8.3×10^{-5} K^{-1}	7.0×10^{-5} K^{-1}
α_{22}	4.7×10^{-5} K^{-1}	4.1×10^{-5} K^{-1}
α_{33}	-2.9×10^{-6} K^{-1}	-7.7×10^{-5} K^{-1}
$C_{3333} \approx 1/S_{3333}$ (at 298 K)	168 GPa	188 GPa
$\partial C_{3333}/\partial T\|_{\sigma 33=0.5\ GPa}$ $\approx -S_{3333}^{-2}\ \partial S_{3333}/\partial T\|_{\sigma 33=0.5\ GPa}$	-0.181 GPa/K	-0.247 GPa/K
$\partial C_{3333}/\partial \sigma_{33}\|_{300K} \approx -S_{3333}^{-2}\ \partial S_{3333}/\partial \sigma_{33}\|_{300K}$	59	32

[a] from Ii et al. [1986, 1986, and 1987].

Table 5.2

Strain dependence of Raman frequencies in PPTA[a]

Frequency (cm^{-1})	$\partial \nu_j/\partial \varepsilon_{33}$ ($cm^{-1}/\%$)	$\Lambda+\Lambda^2$
1649.5	-2.2 ± 0.2	3.65×10^{-4}
1613.5	-4.4 ± 0.2	4.33
1519.2	-4.2 ± 0.7	6.82
1330.9	-3.4 ± 0.3	16.9
1280.1	-3.6 ± 0.3	21.5
1183.7	-0.5 ± 0.3	34.3

[a] from Galiotis et al. [1985].

zero, and take an average value for $K_\nu = -3cm^{-1}/\%$ (i.e. $-300cm^{-1}$). At 298K, we have $h\beta = 0.0048cm$, V_O is $5.26\times10^{-22}cm^3$ (the unit cell volume), N_O is taken to be the 56 atoms for PPTA (two repeat units per unit cell) and $(kT/V_OC_{3333}) = 0.00466$.

Estimation of the Einstein and Debye frequencies of such a material is subjective, at best. Bondi [1968] reports Debye temperatures (Θ_D) between 100° and 400°C for monatomic solids, which corresponds to $\nu_D = k\Theta_D/h$ between $70cm^{-1}$ and $280cm^{-1}$. Values for glassy polymers are on the order of 120°C. Unfortunately, there exist no good estimates for Debye or Einstein temperatures for polymeric crystals. However, guided by those systems for which such data is available, we may presume a conservative value of:

$$\Theta_D = 100°C; \qquad \Theta_E = 0.75\Theta_D = 75°C$$

which corresponds to:

$$\nu_D = 70cm^{-1}; \qquad \nu_E = 52cm^{-1}$$

Einstein Approximation:

$$-(3N_OkT/V_OC_{LMNK})\,(h\beta K_\nu)^2\,[\,\exp(h\beta\nu_E)/(\exp(h\beta\nu_E)-1)\,] = .066 << 1$$

Debye Approximation:

$$-(3N_OkT/V_OC_{LMNK})K_\nu^2/(h\beta\nu_D^3) \int_0^{h\beta\nu_D} x^2\exp(x)/(\exp(x)-1)\,dx = .024 << 1$$

These values would suggest that entropic and kinetic energy contributions to the elastic moduli in polymeric crystals are actually less than 7% of the total response of free energy to deformation, a quarter of that determined from thermomechanical data for axial deformation. In the following sections, we will adhere to calculations of the elastic constants from changes in the potential energy for deformed structures, with the realization that these estimates may be 10% to 30% too high.

5.2 Method of Calculation

In the case of static crystals fully minimized in potential energy with respect to both intramolecular and intermolecular degrees of freedom, the first order coefficients of Equation 5.6 are all zero (i.e. there is no internal residual stress or thermal expansion). To obtain the twenty-one independent C_{LMNK}'s one requires twenty-one deformation "experiments"; these are selected as follows:

3 uniaxial tensions (ε_{LL})
3 simple shears (ε_{LM})
3 biaxial tensions (ε_{LL}, ε_{MM})
3 dual component shears (ε_{LM}, ε_{NK})
9 combined tension/shear (ε_{LL}, ε_{NK})

The first six require the minimum energy configuration plus two deformed configurations ($\pm\varepsilon$), from which an estimate of C_{LNMK} may be calculated using a three point formula. The other fifteen cases each require an additional two deformed configurations ($+\varepsilon_{LM}$,$+\varepsilon_{NK}$ and $-\varepsilon_{LM}$,$-\varepsilon_{NK}$), which in combination with the previous deformed structures yield estimates of C_{LMNK} through use of a seven point formula.

$$\text{3-point: } \partial^2 f/\partial x^2 = \left(f(1,0) - 2f(0,0) + f(-1,0) \right)/(h_x)^2 \tag{5.34}$$

$$\text{7-point: } \partial^2 f/\partial x \partial y = -\left(f(1,0) + f(0,1) + f(-1,0) + f(0,-1) - 2f(0,0) - f(1,1) - f(-1,-1) \right)/2n(h_x)^2 \tag{5.35}$$

h_x is the step size in x, h_y is the step size in y, $n = h_y/h_x > 1$

$\partial^2 f/\partial x \partial y$ provides an estimate of $dU/\varepsilon_{LM}\varepsilon_{NK}$. From Equation 5.9, in the absence of entropic contributions, the elements of the compliance matrix may be obtained as

$$C_{LMNK} = (dU/\varepsilon_{LM}\varepsilon_{NK})\ (\rho_O/M_{ru}) \tag{5.36}$$

Because of the feature of chain alignment within the model, deformation parallel to the chain propagation direction and lateral to it may not be treated identically. Tensile deformation in the latter case is solely a function of intermolecular packing parameters and may be imposed by appropriately straining the packing geometry. Tensile deformation along the chain direction is an implicit function of intramolecular parameters and may be imposed by applying a forcing function to cause deformation of the

chain axis. On the other hand, simple shear in a plane containing the chain axis may be induced by altering the intermolecular description, while shear in a plane cutting the chain axis is precluded by formulation of the model, which defines the z-axis of the global coordinate system as the alignment direction of the chain axes. In the actual "experiments" we impose engineering strains e_{LM} where it is possible to impose deformations of lateral dimensions in the chain direction (i.e. e_{13} and e_{23} may be nonzero). Then $\varepsilon_{LL} = e_{LL}$ and $\varepsilon_{LM} = \varepsilon_{ML} = \frac{1}{2}e_{LM}$. With the imposition of strain and reminimization with respect to intramolecular and intermolecular degrees of freedom, the components of the structure may respond in a nonaffine manner; this process is conceptually consistent with a realistic phenomenon of atomic rearrangement in a system involving bonded and nonbonded atoms.

5.3 Elasticity of Poly(p-phenylene terephthalamide)

5.3.1 Modification of the Chain Description

The model used for PPTA is a modification of the simple chain description used to identify optimal crystal structures. The latter described the single chain using fixed bond lengths, hexagonal planar phenyl rings, and planar sp^2 bond orientations at the amide carbons and nitrogens, requiring only six torsional degrees of freedom and eight valence bond angle degrees of freedom. While this was deemed sufficient internal freedom for the chain to adjust to its preferred packing configuration, this chain description was too restricted to respond realistically to imposed strains acting along the chain axis. The new chain description relaxes the planarity constraint at the amide nitrogens and carbons, resulting in ten torsional degrees of freedom. The rigid phenylene ring was replaced by a planar symmetric ring which may be described using only one bond angle and two bond length degrees of freedom. Finally, the bonds in the chain backbone were allowed to respond to deformation, adding six more bond lengths to the degrees of freedom, for a total of ten bond angle and ten bond length degrees of freedom for the PPTA repeat unit. Valence Force Field potentials [Tashiro et al., 1977] were introduced to describe the potential energy of these deformations, with the equilibrium positions chosen so as to reproduce the original chain upon energy minimization. Table 5.3 shows the correlation between corresponding values for the above mentioned degrees of freedom at the minimum energy cell configuration for PPTA Structure #3 using the two chain descriptions. The intermolecular degrees of freedom remained unchanged (i.e. two periodicity lengths, three periodicity orientation angles, two setting angles, and one translational displacement). The cohesive energy of this structure calculated using the second chain description is within 0.5 kcal/mol of that obtained using the simpler description; this lends further confidence to the accuracy and adequacy of the simpler version for structure and cohesive energy calculations. Lastly, it remains to define the coordinate axes of mechanical deformation. It must be noted that the selection of axes in use at this

Table 5.3

Comparison of the two chain descriptions used for structure and mechanical property calculations

	Type 1 (22 DOF)	Type 2 (38 DOF)
Bond Length (Å)		
$C\text{-}C_{ar,1}$	1.50 (fixed)	1.504, 1.508
$C_{ar,1}\text{-}C_{ar,2}$	1.40 (fixed)	1.404, 1.402
$C_{ar,2}\text{-}C_{ar,3}$	1.40 (fixed)	1.400, 1.396
C-N	1.39 (fixed)	1.385, 1.385
$C_{ar,1}$-N	1.41 (fixed)	1.398, 1.400
Bond Angle (degrees)		
$C_{ar,6}\text{-}C_{ar,1}\text{-}C_{cr,2}$	120 (fixed)	119.4, 120.3
$C_{ar,1}$-C=O	118.9, 118.9	118.9, 119.9
$C_{ar,1}$-C-N	122.0, 121.9	121.8, 122.0
$C_{ar,1}$-N-H	118.1, 118.4	118.1, 118.1
$C_{ar,1}$-N-C	123.1, 122.7	122.9, 122.6
Bond Torsion (degrees)		
$C_{ar,2}\text{-}C_{ar,1}$-C-N	-26.0, -153.7	-25.7, -159.0
$C_{ar,2}\text{-}C_{ar,1}$-C=O	(dependent)	19.0, 172.0
$C_{ar,1}\text{-}C\text{-}N\text{-}C_{ar,1'}$	5.6, -6.6	5.8, -6.9
$C_{ar,2}\text{-}C_{ar,1}$-N-C	-137.3, -43.1	-134.6, -44.4
$C_{ar,2}\text{-}C_{ar,1}$-N-H	(dependent)	137.8, -167.8
Intermolecular		
A (Å)	4.78	4.78
B (Å)	4.90	4.93
α (degrees)	90.3	89.7
β (degrees)	89.9	89.5
γ (degrees)	62.1	61.5
ω_1 (degrees)	101.4	99.5
ω_2 (degrees)	-79.5	-81.4
f_2	0.45	0.45
Density (g/cm^3)	1.46	1.46
Cohesive Energy (kcal/mol)	38.3	37.8

point differ slightly from those used to report crystal structures in Chapter 4. In the mechanical property presentation, as in the model development, the x_3-axis corresponds to the c-axis of the pseudocrystal, along which the chain axes are aligned; the x_1-x_3 plane, i.e. the "2" face, contains the ac-facet of the pseudocrystal wherein lie the hydrogen-bonded sheets; the x_2-axis and the bc-facet are defined by orthogonality and crystal periodicity relationships, respectively. Crystal structures provided in Table 4.6 follow the convention that the hydrogen-bonded sheets lie in the bc-facet; however, this is employed purely for reasons of consistency with the common practice in crystallography of selecting the "a" dimension such that "a" is larger than "b", as has been done for the structures previously reported in the literature.

5.3.2 Determination of Crystallite Compliance and Stiffness Matrices

Initially, the multichain structure was subjected to ±0.4% tensile strains along the crystallographic c (chain) axis, with all other internal and external degrees of freedom allowed to adjust (i.e. lateral contraction of the structure in addition to chain conformation adjustment). The resulting E_{33} modulus was 303 GPa; the resulting densities of the strained structures deviated from the strain free value by ±0.16%, indicative of a slight expansion (compression) of the lattice upon extension (compression).

In a second set of experiments, the full complement of twenty-one deformations was performed, allowing only degrees of freedom internal to the unit cell to relax (i.e. the optionally-strained lattice dimensions a, b, c, and the interaxial angles α, β, and γ were fixed). The complete stiffness matrix is presented below in the 6×6 Voigt format. In this convention, only one subscript is required to identify the appropriate element of stress or strain, and two for the corresponding stiffness and compliance matrices (e.g. $\varepsilon_L = \varepsilon_{LL}$ for L=1,2,3, and $\varepsilon_4 = \varepsilon_{23}$, $\varepsilon_5 = \varepsilon_{13}$, $\varepsilon_6 = \varepsilon_{12}$). The magnitudes of imposed strains were selected to be large enough to give numerically significant differences in potential energy (i.e. e_L = 0.4% for L=3 and 0.8% for L=1,2; e_L = 1.6% for L=4,5,6). The resulting precision in the reported values are on the order of ±5%, or ±1 to 5 GPa. Deformations imposed by e_{33} and e_{23}, representing roughly the extremes of elastic response, where checked for various strain levels; the calculated stiffness elements remained consistent up to 3.2% strain or higher. Removal of the imposed deformation and reminimization of potential energy with respect to the internal coordinate degrees of freedom gives back the original undeformed configuration, ensuring that the strain levels employed are within the domain of elastic response.

The compliance matrix is calculated by inversion of the stiffness matrix:

$$\mathbf{S} = \mathbf{C}^{-1} \tag{5.37}$$

From the compliance matrix are calculated the Young's moduli E_i, the shear moduli G_i, and the first six Poisson's ratios ν_{ij}:

$$E_i = 1/S_{ii} \quad ; i=1,2,3 \tag{5.38a}$$

$$G_j = 1/S_{ii} \quad ; i=4,5,6 \text{ and } j=i-3 \tag{5.38b}$$

$$\nu_{ij} = -S_{ij}/S_{jj} \; ; i,j=1,2,3 \tag{5.38c}$$

For the simulated structure which most closely resembles the thermodynamically stable Modification I reported in the literature, PPTA Structure #3, the full stiffness and compliance matrices are calculated to be:

$$\mathbf{C} = \begin{bmatrix} 40.5 & 23.3 & 12.9 & 0.1 & 1.2 & 2.4 \\ 23.3 & 30.6 & 40.7 & 1.5 & 3.2 & 1.9 \\ 12.9 & 40.7 & 360. & 0.3 & 5.0 & 11.2 \\ 0.1 & 1.5 & 0.3 & 5.5 & 3.7 & 2.7 \\ 1.2 & 3.2 & 5.0 & 3.7 & 22.0 & 3.2 \\ 2.4 & 1.9 & 11.2 & 2.7 & 3.2 & 7.5 \end{bmatrix} \text{ GPa}$$

$$\mathbf{S} = \begin{bmatrix} 4.85 & -4.17 & 0.35 & 1.80 & 0.21 & -1.76 \\ -4.17 & 7.52 & -0.74 & -2.47 & -0.52 & 1.67 \\ 0.35 & -0.74 & 0.37 & 0.50 & 0.02 & -0.66 \\ 1.80 & -2.47 & 0.50 & 25.0 & -2.82 & -8.52 \\ 0.21 & -0.52 & 0.02 & -2.82 & 5.26 & -1.16 \\ -1.76 & 1.67 & -0.66 & -8.52 & -1.16 & 18.0 \end{bmatrix} \times 10^{-2} \text{ GPa}^{-1}$$

$E_1 = 20.6$ GPa	$E_2 = 13.3$ GPa	$E_3 = 270$ GPa
$G_1 = 4.0$ GPa	$G_2 = 19.0$ GPa	$G_3 = 5.6$ GPa
$\nu_{12} = 0.55$	$\nu_{21} = 0.86$	$\nu_{13} = -0.94$
$\nu_{31} = -0.07$	$\nu_{23} = 2.01$	$\nu_{32} = 0.10$

The obvious trends to be noted here are that the transverse moduli E_1 and E_2 are roughly 5% to 8% of the axial modulus E_3. As was presaged in the discussion of interchain total interaction energies within and between hydrogen bonded sheets in Chapter 4, the two transverse moduli are of comparable

magnitude. The shear moduli G_1 and G_3, corresponding to motions of the hydrogen-bonded sheets of chains parallel and perpendicular, respectively, to the chain axes, are roughly 1% to 2% of the axial modulus; the large value calculated for G_2 is indicative of the expected resistance to shear deformation of the hydrogen-bonded sheet structure itself. The values for ν_{ij} satisfy the inequalities for positive strain energy for a body having orthorhombic symmetry [Ward, 1983], which this structure approximates:

$$S_{12}^2 < S_{11}^2 \tag{5.39}$$

$$S_{13}^2 < \tfrac{1}{2} S_{33} (S_{11} + S_{12}) \tag{5.40}$$

5.3.3 Isolated Chain Compliance and Comparison to Crystallite Compliance

For comparison to calculations in the literature, the isolated chain was also subjected to fixed axial strains of ±0.4%, which yielded a chain modulus of 195 GPa. By comparison, Tashiro et al. [1977] calculate a value of 182 GPa for the isolated chain modulus (referred to there as the crystallite modulus). Fielding-Russell [1971] calculates a value of 200 GPa for the all-trans planar conformation. The observed tensile modulus falls in the range 120 GPa to 200 GPa [Tashiro et al., 1977; Gaymans et al., 1976; Kwolek et al., 1987; Allen, 1988]. It is significant that whereas the tensile stiffness C_{3333} calculated for the single chain is in good agreement with previous estimates, that estimated for the packed structure is considerably higher, both with and without inclusion in the optimization parameter list of those variables describing lateral packing (i.e. 303 GPa and 360 GPa, respectively). In order to determine the source of this difference, the component breakdowns of energy contributions in both the single chain and packed chain estimations were computed. For this purpose, the intramolecular contribution was defined as that change in energy attributable to changes in intramolecular variables upon deformation, which includes bond stretching, bond angle bending, torsion angle rotation, intramolecular van der Waals interactions, and intramolecular Coulombic interactions. For the packed structure, intermolecular interaction contributions were defined as changes upon deformation attributable to intermolecular van der Waals and Coulombic interactions. The contributions to changes in energy upon ±0.4% strain along the c-axis (the chain axis) is shown in Table 5.4.

A careful study of these values in the case of the isolated chain indicates that the minimum energy conformation represents a balance between interactions tending to promoted chain compression (i.e. bonds and valence angles) and others promoting chain extension (i.e. torsions and nonbonded interactions); thus small deformations are accompanied by trade-offs in these interactions, such that the total change in internal energy is not large. In the packed chain structure, however, it is the intramolecular and

Table 5.4

Distribution of strain energy among the degrees of freedom of the structure for isolated chain and packed chain simulations

Isolated Chain (intramolecular only)

	ΔE_{bond}	ΔE_{angl}	ΔE_{tors}	ΔE_{vdW}	ΔE_{Coul}	ΔE_{intra}
+0.4%	0.427	0.464	-0.210	-0.597	-0.007	0.078
-0.4%	-0.243	-0.339	0.583	0.002	0.037	0.042

Packed Chains

(Intramolecular)

	ΔE_{bond}	ΔE_{angl}	ΔE_{tors}	ΔE_{vdW}	ΔE_{Coul}	ΔE_{intra}
+0.4%	-0.331	-0.389	0.093	0.649	0.040	0.193
-0.4%	0.421	0.488	-0.007	-0.688	-0.022	0.061

(Intermolecular)

	ΔE_{vdW}	ΔE_{Coul}	ΔE_{inter}	ΔE_{total}
+0.4%	0.030	-0.105	-0.074	0.118
-0.4%	-0.032	0.075	0.042	0.103

intermolecular interactions that compensate each other. Due to impinging intermolecular interactions, the chain conformation is no longer the minimum energy conformation represented by the isolated chain, and as a result the trade-off between intramolecular contributions concurrent with axial strain are no longer balanced, but tend to pay a higher penalty for extension than witnessed previously. On the other hand, intermolecular interactions, primarily the Coulombic interactions, actually favor extension, thus offsetting the higher penalty for conformational extension. This trend may be understood as follows: extension leads to a net separation of atom centers, which decreases the cohesive energy contributions due to van der Waals interactions. However, charge interactions in the packed structure are not randomly oriented, but are so arranged such that attractive interactions predominate. In particular, species of opposite charge are preferentially located closer together. Even an affine extension imposes larger *absolute* changes in charge separation for those species which are *farther* apart, i.e. species of like charge, resulting in a net improvement of the total Coulombic interaction. Nonaffine deformations such as the one performed here will be even more preferential in distributing charge separation. In the sum, both intramolecular and intermolecular interactions contribute to resist compression, while the advantages gained in intermolecular interaction only partially offset the resistance of chain conformation to extension. The net result is the increase in the stiffness constant C_{3333}. This illustrates not only the importance of intermolecular contributions to resistance to deformation, but the complexity of changes in intramolecular response which accompany the changes in conformation that result from interactions with neighboring chains.

5.3.4 Consideration of a Second Allomorph

From the results of the atomistic simulation, several discrete pseudocrystalline polymorphs of comparable energy are obtained. The results presented above correspond to that model structure which most closely resembles the reported most stable crystal structure for PPTA [Northolt, 1974]. However, at least one other crystal allomorph has been isolated by precipitation from acid solution into water under controlled conditions of polymer concentration and postprecipitation heat treatment [Haraguchi, 1979]. Other energetically stable packing geometries may also exist to lesser extents in the actual polymer fiber. The above procedure was repeated for a second model geometry which more closely approximates the second crystal polymorph reported in the literature, although it should be noted that none of the model structures derived by minimization of total potential energy replicated this reported structure to the extent seen in the first case. Shown below is a summary of the stiffness and compliance matrices for the PPTA Structure #5. (It should be noted that negative values for elements of the stiffness matrix are physically impossible, but arise here due to the limit of numerical precision involved in performing the computer strain "experiments".)

$$C = \begin{bmatrix} 54.6 & 18.2 & 0.6 & 17.6 & 9.1 & -4.9 \\ 18.2 & 59.9 & 12.0 & 2.0 & 1.9 & -2.9 \\ 0.6 & 12.0 & 291. & 9.0 & 36.3 & 30.3 \\ 17.6 & 2.0 & 9.0 & 9.4 & 1.5 & 2.6 \\ 9.1 & 1.9 & 36.3 & 1.5 & 20.2 & -2.4 \\ -4.9 & -2.9 & 30.3 & 2.6 & -2.4 & 20.4 \end{bmatrix} \text{ GPa}$$

$$S = \begin{bmatrix} 8.72 & -2.02 & 0.79 & -16.8 & -3.61 & 2.38 \\ -2.02 & 2.20 & -0.32 & 3.48 & 1.01 & -0.03 \\ 0.79 & -0.32 & 0.69 & -1.58 & -1.54 & -0.85 \\ -16.8 & 3.48 & -1.58 & 43.8 & 6.09 & -6.13 \\ -3.61 & 1.01 & -1.54 & 6.09 & 9.00 & 1.84 \\ 2.38 & -0.03 & -0.85 & -6.13 & 1.84 & 7.74 \end{bmatrix} \times 10^{-2} \text{ GPa}^{-1}$$

$E_1 = 11.5$ GPa $\quad E_2 = 45.5$ GPa $\quad E_3 = 146$ GPa

$G_1 = 2.3$ GPa $\quad G_2 = 11.1$ GPa $\quad G_3 = 12.9$ GPa

$\nu_{12} = 0.92$ $\quad \nu_{21} = 0.23$ $\quad \nu_{13} = -1.15$

$\nu_{31} = -0.09$ $\quad \nu_{23} = 0.46$ $\quad \nu_{32} = 0.14$

Significant differences to note between these two model structures are the values for extensional and tranverse moduli, which in the second structure would appear to be considerably smaller for axial deformation but larger for transverse deformation. This would be expected for a chain packing in which the conformation of the individual chains is reduced in pitch (12.87 Å in the second geometry) relative to the most stable isolated chain conformation (13.10 Å in the first geometry) in exchange for more favorable lateral interchain interactions in the packed geometry; in this case, the penalty in energy for extensional deformation of the chain is smaller than that in the previous case, where the chains were closer to a conformational energy minimum, while the penalty in energy for deformation of the lateral interactions is proportionally greater. The range for torsional modulus is roughly the same for both cases.

5.4 Moduli Involving Fiber Symmetry

5.4.1 Derivation of Fiber Symmetry Relations

One may derive estimates for the moduli of the polycrystal mosaic from the complete elastic constant matrices by applying assumptions concerning the crystal packing morphology and the distribution of stress and strain over the packed crystals. For this purpose, we treat the fiber as a polycrystalline structure possessing perfect alignment of the molecular axes along the fiber axis, but random orientation of the crystallites in the planes lateral to the fiber axis. We also presume the absence of any second phase elastic matrix material. We can then calculate the mean elastic constants for the assumed fiber orientation function. If we assume that an imposed strain is distributed uniformly over all elements of the polycrystalline fiber, then we may calculate the fiber stiffness matrix as the cylindrical average of the crystalline stiffness matrix. We invert this matrix to obtain the fiber compliance matrix and obtain the elastic moduli as previously described; this is the volume average of stiffnesses, or Voigt limit, which provides an upper bound to the elastic constants. Alternatively, we may assume that stress, rather than strain, is uniformly distributed, resulting in the analogous volume average of compliances, or Reuss limit. These two assumptions, while neither being exactly correct, provide the upper and lower limits to the elastic constants for the cylindrically symmetric polycrystal "composite", within which the true elastic constants must lie [Arridge, 1985].

In general, the mean value of an element of the stiffness matrix, for example, may be expressed analytically as

$$\langle C_{i'j'k'l'} \rangle = \int\int\int l_{i'i} l_{j'j} l_{k'k} l_{l'l} \, C_{ijkl} \, \Phi(X,\Psi,\Omega) \, \sin X \, dX \, d\Psi \, d\Omega \tag{5.41}$$

where $\Phi(X,\Psi,\Omega)$ is the function describing the distribution of crystallite orientations and the $l_{i'i}$ are given by Arridge [1985]:

$$l_{1'1} = \cos\Omega\cos X\cos\Psi - \sin\Omega\sin\Psi \tag{5.42a}$$

$$l_{1'2} = -\cos\Omega\sin\Psi - \sin\Omega\cos X\cos\Psi \tag{5.42b}$$

$$l_{1'3} = \sin X\cos\Psi \tag{5.42c}$$

$$l_{2'1} = \cos\Omega\cos X\sin\Psi + \sin\Omega\cos\Psi \tag{5.42d}$$

$$l_{2'2} = -\sin\Omega\cos X\sin\Psi + \cos\Omega\cos\Psi \tag{5.42e}$$

$$l_{2'3} = \sin X \sin \Psi \tag{5.42f}$$

$$l_{3'1} = -\cos \Omega \sin X \tag{5.42g}$$

$$l_{3'2} = \sin \Omega \sin X \tag{5.42h}$$

$$l_{3'3} = \cos X \tag{5.42i}$$

For the case of fiber symmetry, where we assume perfect alignment of the crystal elements along the z-axis and a uniform orientation distribution lateral to this axis, we may express the compliance as a function of crystallite orientation in tensorial form as:

$$\mathbf{C}_\Omega = \mathbf{T}_\Omega \, \mathbf{T}_\Omega \, \mathbf{C} \, \mathbf{T}_\Omega^T \, \mathbf{T}_\Omega^T \tag{5.43}$$

where $\mathbf{T}_\Omega$ is the rotation matrix:

$$\mathbf{T}_\Omega = \begin{bmatrix} \cos\Omega & \sin\Omega & 0 \\ -\sin\Omega & \cos\Omega & 0 \\ 0 & 0 & 1 \end{bmatrix} \tag{5.44}$$

Given any three conformable matrices, **A**, **B**, and **C**, it can be shown that

$$\{ \mathbf{A} \, \mathbf{B} \, \mathbf{C} \}_{col} = (\mathbf{A} \otimes \mathbf{C}^T) \{ \mathbf{B} \}_{col} \tag{5.45}$$

where $\{ \}_{col}$ denotes the column array of the elements of the matrix enclosed therein, the elements being arranged in "reading" order, i.e. by rows, and $\otimes$ signifies the direct matrix product. Then the above equation for $\mathbf{C}_\Omega$ becomes:

$$\{ \mathbf{C}_\Omega \}_{col} = (\mathbf{T}_\Omega \otimes \mathbf{T}_\Omega \otimes \mathbf{T}_\Omega \otimes \mathbf{T}_\Omega) \{ \mathbf{C} \}_{col} \tag{5.46}$$

or, using the reduced notation where $\mathbf{T}^{xp}$ indicates the self-direct product of degree p of the matrix **T**

$$\{C_\Omega\} = T_\Omega^{x4} \{C\} \tag{5.47}$$

Then the cylindrical average over Ω becomes:

$$< \{C_\Omega\} > = (1/2\pi) \int_0^{2\pi} T_\Omega^{x4} \{C\} \, d\Omega = < T_\Omega^{x4} > \{C\} \tag{5.48}$$

Upon integration, one obtains 41 nonzero terms in $< T_\Omega^{x4} >$, of which 21 are independent. Taking advantage of the symmetries in C, one can derive simple equations for the six independent terms of the cylindrically averaged stiffness matrix $< C_\Omega >$, which may be collected into Voigt form as shown below:

$$< C_\Omega > = \begin{bmatrix} A & B & C & & & \\ B & A & C & & 0 & \\ C & C & F & & & \\ & & & E & & \\ & 0 & & & E & \\ & & & & & D \end{bmatrix} \quad \text{Voigt Average} \tag{5.49}$$

where
$$A = (1/8)(3C_{11} + 3C_{22} + 2C_{12} + 4C_{66})$$
$$B = (1/8)(C_{11} + C_{22} + 6C_{12} - 4C_{66})$$
$$C = (1/2)(C_{13} + C_{23})$$
$$D = (1/8)(C_{11} + C_{22} - 2C_{12} + 4C_{66})$$
$$E = (1/2)(C_{44} + C_{55})$$
$$F = C_{33}$$

Similarly, the cylindrically averaged compliance matrix may be expressed as:

$$< S_\Omega > = \begin{bmatrix} A & B & C & & & \\ B & A & C & & 0 & \\ C & C & F & & & \\ & & & E & & \\ & 0 & & & E & \\ & & & & & D \end{bmatrix} \quad \text{Reuss Average} \tag{5.50}$$

where $A = (1/8)(3S_{11} + 3S_{22} + 2S_{12} + S_{66})$

$B = (1/8)(S_{11} + S_{22} + 6S_{12} - S_{66})$

$C = (1/2)(S_{13} + S_{23})$

$D = (1/2)(S_{11} + S_{22} - 2S_{12} + S_{66})$

$E = (1/2)(S_{44} + S_{55})$

$F = S_{33}$

These equations are in agreement with the more general orientation equations given by Arridge to describe averaged elasticity matrices where actual crystallite alignment functions are experimentally available. Where only the moduli of the fibers are ultimately required, the number of simulated deformation "experiments" is drastically reduced from forty-two to eighteen. However, the reduced experiment set must be used with caution in those cases where one obtains the compliance matrix by inversion of the stiffness matrix. For structures that are clearly triclinic, some of the elements of the single crsytal stiffness matrix which are not required by Equation 5.49 may nevertheless deviate significantly from zero. This is not a problem for calculating the Voigt average elastic properties. However, in cases where these elements are nonzero, inversion of this estimation of the single crystal stiffness matrix introduces error into the estimation of the single crystal compliance matrix and in turn into the estimation of the Reuss average elastic constants. For this reason, the latter may in some cases be artificially high. In the following, we have only reported Reuss average elastic constants in those cases where the complete twenty-one independent element stiffness matrices were determined.

5.4.2 Voigt and Reuss Limits for PPTA

Applying this approach to the crystallographic stiffness and compliance matrices given previously, we arrive at upper (Voigt) and lower (Reuss) limits for the fiber elastic constants. In Table 5.5, these constants are listed for PPTA Structure #3, using the more usual, experimentally-defined terminology. Also shown are the available experimentally-determined moduli for PPTA (Kevlar) fibers, as well as the results of calculations reported by Northolt and van Aartsen using bond deformation models. Values for G_3 and ν_{31} are not independent, but may be determined easily by the relations:

$$G_3 = \tfrac{1}{2}E_1 / (1+\nu_{12}) \tag{5.51}$$

$$\nu_{31} = \nu_{13}E_1 / E_3 \tag{5.52}$$

Table 5.5

PPTA fiber elastic constants (GPa): theoretical (Structure #3) and experimental

	Voigt	Reuss	Predicted Range[h]	Experiment	Northolt[a]
Extensional Modulus (E_3)	335	272	325 - 215	120 - 200[b,c,d,e]	220
Transverse Modulus (E_1,E_2)	21.8	6.6	21.1 - 5.2	-	16 - 29[f]
Torsional Modulus (G_1,G_2)	13.7	5.2	13.3 - 4.1	2[b], 0.95 - 2.2[g]	2.5 - 5.7[f]
Extensional Poisson's Ratio (ν_{13},ν_{23})	0.46	0.54	-	-	-
Transverse Poisson's Ratio (ν_{12},ν_{21})	0.60	0.66	-	-	-

[a] Northolt and van Aartsen [1977].
[b] Allen [1988].
[c] Tashiro et al. [1977].
[d] Gaymans et al. [1976].
[e] Kwolek et al. [1987].
[f] based on the assumption that linear hydrogen bonds are the dominant interactions between chains
[g] Knoff [1987].
[h] after correction for entropy contributions, upper bound is 97% of the Voigt limit and lower bound is 79% of the Reuss limit.

Table 5.6

PPTA fiber theoretical elastic constants (GPa): Structures #4 and #5

	Structure #4		Structure #5		
	Voigt	Predicted Range[a]	Voigt	Reuss	Predicted Range[a]
Extensional Modulus (E_3)	369	358 - 292	290	146	281 - 115
Transverse Modulus (E_1,E_2)	55.1	53.4 - 43.5	52.2	21.9	50.6 - 17.3
Torsional Modulus (G_1,G_2)	15.8	15.4 - 12.5	14.8	3.8	14.4 - 3.0
Extensional Poisson's Ratio (ν_{13},ν_{23})	-0.19	-	0.08	-0.34	-
Transverse Poisson's Ratio (ν_{12},ν_{21})	0.14	-	0.31	0.24	-

[a] after correction for entropy contributions, upper bound is 97% of the Voigt limit and lower bound is 79% of the Voigt limit for Structure #4 and 79% of the Reuss limit for Structure #5.

The values calculated for the PPTA Structure #3 exhibit considerable spread between the upper (Voigt) and lower (Reuss) bounds. The values for all moduli tend to be somewhat higher than the experimentally measured values, as expected; the former may be as much as 30% higher than the true crystal lattice values, due to neglect of entropic effects, while the latter may be expected to be lower due to imperfections in the bulk. Taking these considerations into effect, the calculated lower bounds for E_3 and G_1 may be as low as 215 GPa and 4.1 GPa, respectively, in excellent agreement with experimental values.

Table 5.6 lists the fiber moduli calculated for two additional predicted structures of PPTA: Structure #4, which is closely related to Structure #3 above and differs primarily in the orientation of neighboring sheets, and Structure #5 previously discussed. It must be noted here that the data for Structure #4 were calculated using the reduced experimental data set. Based on the Voigt averages for Structure #4, one observes similar magnitudes for the extensional and torsional moduli of PPTA structures #3 and #4 but a significant increase in the transverse modulus, probably due to slightly higher hydrogen-bonding energies in the latter geometry. Structure #5, on the other hand, exhibits somewhat lower Reuss bounds than Structure #3 for E_3 and G_1 (based on the full stiffness matrix calculation); the implication is that this structure might lead to a slightly more extensible fiber if predominant in the actual final product (e.g. a predominance of Modification II).

5.5 Estimation of Resistance to Shear

Returning to the discussion of Section 5.3, one may take advantage of the complete stiffness matrix to look at candidates for orientation of failure. It is not possible to draw rigorous conclusions about yield behavior based only on an estimation of the elastic compliance matrix for a body. However, we may attempt to define that mode of deformation for which the required work is a minimum, or the orientation at which the resistance to shear deformation is least. For this purpose, we proceed analogously to the consideration of yield criteria for isotropic bodies. We first define our criteria for imposed strain and the resulting stress response in terms of the first three tensorial invariants, described by equations 5.53, 5.54, and 5.55, in order to establish a condition of equal deformation. We define a constant state of strain using the first three invariants of the matrix α, where α may be strain ε or stress σ:

$$J_1 = (1/3)\mathrm{Tr}(\alpha) \qquad \text{(for } \alpha = \sigma \text{ this is the negative of hydrostatic pressure)} \tag{5.53}$$

$$J_2 = 3\mathrm{Tr}(\alpha - (1/3)\mathrm{Tr}\alpha \mathbf{I}_3)^2 \tag{5.54}$$

$$J_3 = (1/3)\mathrm{Det}(\alpha) \tag{5.55}$$

such that our critical stress criterion may be described as:

$$\Upsilon = f(J_1, J_2, J_3) \tag{5.56}$$

To a first approximation, we assume that the critical mode of shear deformation is independent of the hydrostatic component of stress, as in metals, although this may not be strictly true for polymers. Then, following the approach of von Mises for analysis of yield phenomena, we propose that the critical shear mode does not involve J_3 and that stresses in simple tension and compression are equal (i.e. no Bauschinger effect [Ward, 1983 p340]). This leads to a criterion analogous to the von Mises yield criterion; Equation 5.56 simplifies to:

$$\Upsilon = f(J_2) = \text{constant} \tag{5.57}$$

For a fixed value of J_2 of ε we can then compute σ and J_2 of σ via equations 5.54 and 5.58:

$$\sigma = C \varepsilon \tag{5.58}$$

We propose to define for Υ a "stress resistance", which is independent of the magnitude of $J_2(\varepsilon)$, as the low shear equivalent of the Von Mises Yield Stress (the second invariant of the stress matrix) over the Work Equivalent Shear Strain (the second invariant of the strain matrix):

$$\Upsilon = (J_2(\sigma) / J_2(\varepsilon))^{1/2} \tag{5.59}$$

For simplicity, we take the condition $J_1(\varepsilon) = J_3(\varepsilon) = 0$. The minimum stress resistance, Υ_{min}, may be identified by selecting an arbitrary strain tensor and operating rotations of this tensor on the elastic stiffness tensor describing the response of the elastic body to determine those orientations at which Υ is a minimum. For the calculation of $J_2(\alpha)$ where α is ε or σ, we use:

$$J_2 = (\alpha_{11}-\alpha_{22})^2 + (\alpha_{22}-\alpha_{33})^2 + (\alpha_{33}-\alpha_{11})^2 + 6(\alpha_{12}^2 + \alpha_{23}^2 + \alpha_{13}^2) \quad (5.60)$$

Applying this approach to the stiffness tensor calculated for the PPTA Structure #3, we obtain a minimum shear resistance Υ of 6.9 GPA for a deformation having principle axes and corresponding deformation eigenvalues of:

X	=	+0.4082 $J_2(\varepsilon)$	**X**	=	[	0.486	-0.662	-0.571]
Y	=	-0.4082 $J_2(\varepsilon)$	**Y**	=	[	0.401	0.749	-0.527]
Z	=	0.	**Z**	=	[	0.777	0.027	0.629]

corresponding to the following tensorial strain description:

$$\varepsilon = \pm J_2(\varepsilon) \begin{bmatrix} 0.031 & -0.254 & -0.027 \\ -0.254 & -0.051 & 0.316 \\ -0.027 & 0.316 & 0.020 \end{bmatrix} \quad (5.61)$$

One may immediately observe that the ε_{12} and ε_{23} elements are predominant, indicative of motions primarily of sheet-sheet slip lateral and parallel, respectively, to the chain axis. This could be anticipated from the nearly equal but low magnitudes of the shear moduli G_1 and G_3 relative to that for G_2 for this structure. The plane of this deformation corresponds closely to deformation in the [102] crystallographic plane; this is illustrated in Figure 5.1, showing the calculated unit cell, the [102] plane, and the principle axes of deformation in this plane. From the minimum energy configuration, the lowest energy deformation process involves a motion of the chain simultaneously longitudinal and lateral to neighboring chains in the next hydrogen-bonded sheet. This is consistent with the view that deformation in PPTA occurs with the retention of the integrity of the hydrogen-bonded sheets.

Figure 5.1 Illustration of the mode of least resistance to shear deformation in the simulated PPTA Structure #3. Shown are the unit cell, the orientation of the [102] crystallographic planes which contain this deformation mode, and the principle axes describing the orientation of deformation within this plane.

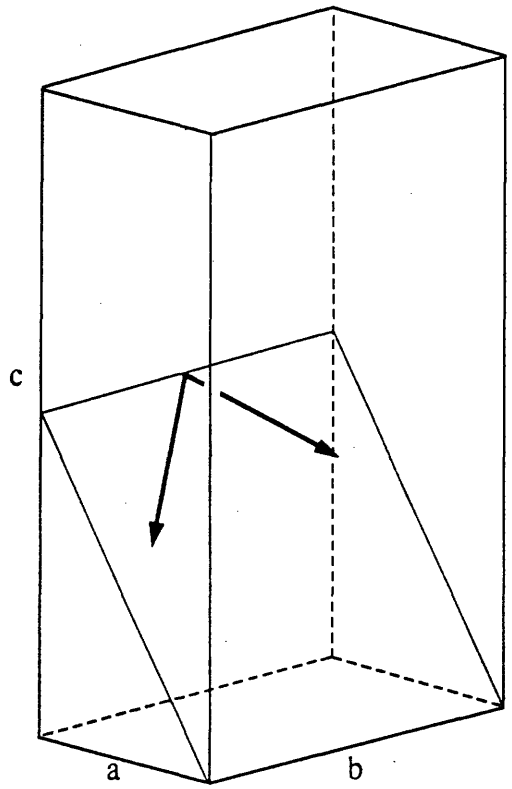

6. FIBER SPINNING AND X-RAY ANALYSIS

6.1 Objective

Simulations of real materials are only as good as the validity of information they provide. Any computational development inherently invokes a series of approximations, whose purpose is to make the problem tractable without sacrificing accuracy. In the end, the validity of the model must be checked against a known material system. For this reason, we found it necessary to undertake an experimental program whereby we could produce aramid polymers of the types to be modelled in a highly ordered form for comparison with simulation results. Our objective did not involve an exhaustive research into the complex interrelationships between material and process conditions, but rather exploitation of the best technology available sufficient for the purpose of producing highly oriented and crystalline samples of PPTA and its derivatives. As was addressed in Chapter 2, the method of choice for this purpose is the dry-jet wet-spinning of aramid fiber from anisotropic solutions. This chapter discusses the criteria behind the design of our embodiment of the dry-jet wet-spinning process, followed by a description of the equipment and the process itself. Experimental procedures and general considerations are discussed prior to a description of the fibers produced from solutions of PPTA in sulfuric acid. Finally, the analysis of fibers via x-ray diffractometry is discussed.

6.2 Equipment Design

6.2.1 Preliminary Considerations

Several requirements guided the choice of process design and selection of methods and materials for our application. These are considered below; where possible, the equipment was constructed to maximize versatility without sacrificing on these minimum requirements.

First, the process must be capable of processing small quantities of polymer into representative fiber. This requirement was based on the limit imposed by current synthetic capabilities in our lab to produce

constitutionally modified and constitutionally isomeric polymers of both sufficient molecular weight and sufficient regularity of structure. The polymers reported by Gentile [1988] and referred to in the section on constitutional isomerism by controlled Homogenous Phase Amidation were in all cases isolated in quantities of less than one gram. The maximum batch size of polymer currently achievable is on the order of five grams, the primary limitation being lack of in-house capability to purify the requisite monomers in sufficient quantity to conduct larger scale polymerizations. The importance of this limit on polymer availability (for the modified polymers) is exacerbated by the nature of fiber spinning, which is inherently a continuous or semicontinuous process. Each trial consists of start-up, steady state, and transition phases; fiber generated during start-up or between changes of operating conditions during the spin is not discussed. One would ideally opt for a process involving the largest quantity of polymer possible, in order to reduce the significance of the start-up phase. As a balance, solution quantities on the order of 5 ml, corresponding to roughly one gram of polymer at 10 wt % in sulfuric acid, were considered to be the appropriate requisite spin dope volume which could be obtained and converted into quality fiber.

Second, the primary feature believed to be responsible for the desirable mechanical properties of aramid fibers and the dominant assumption in the constructions simulated in the model is a high degree of molecular alignment. Two major factors contribute to the development of orientation in aramid fibers. (1) The first factor is the formation of an anisotropic phase prior to filament formation; this may be controlled procedurally, by working at concentrations and temperatures at which liquid crystal phases form. For simplicity, dope preparation may be decoupled from subsequent processing. (2) The second requirement is the capability to control both the spin line speed and the draw-down ratio D_R, defined as the ratio of the linear velocity of the fiber at the collection wheel to that at the die exit, which produces the extensional flow field that causes co-orientation of the directors of the nematic domains.

Third, the corrosive nature of the polymer/solvent system poses special problems. The use of concentrated acids imposes severe restrictions on the selection of materials of construction, and the complete removal of solvent is critical if the fibers are to be exposed to high temperatures, as residual acid will accelerate degradation of the polymer. The use of small filament diameters reduces the magnitude of concentration gradients of solvent within the filament during coagulation and permits more complete removal of solvent from the fiber core. The smaller diameter also ensures a more homogeneous coagulation process, which should minimize the skin/core morphology differentiation often noted in wet-spun fibers. Previous workers typically report the greatest success with spinnerette dies of diameter on the order of 25 μm to 200 μm [Montgomery, 1971; Blades, 1973; Valenti et al., 1981]. The selection of the spinnerette diameter reflects a trade-off between the improved coagulation efficiency possible with small diameter and the ease of handling of larger diameters.

Fourth, the dopes considered are quite viscous. Ideally, one would prefer that the concentration of polymer in the spin dope be as high as possible, in order to promote solution anisotropy and to reduce solvent removal requirements. However, such concentrations lead to very high viscosities in the quiescent solution. Viscosities as high as 4000 poise are reported for PBA (η_{inh} = 3.9 g/dl) in hydrofluoric acid at 0°C [Schaefgen et al., 1979]. Aoki et al. [1980] report viscosity versus shear rate curves for Kevlar® in H_2SO_4 at both 25°C and 60°C, in concentrations up to 12% polymer by weight; this data shows considerable shear thinning behavior (from 30000 poise at a shear rate of 0.01 sec^{-1} down to 300 poise at 8 sec^{-1}) of the anisotropic solution (10 wt % solution) at 25°C, but relatively constant viscosities on the order of 1000 poise or lower at 60°C. We have assumed an representative value of 1000 poise for design purposes.

Fifth, we require certain postspin treatments; these include multiple washing and neutralization steps and heat treatment of the fiber. Postspin treatments are decoupled from the spin line for ease of operation. Washing and neutralization ensure complete removal of acid and prevent later degradation. Annealing at temperatures above 450°C have been shown to produce significant improvements in fiber mechanical properties in aramids. Blades [1973] reports increases in modulus as large as 100% with heat treatments at 550°C for 1 to 6 seconds. Morgan et al. [1983] and Chatzi and Koenig [1987] suggest that the fibers should be elongated by about 0.5% under such conditions with a tension of 6 g/denier (0.8 GPa for PPTA). Kwolek et al. [1977] report increases in modulus for PBA from 450 g/denier (60 GPa) up to 1000 g/denier (132 GPa) at 540°C, and similar increases in tensile strength from 6.5 g/denier (0.86 GPa) to 17 g/denier (2.3 GPa). These large increases in mechanical stiffness are indicative of changes in the morphology of the fibers, presumably in the direction of higher orientation of the molecules or increased crystallinity or both. The morphology change could also reflect a transformation from one polymorph characterized by a low tensile modulus, such as that for PPTA Structure #5 presented in Table 5.6, to another polymorph characterized by a higher tensile modulus, such as that for either PPTA Structure #3 or Structure #4. For purposes of comparison with the results generated under the idealized view presumed by the simulation, experimental data from fibers of greatest molecular orientation and highest degree of crystallinity should prove most appropriate.

6.2.2 Design Specifications

In light of the these considerations, our process as a minimum requires: first, an effective means for forming the highly viscous spin dopes; second, equipment and controls sufficient to spin this dope as a very fine diameter filament under controlled extrusion and wind-up velocity constraints; third, a means for conducting very short duration annealing of the fibers under at least modest tension. The process and requisite apparatus were implemented as follows:

(1) Decoupled dissolution, spinning, and postspin washing, neutralization and heat treatment steps.

(2) Low-shear dope preparation, by means of a special mechanically-driven threaded shaft mixer, to ensure complete polymer dissolution at high concentration without causing shear-induced degradation

(3) Volumetric displacement extruder (syringe and plunger design) for extrusion, rather than a pressure-driven extrusion, in order to ensure accurate control of extrusion velocity regardless of solution inhomogeneities or variations in solution dynamic properties from trial to trial.

(4) Monofilament spinning, to simplify start-up and operation of the spin line

(5) Washing and neutralization of the wet filament while on the collection roller by submersion in agitated baths.

(6) High temperature, short duration heat treatment, by passage of the fiber samples through a furnace at a predetermined velocity to realize the desired residence time, under sufficient tension to maintain the carrier lines taut. This serves to generate high degrees of crystallinity and to mitigate the effects of imperfect process conditions on microstructure.

Figure 6.1 illustrates the entire fiber preparation process, including the prespinning and postspinning treatment steps. During the course of this work, fibers were generated through two different embodiments of this process. However, the fundamental features of process operation and fiber formation did not vary between these two pieces of equipment; the later version included accurate computer control, measurement, and data acquisition of important process variables. Monitored parameters were the extruder and collector drive motor rates, the extruder temperature, and the plunger drive force, from which were calculated extrusion and collection linear velocities, plunger position, and extrusion pressure. The critical components are presented in greater detail in Appendix F. Table 6.1 summarizes the most important design specifications which determine the range of available spin conditions.

6.3 Experimental Procedure

6.3.1 Dope Preparation

Our PPTA solutions consisted exclusively of Kevlar 29®, supplied by E.I. DuPont de Nemours and known to consist primarily of PPTA [Penn et al., 1976; Morgan et al., 1983], redissolved in 100% H_2SO_4. The inherent viscosity of the polymer was 6.1 dl/g in 96% H_2SO_4 (determined using an Ostwald viscometer and a standard concentration of 0.05 g of polymer in 10ml of solvent) at 25°C. Assuming that at concentrations of 0.5 g/dl $\eta_{inh} \approx [\eta]$ and using Mark-Houwink constants of $K = 8\times10^{-5}$ dl/g and $a = 1.09$ [Arpin and Strazielle, 1977], this corresponds to an approximate molecular weight of 30000

Figure 6.1: Schematic of the experimental program for polymer dissolution, fiber spinning, and post-spin heat treatment.

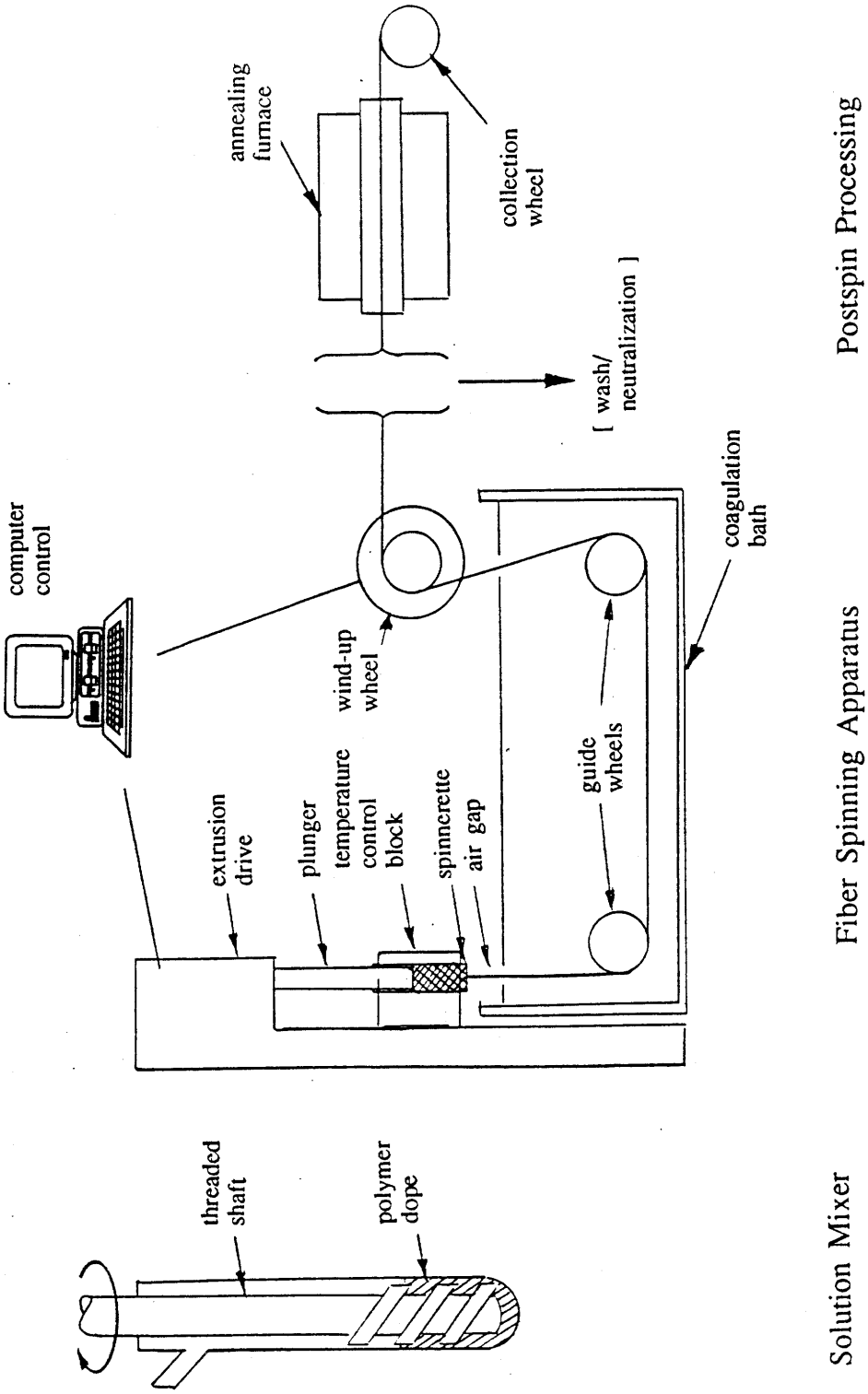

Table 6.1

Equipment design specifications

Syringe volume	6.2 ml
Syringe barrel diameter	10 mm
Spinnerette orifice diameter	50 μm to 120 μm
Spinnerette die profile	2 mm to 1 mm to orifice diameter
Spinnerette temperature	25° to 80°C
Plunger velocity	-42.5 to +42.5 mm/min
Wind-up wheel radius	35 mm
Wind-up velocity	-3000 to +3000 rpm
Maximum plunger force	10,000 N (1.27×10^8 Pa, 1260 atm)

g/mole (DP ≈ 240). The spin dopes were prepared by combining the polymer staple with solvent under an inert atmosphere, heating to 60° to 80°C, and thoroughly mixing by slow stirring (i.e. ≤ 60 rpm) using the threaded mixer. Concentrations from 4.0 wt % to 17.5 wt % were made (V_p^* is about 7 wt % to 8 wt % polymer in sulfuric acid at 25°C); for most trials, a solution of 10 wt % polymer in solvent was used. In some instances, the polymer was first dried at 110°C under vacuum for two hours prior to combination with the solvent, which was then allowed to impregnate the fiber staple overnight before heating was initiated. In either case, homogeneous anisotropic dopes could be prepared in thirty minutes to one hour. Change in molecular weight due to shear-induced degradation or thermal decomposition was checked by viscometry and found to be insignificant. Anisotropy was confirmed by stir opalescence and polarized light microscopy.

6.3.2 Fiber Formation

Approximately 5 ml of the polymer dope was loaded by spatula into a prefilter, which attached to the open end of the assembled syringe barrel. By means of a hand-operated screw which forced the solution through a stainless steel filter screen, the solution was filtered and homogenized while being loaded to the syringe. The dope was then extruded through the die orifice by means of a motor-driven plunger, with the extruded filament falling vertically from the spinnerette die face upon exit. Spinnerette die diameters from 60 μm up to 120 μm were used, but the 60-μm dies were preferred (generally specified to have a 1:1 length to diameter ratio, but in all but a few cases the capillary length could not be confirmed). Operative filament velocities at the orifice ranged from 5 to 80 m/min, depending upon plunger rate and orifice diameter; 40 m/min was typical. The filament passed initially through an air gap of 5 to 10 mm and then through the aqueous coagulation bath at room temperature (24°C), along a path length on the order of 105 cm, at ambient temperature. Finally, the precipitated polymer filament was collected on the wind-up roller, whose rotation speed was selected relative to the linear velocity of the plunger to induce draw-down of the filament. The collected fiber sample was then washed in water, followed by neutralization overnight of residual acid in a 1 wt % NaOH solution bath, followed in turn by a final water wash and drying at 60° to 80°C. This constitutes the denoted "as-spun" fiber. Fiber samples for x-ray analysis were prepared by impregnating a section of the wound filament with epoxy and then cutting a multifilament sample of length 110 mm directly from the collection spool.

6.3.3 Heat Treatment

The samples were optionally tied or glued to long leaders of Kevlar 29® which were used to thread the annealing line prior to heat-up. The sample was drawn through a high temperature zone under inert atmosphere one or more times to produce the denoted "annealed" fiber. A residence time of two seconds

at 500°C was employed, in accordance with recommendations in the literature [Kwolek, 1972; Morgan et al., 1980]. Subsequent annealing passes did not appear to alter the structural characteristics observed by x-ray analysis to any significant extent.

Polarized and unpolarized light microscopy (Nikon Optiphot-pol light microscope with Microflex AFX-II photomicrographic attachment, magnifications of 40x, 200x, and 400x) were used to verify the liquid crystal phase formation and to evaluate fiber diameter variations. Magnifications typically used were 40x for the former and 400x for the latter.

6.4 Spinning Trials for PPTA

The primary factor effecting molecular orientation during the spinning process is the draw-down ratio D_R, a measure of the extensional flow field acting to orient the nematic domains. We generally quote a nominal draw-down ratio, or spin-stretch factor, based on the known extrusion and wind-up linear velocities. The actual extensional flow field depends upon the true draw-down ratio, which is augmented by the tendency for the extruded filament to swell as it exits the spinnerette; this swelling is caused by the relaxation upon transition from confined to free surface flow of residual stresses imposed upon the extrudate by flow through the die geometry. Die swell is defined as the ratio of the diameter of the relaxed fiber to that of the extrudate exiting the die face. In the range of shear rate γ_w, defined as in Equation 6.1, from 6000 to 17200 s^{-1}, Conio et al. [1987] found die swell in PBA (η_{inh} of 1.37 dl/g and 1.85 dl/g) to increase from 1 at very low extrusion speeds up to 1.3 at an extrusion speed of 13 m/min. Jaffe and Jones [1985] report a linear correlation between the logarithms of die swell and shear rate at the wall for PPTA; in the range γ_w = 25000 to 90000 s^{-1}, die swell varied from roughly 1.1 up to 1.7. For a 10% by weight solution of polymer in 100% H_2SO_4 spun at 30°C, we determined that wind-up velocity necessary to match exactly the linear velocity of the swollen filament without inducing draw or allowing slack in the spin line. By assuming that the filament does not undergo additional dimensional changes, other than those due to relaxation, before the collection roller, we may calculate the die swell as the square root of the ratio of linear velocities, as indicated in Equation 6.2. With the assumption of incompressible Newtonian flow behavior in the die capillary, we obtain values for the shear rate and shear stress at the wall of the die using Equations 6.1 and 6.3, respectively:

$$\gamma_w = 8\, v_e / D_{orifice} \tag{6.1}$$

$$\text{die swell} = (v_e / v_w)^{1/2} \tag{6.2}$$

$$\tau_w = D_{orifice} P / 4 L_{orifice} \quad (6.3)$$

P refers to the driving pressure for extrusion, assumed to be equal to the force per unit area at the end of the moving plunger. Figure 6.2 shows the variation of die swell and shear stress with shear rate in the range 30000 $s^{-1} < \gamma_w < 185000\ s^{-1}$ for our apparatus using a spinnerette of diameter 60 μm and capillary length of 100 μm and a 10 wt % polymer dope. Die swell remains essentially constant over the range of shear rates employed in this work, while shear stress increases almost linearly with shear rate. From the slope of the latter curve, we obtain a coefficient of viscosity of 160 poise for the 10 wt % dope at 30°C. The shear thinning behavior under these conditions is considerably less pronounced than that reported by Aoki et al. [1979] for a similar dope at 25°C. However, the shear rates employed here are considerably higher than those reported by Aoki et al., and the calculated coefficient of viscosity is half the value obtained at their ultimate (highest) shear rates; this would suggest a transition from shear thinning to Newtonian behavior at higher shear rates, consistent with some rheological observations for rigid rod polymers [Larson, 1988]. The die swell is somewhat larger than that observed by other investigators; this is probably due to differences in the extrusion geometry and the imposition and relaxation of applied stresses prior to the extruder exit. Conio et al. suggest that this effect should decrease with increasing polymer concentration and higher extrusion temperatures. In agreement with these observations, using a 17.5 wt % solution of PPTA in 100% H_2SO_4 spun at 80°C through the same orifice (i.e. 60 μm x 100 μm), we observe a die swell of only 1.3 in the range 37000 $s^{-1} < \gamma_w < 127000\ s^{-1}$.

Table 6.2 summarizes some results of variations in draw-down ratio. Here we adhere to the use of nominal draw-down ratios and report the estimated die swell, where possible. Unfortunately, we do not have die swell data for fibers spun using the first apparatus; however, based on the similarity of design we expect the phenomenon to be similar to that observed in trials using the second spin apparatus under similar operating conditions. The trends are consistent with those suggested in the literature for the related polymer, polybenzamide [Kwolek et al., 1977]. Specifically, we note that fiber radius decreases with increasing draw-down ratio for as-spun fiber, consistent with dimensional changes normally accompanying extensional flow. Orientation angle, determined as the azimuthal breadth at one half the maximum intensity of the x-ray diffraction peak at $2\theta = 22.5°$, decreases with increasing draw ratio for as-spun fiber; this is in line with expectations for alignment of nematic domains upon exposure to linear accelerations after leaving the spinnerette. Our annealing method produces no measurable dimensional change in the fiber, but results in a decreased orientation angle for those fibers initially spun at low draw ratio. At higher draw ratios we observe a limiting orientation angle which is actually lower (i.e. better alignment) for the 10 wt % polymer dope. At this point, we presume that this discrepancy is due to geometry factors different between the two embodiments of the spin apparatus design. A similar limit in fiber properties is reported by Valenti et al. [1981] for modulus as a function of draw ratio for their work

Figure 6.2: Shear stress at the wall and die swell as functions of shear rate at the wall for the spinning of PPTA from a 10 wt % solution in 100% H_2SO_4 at 30°C using a spinnerette of diameter 60 μm and capillary length 100 μm.

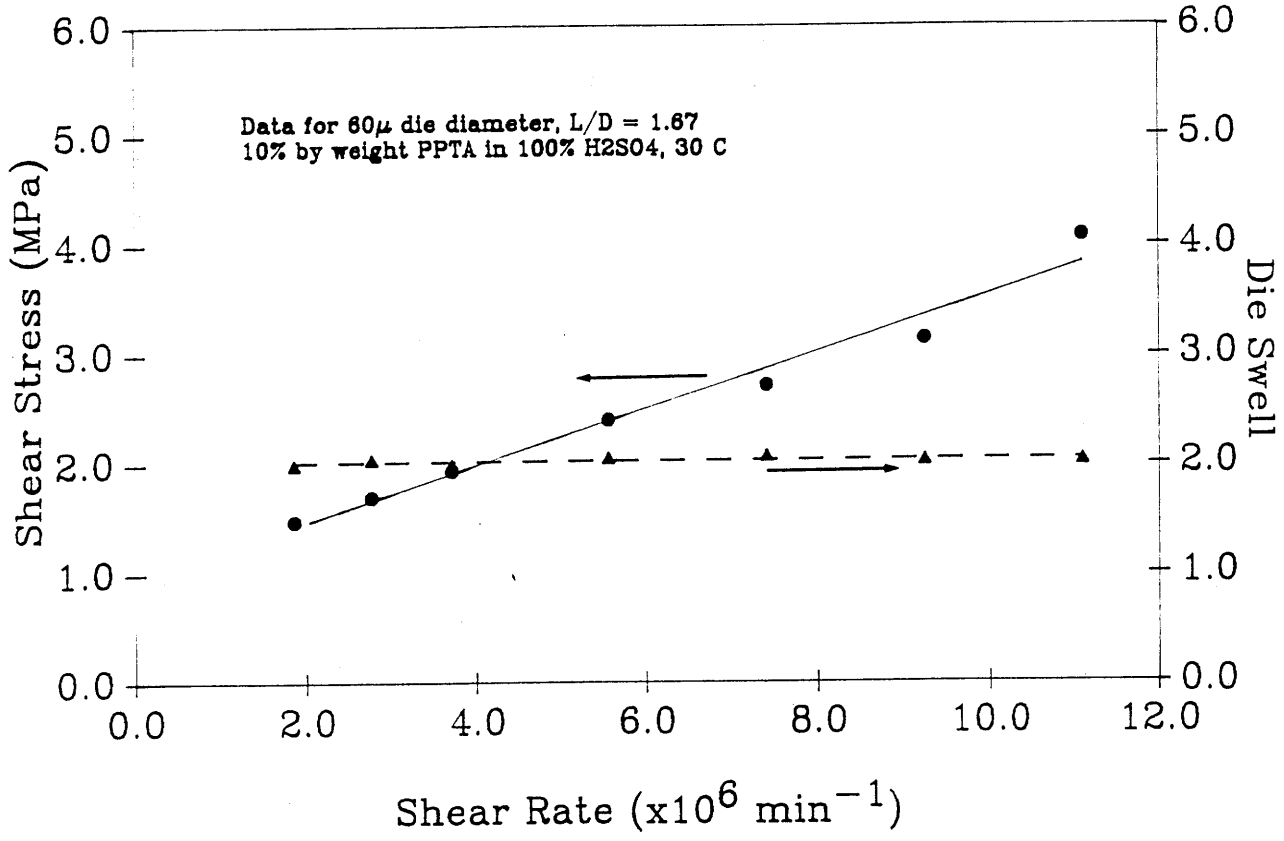

Table 6.2

Summary of Selected Fiber Spinning Trials

			Nominal draw ratio	Dry fiber diameter (μm)	Orientation Angle (degrees) as spun [annealed]
TRIAL 1:	Polymer concentration	: 10 wt %	0.3	28	66
	Extrusion temperature	: 30 °C	0.5	23	43
	Extrusion rate	: 31 m/min			
	Spinnerette diameter	: 55 μm			
	Die swell	: 2.0			
TRIAL 2:	Polymer concentration	: 10 wt %	1.3	38	63 [46]
	Extrusion temperature	: 25 °C	2.0	24	34 [28]
	Extrusion rate	: 36 m/min	2.6	21	20 [20]
	Spinnerette diameter	: 60 μm	2.9	22	25 [20]
	Die swell	: (unknown)	3.2	22	20 [22]
TRIAL 3:	Polymer concentration	: 17.5 wt %	0.9	35	46
	Extrusion temperature	: 80 °C	1.2	32	32
	Extrusion rate	: 30 m/min	1.7	24	30
	Spinnerette diameter	: 63 μm			
	Die swell	: 1.3			
TRIAL 4:	Polymer concentation	: 17.5 wt %	1.0	31	36
	Extrusion temperature	: 80 °C	1.7	25	33
	Extrusion rate	: 60 m/min	2.0	22	35
	Spinnerette diameter	: 63 μm	2.5	19	31
	Die swell	: 1.3 μm	3.0	18	31

on X-500, the polyterephthalamide of p-aminobenzhydrazide, with a break occuring near D_R = 1.5. The ultimate orientation angle values are comparable to values reported in the literature. Hindeleh et al. [1984] report values of 12.4° and 18.9° for commercial Kevlar 49® and Kevlar 29®, respectively, while the original patent of Kwolek [1972] reports values between 11° and 50°. This suggests that our process produces representative fibers. Lastly, we mention that we observe no evidence of an amorphous halo in the x-ray diffraction scans for the annealed fiber. Even in the as-spun fiber, adequate reproductions of the diffraction traces were achieved with the consideration solely of the apparent peaks. From this we conclude that our fiber contains at most a very small amorphous fraction.

6.5 X-ray Analysis

6.5.1 Equipment and Procedures

As our initial interest lies in the analysis of microstructure, wide angle x-ray scattering is the natural choice for evaluation of the quality of fiber spinning and the concurrence between experimental and simulation results. This technique provides the most accurate and direct information about atomic structure and molecular orientation. Infrared absorption provides information about the vibratory freedom of the component atoms and was used as a second independent check for variations in the local atomic environment and for the identification of specific intermolecular interactions such as hydrogen bonds.

Two different WAXS apparatuses were used to gather data during the course of this work. Both machines were rotating anode diffractometers equipped with four-circle goniometers and scintillation counters and employed Cu Kα radiation (λ = 1.5418Å). The first machine was a Rigaku D4148H2 12 kW High Brilliance generator operated at 40 kV and 150 mA, with a 0.1° slit collimator and nickel filtered radiation. The second machine was a Siemens D500 generator with DACO-MP control, operated at 40 kV and 35 mA, with a 1.2 mm pinhole collimator and bent quartz crystal monochromator. Multifilament samples were held together by embedding the filament ends in epoxy. The samples were mounted on a frame suitable for positioning in the incident x-ray beam and were manually extended and fixed to the opposite end of the frame with tape; good filament alignment was thus possible in the fiber holder, but no extensional deformation was applied. Typical sample sizes were 2 mm in diameter and 20 mm long but contained considerable void space. Absorptions of individual samples were determined from a ratio of the scattering intensity of the 2θ = 21.67° peak of polyethylene with and without the sample placed in front of the counter; the absorption (expressed as μt, the linear absorption coefficient μ in cm^{-1} times the sample thickness in cm) was determined using Equation 6.4.

$$(\mu t) \quad = \quad -\ln(I_A / I_O) \tag{6.4}$$

I_O refers to the unmodified intensity and I_A refers to the absorption-modified intensity. Typical values for (μt) were generally about 0.2. At this level of absorption, corrections were deemed unnecessary for our samples in either normal or symmetrical transmission modes [International Tables for X-ray Crystallography, 1968; Tadokoro, 1979].

WAXS analysis of the experimental fiber samples proceeded in two stages. The first was an initial evaluation of crystallinity and molecular order by means of equatorial (perpendicular to the fiber axis) and meridional (parallel to the fiber axis) scans of diffracted intensity versus scattering angle 2θ. This also included a routine scan of diffracted intensity versus azimuthal angle β for a major reflection, generally the intense equatorial reflection at $2\theta = 22.5°$, for purposes of determining orientation angle and crystallite orientation within the fiber sample. Care was taken in all cases to first align the fibers and identify $\beta = 0°$, where the equatorial diffractions are maxima. This analysis provided a rapid evaluation of the fiber spinning process and recommended samples for further evaluation. The second stage entailed the generation of the full two-dimensional fiber diffraction pattern for comparison to simulation results. Scans of intensity versus 2θ were generally in the range of 10° to 55° by steps of 0.1° in 2θ at the desired β. Azimuthal scans were performed in steps of 1° or 2° in β at the desired 2θ. Complete fiber diagrams were recreated from successive radial scans of intensity versus 2θ at different β between 0° and 90°. The full fiber diagram was generated by mirror replication of the first quadrant in the other three quadrants. Counting times were selected to ensure a signal error level (i.e. the square root of intensity divided by intensity) < 5%.

Infrared measurements were made using a Mattson Cygnus 100 FTIR apparatus. Samples were prepared from cut fiber cast in potassium bromide at roughly 2% by weight. Measurements were generally made in the range 4000 cm^{-1} to 400 cm^{-1}.

It is worth noting that neither small angle x-ray scattering nor mechanical property measurement were undertaken within the scope of this work. The first provides information primarily about the macrostructure of the polymer solid on the length scale of tens to hundreds of angstroms, which is beyond the scale of the information currently generated by the model. Mechanical property evaluation of fibers, on the other hand, could perform two useful functions: First, it could provide useful information about the elastic properties of fibers for evaluation of fiber integrity and uniformity; it has been suggested [Prof. P. Smith, UCSB, personal communication] that mechanical behavior is more sensitive to small changes in molecular orientation in the limit of high degrees of order than is the magnitude of the measured orientation angle. Second, the obtained elastic moduli would be available for direct comparison to

simulation predictions, in much the same manner as x-ray scattering has been used to check structure predictions. However, such a program has not been attempted here, due to the sensitivity of such results to many other factors not related to atomic microstructure and for which no account has been made in the theoretical analysis. For example, small imperfections in fiber macrostructure, such as internal or surface voids, are to a large extent invisible to WAXS analysis, but may dominate and grossly distort the conclusions of a mechanical property analysis. A necessary component of any rigorous mechanical property evaluation, especially for purposes of comparison to an idealized model, would be the more extensive evaluation of the fiber spinning process than has been attempted here, concentrating on the development of both microstructure and macrostructure as a function of operating variables.

6.5.2 Methods of Data Analysis

The experimental x-ray diffraction data for fiber patterns were checked visually in the same manner as were the predicted patterns from the simulation structures. The only correction applied was the subtraction of background radiation and normalization of intensities prior to construction of the intensity versus (2θ, β) grid for interpolation and display on the IRIS 4D GT system; all other corrections have already been applied in the calculation of the simulated reflection intensities. The same routines were used to create the visual display as were employed in the cases of the simulated structures; in this manner, comparable fiber diffraction patterns were displayed for both simulated and experimental data sets.

As a further check for experimental accuracy, selected experimental diffraction patterns were analyzed by conventional methods for indexing of significant reflections. This evaluation proceeded by selecting a finite number of Gaussian peaks to fit to the two-dimensional experimental pattern, of the form described by Equations 4.9 and 4.10 used for the representation of reflections generated by the simulated structures. The fitting procedure entailed minimization of the relative deviation, calculated as shown in Equation 6.5; of the complete pattern intensity distribution, as a function of the peak heights A_i, positions $(2\theta_i,\beta_i)$ and widths at half intensity $(\omega_{2\theta},\omega_\beta)$ for all peaks $i=1,n_p$.

$$R_D = \frac{\sum_{i=1}^{n2\theta}\sum_{j=1}^{n\beta}(I_{exp,i,j} - I_{calc,i,j})^2}{\sum_{i=1}^{n2\theta}\sum_{j=1}^{n\beta}(I_{exp,i,j})^2} \qquad (6.5)$$

Allowing all parameters to vary independently describes a set of $5n_p$ independent variables; this set was initially restricted by requiring all peaks to have the same set of peak widths, reducing the independent parameter set to $(3n_p + 2)$. The fitting procedure was initiated with different numbers of peaks and different initial peak assignments, until a best fit (i.e. minimum relative deviation R_D) was achieved; the variance was generally less than 10%. Subsequent reoptimization allowing each peak to vary independently in width did not produce significant improvements in fitting. Figure 6.3 illustrates in one dimension (i.e. 2θ) the quality of fit possible. From the final set of Gaussian peaks describing the best fit to the experimental pattern, the total intensity attributable to each reflection was calculated using Equation 4.9.

6.5.3 Evaluation of PPTA Fibers and Comparison to Simulation

Figures 6.4 (a) and (b) show reconstructed experimental x-ray diffractograms for our D_R = 3.2 fiber (Trial 2, Table 6.2) before and after annealing, respectively. Results from the quantitative analysis and deconvolution of peaks are reported in Table 6.3, along with a summary of the reflection identifications reported by Northolt [1974] and Haraguchi et al. [1979] for Modifications I and II, respectively. In comparing our results with the two crystal modifications reported in the literature, we note the following:

The as-spun fiber exhibits a poorly resolved diffraction pattern, which is to be expected from a morphology determined primarily by kinetic constraints operative during coagulation. Prior to annealing, the possibility for imperfect crystallinity or multiple coexisting crystalline polymorphs is significantly greater. There is no assurance that such a morphology should consist entirely, or even primarily, of the thermodynamically most stable allomorph; it is not expected, then, that the as-spun fiber diffraction pattern must conform to one predicted by simulation calculations. The most notable feature of the as-spun fiber is the appearance of equatorial reflections at 17.9° and 22.6° in 2θ, in agreement with Modification II, and of a new equatorial reflection at 27.7°, indicative of an [hk0] reflection not previously reported; Haraguchi et al. report an off-equatorial reflection of medium intensity that they attribute to the [211] diffraction planes. These reflections are in agreement with a structure possessing chains at the [0,0] and [½,0] locations in the ab-facet of the unit cell, suggestive of the simulation structures #5 through #8. The last three of these, #6, #7 and #8, all possess similarly-rotated phenylene rings with respect to the amide bond plane in the chain conformation, with the resulting generation of significant second layer nonmeridional reflections. This leaves PPTA Structure #5 as that most consistent with the as-spun fiber. This structure also predicts significant reflections attributable to both [210] and [211] sets of diffraction planes; the former, while not noted by Haraguchi et al. in Modification II, is consistent with our as-spun fiber and, in conjunction with the close-lying [211] reflection, reproduces well the intensity previously attributed solely to the [211] planes. However, peak resolution in our as-spun fiber is generally insufficient to justify a more detailed analysis of crystal structure. We do observe that,

Figure 6.3: Experimental and calculated equatorial intensity distributions for a sample of annealed PPTA fiber. The calculated intensity is a summation of fitted Gaussian distributions which best reproduce the experimental trace.

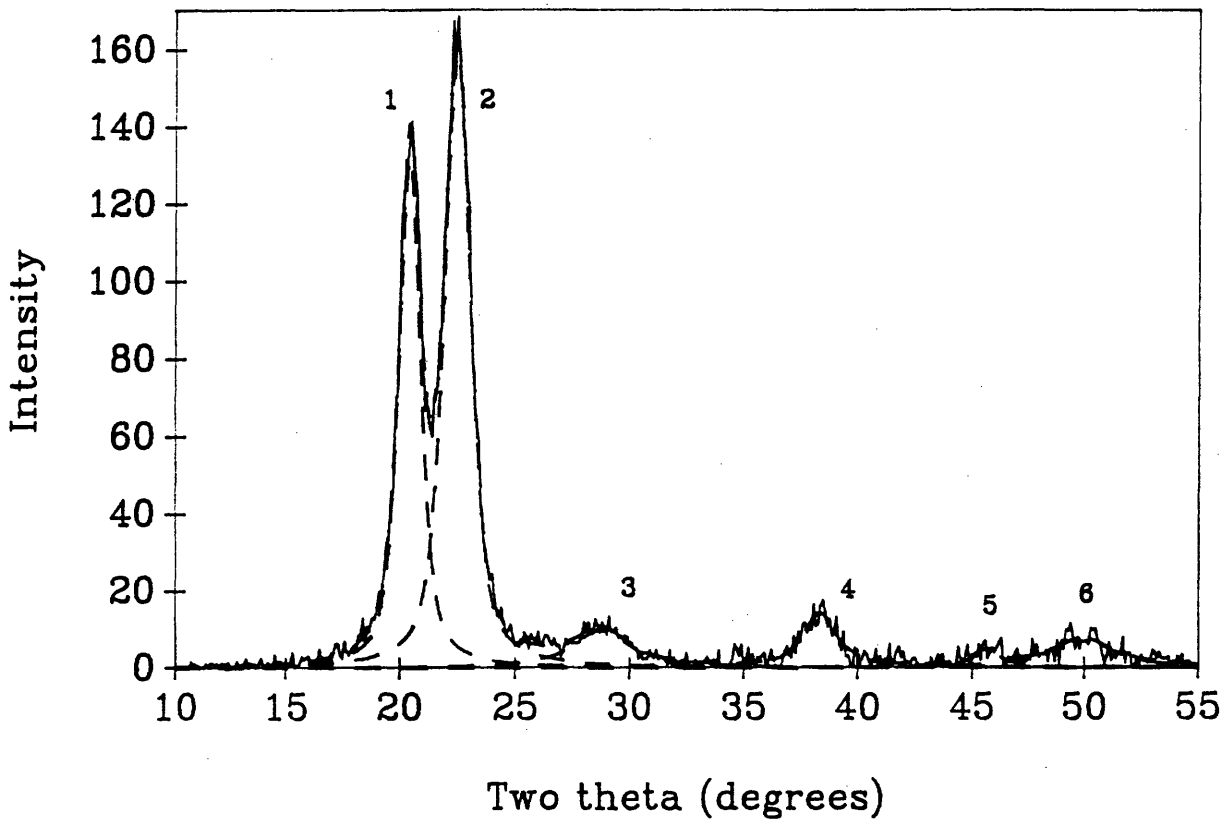

Figure 6.4: Representative x-ray fiber patterns for PPTA fibers spun during the course of this work: (a) as-spun fiber produced at a nominal draw-down ratio of 3.2; (b) same fiber after annealing for 2 sec at 500°C.

(a)

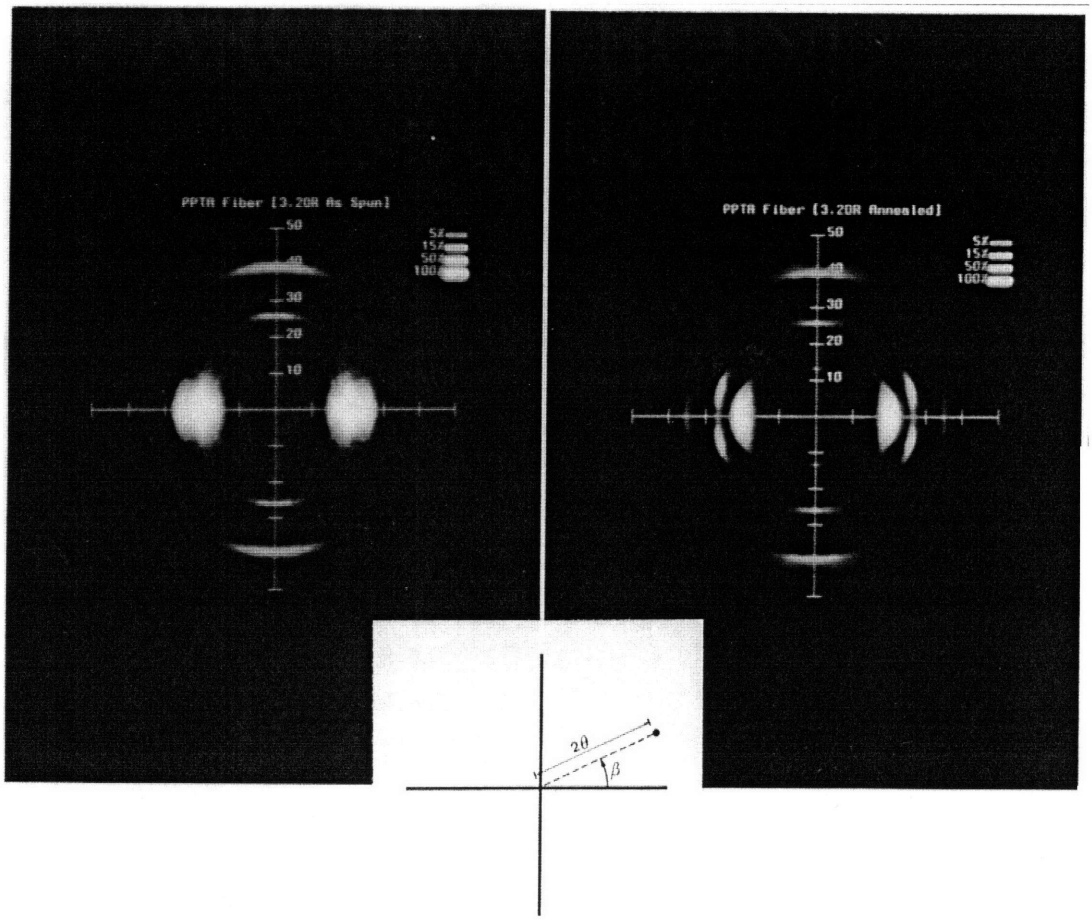

(b)

Table 6.3

Exprimentally determined reflections in PPTA fibers produced in this work and those reported in the literature for Modifications I and II

As-spun fiber[f]			Annealed fiber[f]			Modification I[d]			Modification II[e]		
2θ	β	I	2θ	β	I	2θ	β	I	2θ	β	I
			13.7	84	3	13.7	m	7			
17.9	0	31							17.4	e	s
			20.4	0	81	20.5	e	81			
						21.7	g	8			
22.6	0	100	22.5	0	100	22.6	e	100	22.2	e	vs
27.7	0	45									
28.4	82	13	28.0	86	12	27.7	m	30	27.9	m	m
			29.1	13	23	29.3	g	14	(c)	g	m
			29.8	74	5						
			33.4	57	5						
39.2	72	8									
41.0	29	9	37.3	23	6	37.4	g	4			
			38.4	0	10	38.5	e	4			
43.7	85	35	43.4	85	26	42.0	m	35	(c)	m	m
			45.6	80	15	43.6	g	11			
49.0	15	8				50.0	g	4			
			49.9	0	8	46.1	e	1			
						47.2	g	1			

[a] $\lambda = 1.542$ Å.

[b] e, m, and g refer to equatorial, meridional, and general reflections, respectively, since azimuthal angles of reflection are not reported.

[c] the observed d spacing is not reported.

[d] Northolt [1974].

[e] Haraguchi et al. [1979].

[f] corresponds to 3.2 draw ratio fiber from Trial 2 (Table 6.2)

in agreement with the simulation results, the meridional reflections located at 28.4° and 43.7°, attributable to the [004] and [006] reflections and determined primarily by chain conformation, are indicative of an extended chain conformation.

Upon annealing we note a structural transformation such as that reported by other investigators [Haraguchi et al., 1979; Haraguchi et al., 1979; English, 1986]. The equatorial reflections at 17.9° and 27.7° disappear in favor of a strong reflection at 20.5° and an off-equatorial reflection at 29.1°, characteristic of Modification I. Other strong equatorial reflections occur at 25.5° and 38.4°. Only the [111] reflection predicted to occur at 21.7° fails to appear in our patterns. Reflections along the meridian shift to 28.0° and 43.4°, indicative of a slight extension of the chains during annealing, but remain consistently higher in 2θ than those reported by Northolt [1974]. Intensities of meridional reflections are also lower, but we see increased intensities of off-meridional reflections such as [106] and [104]. The final dominant structure in the annealed fiber agrees well with Modification I.

The same trend in structure transformation was followed using IR spectroscopy, with particular attention paid to the band shifts from 630 cm^{-1} to 673 cm^{-1} and from 720 cm^{-1} to 730 cm^{-1}, reported by Haraguchi et al. [1979] to signal the transition from Modification II to Modification I. However, our IR data was not sensitive to such a transition upon annealing. Rather, we observe an obvious absorption at 720 cm^{-1}, characteristic of Modification II, in both as-spun and annealed fibers, despite the clear predominance suggested by the x-ray results of Modification I over Modification II in the annealed fibers. The breadth of the absorption band between 600 cm^{-1} and 690 cm^{-1} prevented us from drawing any conclusions about a band shift in this range as the result of annealing.

From these results we infer that, prior to annealing, the individual chains are essentially extended and arranged in a reasonably oriented packing array, but that lateral chain packing is not well defined, and two or more such packing modes for the extended chains are probably present. Both of the structures previously reported are partially consistent with the observed diffractogram and could be present in the as-spun fiber. Annealing serves to refine the packing structure in favor of a single dominant packing geometry, as a result of paracrystal-crystal transformation, crystal-crystal transformation, or similar processes.

Of the eight polymorphs suggested by simulation, the PPTA structures identified in Chapter 4 as Structure #3 and Structure #4 bear the greatest resemblance to Modification I and hence to our annealed fiber. With the exception of the overlap of the intense [200] and [110] reflections in the simulated patterns for PPTA Structures #3 and #4 in Figure 4.7(c) and (d), the agreement in position and intensity of the remaining significant reflections is encouraging. Structure #3 most closely approximates the experimental pattern. One notes that in the simulated pattern for Structure #4, the [00*l*] reflections lie off the meridian; this is due to the deviation in the crystallographic angle β from 90°, indicative of a slight

shift between successive sheets of hydrogen-bonded chains. The annealed fiber appears to exhibit characteristics of both polymorphic forms. The reflection "families" (Appendix E, Table E.1) may be compared directly with the integrated intensities for the annealed fiber listed in Table 6.3, deduced from the two-dimensional Gaussian deconvolution procedure. The major reflections are represented in each calculated structure, while the minor reflections could derive from the presence of either or both possible contributors. The weaker meridional reflections predicted by simulation may be traced to the distortion, dictated by local packing constraints, of the 2_1 screw symmetry of the chain conformation. The unit cells deduced by Northolt [1974] and Tashiro et al. [1977] directly from WAXS data on well-annealed fibers are similar to Structure #3 but possess higher crystal symmetry.

7. EXTENSION TO ISOMERS BASED ON DICHLORO-SUBSTITUTED MONOMERS

7.1 Introduction

A primary consideration of model development, and one of the ultimate goals of this work, is the extension of the simulation procedures to the analysis of other similar molecular architectures. At present, the first step in the development of a new model of this type remains the validation of the method using a material of known behavior. This study has been discussed in detail in the previous chapters. However, the real advantage of the method lies in the insight it provides into the connection between chemical structure and material behavior and in its accuracy as a predictive tool and a guide for targeting synthetic efforts. One of the original sources of motivation for this computational development and a running consideration guiding selection of options during development of the model was the more general interest in our group in producing improved, modified aramids which circumvent the weaknesses of the existing list of available stiff chain aramid reinforcement polymers, namely the poor solubility and inferior compressive strength of the Kevlar® family and other rigid rod polymers such as poly(p-phenylene benzobisoxazole) (PBO) and poly(p-phenylene benzobisthiazole) (PBT). The constitutionally isomeric versions of ring-substituted PPTA show promise as reinforcing materials of improved processability, and are especially attractive from the point of view of simulation as materials having controllable atomic-level variations leading to observable macroscopic behavioral changes.

In order to test and demonstrate the extension of the method to new materials, we chose to concentrate on a single representative modification. Variations of interest, based on the previous discussion of constitutional isomerism and the reaction kinetics model, are several: 1) Location of substitution may occur on the phenylene ring of either or both monomers, in order to create the one or two asymmetric monomer units required for control of the reaction kinetics. 2) Substitution may be mono- or di-substitution on one or both carbons, respectively, ortho to the C1 position on the ring. 3) The substituent considered may be either monatomic in nature, such as a halogen, or polyatomic, such as a methoxy group. 4) One may envision an analysis which entails either extreme of order of isomerism (i.e. entirely head-to-head, tail-to-tail linkages or entirely head-to-tail linkages), the completely randomly structured isomer, or some intermediate degree of regularity. We concentrate here on the analysis of modifications involving dual substitution of chlorines in the 2 and 6 positions of the phenylene ring in the limits of complete isomeric regularity, that is, either head-to-head, tail-to-tail (referred to hereafter as

HHTT) or head-to-tail (referred to hereafter as HT). For purposes of model and force field development we consider dichloro-polyamides based on the polymerization of 2,6-dichloro-p-phenylene diamine with terephthalic acid, referred to hereafter as 2,6-DiCl-PPTA, and the polymerization of 2,6-dichloro-terephthalic acid with p-phenylene diamine, referred to hereafter as PP-2,6-DiCl-TA; these dichloro-polyamides will be denoted collectively as Cl-PPTA. For packing calculations, we limit ourselves to the study of the HHTT and HT isomers of 2,6-DiCl-PPTA. One structural repeat unit of each of these two isomers is illustrated in Figure 7.1. Schematically, the symmetric diacid monomer is represented as an open circle and the asymmetric diamine monomer as a filled triangle. Substitution on the diamine monomer was chosen based upon previous successes in the actual synthesis of polymers based on this monomer [Gentile, 1988].

7.2 Chain and Force Field Modification

The selection of Cl-PPTA for the study of controlled variation has the advantage that it requires only minor changes in the chain description and parameterization of the force field and may be considered as a perturbation of the unsubstituted PPTA. In the first instance, it is sufficient to employ the same chain creation and duplication procedure, with the simple removal of pendant hydrogens and replacement by chlorines at appropriate positions along the chain. In practice, this is performed by a delete-and-replace subroutine prior to replication of the parent chain on the lattice. Provisions for generation of packed structures of the random isomer were also implemented by allowing for substitution after chain replication, in randomly selected sequences of head-to-head and head-to-tail orientations, which may differ from chain to chain; however, such calculations will not be discussed within the scope of this work.

Parameterization of the force field requires a redefinition of the set of unique interactions associated with the substituted phenylene ring. In our previous considerations, we treated all the rings as symmetric units. In the modified description, this view is altered to distinguish between a "substituted end" of the ring and an "unsubstituted end" of the ring. In implementation, this requires the definition of a new set of atoms for the phenylene ring, as shown in Figure 7.2: the substituted end consists of the C1 carbon, located between the two chlorines and bonded to the amide moiety, the C2 and C6 carbons, positioned ortho to the C1 carbon and bonded to the two chlorines, and the chlorines themselves; the unsubstituted end consists of the C4 carbon, located between the two hydrogens and bonded to the opposite amide moiety, the C3 and C5 carbons, positioned meta to the C1 carbon and bonded to the two remaining hydrogens, and the hydrogens, for a total of six atomic species, as opposed to the previous description composed of three atomic species. Secondly, we require a new parameterization of the ring-amide torsional interaction potential to describe the modified behavior of the substituted end. For the unmodified ring and the unsubstituted end of the modified ring, we retain the previous torsion potentials

Figure 7.1: Segments of poly(2,6-dichloro-p-phenylene terephthalamide) (2,6-DiCl-PPTA) with all torsion angles in their zero positions: (a) head-to-head, tail-to-tail isomer; (b) head-to-tail isomer.

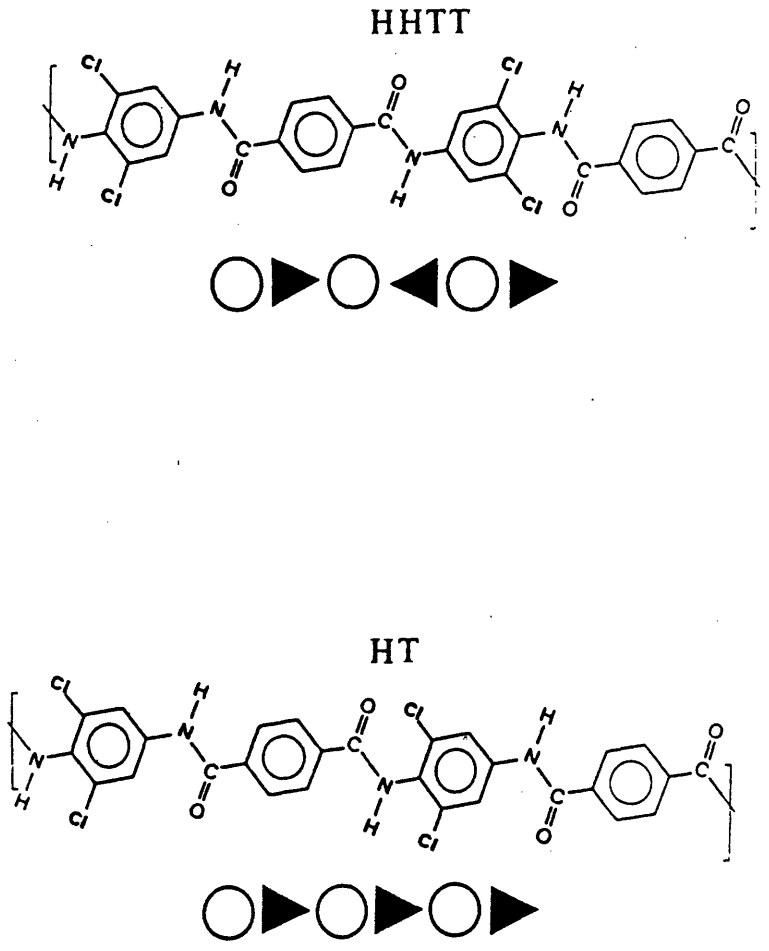

Figure 7.2: Definition of "atom types" for the dihalo-substituted phenylene ring moiety.

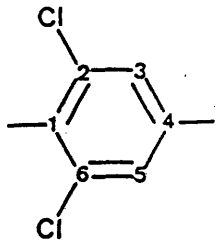

from the PPTA force field. In this way we have tried to incorporate the predominant changes involved in performing the stated ring substitutions with a minimum of changes to the chain construction or the force field description.

The parameters for the modified force field were generated in exactly the same manner as was previously employed for the parameterization of the ring potential for PPTA. The carbon-carbon and carbon-hydrogen bond lengths and the van der Waals radii and well depth parameters r_i and ε_i for carbon and hydrogen were carried over from the PPTA simulation unchanged. The corresponding values for the chlorine atoms were taken from the work of Bernstein and Hagler [1978, 1978] on the crystal structure of the model compound p-(N-chlorobenzylidene)-p-chloroaniline, based on their ab initio quantum mechanical calculations. For partial atomic charges, we again resorted to the procedure of estimation based on AM1 semiempirical quantum mechanical calculations, discussed previously in Chapter 4 and outlined in greater detail in Appendix C. The revised set of atomic nonbonded potential parameters is listed in Table 7.1. The intrinsic torsional energy function was determined for substitution on either the ring of the diamine monomer or the ring of the diacid monomer by appropriate rotations of each ring during AM1 simulations of N-[2,6-dichlorophenyl]-benzamide and 2,6-dichlorobenzanilide, respectively. The variation in potential energy with ring position in each case was best reproduced by the use of a curtate of the form given previously by Equation 4.3. The parameters for these two ring-amide interaction potentials are given in Table 7.2. It is interesting to note that the best fit to the semiempirical AM1 calculations for substitution on the C-N-phenylene torsion requires a significantly increased potential well depth of 32 kcal/mole and a very steep curtate curvature, whereas an adequate fit in the case of the N-C-phenylene torsion is obtained with no additional torsion potential; these curves are shown in Figure 7.3 along with the data points from AM1 calculation. This would imply a significant differentiation between π-bond electron delocalization in the case of the substituted diamine monomer and that in the case of the substituted diacid monomer. However, it would be premature to draw any conclusions concerning electron behavior between moieties based on such a simplified representation. The revised curtates probably reflect a procedural requirement necessitated by the larger hard sphere repulsion of the chlorine atoms in order to emulate the curvature of the rotation potential suggested by AM1, rather than any

Table 7.1

6-12 Nonbonded atomic potential parameters and elementary charges used in the electrostatic potential

Atom	ε (kcal/mole)	r (Å)	q[a] (elementary charge)
C (phenylene, 1)	0.039	1.96	-0.02
C (phenylene, 4)	0.039	1.96	-0.06
C (phenylene, 2 and 6)	0.039	1.96	-0.03
C (phenylene, 3 and 5)	0.039	1.96	-0.12
H (phenylene)	0.038	1.37	+0.17
C (amide)	0.147	2.03	+0.38
H (amide)	0.0	0.0	+0.28
N	0.169	1.96	-0.28
O	0.232	1.60	-0.38
Cl	0.243	1.80	+0.02

[a] The value for the bulk dielectric constant D_B was 3.5, and the Block-Walker crossover distance d^* was 3.3Å.

Table 7.2

Intrinsic torsional energy function parameters[a]

Torsion	V_d[b]	m_d
diacid ring (ϕ_5,ϕ_5-ϕ_1)	0.0	0.0
diamide ring (ϕ_6,ϕ_6-ϕ_3)	32.0	0.8

[a]see text for details, Equation 4.3
[b]all values in kcal/mol

Figure 7.3: Phenylene ring rotation energy functions suggested for dichloro-substituted rings.

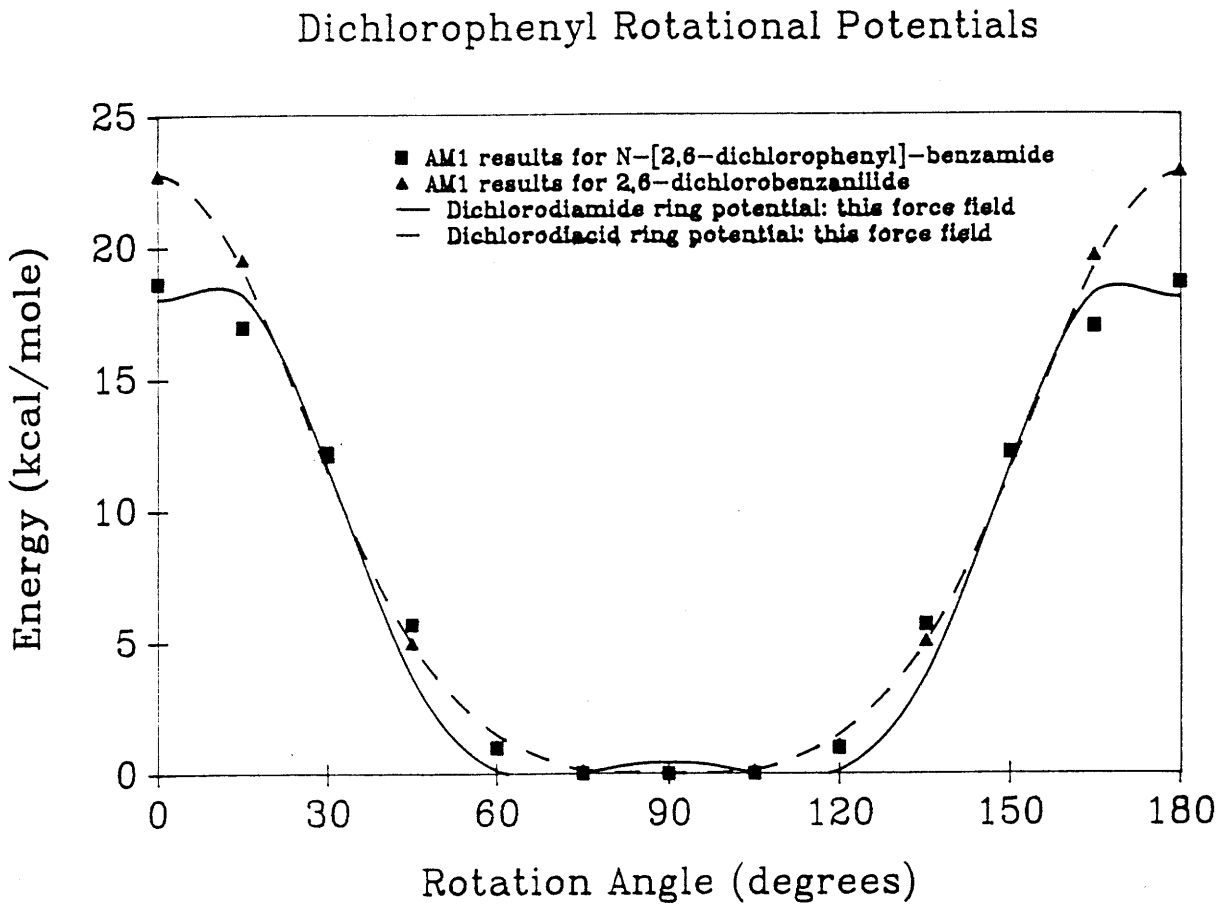

significant redistribution of electron probability; the very low barrier at 90° in the C-N-phenylene case is considered to be of minor significance relative to the general form of the curve. More interesting is the distribution of partial atomic charges among the components of the substituted ring. The pendant chlorines exhibit a very slight positive charge, and appear to effectively counterbalance the tendency for redistribution of electron density to the carbon members of the ring. The pendant hydrogens, on the other hand, retain a significant positive charge, resulting in a notably biased atomic charge distribution at the aromatic C-H bonds. Such assignment of atomic charges accurately reproduces the dipole moment of m-dichlorobenzene (see Appendix C).

7.3 Simulation Results: Single Chain

At this stage, we still consider chains of both 2,6-DiCl-PPTA and PP-2,6-DiCl-TA. As in the case of the unsubstituted polymer PPTA, the isolated chain energetics were first considered in terms of torsion angle triplets. Again, one assumes that intermolecular interactions are essentially decoupled across the rigid phenylene rings. With this simplification, the triplets of the isolated chains of the HHTT isomer and the HT isomer become equivalent; one need only consider the two cases of substitution location. Figures 7.4 and 7.5 show the energy contours for N-[2,6-dichlorophenyl]-benzamide and 2,6-dichlorobenzanilide, respectively, as a function of the phenylene-C-N and C-N-phenylene torsions (ϕ_3 and ϕ_1) with the amide torsion ϕ_2 assuming a position of minimum energy in the vicinity of the trans conformation. As before, contours with the amide torsion in the vicinity of the cis conformation all lie 5 kcal/mole or more above that of the minimum energy conformations. Not surprisingly, the location of the minima and the barrier heights of the unsubstituted rings remain essentially unaltered from the plain benzanilide case. The substituted rings rotate considerably out of the plane of the amide linkage, showing broad minima between 60 and 120 degrees, with very low barriers to rotation within this range. This increased freedom of rotation about the phenylene ring axis should not alter greatly the extensional rigidity of the chain, since it involves rotation about the C1-C4 axis of the ring; this has been confirmed by Gentile [1988] for both random and ordered isomers of Cl-PPTA, which exhibit the onset of a nematic phase at concentrations comparable to those for PPTA of similar molecular weight and consistent with Flory's lattice model for the mesophase transition in rodlike molecules. However, such rotational freedom implies an increase in the entropy of the isolated chains in the solution phase over that for the unsubstituted PPTA.

Figure 7.4: Potential energy contour for N-[2,6-dichlorophenyl]-benzamide as a function of the ring torsions ϕ_1 and ϕ_3.

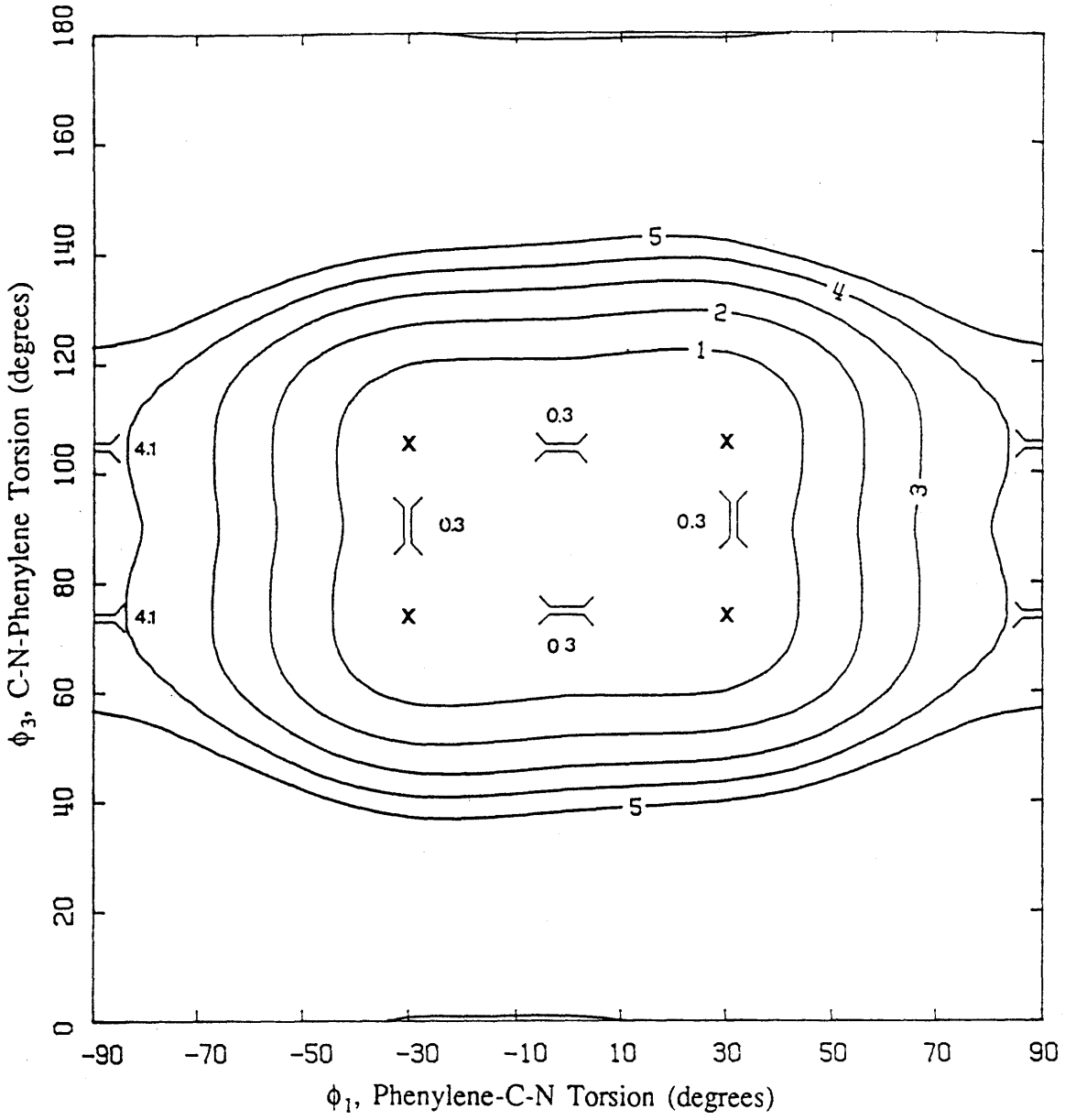

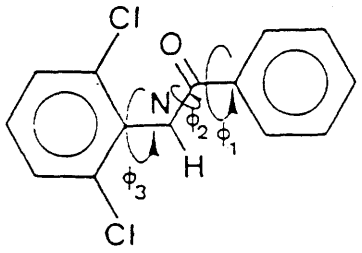

Figure 7.5: Potential energy contour for 2,6-dichlorobenzanilide as a function of the ring torsions ϕ_1 and ϕ_3.

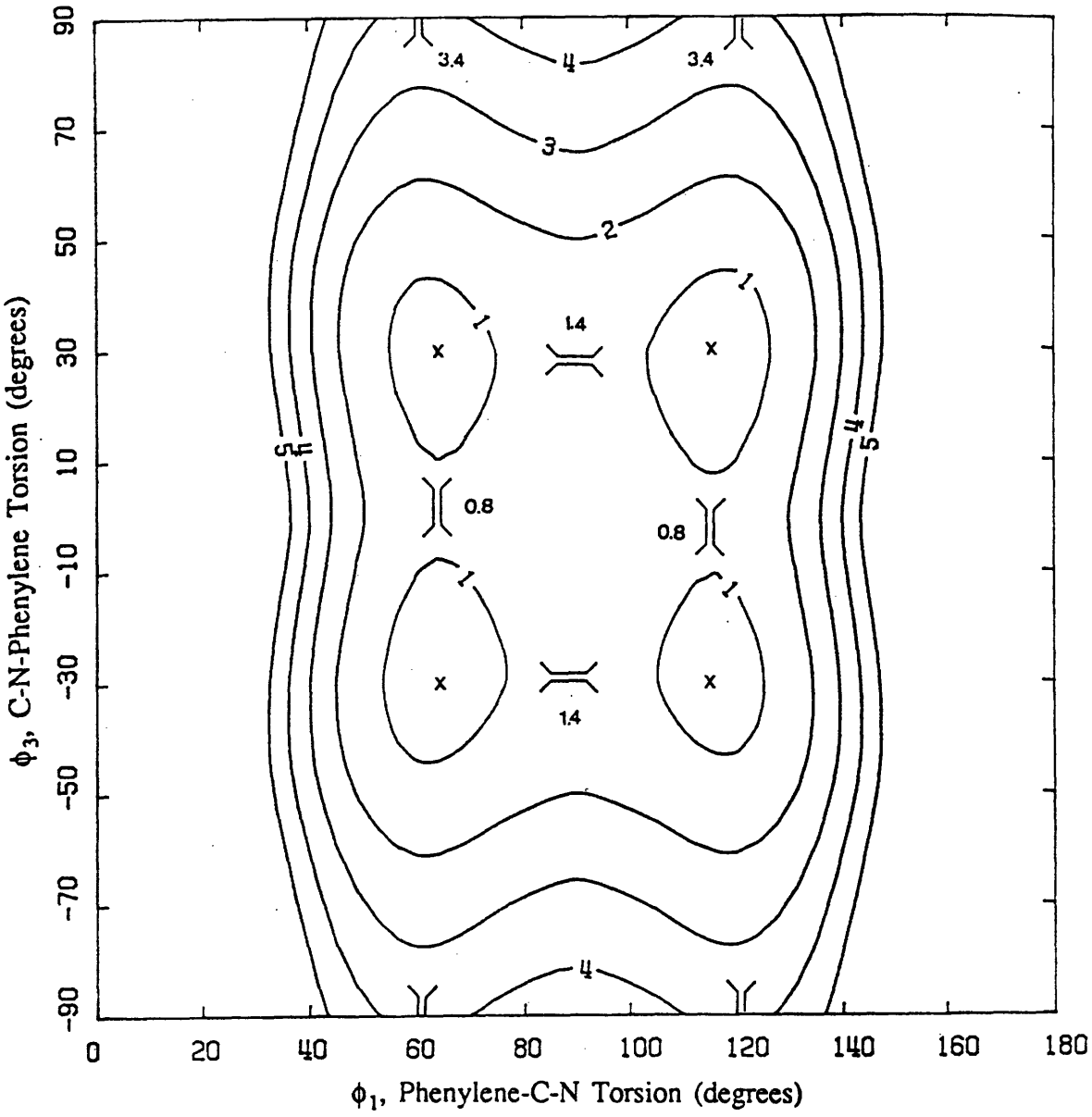

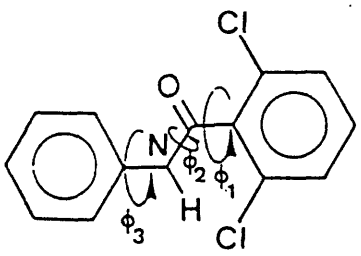

7.4 Simulation Results: Multichain

7.4.1 Approaches to Identification of Minima

At this point we focus on the packing of chains of 2,6-DiCl-PPTA. Two approaches recommend themselves to the identification of the set of structures of local minimum energy likely to occur in nature. The first is a repetition of the process described in Section 4.4 for the initial identification of energy minima in PPTA; this involves a multistep procedure of scanning and searching through the multivariate parameter space. However, equally consistent with the concept of a first principles approach to structure elucidation and considerably less time-consuming is a process of minimization which assumes that the modified structures are likely to exhibit packed geometries which are perturbations of the geometries of the unsubstituted polymer. This assumption obviates the lengthy grid scanning phase and recommends a finite set of minimizations within predetermined regions of parameter space. Its major weakness lies in the implication that the modification does not involve any significant new interactions which would stabilize new, unrelated geometries. In order to determine the comparability of the two methods and in particular the comprehensiveness of the latter, both procedures were followed in the analysis of the HHTT and HT isomers of 2,6-DiCl-PPTA.

7.4.2 Packing of Head-to-Head, Tail-to-Tail Isomers

CRU Definition: For the HHTT isomer, two possible representations of the CRU were initially considered. The first and simplest assumes that the dimer constitutes the basic conformational unit, analogous to PPTA. In a head-tail-tail-head sequence, consisting of four monomers defining two oppositely-directed dimers, the set of conformation-determining angles and torsions are identical for both dimer subunits, regardless of their respective orientations; in this description, the number of independent internal degrees of freedom required to describe the chain remains fourteen. The validity of such a simplification was checked by considering a second representation in which the tetramer constitutes the basic conformational unit, consisting of the complete head-tail-tail-head sequence, or two independently conformable dimers, for a total of twenty-eight internal degrees of freedom.

Location and Description of HHTT Energy Minima: Employing the dimer CRU representation and following the same procedure as described in Chapter 4 with a cut-off criterion of 0.2 for identification of those polymorphs of interest, the analysis suggests a list of four viable crystal polymorphs for the fully ordered HHTT isomer of 2,6-DiCl-PPTA. These are presented in Table 7.3 in the same format as was used for the polymorphs of the unsubstituted PPTA; orthographic projections are provided in Figure 7.6(a)-(d) for ease of visualization. Of these, only Structure #2 derives from one of the eight original

Table 7.3

Multichain energy minimization results: structural parameters for four most probable unit cells of 2,6-dichloro-PPTA; head-to-head, tail-to-tail polymorphs

Structure ID →	1	2	3	4
Structural Parameters ↓				
a (Å)	8.54	8.88	8.53	5.46
b (Å)	6.11	5.79	6.15	4.58
c (Å)	25.4	26.2	26.2	26.2
α (degrees)	107	90	96	107
β (degrees)	87	90	89	88
γ (degrees)	98	82	97	101
Chain Locations (ab projection)	[0,0] [½,½]	[0,0] [½,½]	[0,0] [½,½]	[0,0] -
Chain Setting Angle (degrees) relative to the bc-facet	-20 -20	23 -157	-16 -16	22 22
Inter-sheet Translation (Å)	0.0	6.6	13.1	0.0
Helix Twist Θ_h (degrees)	1	0	1	0
Monomer Phenylene Ring Rotation (degrees)				
diacid ring ϕ_5:	5	-6	5	-6
diamide ring ϕ_6:	61	57	63	60
Cohesive Energy (kcal/mol)	35.8	35.4	35.4	35.1
Density (g/cm^3)	1.63	1.53	1.69	1.69
Parallelepiped Description:				
A (Å)	4.89	5.63	4.95	5.46
B (Å)	5.59	4.95	5.55	4.58
C (Å)	25.4	26.2	26.2	26.2
τ (degrees)	102	90	94	107
υ (degrees)	98	90	93	88
ζ (degrees)	110	66	108	102
ω_1 (degrees)	61	107	78	83
ω_2 (degrees)	61	-73	78	83
f_2	0.0	0.50	1.0	0.0

Figure 7.6: Orthographic perspectives of the four primary structures for the HHTT isomers of 2,6-DiCl-PPTA suggested by simulation. The sets (a) through (d) correspond to the structures labelled 1 through 4, in order, in Table 7.3. Left: z-axis perspective; Middle: perspective perpendicular to the bc-plane; Right: perspective perpendicular to the previous two perspectives.

(a)

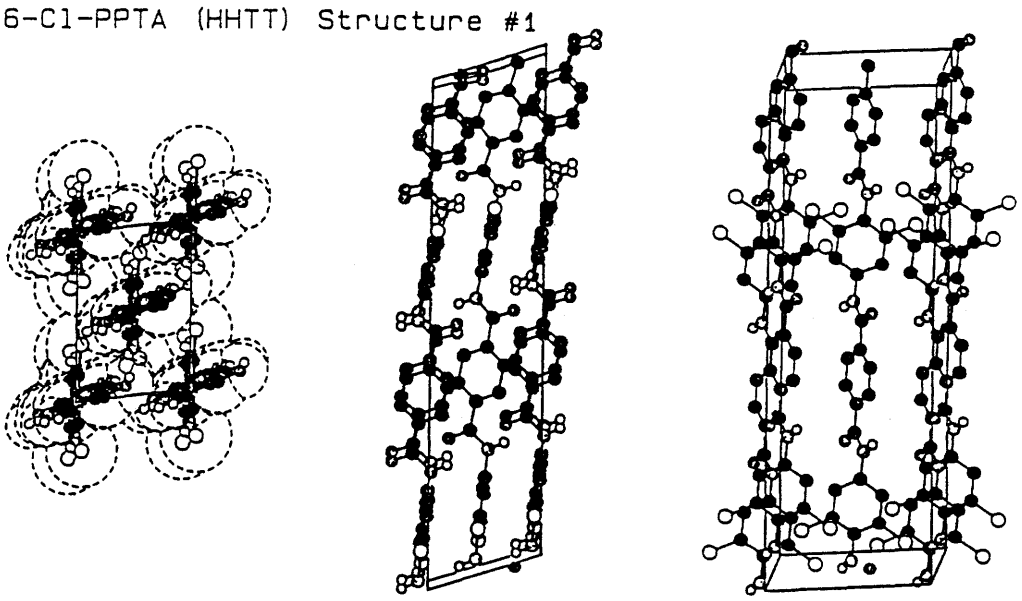

(b)

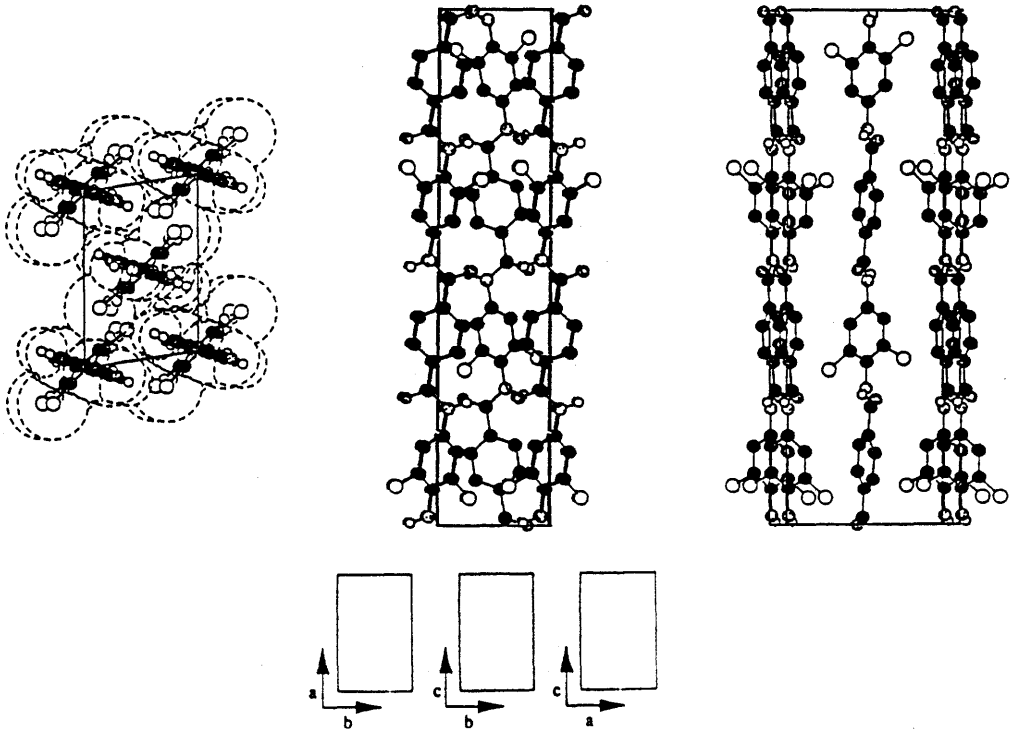

Figure 7.6: Orthographic perspectives of the four primary structures for the HHTT isomers of 2,6-DiCl-PPTA suggested by simulation (continued).

(c)

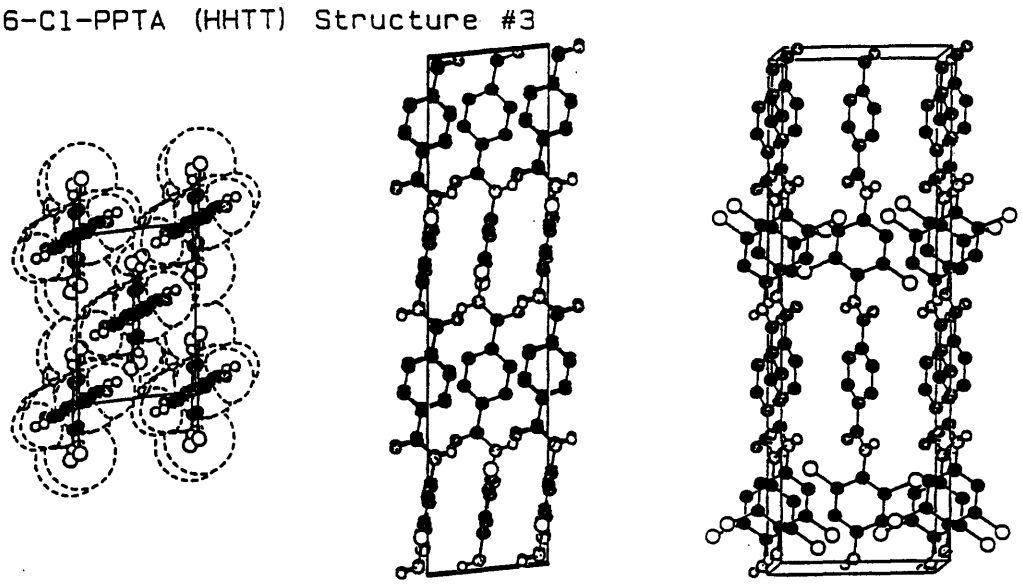

(d)

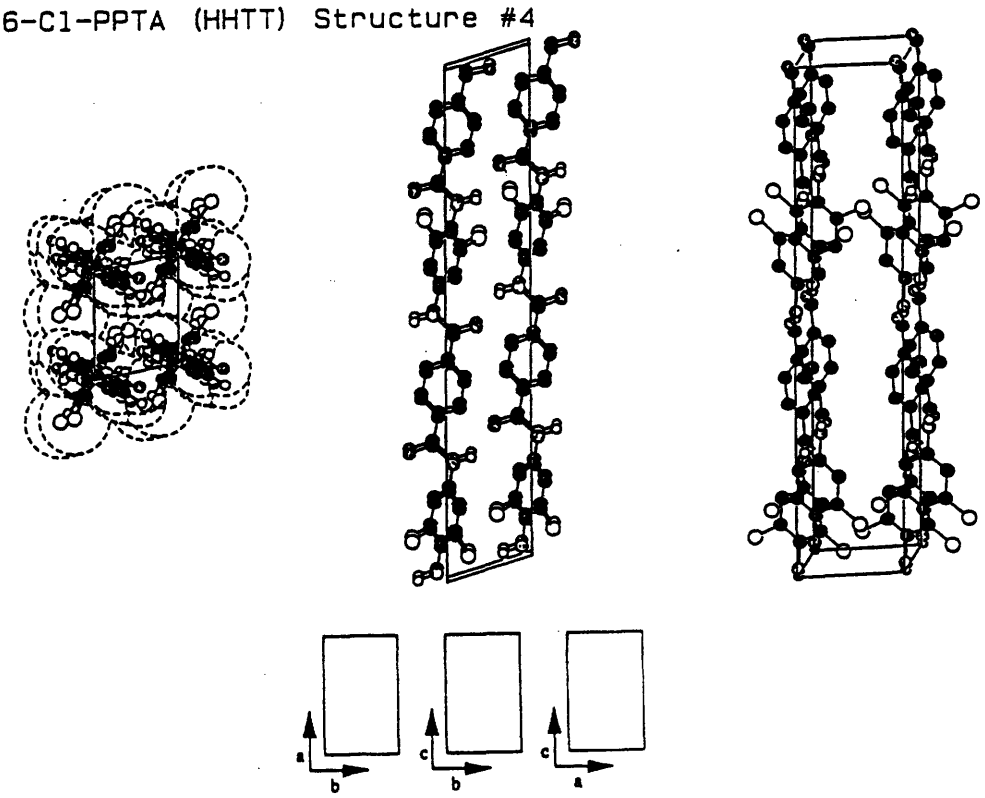

PPTA structures. Significantly, this second structure derives from PPTA Structure #3, the calculated allomorph which bears the greatest likeness to the experimentally-determined Modification I.

Trends in Structure: The density of the HHTT isomers is on the average roughly 10% greater than that of PPTA. Accounting for the higher molecular weight of the substituted polymer, this corresponds to an average increase in unit cell volume of 15% to 20%. One may immediately note that again there is no significant deviation from the fundamental extended conformational behavior of the chain; the helix twist deviates insignificantly from zero degrees. Successive phenylene rings may be either similarly or oppositely rotated with respect to the amide bond plane. However, the trend is for the ring rotation angles to remain within a relatively narrow range of five to six degrees or fifty-seven to sixty-three degrees for the phenylene ring of the diacid monomer or the phenylene ring of the diamine monomer, respectively. This suggests two striking implications for the substituted polymer: First, both rings tend to fall within a very narrow angular range in the packed structure, an unexpected result given the magnitude of the intermolecular forces and the range of low energy angular fluctuation available to the rings suggested by single chain simulations. Second, the unsubstituted ring of the diacid monomer has been forced considerably and consistently away from its minimum energy position for the isolated chain. From these observations, one would conclude that the packing of chains of the HHTT isomer significantly alters and restricts the conformation space of the chain itself; qualitatively, this implies a significantly different environment for both the potential energy and conformational entropy of the chain in the solid state from that in the isolated (e.g. dilute solution) state. Consistent with the PPTA case, the 2,6-DiCl-PPTA HHTT packed chain geometries exhibit a strong correlation between chain setting angles, with the implication again that the chains associate into sheets held together by hydrogen bonds between chains. Within the unit cell, the predominance of hydrogen bonding interactions ensures the maintenance of translational register between amide moieties and phenylene moieties, respectively. Between chains in successive sheets, the substituted phenylene ring may be in register with another substituted ring of like orientation (HHTT structures #1 and #4), with a substituted ring of opposite orientation (HHTT Structure #3), or with an unsubstituted ring (HHTT Structure #2). That is, all three types of register are represented in these four equipotential crystal structures. There does not appear to be any justification for the supposition that the introduction of chlorines on the rings creates or prohibits any specific structural juxtaposition between the modified moieties.

Trends in Potential Energy: The total cohesive energy, expressed on a per dimer basis, is slightly lower than that found for PPTA. Predicted densities range from as low as 1.53 g/cm^3 up to 1.69 g/cm^3. For the set of four HHTT isomer packing geometries, we obtain:

$$E_{coh} = 35.4 \pm 0.5 \text{ kcal/mol}$$

$$13.3\ [cal/cm^3]^{1/2} < \delta < 14.0\ [cal/cm^3]^{1/2}$$

or $$27.1\times10^3\ [J/m^3]^{1/2} < \delta < 28.5\times10^3\ [J/m^3]^{1/2}$$

These values are roughly 90% of the corresponding values predicted for PPTA. Despite the similarities in the nature of interactions between the unsubstituted polymer and the HHTT isomer, the total cohesive forces are measurably smaller in the latter. The implication is that the introduction of ring substituents compels an expansion of the lattice which in turn leads to a weakening of the net cohesive forces. This reduced cohesiveness provides the main argument for the greater solubility of the HHTT isomer over that of the unsubstituted polymer. The new Hildebrand solubility parameter estimates are comparable to those reported for aliphatic polyamides.

These trends are further confirmed by the decomposition of the chain-chain bonding energies (on a per dimer basis) listed in Table 7.4, this time in terms of chains related by crystallographic location; the hydrogen bonded sheets, by earlier convention, lie in the bc-facet in each case. The moiety-specific amide-to-amide electrostatic interaction accounts for 40% to 65% of the total interaction energy between neighboring chains within the bc-facet, corresponding to hydrogen bond energies of 1.5 to 3.0 kcal/mole, in perfect accord with the hydrogen bond energies expressed in PPTA. By contrast, interactions between neighboring chains in the ac-facet exhibit very low total interaction energies. The "diagonal" interactions listed in Table 7.4 refer to the largest interchain interaction energies which cross from one sheet to another. With the exception of Structure #4, intersheet interactions are comparable to intrasheet interactions, with magnitudes of 6.5 to 7.3 kcal/mole. We conclude that the introduction of substitution on the ring appears to alter the magnitude, but not the distribution or moiety-to-moiety specificity, of interaction energy between chains from that seen in the PPTA case.

The Tetramer CRU: The second chain representation, involving four rings in the CRU, was adopted for repetition of the minimizations initiated at the original PPTA structures. The resulting minima realized, on the average, an increase of 1.5 kcal/mole of dimer in cohesive energy. Densities were comparable to those found using the CRU representation with only two rings. The greater freedom allowed to the chain conformation resulted in new twists in the helical structure of the molecule, usually consisting at most of compensating rotations of ±10° to 15° about the virtual bonds spanning the phenylene rings of the two diamine monomer components; such compensating rotations result in a net helix twist close to zero degrees, but with every two successive amide dipoles along the chain contour lying in a plane 15° rotated from the preceding pair. However, this slight variation did not justify the large increase in computational resources required to accommodate the more demanding tetramer calculations. Packing geometry remained essentially unchanged. For this reason, further exploration using this representation was not deemed necessary.

Table 7.4

Chain-to-chain bonding energies for 2,6-dichloro-PPTA; head-to-head, tail-to-tail polymorphs
(all values in kcal/mole of dimer)

Cell ID	1	2	3	4
Cell type[a]	fc	fc	fc	p
ac-facet:				
total 12-6	0.5	0.2	0.5	2.6
total electrostatic	-0.2	0.0	-0.2	0.3
amide-amide elec.	0.0	0.0	0.0	-0.6
phenyl-phenyl elec.	-0.1	0.0	-0.1	0.5
total	0.3	0.2	0.4	2.9
bc-facet:				
total 12-6	2.0	3.1	1.8	3.4
total electrostatic	4.5	4.2	4.6	6.0
amide-amide elec.	3.4	2.8	3.5	6.0
phenyl-phenyl elec.	0.4	0.8	0.4	2.0
total	6.5	7.3	6.4	9.4
diagonal:				
total 12-6	2.7	3.8	2.8	1.4
total electrostatic	4.0	3.2	4.3	1.6
amide-amide elec.	2.8	1.8	2.7	0.7
phenyl-phenyl elec.	1.0	0.2	2.0	0.2
total	6.7	7.0	7.1	3.0

[a] Cell type identifies chain intersections with the ab-facet: fc indicates chains at [0,0] and [½,½]; ec indicates chains at [0,0] and [½,0]; p refers to a primitive cell with chains only at the corners. Intrasheet interactions are consistently in the bc-facet. Closest intersheet interactions are diagonal in the fc cell type but are in the ac-facet in the ec cell type; in the p cell type both types of interactions are intersheet in nature.

7.4.3 Packing of Head-to-Tail Isomers

Chain Directionality: With the HT isomer, the problems of appropriate chain representation are slightly different from those of the HHTT isomer. In this case, it is again reasonable and sufficient to consider only the dimer CRU, as was suggested in the case of the unsubstituted polymer, since there is no distinction of orientation between dimer units along the contour of the chain. However, the HT isomer possesses directionality as a whole. For this reason, one must now consider, instead of multiple representations of the internal chain description, multiple non-interconvertible intermolecular relationships between chain directions during packing. Specifically, we consider two cases: one where all chains pack with parallel directionality, and one where chains may pack with antiparallel directionality. These two cases will be designated as HT(P) and HT(A) variations, respectively. In the latter case, one could as well assume that the two distinguishable chain types (e.g. "up" and "down" chains) have different CRU's, leading again to a doubling of the number of internal degrees of freedom; for simplicity, we have considered only one common CRU for both chain types in all cases. However, we have considered the possibility for the "up" and "down" chain types to be mirror images of one another, effected during simulation by reflecting the parent chain of "up" type through the yz-plane prior to replication and reorientation of a "down" chain.

Location and Definition of HT Energy Minima: Because of the directionality of the HT chain and the consequent escalation in number of variations of packing to be considered, the final list of viable structures is somewhat longer than for the HHTT isomer, even for the same conditions of search and selection. Table 7.5(a) lists the four HT(P) polymorphs, identified through the scan and search procedure; orthographic projections are presented in Figure 7.7(a)-(d). As in the case of the HHTT isomers, the minimizations were also performed based on initial conditions defined by the original eight PPTA structures. Here, as many as three of the four HT(P) allomorphs, structures #1, #2, and #3, derive from the original PPTA structures. Furthermore, these three allomorphs derive in particular from PPTA structures #3, #4 and #7; again, the first of these is that which most closely resembles the experimentally-determined Modification I. This continued recurrence and persistence lends further credence to the accuracy of the PPTA analysis reported in Chapter 4 and hints at the relative importance of this basic geometric unit, in both the substituted and unsubstituted polymers. The HT(P) structures #2 and #3 bear the same relation to #1 as was reported earlier for the corresponding structures in PPTA.

Table 7.5(b) shows the features of the HT(A) isomers, with corresponding orthographic projections in Figure 7.7(e)-(j). These must be considered in common with the HT(P) versions, since these are all structures based on the same chemistry and could be obtained separately or mixed in the actual bulk solid state. Of the structures listed in Table 7.5(b), #5 through #7 contain "up" and "down" chains that are related only by rigid body translation and rotation; #8 through #10 contain chains which are reflected through the yz-plane prior to translation and rotation operations. In this set of antiparallel structures, one

Table 7.5a

Multichain energy minimization results: structural parameters for four most probable unit cells of 2,6-dichloro-PPTA: parallel head-to-tail polymorphs

Structure ID →	1	2	3	4
Structural Parameters ↓				
a (Å)	8.68	8.97	8.04	4.96
b (Å)	5.88	5.60	5.96	5.52
c (Å)	13.1	13.1	13.1	13.0
α (degrees)	90	87	87	91
β (degrees)	85	81	82	92
γ (degrees)	81	80	92	72
Chain Locations (ab projection)	[0,0] [½,½]	[0,0] [½,½]	[0,0] [½,0]	[0,0] -
Chain Setting Angle (degrees) relative to the bc-facet	25 -154	24 24	22 20	32 32
Inter-sheet Translation (Å)	6.6	6.6	6.6	0.0
Helix Twist Θ_h (degrees)	3	2	8	1
Monomer Phenylene Ring Rotation (degrees)				
diacid ring ϕ_5:	-17	-23	18	5
diamide ring ϕ_6:	59	54	60	65
Cohesive Energy (kcal/mol)	36.7	35.2	36.1	34.9
Density (g/cm^3)	1.55	1.59	1.65	1.51
Parallelepiped Description:				
A (Å)	5.60	5.70	7.04	5.51
B (Å)	4.85	4.88	4.02	4.96
C (Å)	13.1	13.1	13.1	13.0
τ (degrees)	86	84	82	92
υ (degrees)	86	81	83	91
ζ (degrees)	68	63	58	72
ω_1 (degrees)	105	107	112	162
ω_2 (degrees)	-76	108	114	162
f_2	0.50	0.50	0.50	0.0

Table 7.5b

Multichain energy minimization results: structural parameters for most probable unit cells of 2,6-dichloro-PPTA: antiparallel head-to-tail polymorphs

Structure ID →	5	6	7	8	9	10
Structural Parameters ↓						
a (Å)	8.73	9.37	7.86	10.06	8.78	8.87
b (Å)	5.68	5.35	5.89	4.65	5.85	6.58
c (Å)	13.1	13.1	13.1	13.1	13.1	13.1
α (degrees)	92	98	92	92	90	83
β (degrees)	81	84	86	82	91	75
γ (degrees)	91	82	90	83	82	115
Chain Locations (ab projection)	[0,0] [½,0]	[0,0] [½,0]	[0,0] [½,0]	[0,0] [½,½]	[0,0] [½,½]	[0,0] [½,0]
Chain Setting Angles (degrees), relative to the bc-facet	21 17	35 74	31 20	18 11	24 -20	10 14
Inter-sheet Translation (Å)	5.3	0.4	6.4	2.9	6.7	0.5
Helix Twist Θ_h (degrees)	1	4	17	2	1	6
Monomer Phenylene Ring Rotation (degrees)						
diacid ring ϕ_5:	-27	-17	12	-34	-7	-29
diamide ring ϕ_6:	60	61	62	55	57	62
Cohesive Energy (kcal/mol)	37.1	37.1	36.0	37.3	35.8	35.3
Density (g/cm^3)	1.59	1.59	1.69	1.71	1.53	1.58
Parallelepiped Description:						
A (Å)	7.13	7.57	3.92	5.81	5.60	6.19
B (Å)	4.37	4.68	7.10	5.26	4.93	4.43
C (Å)	13.1	13.1	13.1	13.1	13.1	13.1
τ (degrees)	92	98	95	96	90	83
υ (degrees)	84	91	92	89	91	69
ζ (degrees)	53	45	56	49	67	74
ω_1 (degrees)	120	99	104	115	113	168
ω_2 (degrees)	168	58	159	-72	108	-42
f_2	0.25	-0.19	0.26	-0.42	0.29	-0.08

Figure 7.7: Orthographic perspectives of the ten primary structures for the HT isomers of 2,6-DiCl-PPTA suggested by simulation. The sets (a) through (j) correspond to the structures labelled 1 through 10, in order, in Tables 7.5a and 7.5b. Left: z-axis perspective; Middle: perspective perpendicular to the bc-plane; Right: perspective perpendicular to the previous two perspectives.

(a)

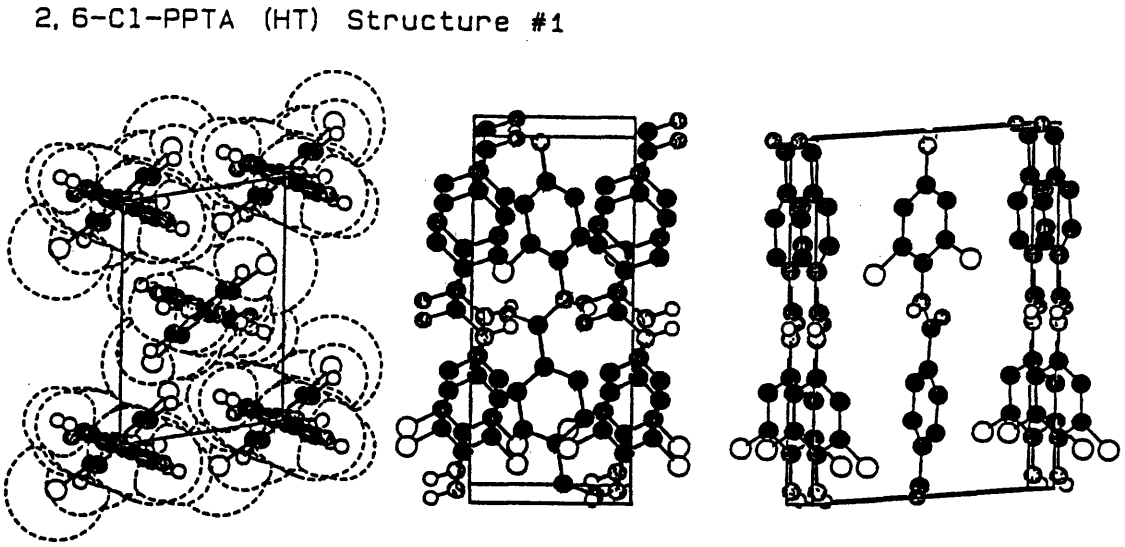

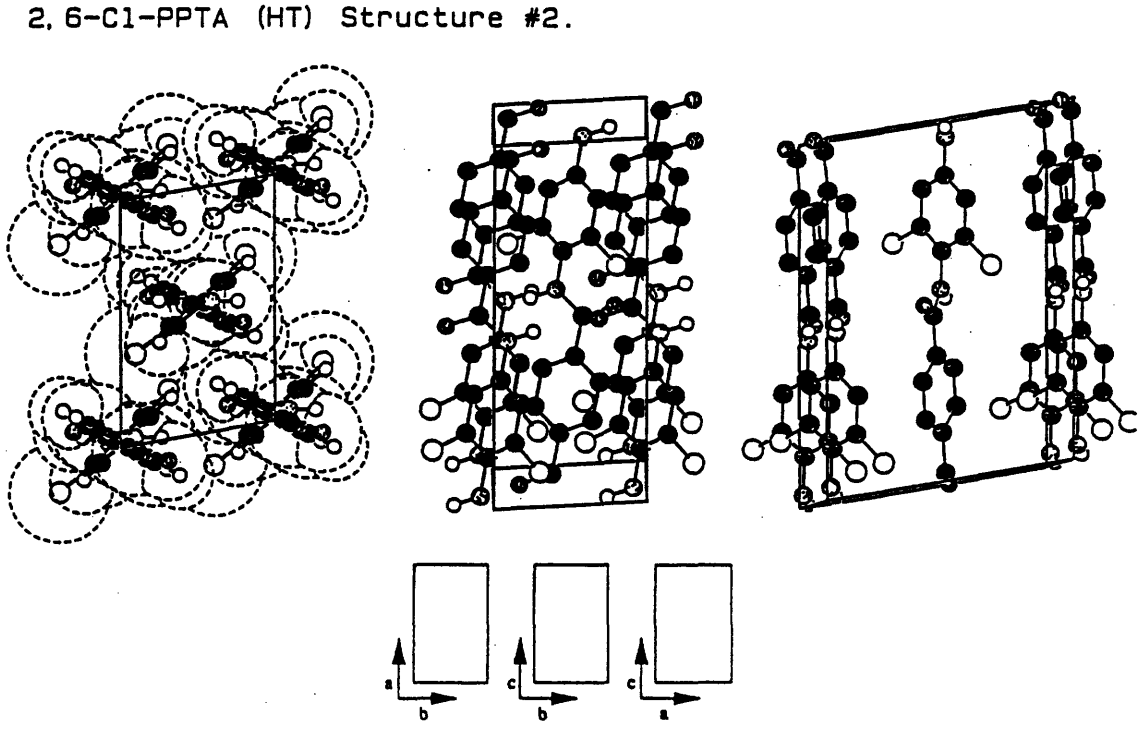

(b)

Figure 7.7: Orthographic perspectives of the ten primary structures for the HT isomers of 2,6-DiCl-PPTA suggested by simulation (continued).

(c)

2, 6-Cl-PPTA (HT) Structure #3

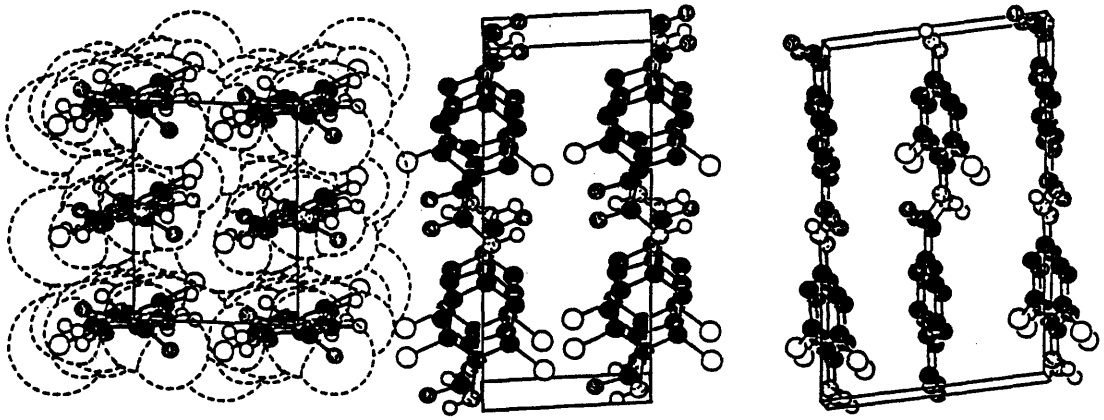

(d) 2, 6-Cl-PPTA (HT) Structure #4

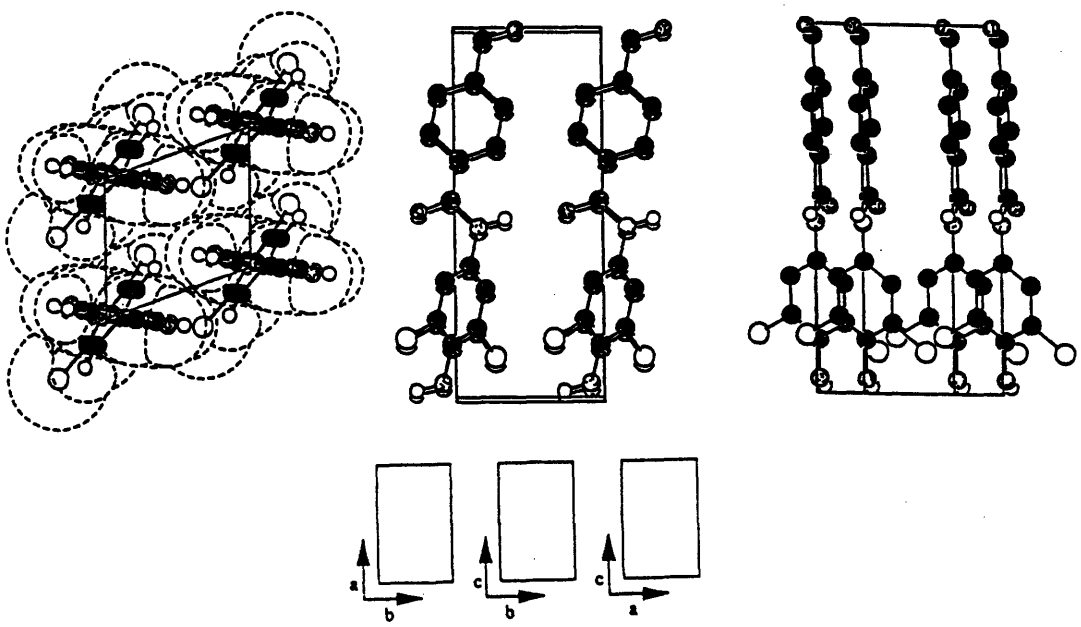

Figure 7.7: Orthographic perspectives of the ten primary structures for the HT isomers of 2,6-DiCl-PPTA suggested by simulation (continued).

(e)

2, 6-Cl-PPTA (HT) Structure #5

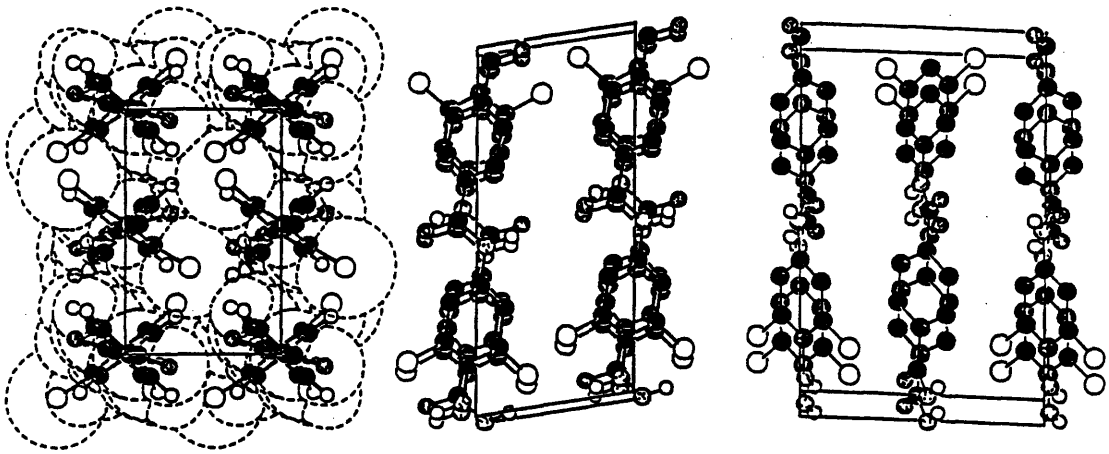

(f)

2, 6-Cl-PPTA (HT) Structure #6.

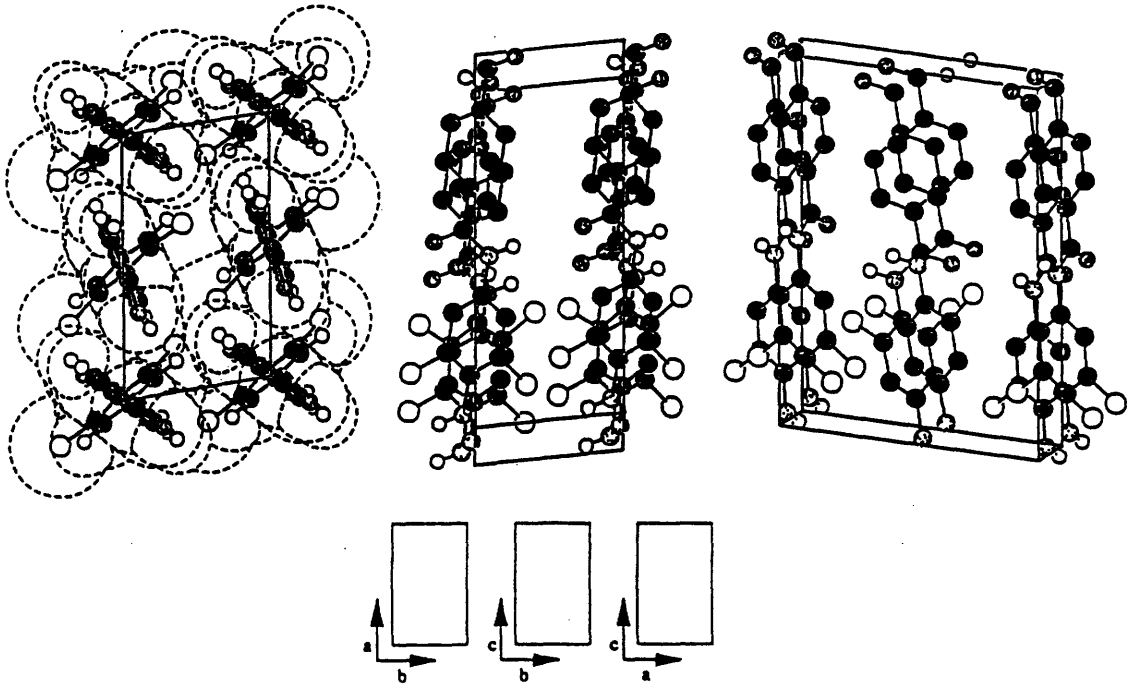

Figure 7.7: Orthographic perspectives of the ten primary structures for the HT isomers of 2,6-DiCl-PPTA suggested by simulation (continued).

(g)

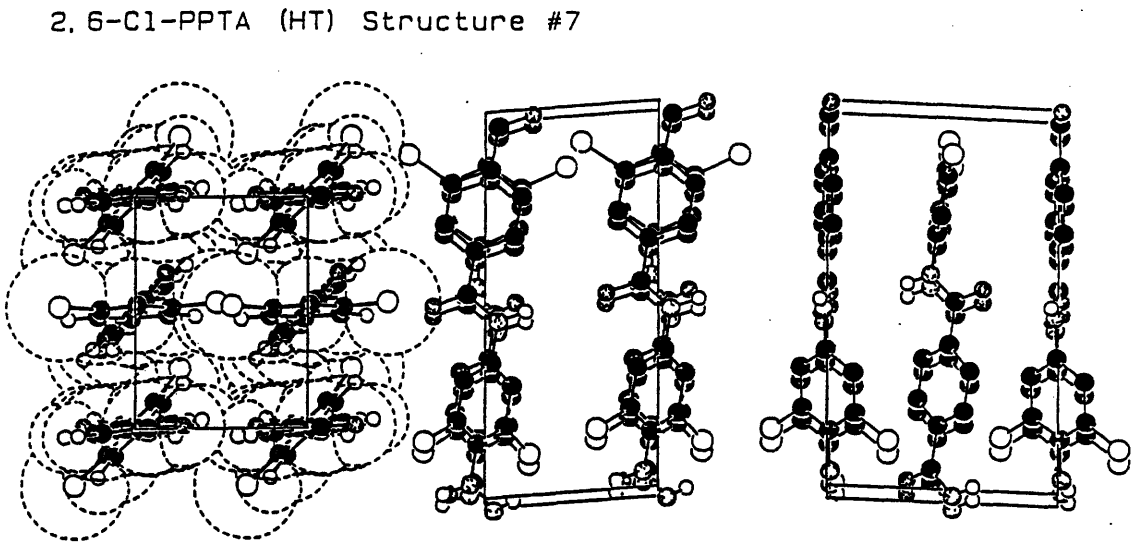

(h)

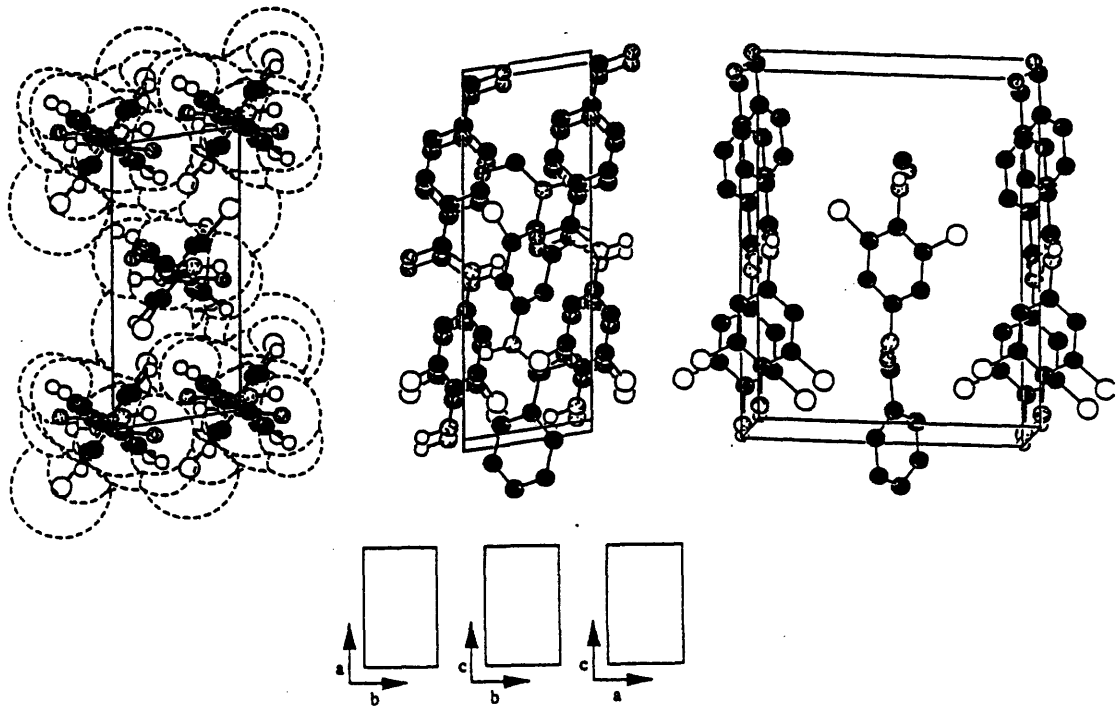

Figure 7.7: Orthographic perspectives of the ten primary structures for the HT isomers of 2,6-DiCl-PPTA suggested by simulation (continued).

(i)

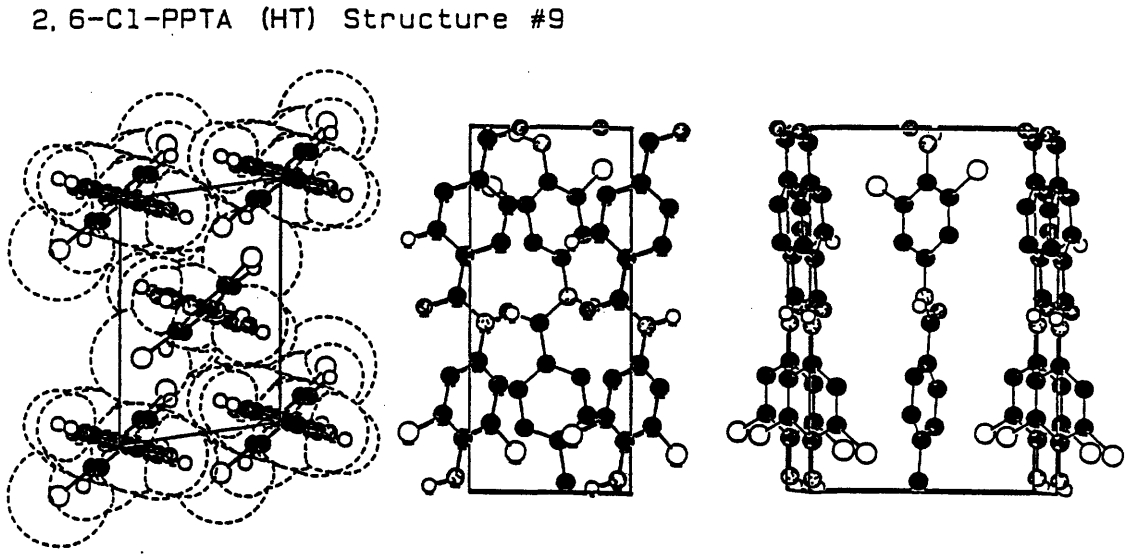

(j)

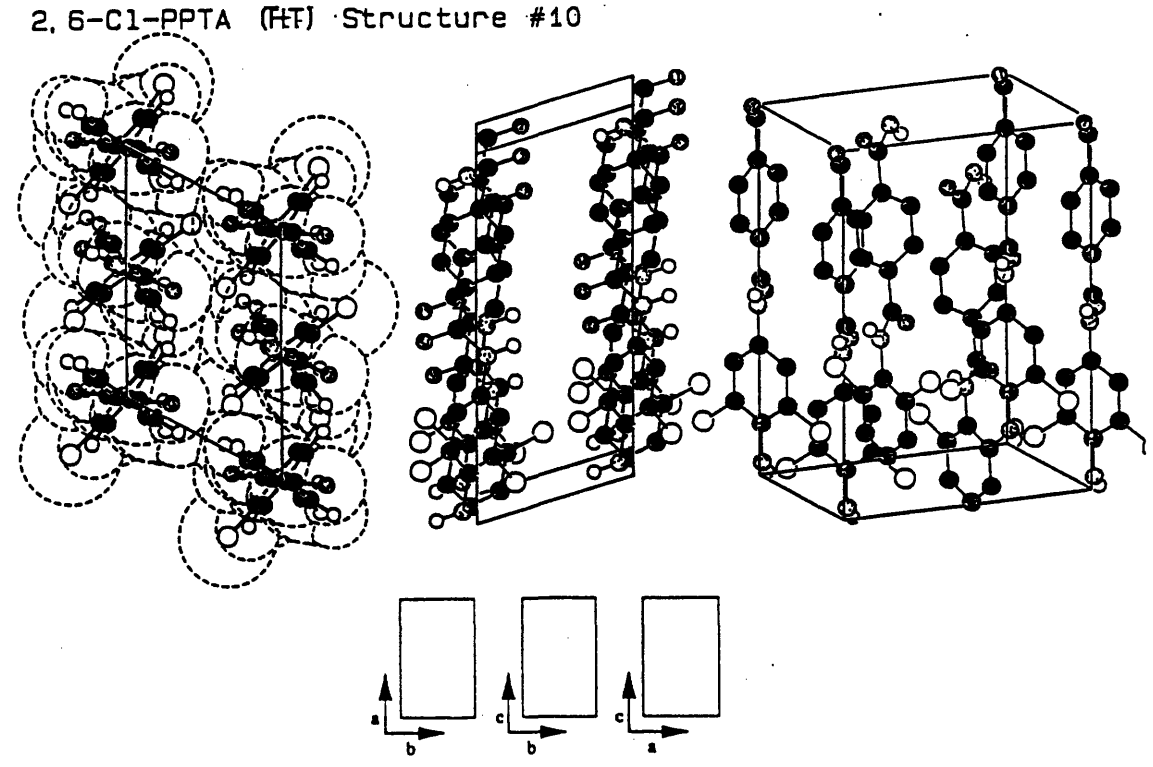

may note that, with the restriction that all chains possess the same conformation, the correlation of chain orientations is significantly altered in order to accommodate steric packing of the large ring moieties. Thus in Structure #5 the identification of hydrogen-bonded sheets is still possible, but with the amide dipoles in one sheet rotated with respect to those in successive sheets, while in structures #6 and #7 the hydrogen bonding between chains in every second (i.e. antiparallel) sheet completely breaks down. It was this observation that led to the suggestion that antiparallel chains based on the same CRU may realize better packing as mirror images; in structures #8 through #10 are again realized the common pattern of correlated chain orientation and hydrogen bonded sheet formation. HT(A) Structures #8 and #9 bear a marked resemblance to the HT(P) Structure #2, and in turn to the PPTA Structure #4, differing primarily in the axial register between sheets. HT(A) Structure #10 exhibits the basic features found also in HT(P) Structure #4 and PPTA Structure #7.

Trends in Potential Energy: Considering these ten HT packing geometries in unison, we observe that the cohesive energy lies intermediate between that of the HHTT isomer geometries and that reported for the PPTA geometries:

$$E_{coh} = 36.2 \pm 1.3 \text{ kcal/mol}$$

The best cohesive energies are found in the HT(A) simulations, although within the margin of accuracy of the energy calculations both parallel and antiparallel packings may be considered feasible. The cohesive energy is roughly 93% of that for PPTA. Calculated densities range from 1.51 g/cm^3 up to 1.71 g/cm^3. The predicted Hildebrand solubility parameters are:

$$13.1 \text{ [cal/cm}^3\text{]}^{1/2} < \delta < 14.4 \text{ [cal/cm}^3\text{]}^{1/2}$$
$$26.7\times10^3 \text{ [J/m}^3\text{]}^{1/2} < \delta < 29.4\times10^3 \text{ [J/m}^3\text{]}^{1/2}$$

The decomposition of the interaction energy into its chain-to-chain contributions is presented in Tables 7.6(a) and (b), in the same manner as before, with identifiable "sheets" parallel to the bc crystallographic facet. Total energies of interaction within sheets range from 6 to 10 kcal/mol. Interactions between sheets vary from 4.5 to 10 kcal/mol depending upon the orientation of interaction. For intrasheet interactions, the trends in hydrogen-bond energies and percentage contributions from each set of moiety-moiety interactions are the same as in the HHTT cases. Contributions vary considerably for interactions between sheets. In both structure and distribution of cohesive forces, the HT isomers exhibit behaviors intermediate between those of PPTA and those of the substituted HHTT counterpart. The HT structures

Table 7.6a

Chain-to-chain bonding energies for 2,6-dichloro-PPTA: parallel head-to-tail polymorphs (all values in kcal/mole of dimer)

Cell ID	1	2	3	4
Cell type[a]	fc	fc	ec	p
ac-facet:				
total 12-6	0.3	0.2	6.1	2.9
total electrostatic	0.0	0.0	3.4	0.0
amide-amide elec.	0.0	0.0	2.8	-0.9
phenyl-phenyl elec.	0.0	0.0	-0.7	0.0
total	0.3	0.2	9.5	2.9
bc-facet:				
total 12-6	3.0	3.6	3.1	3.2
total electrostatic	4.5	4.4	4.7	4.0
amide-amide elec.	3.0	3.2	3.5	2.7
phenyl-phenyl elec.	0.7	0.7	0.7	0.9
total	7.5	8.0	7.8	7.2
diagonal:				
total 12-6	4.0	4.0	1.4	1.8
total electrostatic	3.5	1.6	-0.8	4.5
amide-amide elec.	1.6	1.2	-0.2	3.4
phenyl-phenyl elec.	0.2	0.6	-0.4	0.4
total	7.5	5.6	0.6	6.3

[a] Cell type identifies chain intersections with the ab-facet: fc indicates chains at [0,0] and [½,½]; ec indicates chains at [0,0] and [½,0]; p refers to a primitive cell with chains only at the corners. Intrasheet interactions are consistently in the bc-facet. Closest intersheet interactions are diagonal in the fc cell type but are in the ac-facet in the ec cell type; in the p cell type both types of interactions are intersheet in nature.

Table 7.6b

Chain-to-chain bonding energies for 2,6-dichloro-PPTA: antiparallel head-to-tail polymorphs
(all values in kcal/mole of dimer)

Cell ID	5	6	7	8	9	10
Cell type[a]	ec	ec	ec	fc	fc	ec
ac-facet:						
total 12-6	5.4	4.6	3.0	0.1	2.4	4.6
total electrostatic	4.6	4.1	3.8	0.0	0.0	2.2
amide-amide elec.	2.7	1.4	2.8	0.0	0.0	-1.0
phenyl-phenyl elec.	1.0	1.5	0.6	0.0	0.0	1.0
total	10.0	8.7	6.8	0.1	2.4	6.8
bc-facet:						
total 12-6	3.4	3.2	5.5	3.4	3.1	1.7
total electrostatic	4.1	3.8	4.3	6.5	4.4	4.4
amide-amide elec.	3.7	2.6	3.9	6.8	3.0	2.4
phenyl-phenyl elec.	0.4	0.9	0.4	0.9	0.7	0.2
total	7.5	7.0	9.8	9.9	7.5	6.1
diagonal:						
total 12-6	0.9	0.6	0.1	3.6	3.9	2.7
total electrostatic	-0.8	-0.2	0.2	0.9	3.1	4.9
amide-amide elec.	-0.4	-0.2	0.2	0.7	1.7	2.6
phenyl-phenyl elec.	-0.3	0.0	0.0	1.0	0.2	0.6
total	0.1	0.4	0.3	4.5	7.0	7.6

[a] Cell type identifies chain intersections with the ab-facet: fc indicates chains at [0,0] and [½,½]; ec indicates chains at [0,0] and [½,0]; p refers to a primitive cell with chains only at the corners. Intrasheet interactions are consistently in the bc-facet. Closest intersheet interactions are diagonal in the fc cell type but are in the ac-facet in the ec cell type; in the p cell type both types of interactions are intersheet in nature.

are more clearly perturbations of the unsubstituted polymer, and exhibit a multiplicity of forms. Both parallel and antiparallel arrangements of neighboring chains realize satisfactory cohesive energies. Again, lattice expansion appears to be the primary factor leading to reductions in total cohesive energy relative to the unsubstituted polymer. One may observe that the antiparallel structures are, on the average, roughly ¾ kcal/mol more stable that their parallel-oriented counterparts; however, the long range total dipole moments of the asymmetric chains appear to have relatively little effect at the local scale, where structure definition and stability are primarily determined. We may assert that, in this case of substitution for PPTA, monatomic substitution on every second ring of the chain is *sufficient to force expansion of the lattice*, but the low density of substitution and the specific features of ring orientation within the most probable structures, namely the misalignment of ring edges and the greater or lesser isolation of each modified ring from other modified rings, *preclude any specific interaction, steric or otherwise, which would alter properties anisotropically.*

In the absence of experimental data for direct comparison, and in consideration of the multiplicity of polymorphs for the substituted isomers, we shall not attempt to discuss at this point the calculated x-ray fiber diffraction patterns for the dichloro-substituted polymers. Such predictions have been made, however, and both tabulated intensities and recreated diffractograms are provided in Appendix E for reference purposes.

7.5 Prediction of Fiber Mechanical Properties

By analogy to the study described in Chapter 5 for the prediction of the elastic behavior of PPTA, we may simulate small scale deformation of the dichloro-substituted polymers in order to predict their mechanical behavior. For this purpose, we concentrate on five of the predicted geometries from the total of fourteen viable candidates. These were selected as follows: The first two, HHTT Structure #2 and HT(P) Structure #1, are the modified geometries for the two isomers which are analogous to the PPTA Structure #3 considered in depth in Chapter 5; these were selected for direct comparison to that important PPTA polymorph. The third, HHTT Structure #3, represents a packing geometry wherein the chains have been shifted to bring chlorine substituents on neighboring chains into closest proximity (see Figure 7.6(c)), where they are likely to have the greatest effect on mechanical properties. This structure was selected for comparison to the HHTT Structure #2. The last two, HT(A) Structures #5 and #6, describe packing geometries analogous to PPTA Structure #5 and the related Modification II; the two differ primarily in the axial register of the chlorine substituents between neighboring chains, with the substituents in closest proximity in HT(A) Structure #6 (see Figure 7.7(f)). A comparison of mechanical behavior for these two geometries should describe the largest difference to be observed in the HT isomers attributable to the placement of the monatomic ring substituents.

The modification of the chain description, the method of calculation, and the magnitudes of imposed deformations, were identical to those employed for PPTA and described in depth in Chapter 5. However, rather than generate the full twenty-one element compliance matrix, we concentrated on those elements necessary to determine the Voigt model fiber elastic constants. These are presented in Table 7.7(a) and 7.7(b) for the HHTT isomers and the HT isomers, respectively. In all five cases, the extensional moduli are of the same order of magnitude, ranging from 230 GPa up to 290 GPa. While this range still exceeds the estimated tensile modulus of the isolated chain, it is somewhat lower than the 290 to 370 GPa range of upper limits anticipated for the PPTA structures, indicative of a slight weakening of the load bearing capacity along the fiber axis. Based on the previous discussion, one may conjecture that this slight reduction is due primarily to changes in intermolecular packing interactions. Transverse moduli in the substituted structures HHTT #2 and HT(P) #1 tend to be 50% to 100% greater than the corresponding PPTA #3 transverse modulus. However, the alternate HHTT #3 allomorph involving proximate chlorines again exhibits a transverse modulus comparable to the PPTA value. A comparison of the HHTT structures #5 and #6, which differ primarily in the register between chlorine-modified rings, reveals almost identical sets of elastic constants for these two geometries. In all cases, the torsional moduli are consistently 2% to 5% of the extensional modulus; the absolute values of these moduli are comparable to those for PPTA. It appears that the introduction of chlorines as substituents on every other ring of the chain should have only a moderate effect on the mechanical behavior of the resulting fibers. The simulations suggest that the most likely effect is a slight reduction in the extensional modulus, but little or no change in the torsional modulus. The orientation of the dichloro-substituted rings in each structure appears to preclude the operation of the bulky chlorines as barriers to chain slip. As a result, one should expect to observe little change in shear deformation behavior from that seen previously in PPTA.

Table 7.7a

2,6-DiCl-PPTA HHTT theoretical fiber elastic constants (GPa): Structures #2 and #3

	Structure #2		Structure #3	
	Voigt	Predicted Range[a]	Voigt	Predicted Range[a]
Extensional Modulus (E_3)	288	279 - 228	258	250 - 204
Transverse Modulus (E_1,E_2)	45	44 - 35	20	19 - 15
Torsional Modulus (G_1,G_2)	12	12 - 9.5	13	13 - 10
Extensional Poisson's Ratio (ν_{13},ν_{23})	-0.12	-	0.33	-
Transverse Poisson's Ratio (ν_{12},ν_{21})	0.11	-	0.72	-

[a] after correction for entropic contributions.

Table 7.7b

2,6-DiCl-PPTA HT theoretical fiber elastic constants (GPa): Structures #1, #5 and #6

	Structure #1		Structure #5		Structure #6	
	Voigt	Predicted Range[a]	Voigt	Predicted Range[a]	Voigt	Predicted Range[a]
Extens. Mod (E_3)	232	225 - 183	275	268 - 217	252	244 - 199
Transv. Mod (E_1,E_2)	31	30 - 24	32	31 - 25	31	30 - 24
Tors. Mod (G_1,G_2)	9.4	9.1 - 7.4	7.3	7.1 - 5.8	8.0	7.8 - 6.3
Extens. Poisson's Ratio (ν_{13},ν_{23})	0.29	-	0.08	-	0.27	-
Transv. Poisson's Ratio (ν_{12},ν_{21})	0.36	-	0.39	-	0.49	-

[a] after correction for entropic contributions.

8. CONCLUSION

8.1 Summary

As was proposed at the outset of this work, we have attempted to take advantage of current computational capabilities and unique chemistries in order to address the issues of structure and property prediction relevant to the growing field of engineered polymeric materials. The materials selected for study were the para-linked aramids based on poly(p-phenylene terephthalamide) oriented in the solid state. The contents of this study may be summarized as follows:

(1) A complete methodology was developed for the geometric representation of a general ordered polymer structure composed of many polymer chains aligned along their helical or pseudohelical axes, the generation of requisite parameters for force field potentials, and exploration of the entire multivariate phase space in order to identify the structures of minimum potential energy in a densely packed solid state. The methods used are readily applicable to other helix-forming polymers through a simple change of repeat unit generation and force field calculation routines. The importance of helix imperfection and long range interatomic interactions have been addressed quantitatively. The method is based on atomic-scale considerations and requires no adjustable parameters

(2) Select thermodynamic and phenomenological characteristics, in particular the solid state cohesive energy, Hildebrand solubility parameter, and scattering of x-rays from fiber specimens, were generated deterministically from simulated structures. These predictive methods do not require or presume the availability of experimental data for the material in question, except to the extent that appropriate force field parameterizations may be deduced from data of low molecular weight analogues or other calculational procedures.

(3) The model was validated through application to the study of PPTA, a well-known stiff chain aramid. The results suggest the viability of a plurality of pseudocrystalline forms for PPTA. Predictions of cohesive energy density (39 $\pm$ 1 kcal/mole), Hildebrand solubility parameter (15.3 $[cal/cm^3]^{1/2} < \delta <$ 16.1 $[cal/cm^3]^{1/2}$), and x-ray scattering are in accord with expectations based on available data in the literature. Through a detailed analysis of the polymorphic forms, we are able to distinguish, prioritize, and quantify the features which lead to the development of ordered structure, or lack thereof.

(4) The model description was modified to enable deformation "experiments" of select pseudocrystalline polymorphs. The experiments account only for the potential energy contribution to the elastic stiffnesses, which is shown to overestimate moduli by 3% to 27%. We have calculated the complete twenty-one independent element elastic stiffness and compliance tensors for the general triclinic crystal. We have also predicted the complete set of conventional fiber elastic constants in the Voigt and Reuss limits. Finally, we have proposed a novel approach based on our knowledge of the complete material stiffness tensor for the single crystal to identify the orientation of least resistance to shear.

(5) The design of a fiber spinning apparatus suitable for the production of quality fibers from small (less than one gram) quantities of polymer is presented. The equipment described is suitable for temperature-controlled dry-jet wet spinning (or alternatively, of course, simple wet spinning) of polymer solutions in corrosive solvents up to 100°C, with postspin fiber treatments at temperatures up to 500°C. Representative fibers of PPTA were generated, along with data concerning die swell, draw ratio, and annealing effects in this process. The resulting fibers were analyzed by IR spectroscopy and WAXS for comparison with the model predictions.

(6) The simulation methodology was extended to the study of the effects of controlled atomic variation on solid state structure, cohesive energy density and solubility parameter, x-ray scattering, and mechanical property evaluation. Atomic substitution and the order of substitution along the chain contour were addressed using the regular head-to-head, tail-to-tail and head-to-tail isomers of the polyterephthalamides of 2,6-dichlorophenylene diamine. The results confirm the reduced cohesiveness of these modified pseudocrystalline structures, leading to the observed improvement of solubility in common solvents. Mechanical property predictions suggest that such substitutions should play a relatively minor role in the mechanical behavior of these fibers.

We conclude from this work that the methods of atomistic modelling are applicable to the prediction of detailed structure even in cases where the chemical complexity is considerable. The wealth of thermodynamic, phenomenological, and mechanical property information which may be anticipated by this method makes it especially attractive. Current limitations to applicability result primarily from the numerical difficulties associated with the highly convoluted potential energy hypersurface characteristic of the dense solid state and the limited accuracy in predicting small strain moduli.

8.2 Recommendations for Future Work

Based on our experience developed during the current work, a number of recommendations for improvements and extensions of the methods and ideas described herein may be proposed.

(1) Improvement of the efficiency of the search procedure for minima. To our knowledge, there is no theory or method currently available to guarantee a priori the identification of a *global* minimum; one may only identify a set of local minima, under the assumption that by means of a sufficiently comprehensive search procedure the global minimum is contained therein. However, it would be desireable to develop an "intelligent" search algorithm which recognizes the constraints of the independent parameter set and takes advantage of these to step past irrelevant local minima.

(2) The concepts of paracrystallinity are relevant to the study of crystallinity in polymers; it would be feasible to reformulate the structure generation procedures to incorporate distribution functions which describe distortions of the second kind. It may be possible to redescribe the polymorphism presented in this work in terms of a reduced number of structurally significant parameter distributions employing internal coordinates rather than Cartesian coordinates.

(3) It would be of further value to take advantage of the software and minimum potential energy packing geometries generated within this work to explore specific structure transformation processes such as ring flip motion, chain rotation about or translation parallel to the molecular axis, and deviation from perfect co-alignment of molecular axes. Such analyses could produce information about intermediate activated state geometries and energy barriers to transformation of particular interest to spectroscopic analyses.

(4) The method may be applied to more varied chemistries. The simulation procedure is especially valuable as a guide to proposing modified chemistries in that it can describe the structural changes that occur upon the introduction of chemical changes. Here we have only considered the most minor form of structural modification, the introduction of a larger monatomic species at regular points along the chain contour. Further interesting changes would include the study of random substitutions along the chain contour, the substitution of functional moieties which would force the introduction of a new intermolecular interaction, or introduction into the chain backbone of specific moieties which either reduce the stiffness of the main chain or create a fixed alteration of the chain helicity, which would break down the hydrogen bonded sheets and force the formation of a new set of intermolecular interactions. Specific examples, some of which are currently under pursuit, are the study of the effects of fixed chain twist, such as that found in MPIA, the characterization of solid state crosslinking in a system containing fusible rings, and the analysis of dopant retention in a crystalline polymer.

(5) The experimental apparatus and WAXS scattering procedures are readily applicable to the production of fibers of new materials; a program of experimental work would go hand in hand with the theoretical analysis of proposed new materials suggested by Point 4. Of immediate relevance to the results presented here would be the processing of regularly substituted dichloro-PPTA's into fiber for x-ray and structure analysis and comparison to simulation results. The means currently exist to produce the HHTT isomer with an order parameter of $s < 0.1$; this synthesis and processing effort is currently in progress and will be presented in a later publication. The dipole moment of the repeat unit of the 2,6-DiCl-PPTA isomer is on the order of 2.8 Debye, based on our AM1 calculations for p-(2,6-dichlorophenylene) diformamide. The simulation results presented here suggest the possibility for an electrically active polymer fiber containing parallel arrays of regular HT isomers of 2,6-DiCl-PPTA; Synthetic routes to the HT isomer of this polymer having order parameter $s > 0.9$ are currently under investigation;

(6) A final ambitious recommendation would be a study of the linkage between structure at the atomic scale addressed within this work and structure at the macromorphological scale tenfold or a hundredfold larger than the current simulation scale. Such an undertaking would require the consideration of the extent to which local structure determines long range structure and how kinetic processing parameters influence this determination. The fruits of such a study would include a more accurate predictive method for real mechanical properties and could lend new insight into the formation of macrofeatures in the bulk, such as microfibrils or periodic defect structures.

NOTATION

$\mathbf{a},\mathbf{b},\mathbf{c}$	real space continuation vectors for the crystallographic unit cell.	(Å)
$\mathbf{a}^*,\mathbf{b}^*,\mathbf{c}^*$	reciprocal space continuation vectors for the crystallographic unit cell.	($Å^{-1}$)
$\mathbf{A},\mathbf{B},\mathbf{C}$	lattice continuation vectors in the parallelopiped description.	(Å)
A,B,C	magnitudes of the lattice continuation vectors **A**, **B**, and **C**.	(Å)
A	Helmholtz free energy.	(kcal/mol)
$A_{ij,n}$	the generalized potential function multiplier	
$\mathbf{A_H}$, $\mathbf{B_H}$	helix rotation matrix and translation vector, as defined by Miyazawa et al., describing the helix conformation.	
C_{LMNK}	an element of the material stiffness tensor **C**.	(GPa)
C_ε	Specific heat of a solid at constant strain.	(kcal/mol/K)
d_h	helix pitch, or projected length of one repeat unit on the helix axis.	(Å)
d_{ch}	diameter of the molecular "cylinder".	(Å)
d_{ij}	the interatomic distance between i and j	(Å)
d^*	the critical crossover distance for the distance-dependent dielectric constant	(Å)
D_B	the bulk dielectric constant.	
D_R	the in-line draw-down ratio during fiber spinning, defined as the ratio of the linear velocity of the fiber at collection over the linear velocity at the spinnerette.	
$D_{orifice}$	the diameter of the spinnerette orifice.	(μm)
e_{LM}	an element of the engineering strain tensor **e**.	
E_i	elastic modulus.	(GPa)
E_{coh}	cohesive energy of a multichain geometry.	(kcal/mol)
E^{expl}	the total internal energy calculated in the explicit domain.	(kcal/mol)
E_l^{intra}	the intramolecular internal energy of chain *l*.	(kcal/mol)
$E_{l,l'}^{inter}$	the intermolecular internal energy between chains *l* and *l'*.	(kcal/mol)

$E^{lattice}$	the total internal energy calculated in the outer lattice domain, per repeat unit.	(kcal/mol)
E^{tot}	the total internal energy of a structure, per repeat unit.	(kcal/mol)
E^{unit}	the internal energy of the explicit domain, per repeat unit.	(kcal/mol)
f_i	the fractional translation in the lattice of chain i along its axis.	
$f_j(S)$	the atomic scattering factor for atom type j, which is a function of the length of the scattering vector S.	
F	the helix translation vector, akin to $\mathbf{B_H}$, employed in imposing helical symmetry.	(Å)
$F(S),F_{cr}(S)$	general and crystallographic x-ray structure factor based on atom positions.	
g_a, g_b	induction parameters, in reaction kinetics model for constitutional isomerism.	
G_i	shear modulus.	(GPa)
G(S)	crystallographic x-ray structure factor based on unit cell periodicity.	
G	real space metric tensor, defined by $\mathbf{H^TH}$.	
h	Planck constant (0.662×10^{-33} J·s).	(J·s)
h,k,*l*	Miller indices denoting the sets of crystallographic planes.	
H	coordinate transformation matrix for Cartesian to fractional coordinate systems.	
I_e	the intensity of x-rays scattered by an electron.	
$I(S),I_{cr}(S)$	calculated general and crystallographic intensities of scattered x-ray radiation, as functions of the scattering vector S.	
$I_{obs}(S)$	observed x-ray intensity.	
l_{ru}	the projected "length" of the repeat unit.	(Å)
l_i	the length of bond i.	(Å)
J_1, J_2, J_3	first, second, and third tensorial invariants.	
k	Boltzmann constant (8.31 J/mole·K).	(J/mole·K)
L(hk*l*)	Lorentz Factor for x-ray intensity correction for diffraction from a set of planes hk*l*.	
$L_{orifice}$	the capillary length of the spinnerette orifice.	(μm)
M_w	weight average molecular weight.	(g/mol)

M_{ru}	molecular weight of the repeat unit.	(g/mol)
N_A	Avogadro Number (6.022×10^{23}).	(mol^{-1})
N_{CRU}	the number of atoms in a conformational repeat unit (CRU).	
N_c	the number of independent chains on the lattice.	
N_i	the number of crystallographically unique atoms.	
N_p	the number of additive components of the total nonbonded potential description.	
N_r	the number of repeat units in the chain.	
O	octopole moment of an atomic moiety.	($Å^3$)
P	Pressure.	(Pa)
P(hk*l*)	the polarization factor for x-ray intensity correction for diffraction from a set of planes hk*l*.	
q_i	the partial atomic charge of atom i.	
Q	canonical partition function in statistical mechanics.	
r	relative reactivity of ends of an asymmetric monomer, used in reaction kinetics model for constitutional isomerism.	
r_i	the van der Waals radius of atom i.	(Å)
R_k,r_i	location vectors describing unit cell and atomic positions in an arbitrary frame of reference.	(Å)
s	the order parameter to describe constitutional isomerism.	
s_O,s	the paths of incident and scattered radiation, respectively.	
S	the scattering vector for incident radiation along the path s_O and radiation scattered along the path s.	
S	entropy.	(kcal/mol/K)
S_{LMNK}	an element of the material compliance tensor S.	(GPa^{-1})
T_H	the rotation matrix describing alignment of the helix axis of the polymer chain along the Cartesian z-axis.	
T	temperature.	(°C,K)
u	displacement vector of atomic coordinates describing deformation.	(Å)
U	internal energy.	(kcal/mol)
v_e	linear extrusion velocity of a filament during spinning.	(m/min)

v_w	linear collection, or wind-up, velocity of filament during spinning.	(m/min)
V, V_O	volume (eg. unit cell).	($Å^3$)
V_n	the generalized distance dependent potential function.	(kcal/mol)
V_p^*	the critical volume fraction for anisotropic phase formation.	
$\mathbf{W}_j$	the rotation matrix used to orient the polymer chain j about its center of gravity by means of the appropriate Euler angle rotations χ_j, ψ_j, and ω_j.	
$\hat{\mathbf{W}}$	the helix twist matrix employed in imposing helical symmetry in the lattice summation for potential energy.	
x	aspect ratio of a rigid rod molecule.	
$\mathbf{x}$	the eigenvector matrix for the radius of gyration tensor **H**	
X_n	degree of conversion during polymerizaton.	
$\mathbf{X}$	the vector of Cartesian coordinates for atoms.	(Å)
α,β,γ	real space interaxial angles for the crystallographic unit cell.	(degrees)
α_{PQ}	an element of the thermal expansion tensor α.	$(K)^{-1}$
β	the azimuthal angle of scattered radiation in x-ray scattering.	(degrees)
γ_w	shear rate at the wall of the spinnerette orifice in fiber spinning	(sec^{-1})
γ_{LM}	an element of the Grüneisen tensor γ.	
ζ,ν,τ	interaxial angles describing lattice continuation in the parallelepiped description.	(degrees)
δ	Hildebrandt solubility parameter.	$(cal/cm^3)^{1/2}$
ε_i	the Lennard-Jones potential well depth parameter for atom i.	(kcal/mol)
ε_O	the permittivity of a vacuum.	$(kcal \cdot Å/C^2)^{-1}$
ε_{LM}	an element of the material strain tensor ε.	
η_{inh}	inherent viscosity, approximated at 0.5g polymer per dl.	(dl/g)
θ	the scattering angle in x-ray diffraction, also referred to as half the Bragg angle 2θ.	(degrees)
ϑ_i	the complement of the bond angle at atom i-1, used in describing the location of atom i.	(degrees)
Θ_h	helix twist, or the amount of rotation about the helix axis occuring over one repeat unit.	(degrees)
Θ_E,Θ_D	Einstein and Debye temperatures, defined as $\nu_E h/k$ or $\nu_D h/k$.	(K)

Θ	quadrupole moment of an atomic moiety.	($Å^2$)
κ_T	isothermal compressibility.	(kcal/mol·m^3)
λ	wavelength of radiation.	(Å)
$\lambda_a,\lambda_b,\lambda_c$	summation coefficients along the lattice continuation vectors.	
$\lambda_1,\lambda_2,\lambda_3$	eigenvalues of the radius of gyration tensor Ξ of the finite chain segment.	(Å)
μ	elementary dipole moment of an atomic moiety.	(Å)
$\mu_{s,i}^2,\mu_s^2$	isotropic mean square displacement of atoms due to thermal vibration, for an atom i and universally for all atoms.	(cm^2)
μt	sample absorption in an x-ray beam, as the product of the linear absorption coefficient μ and the sample thickness t	
ν	vibrational frequency.	$(cm)^{-1}$
ν_E	characteristic frequency in the Einstein Approximation.	$(cm)^{-1}$
ν_D	characteristic frequency in the Debye Approximation.	$(cm)^{-1}$
ν_{ij}	Poisson's ratio.	
Ξ	the radius of gyration tensor for the finite chain segment.	(Å)
ρ	density.	(g/cm^3)
ρ_h	helix radius, defined at an arbitrary point on the helix.	(Å)
σ_{LM}	an element of the material stress tensor σ.	(GPa)
τ_w	shear stress at the wall of the spinnerette orifice in fiber spinning.	(Pa)
ϕ_i	the torsion angle between atoms i-2 and i-1, used in describing the location of atom i.	(degrees)
χ_i,ψ_i,ω_i	the Euler angles orienting chain i on the lattice.	(degrees)
X,Ψ,Ω	the Euler angles describing the crystallite orientation	(degrees)

ABBREVIATIONS

AM1	Austin Model 1. AMPAC version available through the Department of Chemistry, Indiana University, Bloomington, Indiana, 47405, QCPE Program #506.
Cl-PPTA	generic reference to chlorine-modified versions of poly(p-phenylene terephthalamide)
CNDO	Complete Neglect of Differential Overlap quantum mechanics package
CPU	Central Procesing Unit
CRU	Conformational Repeat Unit
DP	Degree of Polymerization
HHTT	Constitutional isomer of head-to-head, tail-to-tail alignment of repeat units
HT	Constitutional isomer of head-to-tail alignment of repeat units
IR	Infrared spectroscopy
MNDO	Modified Neglect of Differential Overlap quantum mechanics package
MPIA	Poly(m-phenylene isophthalamide)
PBA	Poly(benzamide)
PE	Polyethylene
PPTA	Poly(p-phenylene terephthalamide)
PP-2,6-DiCl-TA	Poly(p-phenylene 2,6-dichloroterephthalamide)
2,6-DiCl-PPTA	Poly(2,6-dichloro-p-phenylene terephthalamide)
PVC	Poly(vinylchloride)
VFF	Valence Force Field
WAXS	Wide Angle X-ray Scattering

REFERENCES

[1] Adams, W.W.; Eby, R.K. *MRS Bulletin* **1987**, Nov.16/Dec.31, 22.

[2] Alexander, L.E. *X-Ray Diffraction Methods in Polymer Science*, Wiley-Interscience: New York, 1969.

[3] Allcock, H.R.; Lampe, F.W. *Contemporary Polymer Chemistery*, Prentice-Hall: New Jersey, 1981.

[4] Allegra, G.; Benedetti, E.; Pedone, C. *Macromolecules* **1970**, *3*, 727.

[5] Allen, S.R. *Polymer* **1988**, *29*, 1091.

[6] Anand, J.N. *J. Macromol. Sci.-Phys.* **1967**, *B1*, 3, 445.

[7] Aoki, H.; Coffin, D.R.; Hancock, T.A.; Harwood, D.; Lenk, R.S.; Fellers, J.F.; White, J.L. *J. Polym. Sci.: Polym. Symp. 65*, 1978, 29.

[8] Aoki, H.; Onogi, Y.; White, J.L.; Fellers, J.F. *Polym. Eng. and Sci.* **1980**, *20*, 3, 221.

[9] Arpin, M.; Strazielle C.; Weill, G.; Benoit, H. *Polymer* **1977**, *18*, 262.

[10] Arpin, M.; Strazielle, C. *Polymer* **1977**, *18*, 591.

[11] Arridge, R.G.C. *An Introduction to Polymer Mechanics*, Taylor and Francis: London, 1985.

[12] Bair, T.I.; Morgan, P.W.; Killain, F.L. *Macromolecules* **1977**, *10*, 6, 1396.

[13] Balbi, C.; Bianchi, E.; Ciferri, A.; Tealdi, A. *J. Polymer Sci, Polymer Phys. Ed.* **1980**, *18*, 2037.

[14] Barton, R. *J. Macromol. Sci.-Phys.* **1985-1986**, *B24*, 119.

[15] Battaglia, M; Buckingham, A.D.; Williams, J.H. *Chem. Phys. Lett.* **1981**, *78*, 421.

[16] Bernstein, J.; Hagler, A.T. *J. Amer. Chem. Soc.* **1978**, *100*, 673.

[17] Blades, H., U.S. Patent 3767756, Oct. 23 1973.

[18] Blades, H., U.S. Patent 3869430, Mar. 4 1975.

[19] Block, H.; Walker, S.M. *Chem. Phys. Let.* **1973**, *19*, 363.

[20] Bondi, A., *Physical Properties of Molecular Crystals, Liquids, and Glasses*, John Wiley and Sons: New York, 1968.

[21] Boon, J.; Magré, E.P. *Makromol. Chemie* **1970**, *136*, 267.

[22] Brant, D.A.; Flory, P.J. *J. Amer. Chem. Soc.* **1965**, *87*, 2791.

[23] Brisson, J.; Brisse, F. *Macromolecules* **1986**, *19*, 2632.

[24] Carazzolo, G.A. *J. Polym. Sci.:A-1* **1963**, *1*, 1573.

[25] Chatzi, E.G.; Koenig, J.L. *Polym.-Plast. Technol. Eng.* **1987**, *26*, 3&4, 229.

[26] Chung, T. *J. Polym. Sci.: Polymer Let.* **1986**, *24*, 299.

[27] Conio, G.; Bruzzone, R.; Ciferri, A.; Bianchi, E.; Tealdi, A. *Polymer J.* **1987**, *19*, 757.

[28] de Wolff, P.M. *J. Polymer Sci.* **1962**, *60*, S34.

[29] Dobb, M.G.; Johnson, D.J.; Saville, B.P. *J. Polymer Sci: Polymer Symp. 58* **1977**, 237.

[29] Dobb, M.G.; Johnson, D.J.; Saville, B.P. *J. Polym. Sci.: Polym. Phys.* **1977**, *15*, 2201.

[30] English, A.D. *J. Polym. Sci.: Polym. Phys.* **1986**, *24*, 805.

[31] Erman, B.; Flory, J.P.; Hummel, J.P. *Macromolecules* **1980**, *13*, 484.

[32] Fielding-Russell, G.S. *Text. Res. J.* **1971**, *41*, 861.

[33] Fletcher, R.A. AERE Report No. R-7125, Harwell, England; Subroutine VA10A in Harwell Subroutine Library, 1972, Harwell, England.

[34] Flory, P.J. "Molecular Theory of Liquid Crystals", *Advances in Polymer Science 59*, Academic Press, 1984.

[35] Flory, P.J.; Ronca, G. *Mol. Cryst. Liq. Cryst.* **1979**, *54*, 289.

[36] Flory, P.J.; Ronca, G. *Mol. Cryst. Liq. Cryst.* **1979**, *54*, 311.

[37] Flory, P.J. *Proc. Roy. Soc. London* **1956**, *A 234*, 60.

[38] Flory, P.J. *Statistical Mechanics of Chain Molecules*; Interscience: New York, 1969; Chapter 1.

[39] Gado, J.E. "Constitutional Isomerism in Aromatic Polyamides", MS thesis, Massachusetts Institute of Technology, Cambridge, Massachusetts, 1985.

[40] Galiotis, C.; Robinson, I.M.; Young, R.J.; Smith, B.J.E.; Batchelder, D.N. *Polymer Communications* **1985**, *26*, p354.

[41] Gardner, K.H.; Matheson, R.R.; Avakian, P.; Chia, Y.T.; Gierke, T.D., *Polymers for Fibers and Elastomers*, Arthur, J.C., ed., American Chem. Soc., Washington D.C., 1984, 91.

[42] Gaymans, R.J.; Tijssen, J.; Harkema, S.; Bantjes, A. *Polymer* **1976**, *17*, 517.

[43] Gentile, F.T. "Consitutional Isomerism in Liquid Crystalline Polyamides", PhD thesis, Massachusetts Institute of Technology, Cambridge, Massachusetts, 1988.

[44] Gramlich, V. in *X-Ray 76, Diffraction Meeting Oxford Proceedings* **1976**. Paper PII64, 531.

[45] Gray, C.G.; Gubbins, K.E. *Theory of Molecular Fluids, Volume 1: Fundamentals*, Clarendon Press:Oxford, 1984.

[46] Hagler, A.T.; Huler, E.; Lifson, S. *J. Am. Chem. Soc.* **1974**, *96*, 5319.

[47] Hagler, A.T.; Bernstein, J. *J. Amer. Chem. Soc.* **1978**, *100*, 6349.

[48] Hancock, T.A.; Spruiell, J.E.; White, J.L. *J. Appl. Polym. Sci.* **1977**, *21*, 1227.

[49] Haraguchi, K.; Kajiyama, T.; Takayanagi, M. *J. Appl. Polym. Sci.* **1979**, *23*, 903.

[50] Haraguchi, K.; Kajiyama, T.; Takayanagi, M. *J. Appl. Polym. Sci.* **1979**, *23*, 915.

[51] Hindeleh, A.M.; Halim, N.A.; Ziq, K.A. *J. Macromol. Sci.-Phys.* **1984**, *B23*, 3, 289.

[52] Hopfinger, A.J.; Walton, A.G. *J. Macromol. Sci.-Phys.* **1969**, *B3*, 195.

[53] Hosemann, R. and Bagchi, S.N., *Direct Analysis of Diffraction by Matter*, North-Holland Publ. Co.: Amsterdam, 1962.

[54] Hummel, J.P.; Flory, J.P. *Macromolecules* **1980**, *13*, 479.

[55] Ii, T.; Tashiro, K.; Kobayashi, M.; Tadokoro, H. *Macromolecules*, *19*, 7, **1986**, 1772.

[56] Ii, T.; Tashiro, K.; Kobayashi, M.; Tadokoro, H., *Macromolecules* **1986**, *19*, 7, 1809.

[57] Ii, T; Tashiro, K.; Kobayashi, M.; Tadokoro, H. *Macromolecules* **1987**, *20*, 2, 347.

[58] *International Tables for X-Ray Crystallography*, Volume III: Physical and Chemical Tables, K. Lonsdale, ed., The International Unionof Crystallography, Kynoch Press: Birmingham, 1968.

[59] Jadhav, J.Y.; Krigbaum, W.R.; Preston, J. *Macromolecules* **1988**, *21*, 2, 538.

[60] Jaffe, M. *Polymer Preprints* **1978**, *19*, 1, 355.

[61] Jaffe, M.; Jones, R.S. "High Performance Aramid Fibers", *Handbook of Fiber Science and Technology: Volume III*, Lewin, M. and Preston, J., eds., Marcel Decker Inc.: New York, 1985, 349.

[62] Jaffe, M. "High Modulus Polymers", *Encyclopedia of Polymer Science and Engineering*, Mark, H.F, Bikales, N.M., Overberger, C.G., Menges, G., and Kroschwitz, J.I., eds., Volume 7, Wiley Interscience: New Jork, 1987, 699.

[63] Jorgensen, W.L.; Swenson, C.J. *J. Amer. Chem. Soc.* **1985**, *107*, 569.

[64] Kim, B.C.; Hwang, S.S.; Kim, K.U. *Intern. Polym. Processing* **1987**, *2*, 1.

[65] Knoff, W.E. *J. Mat. Sci. Lett.* **1987**, *6*, 1392.

[66] Korshak, V.V.; Vinogradova, S.V.; Vasnev, V.A.; Markova, G.D.; Lecae, T.V. *J. Polymer Sci.* **1975**, *13*, 2741.

[67] Kwolek S., U.S. Patent 3671542, June 20 1972.

[68] Kwolek, S,L.; Morgan, P.W.; Schaefgen, J.R.; Gulrich, L.W. *Macromolecules* **1977**, *10*, 6, 1390.

[69] Kwolek, S; Memeger, W.; Van Trump, J.E. *Int. Symp. on Polymers for Adv. Tech.*, Lewin, M., ed., Int. Union of Pure and Appl. Chem., 1987, 421.

[70] Ladell, J.; Post, B. *Acta. Cryst.* **1974**, *7*, 559.

[71] Larson, R.G. *Constitutive Equations for Polymer Melts and Solutions*; Butterworths: Boston, 1988.

[72] Lauprêtre, F.; Monnerie, L. *Europ. Polymer J.* **1978**, *14*, 415.

[73] Lenk, R.S.; White, J.L.; Fellers, J.F., *J. Appl. Polym. Sci.*, *21*, 1977, 1543.

[74] Lifson, S.; Warshel, A. *J. Chem. Phys.* **1968**, *49*, 5116.

[75] Lifson, S.; Hagler, A.T.; Dauber, P. *J. Am. Chem. Soc.* **1979**, *101*, 5111.

[76] Ludovice, P.J. "Static and Dynamic Atomistic Level Modelling of Polymeric Glasses", PhD thesis, Massachusetts Institute of Technology, Cambridge, Massachusetts, 1989.

[77] Ludovice, P.J.; Suter, U.W. *Polymer Preprints* **1987**, *28*, 295.

[78] Maitland, G.C.; Rigby, M.; Smith, E.B.; Wakeham, W.A. *Intermolecular Forces: Their Origin and Determination*; Clarendon Press: Oxford, 1981.

[79] Mansfield, K.F.; Theodorou, D.N. *Polymer Preprints* **1989**, *30*, 2, 76.

[80] McCullough, R.L. *J. Macromol. Sci.-Phys.* **1974**, *B9*, 97.

[81] McQuarrie D.A. *Statistical Mechanics*, Harper and Row: New York, 1976.

[82] Middleman, S. *Fundamentals of Polymer Processing*, McGraw-Hill: New York 1977, p236.

[83] Millaud, B.; Strazielle, C. *Makromol. Chem.* **1978**, *179*, 1261.

[84] Miyazawa, T. *J. Polymer Sci.* **1961**, *55*, 215.

[85] Moncrieff, R.W. *Man-Made Fibers*, John Wiley & Sons: New York, 1963.

[86] Montgomery, D.E. "The Production and Properties of Some High Performance Synthetic Fibres", PhD thesis, University of Bradford, 1971.

[87] Moore, F.H. *Acta Cryst. Short Communications* **1963**, *16*, 1169.

[88] Morgan, P.W. *Macromolecules*, *10*, 6, 1977, 1381.

[89] Morgan, P.W.; Fletcher, T.C., U.S. Patent 3869419, Mar. 4 1975.

[90] Morgan, P.W. *J. Polym. Sci.: Polym. Symp. 65*, **1978**, 1.

[91] Morgan, P.W.; Pletcher, T.C.; Kwolek, S.L. "Aromatic Azomethine Polymers and Fibers", *Polymers for Fibers and Elastomers*, J.C. Arthur, ed., American Chemical Society, Washington D.C., 1984.

[92] Morgan, R.J.; Mones, E.T.; Steele, W.J.; Deutscher, S.B. *Polymer Preprints* **1980**, *21*, 2, 264.

[93] Morgan, R.J.; Pruneda, C.O.; Steele, W.J. *J. Polym. Sci.: Polym. Phys.* **1983**, *21*, 1757.

[94] Morgan, R.J.; Allred, R.E. *Reference Book for Composites Technology*, Lee, S.M., ed., (in press).

[95] Murano, M. *Polymer J.* **1972**, *3*, 6, 663.

[96] Napolitano, R. *Macromolecules* **1988**, *21*, 622.

[97] Napolitano, R.; Pirozzi, B.; Tuzi, A. *Eur. Polym. J.* **1988**, *24*, 103.

[98] Northolt, M.G. *Europ. Polymer. J.* **1974**, *10*, 799.

[99] Northolt, M.G.; Van Aartsen, J.J. *J. Polym. Sci.:Polym. Symp. 58* **1977**, 283.

[100] Ooi, T.; Scott, R.A.; Vanderkooi, G.; Scheraga, H.A. *J. Chem. Phys.* **1967**, *46*, 4410.

[101] Panar, M.; Beste, L.F. *Macromolecules* **1977**, *10*, 6, 1401.

[102] Panar, M.; Avakian, P.; Blume, R.C.; Gardner, K.H.; Gierke, T.D.; Yang, H.H. *J. Polymer Sci.: Polymer Phys.* **1983**, *21*, 1955.

[103] Papkov, S.P.; Kulichikhin, V.G.; Kalmykova, V.D.; Malkin, A.YA. *J. Polym. Sci.: Polym. Phys.* **1974**, *12*, 1753.

[104] Penn, L.; Newey, H.A.; Chiao, T.T. *J. Mater. Sci.* **1976**, *11*, 190.

[105] Penn, L.; Larsen, F. *J. Appl. Polym. Sci.* **1979**, *23*, 59.

[106] Pertsin, A.J.; Kitaigorodsky, A.I. *The Atom-Atom Potential Method*; Cardona, M., Ed.; Springer Series in Chemical Physics 43; Springer-Verlag:Berlin, 1987.

[107] Pino, P.; Lorenzi, G.P.; Suter, U.W.; Casartelli, P.G.; Steinmann, A.; Bonner, F.J.; Quiroga, J.A. *Macromolecules* **1978**, *11*, 3, 624.

[108] Preston, J.; Hofferbert, W.L. *J. Polym. Sci.: Polym. Symp. 65*, **1978**, 13.

[109] Preston, J. "Polyamides, Aromatic" in *Encyclopedia of Polymer Science and Engineering*; Wiley-Interscience: New York, 1987, 381.

[110] Prevorsek, D.C. "Recent Advances in High-Strength Fibers and Composites", *Polymer Liquid Crystals*, Ciferri, Krigbaum, and Meyers, eds., **1982**, 329.

[111] Prince, E. *Mathematical Techniques in Crystallography and Materials Science*, Springer-Verlag: Berlin, 1982.

[112] Ramachandran and Mitra, *J. Mol. Biol.* **1976**, *197*, 85.

[113] Saruyama, Y. *J. Chem. Phys.* **1985**, *83*, 413.

[114] Saruyama, Y.; Miyaji, H. *J. Polym. Sci.: Polym. Phys.* **1985**, *23*, 1637.

[115] Schaefgen, J.R.; Bair, T.I.; Ballou, J.W.; Kwolek, S.L.; Morgan, P.W.; Panar, M.; Zimmerman, J. "Rigid Chain Polymers: Properties and Solutions and Fibres", *Ultra-High Modulus Polym.*, Meeting date 1977, ed. Ciferri, A., Ward, I.M., Appl. Sci.: Barking, England (1979), 173.

[116] Schmucki, M.; Pino, P.; Suter, U.W. *Macromolecules* **1985**, *18*, 823.

[117] Schroeder, R.; Lippincott, E.R. *J. Phys. Chem.* **1957**, *61*, 921.

[118] Scott, R.A.; Scheraga, H.A. *J. Chem. Phys.* **1966**, *45*, 2091.

[119] Scott, R.A.; Scheraga, H.A. *J. Chem. Phys.* **1966**, *44*, 3054.

[120] Slonim, Y.; Vasnev, V.A.; Bulai, A.K.; Urman, Y.G.; Markova, G.D.; Korshak, V.V.; Vinogradova, S.V. *Vysokomol. soyed.* **1980**, *A22*, 12, 2792.

[121] Sorensen, R.A.; Liau, W.B.; Boyd, R.H. *Macromolecules* **1988**, *21*, 194.

[122] Sorensen, R.A.; Liau, W.B.; Kesner, L.; Boyd, R.H. *Macromolecules* **1988**, *21*, 200.

[123] Steinman, A.; Arber, W.; Schmucki, M.; Suter, U.W.; Lorenzi, G.P.; Pino, P. *Int. Symp. Macromol. Chem. Preprints* **1981**, *1*, 103.

[124] Sugeta, H.; Miyazawa, T. *Biopolymers* **1967**, *5*, 673.

[125] Suter, U.W. *J. Amer. Chem. Soc.* **1979**, *101*, 6481.

[126] Suter, U.W.; Pino, P. *Macromolecules* **1984**, *17*, 2248.

[127] Suter, U.W.; Pino, P. *Macromolecules* **1984**, *17*, 2248.

[128] Tadokoro, H. *Structure of Crystalline Polymers*, Wiley-Interscience: New York, 1979.

[129] Tashiro, K.; Kobayashi, M.; Tadokoro, H. *Macromolecules* **1977**, *4*, 731.

[130] Tashiro, K.; Kobayashi, M.; Tadokoro, H. *Macromolecules* **1977**, *10*, 413.

[131] Tashiro, K.; Kobayashi, M.; Tadokoro, H. *Macromolecules* **1978**, *11*, 908.

[132] Tashiro, K.; Kobayashi, M.; Tadokoro, H. *Macromolecules* **1978**, *11*, 914.

[133] Tashiro, K.; Tadokoro, H. *Macromolecules* **1981**, *14*, 781.

[134] Theodorou, D.N. "Molecular Modelling of Polymeric Glasses", PhD thesis, Massachusetts Institute of Technology, Cambridge, Massachusetts, 1985.

[135] Theodorou, D.N.; Suter, U.W. *Macromolecules* **1985**, *18*, 1206.

[136] Theodorou, D.N.; Suter, U.W. *Macromolecules* **1985**, *18*, 1467.

[137] Theodorou, D.N.; Suter, U.W. *Macromolecules* **1986**, *19*, 139.

[138] Tripathy, S.K.; Hopfinger, A.J.; Taylor, P.L. *J. Phys. Chem.* **1981**, *85*, 1371.

[139] Tsvetkov, V.N. *Polym. Sci. USSR* **1977**, *19*, 2485.

[140] Tsvetkov, V.N.; Shtennikova, I.N. *Macromolecules* **1978**, *11*, 2, 306.

[141] Valenti, B.; Alfonso, G.C.; Ciferri, A.; Giordani, P. *J. Appl. Polym. Sci.* **1981**, *26*, 3643.

[142] Van Krevelen, D.W. *Properties of Polymers*; Elsevier: New York, 1972, p88.

[143] Ward, I.M. *Mechanical Properties of Solid Polymers*, 2nd Edition, Wiley-Interscience: Chichester, 1983.

[144] Warshel, A.; Lifson, S. *J. Chem. Phys.* **1970**, *53*, 582.

[145] Weeks, J.J; Clark, E.S., and Eby, R.K. *Polymer* **1981**, *22*, 1480.

[146] Weiner, J.H. *Statistical Mechanics of Elasticity*, Wiley-Interscience: New York, 1983.

[147] White, J.L.; Fellers, J.F. *J. Appl. Polym. Sci.: Appl. Polym. Symp. 33* **1978**, 137.

[148] Wilfong, R.E.; Zimmerman, J. *J. Appl. Polym. Sci.: Polym. Sci. Symp. 31* **1977**, 1.

[149] Zero, K.; Aharoni, S.M. *Macromolecules* **1987**, *20*, 1957.

APPENDIX A: Helix Representation of Chain Conformation

The helix described entirely in terms of internal bond coordinates may be fairly simple or severely convoluted within a single helical repeat distance and there is no constraint on the rationality of the helix. We derive the corresponding helix rotation matrix $\mathbf{A_H}$ and translation vector $\mathbf{B_H}$ of Miyazawa and Sugeta [Miyazawa, 1961; Sugeta and Miyazawa, 1967] from our earlier generator matrices:

$$\mathbf{A_H} = \mathbf{Y_k}\,\mathbf{Y_j}^{-1} \tag{A.1}$$

$$\mathbf{B_H} = \mathbf{Y_k}\begin{bmatrix}0\\0\\0\\1\end{bmatrix} - \mathbf{Y_j}\begin{bmatrix}0\\0\\0\\1\end{bmatrix} \tag{A.2}$$

where:

$$\mathbf{Y_j} = \mathbf{A_1}\,\mathbf{A_2} \ldots \mathbf{A_{j-1}} \tag{A.3}$$

$$\mathbf{Y_k} = \mathbf{A_1}\,\mathbf{A_2} \ldots \mathbf{A_{j-1}}\mathbf{A_j} \ldots \mathbf{A_{k-1}} \tag{A.4}$$

such that:

$$\mathbf{X_k}^1 = \mathbf{A_H}\;\mathbf{X_j}^1 + \mathbf{B_H} \tag{A.5}$$

$$\mathbf{X_j}^1 = \mathbf{A_H}^T\,\mathbf{X_k}^1 - \mathbf{B_H} \tag{A.6}$$

j and k are the corresponding atoms in two successive conformational repeat units m and m+1, and j is greater than or equal to 3.

From $\mathbf{A_H}$ and $\mathbf{B_H}$ one can calculate the three helix parameters for a uniform, nondegenerate helix and the rotation matrix required to align the helix axis with the z-axis.

$$\mathbf{C} = (\mathbf{A_H}^T - \mathbf{E_4})\mathbf{B_H} \tag{A.7}$$

$$\mathbf{C'} = (\mathbf{E_4} - \mathbf{A_H})\mathbf{B_H} \qquad (\mathbf{E_S} \text{ is the identity matrix of order S}) \tag{A.8}$$

$$B = (\mathbf{B_H}^T\,\mathbf{B_H})^{1/2} \tag{A.9}$$

$$C = (\mathbf{C}^T\,\mathbf{C})^{1/2} \tag{A.10}$$

from which it follows that: (refer to Figure A.1)

Figure A.1: Definition of the vectors **B**, **B'**, **B"**, C, and C' and the helical parameters ρ and Θ (after Sugeta and Miyazawa [1967]).

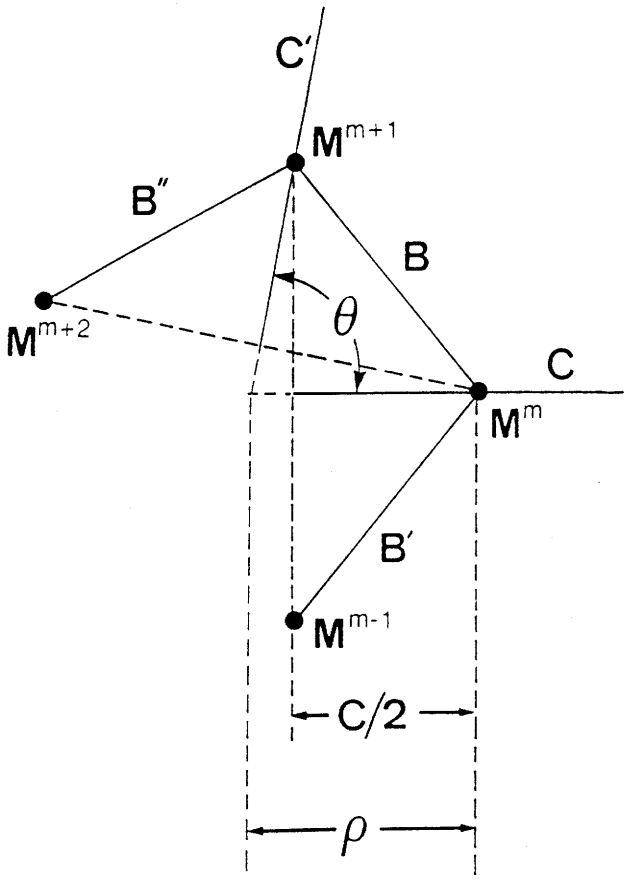

$$\cos\Theta_h = (\mathbf{C}^T\ \mathbf{C}')/C^2 \quad (A.11)$$

$$\rho_h = \tfrac{1}{2}C/(1-\cos\Theta_h) \quad (A.12)$$

$$d_h = \mathbf{B_H}(\mathbf{C}^T\ \mathbf{C}')/(C^2\sin\Theta) \quad (A.13)$$

and then:

$$\mathbf{X}_i^h = \mathbf{T_H}\ \mathbf{X}_i^1 + \mathbf{D} \quad (A.14)$$

where

$$\mathbf{D} = \begin{bmatrix} \rho_h & 0 & 0 \end{bmatrix} \quad (A.15)$$

$$\mathbf{T_H} = \begin{bmatrix} e_1(x) & e_1(y) & e_1(z) \\ e_2(x) & e_2(y) & e_2(z) \\ e_3(x) & e_3(y) & e_3(z) \end{bmatrix} \quad (A.16)$$

$$\mathbf{e}_1 = \mathbf{C}/C \quad (A.17)$$

$$\mathbf{e}_2 = \mathbf{e}_3^T\ \mathbf{e}_1 \quad (A.18)$$

$$\mathbf{e}_3 = (\mathbf{C}^T\ \mathbf{C}')/C^2\sin\Theta_h \quad (A.19)$$

For the special case where $\Theta=180°$, one must substitute an alternative calculation for the pitch and for a section of the orientation matrix:

$$\mathbf{B_H}^* = (\mathbf{A_H} + \mathbf{E})\mathbf{B_H} \quad (A.20)$$

$$d_h = \tfrac{1}{2}\,|\,\mathbf{B_H}^*\,| \quad (A.21)$$

$$\mathbf{e}_3 = \tfrac{1}{2}\,\mathbf{B_H}^*/d_h \quad (A.22)$$

However, in applications involving finite chain lengths, this helical coordinate conversion encounters a singularity in radius ρ_h for the degenerate straight rod helix ($\Theta_h=0$, $C=0$). This singularity produces a discontinuity in helix alignment, whereby conformations infinitesimally displaced from the straight rod become sections of infinitely large spirals, with the result that alignment is rotated by 90° in space. To surmount this numerical problem, we have chosen to substitute in this vicinity of parameter space a coordinate transformation which approximates the helix axis with the major axis of the radius of gyration tensor for the finite chain segment, with a transition between the two transformations at a finite value of

Θ_h. The radius of gyration tensor for the finite chain segment is calculated using only the coordinates of the "backbone" atoms, i.e. those carbon and nitrogen atoms which lie on the backbone bond (and virtual bond) contour of the chain. For a segment containing N_i such atoms, the elements of the radius of gyration tensor are calculated simply by:

$$\Xi_{jk} = \sum_{i=1}^{N_i} (\mathbf{e}_j \cdot \mathbf{r}_i)(\mathbf{e}_k \cdot \mathbf{r}_i)/N_i - \sum_{i=1}^{N_i} (\mathbf{e}_k \cdot \mathbf{r}_i)/N_i \sum_{i=1}^{N_i} (\mathbf{e}_k \cdot \mathbf{r}_i)/N_i \quad \text{(A.23)}$$

Here, $\mathbf{e}_j$ is a coordinate axis unit vector, where j and k take the values 1, 2, and 3, corresponding to the Cartesian x-, y- and z-axes of the real space coordinate system. Diagonalization of Ξ by successive Jacobi transformations yields the eigenvalues (λ_1, λ_2, and λ_3) of this tensor, which correspond to the magnitudes of the principle axes of the chain segment, and the matrix x of eigenvectors, which correspond to the unit vectors of the principle axes. The principle axes are sorted such that $\lambda_3 > \lambda_1 > \lambda_2$ to yield the rotation matrix $\mathbf{T_H} = \mathbf{x}^T$. The helix is centered and aligned such that its primary axis lies along the Cartesian z-axis and the secondary axis lies in the Cartesian xz-plane:

$$\mathbf{X}_i = \mathbf{T_H} \left(\mathbf{r}_i - \sum_{i=1}^{N_i} (\mathbf{e} \cdot \mathbf{r}_i)/N_i \right) \quad \text{(A.24)}$$

This approximation allows the model to handle all cases of chain conformation in a numerically continuous manner for finite chains segments of sufficient length. However, it may readily be seen that the above transformation of coordinates is dependent upon N_i, or the length of the chain segment; this dependence becomes less sensitive as N_i increases for segments which are rodlike in conformation, since λ_3 increases faster than either λ_1 or λ_2. It does not, of course, ensure perfect alignment of the near-rod helices along their true propagation axes except in the limit of extremely large N_i.

Individual chains are characterized by their local Cartesian frames of reference, defined by the helix axis (or the longest principle axis of the radius of gyration) along the z-axis, the first amide bond plane (or the second longest principle axis) in the xz-plane, and the y-axis chosen to form a right-handed orthonormal coordinate system. The chain may then be oriented in general by application of three rotations, χ, ψ, and ω, about the z-axis (counterclockwise), the y'-axis (clockwise), and the z"-axis (counterclockwise), respectively, as shown in Figure A.2. The necessary rotation matrix **W** by this definition is as follows:

$$\mathbf{W} = \mathbf{W}_{\omega}\ \mathbf{W}_{\psi}\ \mathbf{W}_{\chi} \tag{A.25}$$

$$\mathbf{W}_{\chi} = \begin{bmatrix} \cos\chi & -\sin\chi & 0 \\ \sin\chi & \cos\chi & 0 \\ 0 & 0 & 1 \end{bmatrix} \tag{A.26}$$

$$\mathbf{W}_{\psi} = \begin{bmatrix} \cos\psi & 0 & -\sin\psi \\ 0 & 1 & 0 \\ \sin\psi & 0 & \cos\psi \end{bmatrix} \tag{A.27}$$

$$\mathbf{W}_{\omega} = \begin{bmatrix} \cos\omega & -\sin\omega & 0 \\ \sin\omega & \cos\omega & 0 \\ 0 & 0 & 1 \end{bmatrix} \tag{A.28}$$

which, when multiplied as shown in Equation A.25, yield the rotation matrix given by Equation 3.10.

Figure A.2: Definition of Euler angles for orientation of a chain about its center of gravity.

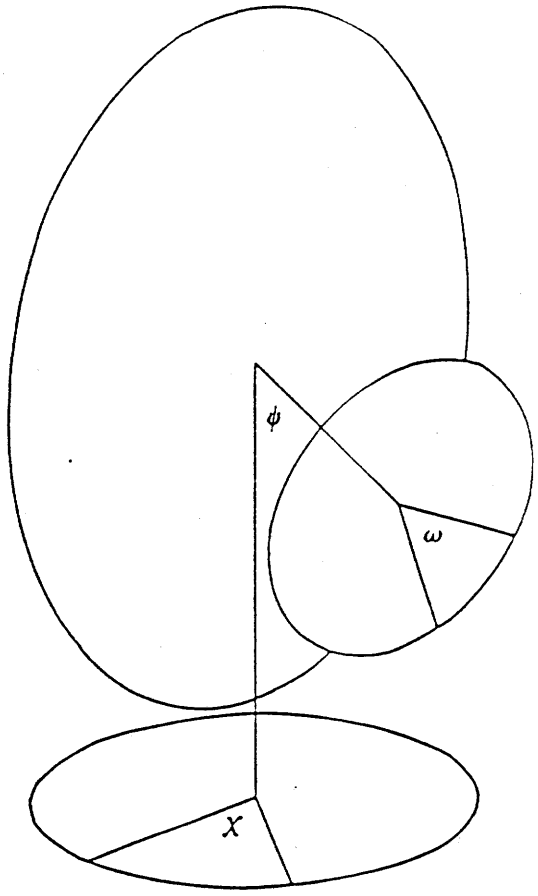

APPENDIX B: Summation Representation of a Periodic Structure and Convergence of Terms

Lattice Summation In general, for a force field of the type described below, with p terms of inverse power m(p) in distance:

$$E = \sum_{p} A_p \, (1/d)^{-m(p)} \tag{B.1}$$

one may write the total energy of interaction of one atom i with an entire lattice of N_j atoms of type j in the form:

$$E_{i=1,j} = \sum_{j} \sum_{p} A_p \, (1/d_{i=1,j})^{-m(p)} \tag{B.2}$$

In general, for a periodic lattice described in three dimensions by the periodicity vectors **a**, **b**, and **c**, the interatomic distance may be described by the lattice point (h,k,*l*) and the vector $\mathbf{d_O}$ locating the j lattice relative to the atom i=1:

$$\mathbf{d}_{1,j}^{\,2} = (\mathbf{d}_{1,j}{}^{T}\mathbf{d}_{1,j}) \tag{B.3}$$

$$= (h\mathbf{a} + k\mathbf{b} + l\mathbf{c} + \mathbf{d_O})^{T}(h\mathbf{a} + k\mathbf{b} + l\mathbf{c} + \mathbf{d_O}) \tag{B.4}$$

$$= (\mathbf{d}_{1,hkl}{}^{T}\mathbf{d}_{1,hkl}) \tag{B.5}$$

which yields, in Cartesian coordinates, for the interaction of the lattice centered on atom j=1 with the atom i=1:

$$E_{1,1} = \sum_{p} \sum_{h} \sum_{k} \sum_{l} A_{1,1,p} \, (\mathbf{d}_{1,hkl}{}^{T}\mathbf{d}_{1,hkl})^{-m(p)/2} \tag{B.6}$$

This may be generalized for a structural unit consisting of N_i atoms interacting with an entire composite lattice having N_j atoms in its simplest subunit. The total energy per unit of N_i atoms is given by Equation B.7; this equation is essentially the lattice summation in the form presented in the text in Equations 3.16, 3.17, and 3.18.

$$E_{lattice} = \sum_{p} \sum_{i}^{N_i} \sum_{j}^{N_j} \left[\sum_{h} \sum_{k} \sum_{l} A_{i,j,p} \left(\mathbf{d}_{1,hkl \text{ of } j}{}^{T} \mathbf{d}_{1,hkl \text{ of } j} \right)^{-m(p)/2} \right] \tag{B.7}$$

Transformation from Cartesian to lattice coordinate system This may be converted into a lattice-based coordinate system (i.e. "fractional coordinates") by means of the transformation matrix **H**

$$\mathbf{X}_c = \mathbf{H}\, \mathbf{x}_f \qquad \text{where } \mathbf{x}_f \text{ refers to the lattice coordinates and } \mathbf{X}_c \text{ refers to the Cartesian coordinates.} \tag{B.8}$$

$$\mathbf{H} = \begin{bmatrix} a\sin\beta & b(\cos\gamma - \cos\alpha\cos\beta)/\sin\beta & 0 \\ 0 & b(\sin^2\beta - \cos^2\gamma - \cos^2\alpha + 2\cos\alpha\cos\beta\cos\gamma)^{1/2} & 0 \\ a\cos\beta & b\cos\alpha & c \end{bmatrix} \tag{B.9}$$

H has been defined with the crystallographic system oriented within the Cartesian system as described in Chapter 3, i.e. **c** parallels the Cartesian z-axis, **a** lies in the xz-plane, and **b** completes a right-handed system. Then we may write:

$$\mathbf{d}_{ij} = \mathbf{X}_{cj} - \mathbf{X}_{ci} = \mathbf{H}\,(\mathbf{x}_{fj} - \mathbf{x}_{fi}) \tag{B.10}$$

In general, the atoms reside at fractional coordinates described by $\mathbf{x}_f = [h \;\; k \;\; l]$ in the lattice-based coordinate system. We redefine the vector $\mathbf{d}_O$ in lattice space as:

$$\mathbf{d}_O = \mathbf{H}\, \mathbf{d}_{fO} \;; \qquad \mathbf{d}_{fO} = [\, h' \;\; k' \;\; l' \,] \tag{B.11}$$

For ease of expression we define the following condensed notation:

$$\mathbf{x}_{hkl\ of\ j} \equiv (\mathbf{x}_{fj} - \mathbf{x}_{fi}) = [\ h+h'\quad k+k'\quad l+l'\ ] \tag{B.12}$$

The summation may be rewritten as:

$$E_{lattice} = \sum_{p}\sum_{i}^{N_i}\sum_{j}^{N_j}\left[\ \sum_{h}\sum_{k}\sum_{l} A_{i,j,p}\ (\mathbf{x}_{hkl\ of\ j}{}^{T}\mathbf{G}\mathbf{x}_{hkl\ of\ j})^{-m(p)/2}\ \right] \tag{B.13}$$

G is the real space metric tensor:

$$\mathbf{G} = \mathbf{H}^{T}\mathbf{H} = \begin{bmatrix} a^2 & ab(\cos\gamma) & ac(\cos\beta) \\ ab(\cos\gamma) & b^2 & bc(\cos\alpha) \\ ac(\cos\beta) & bc(\cos\alpha) & c^2 \end{bmatrix} \tag{B.14}$$

Convergence of Lattice Terms To demonstrate convergence, we write $E_{lattice}$ as a summation of ΔE's from successive triclinic "shells" of atoms N_j

$$E_{lattice} = \Delta E_{shell\ 1} + \Delta E_{shell\ 2} + \Delta E_{shell\ 3} + \ldots + \Delta E_{shell\ n} + \ldots \tag{B.15}$$

We demonstrate convergence of $E_{lattice}$ as n goes to ∞ by scaling arguments. For large h,k,l:

$$|\ \mathbf{x}_{hkl}\ |^2 \approx h^2 + k^2 + l^2 \propto n^2 \tag{B.16}$$

and the number of terms in the shell goes as $(n^3 - (n-2)^3) \propto n^2$. Therefore, $\lim_{n\to\infty} E_{shell\ n}$ is a "p series" of

order of magnitude $O(n^{2-m(p)})$, which converges for $m > 3$ and converges conditionally for $m = 3$.

Thus all induction/dispersion terms and interactions of electrostatic moments higher than dipole/dipole and charge/quadrupole are convergent. The last two are slowly divergent (harmonic) series in the limit $n \to \infty$. The charge/quadrupole term may be discarded in the limit $n \to \infty$ for systems in which the total charge is zero, since separation of charges becomes insignificant in the limit of infinite interaction distance, and only the total charge is important.

The special case of the dipole/dipole term may be written as [Maitland et al., 1981]:

$$E_{d/d} = -(\mu\mu'/r^3)\ (2\cos\theta_1\cos\theta_2 - \sin\theta_1\sin\theta_2\cos\phi) \qquad (B.17)$$

where θ_1, θ_2, and ϕ are angles of orientation defined as in Figure B.1. In the amorphous limit, one may assume that at very large distances, all orientations of the second dipole with respect to the first are sampled equally. In this case, it is easily shown, by integration of θ_2 and ϕ over all possible orientations relative to the first dipole, that the total contribution from each set of interacting dipoles becomes zero. Such an approximation is not rigorous in the case of periodic structures; however, in translationally periodic locations of dipoles of fixed local orientation, as one proceeds through successive shells of radius r and thickness δr, each shell contains an increasing number of dipoles describing a broader range of (discrete) dipole orientations relative to the first dipole, making such an approximation reasonable, if not rigorous, at large distances.

Figure B.1: Definition of angles describing the relative orientation of two linear charge distributions (from Maitland et al., 1981)

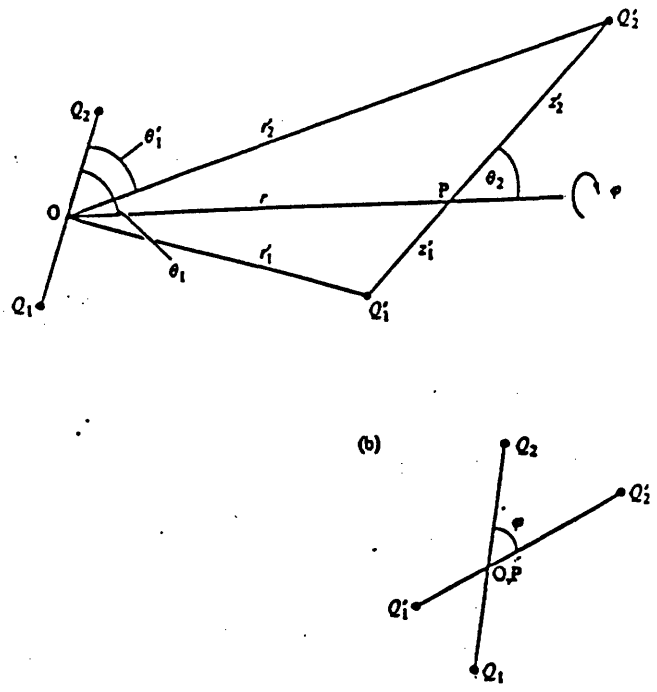

APPENDIX C: Semiempirical Quantum Calculations

Central to the success in application of the atomistic modelling methods is the validity and comprehensiveness of the force fields used to describe internal energy and their dependence on conformational and structural variables. Ideally, one would attempt to achieve the greatest degree of validity and comprehensiveness by applying the most fundamental concepts of interactions between bodies characterized by mass and charge distributions. For this purpose, the theories of quantum mechanics could, in principle, be used to describe the energetics of many body/many electron systems. However, in practice these calculations are far too complex even in relatively small polyatomic molecules for rigorous evaluation. Thus one must strike a balance between rigor and sufficiency. Even *ab initio* quantum calculations on small molecules already involve (albeit well accepted) simplifications of *de rigueur* quantum theory. Next are the semiempirical quantum calculations, which employ approximations of the wave functions to simplify calculations with (hopefully) little loss of validity; however, these approximations must be parameterized using data from real molecules, and thus have individual limits of utility, depending upon the nature of the approximations and parameterizations used. For atomistic modelling of large multichain systems such as are involved in this work, time and calculational constraints mandate even further simplification of the set of equations used to describe the system energetics. Most common are the two-body interaction potentials used to describe the energy of interaction as a function of distance of separation, such as the Lennard-Jones or Buckingham potentials. Other modelling efforts have employed orientation-dependent interactions, such as the "hydrogen bond potential", inductive effects in electrostatics, such as field-induced polarizabilities, or higher moment interactions, such as dipole-dipole or quadrupole-quadrupole interactions.

We have attempted to satisfy the criteria of sufficiency and simplicity entirely through the use of atom-centered, distance-dependent, two-body interactions to describe all nonbonded interactions. Where possible, these potentials are parameterized using experimental data from real systems; where such data is unavailable, we resort to predictions based on the more rigorous semiempirical quantum methods mentioned previously. The validity of these results, in turn, are checked against available structural and electrostatic moments of real molecules. For the aramid system, the following approach was undertaken.

A homologous series of amide, aromatic, and aromatic amide compounds representing subunits of poly(p-phenylene terephthalamide), end-capped with hydrogens, were optimized for heat of formation with respect to geometry. The series consisted of:

(1) formamide (CH_3NO)
(2) benzene (C_6H_6)
(3) benzamide (C_7H_7NO)
(4) formanilide (C_7H_7NO)
(5) terephthalamide ($C_8H_8N_2O_2$)
(6) p-phenylene diformamide ($C_8H_8N_2O_2$)
(7) benzanilide ($C_{13}H_{11}NO$)

The heat of formation of each compound was minimized (using the Davidon-Fletcher-Powell Method) with respect to bond lengths, bond angles, and bond torsions, with the restrictions that equivalent bond lengths and bond angles be equal (e.g. benzene) and all phenylene rings retain a hexagonal planar conformation (consistent with the description of the phenylene ring in the simulations). The results are tabulated in Table C.1(a)-(g), showing atomic charge assignment (in units of "partial atomic charge"), dipole moments, heats of formation, and relevant bond torsions. Initial conformations were chosen with trans-planar amide bonds and phenylene rings rotated by 30° from the plane of the amide bond. In each case, AM1, MNDO, and CNDO (in part) semiempirical quantum calculations were performed and compared. Partial atomic charges for each atom are calculated as the difference between the number of outer shell electrons and the calculated electron density attributed to that atom in the compound. No conformational averaging was involved in any case. The calculated dipoles were compared, where possible, with experimentally measured values. Also noted are the percentages of the dipole moments attributed to hybridization, as these represent that part of the dipole moment not captured by the atom-centered partial charges; a larger calculated percentage hybridization translates into a greater error in using only the stated partial atomic charges to describe the electrostatic moments. Also shown are the final values for the amide and ring torsions.

From this analysis, we note that CNDO tends to predict the smallest charges, and in many cases of different sign from the MNDO and AM1 results, and the largest hybridization percentages. AM1 generally calculates the largest partial atomic charges and the lowest percentage hybridization. CNDO and AM1 both appear to predict reasonably good estimates of dipole moments across the series, but only the AM1 charges comes close to reproducing the experimental quadrupole moment of benzene of -8.7×10^{-26} esu cm^2 [Battaglia et al., 1981]. MNDO performs poorest in estimating dipole moments and generally overestimates the torsions of the amide bond and that about the bond connecting the rings and amide moieties; in this respect, it is worth noting that AM1 was designed specifically to correct problems experienced by MNDO in predicting correct bond geometries in aromatic compounds. Based on these observations, we used AM1 exclusively from this point onward to obtain estimates for partial atomic charges.

Partial atomic charges for use in the 12-6-1 energy function in the polymer crystal simulations were determined as follows. (1) We require a minimum number of distinct atom types; in the unsubstituted polymer, this corresponds to seven atomic species: the amide nitrogen, amide oxygen, amide carbon and

amide hydrogen, the aromatic hydrogen, the aromatic carbons in the para position (no distinction is made between those connected to the amide nitrogen and those connected to the amide carbon), and the aromatic carbons in the ortho position. For these, the weighted average of AM1 charges across the homologous series are given in Table C.2, along with the standard deviations of actual values from the mean. In calculating the averages, charges in the larger compounds, which more closely approximate the electronic structure of the polymer, are preferentially weighted: the last three compounds in the series each contribute fully to the average; the first two are weighted by 1/3, and the second two by 2/3. (2) We require total charge neutrality on each of the N-H and C=O bond groups of the amide moiety (as per Hagler et al., [1974]) and on the phenylene ring. To achieve this, the residual charge for each of these three groups was uniformly redistributed among the elements of the group. This is a subjective correction, but one of only minor significance, given the small magnitude of residual charge in all cases but the N-H bond group. The final "adjusted partial atomic charges" are also listed in Table C.2, along with the charges suggested by the self-consistent force field of Hagler et al. [1974] for the atoms of the amide moiety.

The procedure described above has a significant advantage in that it may be readily extended to the parameterization of chains of modified constitution. This is, of course, a critical advantage to this work, which presumes to analyze chlorine-substituted polymers as an extension of the parent polymer poly-(p-phenylene terephthalamide). This procedure, which is tested for PPTA and with results compared to available experimental data, must be applied blindly to the homologous series based on aromatic amides having chlorines substituted in the ortho position on the ring, as experimental data, other than the dipole moment of m-dichlorobenzene, is essentially nonexistent. In this case, the homologous series consists of:

(1) m-dichlorobenzene ($C_6H_4Cl_2$)
(2) 2,6-dichlorobenzamide ($C_7H_5NOCl_2$)
(3) 2,6-dichloroformanilide ($C_7H_5NOCl_2$)
(4) 2,6-dichloroterephthalamide ($C_8H_6N_2O_2Cl_2$)
(5) p-(2,6-dichloro)phenylene diformamide ($C_8H_6N_2O_2Cl_2$)
(6) N-[2,6-dichlorophenyl]-benzamide ($C_{13}H_9NOCl_2$)
(7) 2,6-dichlorophenylbenzanilide ($C_{13}H_9NOCl_2$)

The set of unique species in the phenylene ring now become: the carbon in the 1 position (between the chlorines), the carbon in the 4 position (between the hydrogens), the carbons in the 2 and 6 positions (bonded to the chlorines), the carbons in the 3 and 5 positions (bonded to the hydrogens), the hydrogens, and the chlorines. As before, the charge and geometry results for each compound in the series are presented in Table C.3(a)-(g); the average, standard deviation, and adjusted partial atomic charges are tabulated in Table C.4.

It is worth noting that the amide charges have changed insignificantly from their values calculated for the unsubstituted compounds, which lends support to the premise that the substituted materials may be

treated as simple modifications of the unsubstituted materials. Secondly, the charges on the 1 and 4 carbons remain very close to zero and the carbon and hydrogn charges of the C-H bonds remain close to their original values (within the confidence limit of the averaging method employed); it is the C-Cl bond species in the ring that alter, to the extent that now charge is actually more evenly distributed between the two bonded atoms than before.

Rotation potentials for the unsubstituted and substituted phenylene rings about the bond connecting to the amide nitrogen or amide carbon were calculated using benzanilide, (2,6-dichlorophenyl)benzamide, and (2,6-dichlorophenyl)formanilide. In the first case, each ring was driven through a 90° rotation in increments of 15°, with the opposite ring fixed at 30° out-of-plane rotation. In the latter cases, only the substituted rings were driven in this manner; it was assumed here, and in the simulation work, that the ring rotation potential was a function only of the connected ring and amide atoms, and not of substitution at the other side of the ring or on the ring across the amide group. These results have been dealt with in greater detail in chapters 4 and 7.

Table C.1

Tabulated results of semiempirical quantum mechanics calculations

(a) **FORMAMIDE**

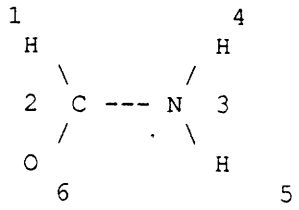

ATOM	**CHARGE**		
	CNDO	MNDO	AM1
H1	-.041	+.056	+.119
C2	+.348	+.376	+.257
N3	-.247	-.430	-.448
H4	+.225	+.182	+.219
H5	+.210	+.187	+.223
O6	-.632	-.371	-.371

DIPOLE MOMENT:	total (% hybrid)			Exp.
	3.728	3.361	3.703	3.37-3.86
	(57.5)	(23.4)	(17.6)	

HEAT OF FORMATION: (kcal/mole)			
	-39.31	-39.05	-44.75

TORSIONS:			
1-2-3-5 :		180°	180°

(b) **BENZENE**

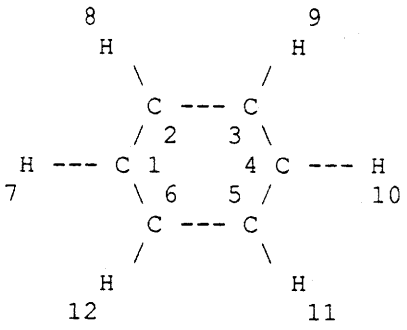

ATOM	**CHARGE**		
	CNDO	MNDO	AM1
C1	+.008	-.059	-.130
C2	+.008	-.059	-.130
C3	+.008	-.059	-.130
C4	+.008	-.059	-.130
C5	+.008	-.059	-.130
C6	+.008	-.059	-.130
H7	-.008	+.059	+.130
H8	-.008	+.059	+.130
H9	-.008	+.059	+.130
H10	-.008	+.059	+.130
H11	-.008	+.059	+.130
H12	-.008	+.059	+.130

DIPOLE MOMENT:	total	(% hybrid)		Exp.
	0.0	0.0	0.0	0.0

HEAT OF FORMATION: (kcal/mole)			
-47.10	21.32	22.02	

(c) **BENZAMIDE**

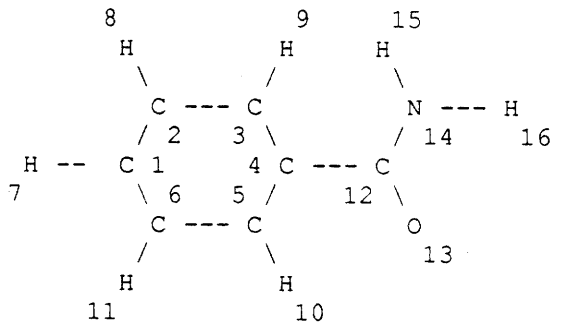

ATOM	**CHARGE**			
	CNDO	MNDO	AM1	
C1	+.018	-.034	-.108	
C2	+.005	-.071	-.140	
C3	+.018	-.007	-.104	
C4	-.027	-.121	-.121	
C5	+.024	-.017	-.077	
C6	+.005	-.069	-.138	
H7	-.005	+.064	+.135	
H8	-.005	+.066	+.136	
H9	-.009	+.071	+.133	
H10	+.006	+.066	+.157	
H11	-.004	+.066	+.139	
C12	+.319	+.361	+.343	
O13	-.353	-.336	-.371	
N14	-.260	-.336	-.434	
H15	+.117	+.146	+.220	
H16	+.128	+.152	+.231	
DIPOLE MOMENT:	total (% hybrid)			Exp.
	3.857	3.411	3.710	3.65-3.88
	(58.2)	(26.8)	(17.4)	
HEAT OF FORMATION: (kcal/mole)				
			-15.69	-16.03
TORSIONS:				
3-4-12-14 :		69°	33°	
13-12-14-15 :		-150°	-174°	

(d) **FORMANILIDE**

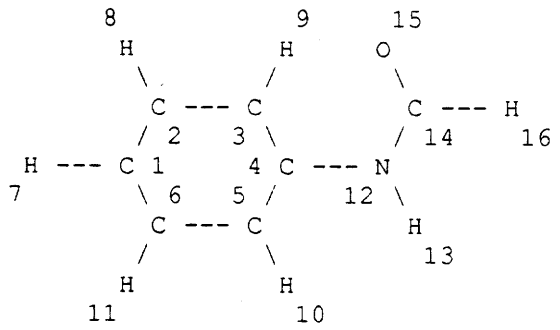

ATOM	**CHARGE**			
	CNDO	MNDO	AM1	
C1	-.014	-.068	-.154	
C2	+.024	-.048	-.106	
C3	-.036	-.046	-.149	
C4	+.141	+.086	+.065	
C5	-.044	-.090	-.181	
C6	+.023	-.046	-.106	
H7	-.003	+.062	+.133	
H8	-.004	+.063	+.135	
H9	+.012	+.076	+.169	
H10	+.002	+.059	+.128	
H11	-.004	+.061	+.131	
N12	-.204	-.370	-.339	
H13	+.101	+.172	+.230	
C14	+.342	+.372	+.267	
O15	-.291	-.343	-.345	
H16	-.042	+.058	+.122	
DIPOLE MOMENT:	total (% hybrid)			Exp.
	3.397 (81.4)	2.849 (32.2)	3.156 (25.0)	3.37
HEAT OF FORMATION: (kcal/mole)				
		-8.334	-9.716	
TORSIONS:				
3-4-12-14 :		60°	17°	
13-12-14-15 :		-168°	-176°	

(e) **TEREPHTHALAMIDE**

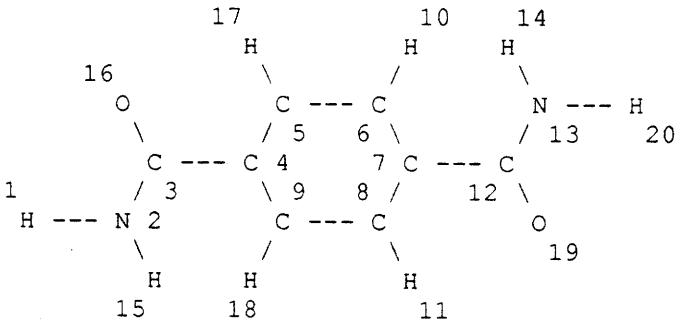

ATOM	**CHARGE**	
	MNDO	AM1
H1	+.160	+.234
N2	-.343	-.432
C3	+.361	+.341
C4	-.094	-.099
C5	-.033	-.089
C6	-.016	-.111
C7	-.095	-.101
C8	-.030	-.089
C9	-.016	-.114
H10	+.077	+.142
H11	+.071	+.159
C12	+.358	+.341
N13	-.337	-.428
H14	+.149	+.221
H15	+.152	+.224
O16	-.334	-.366
H17	+.069	+.159
H18	+.077	+.141
O19	-.332	-.364
H20	+.156	+.231
DIPOLE MOMENT: total (% hybrid)		
	0.248	0.156
	(25.0)	(92.9)
HEAT OF FORMATION: (kcal/mole)		
	-52.30	-16.03
TORSIONS:		
16-3-2-15 :	-153°	-177°
2-3-4-5 :	-98°	-141°
13-12-7-6 :	-75°	-35°
14-13-12-19 :	150°	170°

(f) **P-PHENYLENE DIFORMAMIDE**

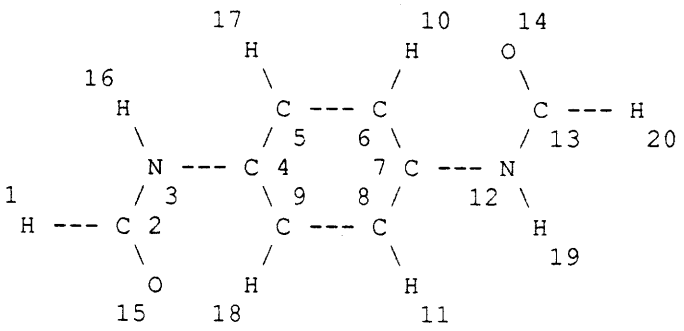

ATOM	**CHARGE**	
	MNDO	AM1
H1	+.058	+.122
C2	+.384	+.266
N3	-.390	-.333
C4	+.097	+.041
C5	-.077	-.156
C6	-.024	-.128
C7	+.072	+.043
C8	-.060	-.156
C9	-.048	-.126
H10	+.074	+.174
H11	+.065	+.134
N12	-.388	-.335
C13	+.379	+.268
O14	-.350	-.350
O15	-.349	-.350
H16	+.182	+.230
H17	+.066	+.133
H18	+.075	+.172
H19	+.178	+.230
H20	+.057	+.121

DIPOLE MOMENT: total (% hybrid)

	0.212	0.138
	(18.9)	(2.9)

HEAT OF FORMATION: (kcal/mole)

	-38.06	-41.56

TORSIONS:

16-3-2-15 :	-172°	-177°
2-3-4-5 :	-127°	-168°
13-12-7-6 :	-74°	-6°
14-13-12-19 :	174°	179°

(g) **BENZANILIDE**

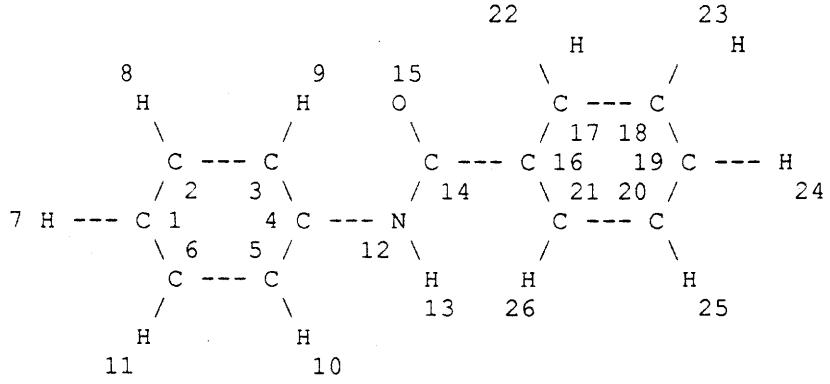

ATOM	**CHARGE**	
	MNDO	AM1
C1	-.056	-.155
C2	-.058	-.107
C3	-.029	-.145
C4	+.070	+.071
C5	-.072	-.181
C6	-.054	-.107
H7	+.062	+.132
H8	+.062	+.135
H9	+.072	+.168
H10	+.059	+.129
H11	+.061	+.130
N12	-.357	-.326
H13	+.171	+.231
C14	+.394	+.351
O15	-.334	-.343
C16	-.118	-.127
C17	-.009	-.105
C18	-.068	-.137
C19	-.035	-.108
C20	-.068	-.137
C21	-.021	-.078
H22	+.069	+.137
H23	+.066	+.138
H24	+.065	+.136
H25	+.065	+.140
H26	+.064	+.155

DIPOLE MOMENT: total (% hybrid)			Exp.
	3.193	3.449	3.38,3.83
	(27.2)	(22.1)	
HEAT OF FORMATION: (kcal/mole)			
	16.19	19.66	
TORSIONS:			
3-4-12-14 :	84°	24°	
15-14-12-13 :	-164°	-172°	
12-14-16-17 :	89°	41°	

Table C.2

Partial atomic charges from AM1 calculations: unsubstituted compounds

Atom type:	H_{amide}	N_{amide}	C_{amide}	O_{amide}	$C_{ph,para}$	$C_{ph,ortho}$	H_{ph}
Weighted average charge	0.226	-0.378	0.309	-0.356	-0.065	-0.124	0.144
Standard deviation	0.005	0.051	0.040	0.011	0.085	0.028	0.015
Residual charge on N-H	-0.151						
Residual charge on C=O	-0.047						
Residual charge on phenylene	-0.050						
"Adjusted" charge	0.302	-0.302	0.333	-0.333	-0.060	-0.119	0.149
HHL charge[a]	0.28	-0.28	0.38	-0.38	-	-	-

[a] values suggested by Hagler, Huler,and Lifson [1974].

Table C.3

Tabulated results of semiempirical quantum mechanical calculations: dichloro compounds

(a) **M-DICHLORO-BENZENE**

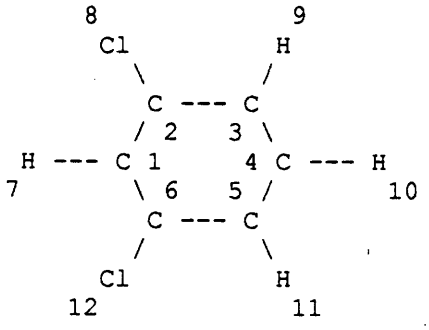

ATOM	**CHARGE**		
	CNDO	MNDO	AM1
C1	+.016	-.020	-.121
C2	+.076	-.000	-.055
C3	+.022	-.033	-.125
C4	+.002	-.052	-.112
C5	+.022	-.033	-.125
C6	+.076	-.000	-.055
H7	+.029	+.094	+.161
C18	-.142	-.096	-.006
H9	+.016	+.081	+.149
H10	+.011	+.076	+.144
H11	+.016	+.081	+.149
C112	-.142	-.096	-.006

DIPOLE MOMENT: total (% hybrid)			Exp.
1.649	1.745	1.222	1.22-1.68
(0.1)	(1.1)	(3.1)	

HEAT OF FORMATION: (kcal/mole)

-----	6.63	8.23

(b) **2,6-DICHLORO-BENZAMIDE**

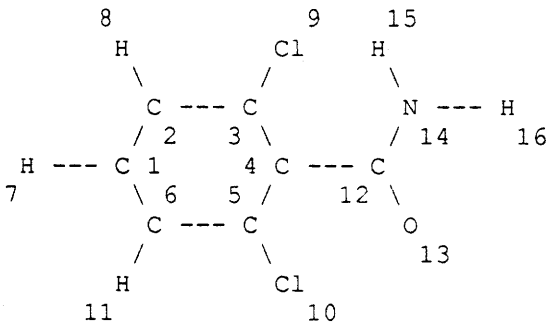

ATOM	**CHARGE** MNDO	AM1
C1	-.033	-.100
C2	-.041	-.130
C3	+.045	-.034
C4	-.076	-.108
C5	+.029	-.023
C6	-.039	-.130
H7	+.077	+.146
H8	+.087	+.155
Cl9	-.075	+.007
Cl10	-.094	+.017
H11	+.087	+.156
C12	+.366	+.352
O13	-.315	-.342
N14	-.326	-.426
H15	+.149	+.226
H16	+.159	+.234

DIPOLE MOMENT: total (% hybrid)

	4.266	4.315
	(22.1)	(12.7)

HEAT OF FORMATION: (kcal/mole)

	-25.83	-25.15

TORSIONS:

3-4-12-14 :	88°	77°
13-12-14-15 :	-152°	177°

(c) **2,6-DICHLORO-FORMANILIDE**

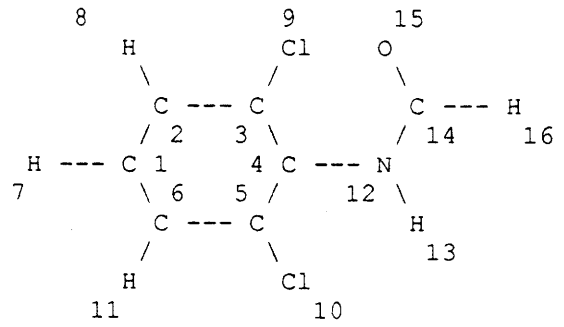

ATOM	**CHARGE**	
	MNDO	AM1
C1	-.051	-.119
C2	-.031	-.116
C3	+.022	-.046
C4	+.113	+.061
C5	-.010	-.079
C6	-.027	-.112
H7	+.075	+.146
H8	+.084	+.153
Cl9	-.080	+.014
Cl10	-.099	-.018
H11	+.084	+.154
N12	-.376	-.344
H13	+.184	+.236
C14	+.380	+.268
O15	-.335	-.326
H16	+.067	+.128

DIPOLE MOMENT: total (% hybrid)

	2.854	2.917
	(30.5)	(24.5)

HEAT OF FORMATION: (kcal/mole)

	-20.35	-19.01

TORSIONS:

3-4-12-14 :	88°	66°
13-12-14-15 :	-163°	-163°

(d) **2,6-DICHLORO-TEREPHTHALAMIDE**

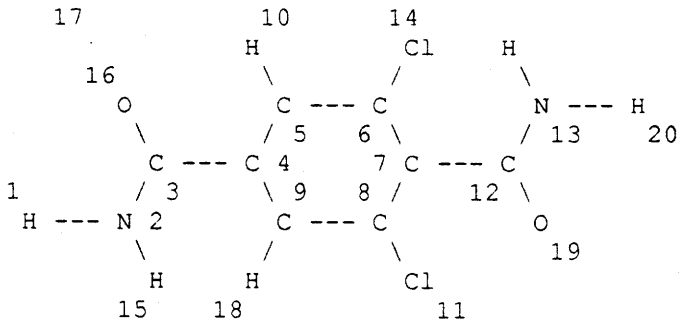

ATOM	**CHARGE**	
	MNDO	AM1
H1	+.162	+.236
N2	-.334	-.429
C3	+.357	+.342
C4	-.092	-.089
C5	-.004	-.084
C6	+.033	-.043
C7	-.054	-.092
C8	+.015	-.032
C9	+.010	-.109
Cl10	-.064	+.024
Cl11	-.082	+.024
C12	+.362	+.348
N13	-.326	-.423
H14	+.152	+.228
H15	+.152	+.226
O16	-.322	-.357
H17	+.089	+.175
H18	+.096	+.158
O19	-.313	-.340
H20	+.162	+.235
DIPOLE MOMENT: total (% hybrid)		
	1.531	1.988
	(18.3)	(12.5)
HEAT OF FORMATION: (kcal/mole)		
	-60.89	-61.70
TORSIONS:		
16-3-2-15 :	-153°	-176°
2-3-4-5 :	-108°	-140°
13-12-7-6 :	-88°	-77°
14-13-12-19 :	151°	-176°

(e) **P-(2,6-DICHLORO-)PHENYLENE DIFORMAMIDE**

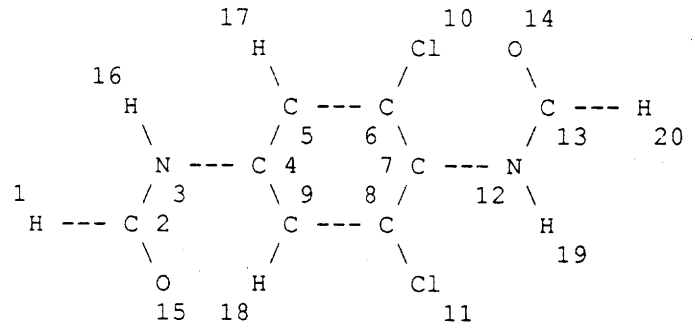

ATOM	**CHARGE**	
	MNDO	AM1
H1	+.067	+.130
C2	+.377	+.268
N3	-.385	-.336
C4	+.101	+.085
C5	-.058	-.175
C6	-.022	-.017
C7	+.117	+.032
C8	+.014	-.050
C9	-.019	-.141
Cl10	+.084	+.013
Cl11	+.084	-.002
N12	-.402	-.346
C13	+.394	+.269
O14	-.345	-.331
O15	-.337	-.336
H16	+.183	+.235
H17	+.084	+.150
H18	+.096	+.189
H19	+.194	+.237
H20	+.066	+.126
DIPOLE MOMENT: total (% hybrid)		
	2.245	2.800
	(29.4)	(14.2)
HEAT OF FORMATION: (kcal/mole)		
	-49.35	-50.18
TORSIONS:		
16-3-2-15 :	-165°	-177°
2-3-4-5 :	-114°	-161°
13-12-7-6 :	-93°	-70°
14-13-12-19 :	178°	167°

(f) **N-[2,6-DICHLOROPHENYL]-BENZAMIDE**

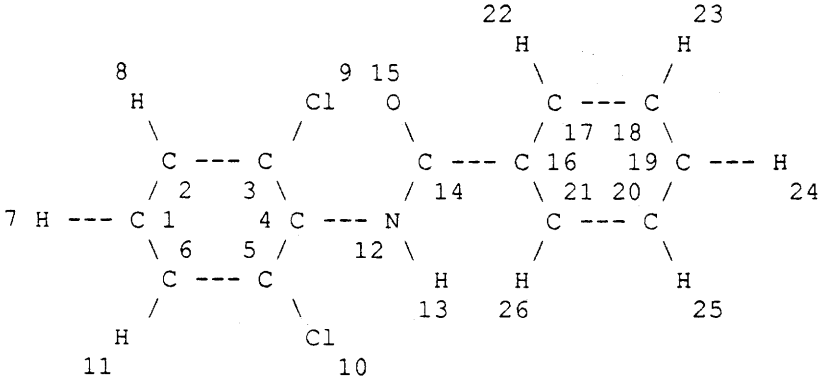

ATOM	**CHARGE**	
	MNDO	AM1
C1	-.054	-.117
C2	-.030	-.119
C3	+.019	-.040
C4	+.124	+.062
C5	-.011	-.075
C6	-.027	-.117
H7	+.075	+.144
H8	+.084	+.153
Cl9	-.085	+.017
Cl10	-.100	-.004
H11	+.083	+.151
N12	-.373	-.337
H13	+.188	+.237
C14	+.413	+.352
O15	-.329	-.326
C16	-.121	-.124
C17	-.009	-.100
C18	-.071	-.139
C19	-.033	-.108
C20	-.070	-.138
C21	-.012	-.080
H22	+.071	+.142
H23	+.067	+.137
H24	+.064	+.136
H25	+.067	+.139
H26	+.068	+.154
DIPOLE MOMENT: total (% hybrid)		
	2.807	2.946
	(28.3)	(22.5)
HEAT OF FORMATION: (kcal/mole)		
	4.50	10.35
TORSIONS:		
3-4-12-14 :	83°	75°
15-14-12-13 :	-163°	-162°
12-14-16-17 :	77°	42°

(g) **2,6-DICHLOROBENZANILIDE**

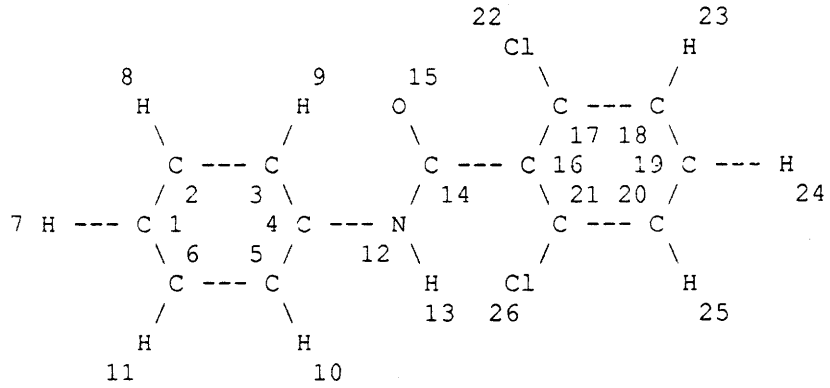

ATOM	**CHARGE**	
	MNDO	AM1
C1	-.065	-.154
C2	-.050	-.107
C3	-.044	-.146
C4	+.092	+.072
C5	-.081	-.178
C6	-.049	-.107
H7	+.062	+.133
H8	+.062	+.135
H9	+.076	+.169
H10	+.062	+.130
H11	+.060	+.131
N12	-.361	-.317
H13	+.181	+.235
C14	+.409	+.360
O15	-.320	-.317
C16	-.079	-.118
C17	+.040	-.027
C18	-.042	-.130
C19	-.033	-.097
C20	-.041	-.130
C21	+.034	-.029
Cl22	-.080	+.018
H23	+.086	+.156
H24	+.078	+.148
H25	+.087	+.156
Cl26	-.086	+.017
DIPOLE MOMENT: total (% hybrid)		
	4.185	4.078
	(20.1)	(17.8)
HEAT OF FORMATION: (kcal/mole)		
	6.64	10.57
TORSIONS:		
3-4-12-14 :	58°	22°
15-14-12-13 :	-169°	-177°
12-14-16-17 :	87°	88°

Table C.4

Partial atomic charges from AM1 calculations: dichloro compounds

Atom type:	H_{amide}	N_{amide}	C_{amide}	O_{amide}	C_1	C_4	$C_{2,6}$	$C_{3,5}$	H_{ph}	Cl_{ph}
Average Charge	0.233	-0.368	0.321	-0.334	-0.033	-0.071	-0.042	-0.125	0.155	0.013
Standard Deviation	0.005	0.045	0.041	0.012	0.082	0.075	0.018	0.021	0.029	0.028
Residual charge on N-H			-0.102							
Residual charge on C=O			-0.136							
Residual charge on phenylene			-0.014							
"Adjusted" Charge	0.301	-0.301	0.328	-0.328	-0.023	-0.061	-0.031	-0.115	0.165	0.023

APPENDIX D: Atomic Scattering Factor Functions

For purposes of calculating the structure factors for the crystal based on the ensemble of atoms and atom coordinates, the atomic scattering factors are required in functional form. Tables of mean atomic scattering values are readily available from the International Tables of X-Ray Crystallography, [Volume III, 1968] page 201. Following Moore [1963], we have used functions of the form:

$$f_j(x_i) = A_j \exp(-a_j x_i^2) + B_j \exp(-b_j x_i^2) + C_j \qquad (D.1)$$

$$j = H, C, N, O, Cl$$

$$x_i = \sin(\theta_i)/\lambda$$

These have been fitted to the mean atomic scattering factors derived by self-consistent or variational wave functions in the range ($0 \leq \sin(\theta_i)/\lambda \leq 1$) using the recommended weighting function for CuKα radiation:

$$w_i = \exp[\ -(x_i - \tfrac{1}{2})^2\ ] \qquad (D.2)$$

The resulting function parameters and the corresponding sum of squares of the regression obtained using the RS1 graphics and statistical analysis software package [BBN Research Systems, Cambridge, MA], are presented in Table D.1. The quality of fit is illustrated in Figure D.1.

Table D.1

Function parameters for atomic scattering factors

Atom type	A_i	a_i	B_i	b_i	C_i	ε
H	0.391	7.483	0.596	30.072	0.011	0.268
C	1.248	2.517	3.678	23.747	1.044	0.414
N	1.778	3.836	3.938	19.226	1.260	0.309
O	2.836	4.423	3.773	17.229	1.373	0.218
Cl	8.066	0.973	7,983	22.093	0.946	---

Figure D.1: Atomic scattering factor functions for hydrogen, carbon, nitrogen, oxygen, and chlorine (in order from bottom to top). Points are recommended mean atomic scattering factors from self-consistent or variational wave functions (from the International Tables for X-Ray Crystallography [1968]); curves are fitted functions of the form given by Equation D.1 using parameters listed in Table D.1.

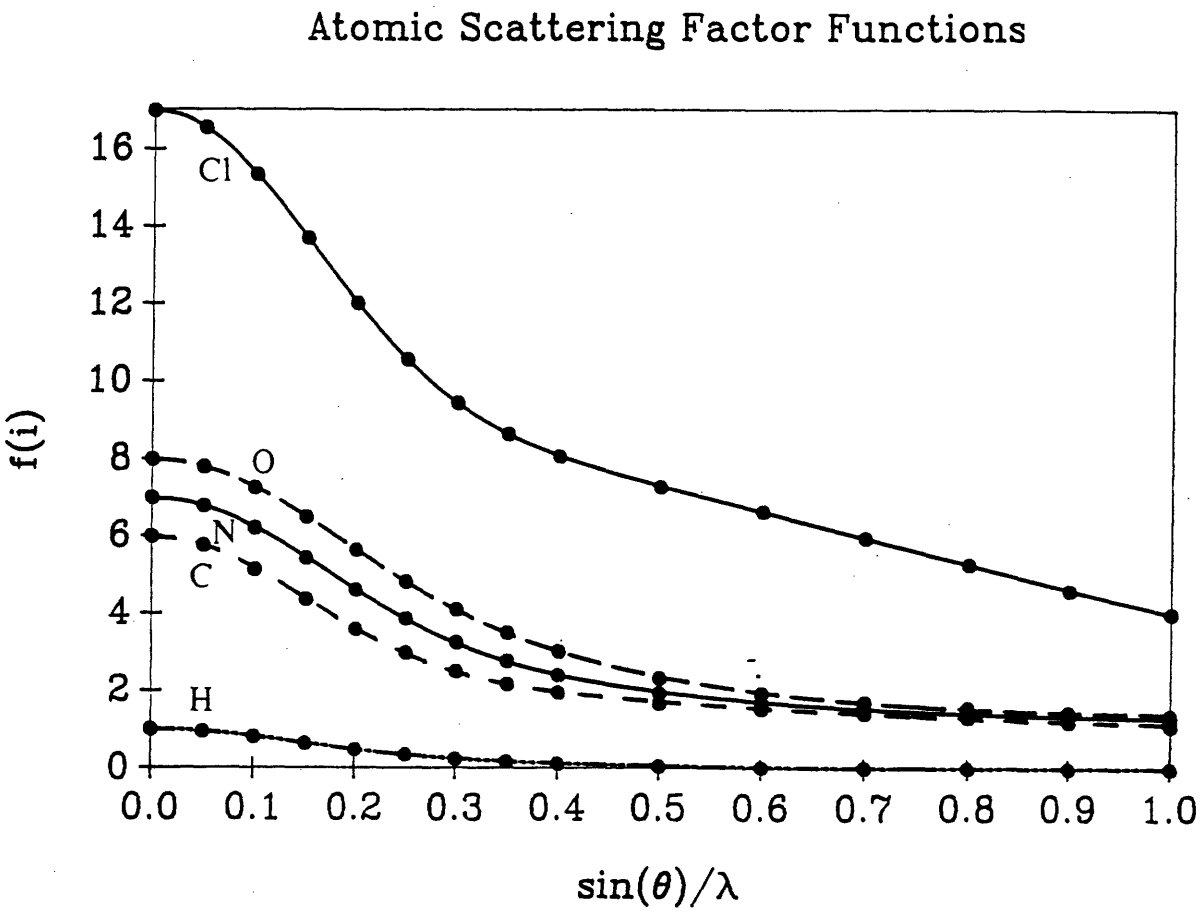

APPENDIX E: Detailed X-ray Scattering Intensities from Simulated Structures and Simulated X-ray Fiber Diffraction Patterns for Chlorine-modified Isomers

Table E.1a

Summary of x-ray reflections in molecular simulation structures of PPTA

	Structure #1			Structure #2			Structure #3			Structure #4		
hkl	2θ	β	I	2θ	β	I	2θ	β	I	2θ	β	I
110	19.6	0	87	20.0	0	72	21.0	0	74	21.0	0	50
$1\bar{1}0$	19.0	0	65	19.3	0	80	20.5	0	23	21.2	0	21
200	26.2	0	100	25.2	0	100	21.4	0	100	21.5	0	100
310	42.1	0	4	41.9	0	2	37.7	0	7	37.3	0	4
$3\bar{1}0$	42.9	0	2	40.8	0	2	36.7	0	1	37.7	0	1
400	54.0	0	1									
$\bar{1}01$										13.8	29	3
011				16.9	24	6				19.0	21	2
$0\bar{1}1$				16.2	25	6				19.9	20	4
111	20.2	20	3				22.1	18	1			
$\bar{1}11$	20.7	19	4									
$1\bar{1}1$	20.7	19	4									
$\bar{1}\bar{1}1$	20.2	19	3				22.1	18	2			
201	27.1	14	1				22.5	18	2			
$\bar{2}01$							22.5	18	2			
211	30.4	13	2	31.2	13	12	29.2	13	4	27.6	14	2
$\bar{2}11$	31.1	12	3	29.8	13	13	28.4	14	5	30.0	13	6
$2\bar{1}1$	31.1	12	3	30.0	13	1	28.5	14	5	28.6	14	4
$\bar{2}\bar{1}1$	30.4	13	2	30.4	13	9	29.2	13	4	30.3	13	7
121				34.6	11	1				38.0	10	1
$1\bar{2}1$				33.0	12	1						
$\bar{3}01$										34.7	11	2
002	28.5	0	1	13.5	86	5	13.5	90	5	13.8	78	5
$1\bar{1}2$				23.4	35	1				24.9	33	2
$\bar{1}\bar{1}2$				23.5	35	2						
202				29.2	28	2						
$\bar{2}02$										27.9	29	2
022				34.2	23	2						
312							40.2	20	1	37.0	22	1
$\bar{3}\bar{1}2$							40.2	20	1			
$\bar{1}32$				50.5	16	1						

Table E.1a (continued)

103										21.4	72	2
$\bar{1}03$										25.3	54	1
013				26.1	51	4				26.7	50	2
$0\bar{1}3$				24.7	55	2						
$\bar{1}13$	28.3	46	2									
$1\bar{1}3$	28.3	46	2									
203							29.8	43	2			
$\bar{2}03$							29.7	44	1			
$2\bar{1}3$				35.8	35	2						
213				37.6	33	1				31.6	40	2
303										35.1	35.8	2
004	27.1	90	17	27.3	86	25	27.2	90	13	27.8	78	17
104				40.0	43	3						
$1\bar{1}4$				33.3	55	2				34.5	52	3
$\bar{1}\bar{1}4$				32.9	56	1						
105									34.5	82	1	
015				38.4	63	2						
006	41.2	90	17	41.4	86	36	41.3	90	9	42.3	78	17
106	43.4	72	1				42.8	75	4			
$\bar{1}06$	43.4	72	1				42.8	75	4			
016	43.7	71	1									
$0\bar{1}6$	43.8	71	1									
116				47.7	61	1				44.3	69	3.4
$\bar{1}16$				46.4	64	2						
206				50.0	57	1				43.7	72	2
$\bar{2}06$				48.2	60	2						

Table E.1b

Summary of x-ray reflections in molecular simulation structures of PPTA

	Structure #5			Structure #6			Structure #7			Structure #8		
hkl	2θ	β	I	2θ	β	I	2θ	β	I	2θ	β	I
100										21.9	0	100
010	18.4	0	49	19.5	0	47	18.1	0	46	18.7	0	31
110										29.8	0	27
200	21.3	0	100	21.1	0	100	21.1	0	100			
020										44.7	0	1
210	28.2	0	11	29.4	0	2				49.9	0	1
$2\bar{1}0$	28.3	0	6	28.3	0	53	28.1	0	35			
$2\bar{2}0$				44.6	0	2	42.8	0	1			
400							43.3	0	1			
$4\bar{1}0$				46.8	0	1						
001	6.9	80	9	6.9	79	4				8.3	55	2
$\bar{1}01$										20.2	20	2
011	18.5	21	1	19.5	20	1						
$0\bar{1}1$	20.8	19	1									
111							21.8	18	1			
$\bar{1}11$	21.5	18	2	21.6	18	1	21.4	18	2			
$1\bar{1}1$							22.8	17	1			
$\bar{1}\bar{1}1$	23.4	17	4									
211	28.5	14	6									
$2\bar{1}1$	29.9	13	3									
$\bar{2}\bar{1}1$	29.9	13	5									
002	13.8	80	5				13.6	84	10	16.6	54.8	2
$\bar{1}02$				16.9	53	1				34.5	23	2
$0\bar{1}2$							23.6	35.0	3			
112				24.9	33	2				27.7	29.4	5
$\bar{1}12$				23.6	35	1						
$1\bar{1}2$	27.1	30	2	28.1	29	11				24.9	33	2
$\bar{1}\bar{1}2$	27.2	30	3									
$\bar{2}02$							24.6	33	4			
212							31.1	26	3	43.6	18	1
$2\bar{1}2$							32.6	25	6	40.5	20	1
122				41.6	19	2						
$1\bar{2}2$										40.6	20	1

Table E.1b (continued)

302	34.9	23	1	35.5	23	3				
$\bar{3}02$	35.3	23	2	34.1	24	4				
312	38.5	21	1	40.2	20	1				
$3\bar{1}2$				41.5	19	2				
$\bar{4}02$							44.7	18	2	
003				20.7	89	1				
103	23.1	62	4							
013				25.8	52	1				
113	27.3	48	4							
$\bar{1}13$				27.2	49	1	27.9	47	1	
$1\bar{1}3$							28.8	45	1	27.4 48 1
$\bar{1}\bar{1}3$	32.2	40	1							
303	38.2	33	1							
004	27.7	80	4	27.7	79	11	27.3	84	13	33.5 55 4
104										27.5 82 8
014										39.3 44 3
$0\bar{1}4$	36.1	50	1	37.0	48	2	34.3	53	2	
114										35.0 52 2
$1\bar{1}4$	37.7	47	1							
$\bar{2}14$				42.5	40	3				
$\bar{2}\bar{1}4$							39.8	44	2	
005	34.9	80	2	34.8	79	2				
015	36.6	70	1	36.8	68	1				
$1\bar{1}5$									38.0	65 1
006	42.1	80	4				41.5	84	15	
106				44.1	70	3	44.1	70	3	42.1 80 4
016	43.1	74	7							
116				45.4	66	2				
$\bar{1}16$				43.8	71	6				
$1\bar{1}6$										45.0 67 2
206							48.3	60	1	57.3 47 3
$\bar{2}16$							48.3	60	1	

Table E.2

Summary of x-ray reflections in molecular simulation structures for 2,6-dichloro-PPTA; head-to-head, tail-to-tail polymorphs

	Structure #1			Structure #2			Structure #3			Structure #4		
hkl	2θ	β	I	2θ	β	I	2θ	β	I	2θ	β	I
100										16.5	0	14
010										20.7	0	1
$\bar{1}10$	17.4	0	2				16.9	0	5	23.9	0	2
110	6.1	0	6	17.2	0	9	19.0	0	15	29.1	0	2
$1\bar{1}0$				19.6	0	22						
200	21.0	0	3	20.2	0	17	21.0	0	5			
020	31.0	0	1				29.4	0	2			
$\bar{2}10$										35.9	0	2
310	37.3	0	1	32.3	0	9	36.7	0	3			
001	3.7	72	100	3.4	90	100				3.6	73	100
$0\bar{1}1$							14.6	13	1			
002	7.3	72	37				6.8	84	100	7.2	73	58
102	22.2	18	1									
$\bar{1}02$	22.4	18	1									
112										31.5	13	2
202							22.0	18	1			
$\bar{2}02$							22.1	18	2			
022							30.9	13	2			
$\bar{2}12$				28.1	14	3						
$2\bar{1}2$				24.7	16	2						
$2\bar{1}\bar{2}$				28.1	14	3						
212				24.7	16	2						
003	11.0	72	37	10.1	90	59				10.8	73	32
$0\bar{1}3$							16.9	37	2			
$\bar{1}03$							14.6	44	1	19.7	32	1
113				20.0	31	1						
$1\bar{1}3$				20.1	30	1						
004				13.5	90	4	13.6	84	3	14.4	73	3
005	18.3	72	8	16.9	90	19				18.0	73	3
$0\bar{1}5$							21.3	53	1			
$\bar{1}05$							20.1	58	1	24.4	45	1
006							20.5	84	3			
$0\bar{1}6$										25.2	55	2
007				23.8	90	2						
008										28.9	73	1

Table E.3

Summary of x-ray reflections in molecular simulation structures for 2,6-dichloro-PPTA; parallel head-to-tail polymorphs

	Structure #1			Structure #2			Structure #3			Structure #4		
hkl	2θ	β	I	2θ	β	I	2θ	β	I	2θ	β	I
010							14.9	0	14	16.9	0	3
100										18.8	0	7
110	17.1	0	13	17.6	0	19				21.1	0	3
$1\bar{1}0$	19.8	0	24	20.5	0	27				29.2	0	1
200	20.8	0	25	20.2	0	37	22.4	0	34			
210							27.6	0	3	36.6	0	2
$2\bar{1}0$	27.8	0	1				26.4	0	25			
220	34.5	0	1	35.5	0	2						
$3\bar{1}0$				37.3	0	2						
310	32.8	0	9	32.1	0	15						
001										6.8	88	100
101	11.9	35	4	11.3	37	8	12.2	34	3			
$\bar{1}01$	12.8	32	2	13.0	31	4	13.8	29	3			
$0\bar{1}1$	16.6	24	1	17.7	22	10						
011				17.4	23	2						
$\bar{1}\bar{1}1$	18.7	21	1				21.1	19	4	22.0	18	1
$1\bar{1}1$	18.2	22	1				19.4	20	2			
$\bar{1}11$							19.7	20	2	30.1	13	1
$2\bar{1}1$	24.4	16	3	23.7	17	6						
$2\bar{1}\bar{1}$	28.2	14	4	28.3	14	8						
$\bar{2}\bar{1}1$	25.3	16	3	25.7	15	4						
$\bar{2}11$	29.1	14	4	29.5	13	6						
121							32.7	12	1			
301	31.6	12	1	30.2	13	3	33.6	12	2			
$3\bar{1}1$							36.3	11	1			
002	13.6	85	100	13.7	81	100	13.7	82	100	13.6	88	20
012							19.7	44	1			
$0\bar{1}2$							20.9	41	5			
$1\bar{1}2$	21.5	39	3	21.1	40	4						
$\bar{1}\bar{1}2$	22.3	37	3	23.5	35	2						
$\bar{1}12$				25.3	32	2						
$1\bar{1}\bar{2}$				24.0	34	1						
$\bar{2}02$				26.2	31	3						

Table E.3 (continued)

212						29.1	28	2		
$2\bar{1}2$						28.7	28	4		
$\bar{2}\bar{1}2$						32.7	25	1		
222			36.7	22	1	39.5	20	1		
$3\bar{1}2$			38.2	21	1					
003									20.5	88 7
103	22.1	67 3	21.6	71	11	22.0	68	7		
013			26.0	52	2					
$0\bar{1}3$	25.4	54 1	26.7	50	5					
$\bar{1}13$	29.4	44 1				28.1	47	3		
$1\bar{1}3$	27.8	47 1				27.1	49	2		
$\bar{1}\bar{1}3$						26.3	51	2		
$\bar{1}\bar{1}\bar{3}$						30.0	43	1		
213			29.2	44	1					
303			34.4	37	1					
004			27.6	81	5					
114	31.8	59 1								
$\bar{1}14$			35.5	50	2					
$\bar{1}\bar{1}4$	32.9	56 1								
$0\bar{2}4$			43.7	39	2	42.5	41	2		
$\bar{2}04$			37.0	48	2	38.2	46	1		
214						36.4	49	1		
314			39.3	45	1					
$3\bar{1}4$			44.2	39	1					
105			34.8	81	6	34.9	79	4		
$\bar{1}05$			37.8	66	3					
115						37.5	66	2		
215			39.4	61	2					
006	41.5	85 10	41.9	81	9	41.8	82	7	41.6	88 2
016						43.8	71	2		
116			43.9	71	3					
$1\bar{1}6$			45.9	65	1					
206			44.1	71	2	44.9	68	2		

Table E.4a

Summary of x-ray reflections in molecular simulation structures for 2,6-dichloro-PPTA; antiparallel head-to-tail polymorphs

	Structure #5			Structure #6			Structure #7		
hkl	2θ	β	I	2θ	β	I	2θ	β	I
010	15.8	0	7	16.8	0	9	15.1	0	11
100							11.3	0	2
$1\bar{1}0$							18.9	0	1
200	20.4	0	7	19.4	0	4	22.7	0	10
210	25.9	0	5	23.8	0	3			
$2\bar{1}0$	25.8	0	5	27.6	0	2	27.3	0	4
220				36.7	0	1			
$2\bar{2}0$							38.3	0	1
001	6.8	80	100	6.9	79	100	6.8	85	100
101							13.4	30	2
$\bar{1}01$				10.9	38	1			
$0\bar{1}1$				18.9	21	2	17.0	23	1
011							16.1	25	1
$\bar{1}\bar{1}1$							20.3	19	2
111	19.3	21	1						
$\bar{1}11$	19.0	21	1						
201							24.0	16	1
$\bar{2}01$							23.4	17	2
211				25.1	16	1			
$2\bar{1}1$	27.6	14	2	29.8	13	2			
$\bar{2}11$	27.3	14	2						
$\bar{2}11$	25.9	15	1						
002				13.8	79	7			
102							18.1	49	1
$\bar{1}02$				15.5	61	1			
112							23.0	36	1
003	20.6	80	3				20.4	85	5
104	29.8	66	1						
$\bar{1}04$	29.1	69	1						
005				34.8	79	3			
006				42.1	79	2	41.5	85	2

Table E.4b

Summary of x-ray reflections in molecular simulation structures for 2,6-dichloro-PPTA; antiparallel head-to-tail polymorphs

	Structure #8			Structure #9			Structure #10		
hkl	2θ	β	I	2θ	β	I	2θ	β	I
010							15.8	0	14
110	20.3	0	6	17.2	0	6			
$1\bar{1}0$	22.6	0	24	19.5	0	14			
200	17.8	0	46	20.4	0	12	22.9	0	6
210							33.7	0	2
$2\bar{1}0$	28.3	0	1				20.8	0	6
$2\bar{2}0$							29.2	0	2
310	31.1	0	14	32.6	0	5			
001	6.9	81	23	6.7	89	100	7.2	69	100
101	11.6	36	5						
$\bar{1}01$	10.9	38	1						
$0\bar{1}1$	21.7	18	1				19.6	20	2
$\bar{1}\bar{1}1$	22.2	18	7	18.4	22	1			
111				18.6	21	1			
$\bar{1}11$	22.5	16	1						
$1\bar{1}1$	24.7	16	3						
201							22.1	18	2
211	25.1	15.8	2	24.9	16	1			
$2\bar{1}1$	30.2	13	4	28.1	14	2			
$\bar{2}11$				24.7	16	1			
$\bar{2}11$	28.2	14	6	28.2	14	2			
$2\bar{2}1$							31.3	13	1
$\bar{2}21$							28.9	14	1
301	28.2	14	4						
311	31.6	13	2						
$3\bar{1}1$	37.2	11	1						
002	13.7	81	100	13.5	89	2	14.5	69	11
102	16.8	54	2						
112	23.2	36	4						
$1\bar{1}2$	26.0	32	1						
$\bar{1}12$	24.5	34	3						
202							23.7	35	2
$\bar{2}02$	21.9	38	3						

Table E.4b (continued)

$2\bar{1}2$	33.4	24	2					
$\bar{2}12$						25.8	32	1
302	31.1	26	1					
$\bar{3}02$	29.5	28	2					
003	20.7	81	11	20.3	89	9		
103	23.0	62	1					
013	26.2	51	2					
$0\bar{1}3$	30.7	42	1					
$\bar{2}03$	26.5	50	3					
303	35.2	36	3					
104	29.7	67	1					
$\bar{1}04$	28.6	73	4					
114	32.4	58	2					
$\bar{1}14$	33.0	56	2			30.5	64	1
$\bar{2}04$	32.1	59	2					
$\bar{2}\bar{1}4$	38.8	45	2					
005	34.8	81	2					
105						35.6	75	1
$\bar{2}05$	38.3	64	2					
006	42.0	81	3	41.3	89	4		
106	43.6	72	2			41.7	83	1
016	43.7	72.0	4					
116						42.3	79	1

Figure E.1: Simulated x-ray fiber diffraction patterns for the four primary structures for 2,6-DiCl-PPTA, head-to-head, tail-to-tail isomers. The sets (a) through (d) correspond to the structures labelled 1 through 4, in order, in Table 7.3.

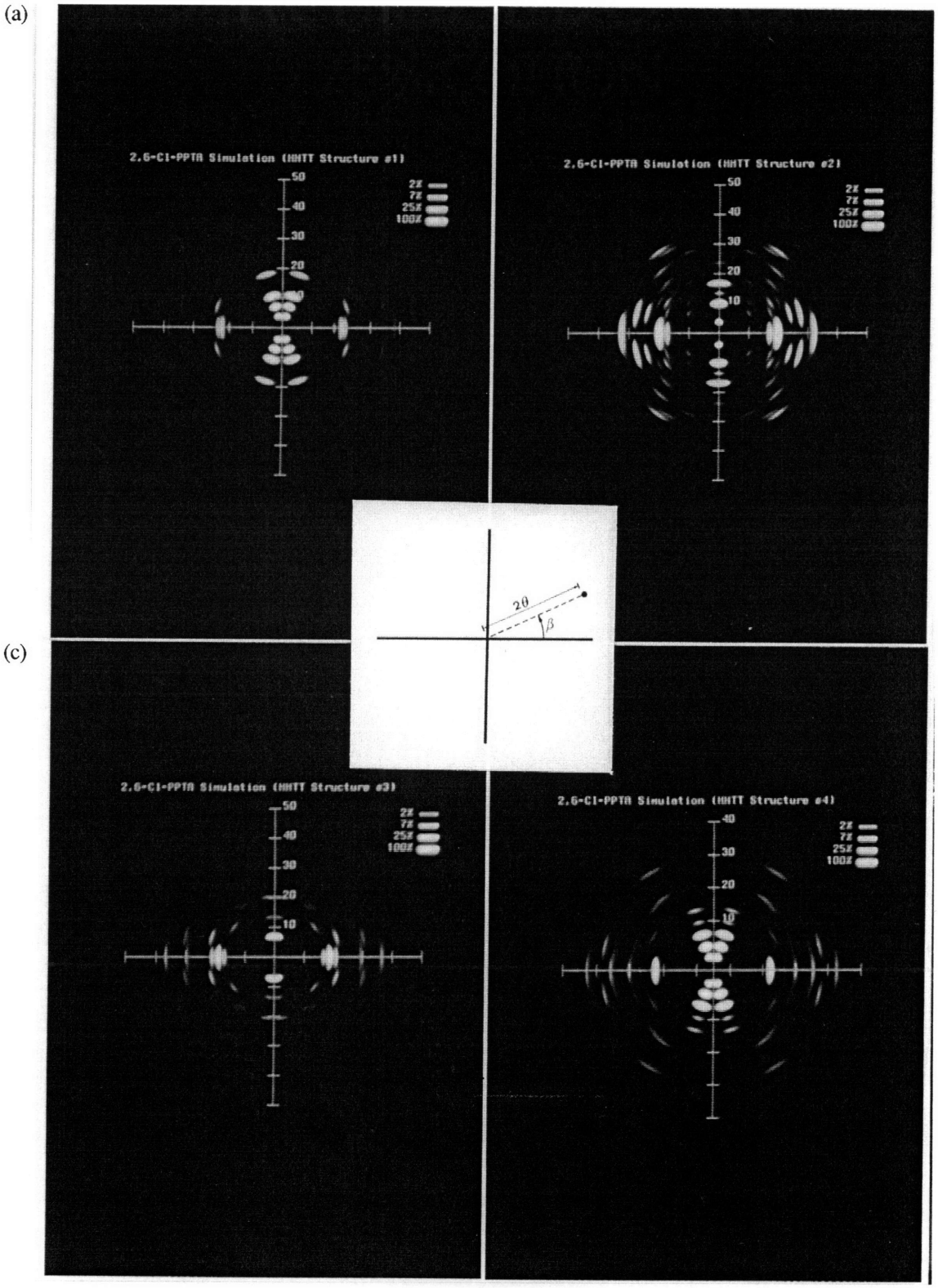

Figure E.2: Simulated x-ray fiber diffraction patterns for the ten primary structures for 2,6-DiCl-PPTA, head-to-tail isomers. The sets (a) through (j) correspond to the structures labelled 1 through 10, in order, in Table 7.5.

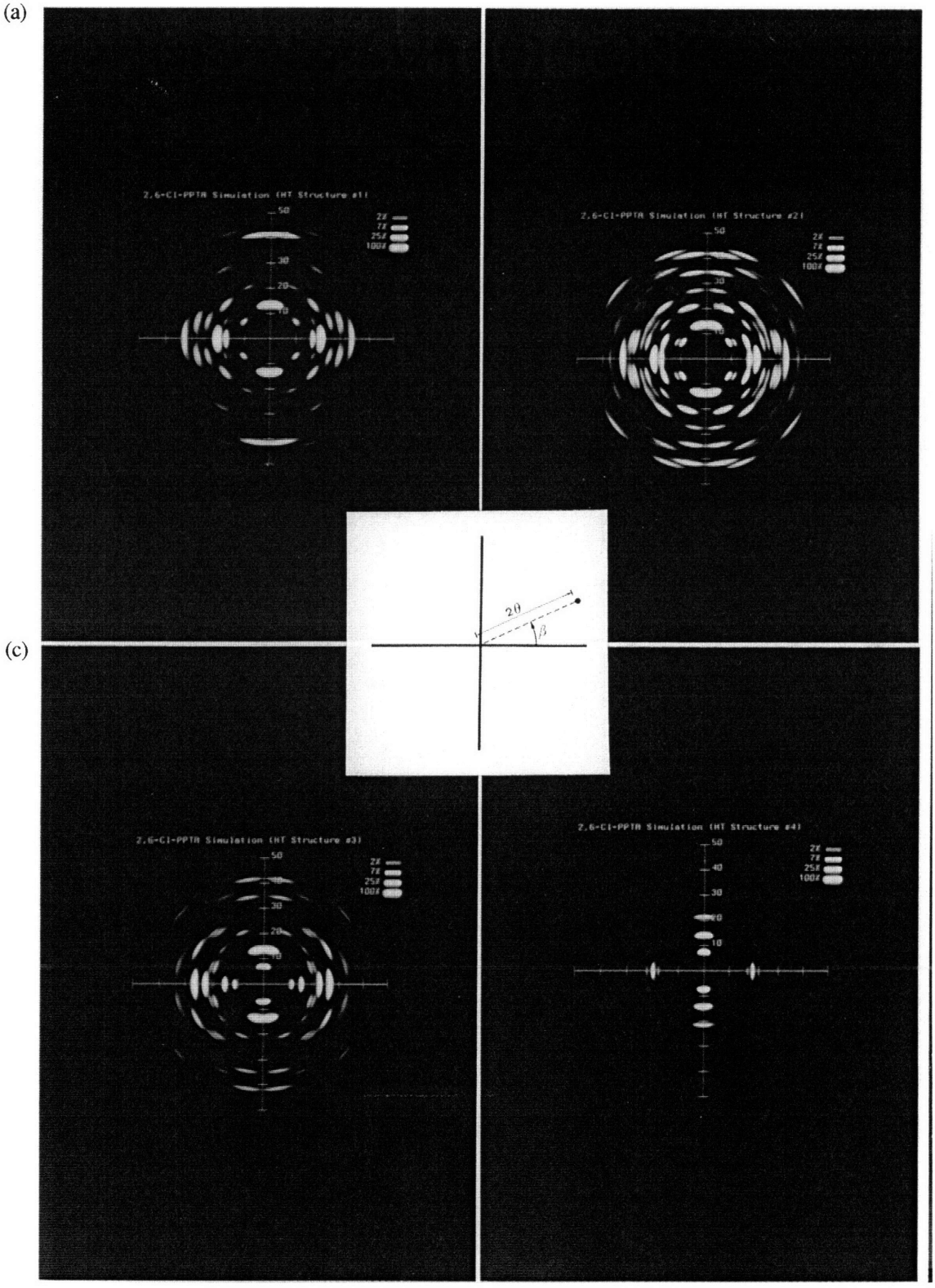

Figure E.2: Simulated x-ray fiber diffraction patterns for the ten primary structures for 2,6-DiCl-PPTA, head-to-tail isomers (continued).

(e) (f)

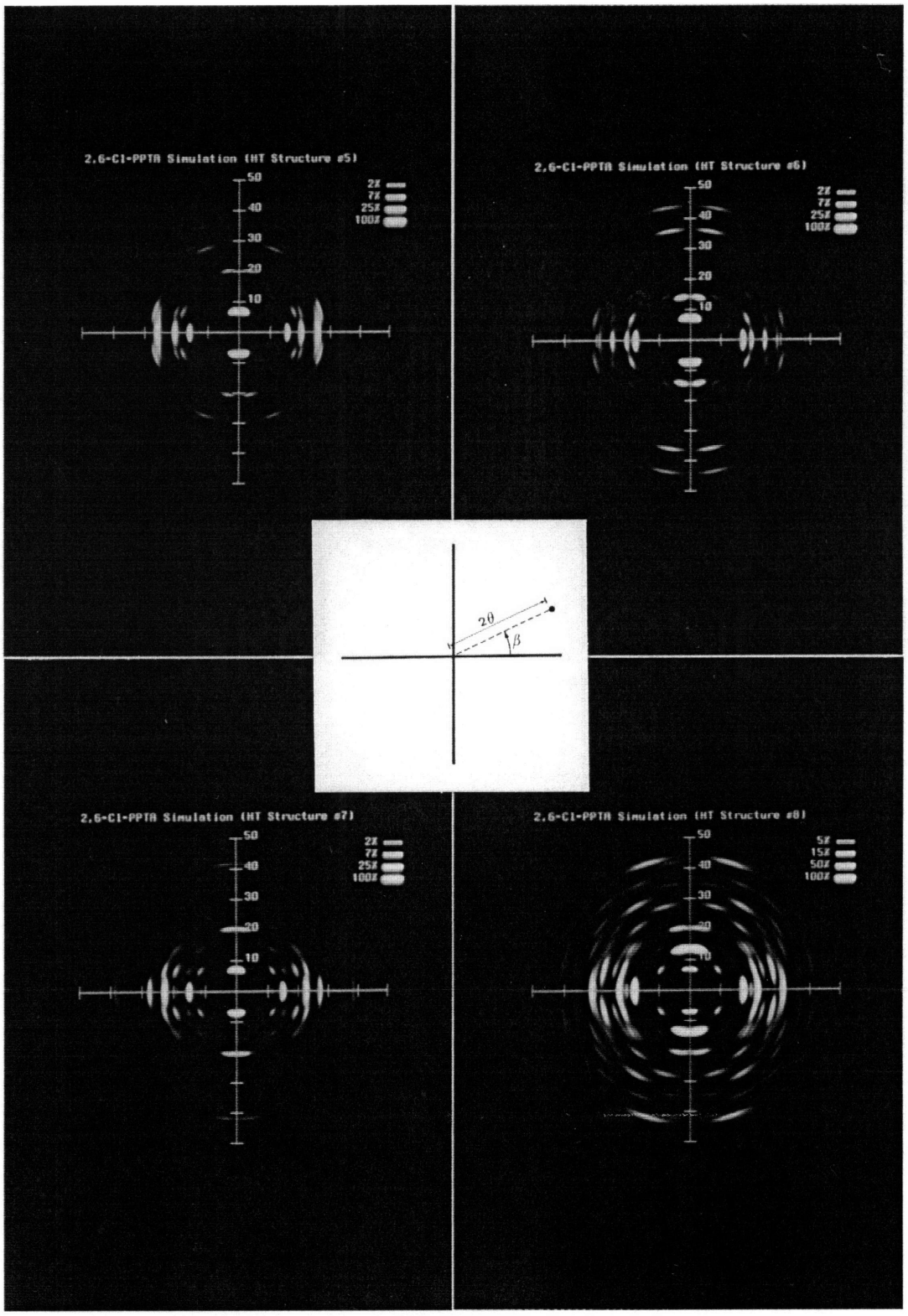

(g) (h)

Figure E.2: Simulated x-ray fiber diffraction patterns for the ten primary structures for 2,6-DiCl-PPTA, head-to-tail isomers (continued).

(i) (j)

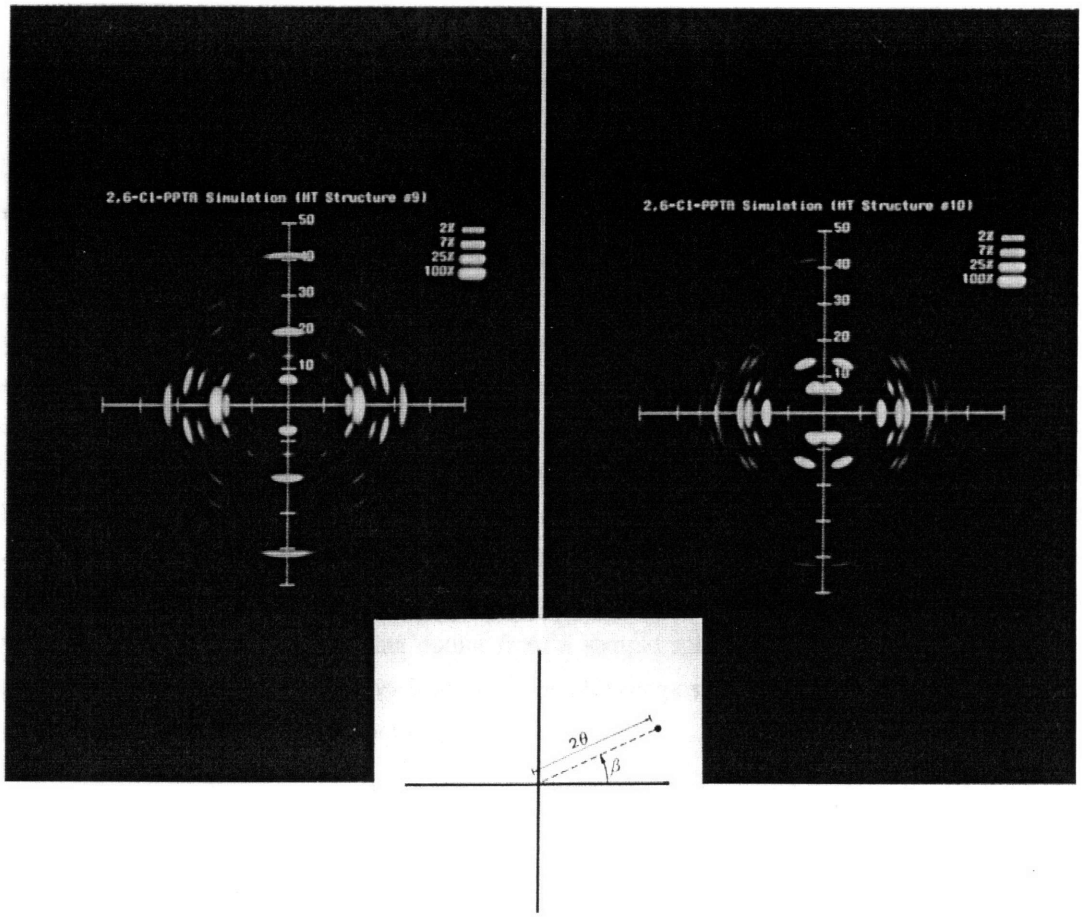

APPENDIX F: Description of Apparatus for Fiber Spinning

The basic process flow has been provided in Chapter 6. Included here are the details of the important components of the process. Figure F.1 shows front and side views of the extrusion apparatus. Figures F.2 through F.6 present, in order, the fiber spinning extruder (F.2), the detail of the syringe-and-plunger design (F.3), the solution pre-filter, used to homogenize and filter the solution while loading to the syringe for spinning (F.4), the control loop for process control and data acquisition (F.5) and the annealing operation (F.6). The dope was prepared using a teflon "screw" mixer, composed of a shaft 9.5 mm in diameter with a thread 6.4 mm in width and height winding the shaft with a pitch of 38.1 mm, fitted into a round-ended glass tube of roughly 30 mm inside diameter. The coagulation tank consisted simply of a plexiglass trough 91.3 cm long by 15.2 cm wide by 20.2 cm deep, with two freely-rotating, grooved wheels 7.6 cm in diameter located 9.0 cm from either end of the trough, to serve as guides for the coagulating filament. Table F.1 lists the parts specifications for the major components of the spinning apparatus. Figure F.7 illustrates the data output from a sample spinning trial, indicating control of temperature and both motor speeds, and monitoring of plunger position and extrusion force required. Finally, a listing of the FORTRAN control program follows.

Table F.1

Equipment parts list for fiber spinning apparatus

Drive Screw	Star Linear-Schlitten #1285-110-02, Traverse: Ausführung B, 240mm Hub	5mm pitch screw
Drive Motor	Sanyo "Super R" R 511-T002E11 DC Servo-Motor Sanyo E500200C31 Optical Shaft Encoder 353:1 Gear Box 4-Quadrant PDT-A03-20 regulator with PS1116 transformer	-3000rpm - +3000rpm 200impulses/rev
Wind-up Motor	Sanyo "Super R" R 301-T011 DC Servo-Motor Litton 820A LDBZ-500-236-12-A Optical Shaft Encoder 4-Quadrant PDT-A01-10 regulator with PS1114 transformer	-3000rpm - +3000rpm 500 impulses/rev
Force Transducer	Hottinger Baldwin Messtechnik C9/10kN with MC3 converter	0-10kN
Heating Elements	VIMO-CNS 200 watt	
Thermocontrol	Pt 100 passive thermal sensing element Amplification to 10mV/°C, accuracy to ±0.1°C PID temperature regulator	0-100°C
Data Acquisition	MetraByte DAS-20 for IBM PC/XT/AT compatibles	

Figure F.1: Front and side views of the extrusion apparatus.

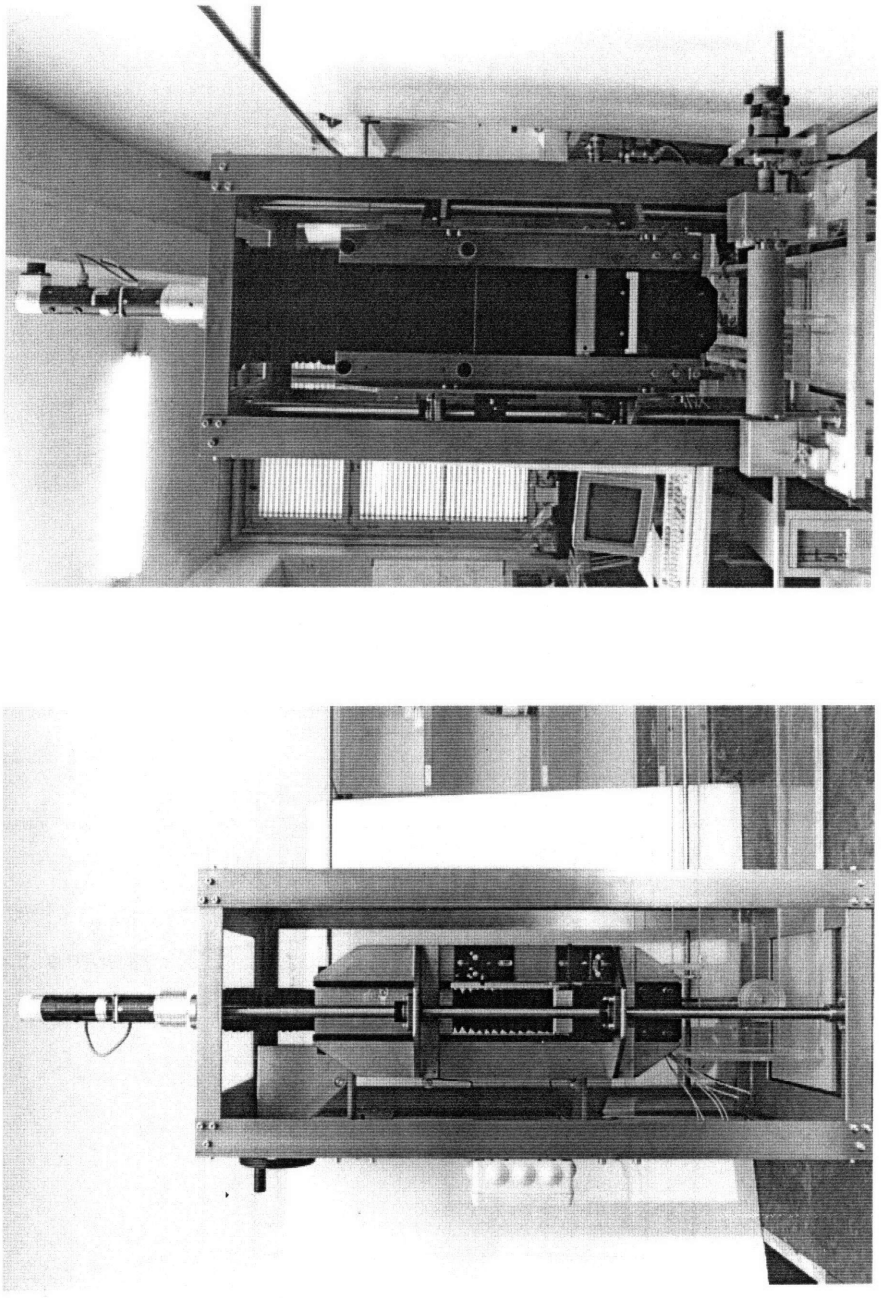

Figure F.2: Diagram of the fiber spinning extrusion apparatus.

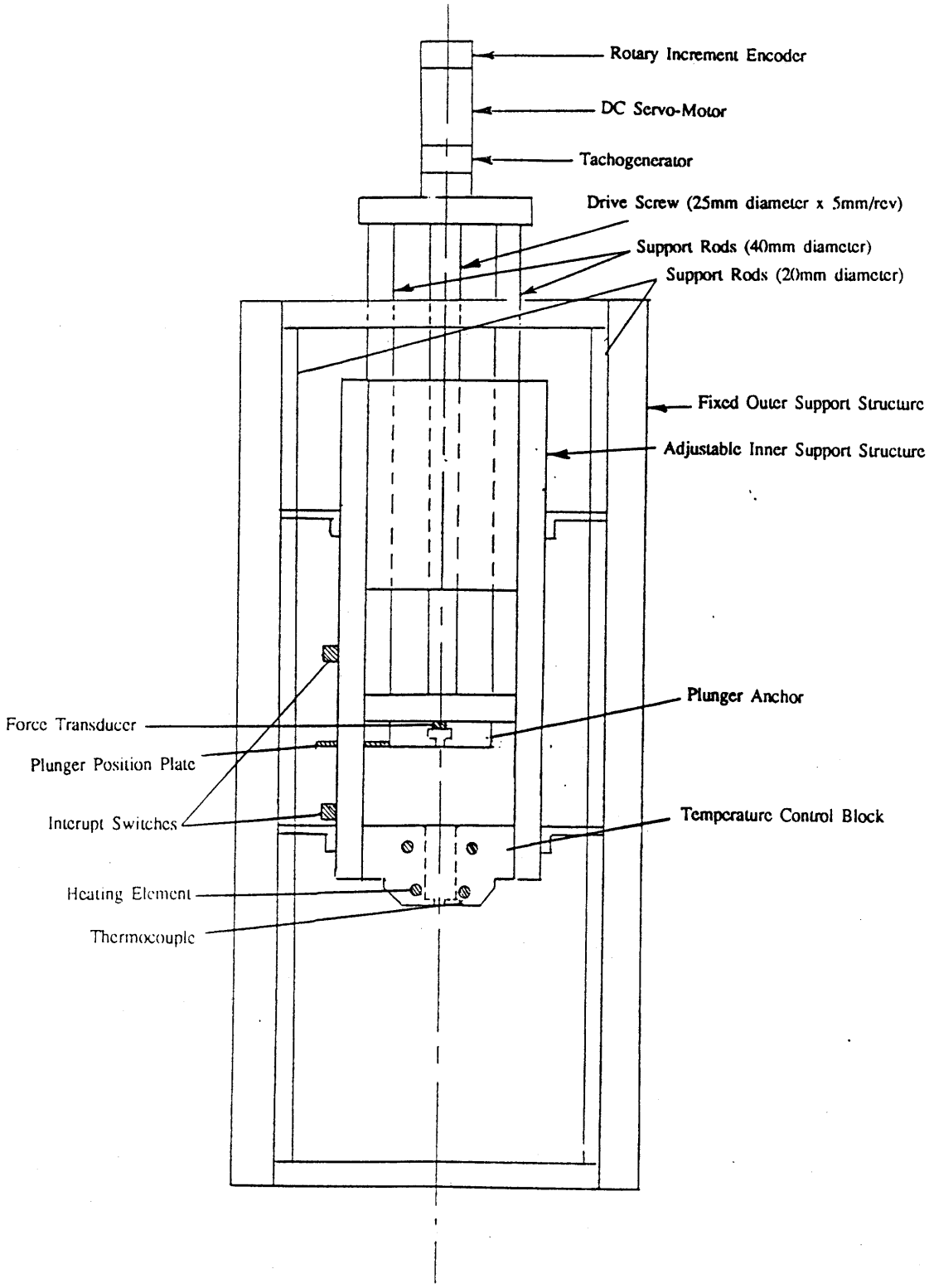

Figure F.3: Diagram of the syringe and plunger design to spin polymer dope.

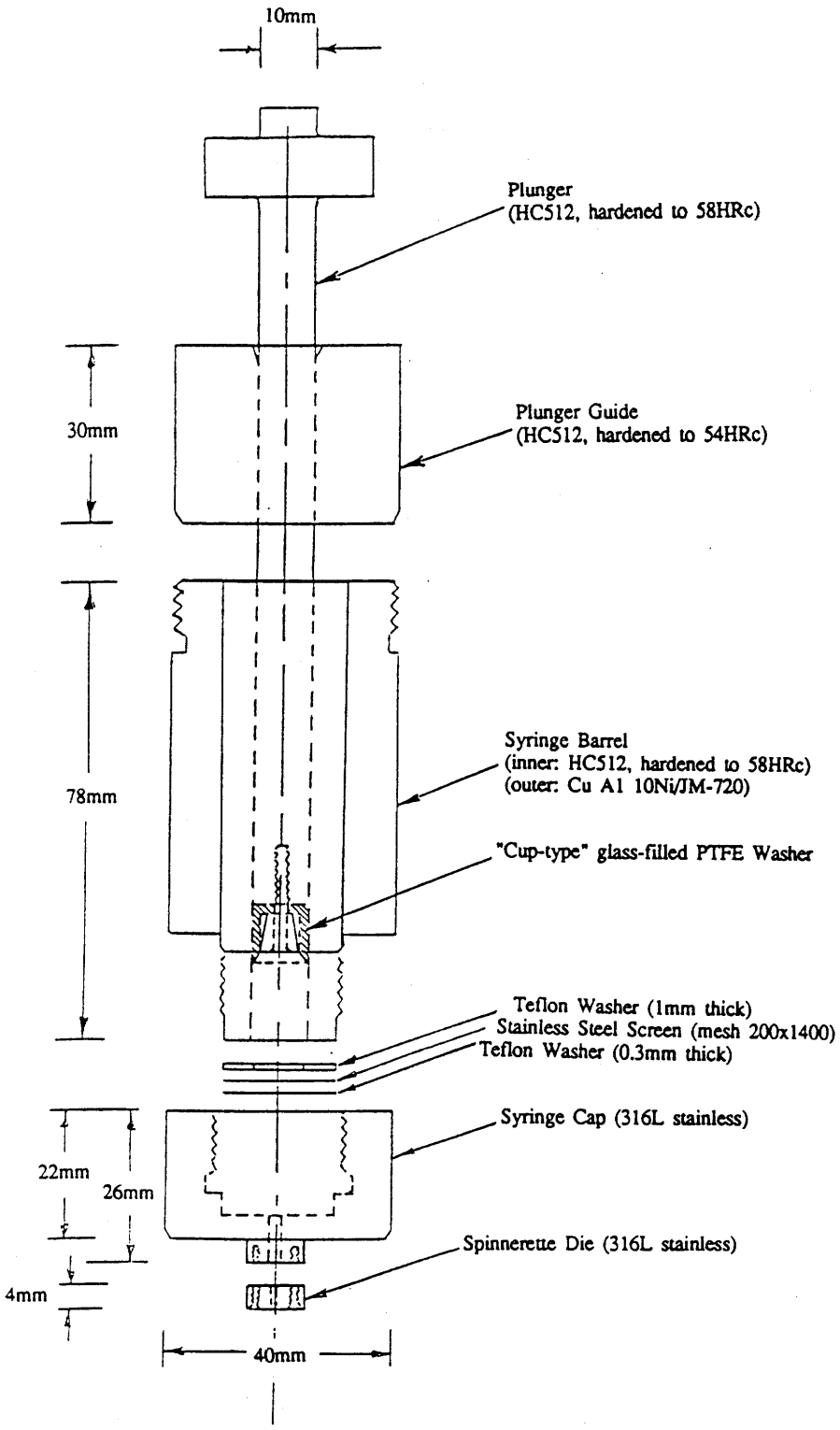

Figure F.4: Diagram of the solution pre-filter for homogenization and loading of the solution to the syringe.

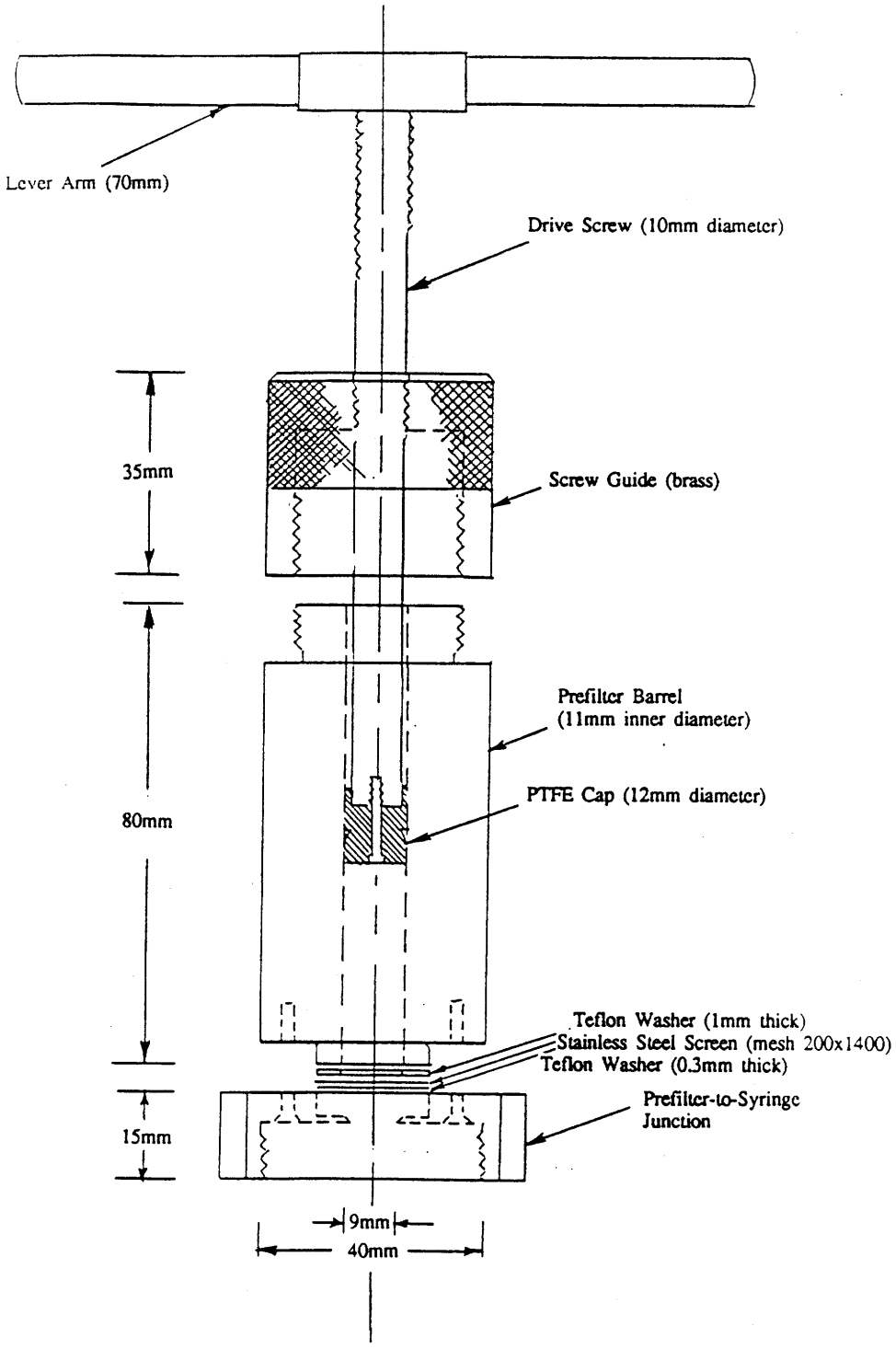

Figure F.5: Schematic of the process control and data acquisition loop for fiber spinning.

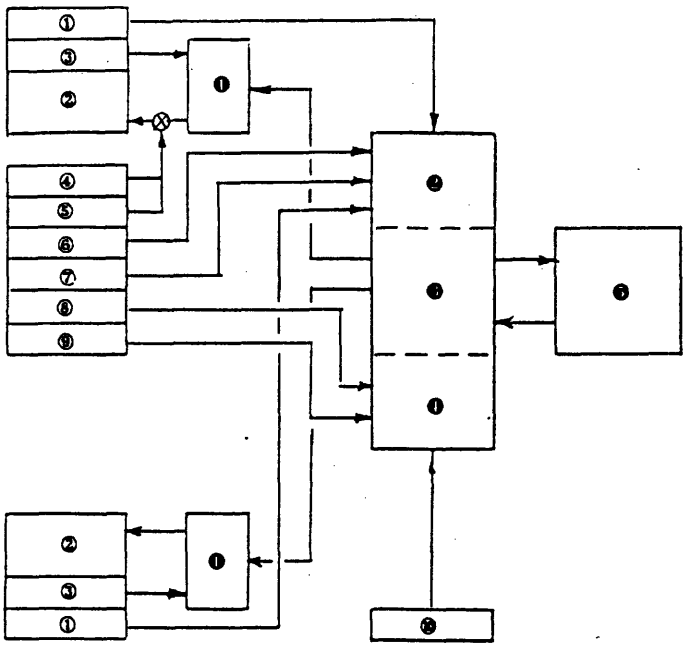

①	Optical Shaft Encoder (A signal, B signal, Reference)
②	DC Servo-Motor
③	Tachogenerator
④	Upper Interrupt Switch for Drive Motor
⑤	Lower Interrupt Switch for Drive Motor
⑥	Plunger Position Reference Switch
⑦	Plunger Stop Switch
⑧	Force
⑨	Temperature
⑩	Program Control Interrupt Switch
❶	Regulator
❷	MBC DAS-20 Digital Input
❸	MBC DAS-20 Analog Output (-10 to +10 volts)
❹	MBC DAS-20 Analog Input (differential input; -10 to +10 volts)
❺	Control Program

Figure F.6: Diagram of the fiber heat treatment process step.

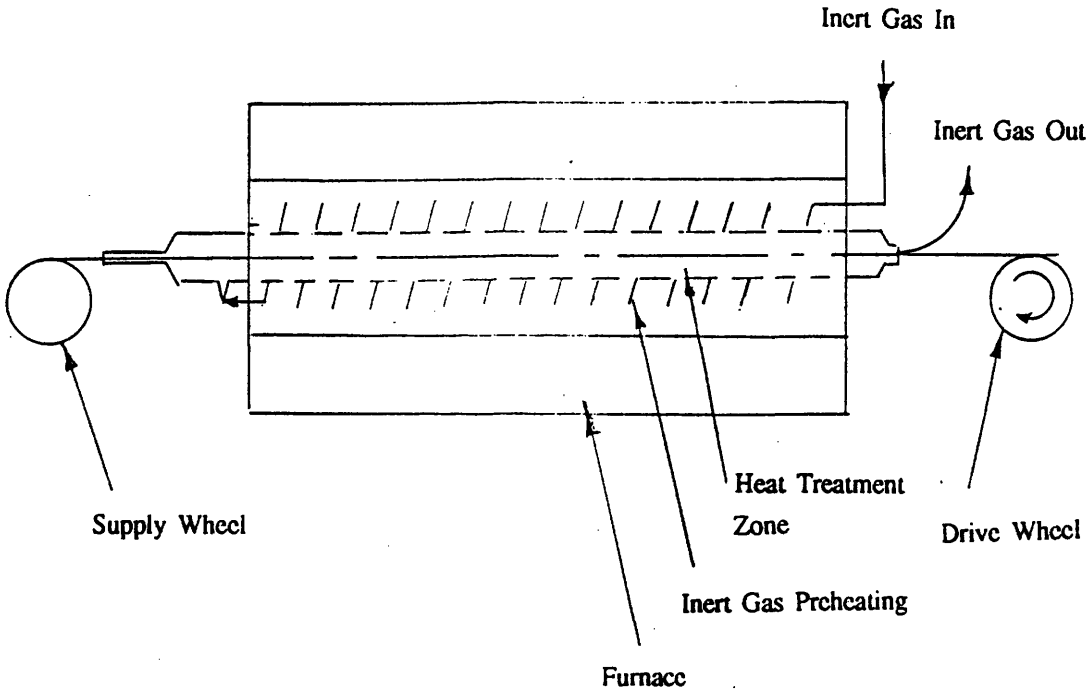

Figure F.7: Data output from a sample spinning experiment illustrating motor control at various rates. The spinnerette used in this example was 120μ in diameter.

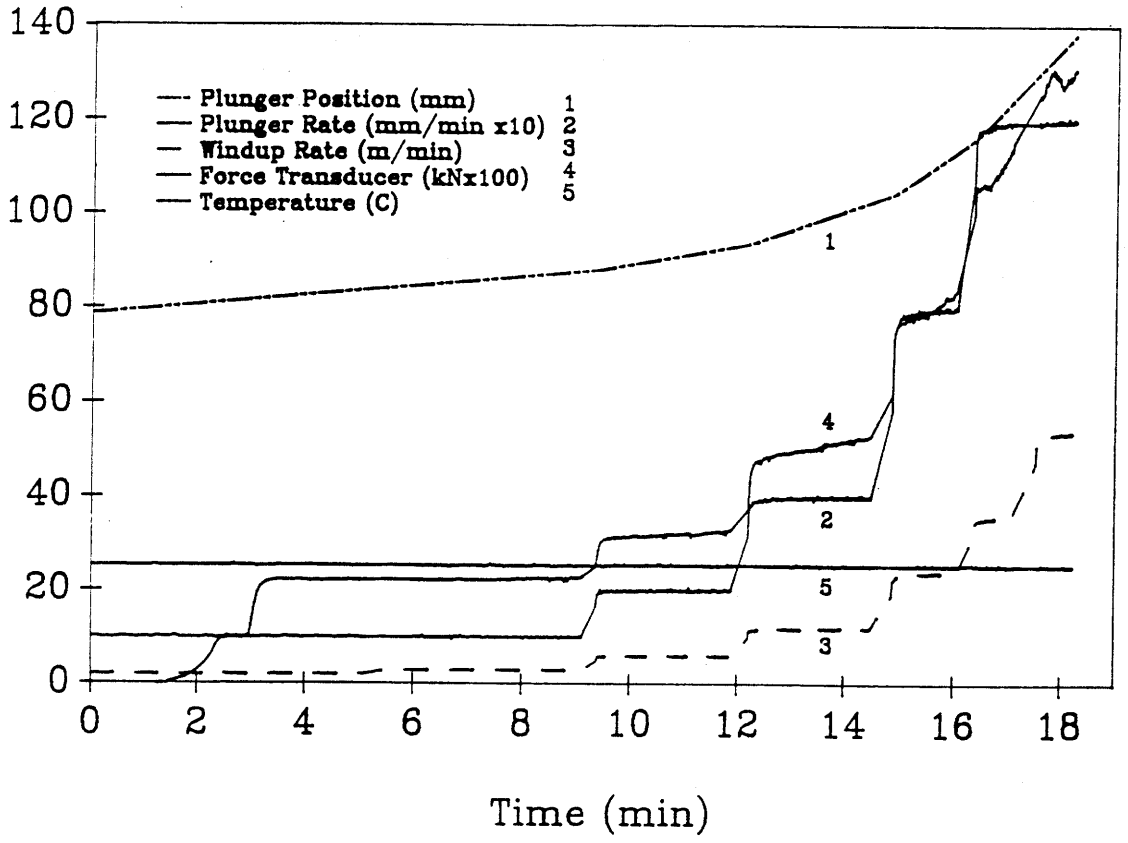

```
      PROGRAM SPINCON
C
C  Control program for operation and data acquisition during fiber
C  spinning experiments.
C
C  Version: December, 1989
C           G.C. Rutledge
C
C  Microsoft FORTRAN77 v4.01
C
C  Motor control via DAS-20 modes 3 (A/D), 7 (D/A), 14 (DI) and 23
C  (Frequency counter).
C
      CHARACTER*10 OUTF1
      CHARACTER*10 OUTF2
      INTEGER*2 DAP1(10),DAP2(10),FRP1(10),FRP2(10),DIP(10),ADP(10)
      INTEGER*2 BASE, INTLEV, DMALEV
      INTEGER*2 IERR, DAMODE, FRMODE, DIMODE, INP, IMODE, ADMODE
      INTEGER*2 DAS20, SEGADR, OFFADR, SEGPTR, OFFPTR
      INTEGER*2 TRIG, RCODE
      INTEGER*2 I, J, K, N
      INTEGER*2 JHR,JMIN,JSEC,JHUN,KHR,KMIN,KSEC,KHUN
      INTEGER*4 JCLOCK
      INTEGER*4 CRATE, BUFFER, ALLOC
      INTEGER*4 WORD1,WORD2,MASK1(16),mask2(16)
      INTEGER*4 BSZ,BSZM1,BSZD
      REAL*8    SRATE, RATE, RLIMIT, PI, Z
      REAL      R301(2),R501(2)
C
C  MASK to identify rotation direction:
C
      DATA MASK1/  0,1,-1,2,-1,0,2,1,1,2,0,-1,2,-1,1,0 /
      DATA MASK2/  0,1,-1,2,-1,0,2,1,1,2,0,-1,2,-1,1,0 /
C
C  R501 and R301 motor calibration curve parameters (in rpm):
C  (eg) DAO = R301(1)*RPM + R301(2)
C
      DATA R501/ 0.6804, -6. /
      DATA R301/ 0.6338, -5. /
      DATA PLDIAM/ 10. /
      DATA DWDIAM/ 35. /
      DATA PLIMIT/ 138.5 /
      DATA VISC /500./
      DATA FSLP,FINT / 1846, -20 /
      DATA TSLP,TINT / 100, 0 /

CONSTANTS
      EPS     = 1E-5
      PI      = 3.1415926535
      SRATE   = 5000000.0
      RLIMIT  = 76.3
      OFFSET  = 0
      BASE    = #300
      INTLEV  = 2
      DMALEV  = 1
      BSZ     = 32766
      BSZD    = 2*BSZ
C
C  Input error message and redistribution
C
      GO TO 50
 60   CONTINUE
      WRITE(*,*) 'Invalid Input.  Please, try again !'
      GO TO (101,201) IERR
 50   CONTINUE

C Initialize DAS-20 Board using mode 0 and allocate buffer:
      IMODE = 0
      DAP1(1) = BASE
      DAP1(2) = INTLEV
      DAP1(3) = DMALEV
```

```
        RCODE = DAS20(IMODE, DAP1)
        IF (RCODE .NE. 0) WRITE(*, 120) IMODE, RCODE
100     CONTINUE
        BUFFER = ALLOC(BSZ)
        IF (BUFFER .EQ. 0) WRITE(*,*) 'Cannot Allocate Buffer'
C
C  Step 0:  Print out experiment configuration and start clock
C
        WRITE(*,*) 'Insert spinnerette diameter (mm) > '
        READ(*,*)  DIEDIAM
        WRITE(*,*) 'Insert capillary length (mm) > '
        READ(*,*)  DIELEN
        WRITE(*,*) 'Spinnerette Diameter (mm) : ',DIEDIAM
        WRITE(*,*) 'Capillary Length (mm)     : ',DIELEN
        WRITE(*,*) 'Approx. Solution Visc (p) : ',VISC
        WRITE(*,*) 'Draw Wheel Diameter (mm)  : ',DWDIAM
        WRITE(*,*) ' '
C
C  "Start" clock
C
        CALL GETTIM( KHR,KMIN,KSEC,KHUN )
        LHR = KHR
        LMIN = KMIN
        LSEC = KSEC
        LHUN = KHUN
C
C  Set modes of operation:
C
        ADMODE = 3
        DAMODE = 7
        FRMODE = 23
        DIMODE = 14
        DAP1(1) = 0
        DAP2(1) = 1
        FRP1(2) = 1
        FRP2(2) = 2
C
C  Initialize motor operation and control:
C
        DR1CRT = 30.
        DR2CRT = 30.
        DR1 = 0.
        DR2 = 0.
        DAP1(2) = NINT( R501(1)*DR1 + R501(2) )
        DAP2(2) = NINT( R301(1)*DR2 + R301(2) )
        RCODE = DAS20( DAMODE,DAP1 )
        RCODE = DAS20( DAMODE,DAP2 )
        FRP1(1) = 125
        FRP2(1) = 125
        RCODE = DAS20( FRMODE,FRP1 )
        RCODE = DAS20( FRMODE,FRP2 )
        FREQ1 = REAL( FRP1(3) )*300./REAL( FRP1(1) )
        FREQ2 = REAL( FRP2(3) )*120./REAL( FRP2(1) )
        POS1 = 0.
        POS2 = 0.
C
C  Zero counters for motor directional control
C
        IDO1  = 0
        IDO2  = 0
        NERR1 = 0
        NERR2 = 0
        KROT1 = 0
        KROT2 = 0
        KDIR1 = SIGN( 1,DR1 )
        KDIR2 = SIGN( 1,DR2 )
C
        NOUT = 0
C
C  Step 1: Raise plunger from current position to Positionschalter
C
```

```
      OUTF1 = 'TSPIN1.DAT'
      OUTF2 = 'CSPIN1.DAT'
      OPEN(UNIT=11,FILE=OUTF1)
      OPEN(UNIT=10,FILE=OUTF2)
  890 CLOSE(UNIT=11)
      CLOSE(UNIT=10)
      DAP2(2) = NINT( R301(2) )
      RCODE = DAS20( DAMODE,DAP2 )
      WRITE(*,*) 'Raising plunger to zero position ... '
      DR1 = -2900.
      DAP1(2) = NINT( R501(1)*DR1 + R501(2) )
      RCODE = DAS20( DAMODE,DAP1 )
  800 RCODE = DAS20( DIMODE,DIP )
      IBIT7 = DIP(1)/128
      IF( IBIT7*KOSHTDN.GT.0 ) GO TO 810
      KOSHTDN = MAX( 0,IBIT7 )
      GO TO 800
  810 CONTINUE
      POS1 = 0.
      WRITE(*,*) 'Plunger position initialized '
C
C  Step 2: Lower plunger to Load Point position (30 mm)
C
      DR1 = 0.
      DAP1(2) = NINT( R501(2) )
      RCODE = DAS20( DAMODE,DAP1 )
      PAUSE  'Hit RET to lower plunger to load point pos. '
      WRITE(*,*) 'Lowering plunger to Load Point ... '
      DR1 = 2500.
      PLOAD = 25.
      DAP1(2) = NINT( R501(1)*DR1 + R501(2) )
      CALL GETTIM( KHR,KMIN,KSEC,KHUN )
      RCODE = DAS20( DAMODE,DAP1 )
  820 CALL GETTIM( JHR,JMIN,JSEC,JHUN )
      JCLOCK = 100*(60*(60*(JHR-KHR) + (JMIN-KMIN)) + (JSEC-KSEC))
     +             + (JHUN-KHUN)
      KHR  = JHR
      KMIN = JMIN
      KSEC = JSEC
      KHUN = JHUN
      DCLOCK = REAL(JCLOCK)/6000.
      POS1 = POS1 + DR1*DCLOCK*5./353.
      IF( POS1.GE.PLOAD ) GO TO 830
      GO TO 820
  830 CONTINUE
      DR1 = 0
      DAP1(2) = NINT( R501(2) )
      RCODE = DAS20( DAMODE,DAP1 )
      RCODE = DAS20( FRMODE,FRP1 )
      RCODE = DAS20( FRMODE,FRP2 )
      FREQ1 = REAL( FRP1(3) )*300./REAL( FRP1(1) )
      FREQ2 = REAL( FRP2(3) )*120./REAL( FRP2(1) )
      IF( FREQ1.GT.2 ) WRITE(*,*) 'Motor 1 not stationary'
      IF( FREQ2.GT.2 ) WRITE(*,*) 'Motor 2 not stationary'
      PAUSE 'Load Plunger and hit RETURN to continue >>> '
C
C  Step 3: Lower plunger into barrel
C
      WRITE(*,*) 'Enter approximate quantity of solution loaded (ml) > '
      READ(*,*) QSOLN
      PFULL = 4000.*QSOLN/PI/PLDIAM**2
      WRITE(*,*) 'Lowering plunger to Solution ... '
      DR1 = 2000.
      PSOLN = PLIMIT - PFULL - 2.
      IF(PLIMIT-PSOLN.LE.0.1) WRITE(*,*) 'WARNING: No Solution'
      DAP1(2) = NINT( R501(1)*DR1 + R501(2) )
      CALL GETTIM( KHR,KMIN,KSEC,KHUN )
      RCODE = DAS20( DAMODE,DAP1 )
  840 CALL GETTIM( JHR,JMIN,JSEC,JHUN )
      JCLOCK = 100*(60*(60*(JHR-KHR) + (JMIN-KMIN)) + (JSEC-KSEC))
     +             + (JHUN-KHUN)
```

```
        KHR  = JHR
        KMIN = JMIN
        KSEC = JSEC
        KHUN = JHUN
        DCLOCK = REAL(JCLOCK)/6000.
        POS1 = POS1 + DR1*DCLOCK*5./353.
        IF( POS1.GE.PSOLN ) GO TO 850
        GO TO 840
  850   CONTINUE
        DR1 = 0.
        DAP1(2) = NINT( R501(2) )
        RCODE = DAS20( DAMODE,DAP1 )
        RCODE = DAS20( FRMODE,FRP1 )
        RCODE = DAS20( FRMODE,FRP2 )
        FREQ1 = REAL( FRP1(3) )*300./REAL( FRP1(1) )
        FREQ2 = REAL( FRP2(3) )*120./REAL( FRP2(1) )
        IF( FREQ1.GT.3 ) WRITE(*,*) 'Motor 1 not stationary'
        IF( FREQ2.GT.3 ) WRITE(*,*) 'Motor 2 not stationary'
        PAUSE 'Plunger in barrel position; hit RETURN to continue >>> '
        NOUT = NOUT + 1
        OUTF1 = 'TSPIN'//CHAR(NOUT + ICHAR('0'))//'.DAT'
        OUTF2 = 'CSPIN'//CHAR(NOUT + ICHAR('0'))//'.DAT'
        OPEN(UNIT=11,FILE=OUTF1)
        OPEN(UNIT=10,FILE=OUTF2)
        WRITE(11,*) '  TIME     POSITION    RATE1     RATE2     FORCE     TEMP'      C
C  Enter loop size
C
        IERR = 1
  101   CONTINUE
        WRITE(*,*) 'Enter size of control loop > '
        READ(*, 132, ERR = 60) NLP
        IF( NLP.LT.1 ) GO TO 60
C
C  Load motor speed setpoint
C  (max range is -42.5 to +42.5 mm/min;
C   maximum is approximated using F = 8(pi)uLv
C   F in newtons, u in poise, L in mm, and v in mm/min
C
        FMAX = 10000.
        FVMAX = 2.387E7*FMAX*(DIEDIAM/PLDIAM)**2/VISC/DIELEN
C
  400   WRITE(*,41)
        WRITE(*,42) FVMAX/1000.
   41   FORMAT(1X,'Input linear extrusion rate ie nom fiber velocity')
   42   FORMAT(1X,'     (up to ',f8.2,' m/min) >')
        READ(*,*) FASER
        VRPM1SET = (DIEDIAM/PLDIAM)**2*FASER*1000.
        RPM1SET = VRPM1SET*70.6
        WRITE(*,*) 'Input draw wheel linear rate ',
     +             '(-329 to +329 m/min) >'
        READ(*,*) VRPM2SET
        IF (ABS(FASER).GE.EPS) THEN
          DRAWRAT = VRPM2SET/FASER
        ELSE
          DRAWRAT = 9999999.
        END IF
        WRITE(*,*) 'Nominal draw ratio:              ',DRAWRAT
        RPM2SET = VRPM2SET*1000./DWDIAM/PI
        WRITE(*,*) 'Is this correct? (0=no,1=yes) > '
        READ(*,*) KORREKT
        CALL GETTIM( JHR,JMIN,JSEC,JHUN )
        LCLOCK = 100*(60*(60*(JHR-LHR) + (JMIN-LMIN)) + (JSEC-LSEC))
     +           + (JHUN-LHUN)
        CUMTIME = REAL(LCLOCK)/100.
        WRITE(10,1) CUMTIME ,faser,vrpm2set,drawrat
        IF(KORREKT.NE.1) GO TO 400
        IF (ABS(FASER).LE.EPS) THEN
          DR1 = 0
          DAP1(2) = NINT( R501(2) )
          RCODE = DAS20( DAMODE,DAP1 )
          RCODE = DAS20( FRMODE,FRP1 )
```

```
          FREQ1 = REAL( FRP1(3) )*300./REAL( FRP1(1) )
        END IF
        IF (ABS(VRPM2SET).LE.EPS) THEN
          DR2 = 0
          DAP2(2) = NINT( R301(2) )
          RCODE = DAS20( DAMODE,DAP2 )
          RCODE = DAS20( FRMODE,FRP2 )
          FREQ2 = REAL( FRP2(3) )*120./REAL( FRP2(1) )
        END IF
        WRITE(*,*) 'Beginning Spin ... '
C
C  Gate interval must be set based on RPM at low RPM:
C  Motor1 sends 200 impulses/cycle; Motor2 sends 500 impulses/cycle
C
        MINCLK  = 50
        MN1GATE = 300*MINCLK/(ABS(RPM1SET) + 1.)
        MN2GATE = 120*MINCLK/(ABS(RPM2SET) + 1.)
        FRP1(1) = MAX( 125,MN1GATE )
        FRP2(1) = MAX( 125,MN2GATE )
        FR1CNV  = 300./REAL( FRP1(1) )
        FR2CNV  = 120./REAL( FRP2(1) )
 450    CONTINUE
C
C  Set a maximum speed step for transitions
C
        STPCNT = 50.
        IBIT6C = 0
        IBIT7C = 0
C
C  Begin Control Loop >>>>>>>>>>>>>>>>>>>>>>>>>>>>>>>>>>>>>>>>>>>>>>>>>>>>>>>>
C
         DO 1000 LP=1,NLP
C
C  Compute signal(s) to send to motor(s) (variable gain):
C
          DELTA1 = RPM1SET - FREQ1*KDIR1
          IF( ABS(DELTA1/(RPM1SET+EPS)).LE.0.025 ) THEN
            GADJ1 = .05
          ELSE IF( ABS(DELTA1/(RPM1SET+EPS)).LE.0.1 ) THEN
            GADJ1 = .2
          ELSE
            GADJ1 = .7
          END IF
          STPMAX = REAL( FREQ1/100 + 1 )*STPCNT
          STPM   = MIN( STPMAX,ABS(DELTA1) )
          SGN    = SIGN( 1.,DELTA1 )
          DGAIN1 = STPM/( DELTA1*SGN + EPS )*GADJ1
          DR1 = ( DELTA1*DGAIN1 + DR1 )
          DR1 = MAX( -3000.,MIN( 3000.,DR1) )
          DAP1(2) = NINT( R501(1)*DR1 + R501(2) )
C
          DELTA2 = RPM2SET - FREQ2*KDIR2
          IF( ABS(DELTA2/(RPM2SET+EPS)).LE.0.025 ) THEN
            GADJ2 = .05
          ELSE IF( ABS(DELTA2/(RPM2SET+EPS)).LE.0.1 ) THEN
            GADJ2 = .2
          ELSE
            GADJ2 = .7
          END IF
          STPMAX = REAL( FREQ2/100 + 1 )*STPCNT
          STPM   = MIN( STPMAX,ABS(DELTA2) )
          SGN    = SIGN( 1.,DELTA2 )
          DGAIN2 = STPM/( DELTA2*SGN + EPS )*GADJ2
          DR2 = ( DELTA2*DGAIN2 + DR2 )
          DR2 = MAX( -3000.,MIN( 3000.,DR2) )
          DAP2(2) = NINT( R301(1)*DR2 + R301(2) )
C
C  Get time of iteration, update postions, and send signal(s)
C
          CALL GETTIM( JHR,JMIN,JSEC,JHUN )
          JCLOCK = 100*(60*(60*(JHR-KHR) + (JMIN-KMIN)) + (JSEC-KSEC))
```

```
     +             + (JHUN-KHUN)
           LCLOCK = 100*(60*(60*(JHR-LHR) + (JMIN-LMIN)) + (JSEC-LSEC))
     +             + (JHUN-LHUN)
           DCLOCK = REAL(JCLOCK)/6000.
           CUMTIME = REAL(LCLOCK)/100.
           POS1 = POS1 + REAL(KDIR1)*FREQ1*DCLOCK*5./353.
        IF( (LP.NE.1).AND.((MAX(REAL(KDIR1)*PLIMIT,0.)-REAL(KDIR1)*POS1)
     +    .LE.0.01) ) GO TO 490
C           POS2 = POS2 + FREQ2*DCLOCK
           RCODE = DAS20( DAMODE,DAP1 )
           RCODE = DAS20( DAMODE,DAP2 )
           KHR  = JHR
           KMIN = JMIN
           KSEC = JSEC
           KHUN = JHUN
C
C  Read frequency counters
C
           RCODE = DAS20( FRMODE,FRP1 )
           RCODE = DAS20( FRMODE,FRP2 )
           FREQ1 = REAL( FRP1(3) )*FR1CNV
           FREQ2 = REAL( FRP2(3) )*FR2CNV
C
C  Force Transducer (CH0), Temperature (CH1) and Program Switch (CH2)
C  ******* For reasons not understood, it appears to be necessary to read
C  ******* each AI twice in succession to get accurate values
C  ******* possibly a board communicaiton problem
C
           ADP(1) = 3
           ADP(2) = 0
           RCODE = DAS20( ADMODE,ADP )
           ADP(1) = 3
           ADP(2) = 0
           RCODE = DAS20( ADMODE,ADP )
           IF(RCODE.NE.0) WRITE(*,*) 'RCODE ERROR ',RCODE
           FVOLTS = ADP(1)*10./4096.
           ADP(1) = 4
           ADP(2) = 1
           RCODE = DAS20( ADMODE,ADP )
           ADP(1) = 4
           ADP(2) = 1
           RCODE = DAS20( ADMODE,ADP )
           IF(RCODE.NE.0) WRITE(*,*) 'RCODE ERROR ',RCODE
           TVOLTS = ADP(1)*1./4096.
           ADP(1) = 1
           ADP(2) = 2
           RCODE = DAS20( ADMODE,ADP )
           ADP(1) = 1
           ADP(2) = 2
           RCODE = DAS20( ADMODE,ADP )
           IF(RCODE.NE.0) WRITE(*,*) 'RCODE ERROR ',RCODE
           SVOLTS = ADP(1)*20./4096.
           INTERUPT = NINT(SVOLTS/5.)
C
C  Record data
C
           CEXP = CUMTIME
           PEXP = POS1
           R1EXP = REAL(KDIR1)*((FREQ1/70.6)*(PLDIAM/DIEDIAM)**2)
     +                 /1000
           R2EXP = REAL(KDIR2)*FREQ2*DWDIAM*PI/1000
           FEXP = FVOLTS*FSLP + FINT
           TEXP = TVOLTS*TSLP + TINT
           WRITE(11,1) CEXP/60,PEXP,R1EXP,R2EXP,FEXP/100,TEXP/10
           WRITE(*,5)  LP,CEXP,PEXP,R1EXP,R2EXP,FEXP,TEXP
C
C  Check for software shutdown endswitches open
C
           RCODE = DAS20( DIMODE,DIP )
           IBIT7 = DIP(1)/128
           NDIP = DIP(1) - IBIT7*128
```

```
          IBIT6 = NDIP/64
          KNSHTDN = KDIR1*( IBIT6 - IBIT7 )
          IF( KNSHTDN*KOSHTDN.GT.0 ) GO TO 490
          KOSHTDN = MAX( 0,KNSHTDN )
          IF(LP.EQ.1) KOSHTDN = 0
C
C  If motor(s) currently run below critical speed, determine direction of
C  rotation (unless motor(s) is essentially idle; ie rpm < 1)
C
          LOW1 = 1
          LOW2 = 1
          IF( (FREQ1.GT.DR1CRT).OR.(FREQ1.LE.2.0) ) LOW1 = 0
          IF( (FREQ2.GT.DR2CRT).OR.(FREQ2.LE.2.0) ) LOW2 = 0
          IF( (LOW1.NE.1).AND.(LOW2.NE.1) ) GO TO 1100
            NCNT = 0
            NDXO1 = 0
            NDXO2 = 0
            NCYC1 = 0
            NCYC2 = 0
            NERR1 = 0
            NERR2 = 0
            KTLY1 = 0
            KTLY2 = 0
            IDO1 = 0
            IDO2 = 0
 1200       RCODE = DAS20( DIMODE,DIP )
C
C  Check for software shutdown endswitches open
C
            IBIT7 = DIP(1)/128
            NDIP = DIP(1) - IBIT7*128
            IBIT6 = NDIP/64
            KNSHTDN = KDIR1*( IBIT6 - IBIT7 )
            IF( KNSHTDN*KOSHTDN.GT.0 ) GO TO 490
            KOSHTDN = MAX( 0,KNSHTDN )
C
C Signal decomposition:
C
            NDIP = NDIP - IBIT6*64
            IBIT5 = NDIP/32
            NDIP = NDIP - IBIT5*32
            IBIT4 = NDIP/16
            NDIP = NDIP - IBIT4*16
            IBIT3 = NDIP/8
            NDIP = NDIP - IBIT3*8
            IBIT2 = NDIP/4
            NDIP = NDIP - IBIT2*4
            IBIT1 = NDIP/2
            IBIT0 = NDIP - IBIT1*2
            IF( LOW1.NE.1) GO TO 1210
              NDXN1 = IBIT0
               NCYC1 = NCYC1 + ABS(NDXN1 - NDXO1)
              IDN1 = 2*IBIT1 + IBIT2
              NELEM = 4*IDO1 + IDN1 + 1
              KDR = MASK1(NELEM)
              NERR1 = NERR1 + KDR/2
                IF( ABS(KDR).EQ.1 ) THEN
                NERR1 = NERR1 + ABS(KDR-KDIR1)/2
                KTLY1 = KTLY1 + KDR
                KDIR1 = SIGN(1,KTLY1)
              END IF
              IDO1 = IDN1
              NDXO1 = NDXN1
              IF(NCYC1.GT.1) LOW1 = 2
 1210         IF( LOW2.NE.1) GO TO 1220
              NDXN2 = IBIT3
              NCYC2 = NCYC2 + ABS(NDXN2 - NDXO2)
              IDN2 = 2*IBIT4 + IBIT5
              NELEM = 4*IDO2 + IDN2 + 1
              KDR = MASK2(NELEM)
              NERR2 = NERR2 + KDR/2
```

```
              IF( ABS(KDR).EQ.1 ) THEN
              NERR2 = NERR2 + ABS(KDR-KDIR2)/2
              KTLY2 = KTLY2 + KDR
              KDIR2 = SIGN(1,KTLY2)
            END IF
            IDO2 = IDN2
            NDXO2 = NDXN2
            IF(NCYC2.GT.1) LOW2 = 2
1220        IF( (LOW1.EQ.1).OR.(LOW2.EQ.1) ) GO TO 1200
            IF( LOW1.EQ.2 ) THEN
            ERROR1 = REAL(NERR1)/REAL(200*NCYC1)
            IF( ERROR1.GT.0.009 ) WRITE(*,*) 'Low speed error 1 = ',
     +      ERROR1
          END IF
          IF( LOW2.EQ.2 ) THEN
            ERROR2 = REAL(NERR2)/REAL(500*NCYC2)
            IF( ERROR2.GT.0.009 ) WRITE(*,*) 'Low speed error 2 = ',
     +      ERROR2
          END IF
        GO TO 1010
1100    CONTINUE
        KDIR1 = SIGN( 1,DR1 )
        KDIR2 = SIGN( 1,DR2 )
1010    IF(INTERUPT.EQ.1) GO TO 220
1000    CONTINUE
220     WRITE(*,*) ' 1,2,3,4,5 - REINITIALIZE, Reset LOOPSIZE, SPEEDS,',
     +           ' REPEAT, END '
        IERR = 2
201     CONTINUE
      READ(*, 132, ERR = 60 ) INP
      IF ((INP .GT. 5) .OR. (INP .LE. 0)) GOTO 60
      GOTO ( 890,101,400,450,600 ) INP

490   CONTINUE
      IF( IBIT6.EQ.1 ) WRITE(*,*) 'Endschalter unten geschlossen'
      IF( IBIT7.EQ.1 ) WRITE(*,*) 'Positionschalter oben geschlossen'
500   CONTINUE
      DAP1(2) = NINT( R501(2) )
      DAP2(2) = NINT( R301(2) )
      RCODE = DAS20( DAMODE,DAP1 )
      RCODE = DAS20( DAMODE,DAP2 )
      GO TO 220
600   CONTINUE
      DAP1(2) = NINT( R501(2) )
      DAP2(2) = NINT( R301(2) )
      RCODE = DAS20( DAMODE,DAP1 )
      RCODE = DAS20( DAMODE,DAP2 )
      STOP

120   FORMAT (' Mode ', I2, ' ,  Error = ', I4)
132   FORMAT (16I7)
  1   FORMAT(1X,F10.2,2X,F6.2,2X,F6.2,2X,F6.2,2X,F7.1,2X,F6.1)
  5   FORMAT(1X,I4,F10.2,2X,F6.2,2X,F6.2,2X,F6.2,2X,F7.1,2X,F6.1)
      END
```

APPENDIX G: FORTRAN Listing of Program for Simulation of Ordered Polymer Structure

This appendix contains one version of the FORTRAN code used to simulate the polymer solid state, calculate potential energy, and minimize with respect to degrees of freedom. It also contains the subroutines required for imposing deformation. The following subroutines are listed for the main program:

CMODEL (main)	UNITCEL	RDSTRAIN	EES
CELGEN	DENS	ATRNS	VECTORIZ
LDVAR	NONBOND	MM	CURTATE
LDCHN	SUBSET	MV	CURINV
RANDS1	ENERGY	VV	MULMAX
COORDN	RTRNS	MT	VA10A
PHENYL	STRAIN	MA	MC11A
HELIX	DATARD	JACOBI	
GYRA	RDWRITE	ELJ	

Following the main code is a listing of the major replacement subroutines required for simulating the modified chain description used to generate mechanical property information. Lastly, sample input files required by the program are provided.

```
      PROGRAM CMODEL
C
C  ********************************************************************
C  *                                                                  *
C  *               POLYMER CRYSTAL SIMULATION PROGRAM                 *
C  *                                                                  *
C  *                      GREGORY C. RUTLEDGE                         *
C  *                                                                  *
C  *               DEPARTMENT OF CHEMICAL ENGINEERING                 *
C  *              MASSACHUSETTS INSTITUTE OF TECHNOLOGY               *
C  *                       NOVEMBER 1989                              *
C  *                                                                  *
C  *                                                                  *
C  *     (C) Copywrite 1989: Gregory C. Rutledge, Ulrich W. Suter     *
C  *                                                                  *
C  ********************************************************************
C
C  The Polymer Crystal Simulation Program (PCSP) is designed for the
C  purpose of conducting general studies into the nature and structure
C  of linearly connected (macromolecular) systems.  The simulation is
C  based upon a Molecular Mechanics interpretation of atomic level
C  energetic interactions.  In simulating crystallinity, the program
C  assumes an infinite connectivity along the backbone of the molecular
C  chain, such that the crystal may be represented by a subset of the
C  molecular architecture which describes a helical curve in space.
C  The program then constructs a regular repetition of this represent-
C  ative unit in three dimensions, subject to variations and con-
C  constraints specified in the material representation.  The internal
C  energy, both intramolecular and intermolecular, of such a material
C  representation is then calculated based on appropriately parameter-
C  ized two-body force interactions between atoms or atomic groups and
C  other functions appropriate to an energetic description of the
C  displacement degrees of freedom available to the atoms in the
C  structure.  Minimization of the total (summed) energy with respect
C  to all degrees of freedom leads then to the prediction of the
C  energetically most stable local material representation.
C
C  The main program serves to control the call and execution of the
C  Polymer Crystal Simulation.  Other subroutines control the genera-
C  tion of atomic coordinates for the representative (parent) chain
C  subset and the corresponding helical parameters for the parent chain
C  conformation (either a true helix or an estimate based on the radius
C  of gyration tensor of the suset).  The parent chain is mapped onto a
C  regular non-orthogonal lattice of chain positions, subject to
C  additional translational and/or orientational variations.  The
C  resulting explicit (and potentially irregular) three dimensional
C  construction may then be "embedded" in an implicit regular three
C  dimensional array of atomic interaction points of unlimited size.
C  The minimum set of energetic interations may then be determined and
C  computed and summed for use by a standard non-derivative minimiza-
C  tion routine.  The code as written here is specific for the simula-
C  tion of isomers of the family of ring-substituted poly-(p-phenylene
C  terephthalamide) as isolated chains or as identical chains packed in
C  a regular lattice.  Program options include scanning of intramolec-
C  ular (conformational) and/or intermolecular (crystal packing)
C  variables and optimization of same.  A fixed strain may be imposed
C  on the unitcell by means of the inut file US.dt, which assumes one
C  of twelve predefined unitcell representations for the general lattice.
C
C  COMMON blocks and PARAMETER statements are set up to enable easy
C  variation of the scale of simulation.  Important dimensions of the
C  simulation are shown below; change of the appropriate dimension in
C  all PARAMETER statements will introduce the change throughout the
C  simulation:
C
C  Description of Program Dimension Parameters
C    NKIND = Numger of atom types of interest
C    NIBB  = Number of internal building blocks per repeat unit
C    MNRU  = Maximum number of repeat units per chain
C    MNCH  = Maximum number of chains (a square number)
C    MNAT  = Maximum number of atoms per chain + 1
```

```
C     MNIC  = Maximum number of independently orientable chains
C     MCOP  = MNIC*5
C     MOPT  = MCOP+6
C
C   Some parameters are specific to the PPTA polymer family
C     NRNG  = Number of rotatable rings per repeat unit = 2
C     NSUB  = Number of substitutions possible per repeat unit = 2
C     MNSB  = NSUB*MNRU
C     NDOF  = NIBB + NRNG
C
C   For the Head-to-Head, Tail-to-Tail isomer, it is possible to
C   reconfigure the code to consider a 56 atom repeat unit:
C        NRNG --> 4
C        NIBB --> 16
C        NDOF --> 20
C        Arrays G,H,W dimension --> 5995
C        LMV(2,9) --> LMV(2,18)
C        VARS(97) --> VARS(109)
C        OMVARS(97) --> OMVARS(109)
C        GRAD(97) --> GRAD(109)
C        disable "NUNIQ = 2" option in DATARD subroutine
C
C
C
C
C   ********************************************************************
C
C   The simulation control proceeds as follows:
C
C                                       MAIN
C     Input Variables, Ranges,            |  <-- DATARD <-- RDSTRAIN
C       and Control Intructions           |
C                                         |
C     Inititialize Parameters             |
C                                         |
C     Loop Over All Lattices:             |
C       Loop Over All Conformations:       <----------------------
C                                         |                       |
C                                       CELGEN                    |
C         Execute Model:              or VA10A,CELGEN             |
C                                         |                       |
C         Load Current Parameters         | <-- LDVAR             |
C         Generate Parent Chain           | <-- COORD <--PHENYL   |
C         Determine Helix                 | <-- HELIX (GYRA)      |
C         Generate Lattice                | <-- UNITCEL <--STRAIN |
C         Initialize Charge and           | <-- NONBOND           |
C                  Connectivity           |                       |
C         [Perform Ring Substitution]     | <-- SUBSET <-- RANDS1 |
C         Load Lattice Multiplicity       | <-- MULMAX            |
C         Calculate Model Energy          | <-- ENERGY <-- ELJ,   |
C                                         |                  EES  |
C                                         |                       |
C         Output Results                  |  <-- RESWR            |
C                                          ---------------------->
C     End                                 |
C
C   ********************************************************************
C
      CHARACTER*10 FNAME
      PARAMETER( NKIND=9,NIBB=8,MNRU=6,MNCH=9,MNAT=179,NRNG=2,NSUB=4,
     +           MNSB=24,NDOF=10,MNIC=9,MCOP=45,MOPT=51 )
      COMMON /CHAINS/ PHI(NIBB),THETA(NIBB),BL(NIBB),PHIR(NRNG),
     +                KSB(4),PCH(4,MNAT),NARU,NRUS,NCH,
     +                A(4,4,MNAT),XYZ(4,MNAT,MNCH),KIND(MNAT,MNCH),
     +                CHRG(MNAT,MNCH),KONEC(MNAT,MNAT),DEE,THT,RHO,
     +                NUNIQ
      COMMON /SCAN/ NSTOT,NSANG,NSCAN(NDOF),SCANO(NDOF),SCAND(NDOF),
     +              NCTOT,NCMUT,NMUT(MOPT),CMUTO(MOPT),CMUTD(MOPT)
      COMMON /CELL/ CELD(3),CELA(3),CHSPEC(5,MNCH),CHLOC(3,MNCH),
     +              NUNIV,KONDENS,TEMP,DENSC
      COMMON /CNTR/ IENTRY1,IENTRY2
```

```
      COMMON G(97),H(4753),W(291)
      COMMON /MINIM/ LMV(2,9),LCV(5,11),OMVARS(97)
      COMMON /OPRS/  NVAR,VARS(97),GRAD(97),GRADNM
      COMMON /STRN/ KUC,KASE,ST(3,3),SUCV(3,3),DINIT,DPRIME,DCON
      DIMENSION PHISTR(NDOF),INDSC(NDOF),SPECSTR(MOPT),INDMU(MOPT),
     +          THESTR(NIBB)
      DIMENSION PHISTRTP(NDOF),INSTR(5)
      EXTERNAL CELGEN
      DEGRAD = 3.1415926535/180.
      IENTRY1 = 0
      IENTRY2 = 0
C
C  Read variable/instruction input file and open output file
C
      MODE = 1
      CALL DATARD( NVAR,INSTR,MODE )
c     WRITE(*,*) ' Input PCSP Results Filename (up to 10 characters)',
c    +           ' > ' )
c     READ(*,2) FNAME
      FNAME = 'U.res'
      OPEN (UNIT=11, FILE=FNAME )
c     WRITE(11,3) FNAME
C
C  Initial values of variables which may be scanned must first be
C  stored for future use.  These variables are the torsion angles
C  (PHI(8) and PHIR(2)) of the repeat unit, loaded into PHISTR and
C  PHISTRTP, and the crystal specifications (CHSPEC(3,J) for the first
C  nine chains,CELD(3),CELA(3)), loaded into SPECSTR.
C
      DO 100 I=1,NDOF
        IF (I.LE.NIBB) THEN
          PHISTR(I) = PHI(I)
          PHISTRTP(I) = PHI(I)
          THESTR(I) = THETA(I)
        ELSE
          PHISTR(I) = PHIR(I-NIBB)
          PHISTRTP(I) = PHIR(I-NIBB)
        END IF
        INDSC(I) = 1
  100 CONTINUE
C
      DO 200 J=1,MNIC
        DO 200 I=1,5
          KK = I+(J-1)*5
          SPECSTR(KK) = CHSPEC(I,J)
          INDMU(KK) = 1
  200 CONTINUE
cvd$  noconcur
      DO 250 I=1,3
        KK = MCOP+I
        SPECSTR(KK) = CELD(I)
        INDMU(KK) = 1
  250 CONTINUE
cvd$  noconcur
      DO 260 I=1,3
        KK = MCOP+3+I
        SPECSTR(KK) = CELA(I)
        INDMU(KK) = 1
  260 CONTINUE

C
C  If optimization is desired, set parameters for VA10A
C
      IF (NVAR.EQ.0) GO TO 300
      TENRGY = 0.
c     MODE = 1
      MAXCL = 10000
      IPRINT = 1
      STEPL = 0.001
      EPSVA = 0.001
  300 CONTINUE
```

```
C
C  ***********************************************************************
C  Here begin the nested loops for scanning of variables.  The complete
C  scan space is divided into two nested loops:  LOOP 1000 scans through
C  all conformational variables; LOOP 1100 scans through all cell
C  packing variables.
C
       DO 1000 LOOPP = 1,NSTOT
         DO 1100 LOOPS = 1,NCTOT
            MXCALL = MAXCL
            IEXIT = 1

C
C  Test for inadmissable angle combinations in CELA(3):
C
            CELANEW = CELA(3)
            TLIM = SIN(CELA(1)*DEGRAD)*SIN(CELA(2)*DEGRAD) +
     +             COS(CELA(1)*DEGRAD)*COS(CELA(2)*DEGRAD)
            BLIM = -SIN(CELA(1)*DEGRAD)*SIN(CELA(2)*DEGRAD) +
     +             COS(CELA(1)*DEGRAD)*COS(CELA(2)*DEGRAD)
            IF( COS((CELA(3)-1.)*DEGRAD).LT.TLIM ) THEN
              IF( COS((CELA(3)+1.)*DEGRAD).GT.BLIM ) THEN
                GO TO 480
              ELSE
                CELANEW = ACOS( BLIM )/DEGRAD - 5.
              END IF
            ELSE
              CELANEW = ACOS( TLIM )/DEGRAD + 5.
            END IF
            IF( ABS(CELANEW-CELA(3)).LE.15.) GO TO 470
              WRITE(11,*) 'Exit due to Inadmissable Cell Angles'
              GO TO 600
  470       CELA(3) = CELANEW
C           WRITE(11,*)'Initial Gamma Angle Correction:Gamma= ',CELA(3)
  480    CONTINUE
C
C  Call Case Simulation using either optimization or no-optimization
C  mode:
C
            IF (NVAR.EQ.0) THEN
C
C  No optimization desired:
C
              CALL CELGEN(NVAR,VARS,TENRGY)
            ELSE
C
C  Optimization desired:
C
C  Load cell parameters into VARS vector and call CELGEN once
C  to get initial values for DEE, RHO, THT before starting VA10A
C
              CALL LDVAR( NVAR,VARS,+1,KMOL )
              CALL CELGEN(NVAR,VARS,TENRGY)
              CALL VA10A(CELGEN,NVAR,VARS,TENRGY,G,H,W,
     +                   0.,OMVARS,STEPL,EPSVA,MODE,
     +                   MXCALL,IPRINT,IEXIT)
              SQGRAD = 0.
              DO 650 I=1,NVAR
                GRAD(I) = G(I)
  650           SQGRAD = SQGRAD + G(I)**2
              GRADNM = SQRT(SQGRAD)
            END IF
C
C  End Case Simulation
C
           CALL LDVAR( NVAR,VARS,-1,KMOL )
            IF (IEXIT.NE.1) WRITE(6,4) IEXIT
C           IF(TENRGY.LE.40.) CALL RESWR( INSTR )
            CALL RESWR( INSTR )
C
C  Set specifications for next cell structure
```

```
C
  600       CONTINUE
            DO 400 NC = 1,MOPT
              N = MOPT+1-NC
              IF(NMUT(N).EQ.0) GO TO 400
              INDMU(N) = INDMU(N) + 1
              IF(INDMU(N).LE.NMUT(N)) GO TO 410
              INDMU(N) = 1
  400       CONTINUE
  410       DO 450 K = 1,MOPT
              IF(K.GT.MCOP) GO TO 420
              J = (INT((K-.01)/5)) + 1
              I = K - (J-1)*5
              CHSPEC(I,J) = SPECSTR(K)
              IF(NMUT(K).EQ.0) GO TO 450
              CHSPEC(I,J) = CMUTO(K) + (INDMU(K)-1)*CMUTD(K)
              GO TO 450
  420         IF(K.GT.(MCOP+3)) GO TO 430
              I = K-MCOP
              CELD(I) = SPECSTR(K)
              IF(NMUT(K).EQ.0) GO TO 450
              CELD(I) = CMUTO(K) + (INDMU(K)-1)*CMUTD(K)
              GO TO 450
  430         I = K-MCOP-3
              CELA(I) = SPECSTR(K)
              IF(NMUT(K).EQ.0) GO TO 450
              CELA(I) = CMUTO(K) + (INDMU(K)-1)*CMUTD(K)
  450       CONTINUE
C
C  Reinitialize conformation parameters:
C
            DO 700 I=1,NDOF
              IF(I.LE.NIBB) THEN
                PHI(I) = PHISTRTP(I)
                THETA(I) = THESTR(I)
              ELSE
                PHIR(I-NIBB) = PHISTRTP(I)
              END IF
  700       CONTINUE
 1100     CONTINUE
C
C  ***************   End of Cell Packing Scan LOOP 1100   ***************
C
C  Set angles for next conformation:
C
          DO 500 ND=1,NDOF
            N = NDOF+1-ND
            IF(NSCAN(N).EQ.0) GO TO 500
            INDSC(N) = INDSC(N) + 1
            IF(INDSC(N).LE.NSCAN(N)) GO TO 510
            INDSC(N) = 1
  500     CONTINUE
  510     DO 550 I=1,NDOF
            IF(I.LE.NIBB) THEN
              PHI(I) = PHISTR(I)
              THETA(I) = THESTR(I)
            ELSE
              PHIR(I-NIBB) = PHISTR(I)
            END IF
            PHISTRTP(I) = PHISTR(I)
            IF(NSCAN(I).EQ.0) GO TO 550
            IF(I.LE.NIBB) THEN
              PHI(I) = SCANO(I) + (INDSC(I)-1)*SCAND(I)
              PHISTRTP(I) = PHI(I)
            ELSE
              PHIR(I-NIBB) = SCANO(I) + (INDSC(I)-1)*SCAND(I)
              PHISTRTP(I) = PHIR(I-NIBB)
            END IF
  550     CONTINUE
 1000   CONTINUE
C
```

```
C  *************   End of Conformation Scan   LOOP 1000   ***************
C
       CLOSE (UNIT=11)
    2  FORMAT( A10 )
    3  FORMAT(1X,' PCSP Simulation Results in File: ',A10 )
    4  FORMAT(1X,'IEXIT = ',I3)
       END


       SUBROUTINE CELGEN( NVAR,VARS,TENRGY )
C
C  Function routine for Polymer Crystal Simulation.  Calls routines
C  required to build a parent chain, determine its primary axis and
C  align the chain along this axis, perform chemical substitutions
C  on the chain, replicate the parent chain in a regular lattice, and
C  calculate a total potential energy for the construction.
C
       PARAMETER( NKIND=9,NIBB=8,MNRU=6,MNCH=9,MNAT=179,NRNG=2,NSUB=4,
     +            MNSB=24,NDOF=10,MNIC=9,MCOP=45,MOPT=51 )
       COMMON /CHAINS/ PHI(NIBB),THETA(NIBB),BL(NIBB),PHIR(NRNG),
     +                 KSB(4),PCH(4,MNAT),NARU,NRUS,NCH,
     +                 A(4,4,MNAT),XYZ(4,MNAT,MNCH),KIND(MNAT,MNCH),
     +                 CHRG(MNAT,MNCH),KONEC(MNAT,MNAT),DEE,THT,RHO,
     +                 NUNIQ
       COMMON /SCAN/ NSTOT,NSANG,NSCAN(NDOF),SCANO(NDOF),SCAND(NDOF),
     +                 NCTOT,NCMUT,NMUT(MOPT),CMUTO(MOPT),CMUTD(MOPT)
       COMMON /CELL/ CELD(3),CELA(3),CHSPEC(5,MNCH),CHLOC(3,MNCH),
     +                 NUNIV,KONDENS,TEMP,DENSC
       COMMON /ENRG/ EDEF,EDEL,ENOB1,ENOB2,ECOU1,ECOU2,EULJ,EUES,
     +                 EULJP,EUESP,ECFF,ETOT
       COMMON /CNTR/ IENTRY1,IENTRY2
       DIMENSION VARS(NVAR),KCMV(56)
C
C  For the helix calculation, NHLXI identifies the first atom of the
C  repeat unit for purposes of helix aligmnent, and the KCMV vector
C  contains a list of atom identities for use in centering the helix
C  in the case of THT = 0 (either by HELIX or GYRA):
C
       NHLXI = 13
       KCM = 0
cvd$ noconcur
       DO 200 I=1,NARU/28
         DO 200 J=1,28
         IX = (I-1)*28
         IF( (J.EQ.1).OR.(J.EQ.2).OR.(J.EQ.11).OR.(J.EQ.13).OR.
     +       (J.EQ.15).OR.(J.EQ.16).OR.(J.EQ.25).OR.(J.EQ.27) ) THEN
           KCM = KCM + 1
           KCMV(KCM) = IX + J
         ELSE
         END IF
  200  CONTINUE
C
       CALL LDVAR(NVAR,VARS,-1,KMOL)
       IF ((NSTOT.EQ.1).AND.(NVAR.EQ.0)) KMOL = 0
       IF ((KMOL.EQ.0).AND.(TENRGY.NE.0.)) GO TO 100
       NFLAG = 0
       CALL COORDN
       NHLXF = NHLXI + NARU
       CALL HELIX( A(1,1,NHLXI),A(1,1,NHLXF),KCM,KCMV,NFLAG )
       IF (NFLAG.EQ.0) CALL GYRA( KCM,KCMV )
       IF (KMOL.EQ.0) CALL LDCHN( 1 )
  100  IF (KMOL.EQ.0) CALL LDCHN( -1 )
       CALL UNITCEL
       CALL NONBOND( IENTRY2 )
       CALL SUBSET( IENTRY1 )
       CALL ENERGY
       TENRGY = ETOT
       RETURN
       END
```

```
      SUBROUTINE LDVAR( NVAR,VARS,LDIR,KMOL )
C
C  If LDIR > 1 : Loads PHI'S, THETA'S, CELD'S, CELA'S, and CHSPEC'S
C                into the variable vector VARS according to the
C                information in LMV and LCV and sets their proper
C                order of magnitude
C  If LDIR < 1 : Loads VARS into the above mentioned arrays according
C                to the information in LMV and LCV
C  Normalizes VARS to the range -180. to +180, where appropriate:
C
      PARAMETER( NKIND=9,NIBB=8,MNRU=6,MNCH=9,MNAT=179,NRNG=2,NSUB=4,
     +           MNSB=24,NDOF=10,MNIC=9,MCOP=45,MOPT=51 )
      COMMON /CHAINS/ PHI(NIBB),THETA(NIBB),BL(NIBB),PHIR(NRNG),
     +                KSB(4),PCH(4,MNAT),NARU,NRUS,NCH,
     +                A(4,4,MNAT),XYZ(4,MNAT,MNCH),KIND(MNAT,MNCH),
     +                CHRG(MNAT,MNCH),KONEC(MNAT,MNAT),DEE,THT,RHO,
     +                NUNIQ
      COMMON /CELL/ CELD(3),CELA(3),CHSPEC(5,MNCH),CHLOC(3,MNCH),
     +                NUNIV,KONDENS,TEMP,DENSC
      COMMON /MINIM/ LMV(2,9),LCV(5,11),OMVARS(97)
      COMMON /SV2/  TVARL
      DIMENSION VARS(NVAR),TROT(9),KCORR(9)
      DO 50 J=1,MNIC
 50     KCORR(J) = 0
C  NORMALIZE, WHERE APPROPRIATE:
      IF (LDIR.GT.0) GO TO 300
      DO 400 I=1,NVAR
        IF (OMVARS(I).NE.100.) GO TO 400
        VARS(I) = MOD(VARS(I),360.)
        IF (VARS(I).LT.-180.) VARS(I) = VARS(I) + 360.
        IF (VARS(I).GT.+180.) VARS(I) = VARS(I) - 360.
 400  CONTINUE
C  LOAD VECTOR/ARRAYS:
 300  NV = 1
      KMOL = 1
      NIBBL = NIBB + NRNG/2
      DO 100 J=1,NIBBL
        DO 100 I=1,2
          IF (LMV(I,J).EQ.0) GO TO 100
          IF (LDIR.LT.0) GO TO 120
            OMVARS(NV) = 100.
            IF (J.GT.NIBB) VARS(NV) = PHIR( (J-NIBB-1)*2 + I )
            IF (J.GT.NIBB) GO TO 130
            IF (I.EQ.1) VARS(NV) = PHI(J)
            IF (I.EQ.2) VARS(NV) = THETA(J)
          GO TO 130
 120        IF (J.GT.NIBB) PHIR( (J-NIBB-1)*2 + I ) = VARS(NV)
            IF (J.GT.NIBB) GO TO 130
            IF (I.EQ.1) PHI(J) = VARS(NV)
            IF (I.EQ.2) THETA(J) = VARS(NV)
 130      NV = NV+1
 100      IF (NV.GT.NVAR) GO TO 500
      IF (NV.EQ.1) KMOL = 0
      DO 200 J=1,11
        DO 200 I=1,5
          IF (LCV(I,J).EQ.0) GO TO 200
          IF (LDIR.LT.0) GO TO 220
            IF (J.GT.MNIC) GO TO 260
              VARS(NV) = CHSPEC(I,J)
              IF (I.EQ.1) OMVARS(NV) = 1.
              IF (I.EQ.2) OMVARS(NV) = 0.1
              IF (I.EQ.2) TVARL = CHSPEC(I,J)
              IF (I.EQ.3) OMVARS(NV) = 100.
              IF (I.EQ.4) OMVARS(NV) = 100.
              IF (I.EQ.5) OMVARS(NV) = 100.
              GO TO 230
 260          IF (J.GT.(MNIC+1)) GO TO 270
              VARS(NV) = CELD(I)
              OMVARS(NV) = 10.
              GO TO 230
 270          VARS(NV) = CELA(I)
```

```
              OMVARS(NV) = 100.
              GO TO 230
  220       IF (J.GT.MNIC) GO TO 620
        IF (I.NE.2) GO TO 450
C  Potential energy minimization appears to be very sensitive to the chain
C  translation variable; VA10A tends to make large steps in CHSPEC(2,J) if
C  the initial guess creates atomic overlap.  For this reason, steps in
C  this variable are limited in magnitude.  The value returned to VA10A is
C  altered; only when VA10A begins to take steps less than STPMX will the
C  corresponding Gradient and Hessian be correct.
C
C  Even then, there may accumulate a significant deviation between the
C  chain translation variable and the correponding VARS variable.  Thus,
C  where the initial condition may be poor and large steps are likely,
C  SFRAC should be restricted, perhaps to 5% (SFRAC = 0.05); where small
C  steps are expected and the corresponding minimization results are
C  intended for reuse, this restriction should be lifted (SFRAC = 1.0)
C
       SFRAC = 1.0
       IF(TVARL.GE.999.) THEN
          CHSPEC(I,J) = VARS(NV)
          TVARL = VARS(NV)
        ELSE
         STPMX = SFRAC*REAL(NUNIQ)
         VDIF  = VARS(NV) - TVARL
         STP   = SIGN( MIN(STPMX,ABS(VDIF)),VDIF )
         IF( (SFRAC.GT.0.9).AND.(ABS(STP-VDIF).GT.1E-5) )
     +     WRITE(11,*) 'WARNING: translation has been restricted'
        CHSPEC(I,J) = CHSPEC(I,J) + STP
       END IF
C
C  Chain translation along the chain axis must be restricted for
C  model chains of finite length; here, helix symmetry may be used
C  to limit translation without imposing constraints on optimization.
C  The appropriate range should center about zero and equal the number
C  of repeat units required to define all unique segments (ie: range
C  = -0.5 to 0.5 for symmetric repeat units or isomers of head-to-tail
C  alignment, = -1.0 to 1.0 for isomers of head-to-head, tail-to-tail
C  alignment.
C
C  Correct translation to the range -0.1 to 0.1:
C  Translation correction may be disabled by setting TURNS = 0.
              TURNS = AINT( CHSPEC(I,J) )
C             TURNS = 0.
              CDIF = CHSPEC(I,J)-TURNS
              IF (NUNIQ.NE.1) GO TO 280
C  For range -0.5 to 0.5, enable the following line:
              IF (ABS(CDIF).GT.0.5) TURNS = TURNS+SIGN(1.,CDIF)
  280         CONTINUE
C
              CHSPEC(I,J) = CHSPEC(I,J) - NUNIQ*TURNS
              TROT(J) = NUNIQ*TURNS*THT
              KCORR(J) = 1
              VARS(NV) = CHSPEC(I,J)
              TVARL = VARS(NV)
              GO TO 230
  620         IF (J.GT.(MNIC+1)) GO TO 630
              CELD(I) = VARS(NV)
              GO TO 230
  630         IF (J.GT.(MNIC+2)) GO TO 230
              CELA(I) = VARS(NV)
              IF (CELA(I).LT.0.) CELA(I) = CELA(I)+180.
              GO TO 230
  450       CHSPEC(I,J) = VARS(NV)
  230       NV = NV+1
  200       IF (NV.GT.NVAR) GO TO 500
  500   DO 510 J=1,MNIC
  510     IF (KCORR(J).EQ.1) CHSPEC(5,J) = CHSPEC(5,J)+TROT(J)
        RETURN
        END
```

```
      SUBROUTINE LDCHN( LDIR )
C
C  If KMOL = 0, it is not necessary to regenerate the parent chain
C  for each iteration; LDCHN is a computational expedient which stores
C  the coordinates of the parent chain for use by later iterations.
C  If LDIR > 0 : loads parent into PCH
C  If LDIR > 0 : loads PCH back into XYZ
C
      PARAMETER( NKIND=9,NIBB=8,MNRU=6,MNCH=9,MNAT=179,NRNG=2,NSUB=4,
     +           MNSB=24,NDOF=10,MNIC=9,MCOP=45,MOPT=51 )
      COMMON /CHAINS/ PHI(NIBB),THETA(NIBB),BL(NIBB),PHIR(NRNG),
     +              KSB(4),PCH(4,MNAT),NARU,NRUS,NCH,
     +              A(4,4,MNAT),XYZ(4,MNAT,MNCH),KIND(MNAT,MNCH),
     +              CHRG(MNAT,MNCH),KONEC(MNAT,MNAT),DEE,THT,RHO,
     +              NUNIQ
      DO 100 I=1,NRUS*NARU+1
        DO 100 J=1,4
          IF(LDIR.GT.0) PCH(J,I) = XYZ(J,I,1)
  100     IF(LDIR.LT.0) XYZ(J,I,1) = PCH(J,I)
      RETURN
      END


      REAL FUNCTION RANDS1(SEED)
C
C     This is a special function for Random number generation
C     on 32-bit machines that do not support long integer
C     multiplication and truncation.  The technique used is to do
C     the multiplication and addition in parts, by splitting all
C     integers in a 'high' and a 'low' part.  The algorithm is
C     exact, and should give machine-independent results.
C
      INTEGER*4 SEED,IA,IB,I1,I2,I3

C     The algorithm implemented is (following D.E. Knuth):
C     seed = seed*1592653589 + 453816691
C     if (seed.lt.0) seed = seed + 1 + 2147483647
C     Note that 1592653589 = 48603*2**15 + 30485

      IA = SEED/32768
      IB = MOD(SEED,32768)
      I1 = IA*30485
      I2 = IB*30485
      I3 = IB*48603
      I1 = MOD(I1,65536)
      I3 = MOD(I3,65536)
      I1 = I1 + I3 + 13849 + I2/32768 + MOD(IA,2)*32763
      I2 = MOD(I2,32768) + 12659
      I1 = I1 + I2/32768
      I2 = MOD(I2,32768)
      I1 = MOD(I1,65536)

      SEED = I1*32768 + I2
      RANDS1 = SEED*4.65661287308D-10
      RETURN
      END
```

```
      SUBROUTINE COORDN
C
C  Builds a Poly(p-phenylene terephthalamide) chain consisting of
C  alternating diacid and diamine units.  The phenyl rings are assumed
C  to be hexagonal planar, and the amide carbons and nitrogens are
C  assumed to form sp2 planar bonds but angles are not required to be
C  120 degrees.
C
C  ***********************************************************************
C  Numbering of internal angles
C  used to place atoms:
C                                                 O
C                                                  \
C                                                   \
C                      H          PHIR(2)           7 C ----
C                       \          ----              /  8
C                        \        /      \        6 /
C         PHIR(1)         3 N ----          ---- N
C           ----           /   4  \        /     5 \
C         /      \      2 /          ----           \
C     ----         ---- C                           H
C         \      /      1 \
C           ----           \
C                           O
C
C  ***********************************************************************
C
C
      PARAMETER( NKIND=9,NIBB=8,MNRU=6,MNCH=9,MNAT=179,NRNG=2,NSUB=4,
     +           MNSB=24,NDOF=10,MNIC=9,MCOP=45,MOPT=51 )
      COMMON /CHAINS/ PHI(NIBB),THETA(NIBB),BL(NIBB),PHIR(NRNG),
     +                KSB(4),PCH(4,MNAT),NARU,NRUS,NCH,
     +                A(4,4,MNAT),XYZ(4,MNAT,MNCH),KIND(MNAT,MNCH),
     +                CHRG(MNAT,MNCH),KONEC(MNAT,MNAT),DEE,THT,RHO,
     +                NUNIQ
      DIMENSION AL(4,4),KATOM(11),XYZL(4,11)
      DATA DCN,DNH,DCO/1.39,1.00,1.24/
      DO 50 I=1,NIBB/8
        KRU = (I - 1)*8
        BL(1+KRU) = DCO
        BL(2+KRU) = DCN
        BL(3+KRU) = DNH
        BL(5+KRU) = DNH
        BL(6+KRU) = DCN
        BL(7+KRU) = DCO
 50   CONTINUE
      NST = 3
      NTYP = 1
C
C  Start building:
C  First phenyl ring lies along the X axis; ring rotation angle must be
C  corrected for PHI(2) = 0 :
C
      PHI2 = PHIR(NTYP)-PHI(2)
      CALL PHENYL( NTYP,PHI2,KATOM,XYZL )
      NTYP = 2
      DO 100 I=1,11
        KIND(I,1) = KATOM(I)
        DO 100 J=1,4
          XYZ(J,I,1) = XYZL(J,I)
100     IF( J.EQ.1 ) XYZ(J,I,1) = XYZ(J,I,1) - XYZL(J,1)
C
C  First amide bond has PHI = 0, first carbonyl has PHI - 180, by
C  default; since no previous A-matrix exits, load both directly:
C
      CALL ATRNS( 180.,THETA(1),XYZ(1,11,1),AL )
      DO 120 I=1,4
        DO 120 J=1,4
120       A(I,J,12) = AL(I,J)
      XYZ(1,12,1) = BL(1)
      XYZ(2,12,1) = 0.
```

```
      XYZ(3,12,1) = 0.
      XYZ(4,12,1) = 1.
      KIND(12,1) = 6
      CALL ATRNS( 0.,THETA(2),XYZ(1,11,1),AL )
      DO 140 I=1,4
        DO 140 J=1,4
140     A(I,J,13) = AL(I,J)
      XYZ(1,13,1) = BL(2)
      XYZ(2,13,1) = 0.
      XYZ(3,13,1) = 0.
      XYZ(4,13,1) = 1.
      KIND(13,1) = 5
      NUMA = 14
      DO 160 I=12,13
160     CALL MV( A(1,1,I),4,3,XYZ(1,I,1),4,XYZ(1,I,1) )
C
C  Loop over all repeat units:
C
      DO 500 NR=1,NRUS
C
C  Loop over all points in repeat unit:
C
        DO 400 NF=NST,NIBB-1,2
          PHI(NF) = PHI(NF+1) + 180.
          NUMAM = NUMA-1
          DO 400 NA=1,2
            NMKR = NF+NA-1
            IF( .NOT.(MOD(NMKR,4).EQ.0) ) GO TO 200
            CALL PHENYL( NTYP,PHIR(NTYP),KATOM,XYZL )
            NTYP = 1 + MOD(NTYP,NRNG)
            BL(NMKR) = XYZL(1,11)
            DO 220 I=1,11
              KIND(NUMA,1) = KATOM(I)
              DO 240 J=1,4
240             XYZ(J,NUMA,1) = XYZL(J,I)
              CALL ATRNS( PHI(NMKR),THETA(NMKR),BL(NF-1),AL )
              CALL MM( A(1,1,NUMAM),AL,A(1,1,NUMA),4,4,4,4,4,4 )
              CALL MV( A(1,1,NUMA),4,3,XYZ(1,NUMA,1),4,XYZ(1,NUMA,1) )
220         NUMA = NUMA+1
            GO TO  400
200         XYZ(1,NUMA,1) = BL(NMKR)
            XYZ(2,NUMA,1) = 0.
            XYZ(3,NUMA,1) = 0.
            XYZ(4,NUMA,1) = 1.
            KIND(NUMA,1) = 4
            IF( MOD(NMKR+2,8).EQ.0 ) KIND(NUMA,1) = 3
            IF( MOD(NMKR+6,8).EQ.0 ) KIND(NUMA,1) = 5
            IF( (MOD(NMKR+7,8).EQ.0).OR.(MOD(NMKR+1,8).EQ.0) )
     +         KIND(NUMA,1) = 6
C
C  For first element of second and successive repeat units, draw upon
C  A-matrix of last atom positioned in previous repeat unit:
C
            IF (NF.EQ.1) THEN
              CALL ATRNS( PHI(NMKR),THETA(NMKR),BL(NIBB),AL )
              CALL MM( A(1,1,NUMAM),AL,A(1,1,NUMA),4,4,4,4,4,4 )
            ELSE
              CALL ATRNS( PHI(NMKR),THETA(NMKR),BL(NF-1),AL )
              CALL MM( A(1,1,NUMAM),AL,A(1,1,NUMA),4,4,4,4,4,4 )
            END IF
C
C  Transform to Frame 0:
C
            CALL MV( A(1,1,NUMA),4,3,XYZ(1,NUMA,1),4,XYZ(1,NUMA,1) )
            NUMA = NUMA+1
400       CONTINUE
          NST = 1
500     CONTINUE
        RETURN
        END
```

```
      SUBROUTINE PHENYL( NTYP,PHI,KATM,XLOC)
C
C  Builds a phenyl ring within the frame of reference of the first
C  atom preceeding the phenyl ring and returns atom types and local
C  coordinates
C
C               10,      6,
C                9       5
C                C ----- C
C               /         \
C              /           \
C       ----- C 1           2 C ----- C (OR N)
C              \           /          11
C               \         /
C                C ----- C
C                7,      3,
C                8       4
C
      DIMENSION KATM(12),RGBL(12),RGPH(12),RGTH(12),XLOC(4,12)
      DIMENSION ALOC(4,4)
      DATA DPH,DCPH,DNPH,DHPH/1.40,1.50,1.41,1.10/
      IF( MOD(NTYP,2).EQ.1 ) THEN
        RGBL(1) = DCPH
      ELSE
        RGBL(1) = DNPH
      END IF
      RGC      = RGBL(1) + DPH
      RGBL(2)  = RGC     + DPH
      RGBL(11) = RGBL(2) + RGBL(1)
      DO 100 I=1,2
  100   KATM(I) = 1
      KATM(11)  = 3
      IF( MOD(NTYP,2).EQ.0 ) KATM(11) = 5
      DO 200 I=3,9,2
        KATM(I) = 1
        RGBL(I) = DPH
        RGPH(I) = PHI
        IF( (I.EQ.5).OR.(I.EQ.9) ) RGPH(I) = RGPH(I) + 180.
        RGTH(I) = 120.
  200   IF( (I.EQ.7).OR.(I.EQ.9) ) RGTH(I) = 60.
      DO 300 I=4,10,2
        KATM(I) = 2
        RGBL(I) = DPH+DHPH
        RGPH(I) = PHI
        IF( (I.EQ.6).OR.(I.EQ.10) ) RGPH(I) = RGPH(I) + 180.
        RGTH(I) = 120.
  300   IF( (I.EQ.8).OR.(I.EQ.10) ) RGTH(I) = 60.
      DO 500 I=1,11
        XLOC(1,I) = RGBL(I)
        XLOC(2,I) = 0.
        XLOC(3,I) = 0.
  500   XLOC(4,I) = 1.
      DO 600 I=3,10
        CALL ATRNS( RGPH(I),RGTH(I),RGC,ALOC )
  600   CALL MV( ALOC,4,3,XLOC(1,I),4,XLOC(1,I) )
      RETURN
      END


      SUBROUTINE HELIX( AO,AX,KCM,KCMV,NFLAG )
C
C  Calculates Helix Parameters (Pitch, Twist, and Radius) and converts
C  XYZ coordinates into a frame of reference wherein the helix axis
C  corresponds to the Z axis.  For this purpose, AO and AX are sectors
C  of the A-matrix locating corresponding atoms in successive molecular
C  repeat units, retrieved for the purpose of calculating the net
C  transformation (AH) per repeat unit and the translation vector (BH)
C  per repeat unit; these are equivalent to the A matrix and B vector
C  of Sugeta & Miyazawa (BIOPOLYMERS,5,673,1967)
C
```

```
C  >>>>>>  MODIFIED TO RETURN COORDINATES UNTRANSFORMED  <<<<<<<
C  >>>>>>           FOR VALUES OF THT BELOW THTCRIT       <<<<<<<
C
        PARAMETER (EPSILON = 1.E-6)
        PARAMETER( NKIND=9,NIBB=8,MNRU=6,MNCH=9,MNAT=179,NRNG=2,NSUB=4,
     +             MNSB=24,NDOF=10,MNIC=9,MCOP=45,MOPT=51 )
        COMMON /CHAINS/ PHI(NIBB),THETA(NIBB),BL(NIBB),PHIR(NRNG),
     +                  KSB(4),PCH(4,MNAT),NARU,NRUS,NCH,
     +                  A(4,4,MNAT),XYZ(4,MNAT,MNCH),KIND(MNAT,MNCH),
     +                  CHRG(MNAT,MNCH),KONEC(MNAT,MNAT),DEE,THT,RHO,
     +                  NUNIQ
        DIMENSION AO(4,4),AX(4,4),AH(4,4),BH(4),AP(4,4),AZ(4,4)
        DIMENSION EMAT(4,4),AT(4,4),CA(4),CB(4),BN(3,2)
        DIMENSION TX(3),TY(3),TZ(3),T(4,4)
        DIMENSION KCMV(KCM)
        THTCRIT = 30.*(3.1415926535/180.)
        KK = 0
C
C  Determine AH and BH:
C  Expeditious choice of AO such that AO = inverse of AO enables the
C  following shortcut:
C
        CALL MM( AX,AO,AH,4,4,4,4,4,4 )
        DO 100 I=1,4
  100     BH(I) = AX(I,4) - AO(I,4)
C
C  Determine helix:
C
        DO 200 I=1,4
          DO 200 J=1,4
            EMAT(I,J) = 0.
  200       IF (I.EQ.J) EMAT(I,J) = 1.
        CALL MT( AH,AT,3,4 )
        CALL MA( AT,EMAT,AT,3,4,-1. )
        CALL MA( EMAT,AH,AP,3,4,-1. )
        CALL MV( AT,4,3,BH,3,CA )
        CALL MV( AP,4,3,BH,3,CB )
        CASQ = CA(1)**2 + CA(2)**2 + CA(3)**2
        CBSQ = CB(1)**2 + CB(2)**2 + CB(3)**2
        CSQ = MAX(CASQ,CBSQ)
        BSQ = BH(1)**2 + BH(2)**2 + BH(3)**2
        CDC  = CA(1)*CB(1)+CA(2)*CB(2)+CA(3)*CB(3)
        IF ( ((1.-AH(1,1)*AH(2,2)*AH(3,3)).GE.(100.*EPSILON)).OR.
     +       ((AH(1,1)+AH(2,2)+AH(3,3)).LT.0.) ) GO TO 300
C
C  Special Case: THT = 0; straight line helix
C
        THT = 0.
        DEE = SQRT( BSQ )
        RHO = 0.
        GO TO 360
C
C  Special Case: BH vector corresponds to helix axis but THT is nonzero
C  ("twisted rod"); for this case, determine THT by applying AH
C  rotation to an arbitrary unit vector normal to axis (valid for BH(1)
C  not equal to zero)
C
  300   CONTINUE
        IF (CSQ.GT.EPSILON) GO TO 320
        IF( BH(1).LT.EPSILON ) WRITE(*,*) 'Invalid Assumption: HELIX'
        BRTO = BH(3)/BH(1)
        BN(1,1) = SQRT( BRTO**2/(1.+BRTO**2) )
        BN(2,1) = 0.
        BN(3,1) = -BN(1,1)/BRTO
        CALL MV( AH,4,3,BN(1,1),3,BN(1,2) )
        BN1SQ = BN(1,1)**2 + BN(2,1)**2 + BN(3,1)**2
        BN2SQ = BN(1,2)**2 + BN(2,2)**2 + BN(3,2)**2
        THT = ACOS( (BN(1,1)*BN(1,2)+BN(2,1)*BN(2,2)+BN(3,1)*BN(3,2))
     +              /SQRT(BN1SQ*BN2SQ) )
        RHO = 0.
        DEE = SQRT( BSQ )
```

```
C
  360   CONTINUE
        DO 350 I=1,3
          TZ(I) = (XYZ(I,NARU+1,1)-XYZ(I,1,1))/DEE
  350     TX(I) = TZ(I)
        IF (ABS(TZ(3)).LT.EPSILON) THEN
          TX(1) = 0.
          TX(2) = 0.
          TX(3) = -1.
        ELSE IF (ABS(TZ(3)-1.).LT.EPSILON) THEN
          TX(1) = 1.
          TX(2) = 0.
          TX(3) = 0.
        ELSE
          ALPHA = ACOS(TZ(3))
          TX(3) = -1.*SQRT(TX(1)**2+TX(2)**2)*TAN(ALPHA)
        END IF
        TXL = SQRT( TX(1)**2 + TX(2)**2 + TX(3)**2 )
        DO 330 I=1,3
  330     TX(I) = TX(I)/TXL
        GO TO 500
  320   CONTINUE
        IF (ABS(CDC/CSQ-1.).LT.EPSILON) THEN
          CDC = CSQ
        ELSE IF (ABS(CDC/CSQ+1.).LT.EPSILON) THEN
          CDC = -CSQ
        ELSE
        END IF
        THT = ACOS( CDC/CSQ )
        RHO = SQRT(CSQ)/( 2*(1.-COS(THT)) )
C
C  Special Case: THT=180; Planar zigzag helix
C
        IF (ABS(THT-3.1415926535).GT.EPSILON) GO TO 400
        CALL MA( AH,EMAT,AZ,3,4,+1. )
        CALL MV( AZ,4,3,BH,3,TZ )
        TZM2 = 0.
        DO 365 I=1,3
  365     TZM2 = TZM2 + TZ(I)**2
        TZM = SQRT(TZM2)
        DEE = TZM/2.
        DO 370 I=1,3
          TX(I) = CA(I)/SQRT( CSQ )
  370     TZ(I) = TZ(I)/TZM
        GO TO 500
  400   CALL VV( CA,CB,TZ,3 )
        BCC = 0.
        DO 310 I=1,3
  310     BCC = BCC + BH(I)*TZ(I)
        DEE = BCC/(CSQ*SIN(THT))
        TZL = SQRT( TZ(1)**2 + TZ(2)**2 + TZ(3)**2 )
        DO 450 I=1,3
          TZ(I) = TZ(I)/TZL
  450     TX(I) = CA(I)/SQRT( CSQ )
  500   CALL VV( TZ,TX,TY,3 )
  750   DO 550 I=1,3
          T(1,I) = TX(I)
          T(2,I) = TY(I)
          T(3,I) = TZ(I)
  550     T(4,I) = 0.
        T(1,4) = RHO
        T(2,4) = 0.
        T(3,4) = 0.
        T(4,4) = 1.
C
C  >>>>>>> MODIFIED RETURN FOR THT < THTCRIT  <<<<<<<
        IF( THT.LT.THTCRIT ) RETURN
C  >>>>>>>>>>>>>>>>>>>>>>>>>><<<<<<<<<<<<<<<<<<<<<<<<<
C
C  Convert from initial coordinates to helix coordinates:
C
```

```
      DO 600 J=1,NARU*NRUS+1
  600   CALL MV( T,4,3,XYZ(1,J,1),4,XYZ(1,J,1) )
      IF (ABS(THT).GT.EPSILON) GO TO 800
C
C  For THT = 0 helix radius is arbitrary;  for this case, center
C  molecule about the average projection of the KCM atoms previously
C  specified in the KCMV vector:
C
      IF (KK.EQ.1) GO TO 800
      NN = 0
      XI = 0.
      YI = 0.
      DO 700 I=1,NARU
        DO 740 J=1,KCM
          IF( I.EQ.KCMV(J) ) THEN
            XI = XI + XYZ(1,I,1)
            YI = YI + XYZ(2,I,1)
            NN = NN + 1
          ELSE
          END IF
  740     CONTINUE
  700   CONTINUE
      XI = XI/NN
      YI = YI/NN
      RHO = SQRT( XI**2 + YI**2 )
      TX(1) = -XI/RHO
      TX(2) = -YI/RHO
      TX(3) = 0.
      TY(1) = YI/RHO
      TY(2) = -XI/RHO
      TY(3) = 0.
      TZ(1) = 0.
      TZ(2) = 0.
      TZ(3) = 1.
      KK = 1
      GO TO 750
  800 THT = THT*180./3.1415926535
      NFLAG = 1
      RETURN
      END


      SUBROUTINE GYRA( KCM,KCMV )
C
C  Calculates the Radius of Gyration matris for a polymer chain and
C  then transforms coordinates to a frame aligning the primary axis
C  of the point distribution along the Z axis
C
      PARAMETER (EPSILON=1.E-6)
      PARAMETER( NKIND=9,NIBB=8,MNRU=6,MNCH=9,MNAT=179,NRNG=2,NSUB=4,
     +           MNSB=24,NDOF=10,MNIC=9,MCOP=45,MOPT=51 )
      COMMON /CHAINS/ PHI(NIBB),THETA(NIBB),BL(NIBB),PHIR(NRNG),
     +                KSB(4),PCH(4,MNAT),NARU,NRUS,NCH,
     +                A(4,4,MNAT),XYZ(4,MNAT,MNCH),KIND(MNAT,MNCH),
     +                CHRG(MNAT,MNCH),KONEC(MNAT,MNAT),DEE,THT,RHO,
     +                NUNIQ
      DIMENSION RG(4,4),RA(4),EVC(4,4),EVT(4,4),EVL(3),BV1(3),
     +          BV2(3),ZV(3),PV1(3),PV2(3)
      DIMENSION KCMV(KCM)
      PI = 3.1415926535
      DO 100 I=1,4
        RA(I) = 0.
      DO 100 J=1,4
        EVC(I,J) = 0.
        EVT(I,J) = 0.
  100   RG(I,J) = 0.
      EVT(4,4) = 1.
C
C  Determine RG of backbone atomic coordinates.
C
      M = 0
```

```
      RGSCALE = 0.
      NBBA = NIBB*NRUS
      DO 200 I=1,NRUS
      DO 200 J=1,NARU
        M = M+1
        DO 200 JCMP=1,KCM
          IF( J.EQ.KCMV(JCMP) ) THEN
            DO 220 K=1,3
              RA(K) = RA(K) + XYZ(K,M,1)/NBBA
            DO 220 L=K,3
              RG(K,L) = RG(K,L)+XYZ(K,M,1)*XYZ(L,M,1)/NBBA
220         CONTINUE
          ELSE
          END IF
200   CONTINUE
      RG(3,1) = RG(1,3)
      RG(2,1) = RG(1,2)
      RG(3,2) = RG(2,3)
      DO 250 K=1,3
      DO 250 L=1,3
250     RG(K,L) = RG(K,L) - RA(K)*RA(L)
C
C  Determine eigenvalues and eigenvectors by method of Jacobi
C  Transformations (Press et.al., NUMERICAL RECIPES, Cambridge
C  University Press, 1986, P342.
C
      CALL JACOBI( RG,3,4,EVL,EVC,NROT )
C
C  Sort eigenvalues in order EVL3 > EVL1 > EVL2 and rearrange eigen-
C  vectors accordingly:
C
      DO 300 I=1,2
        K = I
        T = EVL(I)
        DO 320 J=I+1,3
          IF(EVL(J).LE.T) THEN
            K = J
            T = EVL(J)
          END IF
320     CONTINUE
        IF(K.NE.I) THEN
          EVL(K) = EVL(I)
          EVL(I) = T
          DO 340 J=1,3
            T = EVC(J,I)
            EVC(J,I) = EVC(J,K)
340         EVC(J,K) = T
        END IF
300   CONTINUE
      T = EVL(1)
      EVL(1) = EVL(2)
      EVL(2) = T
      DO 360 J=1,3
        T = EVC(J,1)
        EVC(J,1) = EVC(J,2)
360     EVC(J,2) = T
C
C  Ensure right-handedness of rotation matrix:
C
      DET = EVC(1,1)*EVC(2,2)*EVC(3,3)+EVC(2,1)*EVC(3,2)*EVC(1,3)+
     +      EVC(3,1)*EVC(1,2)*EVC(2,3)-EVC(1,1)*EVC(3,2)*EVC(2,3)-
     +      EVC(2,1)*EVC(1,2)*EVC(3,3)-EVC(3,1)*EVC(2,2)*EVC(1,3)
      IF((ABS(DET)-1.).GT.EPSILON) WRITE(*,*)
     +      'ERROR: Eigenvector Matrix'
      IF(ABS(DET-1.).LE.EPSILON) GO TO 410
      DO 400 I=1,3
400     EVC(I,2) = -EVC(I,2)
410   CONTINUE
C
C  Transform coordinates to Primary Axis frame of reference
C
```

```
      DO 520 I=1,4
      DO 520 J=1,4
  520   EVT(J,I) = EVC(I,J)
      DO 500 I=1,NARU*NRUS+1
        DO 540 J=1,3
  540     XYZ(J,I,1) = XYZ(J,I,1) - RA(J)
        CALL MV( EVT,4,3,XYZ(1,I,1),4,XYZ(1,I,1) )
  500 CONTINUE
C
C  Determine comparable "helix" parameters:
C  (NOTE:  backbone atoms only, code is model specific)
C
      DEE = XYZ(3,NARU+1,1) - XYZ(3,1,1)
      GRHO = 0.
      DO 600 I=1,3
        IF(ABS(EVL(3)-EVL(I)).GT.EPSILON) GRHO = GRHO+EVL(I)
  600 CONTINUE
      RHO = SQRT(GRHO)
C
C  For GTHT determination, the relative rotation of the vertical plane
C  intersecting an arbitrary bond vector (carbonyl C=O) is chosen
C
      N1 = 27
      N2 = 28
      N3 = N1+NARU
      N4 = N2+NARU
      DO 650 I=1,3
        BV1(I) = XYZ(I,N2,1) - XYZ(I,N1,1)
        BV2(I) = XYZ(I,N4,1) - XYZ(I,N3,1)
  650   ZV(I) = 0.
      ZV(3) = 1.
      CALL VV( BV1,ZV,PV1,3 )
      CALL VV( BV2,ZV,PV2,3 )
      DOT = 0.
      PV1M = 0.
      PV2M = 0.
      DO 660 I=1,3
        DOT = DOT + PV1(I)*PV2(I)
        PV1M = PV1M + PV1(I)**2
  660   PV2M = PV2M + PV2(I)**2
      DOT = DOT/SQRT(PV1M*PV2M)
      IF( ABS(ABS(DOT)-1.).LE.EPSILON ) DOT = SIGN(1.,DOT)
      GTHT = ACOS( DOT )
      THT = GTHT*180./PI
      RETURN
      END


      SUBROUTINE UNITCEL
C
C  Creates a unit cell consisting of a regular array of identical chains
C  based on an initial parent chain.  The configuration of the array of
C  chain centers is determined by the dimensions (CELD(1),CELD(2))
C  between the parent (P) and two neighboring chains (N1,N2) and the
C  angle (CELA(3)) between these neighbors (N1-P-N2). The array of
C  centers is oriented relative to the parent axis (Z-axis) by the
C  angles CELA(1) (Z-P-N1) and CELA(2) (Z-P-N2).  Finally, each chain
C  may be rotated about its center and/or translated along its local
C  chain axis independently according to the Eulerian angles and
C  fractional translation values in CHSPEC.
C
C   (Z axis extends out of paper):
C
C               ^ Y                      Angles: Z14 = ALPHA [ CELA(1) ]
C               |                              Z12 = BETA  [ CELA(2) ]
C          5    | 4      3                      412 = GAMMA [ CELA(3) ]
C          * ---- * ---- *
C        /      | /      /          Dimensions: 1-2 = A   [ CELD(1) ]
C       /       |/      /                      1-4 = B   [ CELD(2) ]
C      6* ---- * ---- * -------> X              1-Z = C   [ CELD(3) ]
C     /      /1     /2
```

```
C     /       /       /
C    * ---- * ---- *
C    7       8       9
C
C
C  >>>>>>>>>>>> Modified to impose the following constraints: <<<<<<<<<
C       1. All odd-number designated chains translated identically
C          according to CHSPEC(2,1); all even-number designated chains
C          translated according to CHSPEC(2,2).
C       2. All odd-number designated chains rotated identically
C          according to CHSPEC(3-5,1); all even-number designated chains
C          rotated according to CHSPEC(3-5,2)
C  >>>>>>>>>>>>>>>>>>>>>>>>>>>>>>>>>>>><<<<<<<<<<<<<<<<<<<<<<<<<<<<<<<<
C
        PARAMETER( EPSILON=1.E-6 )
        PARAMETER( NKIND=9,NIBB=8,MNRU=6,MNCH=9,MNAT=179,NRNG=2,NSUB=4,
     +             MNSB=24,NDOF=10,MNIC=9,MCOP=45,MOPT=51 )
        COMMON /CHAINS/ PHI(NIBB),THETA(NIBB),BL(NIBB),PHIR(NRNG),
     +                  KSB(4),PCH(4,MNAT),NARU,NRUS,NCH,
     +                  A(4,4,MNAT),XYZ(4,MNAT,MNCH),KIND(MNAT,MNCH),
     +                  CHRG(MNAT,MNCH),KONEC(MNAT,MNAT),DEE,THT,RHO,
     +                  NUNIQ
        COMMON /CELL/ CELD(3),CELA(3),CHSPEC(5,MNCH),CHLOC(3,MNCH),
     +                  NUNIV,KONDENS,TEMP,DENSC
        COMMON /STRN/ KUC,KASE,ST(3,3),SUCV(3,3),DINIT,DPRIME,DCON
        DIMENSION CROT(4,4),UCV(3,3)
        DEGRAD = 3.1415926535/180.
        CELD(3) = DEE
C
C  >>>>>>>>>>  Modified to allow only two chain types  <<<<<<<<<<<<<<<<<<
C
        DO 50 I=3,NCH,2
          DO 50 J=1,5
            CHSPEC(J,I) = CHSPEC(J,1)
  50        CHSPEC(J,I-1) = CHSPEC(J,2)
        IF(MOD(NCH,2).NE.0) GO TO 55
          CHSPEC(1,NCH) = CHSPEC(1,2)
          CHSPEC(2,NCH) = CHSPEC(2,2)
          CHSPEC(3,NCH) = CHSPEC(3,2)
          CHSPEC(4,NCH) = CHSPEC(4,2)
          CHSPEC(5,NCH) = CHSPEC(5,2)
  55    CONTINUE
C
C  >>>>>>>>>>  End Modification   <<<<<<<<<<<<<<<<<<<<<<<<<<<<<<<<<<<<<<
C
C  Convert unit cell parameters CELD and CELA into placement vectors
C  used to locate chains on a regular periodic lattice: these are the
C  vectors 1-2 and 1-4 (see diagram above) stored in CHLOC(1,2) and
C  CHLOC(1,4), of which all other chain locations are linear
C  combinations
C
        DO 100 I=1,3
          DO 100 J=1,NCH
  100       CHLOC(I,J) = 0.
        CALL VECTORIZ( CELD,CELA,UCV,KERR )
        IF(KERR.EQ.1) WRITE(11,*) 'VECTORIZ ERROR: Invalid Angle Set'
        DO 200 I=1,3
          CHLOC(I,2) = UCV(I,1)
  200     CHLOC(I,4) = UCV(I,2)
C
C  If specified, fix lattice density:
C
        IF(NCH.GT.1)
     +    CALL DENS( CELD,CHLOC(1,2),CHLOC(1,4),TEMP,KONDENS,DENSC )
C
C  Determine location vector CHLOC(I,J) of each chain J up to J = NCH,
C  the total number of chains, in a spiral counterclockwise protocol:
C
C  Here the cell strain is imposed.  CELD and CELA should not be
C  optimized.  This is triggered by KUC not equal to 0.
        IF (KUC.NE.0) CALL STRAIN(KUC,KASE,DINIT,ST,SUCV,CHLOC,DPRIME)
```

```
C
      DO 300 I=1,3
  300   CHLOC(I,3) = CHLOC(I,2) + CHLOC(I,4)
      IF(NCH.GT.4) THEN
        ITRAN = IFIX( (SQRT(FLOAT(NCH))+0.1)/2 )
        JTRAN = 1
        JTRK = -1
        KTRK =  1
        DO 320 NTRK=5,NCH
          DO 340 I=1,3
  340       CHLOC(I,NTRK) = JTRK*CHLOC(I,2) + KTRK*CHLOC(I,4)
          IF(NTRK.GE.((2*JTRAN+1)**2)) JTRAN = JTRAN+1
          IF(     ( JTRAN.EQ.JTRK).AND.( JTRAN.NE.KTRK)) THEN
            KTRK = KTRK+1
          ELSE IF((-JTRAN.NE.JTRK).AND.( JTRAN.EQ.KTRK)) THEN
            JTRK = JTRK-1
          ELSE IF((-JTRAN.EQ.JTRK).AND.(-JTRAN.NE.KTRK)) THEN
            KTRK = KTRK-1
          ELSE IF(( JTRAN.NE.JTRK).AND.(-JTRAN.EQ.KTRK)) THEN
            JTRK = JTRK+1
          ELSE
            JTRK = JTRK+1
          END IF
  320     CONTINUE
      ELSE
      END IF
C
C  For each chain desired, duplicate parent chain and apply
C  specified rotation/translation:
C  -- For Location I: CHSPEC(1,I)= 0. Position not occupied
C                                 = 1. Position occupied
C                     CHSPEC(2,I)= Chain Translation (given as a fraction
C                                  of the C dimension)
C                     CHSPEC(3,I)= the first Eulerian angle (LAMBDA)
C                     CHSPEC(4,I)= the second Eulerian angle (XI)
C                     CHSPEC(5,I)= the third Eulerian angle (OMEGA)
C
C  The order of operations to place each chain is:
C       1.  duplicate chain
C       2.  center about origin
C       3.  rigid body rotation about Eulerian angles
C       4.  translation along crystallographic (CELD) dimensions
C       5.  translation (CHSPEC(2,I)) along chain axis
C
      ZSHFT = ( XYZ(3,NARU*NRUS+1,1)+XYZ(3,1,1) )/2.
      DO 450 I= NCH,1,-1
        ROM = CHSPEC(3,I)*DEGRAD
        RPS = CHSPEC(4,I)*DEGRAD
        RXI = CHSPEC(5,I)*DEGRAD
        CROT(1,1) = COS(RXI)*COS(RPS)*COS(ROM)-SIN(RXI)*SIN(ROM)
        CROT(1,2) = -COS(RXI)*COS(RPS)*SIN(ROM)-SIN(RXI)*COS(ROM)
        CROT(1,3) = -COS(RXI)*SIN(RPS)
        CROT(1,4) = CHLOC(1,I)
        CROT(2,1) = SIN(RXI)*COS(RPS)*COS(ROM)+COS(RXI)*SIN(ROM)
        CROT(2,2) = -SIN(RXI)*COS(RPS)*SIN(ROM)+COS(RXI)*COS(ROM)
        CROT(2,3) = -SIN(RXI)*SIN(RPS)
        CROT(2,4) = CHLOC(2,I)
        CROT(3,1) = SIN(RPS)*COS(ROM)
        CROT(3,2) = -SIN(RPS)*SIN(ROM)
        CROT(3,3) = COS(RPS)
        CROT(3,4) = CHLOC(3,I)
        CROT(4,1) = 0.
        CROT(4,2) = 0.
        CROT(4,3) = 0.
        CROT(4,4) = 1.
        DO 400 J=1,NARU*NRUS
          KIND(J,I) = KIND(J,1)
          XYZ(1,J,I) = XYZ(1,J,1)
          XYZ(2,J,I) = XYZ(2,J,1)
          XYZ(3,J,I) = XYZ(3,J,1) - ZSHFT
          XYZ(4,J,I) = 1.
```

```
            CALL MV( CROT,4,3,XYZ(1,J,I),4,XYZ(1,J,I) )
            XYZ(1,J,I) = XYZ(1,J,I)+CHSPEC(2,I)*DEE*COS(RXI)*SIN(RPS)
            XYZ(2,J,I) = XYZ(2,J,I)+CHSPEC(2,I)*DEE*SIN(RXI)*SIN(RPS)
            XYZ(3,J,I) = XYZ(3,J,I)+CHSPEC(2,I)*DEE*COS(RPS)
            XYZ(4,J,I) = 1.
  400     CONTINUE
  450   CONTINUE
        RETURN
        END


        SUBROUTINE DENS( D,V1,V2,TEMP,KD,DENSC )
C
C  If KD = 1 :  Calculates polymer density based on group additivities
C               and temperature expansion, and determines cell para-
C               meter CELD(1)
C  If KD = 0 :  Computes polymer density based on specified composition
C               and placement vectors
C
        PARAMETER( NKIND=9,NIBB=8,MNRU=6,MNCH=9,MNAT=179,NRNG=2,NSUB=4,
     +             MNSB=24,NDOF=10,MNIC=9,MCOP=45,MOPT=51 )
        COMMON /CHAINS/ PHI(NIBB),THETA(NIBB),BL(NIBB),PHIR(NRNG),
     +                  KSB(4),PCH(4,MNAT),NARU,NRUS,NCH,
     +                  A(4,4,MNAT),XYZ(4,MNAT,MNCH),KIND(MNAT,MNCH),
     +                  CHRG(MNAT,MNCH),KONEC(MNAT,MNAT),DEE,THT,RHO,
     +                  NUNIQ
        DIMENSION V(2),D(3),W(2),V1(3),V2(3),V3(3),V4(3),WX(9),VX(9)
        DATA WPH,WAM /74.,43./
        DATA WX /0.,1.,0.,0.,0.,0.,19.,35.5,79.9 /
        DATA VPH,VAM / 56.3,24.9/
        DATA VX /0.,3.3,0.,0.,0.,0.,10.9,19.9,33.6 /
        DATA GLCR,AA,BB/ 1.07,0.914,0.00029 /
        DEGRAD = 3.1415926535/180.
C
C  Calculate molecular weight and molar volume of glassy repeat unit:
C
        WG0 = 2*( WPH + WAM + 2*WX(2) ) + KSB(4)*WX(KSB(1)) -
     +        KSB(4)*WX(2)
        VG0 = 2*( VPH + VAM + 2*VX(2) ) + KSB(4)*VX(KSB(1)) -
     +        KSB(4)*VX(2)
        WG0 = REAL(NARU/28)*WG0
        VG0 = REAL(NARU/28)*VG0
        VG1 = GLCR/(VG0*(AA+BB*TEMP))
C
C  Compute cell volume:
C
        DO 200 I=1,3
          V1(I) = V1(I)/D(1)
          V2(I) = V2(I)/D(2)
  200     V3(I) = 0.
        V3(3) = 1.
        CALL VV( V1,V2,V4,3 )
        VVOL = 0.
        DO 300 I=1,3
  300     VVOL = VVOL + V3(I)*V4(I)
        VVOL = ABS(VVOL)
        IF( KD.NE.1 ) GO TO 500
C
C  Two Cases for fixed density calculations:
C  1) If D(1).eq.D(2) : fix density such that this equality is
C                       maintained (eg. hexagonal packing calculations
C  2) If D(1).ne.D(2) : (usual case) fix D(2) and density while varying
C                       D(1)
C
        AB = 1./(D(3)*VVOL*.602205*VG1)
        IF(ABS(D(1)-D(2)).LT.1.E-6) GO TO 400
        D(1) = AB/D(2)
        GO TO 500
  400   D(1) = SQRT(AB)
        D(2) = D(1)
  500   CONTINUE
```

```
      DENSC = VG1*WG0
      DO 600 I=1,3
        V1(I) = V1(I)*D(1)
        V2(I) = V2(I)*D(2)
  600 CONTINUE
C
C  Variable density case:
C
      IF(KD.NE.1) DENSC = WG0/(VVOL*D(1)*D(2)*D(3)*.602205)
      RETURN
      END


      SUBROUTINE NONBOND( IENTRY )
C
C  Creates Table of Connectivity and assigns partial atomic charges to
C  atoms of the parent polymer form (PPTA)
C
C  Need be executed only once for a given cell composition, but must
C  be called after all chains have been created
C
      PARAMETER( NKIND=9,NIBB=8,MNRU=6,MNCH=9,MNAT=179,NRNG=2,NSUB=4,
     +           MNSB=24,NDOF=10,MNIC=9,MCOP=45,MOPT=51 )
      COMMON /CHAINS/ PHI(NIBB),THETA(NIBB),BL(NIBB),PHIR(NRNG),
     +              KSB(4),PCH(4,MNAT),NARU,NRUS,NCH,
     +              A(4,4,MNAT),XYZ(4,MNAT,MNCH),KIND(MNAT,MNCH),
     +              CHRG(MNAT,MNCH),KONEC(MNAT,MNAT),DEE,THT,RHO,
     +              NUNIQ
      DATA CHARGC,CHARGO,CHARGN,CHARGH/.38,-.38,-.28,.28/
c     DATA CHARGC,CHARGO,CHARGN,CHARGH/.0,.0,.0,.0/
      DATA CHARGPPC,CHARGNPC,CHARGPH/ -0.06,-0.12,0.15 /
C
      IF( IENTRY.EQ.1 ) RETURN
C
      DO 100 I=1,NARU*NRUS
        DO 120 J=1,NCH
  120   CHRG(I,J) = 0.
        DO 130 J=1,NARU*NRUS
  130     KONEC(I,J) = 0.
  100 CONTINUE
C
C  All atoms within a given phenyl ring or amide bond plane are fixed
C  relative to one another; atoms directly bonded to each ring/plane
C  are fixed relative to that ring/plane
C
C  Amide atom charges are assigned:
C
      NMER = NARU/28
      DO 500 LL = 1,NCH
      KTYP = 10
      MARK = 0
      DO 200 I=1,NMER*NRUS
        DO 200 II=1,4
          DO 300 J=MARK+1,MARK+KTYP
            IF(KTYP.EQ.10) GO TO 310
              IF(KIND(J,LL).EQ.3) THEN
                CHRG(J,LL) = CHARGC
              ELSE IF(KIND(J,LL).EQ.4) THEN
                CHRG(J,LL) = CHARGH
              ELSE IF(KIND(J,LL).EQ.5) THEN
                CHRG(J,LL) = CHARGN
              ELSE IF(KIND(J,LL).EQ.6) THEN
                CHRG(J,LL) = CHARGO
              ELSE
              END IF
  310       CONTINUE
C
C  Three independent charges allowed: carbons 1&4, carbons 2,3,5&6,
C  and all hydrogens
C
```

```
      IF(KTYP.EQ.4) GO TO 315
      IF(J.LE.(MARK+2)) THEN
        CHRG(J,LL) = CHARGPPC
      ELSE
        IF(KIND(J,LL).EQ.1) CHRG(J,LL) = CHARGNPC
        IF(KIND(J,LL).EQ.2) CHRG(J,LL) = CHARGPH
      END IF
  315 CONTINUE
C
            IF(LL.NE.1) GO TO 300
          DO 320 K=J+1,MARK+KTYP+1
  320       KONEC(J,K) = 1
  300     CONTINUE
        IF(LL.EQ.1) THEN
          MARK = MARK+KTYP
          IF(KTYP.NE.10) GO TO 400
          KTYP = 4
          KONEC(MARK-9,MARK+2) = 1
          KONEC(MARK-9,MARK+3) = 1
          KONEC(MARK-9,MARK+4) = 1
          KONEC(MARK-8,MARK+2) = 1
          KONEC(MARK-8,MARK+3) = 1
          KONEC(MARK-8,MARK+4) = 1
          IF( MARK.GE.(NRUS*NARU-4)) GO TO 317
          KONEC(MARK-9,MARK+5) = 1
          KONEC(MARK-9,MARK+6) = 1
          KONEC(MARK-8,MARK+5) = 1
          KONEC(MARK-8,MARK+6) = 1
          IF( MARK.GE.(NRUS*NARU-18)) GO TO 317
          KONEC(MARK-9,MARK+15) = 1
          KONEC(MARK-8,MARK+15) = 1
  317     CONTINUE
          IF( MARK.LE.10 ) GO TO 200
          DO 370 L=1,14
  370       KONEC(MARK-11,MARK-10+L) = 1
          KONEC(MARK-10,MARK-9) = 1
          KONEC(MARK-10,MARK-8) = 1
          KONEC(MARK-10,MARK+1) = 1
          IF(MARK.GE.(NARU*NRUS-4)) GO TO 318
          KONEC(MARK-11,MARK+5) = 1
          KONEC(MARK-11,MARK+6) = 1
          IF(MARK.GE.(NARU*NRUS-18)) GO TO 318
          KONEC(MARK-11,MARK+15) = 1
  318     CONTINUE
          GO TO 200
  400     KTYP = 10
          IF( MARK.EQ.(NARU*NRUS) ) GO TO 200
          KONEC(MARK-2,MARK+2) = 1
          KONEC(MARK-2,MARK+11) = 1
          KONEC(MARK-3,MARK+1) = 1
          KONEC(MARK-3,MARK+2) = 1
          KONEC(MARK-3,MARK+11)= 1
        ELSE
          MARK = MARK+KTYP
          IF(KTYP.EQ.10) THEN
            KTYP = 4
          ELSE
            KTYP = 10
          END IF
        END IF
  200 CONTINUE
  500 CONTINUE
      IENTRY = 1
      RETURN
      END
```

```
      SUBROUTINE SUBSET( IENTRY )
C
C  Generates a key (KSUB) for phenyl ring substitution based on the
C  info in KSB, and then recalculates substituent positions and
C  assigns partial atomic charges.
C
C  >>>>   NOTE: IT IS CURRENTLY ASSUMED THAT THE QHAL DATA       <<<<<<
C  >>>>   STATEMENT CONTAINS THE CORRECT MONO- OR DI-SUB VVALUES  <<<<<<
C
C  All substitution occurs on one ring per repeat unit.
C       KEY:  KSB(1):  Substituent atom/group ID;
C                      2 = H (ie. no substitution)
C                      7 = F, 8 = Cl, 9 = Br
C             KSB(2):  Substition location (1 = acid, 2 = amide)
C             KSB(3):  Substitution order (0 = random, 1 = head-to-head,
C                      tail-to-tail, 2 = head-to-tail)
C             KSB(4):  Substitution type (0 = none, 1 = mono-sub at the
C                      2 position, 2 = di-sub at the 2,6 positions)
C
      INTEGER*4 SEED
      PARAMETER( NKIND=9,NIBB=8,MNRU=6,MNCH=9,MNAT=179,NRNG=2,NSUB=4,
     +           MNSB=24,NDOF=10,MNIC=9,MCOP=45,MOPT=51 )
      COMMON /CHAINS/ PHI(NIBB),THETA(NIBB),BL(NIBB),PHIR(NRNG),
     +                KSB(4),PCH(4,MNAT),NARU,NRUS,NCH,
     +                A(4,4,MNAT),XYZ(4,MNAT,MNCH),KIND(MNAT,MNCH),
     +                CHRG(MNAT,MNCH),KONEC(MNAT,MNAT),DEE,THT,RHO,
     +                NUNIQ
      COMMON /SUBS/ WTED(4)
      DIMENSION KSUB(MNSB,MNCH),DX(9),PV(3),QHAL(10,3)
      SAVE KSUB
      DATA QHAL/ -0.22,0.22,0.22,0.,0.,0.,0.,0.,0.,0.,
     +           -.02,-.06,-.12,-.12,-.03,-.03,+.17,+.17,+.02,+.02,
     +           +.02,-.06,-.09,-.09,-.14,-.14,+.17,+.17,+.08,+.08/
      DATA DX/1.,1.,1.,1.,1.,1.42,1.70,1.87/
C
C  If no substitution required, normalize phenyl ring EDEL weightings
C  and RETURN immediately:
C
      IF( (KSB(1).NE.2).AND.(KSB(4).NE.0) ) GO TO 30
      DO 40 I=1,4
40      WTED(I) = 1.
      RETURN
30    CONTINUE
C
C  Generate substitution vector KSUB (only on initial entry)
C
      IF( IENTRY.EQ.1 ) GO TO 400
        DO 50 I=1,4
50        WTED(I) = 0.
      SEED = 1
      DO 100 J=1,NCH
        DO 100 I=4,2*NRNG*NRUS,4
          KM = 3
          IF( KSB(2).EQ.2 ) KM = 1
          IF( KSB(3).EQ.0 ) THEN
            KS = I - KM + NINT( RANDS1(SEED) )
          ELSE IF( KSB(3).EQ.1 ) THEN
            KS = I - KM + MOD(KS,2)
            IF( I.EQ.4 ) KS = I - KM
          ELSE IF( KSB(3).EQ.2) THEN
            KS = I - KM
          ELSE
            WRITE(*,*) 'ERROR: Invalid KSB value in SUBSET'
          END IF
          DO 200 K=I-3,I
            KSUB(K,J) = 0
            IF( K.EQ.KS ) KSUB(K,J) = KSB(1)
            IF( K.NE.KS ) WTED(K-I+4) = WTED(K-I+4) +
     +                    2./REAL(NRNG*NRUS*NCH)
200       CONTINUE
100   CONTINUE
```

```
      IENTRY = 1
C
  400 CONTINUE
      DO 500 J=1,NCH
        DO 500 I=1,2*NRNG*NRUS
          KSTEP = MOD(I,2)
          IF( KSUB(I,J).EQ.0 ) GO TO 500
C
C  Perform substitution:
C  1) Recalculate group coordinates:
C
          KNRU = (I-1)/4
          KLOC = KNRU*28 + (I-4*KNRU)/3*14 + 3 + MOD(I,2)*4
          DO 300 L=1,KSB(4)
            LLOC = KLOC+(L-1)*2
            PVM2 = 0.
            DO 350 K=1,3
              PV(K) = XYZ(K,LLOC+1,J) - XYZ(K,LLOC,J)
  350         PVM2 = PVM2 + PV(K)**2
            PVM = SQRT( PVM2 )
            DO 360 K=1,3
  360         XYZ(K,LLOC+1,J) = XYZ(K,LLOC,J)+
     +                          PV(K)*DX(KSUB(I,J))/PVM
            KIND(LLOC+1,J) = KSUB(I,J)
  300     CONTINUE
C
C  2) Reassign ring charges according to substitution:
C  Ten independent charges allowed, in the following vector order:
C     C1  C4  C3  C5  C2  C6  H3  H5  X2  X(or H)6
C
          IF(KSTEP.EQ.1) THEN
            CHRG(KLOC-6,J) = QHAL(1,KSUB(I,J)-6)
            CHRG(KLOC-5,J) = QHAL(2,KSUB(I,J)-6)
            CHRG(KLOC-4,J) = QHAL(3,KSUB(I,J)-6)
            CHRG(KLOC-3,J) = QHAL(7,KSUB(I,J)-6)
            CHRG(KLOC-2,J) = QHAL(4,KSUB(I,J)-6)
            CHRG(KLOC-1,J) = QHAL(8,KSUB(I,J)-6)
            CHRG(KLOC  ,J) = QHAL(5,KSUB(I,J)-6)
            CHRG(KLOC+1,J) = QHAL(9,KSUB(I,J)-6)
            CHRG(KLOC+2,J) = QHAL(6,KSUB(I,J)-6)
            CHRG(KLOC+3,J) = QHAL(10,KSUB(I,J)-6)
          ELSE
            CHRG(KLOC-1,J) = QHAL(1,KSUB(I,J)-6)
            CHRG(KLOC-2,J) = QHAL(2,KSUB(I,J)-6)
            CHRG(KLOC+4,J) = QHAL(3,KSUB(I,J)-6)
            CHRG(KLOC+5,J) = QHAL(7,KSUB(I,J)-6)
            CHRG(KLOC+6,J) = QHAL(4,KSUB(I,J)-6)
            CHRG(KLOC+7,J) = QHAL(8,KSUB(I,J)-6)
            CHRG(KLOC  ,J) = QHAL(5,KSUB(I,J)-6)
            CHRG(KLOC+1,J) = QHAL(9,KSUB(I,J)-6)
            CHRG(KLOC+2,J) = QHAL(6,KSUB(I,J)-6)
            CHRG(KLOC+3,J) = QHAL(10,KSUB(I,J)-6)
          END IF
  500 CONTINUE
      RETURN
      END


      SUBROUTINE ENERGY
C
C  Calculates the total potential energy per residue of the simulation
C  stucture, based on a polymer of the PPTA family
C
C  Contributions:  EDEF  (Bond Angle Deformation, Valence FF)
C                  EDEL  (Conjugated Bond Interaction Energy)
C                  ENOB1 (Intramolecular LJ Interaction)
C                  ECOU1 (Intramolecular Coulombic Interactions)
C                  ENOB2 (Intermolecular LJ INTERACTIONS)
C                  ECOU2 (Intermolecular Coulombic Interactions)
C                  EULJP (Intramolec. LJ Lattice Correction)
C                  EUESP (Intramolec. ES lattice Correction)
```

```
C                 EULJ  (Intermolec. LJ Lattice Correction)
C                 EUES  (Intermolec. ES lattice Correction)
C
C  The reference unit for calculating the potential energy depends on
C  the choice of RBASE and the size of the Helical Repeat Unit (HRU):
C
C  Case 1:  Single chain simulation: disregard "helical basis region";
C           calculate interaction of first RBASE residues with rest of
C           chain.
C  Case 2:  THT = 0: HRU is identical to chemical repeat unit, thus
C           similar to Case 1
C  Case 3:  HRU consists of NRUS-2 or fewer structural repeat units;
C           region may be treated exactly
C  Case 4:  HRU exceeds NRUS-2 or is incommensurate: Region is
C           arbitrarily set equal to the chemical repeat unit
C
C  ANGERR is the angular discrepancy allowed in determining the number
C  of turns of the helix required to obtain an integral number of
C  complete 360 degree rotations
C
C  This version of ENERGY provides a compiled toggle option between the
C  two lattice sum methods: 3D Periodicity (LSTOGG=0) or Helical Period-
C  idity (LSTOGG=1, enable MV call in lattice sum section).  On a
C  representative minimization (eg. 9 PPTA chains w/22 degrees of freedom) C  the following
comparison times were obtained
C
        LOGICAL FIRST,REDUND
        PARAMETER( EPSILON=1E-6 )
        PARAMETER( NKIND=9,NIBB=8,MNRU=6,MNCH=9,MNAT=179,NRNG=2,NSUB=4,
     +             MNSB=24,NDOF=10,MNIC=9,MCOP=45,MOPT=51 )
        COMMON /CHAINS/ PHI(NIBB),THETA(NIBB),BL(NIBB),PHIR(NRNG),
     +                  KSB(4),PCH(4,MNAT),NARU,NRUS,NCH,
     +                  A(4,4,MNAT),XYZ(4,MNAT,MNCH),KIND(MNAT,MNCH),
     +                  CHRG(MNAT,MNCH),KONEC(MNAT,MNAT),DEE,THT,RHO,
     +                  NUNIQ
        COMMON /CELL/ CELD(3),CELA(3),CHSPEC(5,MNCH),CHLOC(3,MNCH),
     +                  NUNIV,KONDENS,TEMP,DENSC
        COMMON /ENRG/ EDEF,EDEL,ENOB1,ENOB2,ECOU1,ECOU2,EULJ,EUES,
     +                  EULJP,EUESP,ECFF,ETOT
        COMMON /SUBS/ WTED(4)
        COMMON /STRN/ KUC,KASE,ST(3,3),SUCV(3,3),DINIT,DPRIME,DCON
        DIMENSION ANGZ(12),ANGO(12),DCL(3,3)
        DIMENSION FMULT(MNCH,MNCH)
        DIMENSION VDWR(NKIND),ALPHA(NKIND),EFFNE(NKIND)
        DIMENSION UX(3),UY(3),UZ(3),DVECT(4),R(4,4,21)
        DIMENSION SUM1(3136),SUM6(3136),SUM12(3136),SUM1P(3136),
     +            SUM6P(3136),SUM12P(3136),TMP1(3136),TMP6(3136),
     +            TMP12(3136),TMP1P(3136),TMP6P(3136),TMP12P(3136)
        DATA VDWR/ 1.96,1.37,2.03,1.37,1.96,1.60,1.35,1.80,1.95/
        DATA ALPHA/0.768,0.330,2.16,0., 1.95,1.02,0.38,1.41,3.34/
        DATA EFFNE/5.2,  0.9,  5.2,  0.9,6.1,  7.,   8., 12., 21./
        DATA ANGZ/ .088,.088,.050,.088,.050,.088,.088,.088,
     +                  .088,.050,.050,.088 /
        DATA ANGO/ 120.,120.,120.,120.,120.,120.,120.,120.,
     +             120.,120.,120.,120. /
        DATA B0,B00,C0,C00,B1,B2/9.0,13.0,.2,.4,2.8,21.2 /
        DATA BX0,BX00,CX0,CX00  /0.0,32.0,.0,.8/
        DATA DE/ 3.5 /
        DATA ANGERR/ 5. /
        DATA BWDIST/ 3.3 /
C
        FIRST = .TRUE.
        DEGRAD = 3.1415926535/180.
        LSTOGG = 0
C
C  Initialize VDWR, ALPHA, and EFFNE arrays:
C
        CALL ELJ( NKIND,1,1,VDWR,ALPHA,EFFNE,3.,3.,FIRST,POTINIT )
C
        RBASE = REAL( NUNIQ )
        ECFF = 0.
```

```
        EDEF = 0.
        EDEL = 0.
        ENOB1 = 0.
        ECOU1 = 0.
        ENOB2 = 0.
        ECOU2 = 0.
        EULJ = 0.
        EUES = 0.
        EULJP = 0.
        EUESP = 0.
        NATOMS = NARU*NRUS
        NM1 = NATOMS-1
C
C  Initialize intermolecular interaction multiplier matrix:
C
        NCH2 = NCH**2
        L1MAX = 1
        IF( NCH.NE.1 ) CALL MULMAX( MNCH,NCH,NCH2,L1MAX,MULT )
C
        IF ( (NCH.EQ.1).OR.(ABS(THT).LT.ANGERR) ) GO TO 100
        DO 50 M=1,NRUS-2
          PANG = M*THT/360.
          IPANG = INT(PANG+0.5)
          IF( ABS(PANG-IPANG).LE.(M*ANGERR/360.) ) GO TO 70
  50    CONTINUE
C       WRITE(11,1)
C  1    FORMAT(1X,'HELICAL REPEAT LENGTH EXCEEDS CHAIN LENGTH')
C       NER = NRUS-2
        NER = 1
        GO TO 80
  70    NER = M
        GO TO 80
  100   NER = 1
  80    CONTINUE
        LATM = INT(RBASE*NER*NARU+1.01)
C
C  Bond angle deformation energy:
C
        L = 1
        IF(ABS(CHSPEC(1,L)).NE.1.) GO TO 900
        DO 300 K=1,NARU/28
          KADD = (K-1)*NARU/2
          KADE = (K-1)*NIBB/2
        DO 300 J=1,12
          IF( J.EQ.9 ) THEN
            KA = 12 + KADD
            KB = 13 + KADD
            KC = 11 + KADD
          ELSE IF( J.EQ.10 ) THEN
            KA = 14 + KADD
            KB = 15 + KADD
            KC = 13 + KADD
          ELSE IF( J.EQ.11 ) THEN
            KA = 26 + KADD
            KB = 27 + KADD
            KC = 25 + KADD
          ELSE IF( J.EQ.12 ) THEN
            KA = 28 + KADD
            KB = 29 + KADD
            KC = 27 + KADD
          ELSE
          END IF
          IF( J.LE.8 ) THEN
            EDEF = EDEF+0.5*ANGZ(J)*(THETA(J+KADE)-ANGO(J))**2
          ELSE
            CSQ = (XYZ(1,KA,L)-XYZ(1,KB,L))**2 +
     +            (XYZ(2,KA,L)-XYZ(2,KB,L))**2 +
     +            (XYZ(3,KA,L)-XYZ(3,KB,L))**2
            ASQ = (XYZ(1,KB,L)-XYZ(1,KC,L))**2 +
     +            (XYZ(2,KB,L)-XYZ(2,KC,L))**2 +
     +            (XYZ(3,KB,L)-XYZ(3,KC,L))**2
```

```
            BSQ = (XYZ(1,KC,L)-XYZ(1,KA,L))**2 +
     +            (XYZ(2,KC,L)-XYZ(2,KA,L))**2 +
     +            (XYZ(3,KC,L)-XYZ(3,KA,L))**2
            ANGT= ACOS( (ASQ+BSQ-CSQ)/(2*SQRT(ASQ*BSQ)) )
            ANGT= ANGT/DEGRAD
            EDEF = EDEF+0.5*ANGZ(J)*(ANGT - ANGO(J))**2
          END IF
  300   CONTINUE
C
C  Conjugated bond interaction energy:
C  Note: with the introduction of substitution on the ring (potentially
C  in a random sequence and without equal occurance at the two 'ends'
C  of the ring) with different delocalization potentials, it becomes
C  necessary to compute EDEL weighted by the appropriate loci of
C  substitutions:
C
          NRT = NARU/28
          DO 400 K=1,NRT
            NRR = (K-1)*NRNG/NRT
            NRP = (K-1)*NIBB/NRT
            EDEL = EDEL + WTED(2)*CURTINV( (PHIR(1+NRR)-PHI(2+NRP)),
     +                    B0,C0 )
            EDEL = EDEL + WTED(3)*CURTATE( PHIR(2+NRR),B00,C00 )
            EDEL = EDEL + WTED(4)*CURTATE( (PHIR(2+NRR)-PHI(6+NRP)),
     +                    B00,C00 )
            EDEL = EDEL + WTED(1)*CURTINV( PHIR(1+NRR),B0,C0 )
            EDEL = EDEL + (1.- WTED(2))*CURTATE( (PHIR(1+NRR)-
     +                    PHI(2+NRP)),BX0,CX0 )
            EDEL = EDEL + (1.- WTED(3))*CURTATE( PHIR(2+NRR),BX00,CX00 )
            EDEL = EDEL + (1.- WTED(4))*CURTATE( (PHIR(2+NRR)-
     +                    PHI(6+NRP)),BX00,CX00 )
            EDEL = EDEL + (1.- WTED(1))*CURTATE( PHIR(1+NRR),BX0,CX0 )
            EDEL = EDEL + B1/2*(1.-COS(PHI(4+NRP) *DEGRAD))
     +                  + B2/2*(1.-COS(2*PHI(4+NRP) *DEGRAD))
            EDEL = EDEL + B1/2*(1.-COS(PHI(8+NRP) *DEGRAD))
     +                  + B2/2*(1.-COS(2*PHI(8+NRP) *DEGRAD))
  400     CONTINUE
        DO 500 L1=1,L1MAX
          IF(L1.NE.1) GO TO 530
C
C  Intramolecular nonbonded interactions:
C
          DO 520 I=1,NM1
            IP1 = I+1
            DO 510 J=IP1,NATOMS
              IF( KONEC(I,J).EQ.1 ) GO TO 510
              IF( I.GE.LATM ) GO TO 510
              D2 = (XYZ(1,I,L1)-XYZ(1,J,L1))**2 +
     +             (XYZ(2,I,L1)-XYZ(2,J,L1))**2 +
     +             (XYZ(3,I,L1)-XYZ(3,J,L1))**2
              DIS = SQRT(D2)
              CALL ELJ( NKIND,KIND(I,L1),KIND(J,L1),VDWR,ALPHA,EFFNE,
     +                  D2,D2,FIRST,POTLJ )
              ENOB1 = ENOB1 + POTLJ
              CALL EES( BWDIST,DIS,DE,CHRG(I,L1),CHRG(J,L1),POTES )
              ECOU1 = ECOU1 + POTES
  510       CONTINUE
  520     CONTINUE
  530     CONTINUE
          IF (NCH.EQ.1) GO TO 500
          LP1 = L1+1
C
C  Intermolecular interactions:
C
          DO 550 L2=LP1,NCH
            IF( INT(FMULT(L1,L2)*100.).EQ.0 ) GO TO 550
            IF( INT(ABS(CHSPEC(1,L2))+.01).NE.1 ) GO TO 550
            ENOBT = 0.
            ECOUT = 0.
            DO 570 I=1,NATOMS
              DO 560 J=1,NATOMS
```

```
              IF (I.LT.LATM) THEN
              D2 = (XYZ(1,I,L1)-XYZ(1,J,L2))**2 +
     +             (XYZ(2,I,L1)-XYZ(2,J,L2))**2 +
     +             (XYZ(3,I,L1)-XYZ(3,J,L2))**2
              DIS = SQRT(D2)
              CALL ELJ( NKIND,KIND(I,L1),KIND(J,L2),VDWR,ALPHA,EFFNE,
     +                  D2,D2,FIRST,POTLJ )
              ENOBT = ENOBT + POTLJ
              CALL EES( BWDIST,DIS,DE,CHRG(I,L1),CHRG(J,L2),POTES )
              ECOUT = ECOUT + POTES
              ELSE
              IF (J.LT.LATM) THEN
              D2 = (XYZ(1,I,L1)-XYZ(1,J,L2))**2 +
     +             (XYZ(2,I,L1)-XYZ(2,J,L2))**2 +
     +             (XYZ(3,I,L1)-XYZ(3,J,L2))**2
              DIS = SQRT(D2)
              CALL ELJ( NKIND,KIND(I,L1),KIND(J,L2),VDWR,ALPHA,EFFNE,
     +                  D2,D2,FIRST,POTLJ )
              ENOBT = ENOBT + POTLJ
              CALL EES( BWDIST,DIS,DE,CHRG(I,L1),CHRG(J,L2),POTES )
              ECOUT = ECOUT + POTES
              ELSE
              END IF
              END IF
  560         CONTINUE
  570       CONTINUE
            ENOB2 = ENOB2 + 0.5*ENOBT
            ECOU2 = ECOU2 + 0.5*ECOUT
  550     CONTINUE
  500   CONTINUE
C
C  Infinite Lattice Correction:
C    (specific for two-chain-type lattices, with interchain interactions
C     1-1, 1-2, 2-1, and 2-2 only; of these, only half of the 1-1 and 2-2
C     interactions are unique, and the 1-2 interactions are identical to
C     the 2-1 interactions.  NUNIV represents "infinite" lattice size)
C
        IF( NUNIV.EQ.0 ) GO TO 630
        DO 610 K=1,3
          UX(K) = CHLOC(K,2) - CHLOC(K,4)
          UY(K) = CHLOC(K,2) + CHLOC(K,4)
          UZ(K) = 0.
  610     DVECT(K) = 0.
        UZ(3) = RBASE*REAL(NER)*DEE
        DVECT(4) = 1.
        NCM2 = NINT(SQRT(REAL(NCH))-2)
        NNCM = -NCM2-1
        ESPWR = BWDIST*LOG(DE)
C
C  Set up helix periodicity transforms beforehand:
C
        IF(LSTOGG.EQ.0) GO TO 625
        DO 620 LZN = 1,2*NUNIV+1
          LZ = LZN-NUNIV-1
          RTN = RBASE*REAL(LZ*NER)
          RTH = RTN*THT
          RDE = RTN*DEE
          CALL RTRANS( RTH,RDE,R(1,1,LZN) )
  620   CONTINUE
  625   CONTINUE
C
        DO 600 L1=1,2
        DO 600 L2=L1,2
          KFIJ = L1+L2-1
          LXS = -NUNIV
          IF( KFIJ.NE.2 ) LXS = 0
          NNLX = NUNIV-LXS+1
          NNLY = 2*NUNIV+1
          NNLZ = NNLY
C
C  Zero all atom-atom summations:
```

```
C
          DO 645 I=1,LATM-1
          DO 645 J=1,LATM-1
            NTMP = (I-1)*(LATM-1) + J
            SUM1P(NTMP) = 0.
            SUM6P(NTMP) = 0.
            SUM12P(NTMP) = 0.
            SUM1(NTMP) = 0.
            SUM6(NTMP) = 0.
            SUM12(NTMP) = 0.
  645     CONTINUE
C
C  Loop over all lattice points, checking for redundancy with explicit
C  calculation scheme for L1-L2:
C
cvd$ noconcur
          DO 680 LX=LXS,NUNIV
cvd$ noconcur
          DO 680 LY=-NUNIV,NUNIV
cvd$ noconcur
          DO 680 LZ=-NUNIV,NUNIV
            NRED = (LX-LXS)*NNLY*NNLZ + (LY+NUNIV)*NNLZ +
     +             (LZ+NUNIV) + 1
            IF( (KFIJ.NE.2).AND.(LX.EQ.0).AND.(LY.LE.0) ) THEN
              REDUND = .TRUE.
              GO TO 680
            ELSE
              REDUND = .FALSE.
            END IF
            IF( ABS(LZ).LE.(NRUS-1) ) THEN
              IF (KFIJ.NE.2) THEN
                REDUND = ( (ABS(LX)+ABS(LY)).LE.NCM2 )
              ELSE
                IF( (LX+LY).NE.NCM2 ) THEN
                  REDUND = ( ((ABS(LX)+ABS(LY)).LE.NCM2).OR.
     +             ((LX.LT.0).AND.(LY.LT.0).AND.((LX+LY).EQ.NNCM)) )
                END IF
              END IF
            END IF
            IF( REDUND ) GO TO 680
C
C  Loop over all atoms of the units of L1 and L2 at this lattice point
C  to get inverse distances:
C
          DO 650 I=1,LATM-1
          DO 650 J=1,LATM-1
            NTMP = (I-1)*(LATM-1) + J
C           ESPWR = ( VDWR(KIND(I,L1))+VDWR(KIND(J,L2)) )*LOG(DE)
            IF( LSTOGG.EQ.0 ) THEN
              DVECT(1) = XYZ(1,J,L2) - XYZ(1,I,L1)
              DVECT(2) = XYZ(2,J,L2) - XYZ(2,I,L1)
              DVECT(3) = XYZ(3,J,L2) - XYZ(3,I,L1)
              DVV = (DVECT(1)+LX*UX(1)+LY*UY(1)+LZ*UZ(1))**2
     +            + (DVECT(2)+LX*UX(2)+LY*UY(2)+LZ*UZ(2))**2
     +            + (DVECT(3)+LX*UX(3)+LY*UY(3)+LZ*UZ(3))**2
            ELSE
              LZN = LZ + NUNIV + 1
              DVECT(1) = XYZ(1,J,L2) - CHLOC(1,L2)
              DVECT(2) = XYZ(2,J,L2) - CHLOC(2,L2)
              DVECT(3) = XYZ(3,J,L2) - CHLOC(3,L2)
C  Next line disabled only to allow for better concurrency optimization; C  must be enabled
for use of helical periodicity calculations
C             CALL MV( R(1,1,LZN),4,3,DVECT,4,DVECT )
              DVECT(1) = DVECT(1) + CHLOC(1,L2) - XYZ(1,I,L1)
              DVECT(2) = DVECT(2) + CHLOC(2,L2) - XYZ(2,I,L1)
              DVECT(3) = DVECT(3) + CHLOC(3,L2) - XYZ(3,I,L1)
              DVV = (DVECT(1)+LX*UX(1)+LY*UY(1))**2
     +            + (DVECT(2)+LX*UX(2)+LY*UY(2))**2
     +            + (DVECT(3)+LX*UX(3)+LY*UY(3))**2
            END IF
            DVROOT = SQRT(DVV)
```

```
C  Note: discontinuity in S1 is possible, may have to spline (5/16/88)
              S1 = EXP(ESPWR/DVROOT)/DVROOT
              IF( DVROOT.LE.BWDIST ) S1 = DE/DVROOT
              S6 = 1./DVV**3
              S12 = S6**2
              IF( (KFIJ.NE.2).AND.(LX.EQ.0).AND.(LY.EQ.0) ) THEN
                TMP1P(NTMP) = S1
                TMP6P(NTMP) = S6
                TMP12P(NTMP) = S12
              ELSE
                TMP1(NTMP) = S1
                TMP6(NTMP) = S6
                TMP12(NTMP) = S12
              END IF
  650       CONTINUE
C
C  Add this element to summation
C
            DO 655 I=1,LATM-1
            DO 655 J=1,LATM-1
              NTMP = (I-1)*(LATM-1) + J
              SUM1P(NTMP) = SUM1P(NTMP) + TMP1P(NTMP)
              SUM6P(NTMP) = SUM6P(NTMP) + TMP6P(NTMP)
              SUM12P(NTMP) = SUM12P(NTMP) + TMP12P(NTMP)
              SUM1(NTMP) = SUM1(NTMP) + TMP1(NTMP)
              SUM6(NTMP) = SUM6(NTMP) + TMP6(NTMP)
              SUM12(NTMP) = SUM12(NTMP) + TMP12(NTMP)
  655       CONTINUE
  680     CONTINUE
C
C  Finally, calculate the energies for each atom-atom pair:
C
          DO 665 I=1,LATM-1
          DO 665 J=1,LATM-1
            NTMP = (I-1)*(LATM-1) + J
            CALL ELJ( NKIND,KIND(I,L1),KIND(J,L2),VDWR,ALPHA,EFFNE,
     +                SUM6(NTMP),SUM12(NTMP),FIRST,POTLJ )
            EULJ = EULJ + 0.5*POTLJ
            EUES = EUES + 166.*SUM1(NTMP)*CHRG(I,L1)*CHRG(J,L2)/DE
            IF( (SUM6P(NTMP).EQ.0.).AND.(SUM12P(NTMP).EQ.0.) ) GO TO 665
            CALL ELJ( NKIND,KIND(I,L1),KIND(J,L2),VDWR,ALPHA,EFFNE,
     +                SUM6P(NTMP),SUM12P(NTMP),FIRST,POTLJP )
            EULJP = EULJP + 0.5*POTLJP
            EUESP = EUESP + 166.*SUM1P(NTMP)*CHRG(I,L1)*CHRG(J,L2)/DE
  665     CONTINUE
  600   CONTINUE
  630   CONTINUE
C
C  Here is calculated the penalty function that fixes chain pitch DEE
C
        IF( KUC.NE.0 ) ECFF = DCON*( DEE - DPRIME )**2
C
C  Total energy per residue:
C
        ENOB1 = ENOB1/NER/RBASE
        ENOB2 = ENOB2/NER/RBASE
        ECOU1 = ECOU1/NER/RBASE
        ECOU2 = ECOU2/NER/RBASE
        EULJ = EULJ/NER/RBASE
        EUES = EUES/NER/RBASE
        EULJP = EULJP/NER/RBASE
        EUESP = EUESP/NER/RBASE
        ETOT = EDEF + EDEL + ENOB1 + ENOB2 + ECOU1 + ECOU2 + ECFF +
     +         EULJ + EUES + EULJP + EUESP
        RETURN
  900   CONTINUE
        WRITE(11,*) 'ERROR: No parent chain available'
        RETURN
        END
```

```
      SUBROUTINE RTRANS( TH,D,R )
C  "R" Matrix Generation
C
C           |  N  D  |
C     R  =  |        |
C           |  0  1  |
C
      DIMENSION R(4,4)
      RTH = TH*3.1415926535/180.
      R(1,1) = COS(RTH)
      R(1,2) = -SIN(RTH)
      R(1,3) = 0.
      R(1,4) = 0.
      R(2,1) = SIN(RTH)
      R(2,2) = COS(RTH)
      R(2,3) = 0.
      R(2,4) = 0.
      R(3,1) = 0.
      R(3,2) = 0.
      R(3,3) = 1.
      R(3,4) = D
      R(4,1) = 0.
      R(4,2) = 0.
      R(4,3) = 0.
      R(4,4) = 1.
      RETURN
      END


      SUBROUTINE STRAIN( KUC,KASE,CEE,ST,SUCV,CHLOC,CEEP)
C
C  Invokes a fixed strain on the chain locations.  KUC and KASE specify
C  the unitcell convention and relative orthogonal axes, for frame of
C  reference purposes.  ST is the orthogonal strain tensor (elements of
C  which are fractional change; eg. 0.01).  CHLOC(i,2) and CHLOC(i,4) are
C  used to relate unitcell and are returned in strained form.  Changes
C  along the chain axis dimension must be handled using a penalty
C  function, such that the undeformed length CEE becomes the deformed
C  length CEEP
C
      DIMENSION ST(3,3),STP(3,3),CHLOC(3,9),CRT(3,3),CV(2),DV(2),
     +          SFR(3,3),SFRI(3,3),UCV(3,3),SUCV(3,3)
C
C  First, define placement of unit cell in lattice (Type 1 - 12: see key)
C  and establish coordinate rotation tensor
C
      KONV = 1
      UCV(1,3) = 0.
      UCV(2,3) = 0.
      UCV(3,3) = CEE
 500  CONTINUE
      IF( KUC.EQ.1 ) THEN
C  Type 1: a=1-9, b=1-3
        IF( KONV.EQ.1 ) THEN
          DO 110 I=1,3
            UCV(I,1) = CHLOC(I,2) - CHLOC(I,4)
 110        UCV(I,2) = CHLOC(I,2) + CHLOC(I,4)
        ELSE
          DO 115 I=1,3
            CHLOC(I,2) = 0.5*(UCV(I,2) + UCV(I,1))
 115        CHLOC(I,4) = 0.5*(UCV(I,2) - UCV(I,1))
        END IF
      ELSE IF (KUC.EQ.2 ) THEN
C  Type 2: a=1-9, b=1-51
        IF( KONV.EQ.1 ) THEN
          DO 120 I=1,3
            UCV(I,1) = CHLOC(I,2) - CHLOC(I,4)
 120        UCV(I,2) = 3*CHLOC(I,2) - CHLOC(I,4)
        ELSE
          DO 125 I=1,3
            CHLOC(I,2) = 0.5*(UCV(I,2) - UCV(I,1))
```

```
125           CHLOC(I,4) = 0.5*(UCV(I,2) - 3.*UCV(I,1))
            END IF
          ELSE IF (KUC.EQ.3) THEN
C  Type 3: a=1-9, b=1-35
            IF( KONV.EQ.1 ) THEN
              DO 130 I=1,3
                UCV(I,1) = CHLOC(I,2) - CHLOC(I,4)
130             UCV(I,2) = 3*CHLOC(I,4) - CHLOC(I,2)
            ELSE
              DO 135 I=1,3
                CHLOC(I,2) = 0.5*(UCV(I,2) + 3.*UCV(I,1))
135             CHLOC(I,4) = 0.5*(UCV(I,2) + UCV(I,1))
            END IF
          ELSE IF (KUC.EQ.4 ) THEN
C  Type 4: a=1-9, b=1-11
            IF( KONV.EQ.1 ) THEN
              DO 140 I=1,3
                UCV(I,1) = CHLOC(I,2) - CHLOC(I,4)
140             UCV(I,2) = 2*CHLOC(I,2)
            ELSE
              DO 145 I=1,3
                CHLOC(I,2) = 0.5*UCV(I,2)
145             CHLOC(I,4) = 0.5*UCV(I,2) - UCV(I,1)
            END IF
          ELSE IF (KUC.EQ.5) THEN
C  Type 5: a=1-7, b=1-11
            IF( KONV.EQ.1 ) THEN
              DO 150 I=1,3
                UCV(I,1) = -CHLOC(I,2) - CHLOC(I,4)
150             UCV(I,2) = 2*CHLOC(I,2)
            ELSE
              DO 155 I=1,3
                CHLOC(I,2) = 0.5*UCV(I,2)
155             CHLOC(I,4) = -UCV(I,1) - 0.5*UCV(I,2)
            END IF
          ELSE IF (KUC.EQ.6 ) THEN
C  Type 6: a=1-9, b=1-15
            IF( KONV.EQ.1 ) THEN
              DO 160 I=1,3
                UCV(I,1) = CHLOC(I,2) - CHLOC(I,4)
160             UCV(I,2) = 2*CHLOC(I,4)
            ELSE
              DO 165 I=1,3
                CHLOC(I,2) = UCV(I,1) + 0.5*UCV(I,2)
165             CHLOC(I,4) = 0.5*UCV(I,2)
            END IF
          ELSE IF( KUC.EQ.7 ) THEN
C  Type 7: a=1-3, b=1-15
            IF( KONV.EQ.1 ) THEN
              DO 170 I=1,3
                UCV(I,1) = CHLOC(I,2) + CHLOC(I,4)
170             UCV(I,2) = 2*CHLOC(I,4)
            ELSE
              DO 175 I=1,3
                CHLOC(I,2) = UCV(I,1) - 0.5*UCV(I,2)
175             CHLOC(I,4) = 0.5*UCV(I,2)
            END IF
          ELSE IF (KUC.EQ.8 ) THEN
C  Type 8: a=1-9, b=1-2
            IF( KONV.EQ.1 ) THEN
              DO 180 I=1,3
                UCV(I,1) = CHLOC(I,2) - CHLOC(I,4)
180             UCV(I,2) = CHLOC(I,2)
            ELSE
              DO 185 I=1,3
                CHLOC(I,2) = UCV(I,2)
185             CHLOC(I,4) = UCV(I,2) - UCV(I,1)
            END IF
          ELSE IF (KUC.EQ.9) THEN
C  Type 9: a=1-7, b=1-2
            IF( KONV.EQ.1 ) THEN
```

```
            DO 190 I=1,3
              UCV(I,1) = -CHLOC(I,2) - CHLOC(I,4)
 190          UCV(I,2) = CHLOC(I,2)
            ELSE
              DO 195 I=1,3
                CHLOC(I,2) = UCV(I,2)
 195            CHLOC(I,4) = -UCV(I,2) - UCV(I,1)
            END IF
          ELSE IF (KUC.EQ.10 ) THEN
C  Type 10: a=1-9, b=1-4
            IF( KONV.EQ.1 ) THEN
              DO 200 I=1,3
                UCV(I,1) = CHLOC(I,2) - CHLOC(I,4)
 200            UCV(I,2) = CHLOC(I,4)
            ELSE
              DO 205 I=1,3
                CHLOC(I,2) = UCV(I,2) + UCV(I,1)
 205            CHLOC(I,4) = UCV(I,2)
            END IF
          ELSE IF (KUC.EQ.11) THEN
C  Type 11: a=1-3, b=1-4
            IF( KONV.EQ.1 ) THEN
              DO 210 I=1,3
                UCV(I,1) = CHLOC(I,2) + CHLOC(I,4)
 210            UCV(I,2) = CHLOC(I,4)
            ELSE
              DO 215 I=1,3
                CHLOC(I,2) = UCV(I,1) - UCV(I,2)
 215            CHLOC(I,4) = UCV(I,2)
            END IF
          ELSE IF (KUC.EQ.12 ) THEN
C  Type 12: a=1-2, b=1-4
            IF( KONV.EQ.1 ) THEN
              DO 220 I=1,3
                UCV(I,1) = CHLOC(I,2)
 220            UCV(I,2) = CHLOC(I,4)
            ELSE
              DO 225 I=1,3
                CHLOC(I,2) = UCV(I,1)
 225            CHLOC(I,4) = UCV(I,2)
            END IF
          ELSE
            WRITE(*,*) 'ERROR: invalid cell definition in STRAIN'
          END IF
          IF( KONV.EQ.2 ) GO TO 600
C
C  By convention, strain tensor is given in a Unit Cell Frame of
C  Reference (UCV):
C  2 possibilites: UCV(i,1) lies in ST xz plane (KASE 1)
C                  or: UCV(i,2) lies in ST yz plane (KASE 2)
C  Rotate UCV to correspond to strain tensor F.O.R., deform UCV,
C  rotate back into original F.O.R., then decompose back to CHLOC
C  vectors
C
          DO 300 I=1,3
          DO 300 J=1,3
 300        SFR(I,J) = 0.
          SFR(3,3) = 1.
          CV(1) = UCV(1,KASE)
          CV(2) = UCV(2,KASE)
          CVM = SQRT(CV(1)**2 + CV(2)**2)
          KOTHER = MOD(KASE,2)+1
          SFR(1,1) = CV(KASE)/CVM
          SFR(1,2) = REAL(KOTHER-KASE)*CV(KOTHER)/CVM
          SFR(2,1) = -SFR(1,2)
          SFR(2,2) = SFR(1,1)
C
          DO 400 I=1,3
            DO 450 J=1,3
 450          STP(I,J) = ST(J,I)
 400        STP(I,I) = STP(I,I) + 1.
```

```
C
      CALL MM( SFR,UCV,UCV,3,3,3,3,3,3 )
      CALL MM( STP,UCV,UCV,3,3,3,3,3,3 )
      SFR(1,2) = -SFR(1,2)
      SFR(2,1) = -SFR(2,1)
      CALL MM( SFR,UCV,UCV,3,3,3,3,3,3 )
      CEEP = UCV(3,3)
      KONV = KONV + 1
      GO TO 500
C
 600  CONTINUE
      DO 700 I=1,3
      DO 700 J=1,3
 700    SUCV(I,J) = UCV(I,J)
      RETURN
      END


      SUBROUTINE DATARD( NVAR,INSTR,MODE )
C
C  Reads variable/instruction input file (U.dt) and loads scan range
C  control vectors
C
      PARAMETER( NKIND=9,NIBB=8,MNRU=6,MNCH=9,MNAT=179,NRNG=2,NSUB=4,
     +           MNSB=24,NDOF=10,MNIC=9,MCOP=45,MOPT=51 )
      COMMON /CHAINS/ PHI(NIBB),THETA(NIBB),BL(NIBB),PHIR(NRNG),
     +                KSB(4),PCH(4,MNAT),NARU,NRUS,NCH,
     +                A(4,4,MNAT),XYZ(4,MNAT,MNCH),KIND(MNAT,MNCH),
     +                CHRG(MNAT,MNCH),KONEC(MNAT,MNAT),DEE,THT,RHO,
     +                NUNIQ
      COMMON /CELL/ CELD(3),CELA(3),CHSPEC(5,MNCH),CHLOC(3,MNCH),
     +                NUNIV,KONDENS,TEMP,DENSC
      COMMON /SCAN/ NSTOT,NSANG,NSCAN(NDOF),SCANO(NDOF),SCAND(NDOF),
     +                NCTOT,NCMUT,NMUT(MOPT),CMUTO(MOPT),CMUTD(MOPT)
      COMMON /MINIM/ LMV(2,9),LCV(5,11),OMVARS(97)
      DIMENSION INSTR(5)
      DEGRAD = 3.1415926535/180.
      OPEN (UNIT=10, FILE='U.dt',STATUS='OLD')
C
C  Read output format instruction codes, mode for Hessian in
C  minimization, simulation dimensions, and ring substitution
C
      READ(10,2) (INSTR(I),I=1,5)
      READ(10,2) MODE
      READ(10,1) NARU,NRUS,NCH,NUNIV,KONDENS,TEMP
      IF (NRUS.GT.MNRU) NRUS = MNRU
      READ(10,2) (KSB(I),I=1,4)
C
C  The polymer generation routines create a single polymer type
C  (unsubstituted poly(p-phenylene terephthalamide).  Modifications
C  of the chemistry are intructed by KSB(4), which is translated into
C  a ring substitution sequence by the subroutine SUBSET.
C  Substitution on the ring also affects the number of monomer units
C  required to describe a unique structural unit (ie. one repeat unit
C  if unsubstituted or head-to-tail, two if head-to-head,tail-to-tail);
C  this information is used by LDVAR to limit chain translation during
C  optimization and is passed by NUNIQ.  Here, determine NUNIQ:
C
C  If the 56 atom HHTT isomer representation is used, disable NUNIQ = 2:
C
      NUNIQ = 1
      IF( KSB(3).EQ.1 ) NUNIQ = 2
C
C  Read conformation paramters THETA, PHI, optimization flags for these
C  two variables, and scan instructions for PHI.  Same for PHIR.
C
      DO 100 I=1,NIBB
 100    NSCAN(I) = 0
      NVAR = 0
      NSTOT = 1
      NSANG = 0
```

```
      DO 200 I=1,NIBB
        READ(10,5) THETA(I),PHI(I),(LMV(J,I),J=1,2),
     +             ISCAN,SCO,SCX,SCD
        IF (LMV(1,I).GT.0) NVAR=NVAR+1
        IF (LMV(2,I).GT.0) NVAR=NVAR+1
        IF (ISCAN.LT.1) GO TO 200
        PHI(I) = SCO
        SCANO(I) = SCO
        SCAND(I) = SIGN(SCD,SCX-SCO)
        NSCAN(I) = INT(1.01+(SCX-SCO)/SCAND(I))
        NSANG = NSANG + 1
        NSTOT = NSTOT*NSCAN(I)
  200 CONTINUE
      DO 210 I=1,NRNG
        KTAG = MOD( (I+1),2 ) + 1
        ITAG = NIBB + I/3 + 1
        JTAG = NIBB + I
        READ(10,9) PHIR(I),LMV(KTAG,ITAG),ISCAN,SCO,SCX,SCD
        IF (LMV(KTAG,ITAG).GT.0) NVAR=NVAR+1
        IF (ISCAN.LT.1) GO TO 210
        PHIR(I) = SCO
        SCANO(JTAG) = SCO
        SCAND(JTAG) = SIGN(SCD,SCX-SCO)
        NSCAN(JTAG) = INT(1.01+(SCX-SCO)/SCAND(JTAG))
        NSANG = NSANG + 1
        NSTOT = NSTOT*NSCAN(JTAG)
  210 CONTINUE
C
C  Read cell packing parameters CELD (with optimization flag and scan
C  intructions), CELA (with flag and scan), and CHSPEC (with flag and
C  scan, up to a maximum of first nine chains)
C
      DO 400 I=1,MOPT
  400   NMUT(I) = 0
      NCTOT = 1
      NCMUT = 0
      DO 420 I=1,3
        READ(10,6) CELD(I),LCV(I,MNIC+1),IDVAR,DVO,DVX,DVD
        IF(IDVAR.LT.1) GO TO 420
        KK = MCOP+I
        CELD(I) = DVO
        CMUTO(KK) = DVO
        CMUTD(KK) = SIGN(DVD,DVX-DVO)
        NMUT(KK) = INT(1.01+(DVX-DVO)/CMUTD(KK))
        NCMUT = NCMUT+1
        NCTOT = NCTOT*NMUT(KK)
  420 CONTINUE
      DO 440 I=1,3
        READ(10,6) CELA(I),LCV(I,MNIC+2),IDVAR,DVO,DVX,DVD
        IF(IDVAR.LT.1) GO TO 440
        KK = MCOP+3+I
        CELA(I) = DVO
        CMUTO(KK) = DVO
        CMUTD(KK) = SIGN(DVD,DVX-DVO)
        NMUT(KK) = INT(1.01+(DVX-DVO)/CMUTD(KK))
        NCMUT = NCMUT+1
        NCTOT = NCTOT*NMUT(KK)
  440 CONTINUE
      DO 460 I=1,3
  460   IF(CELD(I).LT.1.) CELD(I) = 1000.
      DO 300 J=1,MNIC
        DO 300 I=1,5
          READ(10,7) CHSPEC(I,J),LCV(I,J),ICVAR,CVO,CVX,CVD
          IF (ICVAR.LT.1) GO TO 300
          KK = I+(J-1)*5
          CHSPEC(I,J) = CVO
          CMUTO(KK) = CVO
          CMUTD(KK) = SIGN(CVD,CVX-CVO)
          NMUT(KK) = INT(1.01+(CVX-CVO)/CMUTD(KK))
          NCMUT = NCMUT+1
          NCTOT = NCTOT*NMUT(KK)
```

```
  300   CONTINUE
        DO 500 J=1,MNIC+2
          DO 500 I=1,5
  500       IF (LCV(I,J).GT.0) NVAR=NVAR+1
        CLOSE (UNIT=10)
C
C  Call strain input file
C
        CALL RDSTRAIN( MODE )
C
        RETURN
    1   FORMAT( 5(I4),F8.3 )
    2   FORMAT( 5(I4) )
    5   FORMAT( 2(F8.3),3(I4,4X),3(F8.3) )
    6   FORMAT( F8.3,2(I4,4X),3(F8.3) )
    7   FORMAT( F8.3,2(I4,4X),3(F8.3) )
    9   FORMAT( F8.3,2(I4,4X),3(F8.3) )
   10   FORMAT( 4(I4) )
        END


        SUBROUTINE RESWR( INSTR )
C
C  Output simulation results to a file opened in the main program,
C  according to instructions contained in INSTR
C
        PARAMETER( NKIND=9,NIBB=8,MNRU=6,MNCH=9,MNAT=179,NRNG=2,NSUB=4,
     +             MNSB=24,NDOF=10,MNIC=9,MCOP=45,MOPT=51 )
        COMMON /CHAINS/ PHI(NIBB),THETA(NIBB),BL(NIBB),PHIR(NRNG),
     +                  KSB(4),PCH(4,MNAT),NARU,NRUS,NCH,
     +                  A(4,4,MNAT),XYZ(4,MNAT,MNCH),KIND(MNAT,MNCH),
     +                  CHRG(MNAT,MNCH),KONEC(MNAT,MNAT),DEE,THT,RHO,
     +                  NUNIQ
        COMMON /CELL/ CELD(3),CELA(3),CHSPEC(5,MNCH),CHLOC(3,MNCH),
     +                  NUNIV,KONDENS,TEMP,DENSC
        COMMON /ENRG/ EDEF,EDEL,ENOB1,ENOB2,ECOU1,ECOU2,EULJ,EUES,
     +                  EULJP,EUESP,ECFF,ETOT
        COMMON /OPRS/ NVAR,VARS(97),GRAD(97),GRADNM
        COMMON G(97),H(4753),W(291)
        COMMON /STRN/ KUC,KASE,ST(3,3),SUCV(3,3),DINIT,DPRIME,DCON
        DIMENSION INSTR(5)
        CHARACTER*2 KAR(NKIND)
        DATA KAR/'C','H','C','H','N','O','F','CL','BR'/
C
        NHELEM = NVAR*(NVAR+1)/2
        IF(INSTR(1).NE.1) GO TO 210
        WRITE(11,1)
        WRITE(11,2)
        NIBB2 = INT(NIBB/2)
        DO 110 J=1,NIBB2
  110     WRITE(11,20) THETA(J),PHI(J),THETA(J+NIBB2),PHI(J+NIBB2)
        WRITE(11,21) (PHIR(I),I=1,NRNG)
        WRITE(11,23) (KSB(I),I=1,4)
  210   IF(INSTR(2).NE.1) GO TO 220
        WRITE(11,4) DEE,RHO,THT
  220   IF(INSTR(3).NE.1) GO TO 230
        WRITE(11,5)
        WRITE(11,24) TEMP,DENSC,NUNIV
        WRITE(11,6) (CELD(I),I=1,3)
        WRITE(11,7) (CELA(I),I=1,3)
        WRITE(11,8)
        DO 200 J=1,2
          IF(ABS(CHSPEC(1,J)).EQ.0.) GO TO 200
          WRITE(11,9) J,(CHSPEC(I,J),I=2,5)
  200   CONTINUE
  230   IF(KUC.EQ.0) GO TO 235
        WRITE(11,31)
        WRITE(11,32) KUC,KASE
        WRITE(11,33) (ST(1,I),I=1,3)
        WRITE(11,33) (ST(2,I),I=1,3)
        WRITE(11,33) (ST(3,I),I=1,3)
```

```
      WRITE(11,34)
      WRITE(11,33) (SUCV(1,I),I=1,3)
      WRITE(11,33) (SUCV(2,I),I=1,3)
      WRITE(11,33) (SUCV(3,I),I=1,3)
      WRITE(11,*)
235   IF(INSTR(4).NE.1) GO TO 240
      EINTRA = EDEF+EDEL+ECFF+ENOB1+ECOU1+EULJP+EUESP
      EINTER = ENOB2+ECOU2+EULJ+EUES
C
C  Keep all energies within bounds for printout:
C
      EDEF = MAX( -999.,MIN( 999.,EDEF ) )
      EDEL = MAX( -999.,MIN( 999.,EDEL ) )
      ECFF = MAX( -999.,MIN( 999.,ECFF ) )
      ENOB1 = MAX( -999.,MIN( 999.,ENOB1 ) )
      ECOU1 = MAX( -999.,MIN( 999.,ECOU1 ) )
      EULJP = MAX( -999.,MIN( 999.,EULJP ) )
      EUESP = MAX( -999.,MIN( 999.,EUESP ) )
      EINTRA = MAX( -999.,MIN( 999.,EINTRA ) )
      ENOB2 = MAX( -9999.,MIN( 9999.,ENOB2 ) )
      ECOU2 = MAX( -9999.,MIN( 9999.,ECOU2 ) )
      EULJ = MAX( -9999.,MIN( 9999.,EULJ ) )
      EUES = MAX( -9999.,MIN( 9999.,EUES ) )
      EINTER = MAX( -9999.,MIN( 9999.,EINTER ) )
      ETOT = MAX( -9999.,MIN( 9999.,ETOT ) )
      WRITE(11,10)
      WRITE(11,11)
      WRITE(11,27) EDEF,EDEL,ECFF,ENOB1,ECOU1,EULJP,EUESP,EINTRA
      WRITE(11,12)
      WRITE(11,28) ENOB2,ECOU2,EULJ,EUES,EINTER,ETOT
      IF (NVAR.NE.0) WRITE(11,22) NVAR,GRADNM
240   IF(INSTR(5).NE.1) GO TO 250
      WRITE(11,13)
      LCNT = 0
      DO 300 L=1,MIN(9,NCH)
        IF(ABS(CHSPEC(1,L)).NE.1.) GO TO 300
        LCNT = LCNT+1
        IO = 1+(LCNT-1)*NARU*NRUS
        IX = LCNT*NARU*NRUS
        DO 350 I=IO,IX
          IM = I-IO+1
          IF ((I.LE.9).AND.(KIND(IM,L).LE.7))
     +        WRITE(11,14) KAR(KIND(IM,L)),I,(XYZ(J,IM,L),J=1,3)
          IF (((I.GT.9).AND.(I.LE.99)).AND.(KIND(IM,L).LE.7))
     +        WRITE(11,15) KAR(KIND(IM,L)),I,(XYZ(J,IM,L),J=1,3)
          IF (((I.GT.99).AND.(I.LE.999)).AND.(KIND(IM,L).LE.7))
     +        WRITE(11,16) KAR(KIND(IM,L)),I,(XYZ(J,IM,L),J=1,3)
          IF ((I.GT.999).AND.(KIND(IM,L).LE.7))
     +        WRITE(11,25) KAR(KIND(IM,L)),I,(XYZ(J,IM,L),J=1,3)
          IF ((I.LE.9).AND.(KIND(IM,L).GT.7))
     +        WRITE(11,17) KAR(KIND(IM,L)),I,(XYZ(J,IM,L),J=1,3)
          IF (((I.GT.9).AND.(I.LE.99)).AND.(KIND(IM,L).GT.7))
     +        WRITE(11,18) KAR(KIND(IM,L)),I,(XYZ(J,IM,L),J=1,3)
          IF (((I.GT.99).AND.(I.LE.999)).AND.(KIND(IM,L).GT.7))
     +        WRITE(11,19) KAR(KIND(IM,L)),I,(XYZ(J,IM,L),J=1,3)
          IF ((I.GT.999).AND.(KIND(IM,L).GT.7))
     +        WRITE(11,26) KAR(KIND(IM,L)),I,(XYZ(J,IM,L),J=1,3)
350     CONTINUE
300   CONTINUE
250   CONTINUE
  1   FORMAT( /1X,'***** RESIDUE INTERNAL PARAMETERS **************' )
  2   FORMAT( 6X,'THETA',5X,' PHI ',9X,'THETA',5X,' PHI ')
  4   FORMAT( 1X,'*****  HELIX PARAMETERS; DEE,RHO,THT:',2X,
     +        3(1X,F9.5))
  5   FORMAT( /1X,'***** UNIT CELL PARAMETERS *********************' )
  6   FORMAT( 3X,' PRINCIPLE AXES;    A,B,C :',10X,3(1X,F9.5) )
  7   FORMAT( 3X,' PRINCIPLES ANGLES; ALPHA,BETA,GAMMA:',3(1X,F9.5) )
  8   FORMAT( 3X,' CHAIN NUMBER   TRANSL          ORIENT/ROTATION')
  9   FORMAT( 6X,I3,9X,F7.5,3X,F6.1,1X,F6.1,2X,F8.3)
 10   FORMAT( 1X,'*****  POTENTIAL ENERGIES  **********************' )
 11   FORMAT( 1X,'* INTRA: EDEF',4X,'EDEL',4X,'ECFF',4X,
```

```
     +          'ENOB1',3X,'ECOU1',3X,'EULJP',3X,'EUESP',3X,'EINTRA')
   27   FORMAT( 1X,8(1X,F7.3) )
   12   FORMAT( 1X,'* INTER: ENOB2',4X,'ECOU2',4X,'EULJ',5X,
     +          'EUES',5X,'EINTER',3X,'ETOT')
   28   FORMAT( 1X,6(1X,F8.3) )
   22   FORMAT( 1X,'* MINIMIZATION: NVAR = ',I3,2X,'GRADIENT NORM = ',
     +          F8.4)
   13   FORMAT( /1X,'***** XYZ COORDINATES, BY ATOM NUMBER **********' )
   14   FORMAT( A1,I1,5X,3F12.4 )
   15   FORMAT( A1,I2,4X,3F12.4 )
   16   FORMAT( A1,I3,3X,3F12.4 )
   17   FORMAT( A2,I1,4X,3F12.4 )
   18   FORMAT( A2,I2,3X,3F12.4 )
   19   FORMAT( A2,I3,2X,3F12.4 )
   25   FORMAT( A1,I4,3X,3F12.4 )
   26   FORMAT( A2,I4,2X,3F12.4 )
C   20   FORMAT( 5X,3(F8.3,2X),5X,3(F8.3,2X) )
   20   FORMAT( 5X,F8.3,2X,F8.3,6X,F8.3,2X,F8.3 )
   21   FORMAT( 4X,'RING ROTATION ANGLES: ',F8.3,2X,F8.3,4X,F8.3,2X,
     +          F8.3 )
   23   FORMAT( 4X,'RING SUBSTITUTION CODE: ',4I3 )
   24   FORMAT( 3X,' TEMP(K), DENS(G/CC), CELL SUM:',8X,2(F9.5,1X),I4)
   31   FORMAT( /1X,' ** IMPOSED STRAIN: CELL TYPE, CASE, STRAIN ',
     +          'TENSOR **' )
   32   FORMAT( 10X,I4,4X,I4 )
   33   FORMAT( 10X,3(F9.4,2X) )
   34   FORMAT( /1X,' ** STRAINED UNIT CELL VECTORS ** ')
 1002   FORMAT( 5E15.7 )
 1003   FORMAT( 2I4 )
        RETURN
        END


        SUBROUTINE RDSTRAIN( MODE )
C
C  Reads special file for unitcell definition and strain tensor
C
        PARAMETER( NKIND=9,NIBB=8,MNRU=6,MNCH=9,MNAT=179,NRNG=2,NSUB=4,
     +             MNSB=24,NDOF=10,MNIC=9,MCOP=45,MOPT=51 )
        COMMON /CHAINS/ PHI(NIBB),THETA(NIBB),BL(NIBB),PHIR(NRNG),
     +                  KSB(4),PCH(4,MNAT),NARU,NRUS,NCH,
     +                  A(4,4,MNAT),XYZ(4,MNAT,MNCH),KIND(MNAT,MNCH),
     +                  CHRG(MNAT,MNCH),KONEC(MNAT,MNAT),DEE,THT,RHO,
     +                  NUNIQ
        COMMON /CELL/ CELD(3),CELA(3),CHSPEC(5,MNCH),CHLOC(3,MNCH),
     +                  NUNIV,KONDENS,TEMP,DENSC
        COMMON /STRN/ KUC,KASE,ST(3,3),SUCV(3,3),DINIT,DPRIME,DCON
        COMMON /MINIM/ LMV(2,9),LCV(5,11),OMVARS(97)
        COMMON /OPRS/ NVAR,VARS(97),GRAD(97),GRADNM
        COMMON G(97),H(4753),W(291)
        COMMON /SV2/ TVARL
        NHELEM = NVAR*(NVAR+1)/2
        OPEN(UNIT=10,FILE='US.dt',STATUS='OLD')
        READ(10,*) KUC,KASE
        READ(10,*) DINIT,DCON
        READ(10,*) (ST(1,I),I=1,3)
        READ(10,*) (ST(2,I),I=1,3)
        READ(10,*) (ST(3,I),I=1,3)
        CLOSE(UNIT=10)
C
C  Read Existing Hessian, if it exists
C
        IF( MODE.EQ.1 ) GO TO 100
        OPEN(UNIT=10,FILE='HESS',STATUS='OLD')
        READ(10,1002) ( H(J),J=1,NHELEM )
 100    CLOSE( UNIT=10 )
C
C  If Hessian exists, read in corresponding geometry
C
        IF( MODE.EQ.1 ) GO TO 300
        OPEN(UNIT=10,FILE='GEOM',STATUS='OLD')
```

```
        READ(10,1002) (VARS(J),J=1,NVAR )
        CLOSE( UNIT=10 )
        TVARL = 1000.
        CALL LDVAR( NVAR,VARS,-1,KMOL)
 1002   FORMAT( 5E15.7 )
 1003   FORMAT( 2I4 )
 300    CONTINUE
        RETURN
        END


      SUBROUTINE ATRNS( PHI,THETA,BL,A )
C
C  "A" Matrix Generation
C  "T"-Matrix as per Flory, STAT. MECH. OF CHAIN MOLECULES, p.21
C
C       |  T   L  |             | BL|
C   A = |         |         L = | 0 |
C       |  0   1  |             | 0 |
C
      DIMENSION A(4,4)
      COMPL(X) = (180.-X)*3.1415926535/180.
C
      TH = COMPL(THETA)
      PH = PHI*3.1415926535/180.
      CT = COS(TH)
      ST = SIN(TH)
      CP = COS(PH)
      SP = SIN(PH)
      A(1,1) = CT
      A(1,2) = ST
      A(1,3) = 0.
      A(1,4) = BL
      A(2,1) = ST*CP
      A(2,2) = -CT*CP
      A(2,3) = SP
      A(2,4) = 0.
      A(3,1) = ST*SP
      A(3,2) = -CT*SP
      A(3,3) = -CP
      A(3,4) = 0.
      A(4,1) = 0.
      A(4,2) = 0.
      A(4,3) = 0.
      A(4,4) = 1.
      RETURN
      END


      SUBROUTINE MV( A,NFORMA,NA,V,N,R )
C
C      - Multiplies matrix with vector: R = A * V
C      - Input : A       NA x N Matrix
C              NFORMA    First dimension of A in calling program
C              NA        Number of rows in A
C              V         Vector of length N
C              N         Length of vector V
C      - Output: R       Resultant vector of length NA, can be V
C
      DIMENSION A(NFORMA,NFORMA), V(N), R(NA), RR(20)
      IF (NA.GT.NFORMA) RETURN
      DO 100 I=1,NA
        X = 0.
        DO 200 K=1,N
  200     X = X + A(I,K)*V(K)
  100   RR(I) = X
      DO 300 I=1,NA
  300   R(I) = RR(I)
      RETURN
      END
```

```
      SUBROUTINE VV( A,B,C,N )
C
C  Calculates the vector cross product C = A X B, where A,B, and C
C  have length N
C
      DIMENSION A(N),B(N),C(N),K(2)
      DO 100 I=1,N
        DO 200 J=1,2
  200     K(J) = MOD( (I+J-1),N ) +1
          C(I) = A(K(1))*B(K(2)) - A(K(2))*B(K(1))
  100 CONTINUE
      RETURN
      END


      SUBROUTINE MM( A,B,C,NFORMA,NFORMB,NFORMC,NA,MA,MB )
C
C      - Multiplies matrix with matrix: C = A X B
C                                (C can be A or B)
C
      DIMENSION CC(20,20),A(NFORMA,NFORMA),B(NFORMB,NFORMB)
      DIMENSION C(NFORMC,NFORMC)
      DO 100 I=1,NA
        DO 100 J=1,MB
          X = 0.
          DO 200 K=1,MA
  200       X = X + A(I,K)*B(K,J)
  100     CC(I,J) = X
      DO 300 I=1,NA
        DO 300 J=1,MB
  300     C(I,J) = CC(I,J)
      RETURN
      END


      SUBROUTINE MT( A,B,N,NP )
C
C  Calculates the transpose of the N x N matrix A contained within
C  the physical array NP x NP, and returns as the matrix B
C
      DIMENSION A(NP,NP),B(NP,NP)
      DO 100 I=1,NP
        DO 100 J=1,NP
  100     B(I,J) = A(I,J)
      DO 200 I=1,N
        DO 200 J=1,I
          B(J,I) = A(I,J)
  200     B(I,J) = A(J,I)
      RETURN
      END


      SUBROUTINE MA( A,B,C,N,NP,S )
C
C  If S = 1 : Adds matrices A and B to form C
C  If S =-1 : Subtracts matrix B from A to form C
C  All matrices are N x N, contained within arrays having physical
C  dimensions NP x NP
C
      DIMENSION A(NP,NP),B(NP,NP),C(NP,NP)
      DO 100 I=1,N
        DO 100 J=1,N
  100     C(I,J) = A(I,J) + S*B(I,J)
      RETURN
      END
```

```
      SUBROUTINE VECTORIZ( SLEN,SANG,VECT,KERR )
C
C  Converts scalar data (lengths, angles) to three placement vectors
C  Convention:  SLEN(3) lies along Z axis
C               SLEN(1) lies within X-Z plane
C               SLEN(2) placement determined by above
C               SANG(i) is the angle between SLEN(j) and SLEN(k), etc.
C  KERR normally equals 0; KERR = 1 if the set of input angles do not
C  make a viable set
C
        DIMENSION SLEN(3),SANG(3),VECT(3,3),ARA(3,3),ARB(3,3)
        COMPL(X) = (90.-X)*3.1415926535/180.
        EPSILON = 1E-6
        DEGRAD = 3.1415926535/180.
        KERR = 0
        DO 100 I=1,3
        DO 100 J=1,3
          ARA(I,J) = 0.
          ARB(I,J) = 0.
  100     VECT(I,J) = 0.
        VECT(1,1) = SLEN(1)
        VECT(1,2) = SLEN(2)
        VECT(3,3) = SLEN(3)
        COSGP = ( COS(SANG(3)*DEGRAD)-COS(SANG(1)*DEGRAD)*COS(SANG(2)
     +          *DEGRAD) )/( SIN(SANG(1)*DEGRAD)*SIN(SANG(2)*DEGRAD) )
       IF((ABS(COSGP)-1.).GT.EPSILON) GO TO 900
       IF(ABS(ABS(COSGP)-1.).LE.EPSILON) COSGP = SIGN(1.,COSGP)
         GP = ACOS(COSGP)
         CA = COMPL(SANG(1))
         CB = COMPL(SANG(2))
         ARA(1,1) = COS(CB)
         ARA(1,3) = -SIN(CB)
         ARA(2,2) = 1.
         ARA(3,1) = SIN(CB)
         ARA(3,3) = COS(CB)
         ARB(1,1) = COSGP*COS(CA)
         ARB(1,2) = -SIN(GP)
         ARB(1,3) = -COSGP*SIN(CA)
         ARB(2,1) = SIN(GP)*COS(CA)
         ARB(2,2) = COSGP
         ARB(2,3) = -SIN(GP)*SIN(CA)
         ARB(3,1) = SIN(CA)
         ARB(3,3) = COS(CA)
         CALL MV( ARA,3,3,VECT(1,1),3,VECT(1,1) )
         CALL MV( ARB,3,3,VECT(1,2),3,VECT(1,2) )
       RETURN
  900  CONTINUE
       KERR = 1
       RETURN
       END


        SUBROUTINE ELJ(NKIND,NUC1,NUC2,VDWR,ALPHA,EFFNE,R2,S2,FIRST,
     +                 POTENT)
C
C  Calculates the 6-12 attraction/repulsion potential between two nuclei
C  separated by the distance R (R2 = R**2)
C  A shifted 3-segment-potential is used:
C  - For R .LE. RCRIT-H/2  :  6-12 potential with R, shifted
C  - For R .GE. RCRIT+H/2  :  0.
C  - For RCRIT-H/2 < R < RCRIT+H/2  : A spline-like cubic polynomial
C                           between these two potentials
C  (NKIND must not exceed MAXA)
C
       LOGICAL FIRST
       PARAMETER( MAXA=9,EPSILON=1E-6 )
       DIMENSION VDWR(NKIND),ALPHA(NKIND),EFFNE(NKIND)
       COMMON /SV1/ A(MAXA,MAXA),C(MAXA,MAXA),EMLH(MAXA,MAXA),
     +              YLH(MAXA,MAXA),YRH(MAXA,MAXA),FSTRL(MAXA,MAXA),
     +              RR,RL,RR2,RL2
C
```

```
C  Note: spline portion not in use...
C
C  Modified to pass two distances, R2 and S2. If R2=S2=distance**2, the
C  routine operates normally, and splining is possible; otherwise, R2
C  represents the inverse 6th order distance sum and S2 represents the
C  inverse 12th order distance sum, as supplied by infinite lattice sum
C  calculations.
C
      DATA RCRIT,H/ .1,1. /
      IF (FIRST) GO TO 500
  100 POTENT = 0.
      IF (ABS(R2/S2-1.).GE.EPSILON) GO TO 300
      IF (R2.GE.RR2) RETURN
      IF (R2.LE.RL2) GO TO 200
      R = SQRT( R2 )
      D1 = RR - R
      D2 = R - RL
      POTENT = EMLH(NUC1,NUC2)*D2*(D1**2)
     +         + YLH(NUC1,NUC2)*(D1**2)*(2.*D2+H)
     +         + YRH(NUC1,NUC2)*(D2**2)*(2.*D1+H) - FSTRL(NUC1,NUC2)
      RETURN
  200 D1 = R2**3
      D2 = D1**2
      POTENT = A(NUC1,NUC2)/D2 - C(NUC1,NUC2)/D1 - FSTRL(NUC1,NUC2)
      RETURN
  300 POTENT = A(NUC1,NUC2)*S2 - C(NUC1,NUC2)*R2
      RETURN
C
C  Initialize potential parameters on first pass
C
  500 CONTINUE
      IF (RCRIT.LT.1.) RCRIT = 500.
      IF (H.LT.0.1) H=0.1
C
C  Calculate A(I,J) and C(I,J):
C
      DO 600 I=1,NKIND
        DO 600 J=1,NKIND
          IF( ((ALPHA(I)-0.).LT.EPSILON).AND.
     +        ((ALPHA(J)-0.).LT.EPSILON) ) THEN
            C(I,J) = 0.
          ELSE
            C(I,J) = 365.*ALPHA(I)*ALPHA(J)/
     +                 (SQRT(ALPHA(I)/EFFNE(I))+SQRT(ALPHA(J)/EFFNE(J)))
          END IF
          A(I,J) = 0.5*C(I,J)*(VDWR(I)+VDWR(J))**6
  600 CONTINUE
C
C  Calculate polynomial parameters:
C
      RL = RCRIT - H/2.
      RR = RCRIT + H/2.
      RL2 = RL**2
      RR2 = RR**2
      RC2 = RCRIT**2
      R6 = RL**6
      R12 = R6**2
      R7 = R6*RL
      R13 = R12*RL
      RC6 = RC2**3
      RC12 = RC6**2
      DO 700 I=1,NKIND
        DO 700 J=1,NKIND
          FSTRL(I,J) = A(I,J)/RC12 - C(I,J)/RC6
          EMLH(I,J) = (-12.*A(I,J)/R13 + 6.*C(I,J)/R7)/(H**2)
          YLH(I,J) = (A(I,J)/R12 - C(I,J)/R6)/(H**3)
          YRH(I,J) = FSTRL(I,J)/(H**3)
  700 CONTINUE
      FIRST = .FALSE.
      GO TO 100
      END
```

```
      SUBROUTINE EES( BWD,DIST,EBULK,AC1,AC2,EEL )
C
C  Calculates Coulombic interaction between two charge centers using
C  a distance-dependent dielectric constant:
C     DIST < Critical Dist (BWD)       : EPS = 1
C     SVDW < DIST < (1+FACT)*BWD       : EPS = Quintic spline
C     DIST > (1+FACT)*BWD              : EPS = Block-Walker Approx.
C
      DATA FACT/ 0.1 /
C
        P12 = BWD*LOG(EBULK)
        RC = BWD + (FACT * BWD)
C
        IF (DIST.LE.BWD) THEN
           EPS=1.
        ELSEIF ((DIST.GT.BWD) .AND. (DIST.LT.RC)) THEN
           DELTA = BWD*FACT
           S = EBULK*EXP(-P12/RC)
           SP = (EBULK*P12/RC**2)*EXP(-P12/RC)
           SDP = ((P12/RC)-2.)*(EBULK*P12/(RC**3))*EXP(-P12/RC)
           D=(10.*(S-1.)/(DELTA**3))-(4*SP/(DELTA**2))+(0.5*SDP/DELTA)
           E=(-15.*(S-1.)/(DELTA**4))+(7.*SP/(DELTA**3))-(SDP/DELTA**2)
           F=(6.*(S-1.)/(DELTA**5))-(3.*SP/(DELTA**4))+(.5*SDP/DELTA**3)
           ETA = DIST - BWD
           EPS = 1.+D*ETA**3+E*ETA**4+F*ETA**5
        ELSE
           EPS = EBULK*EXP(-P12/DIST)
        ENDIF
C
        EEL = 332.*AC1*AC2/EPS/DIST
        RETURN
        END



      SUBROUTINE JACOBI(A,N,NP,D,V,NROT)
C
C  Jacobi Transformation of a symmetric matrix A, having dimensions
C  N x N, stored in an array NP x NP.  On output, upper elements of
C  A are destroyed.  D contains the eigenvalues and V contains the
C  normalized eigenvectors
C  From: Press et.al., NUMERICAL RECIPES, p346.
C
      PARAMETER (NMAX=100,EPSILON=2E-7)
      DIMENSION A(NP,NP),D(NP),V(NP,NP),B(NMAX),Z(NMAX)
      DO 12 IP=1,N
        DO 11 IQ=1,N
          V(IP,IQ)=0.
11      CONTINUE
        V(IP,IP)=1.
12    CONTINUE
      DO 13 IP=1,N
        B(IP)=A(IP,IP)
        D(IP)=B(IP)
        Z(IP)=0.
13    CONTINUE
      NROT=0
      DO 24 I=1,50
        SM=0.
        DO 15 IP=1,N-1
          DO 14 IQ=IP+1,N
            SM=SM+ABS(A(IP,IQ))
14        CONTINUE
15      CONTINUE
C *** Modified for PC where underflow is not set to zero : GCR 10/87 ***
C       IF(SM.EQ.0.)RETURN
      IF(SM.LT.EPSILON) RETURN
C *********************************************************************
        IF(I.LT.4)THEN
```

```
        TRESH=0.2*SM/N**2
      ELSE
        TRESH=0.
      ENDIF
      DO 22 IP=1,N-1
        DO 21 IQ=IP+1,N
          G=100.*ABS(A(IP,IQ))
          IF((I.GT.4).AND.(ABS(D(IP))+G.EQ.ABS(D(IP)))
     *       .AND.(ABS(D(IQ))+G.EQ.ABS(D(IQ))))THEN
            A(IP,IQ)=0.
          ELSE IF(ABS(A(IP,IQ)).GT.TRESH)THEN
            H=D(IQ)-D(IP)
            IF(ABS(H)+G.EQ.ABS(H))THEN
              T=A(IP,IQ)/H
            ELSE
              THETA=0.5*H/A(IP,IQ)
              T=1./(ABS(THETA)+SQRT(1.+THETA**2))
              IF(THETA.LT.0.)T=-T
            ENDIF
            C=1./SQRT(1+T**2)
            S=T*C
            TAU=S/(1.+C)
            H=T*A(IP,IQ)
            Z(IP)=Z(IP)-H
            Z(IQ)=Z(IQ)+H
            D(IP)=D(IP)-H
            D(IQ)=D(IQ)+H
            A(IP,IQ)=0.
            DO 16 J=1,IP-1
              G=A(J,IP)
              H=A(J,IQ)
              A(J,IP)=G-S*(H+G*TAU)
              A(J,IQ)=H+S*(G-H*TAU)
16          CONTINUE
            DO 17 J=IP+1,IQ-1
              G=A(IP,J)
              H=A(J,IQ)
              A(IP,J)=G-S*(H+G*TAU)
              A(J,IQ)=H+S*(G-H*TAU)
17          CONTINUE
            DO 18 J=IQ+1,N
              G=A(IP,J)
              H=A(IQ,J)
              A(IP,J)=G-S*(H+G*TAU)
              A(IQ,J)=H+S*(G-H*TAU)
18          CONTINUE
            DO 19 J=1,N
              G=V(J,IP)
              H=V(J,IQ)
              V(J,IP)=G-S*(H+G*TAU)
              V(J,IQ)=H+S*(G-H*TAU)
19          CONTINUE
            NROT=NROT+1
          ENDIF
21      CONTINUE
22    CONTINUE
      DO 23 IP=1,N
        B(IP)=B(IP)+Z(IP)
        D(IP)=B(IP)
        Z(IP)=0.
23    CONTINUE
24  CONTINUE
    PAUSE '50 iterations should never happen'
    RETURN
    END
```

```
      REAL FUNCTION CURTATE( X,AP,CP )
C
C  Returns the Y value of X of a curtate function described by
C  AP (magnitude) and CP (curvature), X in degrees.
C
      EPS = 1.0E-6
      IMAX = 5000
      DEGRAD = 3.1415926535/180.
C  Find T by iteration:
      XRAD = X*DEGRAD
      T = XRAD
      DO 100 I=1,IMAX
      TINC = 2.*XRAD - T + CP*SIN(T)
      IF( ABS(TINC).LE.EPS ) GO TO 200
  100 T = T+TINC
  200 CONTINUE
      IF( I.GE.IMAX ) WRITE(*,*) 'WARNING: Iteration Limit in Curtate:
     +  TINC = ',TINC
C  Calculate curtate function value:
      CURTATE = (AP/2.)*(1.-COS(T))
      RETURN
      END


      REAL FUNCTION CURTINV( X,AP,CP )
C
C  Returns the Y value of X of an inverted curtate function described
C  by AP (magnitude) and CP (curvature), X in degrees.
C
      EPS = 1.E-6
      IMAX = 5000
      PI = 3.1415926535
      DEGRAD = PI/180.
C  Find T by iteration:
      XRAD = X*DEGRAD
      T = XRAD - PI
      DO 100 I=1,IMAX
      TINC = 2.*XRAD - T + CP*SIN( T ) +PI
      IF(ABS(TINC).LE.EPS) GO TO 200
  100 T = T+TINC
  200 CONTINUE
      IF( I.GE.IMAX ) WRITE(*,*) 'WARNING: Iteration Limit in InvCurt:
     +  TINC = ',TINC
C  Calculate inverted curtate function value:
      CURTINV = (AP/2.)*(1.+COS(T))
      RETURN
      END


      SUBROUTINE MULMAX( MNCH,NCH,NCH2,L1MAX,FMULT )
C
C  For a regular lattice packing geometry having chains of identical
C  placement parameters, intermolecular potential calculations may be
C  expedited by recognition of multiplicative interactions.  For a
C  lattice consisting of only two chain types (designated by odd or even
C  numbering) in an counterclockwise alternating protocol, this routine
C  generates the multiplicity matrix FMULT by which unique energetic
C  interactions must be multiplied to determine relative probabilities
C  of occurance.
C
C  The use of the intermolecular multiplier matrix assumes
C  periodicity within the lattice of the form:
C
C       Two types of chains: all even numbered chains alike
C                            all odd numbered chains alike
C       Chain 1 forms lattice center; chains 2 - 9 form first shell
C       about the center, proceeding counterclockwise from a position
C       "east" of chain 1; chains 10 - 25 form second shell about
C       center, proceeding ccw form a position "east" of chain 9, etc.
C       For a given lattice size (eg. 3x3, 4x4, 5x5) all edge-to-edge
C       intermolecular interactions are ignored (ie. in the 3x3
```

```
C       lattice, interactions between chains separated by a third chain
C       are ignored, in the 4x4 lattice, those separated by two chains
C       are ignored, etc.)
C
C  NOTE:  The Lattice Sum Method does not require an interaction
C       multiplicity correction; however, it does recognize repetitive
C       interactions within the "explicit cell" in order to minimize
C       computation time.  Statements which only serve to correct the
C       (non-zero) MAGNITUDE of the multiplicity correction have been
C       disabled and marked by an asterix
C
C  (NCH must not exceed MAXC, MAXC2 = MAXC**2)
C
      PARAMETER( MAXC=25,MAXC2=625 )
      DIMENSION FMULT(MNCH,MNCH),LOC(2,MAXC),IA(5,MAXC2),FA(MAXC2)
      DO 100 I=1,NCH
        DO 100 J=1,NCH
 100      FMULT(I,J) = 0
      DO 120 I=1,NCH**2
        FA(I) = 0.
        DO 120 J=1,5
  120     IA(J,I) = 0
      NCPS = INT(SQRT(REAL(NCH))+.1)
C***      RUPC = REAL((NCPS-1)**2)
C
C  Build a test array to locate chains:
C
      DO 150 I=1,4
        DO 150 J=1,2
  150     LOC(I,J) = 0
      LOC(1,2) = 1
      LOC(1,3) = 1
      LOC(2,3) = 1
      LOC(2,4) = 1
      IF(NCH.GT.4) THEN
        ITRAN = INT( (REAL(NCPS)+0.1)/2 )
        JTRAN = 1
        JTRK = -1
        KTRK =  1
        DO 200 NTRK=5,NCH
          DO 250 I=1,3
  250       LOC(I,NTRK) = JTRK*LOC(I,2) + KTRK*LOC(I,4)
          IF(NTRK.GE.((2*JTRAN+1)**2)) JTRAN = JTRAN+1
          IF(      ( JTRAN.EQ.JTRK).AND.( JTRAN.NE.KTRK)) THEN
            KTRK = KTRK+1
          ELSE IF((-JTRAN.NE.JTRK).AND.( JTRAN.EQ.KTRK)) THEN
            JTRK = JTRK-1
          ELSE IF((-JTRAN.EQ.JTRK).AND.(-JTRAN.NE.KTRK)) THEN
            KTRK = KTRK-1
          ELSE IF(( JTRAN.NE.JTRK).AND.(-JTRAN.EQ.KTRK)) THEN
            JTRK = JTRK+1
          ELSE
            JTRK = JTRK+1
          END IF
  200   CONTINUE
      ELSE
      END IF
C
C  Loop through all interactions to determine multiplicities of all
C  unique interactions:
C
      NINT = 1
      IA(1,1) = 1
      IA(2,1) = 0
      IA(3,1) = 0
      IA(4,1) = 1
      IA(5,1) = 2
      FA(1) = 1.
      IF( NCH.EQ.4 ) FA(1) = .5
      DO 300 I=1,NCH-1
        IP1 = I+1
```

```
       DO 300 J=IP1,NCH
         IF((I.EQ.1).AND.(J.EQ.2)) GO TO 450
C
C  Determine orientation of present interaction:
C
         NXS = LOC(1,J) - LOC(1,I)
         NYS = LOC(2,J) - LOC(2,I)
         IF( ABS(NXS).LT.ABS(NYS) ) THEN
           NDS = NXS
           NYS = SIGN( (ABS(NYS)-ABS(NXS)),NYS )
           NXS = 0
         ELSE IF( ABS(NXS).GT.ABS(NYS) ) THEN
           NDS = NYS
           NXS = SIGN( (ABS(NXS)-ABS(NYS)),NXS )
           NYS = 0
         ELSE
           NDS = SIGN( NXS,(NXS*NYS) )
           NXS = 0
           NYS = 0
         END IF
C
C  Discard if too distant (ie. edge-to-edge)
C
         IF( NCH.EQ.4 ) GO TO 470
         ND = ABS(NXS) + ABS(NYS) + ABS(NDS)
         IF( ND.GT.(NCPS-2) ) GO TO 450
  470    CONTINUE
C****
C**Determine scale factor (1 if interior, 1/2 if along border of finite
C**cube):
C**
C**     IF( (I.GT.((NCPS-2)**2)).AND.((J-I).LT.NCPS).AND.
C**    +     (NDS.EQ.0) ) THEN
C**           SCALE = .5
C**            ELSE
C**              SCALE = 1.
C**            END IF
C**            IF( (J.EQ.NCH).AND.(NDS.EQ.0) ) SCALE = .5
C****
C  Compare to previous interactions for multiplicity:
C
         DO 400 K=1,NINT
           IF(MOD((I+IA(4,K))/2.,1.).EQ.0.) THEN
             IF((NXS.EQ.IA(1,K)).AND.(NYS.EQ.IA(2,K)).AND.
     +          (NDS.EQ.IA(3,K))) THEN
                FA(K) = FA(K)+SCALE
                GO TO 450
             ELSE
             END IF
           ELSE
           END IF
           IF(MOD((I+IA(5,K))/2.,1.).EQ.0.) THEN
           IF((-NXS.EQ.IA(1,K)).AND.(-NYS.EQ.IA(2,K)).AND.
     +        (-NDS.EQ.IA(3,K)).AND.((NXS.NE.0).OR.(NYS.NE.0))) THEN
             FA(K) = FA(K)+SCALE
             GO TO 450
           ELSE
           END IF
           ELSE
           END IF
  400    CONTINUE
         NINT = NINT+1
         IA(1,NINT) = NXS
         IA(2,NINT) = NYS
         IA(3,NINT) = NDS
         IA(4,NINT) = I
         IA(5,NINT) = J
         FA(NINT) = SCALE
  450    CONTINUE
  300  CONTINUE
C
```

```
C  Load Multiplier matrix:
C
      L1MAX = 1
      DO 500 I=1,NINT
        L1 = IA(4,I)
        L2 = IA(5,I)
        L1MAX = MAX(L1MAX,L1)
  500   FMULT(L1,L2) = FA(I)
C**500   FMULT(L1,L2) = FA(I)/RUPC
      RETURN
      END


      SUBROUTINE VA10A(FUNCT,N,X,F,G,H,W,DFN,XM,HH,EPS,MODE,MAXFN,
     1                 IPRINT,IEXIT)
C  HARWELL - LIBRARY ROUTINE VA10A: OPTIMIZATION WITHOUT DERIVATIVES
C  USING A FLETCHER-POWELL ALGORITHM. ROUTINES REQUIRED: MC11A.
C
C  ARRAY-DIMENSIONS IN THE CALLING ROUTINE:
C  X, XM      : LENGTH N
C  G, H, W    : LENGTH N*(N+1)/2 OR 3*N, WHICHEVER IS LARGER
C
C  CALLING PROCEDURES HAVE BEEN CHANGED FROM THE ORIGINAL ICL-FORTRAN
C  EXTERNAL DECLARATON ADDED FOR PORTABILILTY    GCR 19.4.89
C
      REAL X(1),G(1),H(1),W(1),XM(1)
      EXTERNAL FUNCT
      IF(IPRINT.NE.0)PRINT 1000
 1000 FORMAT('1ENTRY TO VA10A'/)
      NN=N*(N+1)/2
      IG=N
      IGG=N+N
      IS=IGG
      IDIFF=1
      IEXIT=0
      IR=N
      IF(MODE.EQ.3)GOTO15
      IF(MODE.EQ.2)GOTO10
      IJ=NN+1
      DO 5 I=1,N
      DO 6 J=1,I
      IJ=IJ-1
    6 H(IJ)=0.
    5 H(IJ)=1.
      GOTO15
   10 CONTINUE
      CALL MC11B(H,N,G,DUMMY,G,IR,IDUMMY,DUMMY)
      IF(IR.LT.N) RETURN
   15 CONTINUE
      Z=F
      ITN=0
C  ======================================================================
      CALL FUNCT(N,X,F)
C  ======================================================================
      IFN=1
      DF=DFN
      IF(DFN.EQ.0.)DF=F-Z
      IF(DFN.LT.0.)DF=ABS(DF*F)
      IF(DF.LE.0.)DF=1.
   17 CONTINUE
      LINK=1
      IF(IDIFF-1)100,100,110
   18 CONTINUE
      IF(IFN.GE.MAXFN)GOTO90
   20 CONTINUE
      IF(IPRINT.EQ.0)GOTO21
      IF(MOD(ITN,IPRINT).NE.0)GOTO21
      PRINT 1001,ITN,IFN
 1001 FORMAT(24I5)
      PRINT 1002,F
 1002 FORMAT((5E15.7))
```

```
      IF(IPRINT.LT.0)GOTO21
      PRINT 1002,(X(I),I=1,N)
      PRINT 1002,(W(IG+I),I=1,N)
C ******* Statements inserted by GCR to save updates of Hessian *******
      NHELM = NN
      IF(N.LT.5) NHELM = 3*N
      OPEN(UNIT=12,FILE='GEOM')
      WRITE(12,1002) (X(I),I=1,N)
      CLOSE(UNIT=12)
      OPEN(UNIT=12,FILE='HESS')
      WRITE(12,1002) (H(J),J=1,NHELM)
      CLOSE(UNIT=12)
C  *********************************************************************
   21 CONTINUE
      ITN=ITN+1
      DO 22 I=1,N
   22 W(I)=-W(IG+I)
      CALL MC11E(H,N,W,DUMMY,G,IR,IDUMMY,DUMMY)
      Z=0.
      GS0=0.
      DO 29 I=1,N
      W(IS+I)=W(I)
      IF(Z*XM(I).GE.ABS(W(I)))GOTO29
      Z=ABS(W(I))/XM(I)
   29 GS0=GS0+W(IG+I)*W(I)
      AEPS=EPS/Z
      IEXIT=2
      IF(GS0.GE.0.)GOTO92
      ALPHA=-2.*DF/GS0
      IF(ALPHA.GT.1.)ALPHA=1.
      FF=F
      TOT=0.
      INT=0
      IEXIT=1
   30 CONTINUE
      IF(IFN.GE.MAXFN)GOTO90
      DO 31 I=1,N
   31 W(I)=X(I)+ALPHA*W(IS+I)
C  ====================================================================
      CALL FUNCT(N,W,F1)
C  ====================================================================
      IFN=IFN+1
      IF(F1.GE.F)GOTO40
      F2=F
      TOT=TOT+ALPHA
   32 CONTINUE
      DO 33 I=1,N
   33 X(I)=W(I)
      F=F1
      IF(INT-1)35,49,50
   35 CONTINUE
      IF(IFN.GE.MAXFN)GOTO90
      DO 34 I=1,N
   34 W(I)=X(I)+ALPHA*W(IS+I)
C  ====================================================================
      CALL FUNCT(N,W,F1)
C  ====================================================================
      IFN=IFN+1
      IF(F1.GE.F)GOTO50
      IF(F1+F2.GE.F+F.AND.7.*F1+5.*F2.GT.12.*F)INT=2
      TOT=TOT+ALPHA
      ALPHA=2.*ALPHA
      GOTO32
   40 CONTINUE
      IF(ALPHA.LT.AEPS)GOTO92
      IF(IFN.GE.MAXFN)GOTO90
      ALPHA=.5*ALPHA
      DO 41 I=1,N
   41 W(I)=X(I)+ALPHA*W(IS+I)
C  ====================================================================
      CALL FUNCT(N,W,F2)
```

```
C  ================================================================
      IFN=IFN+1
      IF(F2.GE.F)GOTO45
      TOT=TOT+ALPHA
      F=F2
      DO 42 I=1,N
   42 X(I)=W(I)
      GOTO49
   45 CONTINUE
      Z=.1
      IF(F1+F.GT.F2+F2)Z=1.+.5*(F-F1)/(F+F1-F2-F2)
      IF(Z.LT..1)Z=.1
      ALPHA=Z*ALPHA
      INT=1
      GOTO30
   49 CONTINUE
      IF(TOT.LT.AEPS)GOTO92
   50 CONTINUE
      ALPHA=TOT
      DO 56 I=1,N
   56 W(I)=W(IG+I)
      LINK=2
      IF(IDIFF-1)100,100,110
   54 CONTINUE
      IF(IFN.GE.MAXFN)GOTO90
      GYS=0.
      DO 55 I=1,N
      GYS=GYS+W(IG+I)*W(IS+I)
   55 W(IGG+I)=W(I)
      DF=FF-F
      DGS=GYS-GS0
      IF(DGS.LE.0.)GOTO20
      IF(DGS+ALPHA*GS0.GT.0.)GOTO70
C   COMPLEMENTARY DFP FORMULA
      SIG=1./GS0
      IR=-IR
      CALL MC11A(H,N,W,SIG,G,IR,1,0.)
      DO 60 I=1,N
   60 G(I)=W(IG+I)-W(IGG+I)
      SIG=1./(ALPHA*DGS)
      IR=-IR
      CALL MC11A(H,N,G,SIG,W,IR,0,0.)
      GOTO20
   70 CONTINUE
C    DFP FORMULA
      ZZ=ALPHA/(DGS-ALPHA*GS0)
      SIG=-ZZ
      CALL MC11A(H,N,W,SIG,G,IR,1,1E-7)
      Z=DGS*ZZ-1.
      DO 71 I=1,N
   71 G(I)=W(IG+I)+Z*W(IGG+I)
      SIG=1./(ZZ*DGS**2)
      CALL MC11A(H,N,G,SIG,W,IR,0,0.)
      GOTO20
   90 CONTINUE
      IEXIT=3
      GOTO94
   92 CONTINUE
      IF(IDIFF.EQ.2)GOTO94
      IDIFF=2
      GOTO17
   94 CONTINUE
      DO 95 I=1,N
   95 G(I)=W(IG+I)
C  ***************** ATTENTION, NEXT STATEMENT INSERTED BY UWS *********
      MAXFN=IFN
C  ****************TO PASS NUMBER OF FUNCTION CALLS BACK TO CALLER*******
      IF(IPRINT.EQ.0) RETURN
      PRINT 1001,ITN,IFN,IEXIT
      PRINT 1002,F
      PRINT 1002,(X(I),I=1,N)
```

```
      PRINT 1002,(G(I),I=1,N)
C  ******* Statements inserted by GCR to save updates of Hessian *******
      NHELM = NN
      IF(N.LT.5) NHELM = 3*N
      OPEN(UNIT=12,FILE='GEOM')
      WRITE(12,1002) (X(I),I=1,N)
      CLOSE(UNIT=12)
      OPEN(UNIT=12,FILE='HESS')
      WRITE(12,1002) (H(J),J=1,NHELM)
      CLOSE(UNIT=12)
C  **********************************************************************
      RETURN
  100 CONTINUE
      DO 101 I=1,N
      Z=HH*XM(I)
      ZZ=X(I)
      X(I)=ZZ+Z
C  ======================================================================
      CALL FUNCT(N,X,F1)
C  ======================================================================
      W(IG+I)=(F1-F)/Z
  101 X(I)=ZZ
      IFN=IFN+N
      GOTO(18,54),LINK
  110 CONTINUE
      DO 111 I=1,N
      Z=HH*XM(I)
      ZZ=X(I)
      X(I)=ZZ+Z
C  ======================================================================
      CALL FUNCT(N,X,F1)
C  ======================================================================
      X(I)=ZZ-Z
C  ======================================================================
      CALL FUNCT(N,X,F2)
C  ======================================================================
      W(IG+I)=(F1-F2)/(2.*Z)
  111 X(I)=ZZ
      IFN=IFN+N+N
      GOTO(18,54),LINK
      RETURN
      END


      SUBROUTINE MC11A(A,N,Z,SIG,W,IR,MK,EPS)
C  ***********ENTRY STATEMENTS CHANGED FROM ORIGINAL ICL FORTRAN**UWS***
      DIMENSION A(1),Z(1),W(1)
C   UPDATE FACTORS GIVEN IN A BY   SIG*Z*ZTRANSPOSE
      IF(N.GT.1)GOTO1
      A(1)=A(1)+SIG *Z(1)**2
      IR=1
      IF(A(1).GT.0.)RETURN
      A(1)=0.
      IR=0
      RETURN
    1 CONTINUE
      NP=N+1
      IF(SIG.GT.0.)GOTO40
      IF(SIG.EQ.0..OR.IR.EQ.0)RETURN
      TI=1./SIG
      IJ=1
      IF(MK.EQ.0)GOTO10
      DO 7 I=1,N
      IF(A(IJ).NE.0.)TI=TI+W(I)**2/A(IJ)
    7 IJ=IJ+NP-I
      GOTO20
   10 CONTINUE
      DO 11 I=1,N
   11 W(I)=Z(I)
      DO 15 I=1,N
      IP=I+1
```

```
      V=W(I)
      IF(A(IJ).GT.0.)GOTO12
      W(I)=0.
      IJ=IJ+NP-I
      GOTO15
   12 CONTINUE
      TI=TI+V**2/A(IJ)
      IF(I.EQ.N)GOTO14
      DO 13 J=IP,N
      IJ=IJ+1
   13 W(J)=W(J)-V*A(IJ)
   14 IJ=IJ+1
   15 CONTINUE
   20 CONTINUE
      IF(IR.LE.0 )GOTO21
      IF(TI.GT.0.)GOTO22
      IF(MK-1)40,40,23
   21 TI=0.
      IR=-IR-1
      GOTO23
   22 TI=EPS/SIG
      IF(EPS.EQ.0.)IR=IR-1
   23 CONTINUE
      MM=1
      TIM=TI
      DO 30 I=1,N
      J=NP-I
      IJ=IJ-I
      IF(A(IJ).NE.0.)TIM=TI-W(J)**2/A(IJ)
      W(J)=TI
   30 TI=TIM
      GOTO41
   40 CONTINUE
      MM=0
      TIM=1./SIG
   41 CONTINUE
      IJ=1
      DO 66 I=1,N
      IP=I+1
      V=Z(I)
      IF(A(IJ).GT.0.)GOTO53
      IF(IR.GT.0 .OR.SIG.LT.0..OR.V.EQ.0.)GOTO52
      IR=1-IR
      A(IJ)=V**2/TIM
      IF(I.EQ.N)RETURN
      DO 51 J=IP,N
      IJ=IJ+1
   51 A(IJ)=Z(J)/V
      RETURN
   52 CONTINUE
      TI=TIM
      IJ=IJ+NP-I
      GOTO66
   53 CONTINUE
      AL=V/A(IJ)
      IF(MM)54,54,55
   54 TI=TIM+V*AL
      GOTO56
   55 TI=W(I)
   56 CONTINUE
      R=TI/TIM
      A(IJ)=A(IJ)*R
      IF(R.EQ.0.)GOTO70
      IF(I.EQ.N)GOTO70
      B=AL/TI
      IF(R.GT.4.)GOTO62
      DO 61 J=IP,N
      IJ=IJ+1
      Z(J)=Z(J)-V*A(IJ)
   61 A(IJ)=A(IJ)+B*Z(J)
      GOTO64
```

```
   62 GM=TIM/TI
      DO 63 J=IP,N
      IJ=IJ+1
      Y=A(IJ)
      A(IJ)=B*Z(J)+Y*GM
   63 Z(J)=Z(J)-V*Y
   64 CONTINUE
      TIM=TI
      IJ=IJ+1
   66 CONTINUE
   70 CONTINUE
      IF(IR.LT.0)IR=-IR
      RETURN
C    FACTORIZE A MATRIX GIVEN IN A
      ENTRY MC11B(A,N,Z,SIG,W,IR,MK,EPS)
      IR=N
      IF(N.GT.1)GOTO100
      IF(A(1).GT.0.)RETURN
      A(1)=0.
      IR=0
      RETURN
  100 CONTINUE
      NP=N+1
      II=1
      DO 104 I=2,N
      AA=A(II)
      NI=II+NP-I
      IF(AA.GT.0.)GOTO101
      A(II)=0.
      IR=IR-1
      II=NI+1
      GOTO104
  101 CONTINUE
      IP=II+1
      II=NI+1
      JK=II
      DO 103 IJ=IP,NI
      V=A(IJ)/AA
      DO 102 IK=IJ,NI
      A(JK)=A(JK)-A(IK)*V
  102 JK=JK+1
  103 A(IJ)=V
  104 CONTINUE
      IF(A(II).GT.0.)RETURN
      A(II)=0.
      IR=IR-1
      RETURN
C    MULTIPLY OUT THE FACTORS GIVEN IN A
      ENTRY MC11C(A,N,Z,SIG,W,IR,MK,EPS)
      IF(N.EQ.1)RETURN
      NP=N+1
      II=N*NP/2
      DO 202 NIP=2,N
      JK=II
      NI=II-1
      II=II-NIP
      AA=A(II)
      IP=II+1
      IF(AA.GT.0.)GOTO203
      DO 204 IJ=IP,NI
  204 A(IJ)=0.
      GOTO202
  203 CONTINUE
      DO 201 IJ=IP,NI
      V=A(IJ)*AA
      DO 200 IK=IJ,NI
      A(JK)=A(JK)+A(IK)*V
  200 JK=JK+1
  201 A(IJ)=V
  202 CONTINUE
      RETURN
```

```
C   MULTIPLY A VECTOR Z BY THE FACTORS GIVEN IN A
      ENTRY MC11D(A,N,Z,SIG,W,IR,MK,EPS)
      IF(N.GT.1)GOTO300
      Z(1)=Z(1)*A(1)
      W(1)=Z(1)
      RETURN
  300 CONTINUE
      NP=N+1
      II=1
      N1=N-1
      DO 303 I=1,N1
      Y=Z(I)
      IF(A(II).EQ.0.)GOTO302
      IJ=II
      IP=I+1
      DO 301 J=IP,N
      IJ=IJ+1
  301 Y=Y+Z(J)*A(IJ)
  302 Z(I)=Y*A(II)
      W(I)=Z(I)
  303 II=II+NP-I
      Z(N)=Z(N)*A(II)
      W(N)=Z(N)
      DO 311 K=1,N1
      I=N-K
      II=II-NP+I
      IF(Z(I).EQ.0.)GOTO311
      IP=I+1
      IJ=II
      Y=Z(I)
      DO 310 J=IP,N
      IJ=IJ+1
  310 Z(J)=Z(J)+A(IJ)*Z(I)
  311 CONTINUE
      RETURN
C   MULTIPLY A VECTOR Z BY THE INVERSE OF THE FACTORS GIVEN IN A
      ENTRY MC11E(A,N,Z,SIG,W,IR,MK,EPS)
      IF(IR.LT.N)RETURN
      W(1)=Z(1)
      IF(N.GT.1)GOTO400
      Z(1)=Z(1)/A(1)
      RETURN
  400 CONTINUE
      DO 402 I=2,N
      IJ=I
      I1=I-1
      V=Z(I)
      DO 401 J=1,I1
      V=V-A(IJ)*Z(J)
  401 IJ=IJ+N-J
      W(I)=V
  402 Z(I)=V
      Z(N)=Z(N)/A(IJ)
      NP=N+1
      DO 411 NIP=2,N
      I=NP-NIP
      II=IJ-NIP
      V=Z(I)/A(II)
      IP=I+1
      IJ=II
      DO 410 J=IP,N
      II=II+1
  410 V=V-A(II)*Z(J)
  411 Z(I)=V
      RETURN
C   COMPUTE THE INVERSE MATRIX FROM FACTORS GIVEN IN A
      ENTRY MC11F(A,N,Z,SIG,W,IR,MK,EPS)
      IF(IR.LT.N)RETURN
      A(1)=1./A(1)
      IF(N.EQ.1) RETURN
      NP=N+1
```

```
      N1=N-1
      II=2
      DO 511 I=2,N
      A(II)=-A(II)
      IJ=II+1
      IF(I.EQ.N)GOTO502
      DO 501 J=I,N1
      IK=II
      JK=IJ
      V=A(IJ)
      DO 500 K=I,J
      JK=JK+NP-K
      V=V+A(IK)*A(JK)
  500 IK=IK+1
      A(IJ)=-V
  501 IJ=IJ+1
  502 CONTINUE
      A(IJ)=1./A(IJ)
      II=IJ+1
      AA=A(IJ)
      IJ=I
      IP=I+1
      NI=N-I
      DO 511 J=2,I
      V=A(IJ)*AA
      IK=IJ
      K=IJ-IP+J
      I1=IJ-1
      NIP=NI+IJ
      DO 510 JK=K,I1
      A(JK)=A(JK)+V*A(IK)
  510 IK=IK+NIP-JK
      A(IJ)=V
  511 IJ=IJ+NP-J
      RETURN
C---------------------------- END OF OPTIMIZING ROUTINE -----------------
      END
```

```
**************************************************************************
*                                                                        *
*               Select Modifications to PCSP Subroutines                 *
*              Required for Second Chain Type Description                *
*                  for use in Deformation Experiments                    *
*                                                                        *
*                  Gregory C. Rutledge (November 1989)                   *
*                                                                        *
**************************************************************************
```

COMMON blocks and PARAMETER statements are set up to enable easy variation of the scale of simulation. Important dimensions of the simulation are shown below; change of the appropriate dimension in all PARAMETER statements will introduce the change throughout the simulation:

```
  Description of Program Dimension Parameters
    NKIND = Numger of atom types of interest
C*    NIBB  = Number of internal building blocks per repeat unit
    MNARU = Maximum number of atoms per repeat unit
    MNRU  = Maximum number of repeat units per chain
    MNCH  = Maximum number of chains (a square number)
    MNAT  = Maximum number of atoms per chain + 1
    MNIC  = Maximum number of independently orientable chains
    MCOP  = MNIC*5
    MOPT  = MCOP+6

  Some parameters are specific to the PPTA polymer family
    NRNG  = Number of rotatable rings per repeat unit = 2
    NSUB  = Number of substitutions possible per repeat unit = 2
    MNSB  = NSUB*MNRU
C*    NDOF  = NIBB + NRNG
    MDOF = NNARU = 28
```

In the modified chain description, the method of chain description and the numbering of atoms in the chain have been altered. These changes are contained primarily in the routines COORDN, NONBOND, and ENERGY, to reflect the new construction, atom numbering, degrees of freedom, and force field. However, the following routines are also effected through the dimensioning of arrays, the control of DO loop executions, and atomic numbering, but do not differ sufficiently from the previous versions to justify reproduction in their entirety. (*) indicates that only changes to PARAMETER and COMMON statements are required

CMODEL	CELGEN
LDVAR	LDCHN *
DATARD	RESWR
RDSTRAIN *	HELIX *
GYRA *	UNITCELL *
DENS *	SUBSET

```
      SUBROUTINE COORDN
C
C  Generates a chain of poly(p-phenylene terephthalamide) with all
C  bond lengths, valence angles, and torsion angles independently
C  specified.
C  For use in generating elastic constants.  This routine replaces
C  COORDN and PHENYL in previous versions.
C
C  ************************************************************
C
```

```
C  Numbering of Atoms:
C
C
C                                      17              19   28
C                                       H               H    O
C       3              5       14           \          /         \
C       H              H       H              C --- C          27 C ---
C         \          /           \          / 16   18 \         /
C           C --- C              13 N --- C 15        20 C -- N 21
C      1  / 2     4 \             /         \ 24   22 /         \
C   --- C           6 C ---- C 7             C --- C             H 26
C         \10      8 /           \          /         \
C           C --- C                O 12   H 25          H 23
C         /          \
C       H              H
C       11             9
C
C
C  ************************************************************
C
C
        PARAMETER( NKIND=9,NIBB=8,MNRU=6,MNCH=9,MNAT=179,NRNG=2,NSUB=4,
     +             MNSB=24,NDOF=10,MNIC=9,MCOP=45,MOPT=51,MNARU=28 )
        COMMON /CHAINS/ PHI(MNARU),THETA(MNARU),BL(MNARU),PHIR(NRNG),
     +                  KSB(4),PCH(4,MNAT),NARU,NRUS,NCH,
     +                  A(4,4,MNAT),XYZ(4,MNAT,MNCH),KIND(MNAT,MNCH),
     +                  CHRG(MNAT,MNCH),KONEC(MNAT,MNAT),DEE,THT,RHO,
     +                  NUNIQ
        DIMENSION AL(4,4),KATOM(11),XYZL(4,11)
C
C  Constraints:
C  a) planar sp2 hydridization at amide nitrogens and carbons
c       PHI(11) = PHI(12) + 180.
c       PHI(13) = PHI(14) + 180.
c       PHI(25) = PHI(26) + 180.
c       PHI(27) = PHI(28) + 180.
C  b) 1-parameter (angle) ring deformation
        DO 110 I=7,21,14
          ALPHA = THETA(I)
          BETA = 180. - 0.5*ALPHA
          GAMMA = 90. + 0.25*ALPHA
          THETA(I-6) = BETA
          THETA(I-4) = BETA
          THETA(I-2) = BETA
          THETA(I-1) = BETA
          THETA(I+2) = BETA
          THETA(I-5) = GAMMA
          THETA(I-3) = GAMMA
          THETA(I+1) = GAMMA
          THETA(I+3) = GAMMA
  110   CONTINUE
C  c) Selected bond deformation (ring symmetric)
        DO 120 I=1,15,14
          BL(I+5) = BL(I+1)
          BL(I+7) = BL(I+1)
          BL(I+9) = BL(I+3)
  120   CONTINUE
C
C  Start building...
C  All atoms added pair-wise, one "backbone" and one "pendant"
C
        DO 2100 NREP=1,NRUS+1
        DO 2100 NODD=1,MNARU-1,2
        DO 2100 NPAIR=1,2
C
C  Add only first atom of N+1st repeat unit:
C
        IF( (NREP.EQ.(NRUS+1)).AND.((NODD.NE.1).OR.(NPAIR.NE.1)) )
     +    GO TO 2100
          NODD1 = NODD - 1
          NLOC  = NODD1 + NPAIR
```

```
          NLOC1 = NLOC-1
          NCURR  = NLOC+NARU*(NREP-1)
          NCURR1 = NCURR-1
          NATD1 = NCURR-NPAIR
          IF(NLOC1.EQ.0) NLOC1 = 28
C
          XYZ(1,NCURR,1) = BL(NLOC)
          XYZ(2,NCURR,1) = 0.
          XYZ(3,NCURR,1) = 0.
          XYZ(4,NCURR,1) = 1.
          KIND(NCURR,1) = 1
C
C  First atom fixes Cartesian space to coincide with first bond; no
C  further manipulation necessary
C
        IF( NCURR.EQ.1 ) GO TO 2100
C
C  Determine atom type:
C
        IF(MOD(NLOC,2).EQ.1) KIND(NCURR,1) = 2
        IF((NLOC.EQ. 1).OR.(NLOC.EQ.15)) THEN
          KIND(NCURR,1) = 1
        ELSE IF((NLOC.EQ. 7).OR.(NLOC.EQ.27)) THEN
          KIND(NCURR,1) = 3
        ELSE IF((NLOC.EQ.14).OR.(NLOC.EQ.26)) THEN
          KIND(NCURR,1) = 4
        ELSE IF((NLOC.EQ.13).OR.(NLOC.EQ.21)) THEN
          KIND(NCURR,1) = 5
        ELSE IF((NLOC.EQ.12).OR.(NLOC.EQ.28)) THEN
          KIND(NCURR,1) = 6
        END IF
C
C  Second atom placed in xy plane: PHI=0.  Load A matrix directly.
C  Otherwise, obtain A matrix from previous connection
C
        IF(NCURR.EQ.2) THEN
          CALL ATRNS( 0.,THETA(1),BL(1),AL)
          DO 2320 I=1,4
          DO 2320 J=1,4
 2320       A(I,J,NCURR) = AL(I,J)
        ELSE
          IF( ((NLOC.GE.12).AND.(NLOC.LE.16)).OR.
     +         (NLOC.GE.26).OR.(NLOC.LE.2) ) THEN
            IF( (NLOC.EQ.12).OR.(NLOC.EQ.26) ) THEN
              CALL ATRNS( PHI(NLOC1),THETA(NLOC1),BL(NLOC-5),AL)
              CALL MM( A(1,1,NCURR-5),AL,A(1,1,NCURR),4,4,4,4,4,4)
            ELSE IF( (NLOC.EQ.13).OR.(NLOC.EQ.27) ) THEN
              CALL ATRNS( PHI(NLOC1),THETA(NLOC1),BL(NLOC-6),AL)
              CALL MM( A(1,1,NCURR-6),AL,A(1,1,NCURR),4,4,4,4,4,4)
            ELSE
              NLOT = NLOC-MOD(NCURR,2)-1
              IF(NLOC.EQ.1) NLOT = 27
              NATT = NCURR-MOD(NCURR,2)-1
              CALL ATRNS( PHI(NLOC1),THETA(NLOC1),BL(NLOT),AL)
              CALL MM( A(1,1,NATT),AL,A(1,1,NCURR),4,4,4,4,4,4)
            END IF
          ELSE
            CALL ATRNS( PHI(NLOC1),THETA(NLOC1),BL(NODD1),AL)
            CALL MM( A(1,1,NATD1),AL,A(1,1,NCURR),4,4,4,4,4,4)
          END IF
        END IF
C  TRANSFORM TO FRAME 0:
        CALL MV( A(1,1,NCURR),4,3,XYZ(1,NCURR,1),4,XYZ(1,NCURR,1) )
 2100   CONTINUE
        RETURN
        END
```

```
      SUBROUTINE NONBOND( IENTRY )
C
C  Creates Table of Connectivity and assigns partial atomic charges to
C  atoms of the parent polymer form (PPTA)
C
C  Need be executed only once for a given cell composition, but must
C  be called after all chains have been created
C
C  Replaces NONBOND in previous versions involving alternate chain
C  description
C
      PARAMETER( NKIND=9,NIBB=8,MNRU=6,MNCH=9,MNAT=179,NRNG=2,NSUB=4,
     +           MNSB=24,NDOF=10,MNIC=9,MCOP=45,MOPT=51,MNARU=28 )
      COMMON /CHAINS/ PHI(MNARU),THETA(MNARU),BL(MNARU),PHIR(NRNG),
     +                KSB(4),PCH(4,MNAT),NARU,NRUS,NCH,
     +                A(4,4,MNAT),XYZ(4,MNAT,MNCH),KIND(MNAT,MNCH),
     +                CHRG(MNAT,MNCH),KONEC(MNAT,MNAT),DEE,THT,RHO,
     +                NUNIQ
      DATA CHARGC,CHARGO,CHARGN,CHARGH/.38,-.38,-.28,.28/
      DATA CHARGPPC,CHARGNPC,CHARGPH/ -0.06,-0.12,0.15 /
C
      IF( IENTRY.EQ.1 ) RETURN
C
      DO 100 I=1,NARU*NRUS
        DO 120 J=1,NCH
120     CHRG(I,J) = 0.
        DO 130 J=1,NARU*NRUS
130       KONEC(I,J) = 0.
100   CONTINUE
C
C  All atoms within a given phenyl ring or amide bond plane are fixed
C  relative to one another; atoms directly bonded to each ring/plane
C  are fixed relative to that ring/plane
C
C  Amide atom charges are assigned:
C
      NMER = NARU/28
      DO 500 LL = 1,NCH
      KTYP = 10
      MARK = 0
      DO 200 I=1,NMER*NRUS
        DO 200 II=1,4
          DO 300 J=MARK+1,MARK+KTYP
            IF(KTYP.EQ.10) GO TO 310
              JXX = J
              IF(J.EQ.(MARK+1)) JXX = J - 4
              IF(KIND(JXX,LL).EQ.3) THEN
                CHRG(JXX,LL) = CHARGC
              ELSE IF(KIND(JXX,LL).EQ.4) THEN
                CHRG(JXX,LL) = CHARGH
              ELSE IF(KIND(JXX,LL).EQ.5) THEN
                CHRG(JXX,LL) = CHARGN
              ELSE IF(KIND(JXX,LL).EQ.6) THEN
                CHRG(JXX,LL) = CHARGO
              END IF
310         CONTINUE
C
C  Three independent charges allowed: carbons 1&4, carbons 2,3,5&6,
C  and all hydrogens
C
      IF(KTYP.EQ.4) GO TO 315
      IF((J.EQ.(MARK+1)).OR.(J.EQ.(MARK+6))) THEN
        CHRG(J,LL) = CHARGPPC
      ELSE IF (J.EQ.(MARK+7)) THEN
        CHRG(J+4,LL) = CHARGPH
      ELSE IF (KIND(J,LL).EQ.1) THEN
        CHRG(J,LL) = CHARGNPC
      ELSE
        CHRG(J,LL) = CHARGPH
      END IF
315   CONTINUE
```

```
  300       CONTINUE
            MARK = MARK+KTYP
            IF(KTYP.EQ.10) THEN
              KTYP = 4
            ELSE
              KTYP = 10
            END IF
  200     CONTINUE
  500     CONTINUE
C
          MARK = 0
          KEND = 0
          DO 700 I=1,NMER*NRUS
            DO 720 L=0,14,14
            DO 710 J=1,8
            DO 710 K=1,9
              IF( (KEND.EQ.1).AND.((J+K+L).GT.28) ) GO TO 710
              KONEC(MARK+J+L,MARK+J+K+L) = 1
  710       CONTINUE
C
          KONEC(MARK+4+L,MARK+12+L) = 0
          KONEC(MARK+4+L,MARK+13+L) = 0
          KONEC(MARK+8+L,MARK+12+L) = 0
          KONEC(MARK+8+L,MARK+13+L) = 0
          KONEC(MARK+7+L,MARK+16+L) = 0
          KONEC(MARK+6+L,MARK+15+L) = 0
C
            KONEC(MARK+8+L,MARK+17+L) = 0
            KONEC(MARK+1+L,MARK+11+L) = 1
            KONEC(MARK+1+L,MARK+7+L) = 0
            KONEC(MARK+2+L,MARK+9+L) = 0
            KONEC(MARK+4+L,MARK+11+L) = 0
            IF((KEND.EQ.0).AND.(L.EQ.0)) KONEC(MARK+8+L,MARK+16+L) = 0
            KONEC(MARK+7+L,MARK+11+L) = 0
            DO 730 J=1,3
              KONEC(MARK+3+L,MARK+6+J+L) = 0
              KONEC(MARK+3+L,MARK+10+J+L) = 0
              KONEC(MARK+5+L,MARK+8+J+L) = 0
              KONEC(MARK+5+L,MARK+11+J+L) = 0
              IF( (KEND.EQ.1).AND.((J+L).GT.15) ) GO TO 730
              KONEC(MARK+8+L,MARK+13+J+L) = 0
  730       CONTINUE
            KONEC(MARK+9+L,MARK+10+L) = 1
            KONEC(MARK+9+L,MARK+11+L) = 1
            KONEC(MARK+10+L,MARK+11+L) = 1
            DO 740 J=1,3
              IF((KEND.EQ.1).AND.((J+L).GT.16)) GO TO 732
              KONEC(MARK+12+L,MARK+12+J+L) = 1
              KONEC(MARK+13+L,MARK+12+J+L) = 1
  732         IF((KEND.EQ.1).AND.((J+L).GT.15)) GO TO 734
              KONEC(MARK+14+L,MARK+13+J+L) = 1
  734         IF(KEND.EQ.1) GO TO 740
              KONEC(MARK+13+L,MARK+15+J+L) = 1
  740       CONTINUE
          KONEC(MARK+14+L,MARK+16+L) = 0
            IF((KEND.EQ.1).AND.(L.EQ.14)) GO TO 720
            KONEC(MARK+13+L,MARK+22+L) = 1
            KONEC(MARK+13+L,MARK+24+L) = 1
            KONEC(MARK+13+L,MARK+25+L) = 1
  720     CONTINUE
            MARK=MARK+NARU
            IF(I.EQ.(NRUS-1)) KEND = 1
  700     CONTINUE
C
          IENTRY = 1
          RETURN
          END
```

```
      SUBROUTINE ENERGY
C
C  Calculates the total potential energy per residue of the simulation
C  stucture, based on a polymer of the PPTA family
C
C  Contributions:  EDEF  (Bond Angle Deformation, Valence FF)
C                  EDEL  (Conjugated Bond Interaction Energy)
C                  ENOB1 (Intramolecular LJ Interaction)
C                  ECOU1 (Intramolecular Coulombic Interactions)
C                  ENOB2 (Intermolecular LJ INTERACTIONS)
C                  ECOU2 (Intermolecular Coulombic Interactions)
C                  EULJP (Intramolec. LJ Lattice Correction)
C                  EUESP (Intramolec. ES lattice Correction)
C                  EULJ  (Intermolec. LJ Lattice Correction)
C                  EUES  (Intermolec. ES lattice Correction)
C
C  The reference unit for calculating the potential energy depends on
C  the choice of RBASE and the size of the Helical Repeat Unit (HRU):
C
C  Case 1:  Single chain simulation: disregard "helical basis region";
C           calculate interaction of first RBASE residues with rest of
C           chain.
C  Case 2:  THT = 0: HRU is identical to chemical repeat unit, thus
C           similar to Case 1
C  Case 3:  HRU consists of NRUS-2 or fewer structural repeat units;
C           region may be treated exactly
C  Case 4:  HRU exceeds NRUS-2 or is incommensurate: Region is
C           arbitrarily set equal to the chemical repeat unit
C
C  ANGERR is the angular discrepancy allowed in determining the number
C  of turns of the helix required to obtain an integral number of
C  complete 360 degree rotations
C
C  This version of ENERGY provides a compiled toggle option between the
C  two lattice sum methods: 3D Periodicity (LSTOGG=0) or Helical Period-
C  idity (LSTOGG=1, enable MV call in lattice sum section).
C
      LOGICAL FIRST,REDUND
      PARAMETER( EPSILON=1E-6 )
      PARAMETER( NKIND=9,NIBB=8,MNRU=6,MNCH=9,MNAT=179,NRNG=2,NSUB=4,
     +           MNSB=24,NDOF=10,MNIC=9,MCOP=45,MOPT=51,MNARU=28 )
      COMMON /CHAINS/ PHI(MNARU),THETA(MNARU),BL(MNARU),PHIR(NRNG),
     +                KSB(4),PCH(4,MNAT),NARU,NRUS,NCH,
     +                A(4,4,MNAT),XYZ(4,MNAT,MNCH),KIND(MNAT,MNCH),
     +                CHRG(MNAT,MNCH),KONEC(MNAT,MNAT),DEE,THT,RHO,
     +                NUNIQ
      COMMON /CELL/ CELD(3),CELA(3),CHSPEC(5,MNCH),CHLOC(3,MNCH),
     +              NUNIV,KONDENS,TEMP,DENSC
      COMMON /ENRG/ EDEF1,EDEL,ENOB1,ENOB2,ECOU1,ECOU2,EULJ,EUES,
     +              EULJP,EUESP,ECFF,ETOT,EDEF2
      COMMON /SUBS/ WTED(4)
      COMMON /STRN/ KUC,KASE,ST(3,3),SUCV(3,3),DINIT,DPRIME,DCON
C
C     common /atmp/ BX0,BX00,CX0,CX00
C
      DIMENSION ANGZ(12),ANGO(12),DCL(3,3)
      DIMENSION BNDZ(30),BNDO(30),VALZ(48),VALO(48)
      DIMENSION FMULT(MNCH,MNCH)
      DIMENSION VDWR(NKIND),ALPHA(NKIND),EFFNE(NKIND)
      DIMENSION UX(3),UY(3),UZ(3),DVECT(4),R(4,4,21)
      DIMENSION REDUND(125)
      DIMENSION SUM1(3136),SUM6(3136),SUM12(3136),SUM1P(3136),
     +          SUM6P(3136),SUM12P(3136),TMP1(3136),TMP6(3136),
     +          TMP12(3136),TMP1P(3136),TMP6P(3136),TMP12P(3136)
      DATA VDWR/ 1.96,1.37,2.03,1.37,1.96,1.60,1.35,1.80,1.95/
      DATA ALPHA/0.768,0.330,2.16,0., 1.95,1.02,0.38,1.41,3.34/
      DATA EFFNE/5.2,  0.9,  5.2,  0.9,6.1,  7.,   8., 12., 21./
      DATA B0,B00,C0,C00,B1,B2/9.0,13.0,.2,.4,2.8,21.2 /
      DATA BNDZ/ 648.,925.,900.,925.,900.,925.,648.,925.,900.,925.,
     +           900.,1263.,880.,861.,648.,925.,900.,925.,900.,925.,
     +           648.,925.,900.,925.,900.,861.,880.,1263.,925.,925. /
```

```
      DATA BNDO/ 1.48,1.40,1.10,1.40,1.10,1.40,1.48,1.40,1.10,1.40,
     +           1.10,1.24,1.37,1.00,1.38,1.40,1.10,1.40,1.10,1.40,
     +           1.38,1.40,1.10,1.40,1.10,1.00,1.37,1.24,1.40,1.40 /
      DATA VALZ/   0.,  0.,.041,  0.,  0.,.041,.041,.041,.041,  0.,
     +             0.,.041,  0.,  0.,.041,.088,.088,.088,.050,.050,
     +           .088,.041,.041,.041,  0.,  0.,.041,  0.,  0.,.041,
     +           .041,.041,.041,  0.,  0.,.041,  0.,  0.,.041,.050,
     +           .050,.088,.088,.088,.088,.041,.041,.041 /
      DATA VALO/ 120.,120.,119.,120.,120.,119.,119.,119.,122.,120.,
     +           120.,119.,120.,120.,119.,120.,120.,120.,120.,120.,
     +           120.,119.,123.,119.,120.,120.,119.,120.,120.,119.,
     +           119.,119.,123.,120.,120.,119.,120.,120.,119.,120.,
     +           120.,120.,120.,120.,120.,119.,122.,119. /
      DATA PCARBZ,PCARBO/ .0131,180. /
      DATA NHZ,COZ/ .004,.025 /
      DATA BX0,BX00,CX0,CX00  /0.0,32.0,.0,.8/
      DATA DE/ 3.5 /
      DATA ANGERR/ 5. /
      DATA BWDIST/ 3.3 /
C
      FIRST = .TRUE.
      DEGRAD = 3.1415926535/180.
      LSTOGG = 0
C
C  Initialize VDWR, ALPHA, and EFFNE arrays:
C
      CALL ELJ( NKIND,1,1,VDWR,ALPHA,EFFNE,3.,3.,FIRST,POTINIT )
C
      RBASE = REAL( NUNIQ )
      ECFF = 0.
      EDEF1 = 0.
      EDEF2 = 0.
      EDEL = 0.
      ENOB1 = 0.
      ECOU1 = 0.
      ENOB2 = 0.
      ECOU2 = 0.
      EULJ = 0.
      EUES = 0.
      EULJP = 0.
      EUESP = 0.
      NATOMS = NARU*NRUS
      NM1 = NATOMS-1
C
C  Initialize intermolecular interaction multiplier matrix:
C
      NCH2 = NCH**2
      L1MAX = 1
      IF( NCH.NE.1 ) CALL MULMAX( MNCH,NCH,NCH2,L1MAX,FMULT )
C
      IF ( (NCH.EQ.1).OR.(ABS(THT).LT.ANGERR) ) GO TO 100
      DO 50 M=1,NRUS-2
        PANG = M*THT/360.
        IPANG = INT(PANG+0.5)
        IF( ABS(PANG-IPANG).LE.(M*ANGERR/360.) ) GO TO 70
50    CONTINUE
      NER = 1
      GO TO 80
70    NER = M
      GO TO 80
100   NER = 1
80    CONTINUE
      LATM = INT(RBASE*NER*NARU+1.01)
C
C  Bond length deformation: (two extra for ring closure)
C
      DO 3100 I=1,28
        IF( KIND(I,1).EQ.8 ) THEN
          BNDO(I) = 1.70
          RCCL = SQRT( (XYZ(1,I,1)-XYZ(1,I-1,1))**2 +
     +                 (XYZ(2,I,1)-XYZ(2,I-1,1))**2 +
```

```
     +                    (XYZ(3,I,1)-XYZ(3,I-1,1))**2 )
            BL(I) = RCCL
          END IF
          EDEF1 = EDEF1 + 0.5*BNDZ(I)*(BL(I) - BNDO(I))**2
 3100   CONTINUE
        DO 3150 I=1,2
          II = (I-1)*14 + 1
          RCB = SQRT( (XYZ(1,II,1)-XYZ(1,II+9,1))**2 +
     +                (XYZ(2,II,1)-XYZ(2,II+9,1))**2 +
     +                (XYZ(3,II,1)-XYZ(3,II+9,1))**2 )
          EDEF1 = EDEF1 + 0.5*BNDZ(I+28)*(RCB - BNDO(I+28))**2
 3150   CONTINUE
C
C  Valence angle deformation
C
        MKR = 0
        DO 3200 I=1,16
          IHAF = MOD(I,8)
          IA = (I/9)*14 + 2*IHAF
          IB = IA-2
          IC = IA+1
          ID = IA+2
          IF( IHAF.EQ.1 ) THEN
            IB = IA-1
          ELSE IF( IHAF.EQ.5 ) THEN
            ID = IA-9
          ELSE IF( IHAF.EQ.6 ) THEN
            IA = IA-5
            IB = IA-1
            IC = IA+5
            ID = IA+6
          ELSE IF( IHAF.EQ.7 ) THEN
            IA = IA-1
            IB = IA-6
            IC = IA+1
            ID = IA+2
          ELSE IF( IHAF.EQ.0 ) THEN
            IA = (I/9)*14 + 15
            IB = IA-2
            IC = IA+1
            ID = IA+9
          ELSE
          END IF
          MKR = MKR + 1
          CALL ANGL( XYZ(1,IB,1),XYZ(1,IC,1),XYZ(1,IA,1),VA )
          EDEF2 = EDEF2 + 0.5*VALZ(MKR)*( VA - VALO(MKR) )**2
          MKR = MKR + 1
          CALL ANGL( XYZ(1,IC,1),XYZ(1,ID,1),XYZ(1,IA,1),VA )
          EDEF2 = EDEF2 + 0.5*VALZ(MKR)*( VA - VALO(MKR) )**2
          MKR = MKR + 1
          CALL ANGL( XYZ(1,ID,1),XYZ(1,IB,1),XYZ(1,IA,1),VA )
          EDEF2 = EDEF2 + 0.5*VALZ(MKR)*( VA - VALO(MKR) )**2
 3200   CONTINUE
C
C  Conjugated bond interaction energy:
C  Note: with the introduction of substitution on the ring (potentially
C  in a random sequence and without equal occurance at the two 'ends'
C  of the ring) with different delocalization potentials, it becomes
C  necessary to compute EDEL weighted by the appropriate loci of
C  substitutions:
C
          NRT = NARU/28
          DO 400 K=1,NRT
            NRR = (K-1)*NRNG/NRT
            NRP = (K-1)*NIBB/NRT
            EDEL = EDEL + WTED(2)*CURTINV(-PHI(12+NRP),B0,C0 )
            EDEL = EDEL + WTED(3)*CURTATE( (PHI(15+NRP)+180.),B00,C00 )
            EDEL = EDEL + WTED(4)*CURTATE(-PHI(26+NRP),B00,C00 )
            EDEL = EDEL + WTED(1)*CURTINV( (PHI(1+NRP)+180.),B0,C0 )
            EDEL = EDEL + (1.- WTED(2))*CURTATE(-PHI(12+NRP),BX0,CX0 )
            EDEL = EDEL + (1.- WTED(3))*CURTATE( (PHI(15+NRP)+180.),
```

```
     +                    B00,C00 )
            EDEL = EDEL + (1.- WTED(4))*CURTATE(-PHI(26+NRP),B00,C00 )
            EDEL = EDEL + (1.- WTED(1))*CURTATE((PHI(1+NRP)+180.),
     +                    B0,C0 )
            EDEL = EDEL + B1/2*(1.-COS(PHI(14+NRP) *DEGRAD))
     +                  + B2/2*(1.-COS(2*PHI(14+NRP) *DEGRAD))
            EDEL = EDEL + B1/2*(1.-COS(PHI(28+NRP) *DEGRAD))
     +                  + B2/2*(1.-COS(2*PHI(28+NRP) *DEGRAD))
  400       CONTINUE
C
C  Out-of-plane bending for amide N-H and C=O
C
          OOPB1 = ABS( PHI(12) - PHI(11) + SIGN(180.,PHI(11)) )
          OOPB2 = ABS( PHI(14) - PHI(13) + SIGN(180.,PHI(13)) )
          OOPB3 = ABS( PHI(26) - PHI(25) + SIGN(180.,PHI(25)) )
          OOPB4 = ABS( PHI(28) - PHI(27) + SIGN(180.,PHI(27)) )
          IF (OOPB1.GT.180.) OOPB1 = 360. - OOPB1
          IF (OOPB2.GT.180.) OOPB2 = 360. - OOPB2
          IF (OOPB3.GT.180.) OOPB3 = 360. - OOPB3
          IF (OOPB4.GT.180.) OOPB4 = 360. - OOPB4
          EDEF2 = EDEF2 + 0.5*NHZ*( OOPB2**2 + OOPB3**2 )
          EDEF2 = EDEF2 + 0.5*COZ*( OOPB1**2 + OOPB4**2 )
C
C  Add phenyl-cargon torsions (6 per ring)
C
          DO 3300 I=1,NRNG
            IC1 = (I-1)*14
            DO 3300 J=1,6
              IF(J.EQ.1) THEN
                IA = IC1 + 1
                IB = IA + 1
                IC = IB + 2
                ID = IC + 2
              ELSE IF(J.EQ.4) THEN
                IA = J*2 - 2 + IC1
                IB = IA + 2
                IC = IB + 2
                ID = IC - 9
              ELSE IF(J.EQ.5) THEN
                IA = J*2 - 2 + IC1
                IB = IA + 2
                IC = IB - 9
                ID = IC + 1
              ELSE IF(J.EQ.6) THEN
                IA = J*2 - 2 + IC1
                IB = IA - 9
                IC = IB + 1
                ID = IC + 2
              ELSE
                IA = J*2 - 2 + IC1
                IB = IA + 2
                IC = IB + 2
                ID = IC + 2
              END IF
              CALL TORSION( XYZ(1,IA,1),XYZ(1,IB,1),XYZ(1,IC,1),
     +                      XYZ(1,ID,1),BTR )
              IF(BTR.LE.-180.) BTR = BTR + 360.
              IF(BTR.LE.0.) BTR = BTR + 180.
              EDEL = EDEL + 0.5*PCARBZ*(BTR - PCARBO)**2
 3300     CONTINUE
C
          DO 500 L1=1,L1MAX
            IF(L1.NE.1) GO TO 530
C
C  Intramolecular nonbonded interactions:
C
            DO 520 I=1,NM1
              IP1 = I+1
              DO 510 J=IP1,NATOMS
                IF( KONEC(I,J).EQ.1 ) GO TO 510
                IF( I.GE.LATM ) GO TO 510
```

```
              D2 = (XYZ(1,I,L1)-XYZ(1,J,L1))**2 +
     +             (XYZ(2,I,L1)-XYZ(2,J,L1))**2 +
     +             (XYZ(3,I,L1)-XYZ(3,J,L1))**2
              DIS = SQRT(D2)
              CALL ELJ( NKIND,KIND(I,L1),KIND(J,L1),VDWR,ALPHA,EFFNE,
     +                  D2,D2,FIRST,POTLJ )
              ENOB1 = ENOB1 + POTLJ
              CALL EES( BWDIST,DIS,DE,CHRG(I,L1),CHRG(J,L1),POTES )
              ECOU1 = ECOU1 + POTES
  510       CONTINUE
  520     CONTINUE
  530     CONTINUE
          IF (NCH.EQ.1) GO TO 500
          LP1 = L1+1
C
C  Intermolecular interactions:
C
          DO 550 L2=LP1,NCH
            IF( INT(FMULT(L1,L2)*100.).EQ.0 ) GO TO 550
            IF( INT(ABS(CHSPEC(1,L2))+.01).NE.1 ) GO TO 550
            ENOBT = 0.
            ECOUT = 0.
            DO 570 I=1,NATOMS
              DO 560 J=1,NATOMS
              IF (I.LT.LATM) THEN
              D2 = (XYZ(1,I,L1)-XYZ(1,J,L2))**2 +
     +             (XYZ(2,I,L1)-XYZ(2,J,L2))**2 +
     +             (XYZ(3,I,L1)-XYZ(3,J,L2))**2
              DIS = SQRT(D2)
              CALL ELJ( NKIND,KIND(I,L1),KIND(J,L2),VDWR,ALPHA,EFFNE,
     +                  D2,D2,FIRST,POTLJ )
              ENOBT = ENOBT + POTLJ
              CALL EES( BWDIST,DIS,DE,CHRG(I,L1),CHRG(J,L2),POTES )
              ECOUT = ECOUT + POTES
              ELSE
              IF (J.LT.LATM) THEN
              D2 = (XYZ(1,I,L1)-XYZ(1,J,L2))**2 +
     +             (XYZ(2,I,L1)-XYZ(2,J,L2))**2 +
     +             (XYZ(3,I,L1)-XYZ(3,J,L2))**2
              DIS = SQRT(D2)
              CALL ELJ( NKIND,KIND(I,L1),KIND(J,L2),VDWR,ALPHA,EFFNE,
     +                  D2,D2,FIRST,POTLJ )
              ENOBT = ENOBT + POTLJ
              CALL EES( BWDIST,DIS,DE,CHRG(I,L1),CHRG(J,L2),POTES )
              ECOUT = ECOUT + POTES
              ELSE
              END IF
              END IF
  560         CONTINUE
  570       CONTINUE
            ENOB2 = ENOB2 + 0.5*ENOBT
            ECOU2 = ECOU2 + 0.5*ECOUT
  550     CONTINUE
  500   CONTINUE
C
C  Infinite Lattice Correction:
C    (specific for two-chain-type lattices, with interchain interactions
C     1-1, 1-2, 2-1, and 2-2 only; of these, only half of the 1-1 and 2-2
C     interactions are unique, and the 1-2 interactions are identical to
C     the 2-1 interactions.  NUNIV represents "infinite" lattice size)
C
        IF( NUNIV.EQ.0 ) GO TO 630
        DO 610 K=1,3
          UX(K) = CHLOC(K,2) - CHLOC(K,4)
          UY(K) = CHLOC(K,2) + CHLOC(K,4)
          UZ(K) = 0.
  610     DVECT(K) = 0.
        UZ(3) = RBASE*REAL(NER)*DEE
        DVECT(4) = 1.
        NCM2 = NINT(SQRT(REAL(NCH))-2)
        NNCM = -NCM2-1
```

```
        ESPWR = BWDIST*LOG(DE)
C
C  Set up helix periodicity transforms beforehand:
C
        IF(LSTOGG.EQ.0) GO TO 625
        DO 620 LZN = 1,2*NUNIV+1
          LZ = LZN-NUNIV-1
          RTN = RBASE*REAL(LZ*NER)
          RTH = RTN*THT
          RDE = RTN*DEE
          CALL RTRANS( RTH,RDE,R(1,1,LZN) )
  620   CONTINUE
  625   CONTINUE
C
        DO 600 L1=1,2
        DO 600 L2=L1,2
          KFIJ = L1+L2-1
          LXS = -NUNIV
          IF( KFIJ.NE.2 ) LXS = 0
          NNLX = NUNIV-LXS+1
          NNLY = 2*NUNIV+1
          NNLZ = NNLY
C
C  Zero all atom-atom summations:
C
          DO 645 I=1,LATM-1
          DO 645 J=1,LATM-1
            NTMP = (I-1)*(LATM-1) + J
            SUM1P(NTMP) = 0.
            SUM6P(NTMP) = 0.
            SUM12P(NTMP) = 0.
            SUM1(NTMP) = 0.
            SUM6(NTMP) = 0.
            SUM12(NTMP) = 0.
  645     CONTINUE
C
C  Loop over all lattice points, checking for redundancy with explicit
C  calculation scheme for L1-L2:
C
cvd$ noconcur
          DO 680 LX=LXS,NUNIV
cvd$ noconcur
          DO 680 LY=-NUNIV,NUNIV
cvd$ noconcur
          DO 680 LZ=-NUNIV,NUNIV
            NRED = (LX-LXS)*NNLY*NNLZ + (LY+NUNIV)*NNLZ +
     +             (LZ+NUNIV) + 1
            IF( (KFIJ.NE.2).AND.(LX.EQ.0).AND.(LY.LE.0) ) THEN
              REDUND(NRED) = .TRUE.
              GO TO 680
            ELSE
              REDUND(NRED) = .FALSE.
            END IF
            IF( ABS(LZ).LE.(NRUS-1) ) THEN
              IF (KFIJ.NE.2) THEN
                REDUND(NRED) = ( (ABS(LX)+ABS(LY)).LE.NCM2 )
              ELSE
                IF( (LX+LY).NE.NCM2 ) THEN
                  REDUND(NRED) = ( ((ABS(LX)+ABS(LY)).LE.NCM2).OR.
     +             ((LX.LT.0).AND.(LY.LT.0).AND.((LX+LY).EQ.NNCM)) )
                END IF
              END IF
            END IF
            IF( REDUND(NRED) ) GO TO 680
C
C  Loop over all atoms of the units of L1 and L2 at this lattice point
C  to get inverse distances:
C
          DO 650 I=1,LATM-1
          DO 650 J=1,LATM-1
            NTMP = (I-1)*(LATM-1) + J
```

```
C           ESPWR = ( VDWR(KIND(I,L1))+VDWR(KIND(J,L2)) )*LOG(DE)
            IF( LSTOGG.EQ.0 ) THEN
              DVECT(1) = XYZ(1,J,L2) - XYZ(1,I,L1)
              DVECT(2) = XYZ(2,J,L2) - XYZ(2,I,L1)
              DVECT(3) = XYZ(3,J,L2) - XYZ(3,I,L1)
              DVV = (DVECT(1)+LX*UX(1)+LY*UY(1)+LZ*UZ(1))**2
     +            + (DVECT(2)+LX*UX(2)+LY*UY(2)+LZ*UZ(2))**2
     +            + (DVECT(3)+LX*UX(3)+LY*UY(3)+LZ*UZ(3))**2
            ELSE
              LZN = LZ + NUNIV + 1
              DVECT(1) = XYZ(1,J,L2) - CHLOC(1,L2)
              DVECT(2) = XYZ(2,J,L2) - CHLOC(2,L2)
              DVECT(3) = XYZ(3,J,L2) - CHLOC(3,L2)
C             CALL MV( R(1,1,LZN),4,3,DVECT,4,DVECT )
              DVECT(1) = DVECT(1) + CHLOC(1,L2) - XYZ(1,I,L1)
              DVECT(2) = DVECT(2) + CHLOC(2,L2) - XYZ(2,I,L1)
              DVECT(3) = DVECT(3) + CHLOC(3,L2) - XYZ(3,I,L1)
              DVV = (DVECT(1)+LX*UX(1)+LY*UY(1))**2
     +            + (DVECT(2)+LX*UX(2)+LY*UY(2))**2
     +            + (DVECT(3)+LX*UX(3)+LY*UY(3))**2
              END IF
              DVROOT = SQRT(DVV)
C  Note: discontinuity in S1 is possible, may have to spline (5/16/88)
              S1 = EXP(ESPWR/DVROOT)/DVROOT
              IF( DVROOT.LE.BWDIST ) S1 = DE/DVROOT
              S6 = 1./DVV**3
              S12 = S6**2
              IF( (KFIJ.NE.2).AND.(LX.EQ.0).AND.(LY.EQ.0) ) THEN
                TMP1P(NTMP) = S1
                TMP6P(NTMP) = S6
                TMP12P(NTMP) = S12
              ELSE
                TMP1(NTMP) = S1
                TMP6(NTMP) = S6
                TMP12(NTMP) = S12
              END IF
  650       CONTINUE
C
C  Add this element to summation
C
            DO 655 I=1,LATM-1
            DO 655 J=1,LATM-1
              NTMP = (I-1)*(LATM-1) + J
              SUM1P(NTMP) = SUM1P(NTMP) + TMP1P(NTMP)
              SUM6P(NTMP) = SUM6P(NTMP) + TMP6P(NTMP)
              SUM12P(NTMP) = SUM12P(NTMP) + TMP12P(NTMP)
              SUM1(NTMP) = SUM1(NTMP) + TMP1(NTMP)
              SUM6(NTMP) = SUM6(NTMP) + TMP6(NTMP)
              SUM12(NTMP) = SUM12(NTMP) + TMP12(NTMP)
  655       CONTINUE
  680     CONTINUE
C
C  Finally, calculate the energies for each atom-atom pair:
C
          DO 665 I=1,LATM-1
          DO 665 J=1,LATM-1
            NTMP = (I-1)*(LATM-1) + J
            CALL ELJ( NKIND,KIND(I,L1),KIND(J,L2),VDWR,ALPHA,EFFNE,
     +                SUM6(NTMP),SUM12(NTMP),FIRST,POTLJ )
            EULJ = EULJ + 0.5*POTLJ
            EUES = EUES + 166.*SUM1(NTMP)*CHRG(I,L1)*CHRG(J,L2)/DE
            IF( (SUM6P(NTMP).EQ.0.).AND.(SUM12P(NTMP).EQ.0.) ) GO TO 665
            CALL ELJ( NKIND,KIND(I,L1),KIND(J,L2),VDWR,ALPHA,EFFNE,
     +                SUM6P(NTMP),SUM12P(NTMP),FIRST,POTLJP )
            EULJP = EULJP + 0.5*POTLJP
            EUESP = EUESP + 166.*SUM1P(NTMP)*CHRG(I,L1)*CHRG(J,L2)/DE
  665     CONTINUE
  600   CONTINUE
  630   CONTINUE
C
C  Here is calculated the penalty function that fixes chain pitch DEE
```

```
C
      IF( KUC.NE.0 ) ECFF = DCON*( DEE - DPRIME )**2
C
C  Total energy per residue:
C
      ENOB1 = ENOB1/NER/RBASE
      ENOB2 = ENOB2/NER/RBASE
      ECOU1 = ECOU1/NER/RBASE
      ECOU2 = ECOU2/NER/RBASE
      EULJ = EULJ/NER/RBASE
      EUES = EUES/NER/RBASE
      EULJP = EULJP/NER/RBASE
      EUESP = EUESP/NER/RBASE
      ETOT = EDEF1 + EDEL + ENOB1 + ENOB2 + ECOU1 + ECOU2 + ECFF +
     +       EULJ + EUES + EULJP + EUESP + EDEF2
      RETURN
  900 CONTINUE
      WRITE(11,*) 'ERROR: No parent chain available'
      RETURN
      END


      SUBROUTINE ANGL( AA,BB,CC,ANGLE )
C  CALCULATES THE BOND ANGLE AA-CC-BB AND THEN RETURNS THE ENERGY
C  ASSOCIATED WITH DEFORMATION OF THIS ANGLE FROM AO:
      DIMENSION AA(3),BB(3),CC(3)
      ASQ = 0.
      BSQ = 0.
      CSQ = 0.
      DO 100 I=1,3
        CSQ = CSQ+(AA(I)-BB(I))**2
        ASQ = ASQ+(BB(I)-CC(I))**2
  100   BSQ = BSQ+(CC(I)-AA(I))**2
      ANGLE = ACOS( 0.5*(ASQ+BSQ-CSQ)/SQRT(ASQ*BSQ) )
      ANGLE = ANGLE*180./3.1415926535
      RETURN
      END

      SUBROUTINE TORSION( AA,BB,CC,DD,TOR )
C  CALCULATES THE TORSION ANGLE AA-BB-CC-DD AND THEN RETURNS THE ENERGY
C  ASSOCIATED WITH DEFORMATION OF THIS ANGLE FROM TO:
      DIMENSION AA(3),BB(3),CC(3),DD(3),AB(3),BC(3),DC(3)
      DIMENSION ABC(3),BCD(3)
      ABM = 0.
      BCM = 0.
      DCM = 0.
      DOT = 0.
      ABCM = 0.
      BCDM = 0.
      DO 100 I=1,3
        AB(I) = BB(I) - AA(I)
        BC(I) = CC(I) - BB(I)
        DC(I) = CC(I) - DD(I)
        ABM = ABM + AB(I)**2
        BCM = BCM + BC(I)**2
  100   DCM = DCM + DC(I)**2
      DO 200 I=1,3
        AB(I) = AB(I)/SQRT(ABM)
        BC(I) = BC(I)/SQRT(BCM)
  200   DC(I) = DC(I)/SQRT(DCM)
      CALL VV( AB,BC,ABC,3 )
      CALL VV( BC,DC,BCD,3 )
      DO 300 I=1,3
        DOT = DOT + ABC(I)*BCD(I)
        ABCM = ABCM + ABC(I)**2
  300   BCDM = BCDM + BCD(I)**2
      ARG = DOT/SQRT(ABCM*BCDM)
      IF( ABS(ARG-1.).LE.1E-6 ) ARG = 1.
      IF( ABS(ARG+1.).LE.1E-6 ) ARG = -1.
      TOR = ACOS( ARG )*180./3.1415926535
C  DETERMINE TORSION DIRECTION:
```

```
      DTX = 0.
      DO 400 I=1,3
400     DTX    = DTX + AB(I)*BCD(I)
      ARG2 = DTX/SQRT(ABM*BCDM)
      IF( ABS(ARG2-1.).LE.1E-6 ) ARG2 = 1.
      IF( ABS(ARG2+1.).LE.1E-6 ) ARG2 = -1.
      DRX = ACOS( ARG2 )*180./3.1415926535
      TOR = SIGN( TOR,(90.-DRX))
      RETURN
      END
```

Data Input File U.dt:

```
  1   1   1   1   0
  1
 28   6   9   2   0 205.
  2   2   2   2
120.    180.      0       0       0       0.    180.      0.
120.      0.      0       0       0       0.    180.     60.
120.    180.      0       0       0       0.      0.      0.
122.      5.      0       0       0     -10.     10.     10.
120.    180.      0       0       0       0.      0.      0.
122.      0.      0       0       0       0.    180.     60.
120.    180.      0       0       0       0.      0.      0.
120.     -5.      0       0       0     -10.     10.     10.
150.      0       0      25.    155.    130.
 30.      0       0       0.    180.     15.
  4.9     0       0       0.      0.      0.
  4.9     0       0       4.5     9.      1.5
 13.1     0       0       0.      0.      0.
 90.      0       0      90.     60.    -15.
 90.      0       0      90.     60.    -15.
 90.      0       0      30.     90.     15.
  1.      0       0      -1.      1.      2.
  0.      0       0       0.1     0.5     0.2
  0.      0       0       0.      0.      0.
  0.      0       0       0.      0.      0.
120.      0       0       0.    150.     30.
  1.      0       0      -2.      2.      1.
  0.4     0       0      -0.4     0.5     0.1
  0.      0       0       0.      0.      0.
  0.      0       0       0.    180.    180.
-60.      0       0    -180.    150.     30.
  1.      0       0      -1.      1.      2.
  0.      0       0       0.      0.      0.
  0.      0       0       0.      0.      0.
  0.      0       0       0.      0.      0.
  0.      0       0       0.      0.      0.
  1.      0       0      -1.      1.      2.
  0.      0       0       0.      0.      0.
  0.      0       0       0.      0.      0.
  0.      0       0       0.    180.     10.
  1.      0       0      -1.      1.      2.
  0.      0       0       0.      0.      0.
  0.      0       0       0.      0.      0.
  0.      0       0       0.      0.      0.
  0.      0       0       0.      0.      0.
  1.      0       0      -1.      1.      2.
  0.      0       0       0.      0.      0.
  0.      0       0       0.      0.      0.
  0.      0       0       0.      0.      0.
  0.      0       0       0.      0.      0.
  0.      0       0      -1.      1.      2.
  0.      0       0       0.      0.      0.
  0.      0       0       0.      0.      0.
  0.      0       0       0.      0.      0.
  0.      0       0       0.      0.      0.
```

```
0.      0       0       -1.     1.      2.
0.      0       0        0.     0.      0.
0.      0       0        0.     0.      0.
0.      0       0        0.     0.      0.
0.      0       0        0.     0.      0.
0.      0       0       -1.     1.      2.
0.      0       0        0.     0.      0.
0.      0       0        0.     0.      0.
0.      0       0        0.     0.      0.
0.      0       0        0.     0.      0.
```

Data Input File US.dt:

```
 1    1
13.1066   0
 0.0   0.0   0.0
 0.0   0.0   0.0
 0.0   0.0   0.0
```

APPENDIX H: FORTRAN Listing of program to Calculate and Plot X-ray Scattering Diagrams

The following is a listing of one version of the program used to simulate x-ray scattering behavior. This version is appropriate for use with the output file from the structure simulation program and contains graphics subroutines for use with the IRIS 4D-GT multicolor display. This listing contains the following routines:

UCANAL (main)	XRSHADE	MV
UCDRAW	RANDS1	MM
FRCOORD	PALETTE	LUBKSB
STRUFA	VECTORIZ	LUDCMP
PLORG	LATCON	ATSCAT
GOURPLOT	VV	

```
      PROGRAM UCANAL
C
C  ***********************************************************************
C  *                                                                     *
C  *                  POLYMER CRYSTAL X-RAY DIFFRACTION                  *
C  *                                                                     *
C  *                         GREGORY C. RUTLEDGE                         *
C  *                                                                     *
C  *                  DEPARTMENT OF CHEMICAL ENGINEERING                 *
C  *                 MASSACHUSETTS INSTITUTE OF TECHNOLOGY               *
C  *                           NOVEMBER 1989                             *
C  *                                                                     *
C  *     (C) Copywrite 1989: Gregory C. Rutledge, Ulrich W. Suter        *
C  *                                                                     *
C  ***********************************************************************
C
C  This is the driver program to interpret results output by the Polymer
C  Crystal Simulation Program.  Reads simulation crystal variables and
C  Cartesian coordinates of the first four chains, estimates the best
C  unit cell type (out of twelve possibilities provided), converts
C  atom coordinates to fractional coordinates, and outputs a plot file
C  for use by SCHAKAL88 or CHARON (PLUTO derivative) to draw unit cell
C  schematic (in subroutine UCDRAW).
C  If specified, the calculation will proceed to call routines to
C  generate a list of the x-ray diffraction positions and intensities
C  for crystal planes hkl up to a pre-determined limit in h, k, and l;
C  it is assumed that the chain axes lie along the crystallographic c
C  axis, which corresponds in turn to the fiber axis. A representative
C  x-ray fiber diagram may be recreated for display.
C
C  The input file is PCS.IN; Output files are UNCL.OUT for unit cell
C  representation, SF.RES for a listing of the x-ray reflection positions
C  and intensities, and UCDRAW.OUT for the unit cell plot file.
C
C  This version contains markers for modification required to simulate
C  larger repeat units (eg. HHTT isomers) and antiparallel chain types
C  (eg. HT(A) isomers).  These are also marked in the subroutines
C  FRCOORD, UCDRAW, and STRUFA.
C  *** marks modifications for HHTT isomers
C  &&& marks modications for antiparallel chains
C
      CHARACTER*64 TITLE,RARG
      CHARACTER*1 KIND(84,4),GARB1(72),KGB
c***  CHARACTER*1 KIND(168,4),GARB1(72),KGB
      INTEGER*2 LNBLNK
      DIMENSION UCT(3,3),GCT(3,3,12),GCL(3,12),GCA(3,12),GHYB(4),
     +          ARA(3,3),ARB(3,3),SS(3),SA(3)
      DIMENSION XYZ(3,84,4),KCTST(12)
c***  DIMENSION XYZ(3,168,4),KCTST(12)
      COMPL(X) = (90.-X)*3.141526535/180.
      DEGRAD = 3.1415926535/180.
      NARU = 28
c***  NARU = 56
      WRITE(*,*) 'Input Structure Designation (up to 36 characters) >'
      READ(*,1) TITLE
    1 FORMAT( A64 )
  140 WRITE(*,*) 'Do you want to generate or plot x-ray info: [NO] >'
      READ(*,1) RARG
      LEN = LNBLNK(RARG)
      IF( LEN.GE.1 ) THEN
        IF( (RARG(1:1).EQ.'Y').OR.(RARG(1:1).EQ.'y') ) THEN
          KXRFD = 0
        ELSE IF( (RARG(1:1).EQ.'N').OR.(RARG(1:1).EQ.'n') ) THEN
          KXRFD = 1
        ELSE
          GO TO 140
        END IF
      ELSE
        KXRFD = 1
      END IF
      OPEN( UNIT=9,FILE='PCS.IN',STATUS='OLD' )
```

```
        OPEN( UNIT=10,FILE='UNCL.OUT')
        DO 100 I=1,25
        IF(I.EQ.14) THEN
          READ(9,10) (GARB1(J),J=1,40),SS(1),SS(2),SS(3)
        ELSE IF (I.EQ.15) THEN
          READ(9,10) (GARB1(J),J=1,40),SA(1),SA(2),SA(3)
        ELSE IF (I.EQ.17) THEN
          READ(9,11) (GARB1(J),J=1,16),TNUL,(GARB1(J),J=1,18),OM1
        ELSE IF (I.EQ.18) THEN
          READ(9,11) (GARB1(J),J=1,16),TX,(GARB1(J),J=1,18),OM2
        ELSE
          READ(9,12) (GARB1(J),J=1,72)
        END IF
 100    CONTINUE
C
C  For HHTT species, use 56 atom NARU with NRUC=3 and larger arrays
C  For anti-parallel HTHT, must read atoms of even-numbered chains
C  from the opposite end
C
c###    NRUC = 3
        NRUC = 6
        DO 120 I=1,NARU*NRUC*4
          II = I/(NARU*NRUC+1) + 1
          III = I - (II-1)*NARU*NRUC
          IF(III.LE.84) THEN
c***      IF(III.LE.168) THEN
          READ(9,14,ERR=130,END=130) KIND(III,II),(XYZ(J,III,II),J=1,3)
          ELSE
          READ(9,14,ERR=130,END=130) KGB,XGB,YGB,ZGB
          END IF
c&&&      IF(MOD(II,2).EQ.1) THEN
c&&&      IF(III.LE.84) THEN
c&&&      READ(9,14,ERR=130,END=130) KIND(III,II),(XYZ(J,III,II),J=1,3)
c&&&      ELSE
c&&&      READ(9,14,ERR=130,END=130) KGB,XGB,YGB,ZGB
c&&&      END IF
c&&&      ELSE
c&&&      IF(III.LE.84) THEN
c&&&      READ(9,14,ERR=130,END=130) KGB,XGB,YGB,ZGB
c&&&      ELSE
c&&&      IIX = NARU*NRUC-III+1
c&&&      READ(9,14,ERR=130,END=130) KIND(IIX,II),(XYZ(J,IIX,II),J=1,3)
c&&&      END IF
c&&&    END IF
 120   CONTINUE
 130    CONTINUE
        CLOSE( UNIT=9 )
C
C  Convert Simulation variables into corresponding vectors:
C
c***
c***            ss(3) = 2.*ss(3)
        CALL VECTORIZ( SS,SA,UCT )
C
C  12 General Cell Formats:
C    1) 2 CHAINS, FC, GENERAL; a=1-9,b=1-3
C    2) 2 CHAINS, FC, GENERAL; a=1-9,b=1-51
C    3) 2 CHAINS, FC, GENERAL; a=1-9,b=1-35
C    4) 2 CHAINS, EC, GENERAL; a=1-9,b=1-11
C    5) 2 CHAINS, EC, GENERAL; a=1-7,b=1-11
C    6) 2 CHAINS, EC, GENERAL; a=1-9,b=1-15
C    7) 2 CHAINS, EC, GENERAL; a=1-3,b=1-15
C    8) 1 CHAIN, TRANS = 0,1/2; a=1-9,b=1-2
C    9) 1 CHAIN, TRANS = 0,1/2; a=1-7,b=1-2
C    10) 1 CHAIN, TRANS = 0,1/2; a=1-9,b=1-4
C    11) 1 CHAIN, TRANS = 0,1/2; a=1-3,b=1-4
C    12) 1 CHAIN, TRANS = 0,1/2; a=1-2,b=1-4
C
C  Calculate unit cell vectors:
C
        DO 200 I=1,3
```

```
          GCT(I,1,1) = UCT(I,1) - UCT(I,2)
          GCT(I,2,1) = UCT(I,1) + UCT(I,2)
          GCT(I,3,1) = UCT(I,3)
          GCT(I,2,2) = 3.*UCT(I,1) - UCT(I,2)
          GCT(I,2,3) = 3.*UCT(I,2) - UCT(I,1)
          GCT(I,2,4) = 2.*UCT(I,1)
          GCT(I,2,5) = 2.*UCT(I,1)
          GCT(I,2,6) = 2.*UCT(I,2)
          GCT(I,2,7) = 2.*UCT(I,2)
          GCT(I,2,8) = UCT(I,1)
          GCT(I,2,9) = UCT(I,1)
          GCT(I,2,10) = UCT(I,2)
          GCT(I,2,11) = UCT(I,2)
          GCT(I,1,12) = UCT(I,1)
          GCT(I,2,12) = UCT(I,2)
          GCT(I,3,12) = UCT(I,3)
          DO 200 J=2,11
           IF( (J.EQ.5).OR.(J.EQ.9) ) THEN
             GCT(I,1,J) = -UCT(I,1) - UCT(I,2)
           ELSE IF ( (J.EQ.7).OR.(J.EQ.11) ) THEN
             GCT(I,1,J) = UCT(I,1) + UCT(I,2)
           ELSE
             GCT(I,1,J) = GCT(I,1,1)
           END IF
  200      GCT(I,3,J) = UCT(I,3)
C
C  Calculate unit cell scalars: sidelengths and angles:
C
        DO 300 K=1,12
          DOT1 = 0.
          DOT2 = 0.
          DOT3 = 0.
        DO 320 J=1,3
          GCL(J,K) = SQRT( GCT(1,J,K)**2+GCT(2,J,K)**2+GCT(3,J,K)**2 )
          DOT1 = DOT1 + GCT(J,2,K)*GCT(J,3,K)
          DOT2 = DOT2 + GCT(J,3,K)*GCT(J,1,K)
  320     DOT3 = DOT3 + GCT(J,1,K)*GCT(J,2,K)
          GCA(1,K) = ACOS( DOT1/GCL(2,K)/GCL(3,K) )/DEGRAD
          GCA(2,K) = ACOS( DOT2/GCL(3,K)/GCL(1,K) )/DEGRAD
          GCA(3,K) = ACOS( DOT3/GCL(1,K)/GCL(2,K) )/DEGRAD
  300   CONTINUE
C
C  Calculate potential hydrogen bonding orientations, distances, and
C  translational registers:
C
        DOT1 = 0.
        DOT2 = 0.
        DOT3 = 0.
        DOT4 = 0.
        UCT1M = SQRT( UCT(1,1)**2 + UCT(2,1)**2 )
        UCT2M = SQRT( UCT(1,2)**2 + UCT(2,2)**2 )
        GCT1M = SQRT( GCT(1,1,1)**2 + GCT(2,1,1)**2 )
        GCT2M = SQRT( GCT(1,2,1)**2 + GCT(2,2,1)**2 )
        D1M = SQRT((UCT(1,2)-GCT(1,1,1))**2+(UCT(2,2)-GCT(2,1,1))**2)
        DO 400 J=1,2
          DOT1 = DOT1 + UCT(J,1)*GCT(J,1,1)
          DOT2 = DOT2 + UCT(J,1)*GCT(J,2,1)
          DOT3 = DOT3 + UCT(J,1)*(UCT(J,2)-GCT(J,1,1))
  400     DOT4 = DOT4 + UCT(J,1)*UCT(J,2)
        GHYB(1) = OM1 + ACOS( DOT1/UCT1M/GCT1M )/DEGRAD
        GHYB(2) = OM1 - ACOS( DOT2/UCT1M/GCT2M )/DEGRAD
        GHYB(3) = OM1 - ACOS( DOT3/UCT1M/D1M   )/DEGRAD
        GHYB(4) = OM1 - ACOS( DOT4/UCT1M/UCT2M )/DEGRAD
        ASHFT = SS(1)/SS(3)*COS(SA(2)*DEGRAD)
        BSHFT = SS(2)/SS(3)*COS(SA(1)*DEGRAD)
        TXM1 = ASHFT - BSHFT
        TXM2 = ASHFT + BSHFT
        TXM3 = TX - TXM1 + BSHFT
        TXM4 = TX + BSHFT
C
C  Determine the 'best' unit cell representation:
```

```
C
      DO 600 I = 1,12
        KCTST(I) = ((I-1)/7)*5 + 1
        DO 610 J=1,3
  610     KCTST(I) = KCTST(I) + 9-NINT(ABS(GCA(J,I)-90.)/10.)
        IF( ABS(TX).LE..1) GO TO 600
          DO 630 J=8,12
  630       KCTST(J) = 0.
  600   CONTINUE
      KCELL = 1
      KCOUNT = 0
      DO 650 I=1,12
        IF(KCTST(I).LT.KCOUNT) GO TO 650
        KCELL = I
        KCOUNT = KCTST(I)
  650 CONTINUE
  660 WRITE(*,*) 'KCELL = ',KCELL
      WRITE(*,*) 'Do you agree? [Yes] > '
      READ(*,1) RARG
      LEN = LNBLNK(RARG)
      IF( LEN.GE.1 ) THEN
        IF( (RARG(1:1).EQ.'Y').OR.(RARG(1:1).EQ.'y') ) THEN
        ELSE IF( (RARG(1:1).EQ.'N').OR.(RARG(1:1).EQ.'n') ) THEN
          WRITE(*,*) 'Input desired cell type (1 - 12): > '
          READ(*,*) KF
          IF((KF.LT.1).OR.(KF.GT.12)) THEN
            WRITE(*,*) 'Invalid cell ID ... '
            GO TO 660
          ELSE
            KCELL = KF
          END IF
        ELSE
          GO TO 660
        END IF
      ELSE
      END IF
C
C  For selected cell configuration , compute chain setting angles
C  relative to bc facet.
C
      COX = XYZ(1,12,1)-XYZ(1,11,1)
      COY = XYZ(2,12,1)-XYZ(2,11,1)
      SETX = GCT(1,1,KCELL)*COX
      SETY = GCT(2,1,KCELL)*COY
      COM = COX**2 + COY**2
      GCTM = GCT(1,1,KCELL)**2 + GCT(2,1,KCELL)**2
      SETA1 = ACOS( (SETX+SETY)/SQRT(COM*GCTM) )
      SETA1 = SETA1/DEGRAD
      COX = XYZ(1,12,2)-XYZ(1,11,2)
      COY = XYZ(2,12,2)-XYZ(2,11,2)
c&&&  COX = XYZ(1,1,2)-XYZ(1,2,2)
c&&&  COY = XYZ(2,1,2)-XYZ(2,2,2)
      SETX = GCT(1,1,KCELL)*COX
      SETY = GCT(2,1,KCELL)*COY
      COM = COX**2 + COY**2
      GCTM = GCT(1,1,KCELL)**2 + GCT(2,1,KCELL)**2
      SETA2 = ACOS( (SETX+SETY)/SQRT(COM*GCTM) )
      SETA2 = SETA2/DEGRAD
C
      COX = XYZ(1,12,1)-XYZ(1,11,1)
      COY = XYZ(2,12,1)-XYZ(2,11,1)
      SETX = GCT(1,2,KCELL)*COX
      SETY = GCT(2,2,KCELL)*COY
      COM = COX**2 + COY**2
      GCTM = GCT(1,2,KCELL)**2 + GCT(2,2,KCELL)**2
      SETA3 = ACOS( (SETX+SETY)/SQRT(COM*GCTM) )
      SETA3 = SETA3/DEGRAD
      COX = XYZ(1,12,2)-XYZ(1,11,2)
      COY = XYZ(2,12,2)-XYZ(2,11,2)
c&&&  COX = XYZ(1,1,2)-XYZ(1,2,2)
c&&&  COY = XYZ(2,1,2)-XYZ(2,2,2)
```

```
        SETX = GCT(1,2,KCELL)*COX
        SETY = GCT(2,2,KCELL)*COY
        COM = COX**2 + COY**2
        GCTM = GCT(1,2,KCELL)**2 + GCT(2,2,KCELL)**2
        SETA4 = ACOS( (SETX+SETY)/SQRT(COM*GCTM) )
        SETA4 = SETA4/DEGRAD
C
C  Output cell conversion results:
C
        WRITE(10,1) TITLE
        WRITE(10,13) KCELL
        DO 900 K=1,12
        WRITE(10,9) K
        WRITE(10,2) GCL(1,K),GCL(2,K),GCL(3,K)
 900    WRITE(10,3) GCA(1,K),GCA(2,K),GCA(3,K)
        WRITE(10,*)
        WRITE(10,4) GHYB(1),GHYB(2),GHYB(3),GHYB(4)
        WRITE(10,8) GCT1M,GCT2M,D1M,UCT2M
        WRITE(10,7) TXM1,TXM2,TXM3,TXM4
        WRITE(10,5) (OM1-OM2)
        WRITE(10,6) TX
        WRITE(10,*) ' '
        WRITE(10,*) 'SET ANGLES REL TO GCT(1): ',SETA1,SETA2
        WRITE(10,*) 'SET ANGLES REL TO GCT(2): ',SETA3,SETA4
        CLOSE(UNIT=10)

C
C  Generate data file for CHARON plotting and X-Ray fiber diagram:
C
        CALL UCDRAW( KCELL,KIND,XYZ,GCT(1,1,KCELL),GCL(1,KCELL),
     +               GCA(1,KCELL),TITLE,KXRFD )
C
   2    FORMAT(' Sidelengths a,b & c   :',3(F7.2) )
   3    FORMAT(' Cell Angles al,be,ga  :',3(F7.2) )
   4    FORMAT(' 4 Potential H-Bondings:',4(F7.1) )
   5    FORMAT(' Relative Chain Rotate :',F7.1 )
   6    FORMAT(' Relative Chain Transl.:',F7.3 )
   7    FORMAT(' H-Bond Register       :',4(F7.3) )
   8    FORMAT(' H-Bond Chain Distance :',4(F7.2) )
   9    FORMAT(' General Cell Type ',I3 )
  13    FORMAT(' Best Cell Representation: ',I2)
  10    FORMAT(40A1,3F10.5)
  11    FORMAT(16A1,F9.5,18A1,F8.3)
  12    FORMAT(72A1)
  14    FORMAT(A1,6X,3(2X,F10.4))
        END


        SUBROUTINE UCDRAW( KCELL,KIND,XYZ,VECT,SIDE,ANG,PTITLE,KXR )
C
C  Routine to create SCHAKAL88B files for drawing unit cells of PPTA
C  simulations; used in conjunction with UCANAL, which provides
C  parameters necessary for unit cell definition.
C
C  *** marks modifications for HHTT isomers
C
        CHARACTER*1 KIND(84,4),FKIND(28,6)
c***    CHARACTER*1 KIND(168,4),FKIND(56,6)
        CHARACTER*8 FILENAME
        CHARACTER*72 GARB72
        CHARACTER*64 PTITLE
        INTEGER HPLOT
        DIMENSION XYZ(3,84,4),VECT(3,3),PXYZ(3,28,6),VTX(3,8)
c***    DIMENSION XYZ(3,168,4),VECT(3,3),PXYZ(3,56,6),VTX(3,8)
        DIMENSION SIDE(3),ANG(3),FXYZ(3,28,6)
c***    DIMENSION SIDE(3),ANG(3),FXYZ(3,56,6)
        NARU = 28
c***    NARU = 56
C       WRITE(*,*) 'INPUT TITLE >'
C       READ(*,7) PTITLE
C
```

```
C  Calculate unit cell vertices and fractional coordinates
C  of unique atoms (2 chains)
C

        DO 220 I=1,3
  220     VTX(I,1) = ( XYZ(I,NARU+11,1) + XYZ(I,NARU+13,1) )/2.
        D13 = 0.
        D24 = 0.
        DO 200 I=1,3
          VTX(I,2) = VTX(I,1) + VECT(I,1)
          VTX(I,3) = VTX(I,2) + VECT(I,2)
          VTX(I,4) = VTX(I,1) + VECT(I,2)
          VTX(I,5) = VTX(I,1)
          VTX(I,6) = VTX(I,2)
          VTX(I,7) = VTX(I,3)
          VTX(I,8) = VTX(I,4)
          D13 = D13 + (VTX(I,3)-VTX(I,1))**2
  200     D24 = D24 + (VTX(I,4)-VTX(I,2))**2
        DO 250 I=5,8
  250     VTX(3,I) = VTX(3,I) + SIDE(3)
        IF (KCELL.LE.3) THEN
          ZC = 0.5*( VTX(3,3) + VTX(3,1) )
        ELSE IF (KCELL.LE.7) THEN
          ZC = 0.5*( VTX(3,4) + VTX(3,1) )
        ELSE IF (KCELL.LE.11) THEN
          ZC = VTX(3,4)
        ELSE
          ZC = VTX(3,2)
        END IF
        KSECOND = 2
        IF( MOD(INT(KCELL/2),2).EQ.1 ) KSECOND = 4
        IF(KCELL.EQ.2) KSECOND = 2
        DO 240 I=1,3*NARU
          IF (KCELL.NE.2) THEN
            ZRSFT = 0.
          ELSE
            ZRSFT = VECT(3,1)
          END IF
  240     IF((XYZ(3,I,KSECOND)+ZRSFT).GE.ZC) GO TO 260
  260   NC = I - 1
        IF((MOD(NC,NARU).NE.1).AND.(MOD(NC,NARU).NE.15)) GO TO 280
c***    IF((MOD(NC,NARU).NE.1).AND.(MOD(NC,NARU).NE.15).and.
c*** +     (MOD(NC,NARU).NE.29).AND.(MOD(NC,NARU).NE.43)) GO TO 280
        IF( (ZC-ZRSFT-XYZ(3,NC,KSECOND))/(XYZ(3,NC+1,KSECOND)-
     +       XYZ(3,NC,KSECOND)).LT.0.5) THEN
          NC = NC - 1
        ELSE
          NC = NC + 9
        END IF
  280   CONTINUE
        DO 270 J=1,NARU
          J1 = NARU + 12 + J
          J2 = NC + J
          FKIND(J,1) = KIND(J1,1)
          FKIND(J,2) = KIND(J2,2)
          PXYZ(1,J,1) = XYZ(1,J1,1)
          PXYZ(2,J,1) = XYZ(2,J1,1)
          PXYZ(3,J,1) = XYZ(3,J1,1)
          PXYZ(1,J,2) = XYZ(1,J2,KSECOND)
          PXYZ(2,J,2) = XYZ(2,J2,KSECOND)
  270     PXYZ(3,J,2) = XYZ(3,J2,KSECOND)

C
        CALL FRCOORD( PXYZ,VECT,VTX(1,1),3,28,6,3,3,28,2,FXYZ)
c***    CALL FRCOORD( PXYZ,VECT,VTX(1,1),3,56,6,3,3,56,2,FXYZ)
C
C  Generate symmetry related coordinates appropriate to cell specified
C
        IF (KCELL.LE.3) THEN
          NCH = 5
          DO 400 I=1,NARU
```

```
            FKIND(I,3) = FKIND(I,1)
            FKIND(I,4) = FKIND(I,1)
            FKIND(I,5) = FKIND(I,1)
            DO 410 J=1,3
              DO 410 K=3,5
  410         FXYZ(J,I,K) = FXYZ(J,I,1)
           IF(KCELL.EQ.2) FXYZ(1,I,2) = FXYZ(1,I,2) + 1.
           FXYZ(1,I,3) = FXYZ(1,I,3) + 1.
           FXYZ(1,I,4) = FXYZ(1,I,4) + 1.
           FXYZ(2,I,4) = FXYZ(2,I,4) + 1.
  400      FXYZ(2,I,5) = FXYZ(2,I,5) + 1.
         ELSE IF (KCELL.LE.7) THEN
           NCH = 6
           DO 420 I=1,NARU
             FKIND(I,3) = FKIND(I,1)
             FKIND(I,4) = FKIND(I,1)
             FKIND(I,5) = FKIND(I,1)
             FKIND(I,6) = FKIND(I,2)
             DO 430 J=1,3
               FXYZ(J,I,6) = FXYZ(J,I,2)
               DO 430 K=3,5
  430          FXYZ(J,I,K) = FXYZ(J,I,1)
           FXYZ(1,I,3) = FXYZ(1,I,3) + 1.
           FXYZ(1,I,4) = FXYZ(1,I,4) + 1.
           FXYZ(2,I,4) = FXYZ(2,I,4) + 1.
           FXYZ(2,I,5) = FXYZ(2,I,5) + 1.
  420      FXYZ(1,I,6) = FXYZ(1,I,6) + 1.
         ELSE IF (KCELL.LE.11) THEN
           NCH = 4
           DO 440 I=1,NARU
             FKIND(I,3) = FKIND(I,1)
             FKIND(I,4) = FKIND(I,2)
             DO 450 J=1,3
               FXYZ(J,I,3) = FXYZ(J,I,1)
  450          FXYZ(J,I,4) = FXYZ(J,I,2)
           FXYZ(1,I,3) = FXYZ(1,I,3) + 1.
  440      FXYZ(1,I,4) = FXYZ(1,I,4) + 1.
         ELSE
           NCH = 4
           DO 460 I=1,NARU
             FKIND(I,3) = FKIND(I,1)
             FKIND(I,4) = FKIND(I,2)
             DO 470 J=1,3
               FXYZ(J,I,3) = FXYZ(J,I,1)
  470          FXYZ(J,I,4) = FXYZ(J,I,2)
           FXYZ(1,I,3) = FXYZ(1,I,3) + 1.
           FXYZ(2,I,3) = FXYZ(2,I,3) + 1.
           FXYZ(1,I,4) = FXYZ(1,I,4) - 1.
  460      FXYZ(2,I,4) = FXYZ(2,I,4) + 1.
         END IF
C
C  If specified, initiate generation of X-Ray Fiber Diagram:
C
         IF(KXR.EQ.0) CALL STRUFA(NARU,1,2,FKIND,FXYZ,
     +   PTITLE,VECT,SIDE,ANG )
C
         OPEN(UNIT=11,FILE='UCDRAW.OUT')
C
C  This code is specific for the generating SCHAKAL88 plot files
C
         WRITE(11,3) PTITLE
         WRITE(11,10) (SIDE(I),I=1,3),(ANG(I),I=1,3)
         MARK = 0
C         DO 500 N=1,NCH
         N = 0
  510    N = N+1
         DO 500 I=1,NARU
           MARK = MARK + 1
           IF(MARK.LE.9) THEN
             WRITE(11,4) FKIND(I,N),MARK,(FXYZ(J,I,N),J=1,3)
           ELSE IF(MARK.LE.99) THEN
```

```
            WRITE(11,5) FKIND(I,N),MARK,(FXYZ(J,I,N),J=1,3)
          ELSE
            WRITE(11,6) FKIND(I,N),MARK,(FXYZ(J,I,N),J=1,3)
          END IF
  500   CONTINUE
        IF(N.EQ.1) THEN
           WRITE(11,*) 'SYMM X+1,Y,Z'
           WRITE(11,*) 'SYMM X+1,Y+1,Z'
           WRITE(11,*) 'SYMM X,Y+1,Z'
           IF(NCH.GT.4) GO TO 510
        ELSE IF(NCH.EQ.6) THEN
           WRITE(11,*) 'SYMM X+1,Y,Z'
        ELSE
        END IF
        WRITE(11,9)
        CLOSE( UNIT=11 )
C
    2   FORMAT(A1,7X,3(2X,F10.4))
    3   FORMAT('TITLE ',A64)
    4   FORMAT('ATOM ',A1,I1,5X,3(F8.4,2X))
    5   FORMAT('ATOM ',A1,I2,4X,3(F8.4,2X))
    6   FORMAT('ATOM ',A1,I3,3X,3(F8.4,2X))
    7   FORMAT(A64)
    8   FORMAT(A72)
    9   FORMAT('END')
   10   FORMAT('CELL ',6(1X,F6.2) )
        END


        SUBROUTINE FRCOORD( CXYZ,UCV,ORIG,ND,NA,NM,NU,N1,N2,N3,FXYZ)
C
C  Converts coordinates from Cartesian to Fractional:
C  ND x NA x NM is the size of the array containing the Cartesian
C  coordinates: first dimension is coordinate, second dimension is
C  atoms in a molecule, third dimension is number of molecules.
C  N1 x N2 x N3 is the in-use portion of the array.
C  UCV is the unit cell lattice vector array, having phsyical dimensions
C  NU x NU.  ORIG(i) is the Cartesian coordinate of the origin
C
C       DIMENSION CXYZ(ND,NA,NM),FXYZ(ND,NA,NM),UCV(NU,NU),ORIG(NU),
        DIMENSION CXYZ(3,28,6),FXYZ(3,28,6),UCV(3,3),ORIG(3),
c***    DIMENSION CXYZ(3,56,6),FXYZ(3,56,6),UCV(3,3),ORIG(3),
     +            UCM(3),UCVT(3,3),UCVTI(3,3),INDX(3),CSHFT(3)
        DO 100 K=1,N3
          DO 100 J=1,N2
            DO 100 I=1,3
  100         FXYZ(I,J,K) = 0.
C
C  Compute inverse lattice vector matrix:
C
        DO 200 I=1,3
          DO 200 J=1,3
  200       UCVT(J,I) = UCV(J,I)
        DO 220 I=1,3
          DO 210 J=1,3
  210       UCVTI(I,J) = 0.
  220     UCVTI(I,I) = 1.
        CALL LUDCMP( UCVT,3,3,INDX,D )
        DO 230 J=1,3
  230     CALL LUBKSB( UCVT,3,3,INDX,UCVTI(1,J) )
C
C  Convert to fractional coordinates:
C
        DO 300 K = 1,N3
          DO 300 J=1,N2
            DO 310 I=1,3
  310         CSHFT(I) = CXYZ(I,J,K) - ORIG(I)
  300       CALL MV( UCVTI,3,3,CSHFT,3,FXYZ(1,J,K) )
        RETURN
        END
```

```
      SUBROUTINE STRUFA( NARU,NRUC,NCH,FKIND,FXYZ,
     +      TITLE,VECT,SIDE,ANG)
C
C  Program generates theoretical WAXS data for stuctures predicted
C  by Polymer Crystal Model program.  The required input is the
C  Number of Atoms per Repeat Unit, Number of Repeat Units generated per
C  Chain, the Number of CHains per cell, the x-ray WaVeLength, the range
C  of H,K,L of interest, and the identity (atomic number) and cartesian
C  coordinates of each atom in the unit cell, the "primary axes" and
C  "primary interaxial angles" as defined within PCM program.
C  Also used are the "half-beta angle" (Lorentz factor calculation as
C  per Wolff [Alexander,"X-Ray Diffraction Methods in Polymer Science",
C  p41] ) and the Bragg angle for monochromator (polarization factor
C  calculation [Alexander, p40] ).
C
C  The program calculates the conventional crystallographic axes/angles,
C  determines the type of unit cell, converts to fractional coordinates,
C  and calculates the d spacing, 2*theta angle, beta angle, polarization
C  factor, Lorentz factor, structure factor, and reflection intensity for
C  each (H,K,L) of interest.
C
C  If a fiber diagram is requested, the user is prompted for plotting
C  information required by subroutine STIPLOT (for Laserjet printing)
C  or GOURPLOT (for display on IRIS 4D-GT) (via PLORG)
C
      INTEGER H
      LOGICAL FRST
      CHARACTER*64 TITLE,RARG
      CHARACTER*1 FKIND(28,6)
c***  CHARACTER*1 FKIND(56,6)
      INTEGER*2 LNBLNK
      PARAMETER (EPSILON=1E-6,NSPT=1000)
      COMMON /VECT/ CRAX(3,3),RLV(3,3),VOL
      COMMON /PEAKS/ NS,TWOTH(NSPT),BETA(NSPT),AMP(NSPT)
      COMMON /UNICOM/ IOPORT,MODEL,XCORNER,YCORNER,AXL,TTM,ARCRESOL,
     +                SPOTRESOL,PERO
      DIMENSION CXM(3),CAN(3),RHO(3),VECT(3,3),SIDE(3),ANG(3)
      DIMENSION KIND(28,2),FXYZ(3,28,6)
c***  DIMENSION KIND(56,2),FXYZ(3,56,6)
      DIMENSION D(-6:6,-6:6,-6:6),BTA(-6:6,-6:6,-6:6)
c***  DIMENSION D(-9:9,-9:9,-9:9),BTA(-9:9,-9:9,-9:9)
      DIMENSION TTA(-6:6,-6:6,-6:6),F(-6:6,-6:6,-6:6)
c***  DIMENSION TTA(-9:9,-9:9,-9:9),F(-9:9,-9:9,-9:9)
      DIMENSION P(-6:6,-6:6,-6:6),Z(-6:6,-6:6,-6:6),E(-6:6,-6:6,-6:6)
c***  DIMENSION P(-9:9,-9:9,-9:9),Z(-9:9,-9:9,-9:9),E(-9:9,-9:9,-9:9)
      DIMENSION MILLER(3,NSPT)
      PI = 3.1415926535
      BEE  = 5.
      FRST = .TRUE.
      DO 100 I=1,3
        CXM(I) = SIDE(I)
        CAN(I) = ANG(I)*PI/180.
        DO 100 J=1,3
  100     CRAX(I,J) = VECT(I,J)
      DO 120 I=1,2
        DO 120 J=1,NARU
          IF(FKIND(J,I).EQ.'C') THEN
            KIND(J,I) = 6
          ELSE IF(FKIND(J,I).EQ.'H') THEN
            KIND(J,I) = 1
          ELSE IF(FKIND(J,I).EQ.'N') THEN
            KIND(J,I) = 7
          ELSE IF(FKIND(J,I).EQ.'O') THEN
            KIND(J,I) = 8
          ELSE IF(FKIND(J,I).EQ.'L') THEN
            KIND(J,I) = 17
          ELSE
          END IF
  120   CONTINUE
C
```

```
      OPEN (UNIT=11, FILE='SF.RES')
      OPEN (UNIT=12, FILE='SF.PLT')
  200 WRITE(*,*) 'Do you to plot a fiber diagram? [NO] > '
      READ(*,7) RARG
      LEN = LNBLNK(RARG)
      IF( LEN.GE.1 ) THEN
        IF( (RARG(1:1).EQ.'Y').OR.(RARG(1:1).EQ.'y') ) THEN
          KPLOT = 1
        ELSE IF( (RARG(1:1).EQ.'N').OR.(RARG(1:1).EQ.'n') ) THEN
          KPLOT = 0
        ELSE
          GO TO 200
        END IF
      ELSE
        KPLOT = 0
      END IF
      WRITE(*,*) 'Input Wavelength, MO, and MX > '
      READ (*,*) WVL,MO,MX
      WRITE(*,*) 'Input Beta orientation and monochromator angles >'
      READ (*,*) BETAHAF,CHROM
      TEE = 0.815*BETAHAF*PI/180.
      CHROM = CHROM*PI/180.
C
C  Generate reciprocal lattice vectors:
C
      CALL LATCON
C
C  Determine Space Group (1=Cubic, 2=Tetragonal, 3=Orthorhombic,
C  4=Hexagonal, 5=Monoclinic, 6=Triclinic ) Symmetry:
C
      KSG = 1
      IF( (CXM(1).NE.CXM(2)).OR.(CXM(1).NE.CXM(3)).OR.
     +     (CXM(2).NE.CXM(3)) ) KSG = 2
      IF((CXM(1).NE.CXM(2)).AND.(CXM(1).NE.CXM(3)).AND.
     +     (CXM(2).NE.CXM(3))) KSG = 3
      IF( ABS(CAN(3)-PI/2.).GT.EPSILON ) THEN
        IF( ABS(CAN(3)-2.*PI/3.).LE.EPSILON ) THEN
          KSG = 4
        ELSE
          KSG = 5
        END IF
      ELSE
      END IF
      IF( (ABS(CAN(1)-PI/2.).GT.EPSILON).OR.(ABS(CAN(2)-PI/2.).GT.
     +      EPSILON)) KSG = 6

      EHA = 0.
      N = 1
      WRITE(*,*) 'Calculating Intensities...'
      DO 500 H=MO,MX
      DO 500 K=MO,MX
      DO 500 L=0,MX
        IF( (H.EQ.0).AND.(K.EQ.0).AND.(L.EQ.0) ) GO TO 500
        RH = REAL(H)
        RK = REAL(K)
        RL = REAL(L)
        A = 0.
        B = 0.
        DET1 =(RH/CXM(1)+COS(CAN(1))*COS(CAN(2))*RK/CXM(2)+
     +          COS(CAN(3))*COS(CAN(1))*RL/CXM(3))-(RH/CXM(1)*
     +          COS(CAN(1))**2+COS(CAN(3))*RK/CXM(2)+
     +          COS(CAN(2))*RL/CXM(3))
        DET2 =(RK/CXM(2)+COS(CAN(2))*COS(CAN(3))*RL/CXM(3)+
     +          COS(CAN(1))*COS(CAN(2))*RH/CXM(1))-(RK/CXM(2)*
     +          COS(CAN(2))**2+COS(CAN(1))*RL/CXM(3)+
     +          COS(CAN(3))*RH/CXM(1))
        DET3 =(RL/CXM(3)+COS(CAN(3))*COS(CAN(1))*RH/CXM(1)+
     +          COS(CAN(2))*COS(CAN(3))*RK/CXM(2))-(RL/CXM(3)*
     +          COS(CAN(3))**2+COS(CAN(2))*RH/CXM(1)+
     +          COS(CAN(1))*RK/CXM(2))
        DET4 =(1.+2.*COS(CAN(1))*COS(CAN(2))*COS(CAN(3)))-
```

```
     +          (COS(CAN(1))**2+COS(CAN(2))**2+COS(CAN(3))**2)
           D(H,K,L) = 1./(SQRT( (RH*DET1/CXM(1)+RK*DET2/CXM(2)+RL*DET3/
     +                  CXM(3))/DET4))
           IF( (REAL(N)*WVL/2).GT.D(H,K,L) ) GO TO 500
             ORD = REAL(N)/2./D(H,K,L)
             TTA(H,K,L) = ASIN( WVL*ORD )
C
C  Sum over all atoms in the unit cell:
C
             DO 550 NCN=1,NCH
             DO 550 NAT=1,NARU
               FATM = ATSCAT(KIND(NAT,NCN),ORD)
               ARG=RH*FXYZ(1,NAT,NCN)+RK*FXYZ(2,NAT,NCN)+
     +             RL*FXYZ(3,NAT,NCN)
               A = A + FATM*COS(2.*PI*ARG)
               B = B + FATM*SIN(2.*PI*ARG)
  550        CONTINUE
             F(H,K,L) = SQRT( A**2 + B**2 )
C
C  Calculate Lorentz Factor (paratropic, general, or diatropic)
C  and azimuthal angle of reflection beta:
C
             IF (L.EQ.0) THEN
               Z(H,K,L) = 1./( (SIN(TTA(H,K,L)))**2*COS(TTA(H,K,L)) )
               BTA(H,K,L) = 0.
             ELSE
               RHOM = 0.
               PDOT = 0.
               DO 700 I=1,3
                 RHO(I) = RH*RLV(I,1)+RK*RLV(I,2)+
     +                    RL*RLV(I,3)
                 PDOT = PDOT + RHO(I)*CRAX(I,3)
  700            RHOM = RHOM + RHO(I)**2
               PARG = PDOT/CXM(3)/SQRT(RHOM)
               IF(ABS(PARG-1.).LT.EPSILON) PARG = 1.
               PHI = ACOS( PARG )
               BTA(H,K,L) = 90. - PHI*180./PI
               IF( (H.NE.0).OR.(K.NE.0) ) THEN
                 Z(H,K,L) = 1./((SIN(TTA(H,K,L)))**2*COS(TTA(H,K,L))
     +                        *SIN(PHI))
               ELSE
                 Z(H,K,L) = 1./((SIN(TTA(H,K,L)))**2*COS(TTA(H,K,L))*TEE)
               END IF
             END IF
             P(H,K,L) = (1.+(COS(CHROM))**2*(COS(2.*TTA(H,K,L)))**2)/
     +                  (1.+(COS(CHROM))**2)
             THRM     = -2.*BEE*ORD**2
             E(H,K,L) = F(H,K,L)**2*P(H,K,L)*Z(H,K,L)*EXP(THRM)
C
C  Additional intensity correction (2x) required for equatorial and
C  azimuthal reflections due to reflection distribution among half as
C  many spots in the Fiber Diagram Representation, and again (2x) for
C  all reflections L > 0, since these have been omitted from the loops
C  based on symmerty.  Net: Azimuthal reflections doubled...
C
             IF((90.-BTA(H,K,L)).LE.10*EPSILON) E(H,K,L) = 2.*E(H,K,L)
             EHA = MAX( EHA,E(H,K,L) )
  500    CONTINUE
         NS = 0
         DO 650 L=MX,0,-1
         DO 650 K=MX,MO,-1
         DO 650 H=MX,MO,-1
           NS = NS + 1
           MILLER(1,NS) = H
           MILLER(2,NS) = K
           MILLER(3,NS) = L
           TWOTH(NS) = 2.*TTA(H,K,L)*180./PI
           BETA(NS) = BTA(H,K,L)
           AMP(NS) = E(H,K,L)
           IF( (AMP(NS)/EHA).LT.0.00125) THEN
             NS = NS - 1
```

```
            GO TO 650
          ELSE
          END IF
          NSS = NS - 1
          IF( NS.EQ.1 )  GO TO 650
          DO 660 NCMP = 1,NSS
            IF( (ABS(TWOTH(NS)-TWOTH(NCMP)).LT.1E-3).AND.
     +          (ABS(BETA(NS)-BETA(NCMP)).LT.1E-3) ) THEN
              AMP(NCMP) = AMP(NCMP)+AMP(NS)
              NS = NSS
              GO TO 650
            ELSE
            END IF
  660     CONTINUE
  650   CONTINUE
        EHIGH = 0.
        DO 600 N=1,NS
  600     EHIGH = MAX( EHIGH,AMP(N) )
        WRITE(11,14)
        WRITE(11,20) KSG
        WRITE(11,15) (CXM(I),I=1,3)
        WRITE(11,16) ((CAN(I)*180./PI),I=1,3)
        WRITE(11,18) EHIGH
C       WRITE(12,6) TITLE
        WRITE(11,11)
        DO 610 N=1,NS
          AMP(N) = AMP(N)/EHIGH*100.
          IF( AMP(N).GT.0.25 ) THEN
          H = MILLER(1,N)
          K = MILLER(2,N)
          L = MILLER(3,N)
C         WRITE(12,13) H,K,L,P(H,K,L),Z(H,K,L),F(H,K,L),AMP(N)
            WRITE(11,17)H,K,L,TWOTH(N),BETA(N),AMP(N)
            WRITE(12,17)H,K,L,TWOTH(N),BETA(N),AMP(N)
          ELSE
          END IF
  610   CONTINUE
C
C  Plot if desired:
C
        ENDFILE(12)
        REWIND(12)
        IF( KPLOT.GT.0 ) CALL PLORG
C
        CLOSE (UNIT=11)
        CLOSE (UNIT=12)
    1   FORMAT( 3I4,F8.4,2I4 )
    2   FORMAT( 3F8.4 )
    3   FORMAT( I4,3F8.4 )
    4   FORMAT( 2F8.4 )
    5   FORMAT( A72 )
    6   FORMAT( 1X,A72 )
    7   FORMAT( A64)
   11   FORMAT( 1X,'Theoretical Structure Factors F(H,K,L)' )
   12   FORMAT( 1X,3('F(',I1,',',I1,',',I1,') ',F9.3,3X) )
   13   FORMAT( 1X,'H,K,L:M,P,Z,F,E ',3I2,I4,4F9.3 )
   14   FORMAT( 1X,'Crystallographic Unit Cell Parameters')
   15   FORMAT( 1X,'Sidelengths:     ',3F8.3 )
   16   FORMAT( 1X,'Internal Angles: ',3F8.3 )
   17   FORMAT( 1X,3I3,3F9.3 )
   18   FORMAT( 1X,'Max Absolute Intensity: ',E10.3 )
   20   FORMAT( 1X,'Space Group Symmetry:  ',I2 )
        END
```

```
      SUBROUTINE PLORG
C
C  Reformats simulation-generated peaks (discrete intensities at
C  various 2*theta,beta) to a 2*theta,beta grid of intensity
C  appropriate for STIPLOT (for Laserjet output) or GOURPLOT (for IRIS
C  4D-GT display)
C
C  Reflections are converted from Dirac spikes of intensity I to
C  Gaussian distributions through 2 dimensions (beta and two*theta)
C  having volumes equal to I.  The peak shape and resolution to
C  low intensity are controlled by WB and WT (peak widths at 50%
C  amplitude) and CO (cut-off intensity fraction, 0 < CO < 1 )
C
C  Gaussian:    Y = A*exp( -ln2 * ((X - P)/W)**2 )
C
C  Peaks are mapped onto a grid having resolution RB degrees in beta
C  and RT degrees in two*theta
C
      PARAMETER (NMAX=1001,NSPT=1000)
       COMMON /DPLOT/ NT,NB,TGO,TGX,BGO,BGX,Z(NMAX,NMAX)
       COMMON /PEAKS/ NS,TWOTH(NSPT),BETA(NSPT),AMP(NSPT)
       WRITE(*,*) ' '
       WRITE(*,*) 'Input Gaussian Widths (degrees): Two*Theta,Beta >'
       READ(*,*) WT,WB
       WRITE(*,*) 'Input Gaussian cutoff % (between 0 and 1) >'
       READ(*,*) CO
       WRITE(*,*) 'Input Diagram grid stepsize (2T,B) (degrees) >'
       READ(*,*) RT,RB
       PI = 3.1415926535
       DELBT = WB*SQRT( LOG(1./CO)/LOG(2.) )
       DELTT = WT*SQRT( LOG(1./CO)/LOG(2.) )
       DO 100 J=1,NMAX
         DO 100 I=1,NMAX
100        Z(I,J) = 0.
       TGO = 10.
       TGX = 0.
       BGO = 0.
       BGX = 0.
       DO 200 I=1,NS
         IF( AMP(I).LT.0.01 ) GO TO 200
         AMPMAX = MAX( AMPMAX,AMP(I) )
         TGO = MIN( TGO,TWOTH(I) )
         TGX = MAX( TGX,TWOTH(I) )
         BGO = MIN( BGO,BETA(I) )
         BGX = MAX( BGX,BETA(I) )
200    CONTINUE
       SCL = AMPMAX*4.*LOG(2.)/PI/WB/WT/100.
       TGX = MIN( TGX,50. )
       TGO = MAX( TGO,0. )
       WRITE(*,*) ' WARNING: Two Theta Limit in PLORG is 50 degrees'
       BGX = 90.
       BGO = MAX( BGO,0. )
       NT = NINT( (TGX-TGO)/RT ) + 1
       NB = NINT( (BGX-BGO)/RB ) + 1
       NSZB = NINT( DELBT/RB )
       NSZT = NINT( DELTT/RT )
       WRITE(*,*) ' Number of Peaks Predicted          : ',NS
       WRITE(*,*) ' Calculated Grid Size NTxNB         : ',NT,NB
       WRITE(*,*) ' Calculated Peak Grid Size NSZTxNSZB: ',NSZT,NSZB
       DO 500 I=1,NS
         AG = AMP(I)*4.*LOG(2.)/WB/WT/PI/SCL
         KTT = NINT( REAL(NT)*(TWOTH(I)-TGO)/(TGX-TGO) ) +1
         KBT = NINT( REAL(NB)*(BETA(I) -BGO)/(BGX-BGO) ) +1
         DO 520 JB=1,NSZB
           JBG = KBT - NINT(REAL(NSZB)/1.99) + JB
           IF( JBG.LE.0 ) GO TO 520
           IF( JBG.GT.NMAX ) GO TO 520
           DBSQ = ( REAL(JBG-KBT)*RB )**2
           BFUNC = EXP( -LOG(2.)*4.*DBSQ/WB**2 )
           DO 540 JT=1,NSZT
             JTG = KTT - NINT(REAL(NSZT)/1.99) + JT
```

```
            IF( JTG.LE.0 ) GO TO 540
            IF( JTG.GT.NMAX ) GO TO 540
            DTSQ = ( REAL(JTG-KTT)*RT )**2
            TFUNC = EXP( -LOG(2.)*4.*DTSQ/WT**2 )
            Z(JTG,JBG)=Z(JTG,JBG)+BFUNC*TFUNC*AG
  540      CONTINUE
  520    CONTINUE
  500   CONTINUE
C
C  XRC.DAT is the calculated intensity grid file for later comparison
C  to experiment
C
        OPEN( UNIT=10,FILE='XRC.DAT')
        WRITE(10,101) TGO,TGX,NT
        WRITE(10,101) BGO,BGX,NB
        DO 400 J=1,NB
        DO 400 I=1,NT,10
          IP = MIN(NT,I+9)
          WRITE(10,102) (Z(K,J),K=I,IP)
  400   CONTINUE
  101   FORMAT(1X,2F8.2,I4)
  102   FORMAT(10(1X,F7.2))
        CLOSE( UNIT=10)
C
C      CALL STIPLOT
        CALL GOURPLOT
        RETURN
        END


        SUBROUTINE GOURPLOT
C
C  This routine is modified for use with Gouraud shading display on
C  the IRIS workstation
C
C  Generates a stipled-pattern fiber diagram from regulary-gridded
C  X-ray data in 2*theta vs beta format.  The diagram appearance and
C  sensitivity may be adjusted by means of ZCH, ZCL, and NREF;  ZCH is
C  the upper critical percent intensity, above which the diagram is
C  saturated, while ZCL is the lower critical percent intensity, below
C  which intensity is not recorded.  Between these two intensities
C  stipling is controlled by a cubic spline function of raw intensity.
C  NREF is a reference linear dot density at half the radius of the
C  plot.
C
C  Generates all four quadrants
C  Data passed in common block DPLOT
C
        CHARACTER*72 TITLE
        CHARACTER*1 QTITLE(72)
        EQUIVALENCE (QTITLE(1),TITLE)
        PARAMETER (NMAX=1001)
        COMMON /DPLOT/ NT,NB,TGO,TGX,BGO,BGX,Z(NMAX,NMAX)
        DIMENSION X(NMAX,NMAX),Y(NMAX,NMAX)
        DIMENSION KCC,ZCLK(8),ZCHK(8),JSTIP(4)
        DIMENSION CDEF(3,8),ZCDF(8),ZKEY(8)
        DEGRAD = 3.1415926535/180.
C
C  DEFINE PLOTTING PARAMETERS:
C
        WRITE(*,*) ' Enter TITLE of Plot > '
        READ(*,3) TITLE
        WRITE(*,*) ' Enter Origin of Window (X,Y) (pixels) > '
        READ(*,*) XWO,YWO
        WRITE(*,*) ' Enter Window Size (pixels, square) > '
        READ(*,*) WSL
        WRITE(*,*) ' Enter (Fractional) Origin of Plot in Window (X,Y) > '
        READ(*,*) XCO,YCO
        WRITE(*,*) ' Enter Desired Axis Length (Fractional) > '
        READ(*,*) AXL2
        WRITE(*,*) ' Enter Maximum Two*Theta (degrees) > '
```

```
      READ(*,*) TTM
      WRITE(*,*) ' Enter Palette Color Code, ZCL AND ZCH > '
      READ(*,*) KCC,ZCL,ZCH
C
      ZMAX = -1.E6
      ZMIN =  1.E6
      DO 100 J=1,NB
      DO 100 I=1,NT
        ZMAX = MAX( ZMAX,Z(I,J) )
        ZMIN = MIN( ZMIN,Z(I,J) )
  100 CONTINUE
      TGXA = MIN( TGX,TTM )
      TSTP = (TGXA-TGO)/(NT-1)
      BSTP = (BGX-BGO)/(NB-1)
      WRITE(*,*) ' 2*Theta Range  : ',TGO,' to ',TTM
      WRITE(*,*) ' Beta Range     : ',BGO,' to ',BGX
      WRITE(*,*) ' Intensity Range: ',ZMIN,' to ',ZMAX
C
      DO 200 J=0,NB-1
      DO 200 I=0,NT-1
        ZLOC = ( Z(I+1,J+1)-ZMIN )/(ZMAX-ZMIN)
        TLOC = TGO + REAL(I)*TSTP
        BLOC = BGO + REAL(J)*BSTP
       XLOC = TLOC*COS( BLOC*DEGRAD )
       YLOC = TLOC*SIN( BLOC*DEGRAD )
       Z(NT+I,NB+J) = ZLOC
       X(NT+I,NB+J) = XLOC
       Y(NT+I,NB+J) = YLOC
       IF( J.NE.0) THEN
         Z(NT+I,NB-J) = ZLOC
         X(NT+I,NB-J) = XLOC
         Y(NT+I,NB-J) = -YLOC
        END IF
  200 CONTINUE
      NB = 2*NB - 1
      DO 250 J=1,NB
      DO 250 I=1,NT-1
        Z(NT-I,J) = Z(I+NT,J)
        X(NT-I,J) = -X(I+NT,J)
        Y(NT-I,J) = Y(I+NT,J)
  250 CONTINUE
      NT = 2*NT - 1
       ZCL = ZCL/100.
       ZCH = ZCH/100.
       ZDIF = ZCH - ZCL
       ZDF2 = ZDIF**2
       ZDF3 = ZDF2*ZDIF
       ZCL2 = ZCL**2
       AF = -2./ZDF3
       BF = 6.*ZCL/ZDF3 + 3./ZDF2
       CF = -6.*(ZCL2/ZDF3 + ZCL/ZDF2)
       DF = 2.*ZCL2*ZCL/ZDF3 +3.*ZCL2/ZDF2
C
C  Define specific points on the color scale:
C
     CALL PALETTE( KCC,NCOL,CDEF,ZKEY )
     DO 610 NC=1,NCOL
       ZZ = ZKEY(NC)*100.
      ZCDF(NC) = (ZZ - ZCL)/ZDIF
       ZCDF(NC) = ZCDF(NC)/100.
  610 CONTINUE

C
C  Renormalize grid values with new sensitivity range:
C  Loop over grid points:
C
      KPRN = 10
      DO 700 I=1,NB
      DO 700 J=1,NT
        IF( Z(J,I).LE.ZCL ) THEN
          Z(J,I) = 0.
```

```
          ELSE IF( Z(J,I).GE.ZCH ) THEN
             Z(J,I) = 1.
          ELSE
            ZZ = Z(J,I)
            Z(J,I) = (ZZ - ZCL)/ZDIF
          END IF
  700   CONTINUE
        CALL XRSHADE( XWO,YWO,WSL,XCO,YCO,AXL2,KCC,NT,NB,
     +                X,Y,Z,QTITLE,NCOL,ZKEY,ZCDF,CDEF )
        RETURN
C
    1   FORMAT(A25,3F12.5)
    2   FORMAT(5F12.5)
    3   FORMAT( A72 )
        END


        REAL FUNCTION RANDS1(SEED)
C
C       This is a special function for Random number generation
C       on 32-bit machines that do not support long integer
C       multiplication and truncation.  The technique used is to do
C       the multiplication and addition in parts, by splitting all
C       integers in a 'high' and a 'low' part.  The algorithm is
C       exact, and should give machine-independent results.
C
        INTEGER*4 SEED,IA,IB,I1,I2,I3

C       The algorithm implemented is (following D.E. Knuth):
C       seed = seed*1592653589 + 453816691
C       if (seed.lt.0) seed = seed + 1 + 2147483647
C       Note that 1592653589 = 48603*2**15 + 30485

        IA = SEED/32768
        IB = MOD(SEED,32768)
        I1 = IA*30485
        I2 = IB*30485
        I3 = IB*48603
        I1 = MOD(I1,65536)
        I3 = MOD(I3,65536)
        I1 = I1 + I3 + 13849 + I2/32768 + MOD(IA,2)*32768
        I2 = MOD(I2,32768) + 12659
        I1 = I1 + I2/32768
        I2 = MOD(I2,32768)
        I1 = MOD(I1,65536)

        SEED = I1*32768 + I2
        RANDS1 = SEED*4.65661287308D-10
        RETURN
        END


      SUBROUTINE XRSHADE( XWO,YWO,WSL,XCO,YCO,CSL,NPL,
     +                    NPH,NPV,XP,YP,ZP,QTITLE,
     +                    NCOL,ZKEY,ZCDF,CDEF )
C
C  Given a rectangular array of values (XP,YP,ZP), creates a x-ray
C  fiber diagram using Gouraud shading technique
C
      INTEGER*4 KXO,KYO,KXE,KYE
      INTEGER*4 WINOPE
      CHARACTER*72 CHARS
      CHARACTER*1 QTITLE(72),TLAB1,TLAB2,TLAB3,TLAB4,TLAB5
      PARAMETER (NMAX=1001)
      REAL BGD(3),CNO(3),PVTX(3,4),VTXC(3,4)
      REAL CDEF(3,8),ZCDF(8),ZKEY(8)
      REAL XP(NMAX,NMAX),YP(NMAX,NMAX),ZP(NMAX,NMAX)
      REAL XAX(2,2),YAX(2,2),XTIC(4,15),YTIC(4,15)
C
C  First, set array to be "colored" and normalize:
C
```

```
      ZPMAX = -1E6
      ZPMIN =  1E6
      XPMAX = -1E6
      XPMIN =  1E6
      YPMAX = -1E6
      YPMIN =  1E6
C
C  Renormalize data array (range = 0 - 1):
C
      DO 100 J=1,NPV
        DO 110 K=1,NPH
          ZPMAX = MAX(ZPMAX,ZP(K,J))
          ZPMIN = MIN(ZPMIN,ZP(K,J))
          XPMAX = MAX(XPMAX,XP(K,J))
          XPMIN = MIN(XPMIN,XP(K,J))
          YPMAX = MAX(YPMAX,YP(K,J))
          YPMIN = MIN(YPMIN,YP(K,J))
 110    CONTINUE
 100  CONTINUE
      IF(ZPMIN.LT.0.) WRITE(*,*) "ZPMIN less than zero; corrected"
      DO 120 J=1,NPV
        DO 120 I=1,NPH
          IF( ZPMIN.LT.0. ) THEN
            ZP(I,J) = (ZP(I,J)-ZPMIN)/(ZPMAX-ZPMIN)
          ELSE
            ZP(I,J) = ZP(I,J)/ZPMAX
          END IF
 120  CONTINUE
      WRITE(*,*) 'ZPMAX,ZPMIN: ',ZPMAX,ZPMIN
      WRITE(*,*) 'XPMAX,XPMIN: ',XPMAX,XPMIN
      WRITE(*,*) 'YPMAX,YPMIN: ',YPMAX,YPMIN
C
C  Determine axis construction:
C
      TICDIST = 10.
      XCE = XCO + CSL
      YCE = YCO + CSL
      XAX(1,1) = XCO
      XAX(2,1) = YCO + CSL/2.
      XAX(1,2) = XCE
      XAX(2,2) = XAX(2,1)
      YAX(1,1) = XCO + CSL/2.
      YAX(2,1) = YCO
      YAX(1,2) = YAX(1,1)
      YAX(2,2) = YCE
      NXTIC = NINT((XPMAX-XPMIN)/TICDIST) + 1
      NYTIC = NINT((YPMAX-YPMIN)/TICDIST) + 1
      DO 200 I=1,NXTIC
        XTIC(1,I) = XCO + REAL(I-1)/REAL(NXTIC-1)*CSL
        XTIC(2,I) = XAX(2,1) - CSL/50.
        XTIC(3,I) = XTIC(1,I)
 200    XTIC(4,I) = XAX(2,1) + CSL/50.
      DO 220 I=1,NYTIC
        YTIC(1,I) = YAX(1,1) - CSL/50.
        YTIC(2,I) = YCO + REAL(I-1)/REAL(NYTIC-1)*CSL
        YTIC(3,I) = YAX(1,1) + CSL/50.
 220    YTIC(4,I) = YTIC(2,I)
      DO 230 I=1,72
        J = 73-I
        IF(QTITLE(J).NE.' ') GO TO 240
 230  CONTINUE
 240  LENT = J
C
C  Define background and notation colors:
C  backgound corresponds to zero intensity;
C  notation corresponds to complement thereof
C
      DO 250 I=1,3
      BGD(I) = CDEF(I,1)
      CNO(I) = 0.3*(1. - BGD(I))
 250  CONTINUE
```

```
C
C  Open window and transform coordinates; define picture size and
C  configure monitor:
C
      WRITE(*,*) 'Ready to set up plot'
      KXO = INT(XWO)
      KXE = INT(XWO + WSL)
      KYO = INT(YWO)
      KYE = INT(YWO + WSL)
      CALL PREFPO( KXO,KXE,KYO,KYE )
      CALL NOBORD
      STATUS = WINOPE( "COLARRAY PROGRAM",20)
      CALL ORTHO2( 0.,1.,0.,1. )
      CALL RGBMOD
      CALL GCONFI
      CALL C3F(BGD)
      CALL CLEAR
C
C  Loop over all polygons:
C
      NPHM1 = NPH - 1
      NPVM1 = NPV - 1
      XSCL = CSL/(XPMAX - XPMIN)
      YSCL = CSL/(YPMAX - YPMIN)
      DO 300 I=1,NPHM1
      DO 300 J=1,NPVM1
C
C  Test for shading required:
C
        IF( (ZP(I,J).LE.ZCDF(1)).AND.(ZP(I+1,J).LE.ZCDF(1)).AND.
     +      (ZP(I,J+1).LE.ZCDF(1)).AND.(ZP(I+1,J+1).LE.ZCDF(1)) )
     +      GO TO 300
C
C Assign colors to the four vertices:
C
        DO 400 NC=1,NCOL-1
          IF( ZP(I,J).GE.ZCDF(NC) )
     +      NC1 = NC
          IF( ZP(I+1,J).GE.ZCDF(NC) )
     +      NC2 = NC
          IF( ZP(I+1,J+1).GE.ZCDF(NC) )
     +      NC3 = NC
          IF( ZP(I,J+1).GE.ZCDF(NC) )
     +      NC4 = NC
 400    CONTINUE
C
        PAR1 = (ZP(I,J)-ZCDF(NC1))/(ZCDF(NC1+1)-ZCDF(NC1))
        PAR2 = (ZP(I+1,J)-ZCDF(NC2))/(ZCDF(NC2+1)-ZCDF(NC2))
        PAR3 = (ZP(I+1,J+1)-ZCDF(NC3))/(ZCDF(NC3+1)-ZCDF(NC3))
        PAR4 = (ZP(I,J+1)-ZCDF(NC4))/(ZCDF(NC4+1)-ZCDF(NC4))
        DO 450 K=1,3
          VTXC(K,1) = CDEF(K,NC1)+PAR1*(CDEF(K,NC1+1)-CDEF(K,NC1))
          VTXC(K,2) = CDEF(K,NC2)+PAR2*(CDEF(K,NC2+1)-CDEF(K,NC2))
          VTXC(K,3) = CDEF(K,NC3)+PAR3*(CDEF(K,NC3+1)-CDEF(K,NC3))
          VTXC(K,4) = CDEF(K,NC4)+PAR4*(CDEF(K,NC4+1)-CDEF(K,NC4))
 450    CONTINUE
C
C  Place this polygon:
C
        PVTX(1,1) = (XP(I,J) - XPMIN)*XSCL + XCO
        PVTX(2,1) = (YP(I,J) - YPMIN)*YSCL + YCO
        PVTX(1,2) = (XP(I+1,J) - XPMIN)*XSCL + XCO
        PVTX(2,2) = (YP(I+1,J) - YPMIN)*YSCL + YCO
        PVTX(1,3) = (XP(I+1,J+1) - XPMIN)*XSCL + XCO
        PVTX(2,3) = (YP(I+1,J+1) - YPMIN)*YSCL + YCO
        PVTX(1,4) = (XP(I,J+1) - XPMIN)*XSCL + XCO
        PVTX(2,4) = (YP(I,J+1) - YPMIN)*YSCL + YCO
C
C  Color Polygon (Gouraud Shading)
C
        CALL BGNPOL()
```

```
        CALL C3F(VTXC(1,1))
        CALL V2F(PVTX(1,1))
        CALL C3F(VTXC(1,2))
        CALL V2F(PVTX(1,2))
        CALL C3F(VTXC(1,3))
        CALL V2F(PVTX(1,3))
        CALL C3F(VTXC(1,4))
        CALL V2F(PVTX(1,4))
        CALL ENDPOL()
 300  CONTINUE
C
C  Draw Equatorial Axis
C
      CALL C3F(CNO)
      CALL BGNLIN
      CALL V2F(XAX(1,1))
      CALL V2F(XAX(1,2))
      CALL ENDLIN
      DO 500 I=1,NXTIC
        CALL BGNLIN
        CALL V2F(XTIC(1,I))
        CALL V2F(XTIC(3,I))
        CALL ENDLIN
  500 CONTINUE
C
C  Draw Azimuthal Axis
C
      CALL BGNLIN
      CALL V2F(YAX(1,1))
      CALL V2F(YAX(1,2))
      CALL ENDLIN
      DO 520 I=1,NYTIC
        CALL BGNLIN
        CALL V2F(YTIC(1,I))
        CALL V2F(YTIC(3,I))
        CALL ENDLIN
  520 CONTINUE
C
C  Label Upper Half of Azimuth
C
      NLAB = (NYTIC - 1)/2
      DO 530 I=1,NLAB
        J = I + NYTIC - NLAB
        PLAB1 = YTIC(3,J) + CSL/100.
        PLAB2 = YTIC(4,J)
        TLAB1 = CHAR(I+ICHAR('0'))
        TLAB2 = '0'
        CALL CMOV2( PLAB1,PLAB2 )
        CALL CHARST( TLAB1,1 )
        CALL CHARST( TLAB2,1 )
  530 CONTINUE
C
C  Draw Title
C
      PLAB1 = XCO + CSL/2. - REAL(LENT/2)*(CSL/WSL)*25.
      PLAB2 = YCE + 25./WSL
      CALL CMOV2( PLAB1,PLAB2 )
      DO 540 I=1,LENT
        CALL CHARST( QTITLE(I),1 )
  540 CONTINUE
C
C  Create Key
C
      PLAB1 = XCE - 60.*CSL/WSL - 60*CSL/WSL
      PLAB2 = YCE - 25.*CSL/WSL
      DO 600 I=2,NCOL
        CALL C3F(CNO)
        CALL CMOV2( PLAB1,PLAB2 )
       TKEY = ZKEY(I)*100.
        IF( TKEY.GE.100. ) THEN
          KEY = INT(TKEY)
```

```
          KEY1 = KEY/100
          KEY2 = (KEY-KEY1*100)/10
          KEY3 = KEY-KEY1*100-KEY2*10
        ELSE IF( TKEY.GE.10. ) THEN
          KEY = INT(TKEY)
          KEY1 = ICHAR(' ') - ICHAR('0')
          KEY2 = KEY/10
          KEY3 = KEY-KEY2*10
        ELSE IF( TKEY.GE.1. ) THEN
          KEY1 = ICHAR(' ') - ICHAR('0')
          KEY2 = ICHAR(' ') - ICHAR('0')
          KEY3 = INT(TKEY)
        ELSE
          KEY1 = INT(TKEY)
          KEY2 = ICHAR('.') - ICHAR('0')
          KEY3 = INT(TKEY*10.) - KEY1*10
        END IF
        TLAB1 = CHAR(KEY1+ICHAR('0'))
        TLAB2 = CHAR(KEY2+ICHAR('0'))
        TLAB3 = CHAR(KEY3+ICHAR('0'))
        TLAB4 = '%'
        TLAB5 = ' '
        CALL CMOV2( PLAB1,PLAB2 )
        CALL CHARST( TLAB1,1 )
        CALL CHARST( TLAB2,1 )
        CALL CHARST( TLAB3,1 )
        CALL CHARST( TLAB4,1 )
        CALL CHARST( TLAB5,1 )
        PKXLO = PLAB1 + 110.*CSL/WSL
        PKYLO = PLAB2
        PKXHI = PKXLO + 60.*CSL/WSL
        PKYHI = PKYLO + 9.*CSL/WSL
        CALL C3F(CDEF(1,I))
        CALL RECTF( PKXLO,PKYLO,PKXHI,PKYHI )
        PLAB2 = PLAB2 - 40.*CSL/WSL
  600 CONTINUE
C
C Wait 10 seconds (or pause indefinitely)
C     CALL SLEEP(10)
      PAUSE
C and exit
      END


      SUBROUTINE PALETTE( NPL,N,A,Z )
      REAL A(3,8),Z(8)
C
      DO 75 J=1,4
        Z(J) = 0.
        DO 75 I=1,3
          A(I,J) = 0.
   75 CONTINUE
      GO TO ( 10,20,30,40,50,60,70,80,90,100,110,120,130,140,
     +        150 ) NPL
C Black to White:
   10 CONTINUE
      N = 2
      Z(2) = 1.
      DO 11 I=1,3
        A(I,2) = 1.
   11 CONTINUE
      GO TO 9999
C Black to Red:
   20 CONTINUE
      N = 2
      Z(2) = 1.
      A(1,2) = 1.
      GO TO 9999
C Black to Green:
   30 CONTINUE
      N = 2
```

```
      Z(2) = 1.
      A(2,2) = 1.
      GO TO 9999
C Black to Blue:
  40  CONTINUE
      N = 2
      Z(2) = 1.
      A(3,2) = 1.
      GO TO 9999
C Red to White:
  50  CONTINUE
      N = 2
      Z(2) = 1.
      A(1,1) = 1.
      DO 51 I=1,3
 51     A(I,2) = 1.
      GO TO 9999
C Green to White:
  60  CONTINUE
      N = 2
      Z(2) = 1.
      A(2,1) = 1.
      DO 61 I=1,3
 61   A(I,2) = 1.
      GO TO 9999
C Blue to White:
  70  CONTINUE
      N = 2
      Z(2) = 1.
      A(3,1) = 1.
      DO 71 I=1,3
 71     A(I,2) = 1.
      GO TO 9999
C Blue to Red:
  80  CONTINUE
      N = 2
      Z(2) = 1.
      A(3,1) = 1.
      A(1,2) = 1.
      GO TO 9999
C Cyan to Magenta:
  90  CONTINUE
      N = 2
      Z(2) = 1.
      A(2,1) = 1.
      A(3,1) = 1.
      A(1,2) = 1.
      A(3,2) = 1.
      GO TO 9999
C Black to Blue to Cyan to Green to Yellow to Red to Magenta to White
  100 CONTINUE
      N = 8
      DO 101 I=2,N
  101   Z(I) = REAL(I-1)/REAL(N-1)
      A(3,2) = 1.
      A(3,3) = 1.
      A(2,3) = 1.
      A(2,4) = 1.
      A(2,5) = 1.
      A(1,5) = 1.
      A(1,6) = 1.
      A(1,7) = 1.
      A(3,7) = 1.
      A(1,8) = 1.
      A(2,8) = 1.
      A(3,8) = 1.
      GO TO 9999
C Variable distribution of colors: black-gray1-gray2-gray3-white
  110 CONTINUE
      N = 5
      WRITE(*,*) '5 GRAYS: DEFINE INTENSITY LEVELS (0 - 1) >'
```

```
      READ(*,*) (Z(I),I=1,5)
      IF(Z(1).GT.0.) Z(1) = 0.
      DO 111 I=1,3
        A(I,2) = 0.25
        A(I,3) = 0.50
        A(I,4) = 0.75
        A(I,5) = 1.
  111 CONTINUE
      GO TO 9999
C Variable distribution of colors: black-red1-red2-red3-red4
  120 CONTINUE
      N = 5
      WRITE(*,*) '5 REDS: DEFINE INTENSITY LEVELS (0 - 1) >'
      READ(*,*) (Z(I),I=1,5)
      IF(Z(1).GT.0.) Z(1) = 0.
      A(1,2) = 0.25
      A(1,3) = 0.50
      A(1,4) = 0.75
      A(1,5) = 1.
      GO TO 9999
C Variable distribution of colors: black-red-magenta-yellow-white
  130 CONTINUE
      N = 5
      WRITE(*,*) '5 COLORS: DEFINE INTENSITY LEVELS (0 - 1) >'
      READ(*,*) (Z(I),I=1,5)
      IF(Z(1).GT.0.) Z(1) = 0.
      A(1,2) = 1.
      A(1,3) = 1.
      A(3,3) = 1.
      A(1,4) = 1.
      A(2,4) = 1.
      A(1,5) = 1.
      A(2,5) = 1.
      A(3,5) = 1.
      GO TO 9999
C Variable distribution of colors: black-blue-cyan-yellow-white
  140 CONTINUE
      N = 5
      WRITE(*,*) '5 COLORS: DEFINE INTENSITY LEVELS (0 - 1) >'
      READ(*,*) (Z(I),I=1,5)
      IF(Z(1).GT.0.) Z(1) = 0.
      A(3,2) = 1.
      A(2,3) = 1.
      A(3,3) = 1.
      A(1,4) = 1.
      A(2,4) = 1.
      A(1,5) = 1.
      A(2,5) = 1.
      A(3,5) = 1.
      GO TO 9999
C
C Variable distribution of colors: black-blue-cyan-yellow-white
  150 CONTINUE
      N = 5
      WRITE(*,*) '5 COLORS: DEFINE INTENSITY LEVELS (0 - 1) >'
      READ(*,*) (Z(I),I=1,N)
      IF(Z(1).GT.0.) Z(1) = 0.
      A(1,1) = .25
      A(2,1) = .25
      A(3,1) = .25
      A(3,2) = .75
      A(1,3) = .8
      A(2,3) = .5
      A(3,3) = .85
      A(2,4) = 1.
      A(3,4) = A(3,3)
      A(1,5) = 1.
      A(2,5) = A(2,4)
      A(3,5) = A(3,4)
      GO TO 9999
C
```

```
 9999 CONTINUE
      RETURN
      END


        SUBROUTINE VECTORIZ( SLEN,SANG,VECT )
C
C  Converts scalar data (lengths, angles) to three placement vectors
C  Convention:  SLEN(3) lies along Z axis
C               SLEN(1) lies within X-Z plane
C               SLEN(2) placement determined by above
C               SANG(i) is the angle between SLEN(j) and SLEN(k), etc.
C
        DIMENSION SLEN(3),SANG(3),VECT(3,3),ARA(3,3),ARB(3,3)
        COMPL(X) = (90.-X)*3.1415926535/180.
        DEGRAD = 3.1415926535/180.
        DO 100 I=1,3
        DO 100 J=1,3
          ARA(I,J) = 0.
          ARB(I,J) = 0.
  100     VECT(I,J) = 0.
        VECT(1,1) = SLEN(1)
        VECT(1,2) = SLEN(2)
        VECT(3,3) = SLEN(3)
        COSGP = ( COS(SANG(3)*DEGRAD)-COS(SANG(1)*DEGRAD)*COS(SANG(2)
     +          *DEGRAD) )/( SIN(SANG(1)*DEGRAD)*SIN(SANG(2)*DEGRAD) )
        GP = ACOS(COSGP)
        CA = COMPL(SANG(1))
        CB = COMPL(SANG(2))
        ARA(1,1) = COS(CB)
        ARA(1,3) = -SIN(CB)
        ARA(2,2) = 1.
        ARA(3,1) = SIN(CB)
        ARA(3,3) = COS(CB)
        ARB(1,1) = COSGP*COS(CA)
        ARB(1,2) = -SIN(GP)
        ARB(1,3) = -COSGP*SIN(CA)
        ARB(2,1) = SIN(GP)*COS(CA)
        ARB(2,2) = COSGP
        ARB(2,3) = -SIN(GP)*SIN(CA)
        ARB(3,1) = SIN(CA)
        ARB(3,3) = COS(CA)
        CALL MV( ARA,3,3,VECT(1,1),3,VECT(1,1) )
        CALL MV( ARB,3,3,VECT(1,2),3,VECT(1,2) )
        RETURN
        END


        SUBROUTINE LATCON
C
C  This subroutine generate the unit cell volume and reciprocal lattice
C  vectors from unit cell vectors.  Cell vectors should be defined such
C  that the c axis coincides with the z axis.
C
        COMMON /VECT/ CRAX(3,3),RLV(3,3),VOL
        DIMENSION TEMP(3)
        CALL VV(CRAX(1,2),CRAX(1,3),TEMP,3)
        VOL = 0.
        DO 100 I=1,3
  100     VOL = CRAX(I,1)*TEMP(I) + VOL
        DO 300 J=1,3
          JP1 = MOD( J,3 ) +1
          JP2 = MOD( (J+1),3 ) +1
          CALL VV(CRAX(1,J),CRAX(1,JP1),TEMP,3)
          DO 200 I=1,3
  200       RLV(I,JP2) = TEMP(I)/VOL
  300   CONTINUE
        RETURN
        END
```

```
      SUBROUTINE VV( A,B,C,N )
C
C  Calculates the vector cross product C = A x B, where A,B, and C
C  have length N
C
      DIMENSION A(N),B(N),C(N),K(2)
      DO 100 I=1,N
        DO 200 J=1,2
  200     K(J) = MOD( (I+J-1),N ) +1
        C(I) = A(K(1))*B(K(2)) - A(K(2))*B(K(1))
  100 CONTINUE
      RETURN
      END


      SUBROUTINE MV( A,NFORMA,NA,V,N,R )
C
C  Multiplies matrix and vector: R = A * V
C  Input:  A           NA x N matrix
C          NFORMA      First dimension of A in calling program
C          NA          Number of rows in A
C          V           Vector of length N
C          N           Length of vector V
C  Output: R           Resultant vector of length NA, can be A
C
      DIMENSION A(NFORMA,NFORMA), V(N), R(NA), RR(20)
      IF (NA.GT.NFORMA) RETURN
      DO 100 I=1,NA
        X = 0.
        DO 200 K=1,N
  200     X = X + A(I,K)*V(K)
  100   RR(I) = X
      DO 300 I=1,NA
  300   R(I) = RR(I)
      RETURN
      END


      SUBROUTINE MM( A,B,C,NFORMA,NFORMB,NFORMC,NA,MA,MB )
C
C      - Multiplies matrix with matrix: C = A X B
C                                       (C can be A or B)
C
      DIMENSION CC(20,20),A(NFORMA,NFORMA),B(NFORMB,NFORMB)
      DIMENSION C(NFORMC,NFORMC)
      DO 100 I=1,NA
        DO 100 J=1,MB
          X = 0.
          DO 200 K=1,MA
  200       X = X + A(I,K)*B(K,J)
  100     CC(I,J) = X
      DO 300 I=1,NA
        DO 300 J=1,MB
  300     C(I,J) = CC(I,J)
      RETURN
      END


      FUNCTION ATSCAT( KA,X )
C
C  Calculates atomic scattering factor, given atom type and ordinate
C  function sin(theta)/lambda , where theta is scattering angle and
C  lambda is the incident x-ray wavelength.  the scattering factors
C  are calculated from a best fit curve of the form:
C
C      F(X) = P(1)*EXP(-P(2)*X**2) + P(3)*EXP(-P(4)*X**2) + P(5)
C
C  Applied to values provided by L.E. Alexander, 'X-ray Diffraction
C  Methods in Polymer Science', Wiley-Interscience,1969,p533, taken
C  in turn from 'International Tables for X-ray Crystallography',
C  Volume III, p202.
```

```
C       ordinate range = 0.0 - 1.0
C       weighting factor = exp( -(x-0.5)**2 )
C  Data in P array correspond to: P(i,1) = carbon
C                                 P(i,2) = hydrogen
C                                 P(i,3) = nitrogen
C                                 P(i,4) = oxygen
C                                 P(i,5) = [empty]
C                                 P(i,6) = chlorine
C                                 P(i,7) = bromine
C
        DIMENSION P(5,7)
        DATA P/1.248 ,2.517,3.678 ,23.747,1.044,
     +         0.3916,7.483,0.5958,30.072,0.0107,
     +         1.778 ,3.836,3.938 ,19.226,1.260,
     +         2.836 ,4.423,3.773 ,17.229,1.373,
     +         0.,0.,0.,0.,0.,
     +         8.066 ,0.9734,7.983,22.093,0.9458,
     +         19.47 ,2.192,8.390 ,27.804,7.083/
C
C  Convert atomic numbers to array identification:
C
      IF( KA.EQ.6 ) THEN
        K = 1
      ELSE IF( KA.EQ.1 ) THEN
        K = 2
      ELSE IF( KA.EQ.7 ) THEN
        K = 3
      ELSE IF( KA.EQ.8 ) THEN
        K = 4
      ELSE IF( KA.EQ.9 ) THEN
        K = 5
      ELSE IF( KA.EQ.17 ) THEN
        K = 6
      ELSE IF( KA.EQ.35 ) THEN
        K = 7
      ELSE
        WRITE(*,*) 'ERROR: Atomic Scattering Curve Not Available'
      END IF
      ATSCAT=P(1,K)*EXP(-P(2,K)*X**2)+P(3,K)*EXP(-P(4,K)*X**2)+P(5,K)
      RETURN
      END


      SUBROUTINE LUBKSB(A,N,NP,INDX,B)
      DIMENSION A(NP,NP),INDX(N),B(N)
      II=0
      DO 12 I=1,N
        LL=INDX(I)
        SUM=B(LL)
        B(LL)=B(I)
        IF (II.NE.0)THEN
          DO 11 J=II,I-1
            SUM=SUM-A(I,J)*B(J)
11        CONTINUE
        ELSE IF (SUM.NE.0.) THEN
          II=I
        ENDIF
        B(I)=SUM
12    CONTINUE
      DO 14 I=N,1,-1
        SUM=B(I)
        IF(I.LT.N)THEN
          DO 13 J=I+1,N
            SUM=SUM-A(I,J)*B(J)
13        CONTINUE
        ENDIF
        B(I)=SUM/A(I,I)
14    CONTINUE
      RETURN
      END
```

```
      SUBROUTINE LUDCMP(A,N,NP,INDX,D)
      PARAMETER (NMAX=100,TINY=1.0E-20)
      DIMENSION A(NP,NP),INDX(N),VV(NMAX)
      D=1.
      DO 12 I=1,N
        AAMAX=0.
        DO 11 J=1,N
          IF (ABS(A(I,J)).GT.AAMAX) AAMAX=ABS(A(I,J))
11      CONTINUE
        IF (AAMAX.EQ.0.) PAUSE 'Singular matrix.'
        VV(I)=1./AAMAX
12    CONTINUE
      DO 19 J=1,N
        IF (J.GT.1) THEN
          DO 14 I=1,J-1
            SUM=A(I,J)
            IF (I.GT.1)THEN
              DO 13 K=1,I-1
                SUM=SUM-A(I,K)*A(K,J)
13            CONTINUE
              A(I,J)=SUM
            ENDIF
14        CONTINUE
        ENDIF
        AAMAX=0.
        DO 16 I=J,N
          SUM=A(I,J)
          IF (J.GT.1)THEN
            DO 15 K=1,J-1
              SUM=SUM-A(I,K)*A(K,J)
15          CONTINUE
            A(I,J)=SUM
          ENDIF
          DUM=VV(I)*ABS(SUM)
          IF (DUM.GE.AAMAX) THEN
            IMAX=I
            AAMAX=DUM
          ENDIF
16      CONTINUE
        IF (J.NE.IMAX)THEN
          DO 17 K=1,N
            DUM=A(IMAX,K)
            A(IMAX,K)=A(J,K)
            A(J,K)=DUM
17        CONTINUE
          D=-D
          VV(IMAX)=VV(J)
        ENDIF
        INDX(J)=IMAX
        IF(J.NE.N)THEN
          IF(A(J,J).EQ.0.)A(J,J)=TINY
          DUM=1./A(J,J)
          DO 18 I=J+1,N
            A(I,J)=A(I,J)*DUM
18        CONTINUE
        ENDIF
19    CONTINUE
      IF(A(N,N).EQ.0.)A(N,N)=TINY
      RETURN
      END
```